Ninth International Workshop on Laser Ranging Instrumentation

incorporating a

Symposium on Western Pacific Laser Ranging Network

WPLS '94

Canberra 1994

VOLUME 1

Compiled and edited by John McK. Luck
with assistance from Georgina R. Luck, Mark J. Elphick, Robbie Horn

Australian Government Publishing Service
Canberra

ISBN 0 644 47424 6 (Vol. 1)
ISBN 0 644 47427 0 (Set)

The Ninth International Workshop on Laser Ranging Instrumentation, incorporating WPLS '94, was held at Becker House, Canberra, Australia, from 7 to 11 November 1994.

Workshop sponsors: Auslig, EOS, Qantas

Symposium sponsor: STA, Japan

Papers compiled and edited by:
John McK. Luck
Orroral Geodetic Observatory
Australian Surveying and Land Information Group
Canberra ACT, Australia

Cover photograph: Orroral Observatory, Australia
Photographer: Anthony Willing

Produced by the Australian Government Publishing Service

TABLE OF CONTENTS

VOLUME 1

VOLUME 2

VOLUME 3

SYMPOSIUM on Western Pacific Laser Ranging Network (WPLS'94)
Convenor: Hiroo Kunimori
Papers presented during Workshop sessions are noted by (W) in Table of Contents for Volumes 1 & 2.

Viewgraph Presentations

Future Science Applications—Christian Veillet

Presentations Not Recorded in the Proceedings
Invited Paper: *25 Years of LLR,* C. Alley

ZIMLAT: The New Zimmerwald Laser and Astrographic Telescope, W. Gurtner, E. Pop, T. Schildknecht, J. Utzinger, U Wild

Transmit/Receive Electronics for SLR 2000, T. Varghese, R. Eichinger, C. Steggerda, H. Donovan, J. Degnan

Development of an Automated Q/C Model for NASA SLR Data, J. Horvath, V. Husson

Automatic and Remote Control of SLR Systems, B. Greene, T. May, J. Luck, H. Kunimori

INTRODUCTION

The Ninth International Workshop on Laser Ranging Instrumentation was held at Becker House, Acton in the centre of Canberra, The Australian Capital Territory on 7-11 November, 1994. There were 142 attendees from overseas and about 30 from Australia. We heartily thank the participants, the organisers and their bands of helpers, and the speakers for making it a very special and happy occasion.

Very special thanks go to Nerida Dunn, Events Coordinator of the Australian Academy of Science, and to her staff, for organising and setting up Becker House as such a magnificent venue for the Workshop, and being on hand throughout the whole week, including nights, to attend to the many little problems and requests which arose. She was instrumental in coordinating the rather splendid lunches and morning and afternoon teas which were available each day, and in facilitating photocopying and communications services including fax and E-mail.

Extra special thanks go to Anne Smith of EOS and Gordon Baker of Orroral, for doing very nearly all the hard work before and during the Workshop, such as dealing with registrations, hotel and travel arrangements, maintaining the accounts, providing transportation, organising all the food including the Great Orroral Barbecue, and the one hundred and one other things needed to make such an event work and run smoothly. They received a great deal of support from colleagues in their respective organisations, but theirs were the vital contributions. Other important contributors were Mark Elphick of Orroral, especially in preparing the Circulars, and Steve Cootes of Orroral for managing the communications links.

Our guests were welcomed by the windiest period of weather in Canberra's history, which even prevented some arrivals at Canberra Airport. It got worse in time for the Barbecue at Orroral Observatory, when the wind turned icy and snow fell. Fortunately, the second half of the week produced the lovely mild Spring days and clear, cool evenings which had been advertised in the Workshop Circulars.

A feature of the Canberra Workshop was the Symposium on Western Pacific Satellite Laser Ranging Network (WPLS'94) held in the evening of Monday 7 November, sponsored by the Science and Technology Agency of Japan. This brought many delegates from Japan and China in particular, and led to the establishment of the Western Pacific Laser Tracking Network (WPLTN). Hiroo Kunimori did a great job organising the Symposium and meshing it in with the Workshop.

This was the first Workshop held outside USA and Europe. An underlying theme was the development of the technique in the Asia-Pacific Region. Besides numerous presentations from the region, there was a very fruitful invitational discussion on the Asia-Pacific Space Geodynamics Project immediately after the Workshop, led by Yang Fu-Min of Shanghai Observatory, at which parameters for the development of the concept were set.

We hope that the following Proceedings will help re-live a very special occasion in all our lives.

Ben Greene
Chairman, Program Committee

John Luck
Local Organising Committee

EDITORIAL NOTE

I would like to thank all the Session Chairpeople for collating the papers in the Sessions and forwarding them on to me, and for hounding delinquent authors. The efforts of Jan McGarry were outstanding - she had collected all the papers in her session within three months, and provided comprehensive lists to make an Editor's lot easier.

The Program Committee resolved that, where full manuscripts were not available, copies of viewgraphs would be accepted for publication in these Proceedings, if in reasonable condition. This policy has been adopted, with a few viewgraphs being edited or re-typed when necessary, or simply omitted. The Editor has unilaterally decided that such presentations, and abstracts when full manuscripts were unavailable, will be placed at the rear of the Proceedings, but in order of presentation.

These Proceedings incorporate papers submitted from the Symposium WPLS'94.

Due to the great quantity of material, it is necessary to break the Proceedings into three volumes. **Volume 1 and 2** contain the Workshop papers for which full manuscripts were submitted plus the Business of the Ninth International Workshop. **Volume 3** contains papers from the Symposium WPLS'94 followed by viewgraph presentations and abstracts from the Ninth Workshop, and the List of Participants. Full-manuscript papers prepared under the sponsorship of WPLS'94 by the Science and Technology Agency of Japan but presented in Workshop sessions are included in Volume I, annotated by **W** in the Table of Contents.

I apologize deeply for the delay in publication. When accepting the role, I had little idea of the magnitudes of the task, the material and the cost involved, nor of the near-impossibility of finding time intervals of the required length to focus upon the task. Without the help of my daughter Georgina, my colleague Mark Elphick and our friend Robbie Horn from EOS, the delay would have been even much longer. With the recent huge expansion of the World Wide Web we considered using it, but not all participants would have access to it yet and anyway we are still on the learning curve in its use so the delay might have been greater.

In view of these experiences, I would strongly urge the Program Committee for the next Workshop to consider yet again its publication policy, and to appoint an Editor with both the firmness and the full facilities to ensure rapid publication. The institution of a fully professional journal for publishing in our field, as propounded during the Canberra Workshop, should be fully explored. Also, the time is now ripe for considering electronic publication. If adopted, complete specifications and instructions must be prepared in advance, with allowance made for authors without access to the required facilities or still struggling to master them.

Despite the difficulties and delays, this has been an intensely enjoyable burden. Having handled so much good material, I can hardly wait to find a few thousand relaxing moments to sit down and read them all myself! I hope that you do, too.

John McK. Luck
Editor
16 May 1996

PROGRAM COMMITTEE

Ben Greene, Electro Optic Systems (Chairman)
Karel Hamal, Czech Technical University
John Degnan, NASA
John Luck, Orroral Observatory
Christian Veillet, CERGA
Carroll Alley, University of Maryland
Mike Pearlman, Smithsonian Astrophysical Observatory

LOCAL ORGANISING COMMITTEE

Ben Greene, Electro Optic Systems (Chairman)
John Luck, Orroral Observatory
Anne Smith, Electro Optic Systems (Secretary)
Gordon Baker, Orroral Observatory (Treasurer)
Mark Elphick, Orroral Observatory (Publicity)

Plus the staffs of Electro Optic Systems and Orroral Observatory

EDITORIAL COMMITTEE

John Luck, Orroral Observatory (Editor)
Georgina Luck, Consultant (Assistant Editor)
Mark Elphick, Orroral Observatory and Robbie Horn, Electro Optic Systems

WORKSHOP PROGRAM

Ninth International Workshop on Laser Ranging Instrumentation
Becker House, Acton ACT, Australia
November 1994

Date	Session/Activity	Chairperson
Sunday 6	**Pre-Registration Gathering,** in Drawing Room at University House, The Australian National University	
	Program Committee and Session Chairpersons Meeting, in Common Room, University House, The Australian National University	
Monday 7	**Opening Session:**	B. Greene
	Laser Ranging: Technical Achievements & Scientific Contributions:	.Gaignebet
	Future Science Applications:	C. Veillet
	Target Signatures and Biasses:	A. Sinclair
Evening:		
	EUROLAS Meeting:	A. Sinclair
	Symposium on Western Pacific Laser Ranging Network (WPLS'94):	H. Kunimori
Tuesday 8	**New Mobile Stations:**	E. Vermaat
	New Fixed Stations:	Yang Fu-Min
	Timing Devices and Calibration:	H. Kunimori
	Lunar Laser Ranging:	P. Shelus
Evening:		
	Great Orroral Barbecue, at Orroral Observatory	
Wednesday 9	**Eyesafe Systems:**	J. Luck
	Data Analysis and Models:	G. Bianco
	Detectors and Spectral Filters:	U. Schreiber
	Laser Technology Development:	K. Hamal
Evening:		
	CSTG SLR Subcommission Meeting:	J. Degnan
Thursday 10	**Streak Camera Systems:**	I. Prochazka
	Atmospheric Sensing and Models:	G. Kirchner
	System Automation and Operational Software:	J. McGarry
	Future Roles for Laser Ranging Instrumentation, Panel Discussion#1:	K.Lambeck
Evening:		
	Workshop Banquet, at Tower Restaurant, Black Mountain	
Friday 11	**Future Technologies and Missions,** Panel Discussion #2:	M. Pearlman
	Workshop Summary and Resolutions:	B. Greene
	Business Meeting and Next Workshop:	P. Dunn
Afternoon:		
	Western Pacific Laser Tracking Network Steering Committee, at Lakeside Hotel	
	Asia-Pacific Space Geodynamics Project Discussion	D. White

OPENING SESSION

Chairperson : Ben Greene

9TH INTERNATIONAL WORKSHOP ON LASER RANGING INSTRUMENTATION
7-11 NOVEMBER 1994

MINISTER'S OPENING ADDRESS
The Hon. Frank Walker, MP
Minister for Administrative Services

Thank you Graham, and good morning ladies and gentlemen.

I'm honoured to have the opportunity to address this important forum.

Firstly, on behalf of the Australian Government, let me extend a warm welcome to all delegates and in particular, to the many international delegates who have made the journey to attend this workshop.

We're delighted to have 18 countries represented here today.

My Government is proud to be associated with this event and we wish you well for what promises to be a challenging, informative and enjoyable week.

Workshops held over the past 20 years have been singularly successful in promoting technological advances, establishing performance standards and in fostering a very high level of international collaboration.

This ninth workshop will continue that pattern -- focussing on new technology and on opportunities for laser ranging to diversify into new fields such as precise time measurement, pollution monitoring and optical communications.

This workshop is historic as it's the first to be held outside Europe or the USA and consequently, the first to be held in the Southern Hemisphere.

It's an important milestone for two other reasons--

- firstly because of its focus on developing eye-safe and remotely controlled laser ranging systems; and

- secondly because of a growing realisation that laser ranging technology is the key to solving the problem of measuring 'height above sea level' with the millimetre accuracy needed for studies of climate change and global warming.

Your presence here will help foster interest in laser ranging in Australia and the region.

This year marks 30 years of satellite laser ranging and 25 years of lunar laser ranging. These programs have made steady and at times spectacular progress in understanding how the Earth and Moon behave.

Success has been achieved by close collaboration between institutions around the world. It has brought together people using different methods -- optical and radio astronomy -- to study similar problems.

I understand that you will be given a fascinating glimpse of the history of these activities later this morning.

Laser ranging to non-technical people such as myself is a bit of a mystery.

The ability to measure distances to reflector mirrors on satellites or the Moon with centimetre accuracy seems almost fanciful, but I'm assured that it can be done, and that even millimetre accuracy is attainable.

Achieving these measurements is one thing and, of course, it's of vital interest to all of you. The **use** to which these measurements are applied, however, is of interest to a much broader community.

Geodesists, geophysicists, geodynamicists and others in the scientific community use these measurements to monitor changes in the Earth's rotation and movement of the tectonic plates.

I was very surprised to discover quite recently that Australia is not the stable place I thought it was. I was told that it is sliding across the Earth's surface in a north easterly direction at the amazing rate of about seven centimetres per year.

This may be of great interest to politicians. When we're accused of shifting ground, perhaps we can now blame continental drift or crustal motion.

Monitoring movements of the Earth's crust and related measurements, of course, have more serious implications. Scientists can learn more about earthquakes and volcanic activity, environmental change arising from the greenhouse effect and changes in sea level height, induced by global warming.

This knowledge may lead to better predictions and hence long-term management of drought, coastal flooding and earthquake and volcano disasters.

Laser ranging occupies a central position within mapping networks and provides a more accurate overall picture of each continent and the globe.

Laser ranging measurements also provide key information on satellite motion.

With the increasing usage of satellites for communication, navigation, positioning and remote sensing, knowledge about the "health" or stability of satellites has become more important.

Analysis of their motions tells us pretty well what the force of gravity is at every point on the globe, and even how the "equatorial bulge" is changing.

In effect, the measurements obtained by laser ranging have scientific, environmental and economic implications that are likely to touch, in some way, the lives of most people in the world.

This is not well known by everyone. The scientists, engineers, technicians and observers toil away in isolated places and results to into the very fundamental parts of national and global technological infrastructures. Those of us who know, appreciate the significance of your work.

Australia is very much aware of the unique role that it plays in international laser ranging. With the only fixed stations in the southern hemisphere, Australia's involvement is critical to many satellite tracking programs.

My Government recognises the valuable contribution that these programs bring to global science and is committed to a continuation of the existing arrangements.

At the same time, I believe Australia should broaden its focus to include more active participation in laser ranging activities in the West Pacific and Asia.

In view of this, it's pleasing to see that the Symposium on Western Pacific Satellite Laser Ranging Network is being held in conjunction with this workshop.

I have also been advised about a proposal for an 'Asia Pacific Space Geodynamics Project' to bring together the strands of your studies in this part of the world, perhaps similar to the way that outstandingly successful programs have been co-ordinated in the USA and Europe.

It's very pleasing to see such a strong representation here from China and Japan and I hope that your discussions on these collaborations are fruitful.

Now let me say something about your co-hosts for this week -- the Australian Surveying and Land Information Group or AUSLIG as it's better known, and Electro Optic Systems or EOS.

AUSLIG is Australia's national surveying and mapping agency with responsibilities for topographic and thematic mapping, geodetic surveying, acquisition and processing of remote sensing image data and co-ordination of related national activities.

It operates the Orroral Geodetic Observatory with which most of you are familiar or will soon become familiar in the next day or two.

EOS is Australia's leading exporter of satellite laser ranging systems and laser gun sights. It's a private company spawned in 1986 by one of AUSLIG's predecessors -- a classic example of government activity leading to the creation of a viable leading-edge export industry.

EOS has continued its relationship with AUSLIG and in 1991, in co-operation with AUSLIG and a substantial grant from the Government's Industry Research and Development Board, undertook a substantial upgrade of Orroral systems.

This form of Government/industry collaboration benefits all parties -- Orroral's productivity has doubled each year since the upgrade, while Ben Greene here claims a leverage factor of 10 in the sales benefits from technology advances produced.

AUSLIG values advice from industry and academia in the running of Orroral Observatory and has formalised this through the establishment of an advisory committee which includes representatives from industry and academic sectors.

Another example of the spirited co-operation that exists in the laser ranging world is the formation of an Australian company, SLR Research Pty Ltd, to make satellite ranging systems based on Latvian technology. SLR Research was formed in association with the Curtin University of Technology in Perth, Western Australia and the University of Latvia in Riga.

Co-operation and good will seem to go hand in hand with laser ranging. With these ingredients, the success of your workshop is assured.

I would now like to declare the 9th International Workshop on Laser Ranging Instrumentation formally open and wish you a week to remember.

LASER RANGING : TECHNICAL ACHIEVEMENTS AND SCIENTIFIC CONTRIBUTIONS

Chairperson : Jean Gaignebet

THIRTY YEARS OF SATELLITE LASER RANGING

John J. Degnan
Code 920.1/Laboratory for Terrestrial Physics
NASA Goddard Space Flight Center
Greenbelt, MD 20771 USA

ABSTRACT

Laser ranging to an artificial satellite equipped with retroreflectors (Beacon Explorer B) was first successfully demonstrated by a team of engineers and scientists from the NASA Goddard Space Flight Center (GSFC) in 1964. Compared to the 50 or more meter accuracy of microwave radars of the period, the 2 to 3 meter accuracies of these early experiments represented a quantum leap in capability for precise orbit determination. The author, who was a junior member of the GSFC team in 1964, provides a retrospective of those early NASA experiments with an emphasis on the key people, hardware, and early data. This is followed by a decadal review of the key scientific, technologic, and programmatic milestones in the history of SLR.

Over the past three decades, SLR has contributed to an ever expanding set of science and engineering applications as system precisions have dramatically improved from a few meters to a few millimeters. Counting both fixed and mobile sites, SLR contributes well over 100 sites, whose locations are known with centimeter accuracy and whose velocities have been established with mm/yr precision, to the International Terrestrial Reference Frame (TRF) and, uniquely among the space geodetic techniques, SLR defines the frame origin (Earth center of mass) with subcentimeter accuracy. SLR provides the longest (17 years), high accuracy (submilliarcsecond) record of the orientation of the Earth's spin axis as well as periodic and secular variations in its spin rate. Changes in spin axis orientation and rotation rate can be associated with the exchange of angular momentum or the movement of mass between or within the solid, liquid, or gaseous components of the Earth making SLR highly relevant to studies of global change. SLR data is predominant in the determination of the static long wavelength components of the Earth's gravity field as well as temporal variations. In addition to providing basic reference frame and gravity (geoid) information, SLR further supports oceanographic and ice missions, such as TOPEX/Poseidon and ERS-1, through precise determination of the satellite orbit in a geocentric reference frame and periodic calibration of onboard microwave altimeters.

Along with Very Long Baseline Interferometry (VLBI), SLR has successfully verified that the Earth's tectonic plates are in constant motion and that contemporary plate velocities are within a few percent of the long term average motion inferred from the geologic record. Complicated motions resulting from deformations occurring at plate boundaries have been observed in the Southwest United States and Mexico, in Southern Europe, and the Far East. SLR has also found a role in subnanosecond intercontinental time transfer, the measurement of fundamental physical constants, and studies of general relativity.

Today, the capability of SLR in precise orbit determination and some areas of geophysics is being augmented by several new and relatively inexpensive radionavigation systems. SLR has provided the "ground truth" against which these emerging systems (such as GPS, GLONASS, TDRSS, DORIS, and PRARE) have been compared and calibrated. Despite the formidable cost competition from radio techniques, several important applications remain, at least for the foreseeable future, which are squarely within the sole dominion of SLR. Furthermore, the presence of several orbiting satellites having both retroreflectors and one or more radionavigation transmitters/receivers presents a unique opportunity for the synergistic combination of laser and radiowave datasets to achieve an absolute accuracy, unification of terrestrial frames, and densification of data which could not be achieved by a single technique.

1. INTRODUCTION

The first ruby laser was invented by Thomas Maiman of Hughes Aircraft Laboratories in 1960. Only four years later, in 1964, NASA scientists and engineers successfully used a ruby laser to range with few meter precision to an artificial satellite, and the field of Satellite Laser Ranging (SLR) was born. It is doubtful anyone could have predicted in 1964 how rapidly the technology and international involvement would evolve and how widespread and interdisciplinary the science applications would become. Yet, as we convene in this Ninth Workshop on Laser Ranging Instrumentation in Canberra, one has to look back and marvel at what has been accomplished by the international community in the fields of geodynamics, gravity, oceanography, relativity, fundamental physics, lunar science, etc. in their pursuit to understand the "signal" content in these very precise range measurements.

I was surprised and honored when the Workshop Program Committee asked me to deliver the keynote address on this thirtieth anniversary of SLR. Apparently, my principal claim to this distinction is extreme longevity in the field. I participated as a junior member of the NASA SLR team in 1964 and am again very active in the field today thanks to my appointments as Deputy Manager for the NASA Crustal Dynamics Project in 1989 and as CSTG SLR Subcommission Chairman in 1992. However, during the intervening 25 years, I had been only occasionally and peripherally involved in the international SLR program, largely through my engineering activities at NASA which often meandered between laser ranging, communications, and remote sensing. I contributed to the 1978 Third International Workshop in Greece "in absentia" (i.e. Tom McGunigal read my papers) but finally, in 1981, I was able to participate fully in the Fourth Workshop in Austin, Texas (the first held in the United States). As a result, there may be large temporal gaps in my memory of key events (especially those which are international in nature). I trust the reader will forgive me if the upcoming brief history of the international SLR program is not totally accurate or if I have unwittingly failed to give appropriate credit to key individuals and/or institutions. However, in an attempt to keep these omissions at a minimum, I solicited and received information from several SLR pioneers in the international community in preparing the synopsis on the 30 year history of SLR. These individuals are listed in the Acknowledgements section.

In this paper, I briefly describe the earliest SLR experiments and campaigns and review, decade by decade, the key technological, scientific, and programmatic events that shaped the development of the SLR technique and the supporting international network. I then provide a summary of the scientific applications to date and discuss some future directions of SLR. More detailed descriptions can be found in a recently published series of AGU monographs [Smith and Turcotte, 1993] and in the report of the 1994 Belmont Workshop [Degnan, 1994], which was convened by NASA to plan its SLR program for the 1990's.

2. THE FIRST SLR EXPERIMENT

The first SLR satellite, Explorer 22/Beacon Explorer-B, was launched by NASA on October 9, 1964. The satellite entered into an orbit with an inclination of 79.7° , an apogee of 1100 Km, and a perigee of 939 Km. The spacecraft attitude was magnetically stabilized, presenting its panels of fused quartz optical retroreflectors only to observers in the Northern Hemi sphere. The array had an optical radar cross-section of approximately 5 million square meters.

A few weeks later, at 10:26 GMT on the morning of 31 October 1964 , a team of engineers and scientists at NASA's Goddard Space Flight Center (GSFC) recorded the first weak laser echoes from Explorer 22 BE-B [Plotkin et al, 1965]. In these first experiments, the output of the 9558A photomultiplier tube was recorded on an oscilloscope, and only four verifiable returns were recorded in approximately 200 oscilloscope traces. In subsequent experiments, the laser returns were also recorded on photographic film and as actual range measurements.

The telescope for the GODLAS system, short for Goddard Laser, was pointed by a modified Nike-Ajax missile tracking mount controlled by two operators guiding on the sunlit satellite under joystick control.

One operator controlled azimuth and the other controlled elevation. The receive telescope had a 16 inch diameter primary and a 300 inch focal length. Background noise was reduced by a 10 Angstrom bandpass filter. The ruby laser transmitter, built by General Electric, was air-cooled and utilized a rotating prism Q-switch to generate an approximate 20 nanosecond pulsewidth. The laser operated at a 1 Hz rate with a single pulse output energy of 0.8 Joules.

The NASA SLR team in 1964 was led by Dr. Henry Plotkin, then Head of the Optical Systems Branch (Code 524) at GSFC. The other NASA team members were Thomas Johnson , Paul Spadin, John Moye, Walter Carrion, Nelson McAvoy, Howard Genatt, Louis Caudill, John Degnan, Edward Reid, and Charles Peruso. In 1965, an SAO team, also using a laser provided by General Electric Corporation, received its first laser returns from Explorer 22 BE-B at its optical tracking site at Organ Pass, New Mexico.

3. A BRIEF HISTORICAL OVERVIEW

The first international SLR measurement campaign, in support of the National Geodetic Satellite Program (NGSP), took place in the Spring of 1967. By this time, six retroreflector-equipped satellites had been launched - four of the NASA Explorer series (22, 27, 29, and 36) and the French Diadem 1 and 2 satellites. During this first campaign, the Centre National d'Etudes Spatiales (CNES) in France operated three laser sites in Haute Provence (France), Colomb-Bechir (Algeria), and Stephanion (Greece). NASA operated its station in Greenbelt, Maryland [Johnson et al, 1967]and SAO operated a fifth site in Organ Pass, New Mexico. The campaign resulted in formal position errors of 5 meters at the laser sites. This represented approximately a factor of four better precision than that obtained from the more conventional Baker-Nunn optical observations which were carried out concurrently with the laser measurements. The laser and other optical data taken during this campaign resulted in a gravity model, the SAO Standard Earth Model, which was completed to degree and order 16 and included 14 pairs of higher degree coefficients. The development of this model was an important milestone in the burgeoning, yet infant, science of satellite geodesy.

A year later, in 1968, SAO sponsored another major campaign centered around the GEOS-2 satellite which had been launched as a test platform for comparing the performance of contemporary radars, lasers, and conventional optical tracking techniques. In the same year, the SAO network prototype laser was installed at the Mt. Hopkins Observatory, and the original Organ Pass system was moved to Mt. Haleakala on the island of Maui in Hawaii. In 1969, NASA/GSFC reported the first daylight laser ranging [Premo and O'Neill, 1969].

In July 1969, the Apollo 11 spacecraft carried the first laser retroreflector array to the moon. In competition with other groups around the world, the Lunar Ranging Experiment (LURE) team, working at the 2.7 meter telescope at the McDonald Observatory at the University of Texas, were the first to successfully record signals from the Apollo 11 retroreflector, and, for the next 15 years, McDonald would provide virtually all of the operational data to the growing lunar laser ranging community. Within a few years, four additional arrays would be placed on the lunar surface by the manned NASA Apollo 14 and 15 missions and by the unmanned Soviet Lunakhod I and II missions carrying French-built reflector panels. An updated 25 year history of the LLR program is provided by Dr. Carroll Alley of the original LURE team in a second invited talk and hopefully a companion article in these Proceedings [Alley, 1994].

In August 1969, NASA organized a major international conference in Williamstown, Massachusetts to formulate a long range plan for the application of space techniques, including SLR, to the improved understanding of solid Earth dynamics. It was at this conference, chaired by William Kaula, that the requirement for one centimeter accuracy laser ranging was first specified [Kaula, 1969].

During the period October 1969 to January 1970, the NASA MOBLAS-1 system participated in the first SLR collocation with an SAO system at the Mount Hopkins Observatory in Arizona. Range biases of 1 to 2 meters were observed, and the bias changed sign several times during collocation.

Following the launch of the PEOLE satellite by France in late 1970, SAO and CNES continued to organize a series of international measurement campaigns to further develop the geodetic reference frame and improve the gravity models. The most important of these was the International Satellite Geodesy Experiment (ISAGEX) in 1971. With NASA support, SAO deployed several submeter-quality SLR systems [Pearlman et al, 1975] at its existing Baker-Nunn camera sites in Arequipa (Peru), Natal (Brazil), and Olifantstein (South Africa). By 1973, following the assimilation of these data, the goals of the NGSP program, i.e. a unified global datum with ± 5 meter accuracy, had been met. After SAO published its final Standard Earth Model, SE-III, which was the first gravity model to use significant amounts of laser data, gravity model work in the United States was turned over to the NASA Goddard Space Flight Center.

In 1972, the first of the INTERKOSMOS network stations began successful operations in Ondrejov, Czechoslovakia under the technical leadership of the Czech Technical University in Prague [Masevitsch and Hamal, 1975]. First generation stations were later deployed internationally at several Soviet AFU 75 optical camera sites, including sites in Poland, Latvia, Bolivia, Cuba, and India. Under a joint program between SAO, the Technical University of Prague, the Soviet Academy of Sciences , and the Helwan Institute for Astronomy and Geophysics , an SLR station was established in Helwan, Egypt, which has since been upgraded to subcentimeter status by Dr. Hamal. European interest in SLR was strong in these early years, and the first three International Workshops on Laser Ranging Instrumentation were held in Lagonissi, Greece in May 1973, Prague , Czechoslovakia in August 1975, and Athens, Greece in July 1978

In 1975, CNES in France launched the first satellite dedicated solely to laser ranging , Starlette., to further improve the gravity field and improve station position estimates. NASA also launched GEOS-3, the first operational radar altimeter satellite equipped with retroreflectors and reported the first SLR system to achieve a precision better than ten cms[McGunigal et al, 1975]. Laser tracking of GEOS-3 was augmented by U.S. Navy Doppler and C-band radar. International tracking campaigns were organized for the two satellites and led to a much refined geoid. Initial acquisition of the two satellites was obtained optically using the international network of Baker-Nunn cameras. During this same time period, the SAO station in Olifantstein, South Africa was relocated to the Orroral Valley in Australia at a site not far from the current observatory.

The launch of the second dedicated SLR satellite, LAGEOS, by NASA in 1976 further fanned international interest in the SLR technique by providing a stable, high altitude, low drag inertial platform which lent itself extremely well to still more precise geodetic and gravity field studies. Starlette and LAGEOS would serve as the primary tools of the SLR community for well over a decade. The STALAS (for Standard Laser) system at GSFC set a new performance standard in 1976 by achieving single shot precisions of about 7 cm with the first use of a modelocked Nd:YAG laser. The laser was engineered by Bud Erickson of the Sylvania Corporation and integrated into the STALAS system by John Degnan and H. Edward Rowe of GSFC. The rather complex transmitter consisted of a CW-pumped acousto-optically modelocked oscillator, followed by an electro-optic switch, a multipass regenerative amplifier, three single pass amplifiers, and a doubling crystal [Johnson et al, 1978]. An identical laser was later installed in Wettzell, Germany. At about the same time, as part of the Earth and Oceans Dynamics Applications Program (EODAP), NASA built five new SLR systems (MOBLAS 4 through 8) to provide precise orbit determination support to the SEASAT ocean altimeter mission. Although SEASAT failed prematurely in October 1978 after only three months of operation, the data retrieved during that brief period kept analysts occupied for years. The five systems were later turned over in 1979 to NASA's fledgling Crustal Dynamics Project (CDP) under the direction of Dr. Robert Coates at the Goddard Space Flight Center.

In 1981, at the request of Chris Stephanides, SLR Manager for the CDP, a NASA engineering team, led by the author, was tasked to upgrade the MOBLAS-4 system at GSFC. The team installed a custom-built passively modelocked Quantel laser and a prototype microchannel plate photomultiplier (QE= 5%) built by ITT, raised the repetition rate from 1 Hz to 5 Hz, and demonstrated both an unprecedented single shot precision of 1.5 cm and a greatly increased data set [Degnan and Adelman, 1981; Degnan et al,

1984]. The team further recommended that the CDP, as part of a general NASA network upgrade, install a new Tennelec discriminator and a new Hewlett Packard time interval unit because these devices had yielded subcentimeter results in earlier ground tests. By the mid-to-late 80's, the upgraded hardware was implemented throughout the NASA SLR network, along with some additional improvements developed by Dr. Thomas Varghese and his Bendix Field Engineering Corporation (BFEC) team, and was routinely recording subcentimeter precision satellite data [Varghese and Heinick, 1986]. By the end of the decade, the Prague group had developed an alternative approach to subcentimeter ranging which made use of ultrashort pulse lasers and Single Photon Avalanche Photodiodes, or SPAD's, which did not require the use of a discriminator [Prochazka et al, 1990].

Also in the early 1980's, Dr. Eric Silverberg and his team at the University of Texas had developed the first highly transportable SLR station, TLRS-1, which was totally housed within a camping van [Silverberg and Byrd, 1981]. In a parallel development, GSFC's Thomas Johnson and his development team were conducting field tests of the TLRS-2 system which was designed to be shipped to remote sites like Easter Island in standard aircraft containers. The latter system was later upgraded by the author in 1985. By 1981, the number of international SLR geodetic sites had grown markedly, due largely to the mobile operations of the NASA MOBLAS systems and the new transportables TLRS-1 and 2, but also augmented by a growing network of fixed stations, including sites in Australia (Yarragadee and Orroral), Africa (the Czech Helwan station), and Asia (Tokyo).

By the end of the 1980's, seven transportables were operating successfully - four by NASA (TLRS-1 through 4), one by Germany (MTLRS-1), one by the Netherlands (MTLRS-2), and one by Japan (HTLRS). The MTLRS-1 system, in particular, routinely demonstrated high efficiency in data gathering, even in daylight. NASA "parked" its larger MOBLAS systems at fixed sites and turned over regional measurements to the more nimble transportables. The American and European transportables participated in cooperative and very successful campaigns to measure the complex tectonics in Southern Europe (as part of the WEGENER/MEDLAS program) and to better understand the spreading of the Gulf of California through occupations in the Southwest U.S. and Mexico. The European studies were augmented by a sizable increase in the number of fixed national stations in Europe. The Japanese HTLRS system concentrated on geodetic mapping of farflung Japanese islands.

During the same decade, major SLR developments were occurring in the former USSR. Three Soviet "Crimea" stations, under the leadership of Dr. Yuri Kokurin of the Lebedev Institute in Moscow, became part of the international SLR network and were operating in the Ukraine at Simeiz and Katzively and in Latvia at Riga under the auspices of the Soviet Academy of Science. As part of a massive national geodetics and space navigation program, the USSR launched several series of retroreflector-equipped satellites including GEOICA, GLONASS, and ETALON. These national satellites were supported by a vast ground network of 25 mobile and 5 permanent SLR stations distributed across the USSR.

The 1980's also saw the development of two new lunar stations at Grasse in France and Mt. Haleakala on the island of Maui in Hawaii. By the mid-80's, the CERGA lunar station at Grasse had surpassed MLRS as the dominant provider of lunar laser ranging data.

As we entered the decade of the 1990's, SLR began to see intense competition from radio techiques such as the American Global Positioning System (GPS), the Russian Global Navigation Satellite System (GLONASS), the French Doppler Orbitography in Space (DORIS) system, and most recently the German Precise Range and Range-rate Equipment (PRARE). As GPS demonstrated a capability to perform regional crustal deformation measurements in a more cost effective manner and with accuracies comparable to SLR and VLBI, NASA began to restrict the mobility of its TLRS systems.

Despite the new competition, international interest in SLR has remained high as evidenced by several developments. . By 1994, the number of SLR systems had grown to approximately 45, with both Russia and China expanding the size of their scientific networks. Additional stations are currently being developed by Germany, Russia, China, France, Japan, Poland, and Saudi Arabia. Over the past decade,

the number of satellites routinely supported by SLR has grown dramatically from only two (LAGEOS and Starlette) in 1984 to thirteen in 1994 and is expected to grow to over twenty satellites by 1996. The first half of the decade has seen the launch of two new dedicated geodetic satellites (LAGEOS 2 and Stella) and two high precision altimetric missions (ERS-1 and TOPEX/POSEIDON) which rely heavily on SLR. Several additional missions are anticipated in the next two years (e.g. GFZ-1, ERS-2, ADEOS, GFO-1, etc.). The growth in the SLR constellation has been matched by a corresponding growth in the data yield from the international SLR network which has also benefited from more shift hours (largely due to the additional support provided by the TOPEX/POSEIDON mission) as well as increased automation and operational efficiency at many sites .

4. SCIENCE APPLICATIONS OF SLR

The two to three meter precisions of the earliest SLR systems represented a better than order of magnitude improvement over the conventional microwave radars of the day. The potential role of SLR in providing precise orbits and geodetic positioning of stations and their subsequent impact on our knowledge of the gravity field was rapidly recognized by the science community following the early international campaigns and the NGSP was established to exploit these technological developments. In 1969, the proceedings of a conference held in Williamstown, Massachusetts, laid out many of the scientific objectives which would ultimately be achieved over the next two decades [Kaula, 1969]. As the precision of the SLR technique improved from a few meters to a few millimeters at the approximate rate of an order of magnitude per decade, many new scientific opportunities presented themselves.

The earliest plate motion experiment was the San Andreas Fault Experiment (SAFE) in which NASA placed two SLR stations on opposite sides of the fault in California and measured the relative rate of motion through laser tracking of the Beacon Explorer-C satellite. The launch of LAGEOS in 1976 provided an ultra-stable inertial platform which enabled highly accurate geodetic measurements of the three-dimensional station positions and site motions, Earth orientation parameters such as polar motion and length of day (LOD), and the Earth's gravity field. Centimeter precision positioning was rapidly achieved using LAGEOS and confirmed the earlier SAFE results. Tectonophysicists and geophysicists were soon puzzling over the so-called "San Andreas Anomaly" [Minster and Jordan, 1978], i.e. a baseline rate half as large as anticipated from rigid plate models, and this led to increased scientific interest in the study of regional crustal deformation near plate boundaries.

The formation of NASA's Crustal Dynamics Project (CDP) in 1979 provided a programmatic focus for the international Earth science community and harnessed the necessary financial, facilities, and manpower resources to enable the first study of contemporary tectonic plate motion on a global scale. For the next twelve years, the CDP pursued its stated science goals with its international partners using the two most accurate space geodetic technologies of the day - Satellite Laser Ranging (SLR) and Very Long Baseline Interferometry (VLBI)[Bosworth et al, 1994]. The CDP goals included contemporary measurements of:

1) Global tectonic plate motion
2) Regional crustal deformation
3) Earth gravity field and
4) Earth orientation parameters (EOP)

Following termination of the CDP in December 1991, the measurements continued under the NASA Dynamics of the Solid Earth (DOSE) Program and an expanded WEGENER program supporting a more detailed study of European/ Mediterranean tectonic processes using the three primary space geodetic techniques, i.e. VLBI, SLR, and GPS.

Along with VLBI, SLR successfully demonstrated that the Earth's tectonic plates exhibit steady state motion and that contemporary plate velocities are typically within a few percent of their long term average motion as determined by geological evidence averaged over the last three million years. The velocities for

all of the major plates were determined, and together the two techniques defined the Terrestrial Reference Frame (TRF) which is maintained by the International Earth Rotation Service (IERS) in Paris, France.[1] By itself, SLR has contributed over 100 site positions to the TRF, has established well-resolved kinematic motion at over 50 sites, and uniquely provides the frame origin (Earth center of mass) with subcentimeter accuracy relative to the global SLR network. In a highly successful collaboration of CDP with the WEGENER/MEDLAS consortium in Europe, detailed studies of regional crustal deformation in the Mediterranean countries of southern Europe (notably Italy, Greece, and Turkey) were determined by the three SLR transportables, TLRS-1, MTLRS-1, and MTLRS-2 working together with several fixed SLR stations in the region. Similar studies were carried out jointly in the southwest United States and Mexico.

Because of its unique access to the Celestial Reference Frame (CRF) defined by the distant quasars, VLBI provides the only long term tie between the celestial and terrestrial reference frames through its regular monitoring of the full suite of Earth Orientation Parameters (EOP), i.e. precession, nutation, polar motion, and Universal Time (UT1). However, because of the temporal gaps between routine VLBI operations, the centimeter accuracy measurement of SLR site positions would not have been possible without simultaneously solving for the short term effects of polar motion as well as variations in the Earth rotation rate (or length of day). Thus, beginning with the MERIT campaign in 1980, short term EOP parameters became natural and important byproducts of the SLR geodynamics analysis. Consequently, LAGEOS is today the most rapid source of polar motion and length of day (LOD) data and has provided the longest-running record of high frequency polar motion and UT1. However, the ability of SLR to sustain UT1 over long periods, without periodic updates by VLBI, is limited by errors in the LAGEOS dynamic models [Eanes, 1994].

The pole orientation and rotation rate of the solid Earth varies due to exchanges of angular momentum with the sun, moon, atmospheres, and oceans and the effects of mass redistribution on the Earth moment-of-inertia tensor. Mass redistribution also changes the Earth's gravity field. The physical mechanisms by which mass is redistributed are many and include: tidal forcing caused by the gravitational attraction of the sun and moon, variations in oceanic and atmospheric circulation , the melting of polar and glacial ice, precipitation, earthquakes and other tectonic movements, post-glacial rebound of the Earth's crust , redistribution of ground waters , and long term mantle convection and core activities. While tidal and seasonal effects are periodic with well-defined frequencies, others such as postglacial rebound introduce long term secular changes in both the LOD and the gravity field.

For over 15 years, high frequency variations in the length of day, as determined from LAGEOS ranging, have shown excellent correlation with seasonal and subseasonal variations in the global atmospheric angular momentum. Short term variations are largely explained by exchanges of angular momentum between the solid Earth and atmosphere and by tidal processes. Long term decadal signals have been attributed to angular momentum coupling at the core-mantle boundary and to the effects of postglacial uplift. Ocean circulation models are now being analyzed as possible sources of the residual signals.

Our knowledge of the long wavelength components of the Earth's gravity field improved dramatically over the past three decades as new and better satellites were launched into a wide variety of orbital planes and altitudes and the distribution and precision of SLR systems continued to improve. SLR tracking of LAGEOS had the greatest impact on gravity modeling improvements in the first half of the 1980's [Lerch et al, 1982; Reigber et al, 1985] and, in the second half, led to a better understanding of nonconservative forces acting on the satellite, such as thermal, neutral density, and charged particle drag and the effects of solar and Earth radiation pressure [Rubincam, 1990; Marshall et al, 1995]. In the early 1990's, the inclusion of data from surface gravimetry and earlier altimetric satellites produced a series of Goddard Earth Models (e.g. GEM-T2, GEM-T3) and the Joint Gravity Model JGM-1, produced jointly by GSFC and the University of Texas Center for Space Research in anticipation of the TOPEX/POSEIDON oceanographic mission. The most recent model, JGM-3, takes into account SLR data from the recently

[1] GPS was added to the TRF in 1992 and DORIS petitioned for inclusion in 1994.

launched LAGEOS-2 and Stella satellites in addition to SLR, GPS, and DORIS tracking of TOPEX/POSEIDON and its high accuracy altimetry data [Tapley et al, 1994].

Temporal variations in the low order zonal harmonics of the Earth's gravity field (e.g. J_2, J_3, and J_4) have been monitored monthly for over 15 years through SLR tracking of LAGEOS and are attributable to movements of mass within the closed solid Earth-oceans-atmosphere system over large spatial scales on the order of 10,000 Km. The short term seasonal and subseasonal variations in J_2 are well-correlated with the distribution of atmospheric mass as determined independently by global measurements of the pressure field as provided, for example, by the European Center for Medium Range Weather Forecasts (ECMWF) [Chou and Au, 1991]. The model agreement is improved by including the displacement of the ocean surface by the atmospheric pressure ("inverse barometer effect") but the true response of the oceans is somewhere in between [Nerem et al, 1993a]. However , atmospheric pressure models alone cannot account for the observed temporal variations in J_3. Large annual residuals in the latter zonal have been attributed to variations in the ocean mass distribution [Marshall and Pavlis, 1993] while other signals appear to be associated with radiationally-forced atmospheric tides, such as the S_1 tide with an approximate 560 day cycle [Nerem et al, 1993b]. If these explanations are confirmed, SLR may provide an important means of monitoring the response of the atmosphere to solar radiation and of testing and discriminating between multilayer ocean circulation models. Furthermore, accurate zonal rates are essential in constraining post-glacial rebound models [Miltrovica and Peltier, 1993] and ice mass balance models [Trupin, 1993].

With the launches of ERS-1 by ESA in 1991 and TOPEX/POSEIDON in 1992, SLR again became a major contributor to the study of sea and ice surface topography. Both missions have been a great success - due in no small part to the contributions of SLR. In spite of the unfortunate failure of the onboard PRARE transceiver and a relatively low (800Km) high drag orbit, ERS-1 orbits have been maintained at roughly the 15 cm level radially with the sole support of the international SLR network. Using the combined SLR and DORIS data sets and a much-improved JGM-3 gravity field, the higher (1375 Km) TOPEX/POSEIDON orbits are generally believed to be accurate to 2 to 3 cm radially - significantly surpassing the original mission requirement of 13 cm. Efforts are underway by the TOPEX/POSEIDON POD Team to improve the radial accuracy to between 1 and 2 cm by applying a heavier relative weighting to the SLR data [S. Klosko, private communication].

The goal of oceanographic missions is to measure the sea surface topography defined as the difference between the local sea surface height and the local geoid (reference gravity equipotential surface). From the two-dimensional slope of sea surface topography, one can compute the global ocean circulation. SLR contributes to sea surface topography in several ways.

(1) By tracking LAGEOS 1 and 2, SLR establishes the positions of the tracking stations with centimeter accuracy in a geocentric reference frame.

(2) SLR provides centimeter accuracy range measurements between the satellite and the station.

(3) The combination of site position and accurate range establishes the altimeter orbital ephemerides with respect to the Earth center-of-mass with centimeter accuracy.

(4) The tracking of the full constellation of SLR satellites provides the longer wavelengths of the gravity field and hence the marine geoid. Knowledge of the gravity field assists in space navigation when laser tracking is sparce, and the geoid surface is essential for computing sea surface topography and ocean circulation.

(5) Because of its insensitivity to the two most dynamic components of the atmosphere, i.e. the ionosphere and the "wet" troposphere, SLR is ideally suited to the calibration and correction of the onboard microwave altimeters during periodic overflights. Long term drifts in altimeter bias can be easily mistaken for changes in sea level.

Recent TOPEX results suggest that the mean sea level is rising at a rate of 2.9 ± 0.9 mm/yr [Nerem et al, 1994] in approximate agreement with earlier estimates based on global tide gauge measurements .

For the sake of completeness, one should also mention the use of SLR in global time transfer and relativity experiments and in the measurement of fundamental physical constants. In the LASSO experiment, coordinated by Dr. Christian Veillet of CERGA, successful subnanosecond time transfer experiments were carried out between the French SLR station at Grasse and the American station at McDonald Observatory in Texas using an intermediary detector, clock, retroreflector array, and telemetry system on the METEOSAT-P2 satellite[Veillet and Fridelance, 1993]. Earlier aircraft experiments conducted by Professor Carroll Alley and his students at the University of Maryland in the late 1970's successfully used a laser ranging system to transfer time between a set of atomic clocks on the ground and a set of clocks on an aircraft [Alley, 1983]. During a flight that lasted approximately thirty hours, the airborne clocks ran faster than the ground clocks due to the reduced gravity field (as expected from Einstein's theory of general relativity) and the change of rate with altitude could be easily seen. Similar NASA/SAO experiments will be carried out over longer time intervals in upcoming missions on the Russian MIR spacecraft to test the performance of hydrogen masers in space. LLR experiments have provided tests of competing relativistic theories, verified the strong equivalence principle in Einstein's formulation of General Relativity, and placed an upper limit on the rate of change in the gravitational constant G [Reis, 1994].

5. FUTURE ROLE OF SLR

The precision of the SLR technique has improved by an order of magnitude in each of its three decades of existence. Approximately 30 countries worldwide are presently active in SLR, and the present network of 45 stations continues to expand as does the SLR constellation which is expected to surpass twenty operational satellites by 1996.

SLR remains crucial to the maintenance of the Terrestrial Reference Frame through its unique subcentimeter determination of the Earth center-of-mass and orbital scale. Laser tracking of LAGEOS has provided the most accurate measurement of the Earth's gravitational coefficient (GM) and has demonstrated the importance of considering the relativistic consequences of the definition of time in the various reference frames {Reis, 1994]. The accurate determination of GM is critical in determining the absolute scale of the geocentric reference frame and affects the intercomparisons of site locations determined independently by SLR and VLBI and the determination of absolute ocean height using altimetric satellites. This has important implications in science applications which have a need for absolute vertical height information such as mean sea level, ice mass monitoring, postglacial uplift, tide gauge monitoring, etc.

Because it uses relatively "clean" cannonball satellites, SLR is presently the best technique for separating conservative from non-conservative forces acting on near-Earth satellites and is presently the only source of information on the time varying gravity field which has potentially major implications for ocean and atmospheric modeling ice mass balance, and other Global Change related science. SLR continues to make unique and important contributions to all elements of Earth science including the solid Earth, oceans, cryosphere, atmosphere, and Earth-lunar dynamics.

The demonstrated capability of SLR to transfer time over global distances with an accuracy measured in tens of picoseconds could have significant scientific and engineering impacts in the not too distant future. In addition to the LASSO experiment discussed previously, SLR tracking of the GPS and GLONASS satellites is presently being used to test the performance of the onboard atomic clocks and to verify the proper handling of certain relativistic effects in ground operations. Over the next few years, spacecraft experiments plan to use SLR to monitor the performance of hydrogen masers in space and to study

longterm relativistic effects on spaceborne clocks. There may be commercial applications of time transfer as well. As larger datasets are merged and transmitted electronically around the globe via groundbased optical fibres or wideband communication satellites, the need for improved absolute timing at the sending and receiving stations will grow proportionately.

Today, the traditional role of SLR in precise orbit determination and some areas of geophysics is being challenged by several new and relatively inexpensive radionavigation systems. Because of its simple and unambiguous range observable and its insensitivity to the dynamic ionosphere and "wet" troposphere, SLR has provided the "ground truth" against which these emerging systems (such as GPS, GLONASS, TDRSS, DORIS, and PRARE) have been compared and calibrated. Despite the formidable competition from radio techniques, several important applications remain, at least for the foreseeable future, which are squarely within the sole dominion of SLR. Nevertheless, SLR must continue to improve its data product, both in accuracy and timeliness, and to move rapidly toward automated field stations and data processing centers in order to be competitive with low cost radio systems.

The presence of several orbiting satellites having both retroreflectors and one or more radionavigation transmitters/receivers presents a unique opportunity for the synergistic combination of laser and radiowave datasets to achieve an absolute accuracy and densification of data which could not be achieved by one technique alone. For example, it is likely that continued SLR tracking of the GPS-35 and GPS-36 satellites will isolate the source of observed biases, ultimately improve the modeling of the onboard atomic clocks as well as the nonconservative forces acting on the GPS spacecraft, and lead to improved accuracy in future GPS measurements. Furthermore, SLR's totally passive space segment provides fail-safe redundancy in high profile altimetric or other spacecraft missions.

In the 1994 Belmont Workshop report [Degnan, 1994], NASA proposed eight programmatic goals which should be pursued by the agency and its international partners over the remainder of this decade. These were:

1) Standardize the performance of the global network.
2) Improve the geographic distribution of SLR stations
3) Reduce the cost of field and data operations through increased standardization and automation
4) Expand the temporal coverage to better serve the growing satellite constellation
5) Improve the absolute accuracy to 2 mm at key sites via two color techniques
6) Continue to improve the satellite force, station motion, and atmospheric propagation modelling
7)Support technique intercomparisons and the Terrestrial Reference Frame through global collocations
8) Investigate potential synergisms between GPS and SLR

In summary, the international SLR community can be justifiably proud of its many technological and scientific accomplishments over the past three decades. The high precisions achieved at several stations have resulted in many new and exciting science applications. However, we must work as a community to proliferate these existing capabilities to other stations which have fallen behind technologically and to establish new stations outside our national borders where they are desperately needed. In an era of falling science budgets and increased competition from the radio techniques in performing traditional SLR tasks, we must continue to improve the quality and timely delivery of the range observable and make it more cost effective through increased automation. With picosecond resolution two color satellite ranging becoming a reality at several stations [Zagwodzki et al., 1994], subpicosecond lasers and streak camera detectors already demonstrated in the laboratory, and new millimeter satellite array designs on the drawing boards [Degnan, 1993], there is no reason to believe that the next order of magnitude improvement in range accuracy and precision is beyond our grasp.

ACKNOWLEDGEMENTS

The author wishes to acknowledge the following people who provided historical material and references for this review and/or critiqued the final manuscript: Dr. Henry Plotkin (recently retired from the NASA Goddard Space Flight Center), Louis Caudill (NASA Headquarters), Dr. Michael Pearlman (Smithsonian Astrophysical Observatory), Steve Klosko and Peter Dunn (Hughes STX), Dr. Yuri Kokurin (Moscow Lebedev Institute), Professor Victor Shargorodsky (Science-Research Institute for Precision Device Engineering, Moscow), and Dr. Karel Hamal (Czech Technical University of Prague). Mark Torrence of Hughes STX provided many of the colorful science visuals used in my presentation which unfortunately cannot be reproduced here but were made available in a color brochure distributed to participants at the Workshop. Additional copies of the brochure, "Satellite laser ranging contributions to Earth science: a synopsis of the 1994 Belmont SLR Workshop", or the full report [Degnan, 1994] can be obtained from the author.

REFERENCES

Alley, C. O., "Proper time experiments in gravitational fields, with atomic clocks, aircraft, and laser light pulses", in Quantum Optics, Experimental Gravity and Measurement Theory, P. Meystre and M. Scully (Eds.), Plenum Publishing Corporation, pp. 363-427, 1983.

Alley, C. O., "Twenty-five Years of Lunar Laser Ranging", these proceedings, 1994.

Bosworth, J. M., R. J. Coates, and T. L. Fischetti, "The development of NASA's Crustal Dynamics Project", in Contributions of Space Geodesy to Geodynamics, D.E. Smith and D. L. Turcotte (Eds.), AGU Geodynamics Series, Vol. 25, pp. 1-20, 1993.

Chao, B. F. and A. Y. Au, "Temporal variation of the Earth's low degree zonal gravitational field caused by atmospheric mass distribution: 1980-1988", J. Geophysical Research, 96 (B4), pp. 6569-6575, 1991.

Degnan, J.J. and A. Adelman, "Upgrade and integration of the NASA laser tracking network", Proc. 4th International Workshop on Laser Ranging Instrumentation, University of Texas in Austin, Austin, Texas, USA, pp. 2-11, October 12-16, 1981.

Degnan, J.J., T. W. Zagwodzki, and H. E. Rowe, "Satellite laser ranging experiments with an upgraded MOBLAS station", in Proc. 5th International Workshop on Laser Ranging Instrumentation, Royal Greenwich Observatory, East Sussex, England, pp. Sept. 10-14, 1984.

Degnan, J. J., "Millimeter accuracy satellite laser ranging: a review", in Contributions of Space Geodesy to Geodynamics, D.E. Smith and D. L. Turcotte (Eds.), AGU Geodynamics Series, Vol. 25, pp. 133-162, 1993.

Degnan, J. J. (Ed.), "Satellite laser ranging in the 1990's: Report of the 1994 Belmont Workshop", NASA Conference Publication 3283, 1994.

Eanes, R., "Earth Orientation Parameters" , in "Satellite laser ranging in the 1990's: Report of the 1994 Belmont Workshop", J.J. Degnan (Ed.), NASA Conference Publication 3283, pp. 61-63, 1994.

Johnson, T. S., H. H. Plotkin, and P. L. Spadin, "A laser satellite ranging system - Part 1: equipment description", IEEE J. Quantum Electronics, QE-3, pp. 435-439, 1967.

Johnson, T. S., J. J. Degnan, and T. S. McGunigal, "200 picosecond laser development - a status report", Proc. Third International Workshop on Laser Ranging Instrumentation, Session 6A, Lagonissi, Greece, 1978.

Kaula, W. (Ed.), "The Terrestrial Environment: Solid Earth and Ocean Physics; Applications of Space and Astronomic Techniques", published by NASA/MIT, Cambridge, Massachusetts, August, 1969.

Lerch, F. J., S. M. Klosko, and G. B. Patel, "Gravity model development from LAGEOS" , Geophysical Research Letters, 9, pp. 1263-1266, 1982.

Marshall, J. A. and N. K. Pavlis, "Ocean mass transport and its impact on temporal variations of the Earth's gravity field", EOS Trans., AGU, 74 (16), p. 102, 1993.

Marshall, J. A. , S. M. Klosko, and J. C. Ries, "Dynamics of SLR Tracked Satellites", to be published in U.S. National Report to the IUGG 1991-1994, Dynamics of the Solid Earth and other Planets, 1995.

Masevitsch, A. G. and K. Hamal, "Interkosmos laser radar network", Proceedings of the Second International Workshop on Laser Ranging Instrumentation, Prague, August 11-16, 1975.

McGunigal, T. E. , W. J. Carrion, L. O. Caudill, C. R. Grant, T. S. Johnson, D. A. Premo, P. L. Spadin, and G. C. Winston, "Satellite laser ranging work at the Goddard Space Flight Center", Proceedings of the Second International Workshop on Laser Ranging Instrumentation, Prague, August 11-16, 1975.

Minster, J. B., and T. H. Jordan, "Present day plate motion", J. Geophysical research, 83, pp. 5331-5354, 1978.

Mitrovica, J. X. and W. R. Peltier, "Present day secular variations in the zonal harmonics of the Earth's geopotential", J. geophysical research, 98(B3), pp. 4509-4526, 1993.

Nerem, R. S. , B. F. Chao, A.Y. Au, J. C. Chan, S. M. Klosko, N. K. Pavlis, and R. G. Williamson, "Time variations of the Earth's gravitational field from satellite laser ranging to LAGEOS", Geophysical Research Letters, 20(7), pp. 595-598, 1993a.

Nerem, R. S., B. F. Chao, J. C. Chan, S. M. Klosko, N. K. Pavlis, and R.G. Williamson, " Temporal variations of the Earth's gravitational field: measurement and geophysical modeling", Annales Geophysicae, 11 (1), p. C110, 1993b.

Nerem, R. S., C. J. Koblinsky, S. M. Klosko, B. D. Beckley, K. E. Rachlin, and R. G. Williamson, "The TOPEX/POSEIDON Mission: Results from the first two years", EOS Transactions, 75, p.51, Supplement, November 1, 1994.

Pearlman, M. R. , C. G. Lehr, N. W. Lanham, and J. Wohn, "The Smithsonian satellite ranging laser system", Proceedings of the Second Internationaol Workshop on Laser Ranging Instrumentation, Prague, August 11-16, 1975.

Plotkin, H.H., T.S. Johnson, P. Spadin, and J. Moye, " Reflection of Ruby Laser Radiation from Explorer XXII", Proc. IEEE, pp.301-302, March, 1965.

Premo, D. A. and B. O'Neill, "Daylight tracking with a pulsed ruby laser", presented at AGU Fall Meeting, San Francisco, CA, December 15-18, 1969.

Prochazka, I., K. Hamal, and B. Sopko, "Subcentimeter single photon ranging all solid state detection package", Internal Report, Czech Technical University, July 1990.

Reigber, C., G. Balmino, H. Muller, W. Bosch, and B. Moynot, " GRIM Ggravity model improvement using LAGEOS (GRIM3-L1)", J. Geophysical Research, 90, pp. 9285-9300, 1985.

Reis, J., R. Eanes, C. Shum, and M. Watkins, "Progress in the determination of the gravitational coefficient of the Earth", Geophysical Research Letters, 19, pp. 529-, 1992.

Reis, J., "The role of SLR and LLR in relativity", in "Satellite laser ranging in the 1990's: Report of the 1994 Belmont Workshop", J.J. Degnan (Ed.), NASA Conference Publication 3283, pp. 77-80, 1994.

Rubincam, D. P., "Drag on the LAGEOS satellite", J. Geophysical Research, 95, pp. 4881-4886, 1990.

Silverberg, E. C. and D. L. Byrd, "A mobile telescope for measuring continental drift", Sky and Telescope, 61, pp. 405-408, May, 1981.

Smith, D. E. and D. L. Turcotte (Eds.), Contributions of Space Geodesy to Geodynamics, AGU Geodynamics Series, Vols. 23-25, 1993.

Tapley, B. D., M. M. watkins, J. C. Ries, G. W. Davis, R. J. Eanes, S. Poole, H. J. Rim, B. E. Schutz, C. K. Shum, R. S. Nerem, F. J. Lerch, E. C. Pavlis, S. M. Klosko, N. K. Pavlis, and R. G. Williamson , "The JGM-3 gravity model", paper presented to the European Geophysical Society XIX General Assembly, Grenoble, France, April 1994.

Trupin, A. S., "Effects of polar ice on the Earth's rotation and gravitational potential", Geophys. J. Intl., 113, 273-283, 1993.

Varghese, T. and M. Heinick, "Subcentimeter multiphotoelectron satellite laser ranging", Proc. Sixth International Workshop on Laser Ranging Instrumentation, Antibes-Juan Les Pins, France, Sept.22-26, 1986.

Veillet, C., and P. Fridelance, "Time transfer between USA and France through LASSO", 7th European Frequency and Time Forum, Neuchatel, March 16-18, 1993.

Zagwodzki, T. W. , J. F. McGarry, J. J. Degnan, and T. Varghese, "Two color satellite laser ranging at NASA's 1.2 meter telescope facility", these proceedings, 1994.

FUTURE SCIENCE APPLICATIONS

Chairperson : Christian Veillet

GRAVITY AND ATMOSPHERE ASPECTS BY THE LOW ALTITUDE TARGET GFZ-1

Ch. Reigber, R. König
GeoForschungsZentrum Potsdam (GFZ), Dept. Kinematics and Dynamics of the Earth, Potsdam, Germany

Under GFZ contract a new laser satellite called GFZ-1 is being built. In March 1995 GFZ-1 will be transported to the MIR station and then released into space. The spherical satellite with a diameter of 21.5 cm and a mass of 20 kg carries 60 laser retroreflectors. As Lageos and other similar geodetic satellites, GFZ-1 belongs to the passive laser target class but will be the one with the lowest altitude. Thus GFZ-1 will contribute to the improvement of modelling the Earth's gravity field. GFZ-1 will slowly decay within it's expected lifetime of 5 years from 400 km altitude to 300 km moving through various resonance regimes of the gravity field. The restitution of recent gravity fields approaches approximately degree 70 of the spherical expansion. GFZ-1 will be sensitive up to degree 100 and more in specific resonant orders. However non-conservative forces at this low altitudes exert considerable perturbations. Simulations are carried out on the separability of the gravity signals from atmospheric effects in precise orbit determination. It can be seen that the uncertainties of atmosphere models can effectively be taken into account by proper parametrizations as long as sufficient SLR tracking is available.

1. INTRODUCTION

Since decades geodesists around the world are demanding a low altitude satellite mission for various reasons as f.i. expanding the restitution of gravity field models derived from satellite orbit perturbations. Up to now their efforts have been put into a number of studies, but the realization of all projects was abandoned mostly due to budget reasons. The recent approach having a good chance to be realized is the STEP satellite not to be launched before the year 2003 (see *Schwintzer et. al.* [1994]). In view of this situation, GFZ decided to finance an intermediate, alternate mission with a fantastic short time span from design to space deployment of one year only. The GFZ-1 satellite is designed as a classical passive laser satellite as Lageos, Starlette etc., but will have the lowest altitude among those. The mission will add considerable improvements to the knowledge of the gravity field. At the low altitudes of the GFZ-1 orbit, surface forces play a major role in the compilation of orbit perturbations. As GFZ-1 should sense gravity signals, the impacts from the surface forces have to be separated.

The following investigations try to quantify the errors that can be expected from the atmospheric models. Simulations are carried out on how the atmospheric model errors can be taken care of by certain parameters.

More background information on GFZ-1 may be found in *Reigber et. al.* [1994]. An analysis of orbit prediction capabilities can be found in *König and Chen* [1994].

2. THE GFZ-1 MISSION

GFZ-1 is sphere of approximately 21.5 cm diameter and weights approximately 20 kg. Its surface is covered with 60 laser retroreflectors. A quite schematic picture of the satellite is given in Figure 1.

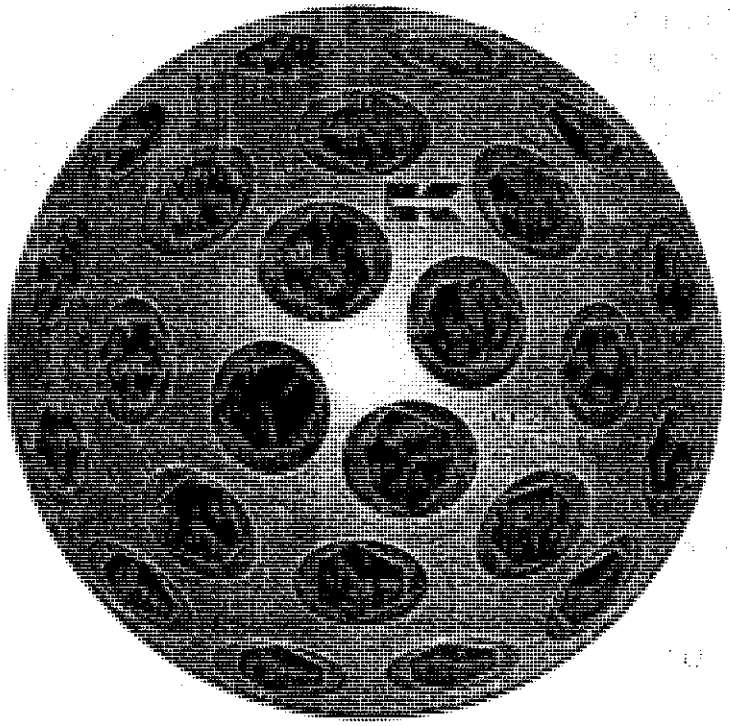

Figure 1 Schematic picture of GFZ-1

GFZ-1 will be transported by a PROGRESS spacecraft to the MIR station and then released into space. So the inclination will be approximately 51.6 deg. From an initial altitude of approximately 400 km after the launch in March 1995, the satellite will slowly decay to 300 km within approximately 5 years touching various resonance regimes of the gravity field. The knowledge of recent gravity fields derived from satellite orbit perturbations lasts to approximately degree 70 of the spherical expansion. This can be seen in Figure 2 where the sensitivity w.r.t. gravity for ERS-1 is depicted. The altitude of ERS-1 is the lowest one with approximately 800 km currently being included in gravity field solutions.

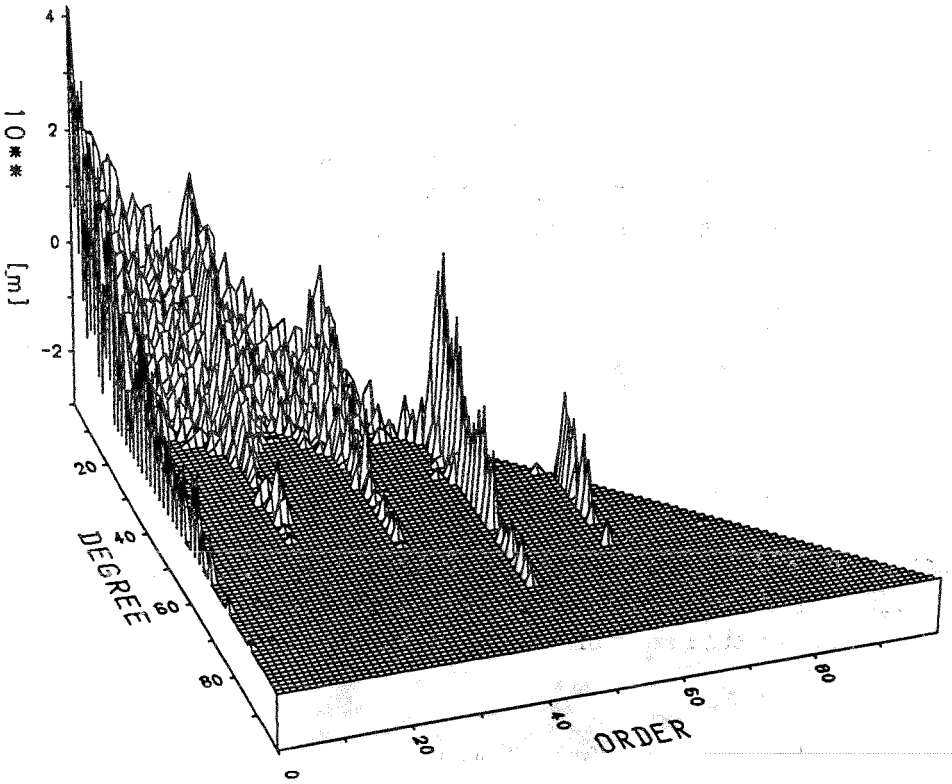

Figure 2 ERS-1 Sensitivity to Gravity

Figure 3 tells the same for GFZ-1 at 350 km altitude. The sensitivity comes now up to degree 100 at certain orders.

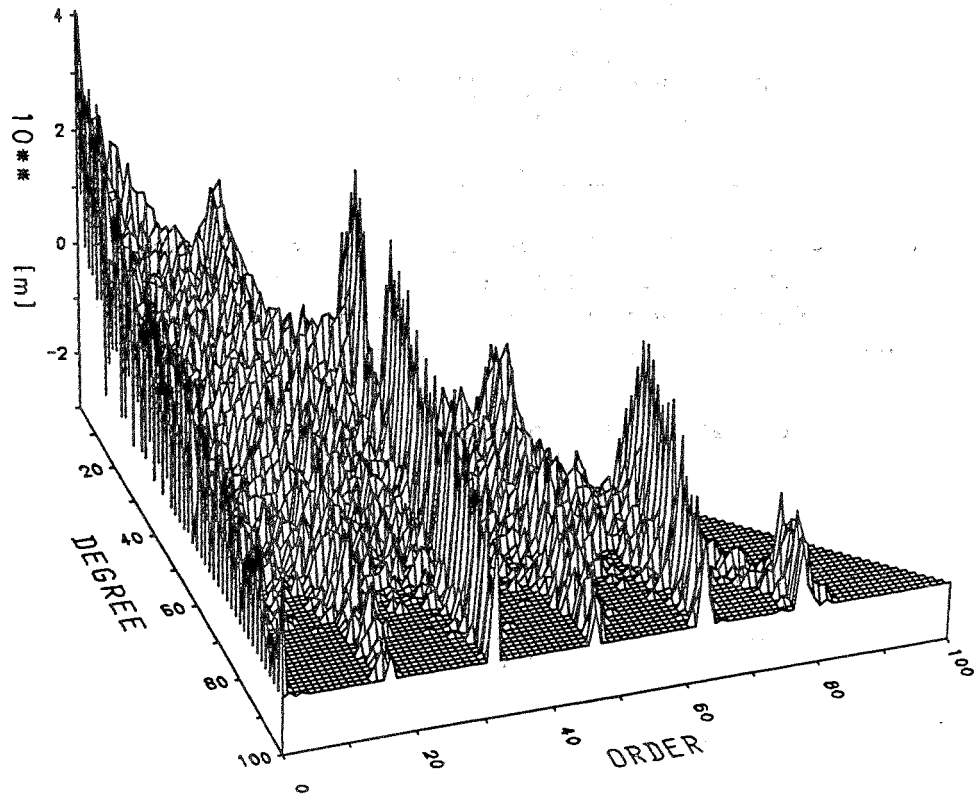

Figure 3 GFZ-1 Sensitivity to Gravity

The time span of the GFZ-1 mission coincides with the ascending part of the solar activity cycle. Initially at the highest altitudes the solar activity is low. The solar activity will increase during the 5 years lifetime of GFZ-1, whereas the altitude of the satellite will decrease. This will multiply the impact of the surface forces and will therefore make the precise orbit determination process more difficult.

3. FORCES AND ATMOSPHERIC MODELS

3.1 *Conservative and Non-conservative Forces*

Table 1 lists some forces acting on GFZ-1 at an altitude of 400 km during the period of low solar activity i.e. at the beginning of the mission. A column for an area to mass ratio like that of Starlette is added in order to relate the numbers to a known mission.

Table 1: Various Forces at One Instant

Source	Acceleration (m/s/s)	
	A/M GFZ-1	A/M Starlette
Potential	0.23 *10**-3	0.23 *10**-3
3rd Bodies	0.65 *10**-6	0.65 *10**-6
Tides	0.26 *10**-6	0.26 *10**-6
Drag	0.34 *10**-6	0.18 *10**-6
Radiation	2.65 *10**-9	1.39 *10**-9
Albedo	1.26 *10**-9	0.66 *10**-9

The magnitude of the surface forces acting on GFZ-1 reaches already the magnitude of the forces imposed by sun, moon, planets and earth and ocean tides. The GFZ-1 surface forces are twice as large as for the Starlette design corresponding to the ratio of the area to mass ratios of the two designs.

Table 2 lists the drag forces for the begin and towards the end of the mission for the two atmospheric models CIRA'86 and DTM.

Table 2: Drag Forces

Alt (km)	SolAct	Acceleration (m/s/s)	
		CIRA'86	DTM
400	Low	0.34 *10**-6	0.30 *10**-6
350	High	1.52 *10**-6	1.57 *10**-6

Towards the end of the mission the drag forces will be 5 times as large as at the beginning. The difference of the two atmospheric models amounts to 3 to 10 %.

3.2 *Area to Mass Ratios and Atmospheric models*

Orbit integrations are carried out to study the effects of different area to mass ratios. Table 3 compiles orbit differences after 3 days if area to mass ratios of either GFZ-1 or of Starlette are used for orbit modelling. The results are given at the beginning and towards the end of the mission and for the two atmospheric models introduced already above.

Table 3: Area to mass ratios

Alt (km)	SolAct	AtmMod	Rad (m)	Cross (m)	Along (m)
400	Low	CIRA'86	97	754	14677
		DTM	113	838	16313
350	High	CIRA'86	551	3000	59449
		DTM	722	3600	71349

The major differences result in along-track direction which would become visible to an observer on the Earth as a shift in the rise time of the satellite. The delay of GFZ-1 w.r.t. a more favourable area to mass ratio design like that of Starlette amounts to roughly 2 seconds in time after 3 days at the beginning of the mission. Towards the end of the mission this increases to 10 seconds. The difference between the atmospheric models lies in the order of 10 to 20 %.

Table 4 compiles orbit differences after 3d if the atmospheric models CIRA'86 or DTM are used. The results are again given at the beginning and towards the end of the mission. They are divided for the two different area to mass ratios also used in the above.

Table 4: Atmospheric models

Alt (km)	SolAct	A/M	Rad (m)	Cross (m)	Along (m)
400	Low	Starlette	15	94	1821
		GFZ-1	28	178	3458
350	High	Starlette	86	664	13168
		GFZ-1	186	1263	25070

Again it can be seen that GFZ-1 is influenced twice as much as in case of a Starlette-like area to mass ratio. During the course of the mission the influence of the atmosphere in-

creases by nearly a factor of 10. Considerable different orbits demonstrate the uncertainties of the two atmospheric models.

4. ATMOSPHERIC MODEL ERROR PARAMETRIZATION

The inherent errors of atmospheric models can only be accounted for by a proper selection of the parameters solved for in the precise orbit determination task. From the simulations in the following conclusions can be drawn on the optimal parametrization of the least squares problem. Also the impacts of data availablity can be checked.

4.1 *Strategy*

Laser tracking data were simulated under the assumption that only a few stations worldwide are able to track this low target. It was further assumed that only 20 % of all possible passes can be acquired. The standard deviations of ranges was generally set to 1 cm. The atmospheric model CIRA'86 was used in generating the laser tracking passes.

For the recovery of the orbit on the basis of the simulated observations the atmospheric model DTM was introduced. So the uncertainties of the atmospheric models were taken into account. Various combinations of parameters were solved for in order to find an optimal combination of parameters that efficiently takes care of the surface forces.

All runs were carried out for periods at the beginning and towards the end of the mission. The simulated observations are sparsely distributed in space and time. The observed ground tracks are displayed in Figure 4 where also the chosen stations are depicted.

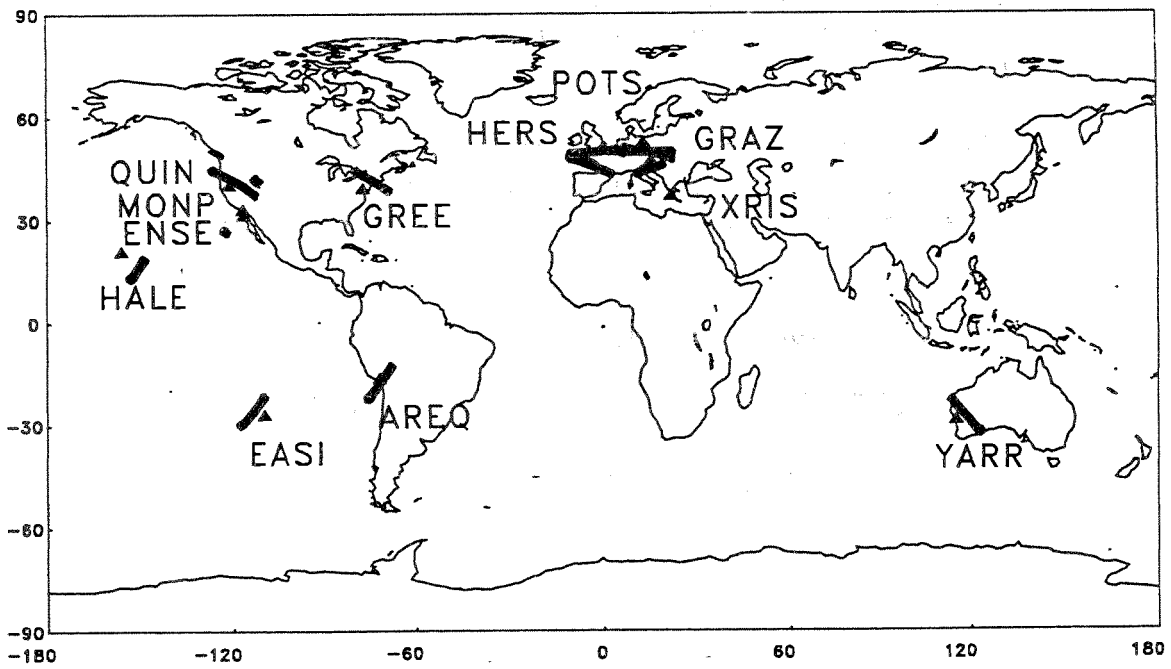

Figure 4 Simulated Passes in Space

The timely distribution of the observations is displayed in Figure 5. There are no observations at the first day which causes some troubles in precise orbit determination. A discussion follows below.

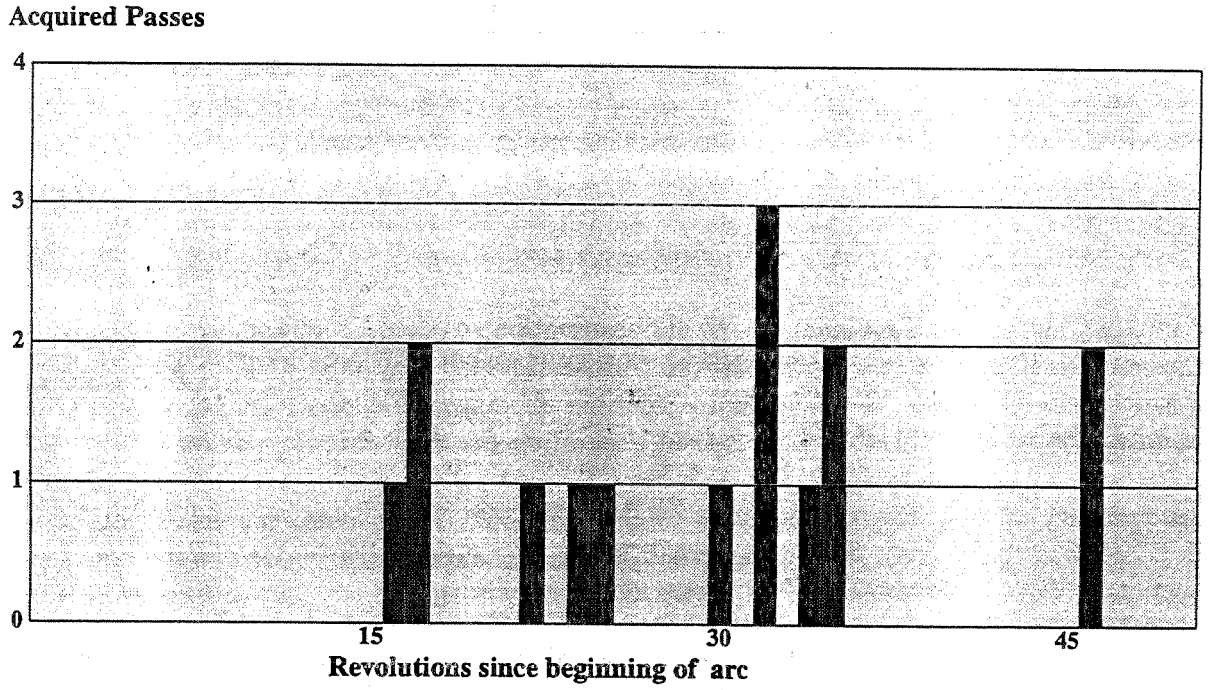

Figure 5 Simulated Passes in Time

4.2 *Effect of Data Gaps*

The following is computed for an altitude of 350 km and high solar activity i.e. towards the end of the mission. The parameters solved for are the initial state vector, one global radiation coefficient, two one-cycle-per-revolution (1CPR) empirical along-track acceleration parameters and drag coefficients (CD) as shown. Table 5 lists the accuracies of the orbit recovery where the one day data gap is part of the arc. The table gives the orbital fits of the precise orbit determination and the differences of the recovered orbit w.r.t. the reference orbit.

Table 5: Recovery accuracy with one day data gap

CD	Orbital Fit (m)	Reference vs. Recovered Orbit Radial (m)	Cross (m)	Along (m)
1	9.02	7.61	21.31	32.93
1/d	1.74	2.06	5.76	139.50

For the generation of the results in Table 6, the arc has been shortened so that the one day data gap has been excluded.

Table 6: Recovery accuracy without data gap

CD	Orbital Fit (m)	Reference vs. Recovered Orbit Radial (m)	Cross (m)	Along (m)
1	9.50	8.04	11.26	37.55
1/d	0.25	1.15	0.76	8.68

With one global CD the data gap does not influence the orbit recovery accuracy. If daily CDs are solved the CD within the data gap can hardly be estimated. Though the orbital fit improves drastically, the correlations among the parameters introduce a peak deviation from the reference orbit around the period where no data are available particularly visible in along-track direction. If the arc is shortened to the period covered more densely with observations, orbital fit and recovery accuracy become much better. However orbital fit and recovery accuracy disagree by approximately 300 %. The orbital fit values do therefore not show the orbit modelling accuracy over the whole arc period. They rather indicate the better physical modelling if they decrease between different parametrizations.

4.3 *Effect of Drag Coefficients Density*

In the following the parameters solved for are the initial state vector, one global radiation coefficient, two 1CPR parameters and drag coefficients as given below.

Table 7 shows the orbit recovery accuracy for an increasing density of drag coefficients for the early mission phase at 400 km altitude and low solar activity.

Table 7: Recovery accuracy w.r.t. CDs (early mission phase)

CD	Orbital Fit (m)	Reference vs. Recovered Orbit Radial (m)	Cross (m)	Along (m)
1	4.59	5.52	2.82	29.31
1/d	0.32	2.26	0.57	15.03
2/d	0.07	0.18	0.07	1.28

Table 8 holds for an orbit at 350 km altitude and high solar activity towards the end of the mission.

Table 8: Recovery accuracy w.r.t. CDs (late mission phase)

CD	Orbital Fit (m)	Reference vs. Recovered Orbit Radial (m)	Cross (m)	Along (m)
1	9.50	8.04	11.26	37.55
1/d	0.25	1.15	0.76	8.68
2/d	0.15	0.82	0.32	9.35

It becomes obvious that more CDs effectively take care of the atmospheric effects. It has to be pointed out however that they may only be used more densely where respectively dense tracking is available. Otherwise large correlations may introduce artificial effects. At the beginning of the mission the recovery accuracy is a factor of 10 better than later on. The situation for lower altitudes and higher solar activities may not be seen so pessimistic as one could probably rely on the learning effect during the course of the mission.

4.4 *Effect of 1CPR Parameters*

The parameters solved for in the following investigations consist of the initial state vector, one global radiation coefficient and two drag coefficients per day. In order to assess the effect of the 1CPR parameters, runs were carried out where they have been estimated and runs where not. For the initial phase of the mission, Table 9 compiles the recovery results for an altitude of the orbit of 400 km and for low solar activity at the beginning of the mission.

Table 9: Recovery accuracy w.r.t. 1CPR (early mission phase)

1CPR Estim	Orbital Fit (m)	Reference vs. Recovered Orbit Radial (m)	Cross (m)	Along (m)
yes	0.07	0.18	0.07	1.28
no	0.18	1.16	0.28	6.93

Table 10 continues the compilation of Table 9 for the orbit at 350 km altitude and high solar activity for the period towards the end of the mission.

Table 10: Recovery accuracy w.r.t. 1CPR (late mission phase)

1CPR Estim	Orbital Fit (m)	Reference vs. Recovered Orbit Radial (m)	Cross (m)	Along (m)
yes	0.15	0.82	0.32	9.35
no	0.54	2.48	1.20	18.11

It becomes clear that the inclusion of the 1CPR parameters is essential for an accurate orbit recovery. The gain ranges from a factor of 2 to a factor of 5.

5. CONCLUSIONS

The restitution of recent satellite gravity fields reaches approximately degree 70 of the spherical expansion. The sensitivity of GFZ-1 comes up to degree 100 and more. The surface forces at the altitudes of GFZ-1 have dramatic impacts into the precise orbit determination process. The magnitudes of the surface forces range at the orders of magnitudes of 3rd bodies and tide forces. The influence of the surface forces on GFZ-1 is twice as large as for a area to mass ratio of Starlette type. Recent atmospheric models differ up to 20 % within the mission scenario of GFZ-1. High solar activities and lower orbit altitudes towards the end of the mission magnify the impact of the surface forces by a factor of 10. However appropriate parameters can effectively account for a large portion of the atmospheric model errors. It has to be outlined that the recovery of the orbit becomes uncertain where data gaps of approximately one day exist. Intensive efforts to acquire dense laser tracking data are therefore a prerequisite for a successful mission.

REFERENCES

König, R., Chen, Z., "Probable Qualities of GFZ-1 Orbit Predictions," this volume (1994)

Reigber, Ch., König, R., Massmann, F.-H., "The GFZ-1, the ERS-1 and the ERS-1/ERS-2 Tandem Mission," this volume (1994)

Schwintzer, P., Rummel, R., Sneeuw, N., "Geodesy with STEP," Annales Geophysicae, Suppl. I to Vol. 12, Part I, Solid Earth Geophysics and Natural Hazards, p. C 184 (1994)

THE RETROREFLECTOR IN SPACE (RIS) - A NEW FACILITY FOR SLR

Nobuo Sugimoto and Atsushi Minato

National Institute for Environmental Studies
16-2 Onogawa, Tsukuba, Ibaraki 305 Japan
Phone: 81-298-51-6111 Facsimile: 81-298-51-4732
E-mail: nsugimot@nies.go.jp

A large single-element retroreflector named Retroreflector In Space (RIS) is to be loaded on the Advanced Earth Observing Satellite (ADEOS) which is scheduled for launch in February 1996. RIS is an instrument provided by Environment Agency of Japan (JEA) for experiments on laser long-path absorption measurement of atmospheric trace species. Measurements of atmospheric trace species such as O_3, CFC12, HNO_3, CO, N_2O, and CH_4 will be carried out with CO_2 lasers from Tokyo by the National Institute for Environmental Studies (NIES) in cooperation with the Communications Research Laboratory (CRL).

ADEOS is a Japanese polar-orbit satellite which carries seven earth-observing sensors besides RIS. Table 1 lists the orbital characteristics of ADEOS.

Table 1. Characteristics of the ADEOS orbit.

Category	Sunsynchronous sub-recurrent orbit
Local Sun Time	10:30+/-15
Recurrent Period	41 days
Altitude	Approx. 797 km
Inclination	Approx. 98.6 deg
Period	Approx. 101 minutes

Figure 1 and Fig. 2 show the structure of RIS. RIS has a new retroreflector design which has a spherical mirror for optimizing the pattern of the reflected beam. The effects of the spherical mirror and spoiled dihedral angles compensate the velocity aberration caused by the satellite movement. Because RIS has a single element, there are no speckle effect and temporal jitter in reflected pulses. Also, RIS has high reflectance in a wide wavelength range from 350 nm to 14 μm, and the reflection of RIS is much brighter than existing SLR targets. Therefore, RIS is also useful as a target for experiments on laser ranging.

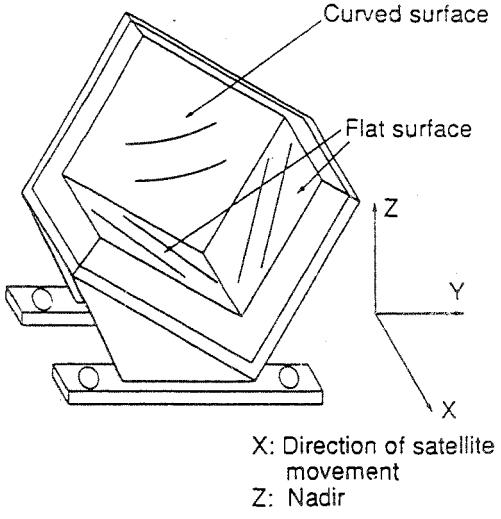

Fig. 1. Structure of RIS.

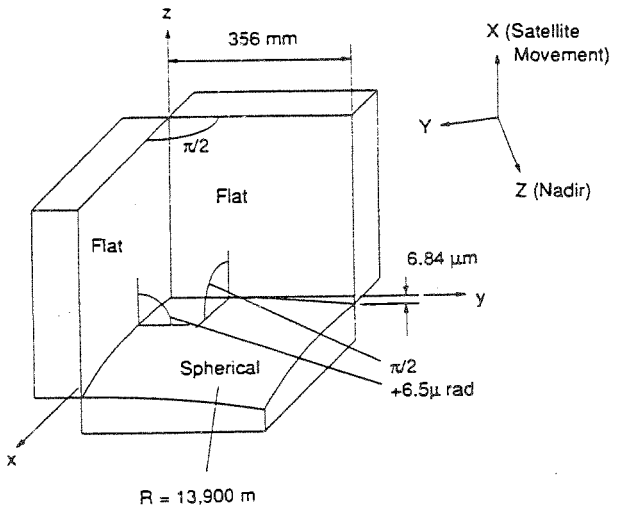

Fig. 2. Surface parameter for RIS.

Figure 3 and Fig.4 shows calculated and measured wavefront of the reflected beam of RIS at 632.8 nm. Figure 5(a) and 5(b) show the ground pattern of reflected beam at 532 nm and 10.6 mm, respectively.

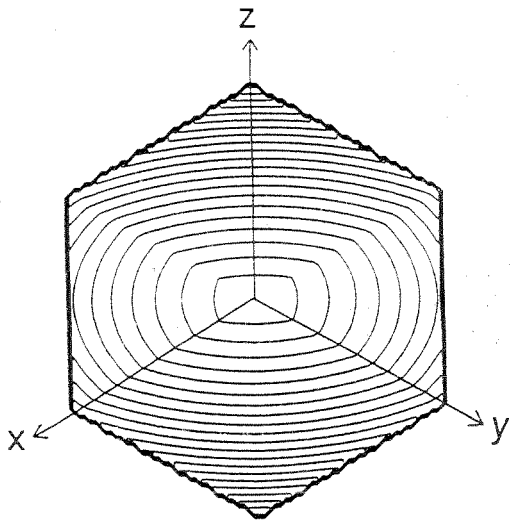

Fig. 3. Calculated interference fringe of RIS.

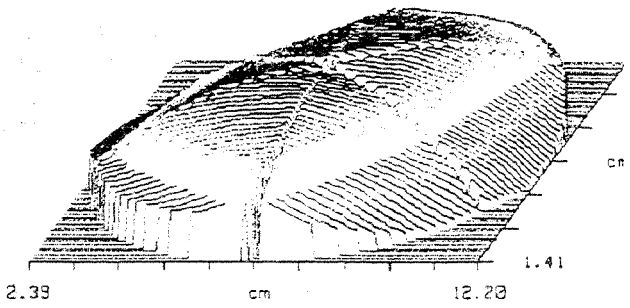

Fig. 4. Wave front of engineering model of RIS measured with a 6 inch interferometer.

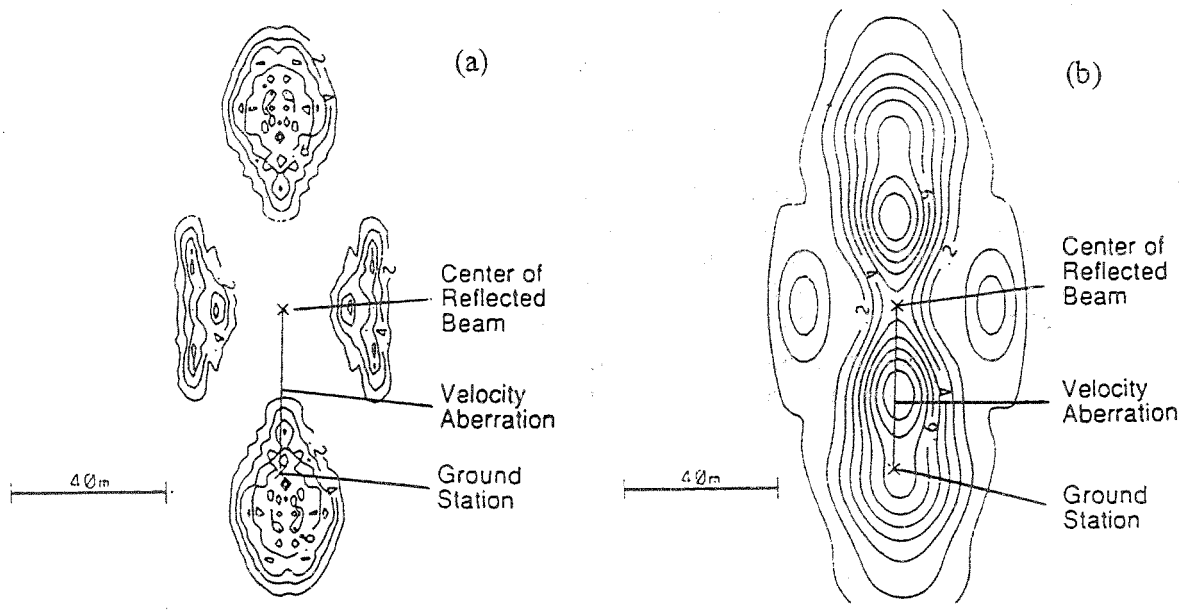

Fig. 5. Ground pattern of reflected beam at (a) 532 nm and (b) 10 μm.

The direction cosine of the optical axis of RIS on ADEOS is (0.508, -0.279, 0.815). Figure 6 shows intensity of reflected beam from RIS as a function of the position of ADEOS relative to a ground station for the descending paths at (a) 532 nm and (b) 10 μm. The quantity indicated is η which is defined so that the received power is calculated by

$$P = (16/\pi^2)\,(P_0/\theta_t^2)\,T^2\,\eta_{RIS}\,A_r\,\eta_{sys}\,\eta, \qquad (1)$$

where P_0, θ_t, T, η_{RIS}, A_r, and η_{sys} represent transmitted power, divergence of the transmitted beam, transmittance of the atmosphere, reflectance of RIS (~0.8), aperture of receiver, and efficiency of the receiver, respectively.

The efficiency, η, for RIS is compared with existing SLR targets in Table 2. RIS is approximately ten times brighter than Ajisai and there is no jitter because it is single element.

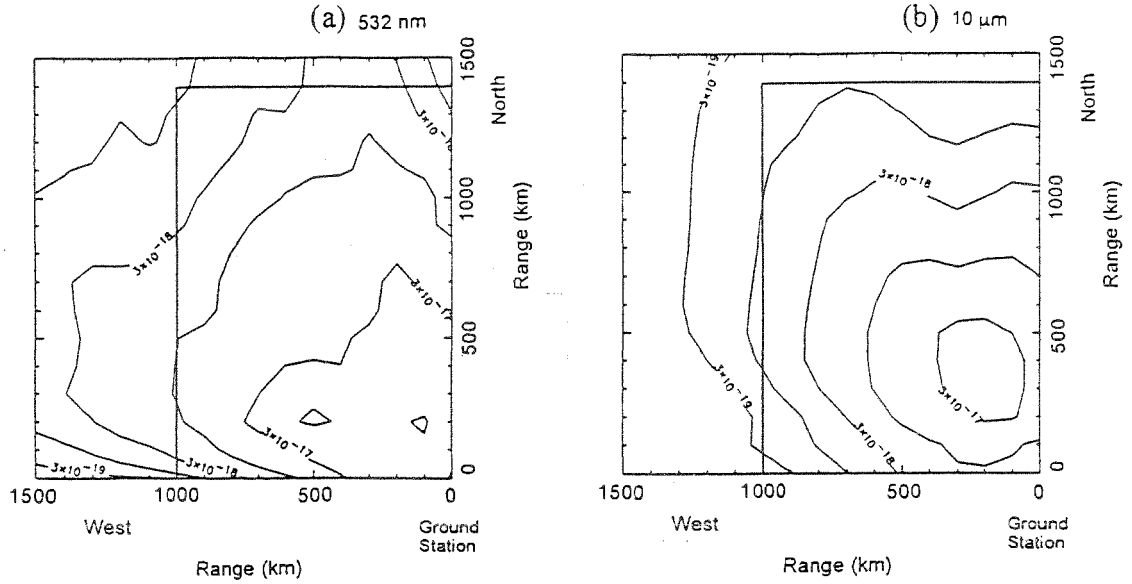

Fig. 6. Intensity of the reflected beam as a function of the satellite position at (a) 532 mn and (b) 10 μm.

Table 2. Optical characteristics of satellite retroreflectors.

Satellite	EGS (Ajisai)	LAGEOS	ETALON	RIS
Distance (km)	2000	8000	25000	800 - 2000
Effective Area (m^2)	0.04 (multiple)	0.04 (multiple)	0.04 (multiple)	0.2 (single)
Divergence of Reflected Beam (μrad)	30	30	30	~80
Reflection Efficiency η (m^{-2})	$2.7x10^{-18}$ (multiple)	$1.1x10^{-20}$ (multiple)	$1.1x10^{-22}$ (multiple)	$\sim 4.6x10^{-17}$ (single)

Figure 7 shows a schematic diagram of the ground system for laser long-path absorption experiments. The system consists of a tracking system, a laser ranging system, and a laser transmitter/receiver system for spectroscopic measurements. The satellite tracking system with a 1.5-m diameter telescope at CRL will be used in the experiment.

For the spectroscopic measurements, we developed a method which utilize the Doppler shift of the reflected beam resulting from the satellite movement. Two single-longitudinal-mode TEA-CO_2 lasers are used. One of the lasers is tuned to the laser lines close to the absorption lines of the target molecule. The other is used for measuring the reference signals to correct atmospheric effects. The magnitude of the Doppler shift of the reflected light is 0 - 0.04 cm^{-1} at 10 μm, which depends on the satellite position relative to the ground station. High-resolution transmission spectra of the atmosphere is measured by using the change in the wavelength of the Doppler-shifted return beam.

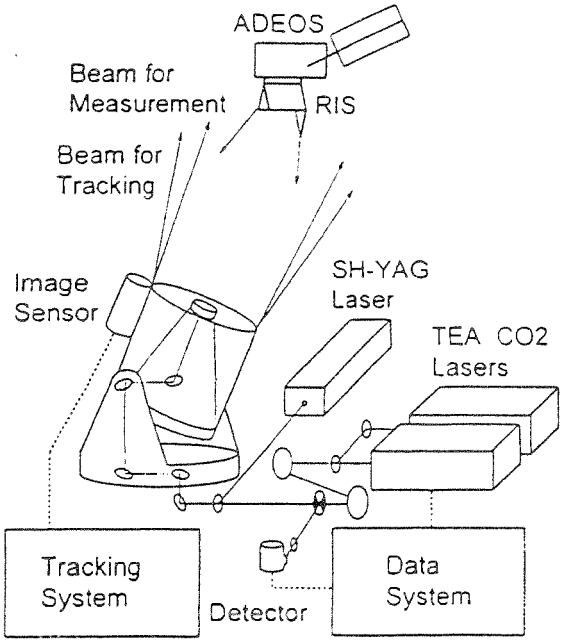

Fig. 7. Ground system for the RIS experiment.

Figure 8 shows an example of the atmospheric transmission spectrum and the laser lines for the measurement of ozone. The wavelength of the laser will be switched alternately between P(18) and P(20) during the measurement, and the spectra in the three wavelength regions indicated in Fig.8 will be measured.

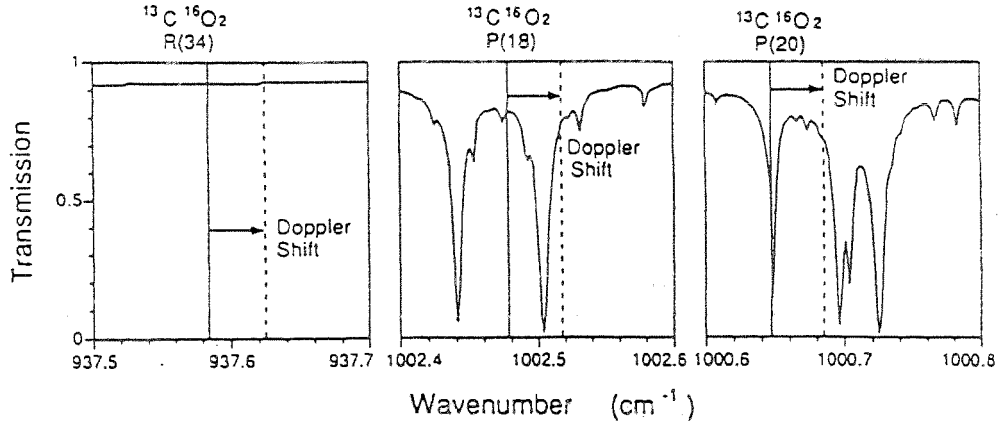

Fig. 8. Synthesized atmospheric transmission spectrum (ground-satellite one-way path; elevation angle, 60 deg.) and the laser lines for measurement of ozone.

Target molecules with isotope TEA-CO_2 lasers ($^{12}C^{16}O_2$, $^{13}C^{16}O_2$) and their second and third harmonics are listed in Table 3. The vertical profiles will be obtained by inversion method using absorption line shape for the molecules with large absorption such as ozone and methane. The column contents will be obtained for other molecules by means of the least squares method with the assumption on the vertical distribution. Measurement method and data reduction method for CFC12 are different because absorption spectrum of CFC12 is almost continuum. In this case, the absorption at the multiple laser lines will be measured by switching laser lines, and the column content will be derived by the multiple wavelength differential absorption method.

Table 3. Target molecules and CO_2 laser lines for the measurement.

Molecule	Laser line	CO_2 isotope	Wavenumber (cm^{-1})
O_3	P(18)	636	1002.4778
	P(20)	636	1000.6473
CO_2	P(26)	626	938.6883
	R(36)	636	938.7776
HNO_3	P(8)	636	907.0528
CFC12	R(6) - R(12)	636	918.74 - 923.11
CO	R(28) SH*	626	2166.96
	R(30) SH	626	2169.27
N_2O	R(38) SH	626	2178.002
CH_4	R(14) TH**	626	2915.79
	R(16) TH	626	2919.87
Reference	R(34)	636	937.5844
	R(8) SH	626	2140.925
	R(26) TH	626	2939.12

*SH, second harmonics; **TH, third harmonics.

Figure 9 shows an example of the simulated return signals calculated by a simulator program which includes the actual system parameters and the simulation results for the reflection characteristics of the RIS. In this example, the line of one of the CO_2 lasers is switched every one second. The parameters for the ground system is listed in Table 4. Figure 10 shows the ozone profile retrieved from the simulated signals shown in Fig.9. The retrieved ozone profile agreed well with the profile given in the simulation. We obtained a good result also for the measurement of methane.

Table 4. Ground system parameters.

TransmittedLaser Energy	100 mJ	(10 μm)
	10 mJ	(5 μm)
	5 mJ	(3 μm)
	100 mJ	(532 nm, for laser ranging)
Transmitted Beam Divergence	100 μrad	(3 - 10 μm)
Receiver Telescope Diameter	1.5 m	
Efficiency of optical system	0.01	
Detectivity of detectors	7×10^{10} $cmHz^{1/2}/W$	(10 μm, HgCdTe)
	1×10^{11} $cmHz^{1/2}/W$	(5 μm, InSb)
	6×10^{10} $cmHz^{1/2}/W$	(3 μm, InSb)
Detector Area	0.001 cm^2	
Time Constant	1 μsec	
Quantum Efficiency	0.6	

Beside the experiment planned by NIES and CRL from Tokyo, research themes are solicited by the ADEOS Research Announcement by NASDA and JEA. Table 5 lists selected proposals. The first three themes are experiments from independent ground stations. We formed the RIS Science team for these experiments. Table 6 lists the members. The reaserch announcement is still open for proposals, and we welcome proposals on experiments using RIS. Also, to perform these experiments successfully, accurate orbital prediction based on laser ranging is indispensable, and we would like to ask for tracking suport of international SLR community.

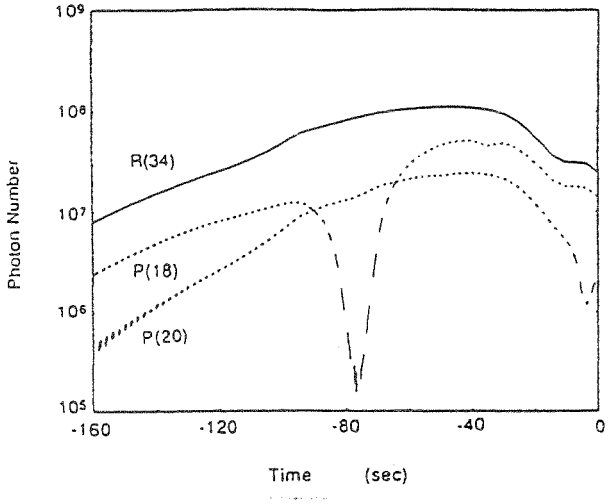

Fig.9. Simulated return signal (photonnumber per shot) in the ozone measurement.

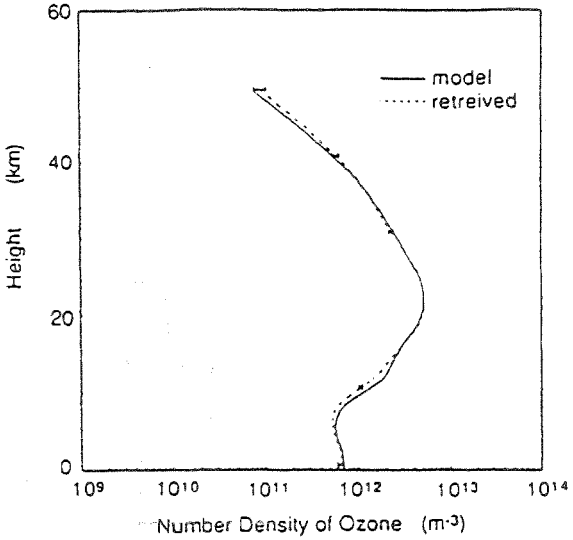

Fig. 10. Ozone profile retrieved from the simulated signal.

Table 5. Selected proposal to the ADEOS research announcement.

Theme	Laser Ranging and Atmospheric Measurements Using RIS from the UK
PI	M. J.T. Milton (National Physical Laboratory, United Kingdom)
Theme	Dualcolor Satellite Laser Ranging Measurements Using RIS
PI	U. Schreiber (Research Establishment Satellite Geodesy of the Technical University of Munich, Germany)
Theme	Precise Determination of the ADEOS Orbit by Laser Ranging Technique
PI	T. Tatsuno (Hydrographic Department Maritime Safety Agency, Japan)
Theme	Retrieval of Vertical Profiles and Column Amounts of Atmospheric Constituents from High Resolution Spectra Taken by RIS Experiments
PI	F. J. Murcray (University of Denver, U. S. A.)
Theme	Elaboration of Information Retrieval System for Analysis of the CO_2-Laser Radiation Extinction by the Atmospheric Gases
PI	O. K. Voitsekhovskaya (Institute of Atmosheric Optics, Russia)

Table 6. RIS science team members.

Nobuo Sugimoto	NIES (National Institute for Environmental Studies)
Atsushi Minato	NIES
Ichiro Matsui	NIES
Yasuhiro Sasano	NIES
Hideaki Nakane	NIES
Toshikazu Itabe	CRL (Communications Research Laboratory)
Tadashi Aruga	CRL
Norihisa Hiromoto	CRL
Masao Takabe	CRL
Hiroo Kunimori	CRL

(continued on the next page)

Table 6. (continued)

Tetsuo Aoki	CRL
Masahiro Toyoda	CRL
Tadao Tatsuno	JHD (Hydrographic Department of Japan)
Masayuki Fujita	JHD
Arata Sengoku	JHD
Minoru Sasaki	JHD
Osamu Uchino	Meteorological Research Institute
Takao Kobayashi	Fukui University
Ryuji Koga	Okayama University
Kazuhiro Asai	Tohoku Institute of Technology
Shoich Okano	Tohoku University
Yasunori Saito	Shinshyu University
Hiroyuki Ohshima	Int. Met. & Oceanogr. Consultant Co., LTD.
Martin J.T. Milton	National Physical Laboratory, U.K.
Robert Nordstrom	Laser Science, Inc., U.S.A.
Zvi Bleier	PLX Inc., U.S.A
Ulrich Schreiber	Techn. Univ. Muenchen, Germany
Frank J. Murcray	University of Denver, USA
Olga K. Voitsekhovskaya	Inst. Atmosheric Optics, Russia

REFERENCES

1. National Space Development Agency of Japan (NASDA), ADEOS pamphlet (1992).
2. N. Sugimoto, A. Minato, and Y. Sasano: Retroreflector In Space for the ADEOS Satellite, CLEO'91, Baltimore, p.450 (1991).
3. A. Minato, N. Sugimoto, and Y. Sasano: Optical Design of Cube-Corner Retroreflectors Having Curved Mirror Surfaces, Appl. Opt. **31**, 6016-6020 (1992).
4. N. Sugimoto and A. Minato: Method for Measuring Dihedral Angles of a Cube-Corner Retroreflector Having Curved Mirror Surfaces, Opt. Eng. **33**, 1187-1192 (1994).
5. N. Sugiomoto: The Retroreflector in Space (RIS) Experiment, Abstracts of Papers 17th Int. Laser Radar Conf. pp.181-183 (1994).
6. A. Minato, N. Sugimoto, and Y. Sasano: Spectroscopic Method for Atmospheric Trace Species Measurement Using a Satellite Retroreflector (RIS), Rev. Laser Eng. **19**, 1153-1163 (1991). (in Japanese)
7. A. Minato, H. Ohshima, Y. Sasano and N. Sugimoto: Data Reduction Algorithm for Earth-Satellite Laser Long-Path Absorption Measurement Using RIS, Abstracts of Papers 17th Int. Laser Radar Conf. pp.559-560 (1994).
8. R.J.Nordstrom, L.J.Berg, A.F.DeSimone, and N.Sugimoto: Time-Gated Gain Cell for Frequency-Stable, Single-Longitudinal-Mode Operation of a TEA CO_2 Laser, Rev. Sci. Instr. **64**, 1663-1664 (1993).
9. R.J.Nordstrom, L.J.Berg, A.F.DeSimone, and N.Sugimoto: Single-Longitudinal-Mode Operation of a TEA CO_2 Laser Using a Time-Gated Gain Cell, Rev. Laser Eng. **22**, 132-139 (1994).

Ninth International Workshop On Laser Ranging Instrumentation, 7-11 November 1994, Camberra, Australia

Session : "Target Signature and Biases"

A NEW CONCEPT OF SPATIAL RETROREFLECTORS FOR HIGH PRECISION SATELLITE LASER RANGING

Michel KASSER[1]
Glenn LUND[2]

[1] M. K.: ESGT-CNAM, 18 Allée Jean ROSTAND, 91025 EVRY Cedex, France, fax (331) 69 36 73 05
IGN-LOEMI, 2 Av. Pasteur, BP 68, 94160 Saint-Mandé, France, fax (331) 43 98 85 81

[2] G. L.: Aerospatiale, 100 Boulevard du Midi, BP 99, 06 322 CANNES-LA BOCCA Cedex, France, fax (33) 9292 7160

Abstract

A new design for optical retroreflectors is presented, the aim of which is to provide solutions for two problems typical to high precision SLR : the first concerns apparent centre of mass range variations incurred by variations in the corner cube incidence geometry, and the second deals with the problem of velocity aberration correction combined with the need for high optical efficiency and the use of technologies suitable for space environment.

I/ Space geodesy, the future of SLR and geophysical needs.

The past few years have shown an impressive degree of activity concentrated on improving the performances of space geodesy techniques, the most outstanding obviously being that of GPS. While VLBI has the exclusive advantage of its unsurpassed precision and of tying terrestrial and extragalactic frames together, GPS - since IGS is operational - provides, to a comparable degree of cost effectiveness, precisions close to that of SLR, if not better, for most of the surveyed parameters (Earth rotation, orbits, station positions). The only feature which, in terms of absolute accuracy, will continue to require SLR in the foreseeable future is the link provided with the gravity centre of the Earth. The need to survey this parameter is however not so imperative as to justify the costly methoddlogy involved in the continued exploitation of a large number of stations around the globe.

It is thus of the utmost importance for the scientific community to carefully appraise the full potential of SLR technology and its application to the survey of geophysical parameters, since if no significant justification can be found for its continued implementation, the use of this technology is likely to disappear within the next few years. It is now commonly thought that this may be our last chance to reexamine the potential of SLR in the context of requirements of sciences other than geophysics, and that decision should be made to adapt its capabilities to meet such goals and requirements. In case of failure the enormous know-how associated with this technology may disappear along with its engineering development and support teams.

Following a joint request from the French space and geophysics agencies (CNES and INSU), a general survey of the future of spatial geodesy was carried out in France one year ago (Ref. 1), and (following long discussions) the basic requirements of neighbouring sciences related to geodesy were appraised. One of the concluding statements of particular interest is quoted here :

"For studies involving altitude variations (mountainous chain formations, subsidence or uplift movements at continental scales such as post-glacial rebound and ocean loading over continental margins, etc...) there are other very important goals for earth sciences, similar to the tectonic aspects already mentioned. For these purposes it will be necessary to measure absolute heights with respect to the Earth's centre of mass, with an accuracy of one millimetre.

With regard to SLR, the following statements were made :

"Concerning SLR (Satellite Laser Ranging), this technology has benefitted from only minor improvements in the last 10 years. It corresponds to a methodology which is one of the most accurate for the computation of a satellite's orbit (locally within a few millimetres), and there exist, devoted exclusively to SLR, around twelve specialised satellites, each of which are considered equivalent to a dense point within the Earth's gravity field, such that their orbits have only a low sensitivity (when compared with other satellites) to non-gravitational forces. The installation cost of a laser reflector on a satellite is quite low, and in any case the useful lifetime of orbital components involved in SLR is far greater than that of other space-borne methodologies. SLR stations number about 30 on earth, are quite different from one another in terms of performance, and provide a non optimal overall accuracy because of their poor global distribution (they are located mainly in Europe and the USA). The measured orbits are used to improve our knowledge of Earth's gravity field and its temporal variations, to contribute to the determinations of the Earth's rotation (until 1992 this was the major source of input into global solutions), and as a by-product they enable absolute positioning to be achieved to within 1 to 2 cm.

The limiting factors in system precision are, in decreasing order of importance, the rather inhomogeneous distribution of stations over the globe, the use of technologies with systematic biases, the geometry of satellite reflectors -now poorly adapted to the required level of performance-, and finally the tropospheric error on the mean refractive index (which we know may be corrected by the simultaneous use of two different wavelengths - Ref. 2). All of these limits are technological ones. Today, the SLR is the only space geodesy technique whose fundamental limitations, including those related to the measurement of vertical components, lie within the millimetric realm. Nevertheless a significant effort will need to be made before reaching this level of accuracy, which is considered to be unattainable by any of the other candidate technologies. On the other hand, SLR will find itself in a very awkward situation if its global performance does not undergo major improvements, such as the transition towards fully automated operationality (to reduce functioning costs), and thereby the adoption of eye-safe solutions."

In the following we present the results of our very specific research into new retroreflector satellite concepts. The main body of the work presented here is devoted to three principal aspects of the design requirements :

- In the case of a classical SLR satellite, a single incident pulse results in a large number of randomly phased, quasi-simultaneous return pulses which combine coherently at the receiver to produce a temporally complex waveform. On a shot to shot basis, this received signal cannot be accurately and unambiguously correlated to the satellite center of mass, and is thereby responsible for a large proportion of the total range measurement uncertainties. An alternative, small geodetic satellite concept, based on the use of eight large hollow cube-corner retroreflectors with *mutually exclusive fields of view* is proposed.

- Such retroreflectors will, for reasons of return signal strength, need to be relatively large in size. This requirement will imply the need for more attractive techniques than those offered by classical or already known solutions (either spoiling the angles, or using a spherical surface (Ref. 3) in the cube-corner), for the compensation of *velocity aberration* effects.

- While the rotation of the satellite around its centre of mass **G** is considered to be unknown, we have looked into the design of a correcting device to be placed in front of each of the satellite cube corners (CC), so that the apparent (angularly dependant) variations in center of mass range are minimised.

II/ LIMITATIONS IMPOSED BY CURRENT SATELLITE SIGNATURES

The time domain behaviour of a "modern" round-trip SLR pulse can be thought of as an initially narrow Gaussian pulse which is convolved successively by the atmospheric transfer function (scintillation due to refractive index dispersion), the "forest" of Diracs corresponding to each of the satellite reflectors "visible" at the ranging instant, (again) the atmospheric transfer function, and finally the detector transfer function. Whereas the emission, detection and atmospheric functions could well provide a global received pulse FWHM of not more than 30 ps, current satellite signatures are typically an order of magnitude greater in duration, due to the large number of CCs visible at any one instant in time.

The practically indetermined nature of this type of signature imposes a lower limit on the residual range uncertainty, which varies between 1 and 5 cm (only in the case of Topex Poseidon and Lageos 2 has an extensive pre-characterisation campaign enabled systematic bias effects to be fully modelised). The extent of this uncertainty depends mainly on the size and characteristics of the ranged satellite, and to a lesser extent on the time response characteristics of the detector and the timing methodology.

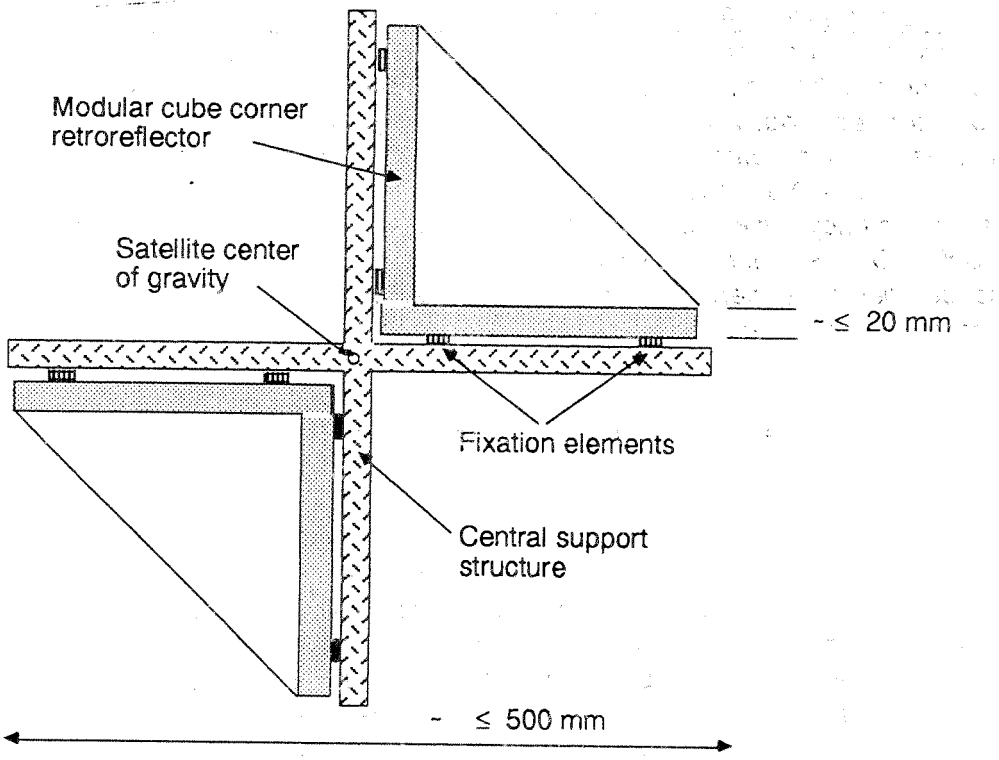

Schematic sectional view of a possible implementation of a geodetic satellite using a central support structure and **eight** modular cube corner retroreflectors. Only two of the retroreflectors are shown here, for reasons of clarity.

The main objective of the proposed retroreflector design (Fig. 1) is to eliminate the above-mentioned drawbacks incurred by the presence of complex multiple-retroreflector signatures. This is achieved by means of a classical set of eight retroreflectors, exhibiting negligeable local FOV overlap, arranged in such a way as to provide a single return echo for each incident pulse.

Link budget requirements can be satisfied by such a single retroreflector provided it has sufficiently large dimensions (typically a few tens of centimetres free aperture), velocity aberration effects can be corrected for by means of the generation of an appropriate far field diffraction pattern, and incident angle dependant range errors can be passively compensated for. These aspects are treated in the following sections.

The proposed use of large hollow CCs opens up the possibilities for using materials other than glass for the retroreflector facets; as an example, SiC could be used for its excellent thermo-elastic properties, or even appropriately chosen dense metals could be envisaged in order to improve the overall mass-to-surface ratio of the satellite. The mechanical robustness of the structural elements, in particular the glass correcting plates, would have to be studied carefully for reasons of acoustic and vibration resistance during launch. Thermo-mechanical behaviour of the reflecting optical surfaces would also require particular attention, in order to ensure minimal deformations of the reflected diffraction patterns.

III/ TOWARDS GEOMETRY CENTRE OF MASS CORRECTIONS MINIMAL FLUCTUATIONS.

Ideally, in any given laser satellite, the apexes of each retroreflecting cube corner would be mutually co-located at the satellite's centre of mass. In practice, this requirement cannot be exactly met for more than one retroreflector, because of the mechanical thickness of the reflector facets. The true center of mass range is thus related to the apparent (retroreflector apex) range by a quantity which varies in accordance with changes in local incidence angle. In order to avoid this difficulty, we have analysed many different devices, including :

- A glass sphere of high refractive index (n = 2),

- Correcting plates in front of a classical solid glass CC, or

- Correcting plates in front of 3 mutually orthogonal, back-silvered parallel plates forming a CC or,

- Correcting plates in front of a classical hollow CC.

The last solution appears to be the most satisfying one, and more detailed studies have been made to investigate its industrial feasability. The analysis begins by considering a classical hollow CC whose apex C is separated from G by a given distance D, due to the mechanical thickness of the constituting CC plates. Three orthogonally aligned, parallel plates of thickness **e** are introduced so as to form an inverted, transparent CC in front or each reflecting CC. When eight such CC sets are assembled together, the transparent CC elements can be joined together so as to form a sort of contiguous glass "cage" around the basic retroreflecting octahedron. The general appearance of the optical components of such an assembly is depicted schematically, in figure 2 hereafter.

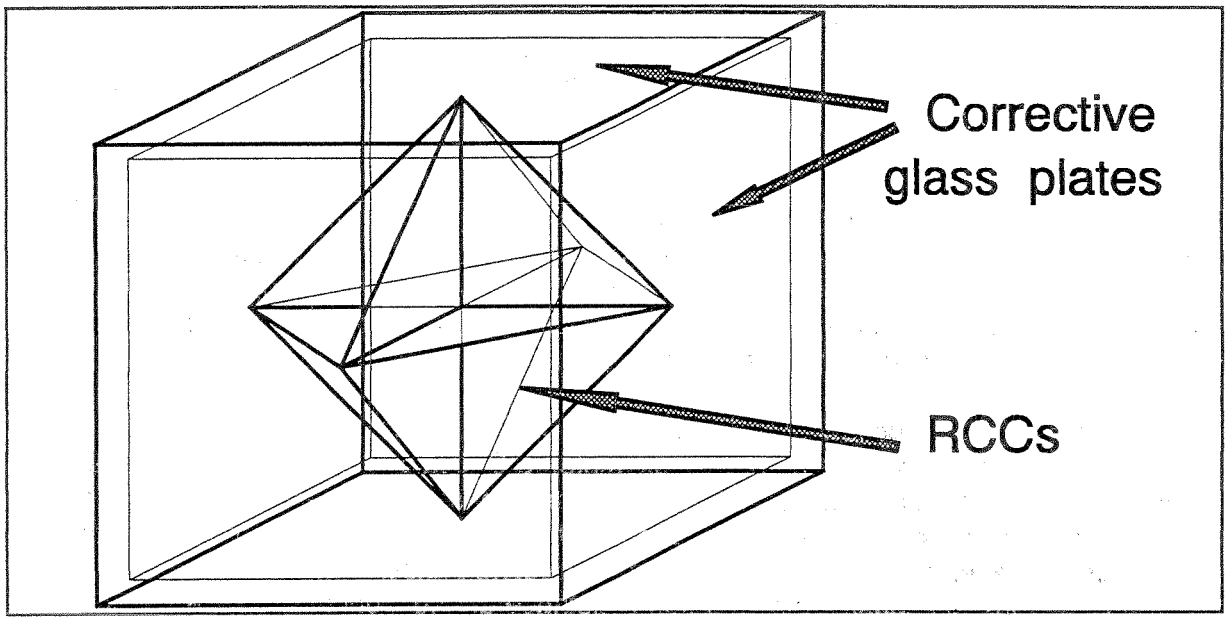

Figure 2

For a given retroreflector, it can be seen from simple geometric reasoning that whenever there is an increase in incident beam angle (defined as that between the direction of the incident beam and the CC axis of symmetry), the apparent difference between the measured distance of C and that of the satellite centre of mass (G) decreases. The correction principle described here (Ref. 4) is based on the fact that the same change in incidence angle gives rise to an increase in optical path length, because the (glass cage) parallel plate is traversed at higher angles of incidence. The resulting global correction used to determine the range of G can thus be rendered, by appropriate balancing of these two effects, virtually independant of incidence angle.

This result can be demonstrated quite easily, as shown in the following : For example, we consider that the reflecting surfaces are parallel to the coordinates planes (x = **a**, y = **a**, z = **a**) and that the correcting plate is parallel to z = 0 plane. Let us take the unit vector components of the optical ray expressed as :

cos α **. sin i**
sin α **. sin i**
cos i

Then **i** is also the value of the incidence angle for the ray over the correcting glass. The correction **cor** to take into account when ranging at the RCC is then :

$$cor = a \,.\, (\sin i (\cos \alpha + \sin \alpha) + \cos i) - e \, (\sqrt{n^2 - \sin^2 i} - \cos i)$$

These values of **cor** against **i** form a set of curves (cf fig. 3), whose minimum may be adjusted to **i** = 45° (in this case, the **cor** has an extremely small variation in a few degrees), but each class of values for **i** will provide a different optimum for **e** (for a variation of 30° the optimum is not the same as for a variation of 45°).

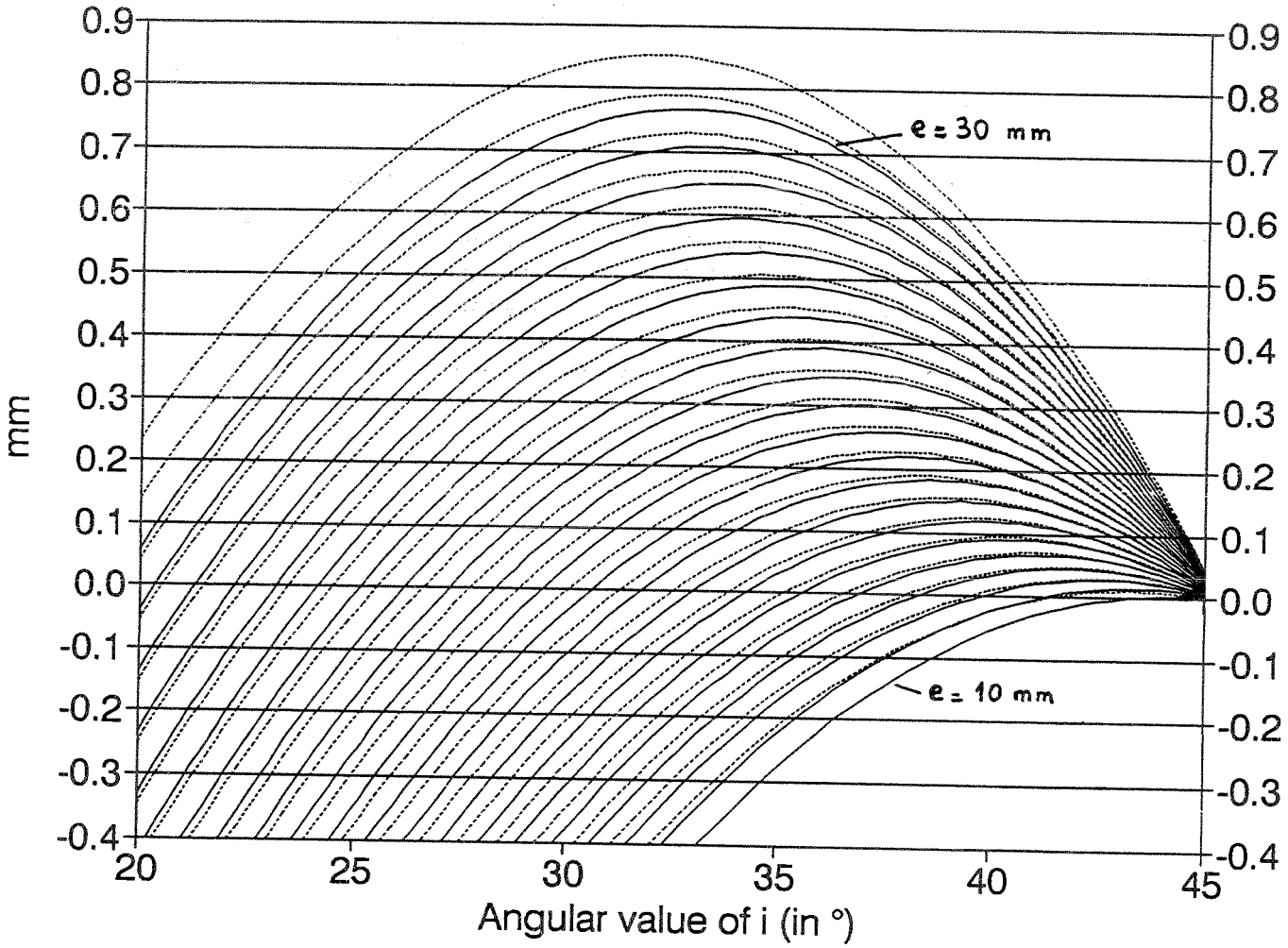

Fig. 3 : Variation of **cor** against **i** with respect to its value at **i** = 45°, for two values of α (45° in solid line, 30° in dashed line). The lines vary from **e** = 10 mm to 30 mm by 1 mm steps, and the value of **a** is 10 mm.

As an example, simulations show that for **d** = 17.32 mm (**a** $\sqrt{3}$ with **a** = 10 mm) and a value of **n** = 1.5 (glass), the optimal value for **e** is around 16 mm. Under these conditions, the correction is stable to within ±0.3 mm, for incidence angles up to ±20°. If an optimisation is required over ±35°, the best value for **e** is around 38 mm, and the correction then remains stable to within ±0.8 mm. However, it is clearly of little practical interest to compensate for such a large field of view, because the hollow RCC has an optical efficiency which falls to zero at about 40° from the axis of symmetry.

IV/ VELOCITY ABERRATION CORRECTION FOR LARGE RETROREFLECTORS.

One of the main difficulties implied by large reflector dimensions in a reflector satellite is that of appropriate compensation for velocity aberration effects, as described in the following. Velocity aberration correction is needed at retroreflector level, in all geodetic satellites, in order to compensate for the relative angular displacement between the station and satellite during the reflected pulse flight time.

In the case of existing SLR satellites, the CCs are designed to generate 6 slightly off-axis (typically less than 10 arcsecond) individual lobes, as shown in Fig. 4. This is referred to here as the "classical" velocity aberration correcting pattern. When the CCs are small in size (≤ 3 cm), the resulting lobes tend, because of diffraction effects, to merge into one another further than shown in the figure. Ranging to any of the existing (multiple echo) reflector satellites results in the production of several such patterns (one per "visible" CC), of mutually random azimuthal orientation. The net result is an approximately uniform annular energy distribution, such that all incident pulses produce an adequate return echo in the direction of the receiving telescope.

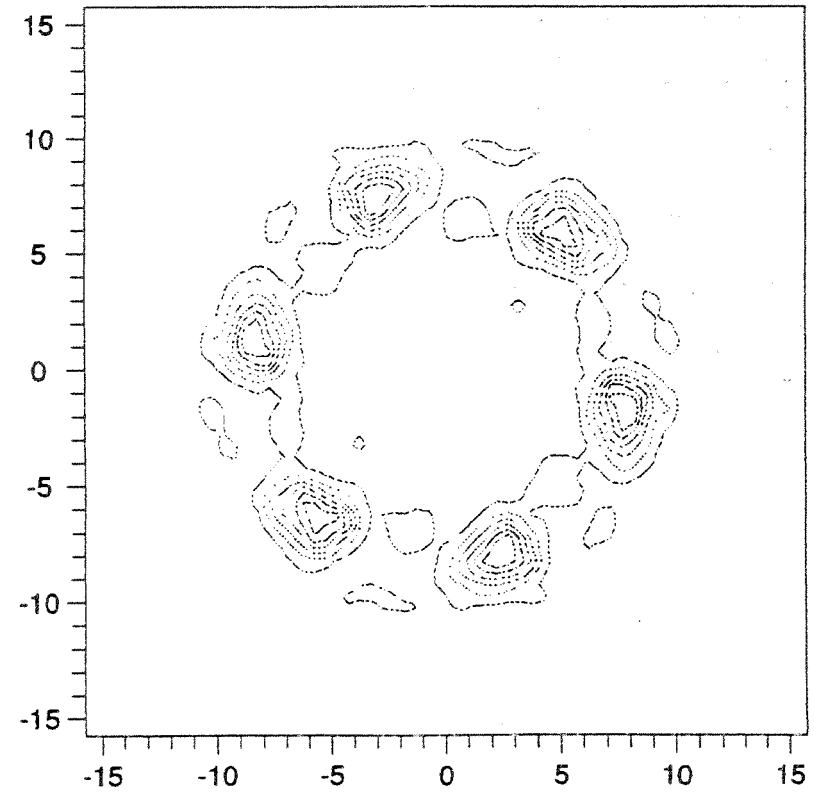

Fig. 4

In the case of a single large RR designed with the same optical compensation principle, the 6 lobes would be considerably smaller and more intense than in Fig. 4., leaving increasingly significant zones (i.e. azimuthal directions) of low energy return. As the absence of any attitude control of the reflector satellite results (in general) in a slowly varying (and uncontrolled) change in the azimuthal orientation of the return diffraction pattern, on average only a small fraction of all emitted pulses would be likely to generate a return signal of adequate strength. The resulting irregularity of the detected echos would be unsatisfactory for good SLR, which requires regularly spaced ($\geq$ 1 Hz) return echos of similar intensity. It is for this reason that the implementation of large CCs in a reflector satellite should accompanied by appropriate engineering of the reflected energy, in order to produce a uniform diffraction ring, rather than a sparse population of intense diffraction lobes.

It is proposed to approach the "regular ring" diffraction requirement by means of a slight modification to the nominally flat shape of the RR reflecting facets (ref. 5), so as to fill in the otherwise "empty" zones between the 6 discrete diffraction lobes. Numerical simlations have shown that an excellent solution is provided by introducing a very slight conical deformation to the reflected wavefront, and that this deformation can be achieved by means of conical deformations on the reflecting surfaces.

A variant to this solution, characterised by the advantage of considerably simplified engineering (polishing) requirements, is provided by replacing the ideal conical shape by a piecewise flat sub-facet approximation. The resulting shape could be thought of as representing a (nearly) flattened section of a Japanese umbrella in which contiguous, triangular sub-facets generate small equal angles along their lines of intersection. When the number of sub-facets is reduced to 1, the classical solution to velocity aberration compensation is found, i.e. a small angular offset of each facet with respect to the perfect corner cube value of 90°.

Fig. 5 illustrates the case of a 2 sub-facet solution.

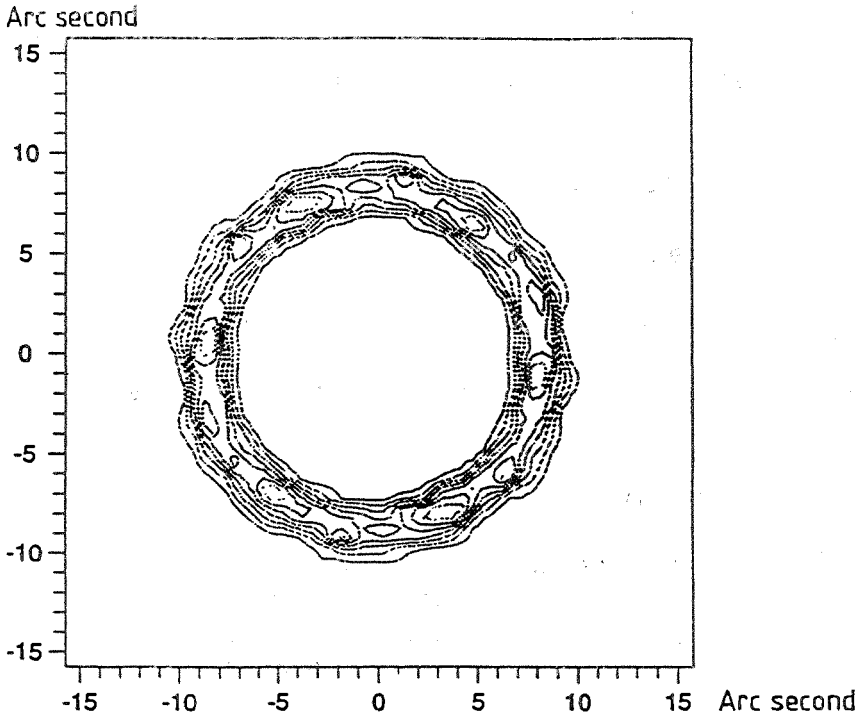

Simulations show that, in the case of a 10cm RR aperture, a nearly uniform, continuous annular pattern is obtained with such a solution. This result is illustrated in Fig. 5, where the computed diffraction pattern is seen to be a suitably regular ring. Close inspection of the contour plot reveals that there are indeed 12 slight local maxima. The thickness of the ring is an inverse function of the size of the RCC.

In conclusion, a near-uniform diffraction ring can be generated by a hollow RR of any size, given appropriate polishing of its constituent facets into 2 or more sub-facets. The azimuthal dependance of the ranging (energy) link budget is thus minimised, ensuring good overall performance of the payload for most instantaneous orientations with respect to incident ranging pulses.

Other solutions which also generate a suitable ring pattern have been found, and are briefly described here:

- Only one of the CC facets is modified, by polishing its surface so as to produce a slightly conical shape whose axis of symmetry is normal to the facet (rather than being parallel with the CC axis as in the Japanese umbrella solution).

- The above solution is modified by applying an elliptical, rather than conical deformation to the facet's surface.

- The three facets are polished with a slightly conic shape, but here the summit of the cone is in the corner **C** and for one facet the revolution axis of the cone is close to the intersection of the two other facets.

- etc...

The result is that even for a very large RCC (even more than 50 cm of aperture), the far field pattern is quite close to a ring, so that it is possible to provide an excellent energy level to the SLR stations. As a consequence, it is acceptable to use a set of 8 hollow large RCC (cf. ref. 6), not necessarily in glass (Si-C could be used for its excellent thermal behaviour ; or even Al-plated wolfram so as to get an important mass within a small volume), with a cubic glass plates cage around it.

The benefits are quite considerable, as :

- the optical efficiency is very high,

- Only one RCC is active at one time,

- The geometric correction is nearly independent of the orientation.

V/ LINK BUDGET COMPARISONS

In the following we compute the expected link budget for a SLR station with a ϕ_1 = 50 cm diameter telescope, α = 20" output divergence for the laser, aiming over a distance **D** = 10 000 km at a large retroreflector of ϕ_2 = 50 cm diameter. The diffracted energy is considered to fall within a ring of radius of ρ = 35 µrd and thickness $d\rho$ = 3 µrd thickness. With

an overall optical efficiency of $\tau = 0.08$ (including lenses, mirrors, interference filters, and the two-way atmospheric transmission) the received to emitted energy ratio amounts to :

$$\tau \cdot \frac{\frac{\pi}{4}\phi_1^2}{\alpha^2 \cdot D^2} \cdot \frac{\frac{\pi}{4}\phi_2^2}{2\pi\rho\, d\rho \cdot D^2} \quad \text{, close to } 5 \cdot 10^{-14}$$

Using similar hypotheses, but with a satellite design equivalent to that of Lageos, we can assume an average of $n = 10$ fully illuminated RCCs, whose radius of angular diffraction limit β is the one of $1/6^{th}$ of a circular aperture of 42 mm diameter. For $\lambda = 0.5$ µm, it means $\beta = 35$ µrd. The received to emitted energy ratio would have been then :

$$\tau \cdot \frac{n\frac{\pi}{4}\phi_1^2}{\alpha^2 \cdot D^2} \cdot \frac{\frac{\pi}{4}\phi_2^2}{\pi\beta^2 D^2} \quad \text{, close to } 5 \cdot 10^{-16}$$

The hypotheses may be discussed, and the absolutes values found should be used only as elements of comparison, but there is an obvious advantage to be gained from such a RCC design, owing to its large optical cross-section and consequently narrow ring-shaped diffraction pattern.

In conclusion, well implemented engineering of the exact CC shape can enable very large single reflectors to be used, with excellent energy levels being provided at the SLR station. The CC should be hollow, in order to avoid the major homogeneity (thermal gradient / refractive index) problems which could occur in large soiid CCs. The CC facets could be made with materials other than glass, such as SiC (for its excellent thermo-mechanical properties) or (Al plated) Tungsten (to improve the satellite's mean density).

CONCLUSION

An alternative approach to the design of second generation geodetic satellites has been suggested, in which the use of a small number of large, hollow cube corner retroreflectors ensures the systematic return of optimally clean (i.e. unique) echos. The mutual orientation of the respective retroreflectors allows only one of them to respond to any given incoming pulse. This approach is fundamental in obtaining millimetric range accuracies tied to the satellite's centre of mass.

The engineering of appropriate retroreflector velocity aberration compensation is an important factor in achieving an adequate station-to-satellite energy link budget, and the proposed solution can theoretically be applied to a hollow cube corner retroreflector of very large size.

Incidence angle variations in the apparent satellite range can be compensated for by means of passive optical components, or in some cases by means of a posteriori corrections to the recorded data.

It is our belief that the described new concepts for retroreflector satellites offer an opportunity to overcome one of the major limitations of SLR. Of course, other technological sources of

errors must also be pushed back to their limit. We can nevertheless observe that alone with the present reflector satellite, it would with today's SLR stations be possible to obtain a far greater optical efficiency by virtue of the Dirac nature of its temporal signatures. This result suggests that we may investigate completely different methodologies of which, in our opinion, a very promising one could be phase detection ranging with continuous lasers, using a very high frequency modulation of the beam polarisation. This is a well-proven technology which has been used for more than 20 years for very high accuracy (up to 0.1 mm) terrestrial geodesy, and which could be implemented with minor modifications, provided there is adequate strength in the optical return signal. The main advantage of this technique is its immunity from any systematic bias errors or variations in calibration. This type of implementation could quite readily be extended to dual wavelength ranging, in order to improve the accuracy of atmospheric corrections (as it has already be developed for terrestrial geodesy since 15 years).

It is proposed that at the earliest possible opportunity a low cost, experimental prototype be developed and launched (in piggy-back along with an existing launch program), in order to ascertain the full potential of such a payload in terms of millimetric absolute ranging accuracies.

REFERENCES

(1) M. KASSER, G. PERRIER
"Etat de la recherche française en géodésie"
CNES/INSU Report, July 1993, 13 p.

(2) M. KASSER
Improvement of SLR accuracy: a possible new step
8th Symposium on laser ranging instrumentation, 18-22 May 1992, Annapolis
pp 8-23 to 8-29, NASA Conference publication N° 3214

(3) MINATO, SUGIMOTO, SASANO
Optical Design of Cube-Corner Retroreflector Having Curved Mirror Surfaces
Appl. Opt., Vol 31, N° 8, p. 6015, 1992

(4) KASSER, LUND
Réflecteurs laser pour télémétrie laser sur satellites de très haute précision.
Patent ref. FR 94-02773 (10-3-1994).

(5) LUND
Rétroréflecteur pour géodésie laser, à correction omnidirectionnelle d'aberration de vitesse
Patent ref. FR 93-15973 (31-12-1993).

(6) G. LUND
New perspectives for high accuracy SLR with second generation geodesic satellites.
8th Symposium on laser ranging instrumentation, 18-22 May 1992, Annapolis
NASA Conference publication N° 3214

Future science applications

SPACE LASER COMMUNICATION EXPERIMENTS AT CRL AND THE POSSIBILITY OF COOPERATION WITH SLR NETWORK

Yoshinori Arimoto and Kenichi Araki
Communications Research Laboratory, 4-2-1 Nukui-Kita, Koganei, 184 Japan
Tel: +81 423 27 7614, Fax: +81 423 27 6696, e-mail: arimoto@crl.go.jp

1. Introduction

Laser communication will play an important role in the future space activities and has various advantages such as providing a high data rate and large communication capacity, requiring only compact and light-weight equipment, and being free from mutual interference. Several organizations are doing research on such systems for future data relay satellites and plan experiments using a satellite. The Communications Research Laboratory (CRL) began the research and development of such a space laser transmission technology in the early 1970's.[1,2] As a next step of such activities, the basic laser communication experiments using a geostationary satellite is under progress. CRL also plans to perform experiments in laser communication between a ground station and low-earth-orbiting satellite.

This winter the first experiment at CRL will be performed using the Japanese Engineering Test Satellite-VI (ETS-VI), which was developed as a geostationary satellite, with an optical communication payload called LCE (for Laser Communication Equipment). The objectives of the ETS-VI/LCE experiment are to demonstrate the basic technologies for an optical intersatellite communications system and to acquire technical data for the future optical system through miscellaneous scientific and engineering experiments using an onboard optical system. ETS-VI was launched on 28 August 1994, but its current orbit is highly elliptic rather than geostationary because of a failure in the liquid propellant apogee system.

The second satellite for the laser communication experiment is the Optical Interorbit Communications Engineering Test Satellite (OICETS) that is being developed by the National Space Development Agency (NASDA) of Japan and that will be launched into low earth orbit about 1998. In cooperation with the European Space Agency (ESA), the in-orbit demonstrations of pointing, acquisition, and tracking technology, and other key technology elements for optical interorbit communications will be conducted with ESA's ARTEMIS geostationary satellite. CRL will take part in the experiment using the main optical ground station.

This paper describes the laser communication payloads for ETS-VI, shows current status of the ETS-VI/LCE experiment and the future plan of laser communication experiment using OICETS satellite, and discusses the possibility of cooperation with the SLR network.

2. ETS-VI Laser Communications Experiment

The concept of the laser communication experiments using ETS-VI is shown in Figure 1. ETS-VI was injected into highly elliptic orbit, but it will be moved into a three days

recurrent orbit by raising its perigee height in November 1994. The experiment will be performed using a ground station as a counterpart to the communication link when the satellite is visible from the ground station and the satellite attitude is maintained to point the ground station. A laser diode with a wavelength of 0.83 μm is used for down-link transmission, and an argon ion laser with a wavelength of 0.5145 μm is used for up-link transmission. The main optical ground station is located at the CRL site in Tokyo.

2.1 Objectives of the Experiment

The experimental items to be performed using ETS-VI/LCE are as follows[3]:
(1) Initial Acquisition and Tracking By using a ground-based laser beacon, the initial acquisition and coarse tracking subsystem will be verified at the first stage of the experiment. Next, the fine tracking subsystem and point-ahead mechanism will be tested.
(2) Bi-directional Laser Communications A bi-directional communication experiment between ETS-VI and the ground station, based on intensity modulation/direct detection technique will be performed. Transmission data rate is 1.024 Mbps for both up-link and down-link.
(3) Satellite Attitude Measurement The pitch and roll axis error can be detected from the pointing errors of the received laser beacon and the yaw axis error can be detected from the polarization of the beacon. This experiment will inform us a high-frequency satellite's vibration, caused by the thruster jets or the torque flutter in driving the solar array and RF antennas in orbit.
(4) Laser Beam Propagation It is possible to measure the receiving laser power for both up-link and down-link. The optical beam propagation characteristics obtained in this experiment will be useful for future laser communication between outer space and the ground.
(5) Optical Device Tests in Space It is planed to obtain preliminary data on the performance and the lifetime of optical devices in space. The long-term characteristics of LDs, photo detectors will be monitored.

2.2 Optical Payload for the ETS-VI[4]

An optical payload for the ETS-VI called LCE. Figure 2 is a block diagram of the LCE. The main feature of the LCE are summarized in Table 1. The optical part of the LCE is installed in the corner of the earth-oriented panel of the ETS-VI. Some electrical components are installed inside the satellite.

Figure 3 schematically shows the layout of the optical part. There are a two-axis gimbal mirror, a 7.5 cm diameter telescope, and acquisition sensor (CCD), a fine pointing mechanism and a tracking sensor (4QD: four quadrant detector), a communications element which includes LDs, APD (Avalanche Photo-Diode), PAM (Point Ahead Mechanism), and 4QD for PAM control.

The coarse tracking system, which consists of a two-axis gimbal mirror and a CCD tracking sensor, has an acquisition range of ± 1.5 degrees with resolution of 0.012 degrees. Coarse tracking is achieved with 33 μrad accuracy, if the up-link spot image is captured in the CCD's field of view of 8 mrad. With received power of -62 dBm to the 4QD, the fine tracking loop is designed to have approximately 2 μrad (3σ) accuracy under the vibration environment of the satellite.

Two LDs are installed, each of which output power is 13.8 mW in average. The down-link beams are circular polarized and are 30 and 60 μrad in $1/e^2$-power beam width. The beam direction is precisely controlled by a PAM in which piezo-electric actuators are used for deflection mirrors. The deflection angle ranges more than 300 μrad with resolution of 2 μrad. Using the PAM, the beam pattern can be measured by the ground receiver. Manchester coded pulse modulation for communication and 20% amplitude modulation at 8 kHz for beacon are superimposed in the transmitted LD light. The down-link bit rate is 1.024 Mbps. Data for down-link transmission is selected out of the LCE generating PN coded signal, demodulated signal of the received up-link signal, and measured data at 2 msec. interval for the LCE attitude measurement and the beam propagation characteristics measurement.

The LCE receives visible light spectrum of about 10 nm bandwidth around 0.51 μm argon laser light. The received light is split to the optical sensors according to their sensitivity. If the up-link beam is modulated at 315 Hz, a 4QD for the PAM control can detect the received light direction. In front of the APD, the receiver has a polarizer of which reference axis is parallel to the LCE base plate. If the received light polarization angle is rotated, the receiver output is modulated sinusoidally at the frequency twice the polarization angle rotating frequency. The intensity modulated 1.024 Mbps up-link optical signal is demodulated by the APD receiver. The bit error rate is measured by the onboard processor. The received power level is measured at 2 msec. intervals with dynamic range of more than 20 dB.

2.3 Current Status of the ETS-VI

LCE was designed to be used only with the main ground station at CRL and the acquisition area is limited to 0.2 degrees around its target, but the failure of ETS-VI's injection into geostationary orbit makes LCE visible from all over the world. LCE can therefore be accessed from anywhere in the world if the satellite attitude can be maintained to point to the target ground station. Figure 4 shows the sub-satellite point prediction of possible 3-days recurrent orbit of ETS-VI from November 31, 1994. Experimental time for one satellite pass will be more than two hours. Figure 5 is another view of the same orbit based on earth fixed coordinate. We expect the laser communication experiment will be able to execute even in such a highly elliptic orbit and especially in this winter season, from December 1994 to February 1995, we will have to perform most part of the experiment because of the degradation of the onboard equipment under severe radiation environment. We are expecting the satellite life to be more than one and half years.

3. Laser Communication Experiment Using OICETS at CRL

The OICETS will be launched into low earth orbit about 1998 or later. Figure 6 shows the concept of optical inter-orbit communication experiment using OICETS. The overall system for optical inter-orbit link experiments will consists of OICETS, Communications and broadcasting Engineering Test Satellite (COMETS), NASDA's tracking and control ground stations, and ESA's ARTEMIS[5] and ground stations. CRL will take part in the experiment using the main optical ground station developed for ETS-VI experiment.

Figure 7 shows the configuration of the satellite. Table 2 lists tentative characteristics. OICETS's laser communication payload is designed to point the ESA's geostationary

satellite, ARTEMIS. It is very difficult to point to the ground station in the normal three-axis-stabilized configuration, but satellite attitude is to be reversed near the end of the mission life in order to make the optical link between OICETS and the ground station.

For precise laser ranging experiments between OICETS and the optical ground station, the OICETS has a corner cube reflector system (CCR) on its earth-facing panel. Effective cross section of the CCR is more than 1 cm^2 with an incident angle of less than 55 degrees, and operation wavelength is 0.5145 μm, 0.532 μm and 0.8 μm.

4. Possibility of Cooperation with SLR Network

LCE and OICETS are designed to be used for laser communication experiments, but both onboard packages are capable of laser reception, incident laser beam tracking, and optical power measurement. These capability will be used in measuring the up-link laser beam quality, such as far field beam pattern and light power attenuation due to atmospheric turbulences. For example, LCE's tracking sensors have optical filters of about 10 nm bandwidth around 0.51 μm, but the 2nd harmonics (0.532 μm) of NdYAG laser light can be detected with an attenuation of -17 dB.

Transmitted laser light from the satellites can be thought of as an artificial guide star in an adaptive optics system, and adaptive optics will be able to decrease the severe attenuation (due to atmospheric turbulence) of up-link laser light in the ground-based laser communication experiment. Figure 8 shows the concept using adaptive optics system for the laser communication experiment.

The onboard laser communication equipment and adaptive optics can thus be used in developing a satellite laser-ranging system.

5. Conclusion

This paper described the laser communication payloads of ETS-VI and OICETS, reported the present status of the ETS-VI/LCE experiment, and discussed the possibility of cooperation with the SLR network. In this December, we are going to start the laser communication experiment using ETS-VI and we hope the LCE will be used effectively by the people who is developing satellite laser ranging system and adaptive optics system.

References

1. T. Aruga, K. Araki, T. Igarashi, F. Imai, Y. Yamamoto and H. Sakagami, "Earth-to-space Laser Beam Transmission for Spacecraft Attitude Measurement," Appl. Opt., vol. 23, pp. 143-147, 1984.
2. T. Aruga, K. Araki, R. Hayashi, T. Iwabuchi, M. Takahashi and S. Nakamura, "Earth-to-Geosynchronous Satellite Laser Beam Transmission," Appl. Opt., vol. 24, pp. 53-56, 1985.
3. Y. Arimoto, M. Shikatani, S. Yoshikado, Y. Suzuki and T. Aruga, "Development of Space Optical Communication Equipment for ETS-VI," 17th ISTS, Tokyo, 1990.
4. K. Araki, Y. Arimoto, M. Shikatani, M. Toyoda and T. Aruga, "ETS-VI Laser Communications Experiment System," AIAA 14th International Communications Satellite Systems Conference, AIAA-92-1833-CP, March 1992.

5. A. F. Popescu and B. Furch, "Status of the European developments for laser intersatellite communications," Free-Space Laser Communication Technologies V, proc. SPIE vol. 1866, pp.10-20, January 1993.

Table 1. Major Specification of the LCE.

Weight	22.4 kg
Power	90.4 W (Max.)
Transmitting part:	
Telescope diameter	7.5 cm
Magnification	15
Laser	LD (AlGaAs)
Wavelength	0.83 μm
Power	13.8 mW (Average)
Beam divergence	30 μrad and 60 μrad
Data rate	1.024 Mbps
Receiving part:	
Telescope	Common to Tx part
Wavelength	0.51 μm
Detector	Si-APD
Data rate	1.024 Mbps
Coarse pointing subsystem:	
Detector	CCD
Acquisition range	± 1.5 deg.
Field of view	8 mrad
Sensitivity	-83.5 dBm
Actuator	Two-axis gimbals
Fine pointing subsystem:	
Detector	Si-PD QD
Field of view	0.4 mrad
Sensitivity	-62 dBm

Table 2. OICETS Main Characteristics (Tentative).

Launch Date	No earlier than Japanese Fiscal 1997		
Launch Vehicle	Three-stage J-1 rocket		
Mission Duration	Approx. one year		
Orbit Altitude	Approx. 550 km		
Orbit Inclination	35 degrees		
Satellite Bus Shape	Box		
Dimension	Approx. 0.78x1.1x1.5 m		
Weight	Approx. 550 kg		
Optical Link Specifications			
	Wavelength	Data rate	Modulation
Laser Beacon	801 -4/+7 nm	N/A	N/A
Receive	819 -4/+6 nm	2 Mbps	2PPM
Transmit	847 -4/+6 nm	50 Mbps	NRZ

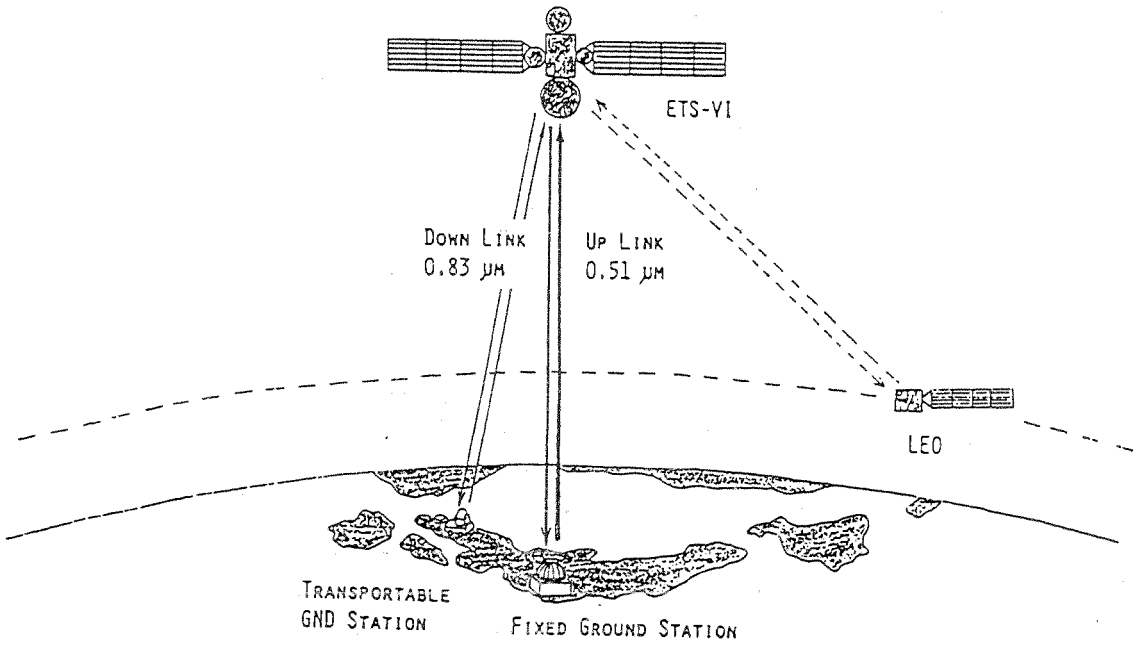

Figure 1. The concept of laser communication experiment using ETS-VI.

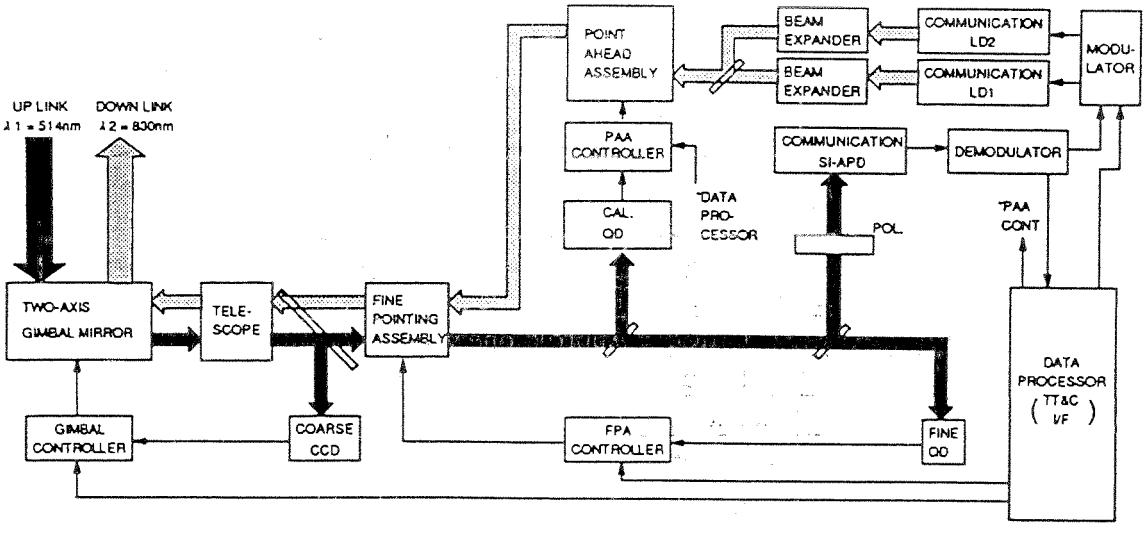

Figure 2. The LCE (Laser Communication Equipment) onboard the ETS-VI satellite.

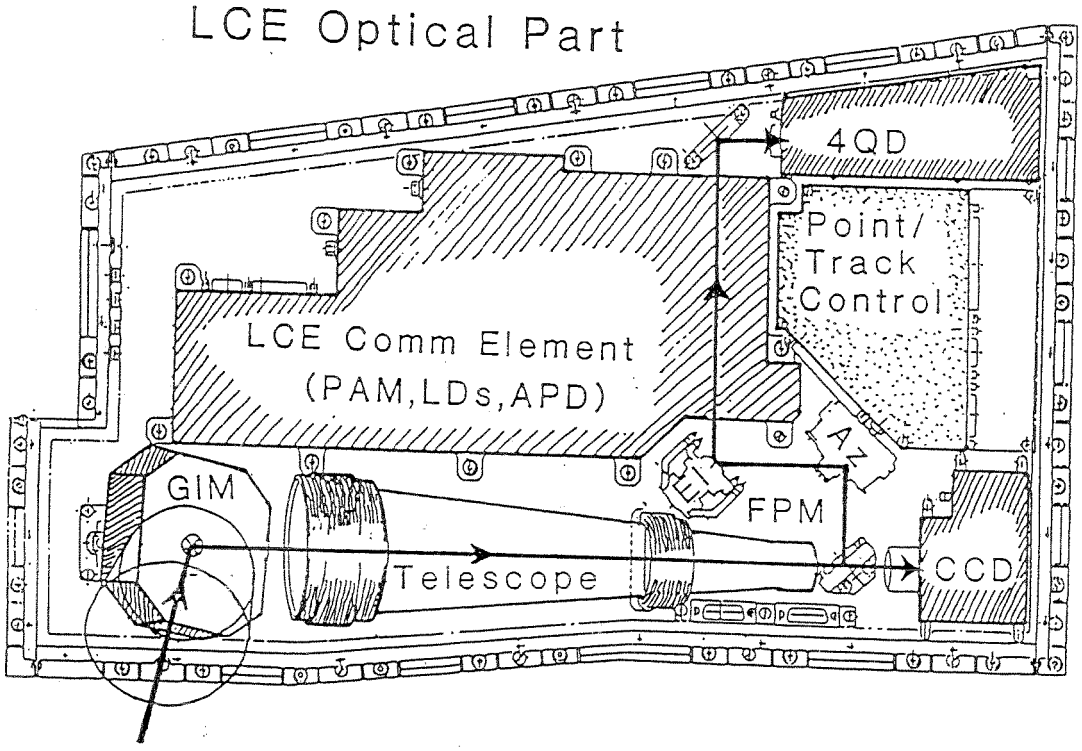

Figure 3. Layout of the LCE optical part.

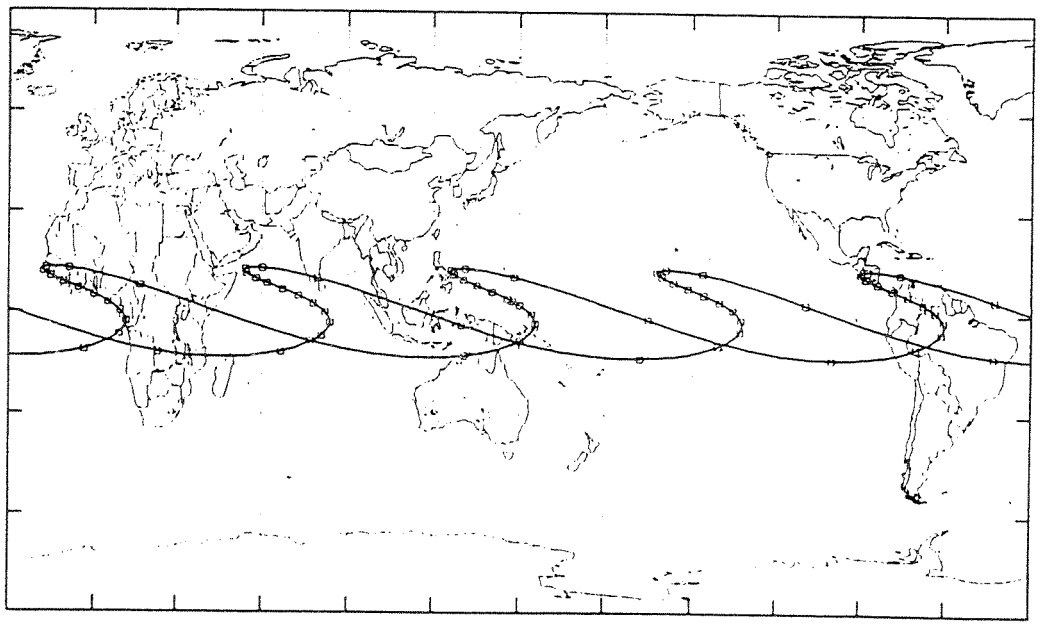

Figure 4. Possible 3-days recurrent orbit of ETS-VI
(3-days prediction of sub-satellite point from Nov. 31, 1994. Marker interval: 1 hour)

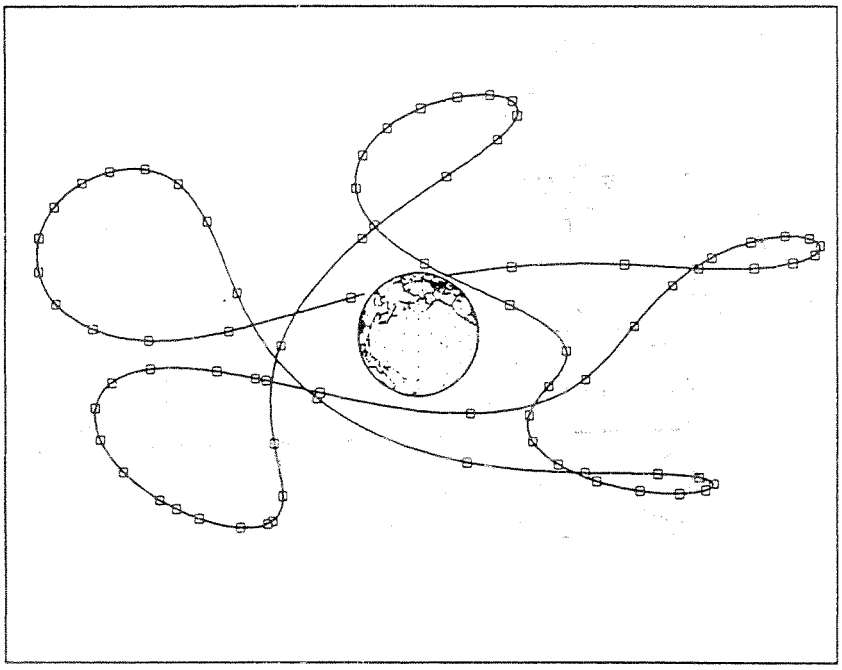

Figure 5. Orbit of ETS-VI based on earth fixed coordinate.
(View point longitude=180 degE, latitude=30 degN, height=320,000 km)

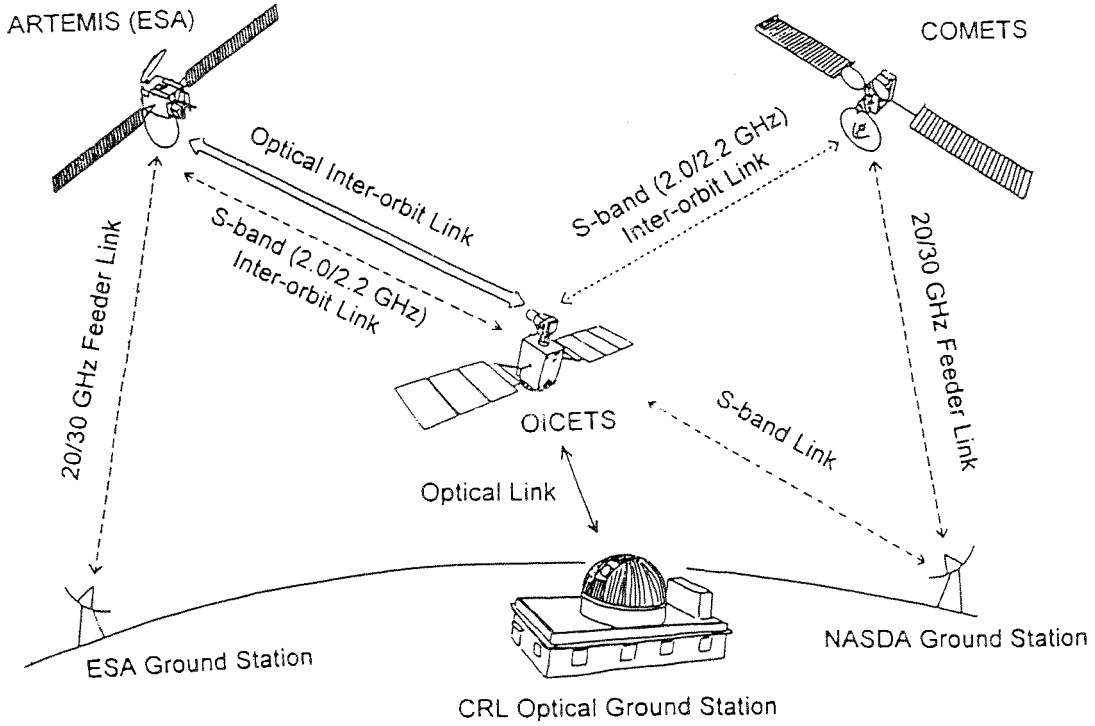

Figure 6. Concept of optical interorbit communication experiment using OICETS.

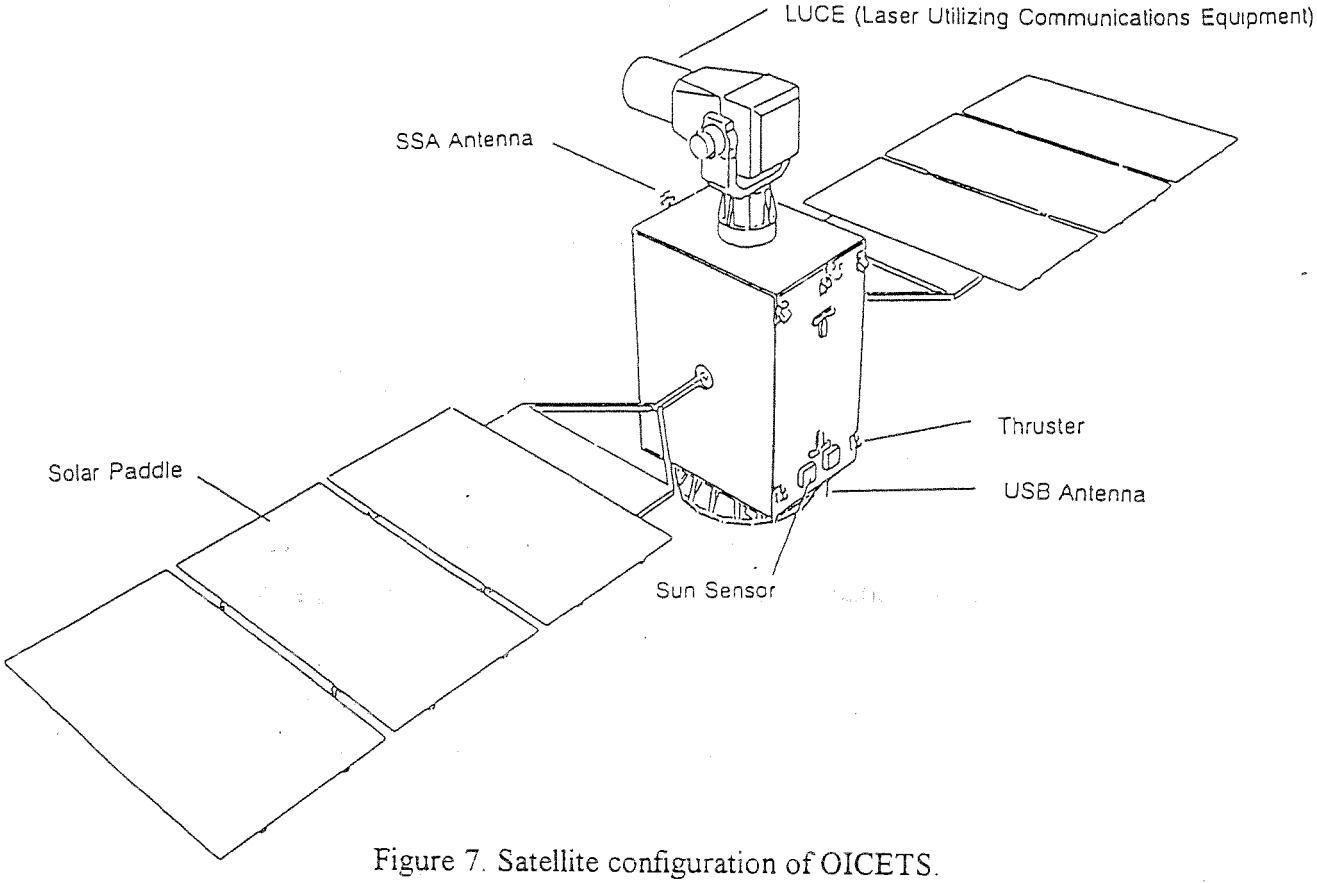

Figure 7. Satellite configuration of OICETS.

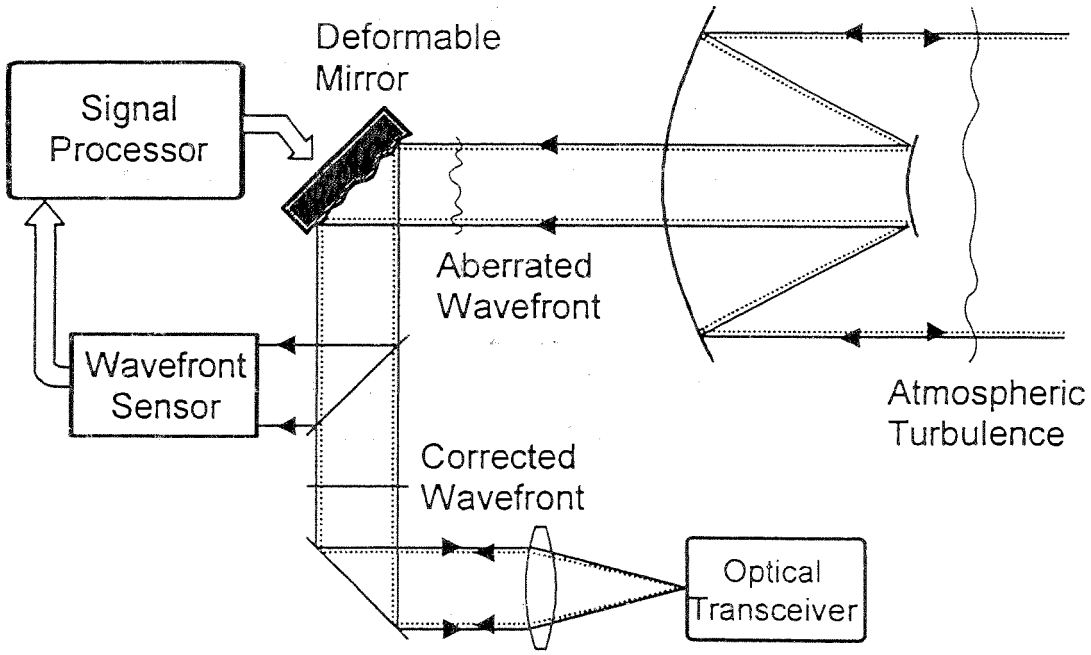

Figure 8. Application of an adaptive optics for laser communication.

Free Space CO_2 Laser Communication Using CdTe/GaAs/CdTe Electrooptic Modulation

Manuscript Presentators
Dominique Souilhac and Dominique Billerey

Institut National Polytechnique de Lorraine
Laboratoire d'Electricité et de Mécanique Théorique et Appliqué
2 Avenue de la Forêt de Haye
54500 Vandoeuvre-lès-Nancy, France

ABSTRACT

The desired goal of this paper is to become familiar with the applications and limitations of a free space CO_2 laser communication system using electrooptic modulation.

We first describe the AM/FM low frequency (1KHz-300KHz) testing of our electrooptic device, using a butterworth low pass filter, a FM modulator and a phase-lock-loop FM demodulator.

We then describe the design of a traveling-wave CdTe/GaAs/CdTe electrooptic waveguide modulator for the CO_2 laser for broadband operation up to 20GHz, performed at the University of Connecticut by Dr K. Cheo. The parallel microstrip gold stripline electrodes are designed for 16GHz center frequency and has a characteristic impedance of 48Ω. The CdTe/GaAs/CdTe electrooptic modulator was tested in the high frequency range using a CO_2 laser and a white cell filled with air (T=60°, P=35Torr) over a bandwidth of 20GHz.

Finally, laser pointing, tracking and spatial acquisition are briefly discussed.

1. INTRODUCTION.

The main advantage of using optical frequencies in free-space communication systems is the high directivity of the propagating optical beam. The diffraction angle is directly proportional to the radiation wavelength and inversely proportional to the antenna size.

First, we describe a low frequency (1KHz-300KHz) electrooptic modulation experiment, using electrooptic laser modulation, performed at McGill University and

capable of transmitting the audio part of a CATV spectrum in free space laser communication.

We then describe a high frequency (up to 20GHz) CdTe/GaAs/CdTe electrooptic modulation experiment capable of transmitting with a CO_2 laser more than 100 video pictures in FM or digital formats, in free space near orbit interlink communication. (Fig.1). The CATV TV spectrum in North America is shown in Fig.2.

10.6μm laser wavelength is too long for deep space communication since that would result in larger diffraction of the propagating beam. It is also lesssuitable for atmospheric propagation since the absorption due to the water continuum is 100 times larger than forthe Ho-Yag laser at 2.1μm.

Section 2 describes the low frequency audio AM/FM audio electrooptic modulation experiment, using a butterworth low pass filter, an electronic FM modulator and a phase lock loop FM demodulator.

Section 3 describes the high frequency testing of the CdTe/GaAs/CdTe electrooptic modulation experiment for the CO_2 laser.

Section 4 concludes with a brief discussion about accurate laser pointing and tracking problems and Interplanetary laser communications limits in free space laser communications.

2. LOW FREQUENCY (1KHz-300KHz) ELECTROOPTIC MODULATION FOR THE CO_2 LASER.

The realization of the AM/FM electrooptic laser modulation is well known and is described in Ref.[1] .

Quality transmission of the information signal was the main objective in our AM/FM electrooptic modulation experiment.

In the AM electrooptic modulation experiment, a single frequency (5KHz) sinusoid of 6 Volts peak to peak was chosen as the signal to be modulated. On this basis a bandpass filter of center frequency 5KHz (BW=100Hz, Q=50, gain=10) was inserted at the output of the photodetector which eliminated noise and harmonic present within the transmission system. (Fig.4 shows the Butterworth bandpass filter and Table 1 the losses measured at different points within the transmission system.)

The input and output signals after bandpass filtering are shown in Fig.3,4.

The combitional AM/FM modulation of the CO_2 laser consisted of AM modulating the laser light by an FM coded or modulated information signal subcarrier. This modulation method is more easily comprehended if one observes the box diagram of the system layout. The FM modulator consisted of the NE 566 function generator (Fig.7). The FM demodulator consisted of the NE 565 phase locked loop (PLL), with the general purpose self contained adaptive filter and demodulator designed for highly linear FM demodulation in the frequency range 0.001Hz to 500KHz (Fig.8). Additional low-pass filtering was necessary at the output of the PLL FM demodulator in order to eliminate the noise and high frequency harmonics present in the system. Essentially, the 300Hz sinewave is the reconstructed information signal wanted. Hence, a 1KHz cut-off frequency Butterworth low-pass filter was chosen to perform this operation.

3. HIGH FREQUENCY CdTE/GaAs/CdTe ELECTROOPTIC MODULATION OF THE CO_2 LASER.

Fig.10-28 describe the design and testing of the 20GHz CdTe/GaAs/CdTe traveling-wave CdTe/GaAs/CdTe electrooptic waveguide modulator, performed at the University of Connecticut by Dr P.K. Cheo. Broadband traveling-wave electrooptic waveguides have been previously analysed [3,4]

A cross-section of the CdTe/GaAs/CdTe waveguide modulator is shown in Fig.13

The optical coupling into the TE_o or TE_1 modes is done with a Ge prism (Fig.17).

The loss in dB for the TE modes with 3μm and 1μm buffer layers is shown in Fig.14

The ideal lossless frequency response, microstrip electrode loss calculation and insertion loss measurement of the paralell gold stripline electrodes with its 48 Ω transformer are shown in Fig. 18-22.

The traveling-wave double-sideband GaAs modulator sub-asemblies and 15GHz output spectra through a white cell (T=60°C,P=35Torr) are shown in Fig.23-28

4.DISCUSSION ON LASER POINTING,TRACKING AND ON SPATIAL ACQUISITION.

While one of the main advantages of laser communication is the antenna gain (narrow beams), this can only be utilized if the beam can be accurately pointed. Contributions to overall pointing errors include:[5,6]

-optical tracking sensor noise equivalent angle

-Inertial sensor noise versus feedforward error (if used)

-Residual uncompensated platform motion and vibration.

-Line-of-sight motion (acceleration) between the two terminals

-Errors in alignment between subsystems (bias errors)

-Error in computation of point-ahead angle

If we assume the different error components are independent, often the components are root-square summed to estimate the total error.

The options for optical tracking sensors include quadrant trackers and area array sensors (FPA's):

-Quadrant APD's have greatest sensitivity, but have limited angular dynamic range (±0.5 spot), are difficult to control gain uniformity and have a dead zone between elements (≈50μm) [7].

-FPA's have greater angular dynamic range than quadrant detectors, can perform both acquisition and tracking, but have somewhat reduced sensitivity and bandwidth.[8,13]

The bandwidth requirements for optical tracking sensors can sometimes be reduced by incorporating inertial sensors such as gyros (conventional or fiber optic), or angular displacement sensors (ADS). Augmenting the optical tracking sensors with an inertial sensor can be particularly advantageous for FPA tracking sensors.[5,6]

The input beam scans a narrow transmitter beam across an uncertainty cone until the other terminal is illuminated. The receiver focal plane array for acquisition and tracking (MxM array) stares into the entire Θ (uncertainty) cone (if small enough) and waits to be illuminated. The subarray (NxN) reads out for tracking. Tracking uses a centroid algorithm. The frame rate increases for tracking as M^2/N^2 . Scanning uses a spiral or raster scan produced by a two dimensional acoustooptic deflector [9]. The number of acquisition cells is equal to $N=(\Theta_{unc}/\Theta_T)^2$. In the latter expression, Θ_T is the angular spread of the received laser beam on the FPA. The dwell time per cell equals t_D. It conveys the pixel integration time during the array acquisition period. It must be long enough to allow 4-5 servo-centering steps. The acquisition time is equal to Nt_D. Each pixel can supply a false alarm in each of the N acquisition cells. The number of false alarm is approximately equal to M^2xN. For 400x500 elements, $M^2 = 2.0x10^5$. For NASA satellites, $\Theta_{unc}=0.5°$. It is dominated by the spacecraft uncertainty in its own attitude during pointing.The maximun number of acquisition cells is of the order of N=0.5°/130μrad= 5000. The probability of success for full acquisition is $P_{acq}=P_d(1-P_{fa})^{M^2N}=0.99$. Hence P_d (detection probability)=0.995. If $P_{fa}=5x10^{-12}$;then we obtain from Ref.[10], SNR=10.6.

The basic link propagation geometry is described in Appendix A.

5. CONCLUSION.

Investigation of AM/FM electrooptic modulation using CdTe/GaAs/CdTe waveguide, up to 20GHz has been reported here with more than 50% sideband power conversion and 20W microwave drive power, using a CO_2 laser with a modest amount of transmitted power (1Watt).

The main applications envisionned for CO_2 laser GEO-GEO links are in the area of commercial telephone and television transmission, tracking and data relay satellites for various space missions, and military communication networks. Because of the relatively short distances involved in intersatellite communication (10^3-10^5 km), high data rate systems can be implemented with a modest amount of transmitted power (less than one Watt) and relatively small (10-50cm) transmitter and receiver telescopes. Thus CO_2 optical systems may offer smaller size and weight and require less power than similar links in the microwave region[11].

CO_2 laser communication through the atmosphere has been abandonned because the average noise exceeds the average signal after propagating distances less than 80km at 1dB/km atmospheric attenuation[12]. Heterodyne coherent detection in this case is not practical because atmospheric effects limit the area over which the signal beam remains coherent to a size that is much smaller than the receiver telescope aperture[14]. Employing a direct detection receiver and concentrating the signal energy into high peak pulses, using a Nd-Yag laser (1.06μm), frequency doubled (0.53μm) one can overcome the background noise. A popular choice of modulation format is the M-ary pulse position modulation (PPM) chosen for deep space communication as well as for Earth-Space links in the future[2 15 16 17]. Impact of weather statistics on laser propagation is discussed in Appendix B and advanced topics in free space communications in Ref.[5 6 18]

6. APPENDIX A.

Link Propagation Geometry:

The diffraction-limited angular beam profile for an uniformly illuminated circular emitting aperture (diameter D_τ) is given by the Airy intensity distribution:

$$I(\theta) = I_o\left(2J_1(x)/x\right)^2 \quad \text{where } x = 2.44\pi\theta/\theta_\tau$$

The beamwidth is equal to: $\theta_\tau = 2.44\lambda/D_\tau$ (Full Airy lobe width to first nulls)(Fig.A_1).

We assume the Airy intensity pattern is centered on the circular receiver aperture (diameter D_R). We need to calculate the expression for the power contained within a radius $D_R/2$ at a distance R from the transmitter.

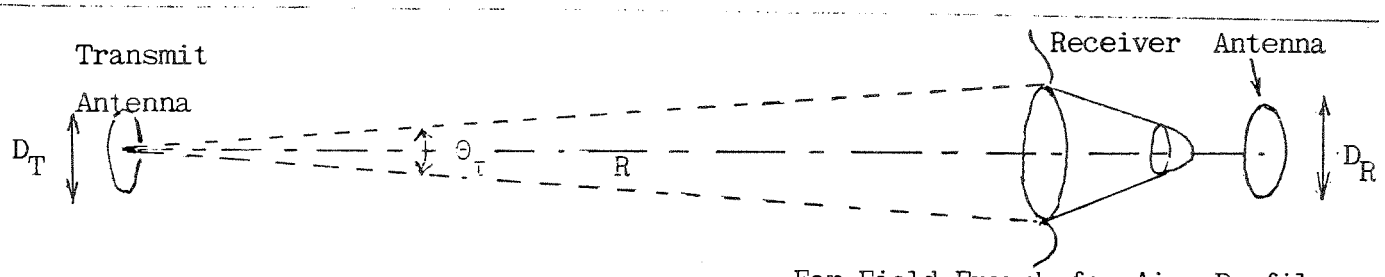

Far Field Fraunhofer Airy Profile

The power contained within the $D_R/2$ radius in the receiver plane, corresponds to the power contained within an angular radius of $D_R/2$ in the transmitter plane (small angles).

Integrating the Airy profile from 0 to $D_R/2$ yields the fraction of power given by:

$$L(D_R/2R) = 1-J_o^2(\pi D_T D_R/2\lambda R) \qquad (A_1)$$

For far field propagation distances, we use a small argument approximation:

$$J_o(x) = 1-x^2/4 \quad \text{and} \quad J_1(x) = x/2 - x^2/2$$

Then $1 - J_o^2(x) - J_1^2(x) \approx x^2/4 + x^3/2 - 5x^4/16 \approx x^2/4$

The received power is:

$$P_R = P_T L(D_R/2R) \approx P_T\left[\frac{1}{4}\left(\frac{\pi D_T D_R}{2\lambda R}\right)^2\right] \qquad (A_2)$$

We rewrite the former equation with the transmitting and receiving areas:

$$A_R = \frac{\pi D_R^2}{4} \quad \text{and} \quad A_T = \frac{\pi D_T^2}{4}$$

$$P_R = \frac{A_R A_T}{\lambda R^2} P_T \qquad (A_3)$$

We note an inverse square λ dependance which is meaningful of an optical narrow beam advantage.

$$P_R = \left(\frac{4\pi A_R}{\lambda^2}\right)\left(\frac{4\pi A_T}{\lambda^2}\right)\left(\frac{\lambda}{4\pi R}\right)^2 P_T = G_R G_T (\lambda/4\pi R)^2 P_T \qquad (A_4)$$

$G_T = (2.44/\Theta_T)^2$ for an ideal diffraction limited Airy lobe Θ_T.

The relation for the propagation of electromagnetic energy is the same for the optical or the radiofrequency wave.

For a Gaussian angular beam profile with a full width $1/e^2$ beamwidth :

$$I = I_o \exp(-8\Theta^2/\Theta_T^2) \quad \text{and} \quad G_T = (32/\Theta_T^2) \qquad (A_5)$$

For an uniform ("top hat") angular beam profile with a full beamwidth Θ_T: $G_T = \left(\frac{4}{\Theta_T}\right)^2$

APPENDIX B.

Weather Statistics.

Weather statistics impact CO_2 laser propagation performance. A key parameter is the atmpospheric transmission coefficient $\alpha(km^{-1}) = (dB/Km)/4.3$. Lowtran 7 is the accurate computer program for the determination of range at which laser communication design provides a $SNR_p = 64$ (18dB) for example. Atmospheric turbulence and system parameters are combined in the computer program in order to calculate the required laser power to acheive a range measurement.

The atmospheric transmittance is given by: $\tau = \exp(-\alpha L)$. α has also contributions from molecular scattering, aerosol scattering, molecular absorption and aerosol absorption.

$$\alpha = \sigma_m + \sigma_a + k_m + k_a \qquad (B_1)$$

For molecular scattering, σ_m is proportional to λ^{-4} (blue sky). Molecular absorption (k_m) can be avoided by choosing the laser wavelength outside of the specific absorption bands. The transmittance can be expressed as: attenuation = 4.3 αdB/km. At 1.06μm and 10.6 μm the atmospheric attenuation varies respectively from 0.384 to 1.72 in clear summer season, to 1.86 and 0.627 (dB/km) in winter hazy conditions. (Table 4).

Atmospheric scintillation is caused by the variations of the index of refraction which creates multipath summation of signals at the receiver, each with different phase (and arrival angles). Optical intensity fluctuates around the zero mean without reducing the average intensity. The atmospheric structure function (Cn_2) characterizes the stength of the turbulence as a function of the altitude (Hugnagel-Valley model). For a weak turbulence, the intensity fluctuations are described by a lognormal intensity statistics and the log intensity variance is given by:

$$\sigma^2_{lnI} = 2.24k^{7/6}\int_0^L C_n^2(x)\left(\frac{x}{L}\right)^{5/6}(L-x)^{5/6}dx \ , \quad \sigma^2_{lnI} \ll 1; \ k = 2\pi/\lambda \qquad (B_2)$$

In order to calculate the fade margin necessary to compute a probability that the signal will not fade below the minimum level necessary for the receiver, the cumulative density function of the log-normal distribution is given by:

$$P(I) = \frac{1}{2} + \frac{1}{2}\Phi\left\{\left[\ln(I/\bar{I}) + \frac{1}{2}\sigma^2_{lnI}\right]/(\sqrt{2}\sigma_{lnI})\right\} \text{ where } \Phi(x) = (2/\sqrt{\pi})\int_0^L e^{-t^2}dt \qquad (B_3)$$

As an example of fade margin calculation, we assume that saturated scintillation requires 95% of the time that received intensity is greater than or equal to the signal level required by the receiver. In this case $\sigma^2_{\ln I} > 1$ and:

$P(I) = 1-\exp(-I/\bar{I})$ and $0.05 = 1-\exp(-I/\bar{I})$, hence $I/\bar{I} = 0.05 = 13\text{dB}$

Hence, 13dB of additional signal power (fade margin) is needed to ensure that 95% of the time there is adequate signal to be detected by the receiver.

Aperture averaging can mitigate the effects of scintillation and occurs when the receiver diameter is greater than the average size of a "turble". This can sometimes occur even for modest apertures of a few inches.

Another laser beam turbulence is the case of beam spreading which occurs when transmitting through an aircraft boundary layer which causes a random phase screen in front of a transmitter located on the aircraft. Beam spreading can be described by the Strehl ratio of the on-axis intensity without aberration:

$$I/I_o = \exp(-\sigma_\phi^2 k^2) \qquad (B_4)$$

where I_o = on-axis intensity without aberration

k = optical wavenumber = $2\pi/\lambda$

σ_ϕ = variance of optical path length

For example, an aircraft at Mach 0.6 at 8-10km altitude has $\sigma_\phi = 0.08$ waves at 0.89μm, Strehl =0.79. Another case where beam spreding can be significant is for uplinks from ground to aircraft or satellite.

7. ACKNOWLEDGMENTS.

We acknowledge the Department of Electrical Engineering of McGill University for fruitful discussions and experimental support. We are especially grateful to Dr K.Cheo, University of Connecticut for the excellence of the results obtained on broadband electrooptic waveguide modulation for the CO_2 laser and Dr G.S. Mecherle.

8. REFERENCES.

1.W.K.Pratt,"Laser Communication Systems", Ed.John Wiley & Sons, Inc., 1969.

2.J.Katz, "Optoelectronic Technology and Lightwave Communications Systems", Ed. Chinlon Lin, Bellcore, New Jersey.

3.Masayuki Izutsu, Yasukuni Yamane, Tadasi Sueta, "Broadband Traveling-Wave Modulator

Using a $LiNbO_3$ Optical Waveguide", J. Quant. Electron., Vol.QE-13, N°4, pp.287-290, 1977.

4. Haeyang Chung, William S.C. Chang and Eric L. Adler, Modelling and Optimization of Travelling-Wave $LiNbO_3$ Interferometric Modulators", IEEE J. Quant. Electron. Vol 27, N°3, pp.608-617, 1991.

5. L.A. Stockum and C.R. Carroll, "Precision Stabilized Platforms for Shipboard Elect-ro-Optic Systems", Proceedings of the Society of Photo-Optical Instrumentation Engineers, Vol.493, June 1984.

6. R.A. Laskin and S.W. Stirlin, "Future Payload Isolation and Pointing System Technology"Journal of Guidance Control and Dynamics, Vol.9, N°4, July-August 1986, pp.469-477.

7. R.M. Gagliardi and S. Karp, "Optical Communications", Wiley, New York, pp.391, 1976.

8. Gordon Walker, Astronomical Observations an Optical Perspective", Cambridge University Press, Chapter 68, 1987.

9. D.Souilhac, D.Billerey and A.Gundjian, "Two Dimensional Acoustooptic Deflector Using a Crystal of Tellurium for the CO_2 Laser", Appl. Opt., Vol.29 (12), pp.1798-1804, 1992.

10. R.J. Becherer, "Introduction to Laser Radar and Lidar", Course Notes, SPIE's OE/Aerospace Sensing, Orlando' 92.

11. J.H. McElroy, N.McAvoy, E.H. Johnson, J.J. Degan, F.E. Goodwin, D.M. Henderson, T.A. Nussmeir, L.S. Stokes, B.J. Peyton and T. Flattan, "CO_2 Laser Communication systems for near-Earth space applications", Proc. IEEE, 65, pp.221-251, 1977; E. Bonek and H. Lutz, "CO_2 laser communication technology for intersatellite data links, "ESA J., 5, pp.83-98, 1981.

12. A. Waksberg, "Range predictions for a CO_2 laser communication system". Appl. Opt. Vol. 20, N°15, pp.2688-2693, 1981.

13. William J.Parrish, "Advanced Topics in Infrared Focal Plane Electronics", Course Notes, Amber Engineering Inc., SPIE's OE/Aerospace Sensing, Orlando 1993.

14. Richard J.Becherer, "Applications of Laser Radar", Course Notes SPIE's OE/Aerospace Sensing, Orlando 1992.

15. Charles H. Townes, "Infrared SETI", PIE Vol.1867, pp.121-125, 1993.

16. Stuart A. Kingsley,"Amateur Optical SETI", SPIE Vol.1867, pp.178-208, 1993.

17. Stuart Kingsley,"The Search for Extraterrestrial Intelligence (SETI) in the Optical Spectrum", A Review, SPIE Vol.1867, pp.75-113,1993.

18. L.G.Kazovsky,"Fundamentals of Coherent Lightwave Systems".Course Notes SPIE's 1991, Boston.

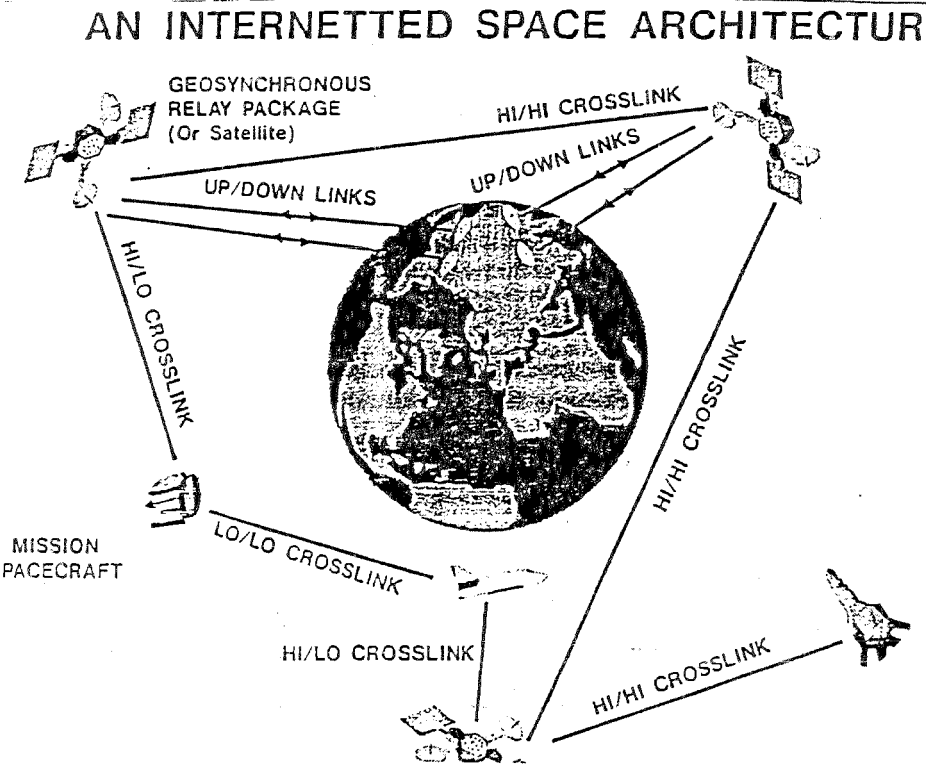

Fig.1. Free Space Near Orbit Interlink Laser Communication.

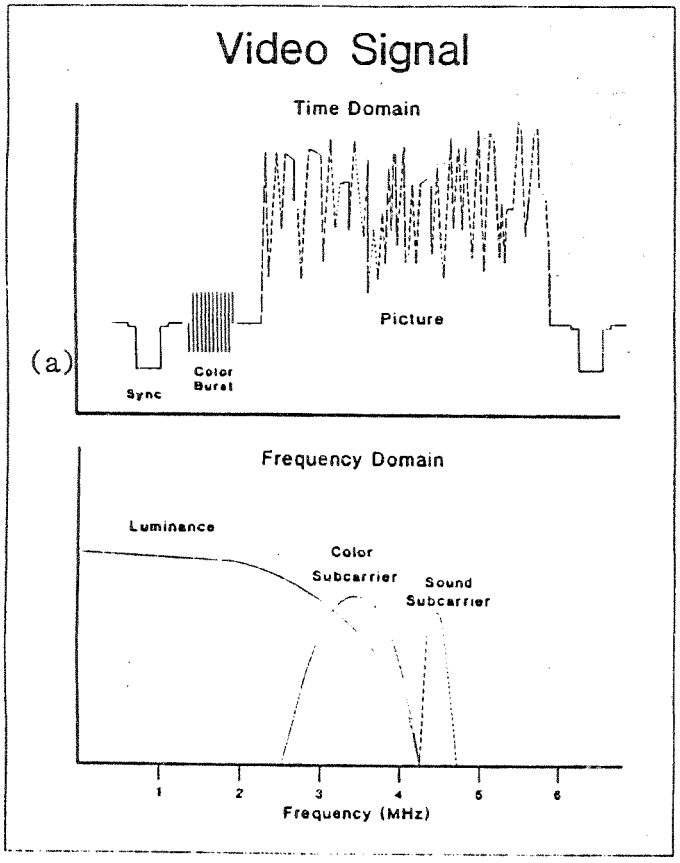

Fig.2a,b.CATV Spectrum

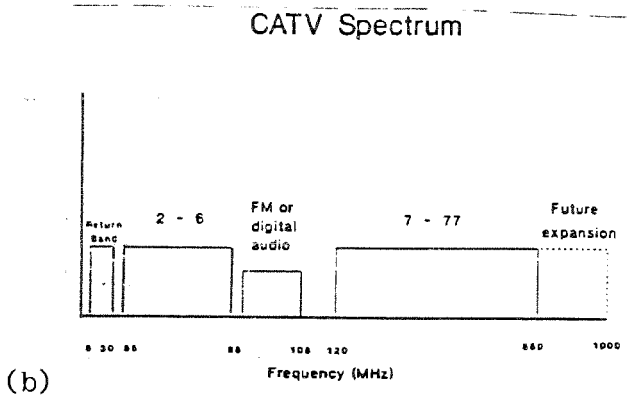

Channel Assignments
North America

- Standard
  Most channels have Fc=1.25+n•6 MHz
  Channels 5 and 6 offset 4 MHz
- IRC (Incrementally Related Carrier)
  All channels have Fc=1.25+n•6 MHz
  Phaselock and non-phaselock
- HRC (Harmonically Related Carrier)
  All channels have Fc=n•6 MHz
  Phase locked to reference

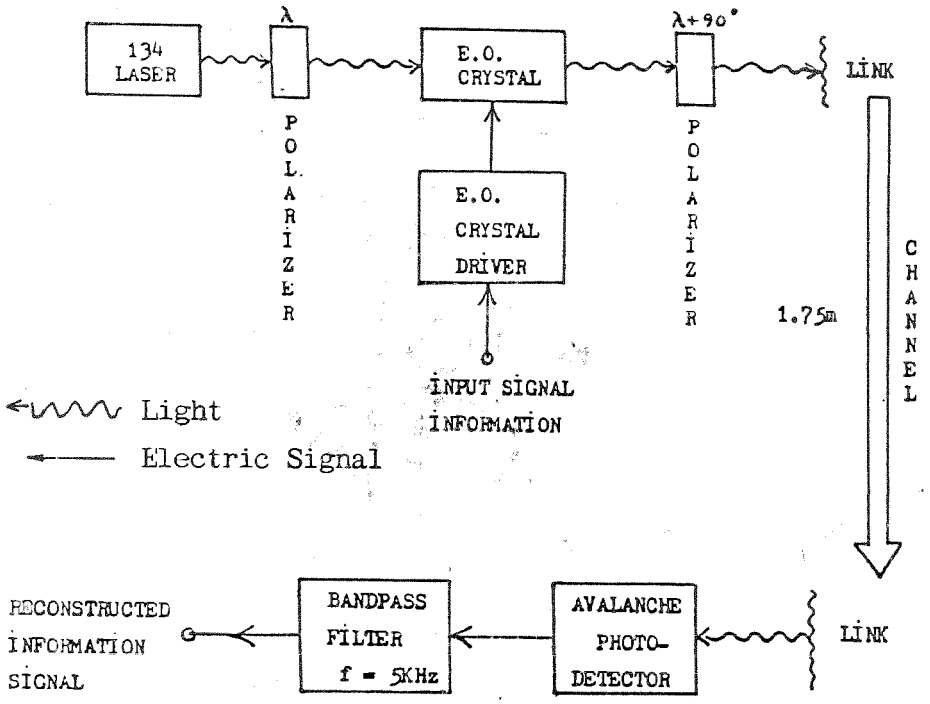

Fig.3. AM Electrooptic Laser Communication Experiment.

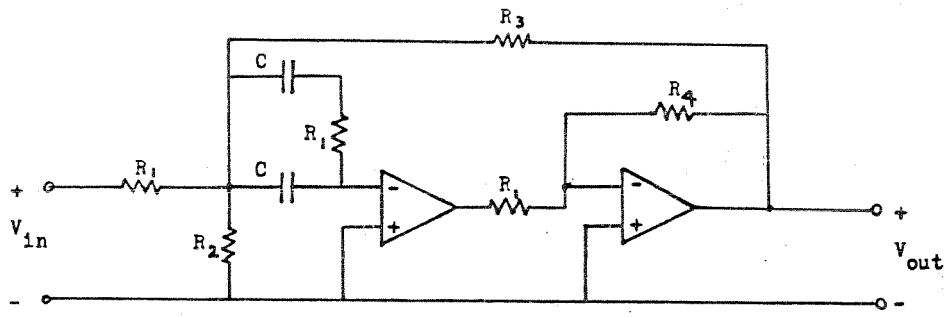

GAİN = 10 = 20 db

B.W. = 100 Hz

f = 5 KHz

Q = 50

R_1 = 10 K

R_2 = 1.6 K

R_3 = 3.3 K

R_4 = 6.3 K

C = 0.01 uf

Fig.4. Butterworth Bandpass Filter.

LOCATION OUTPUT	OUTPUT POWER (Watts)	POWER LOSS db
134 laser	6.31×10^{-3}	—
first polarizer	1.42×10^{-3}	12.95
E.O. crystal	4.73×10^{-4}	22.50
Analyzer	7.85×10^{-5}	38.10

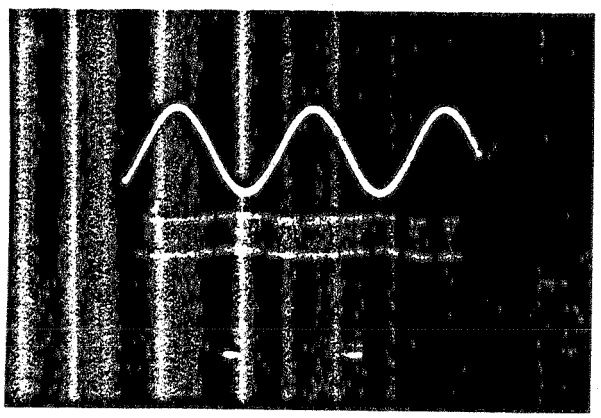

Fig.5a (Top) Input $6V_{p-p}$, at 5 KHz
(Bottom) Output before bandpass filtering.

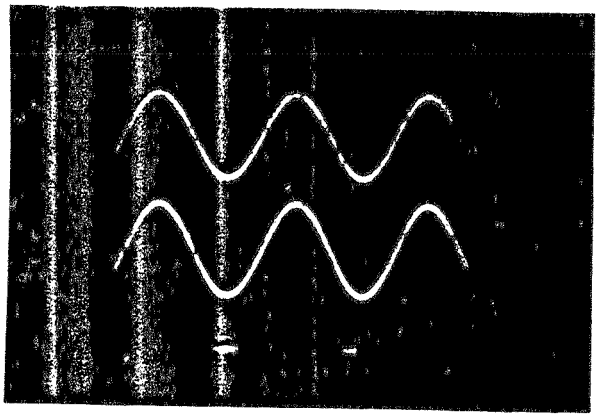

Fig.5b (Top) Input
(Bottom) Output demodulation
1.0% distorsion.

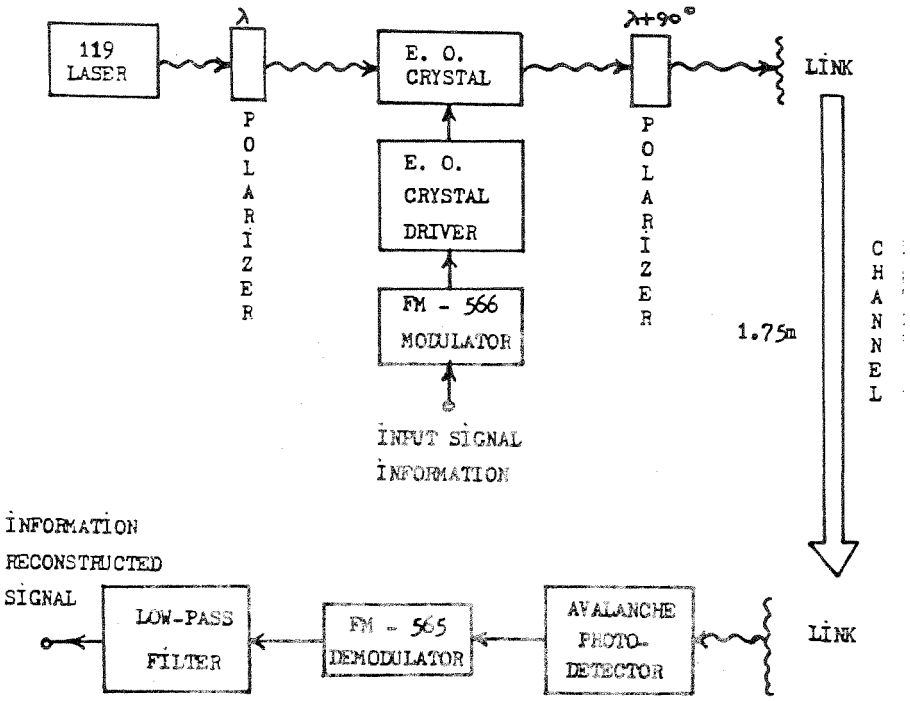

Fig.6. AM/FM Electrooptic Laser Modulation.

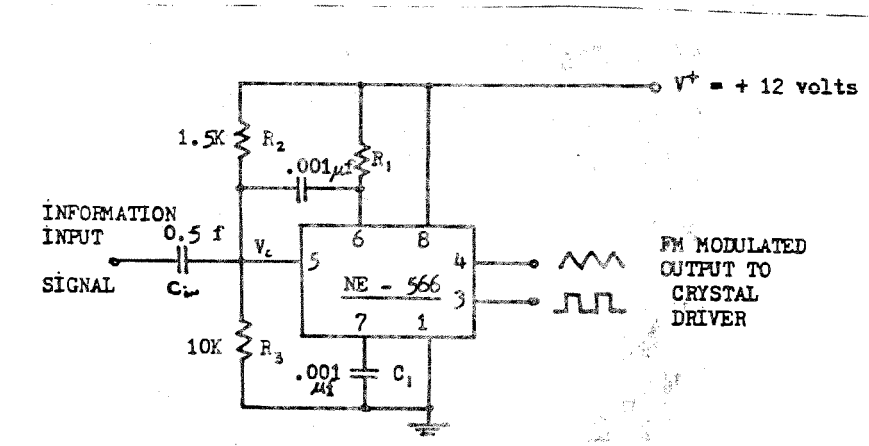

Fig.7 NE 566 Function Generator.

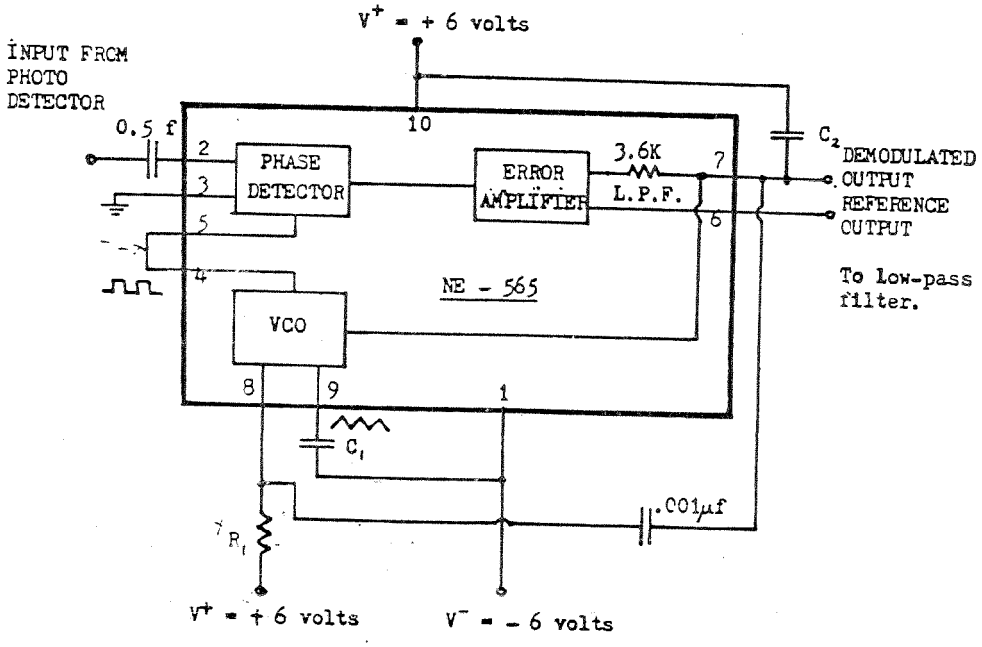

Fig.8. NE 565 Phase-Locked-Loop (PLL)

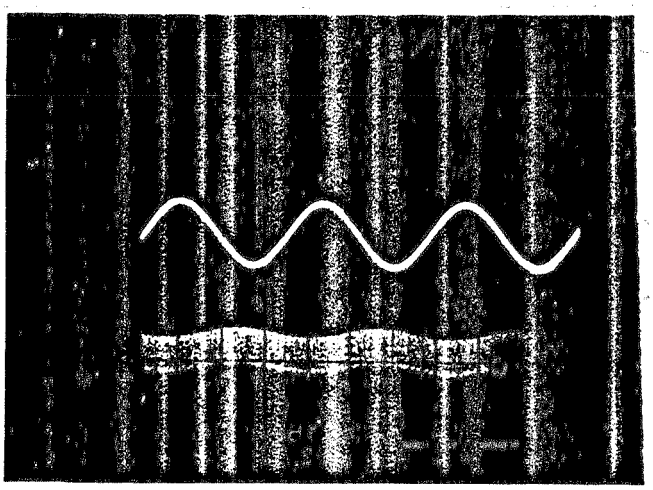

Fig.9a (Top) Input $2V_{p-p}$ at 30KHz
(Bottom) Output before low-pass filtering.

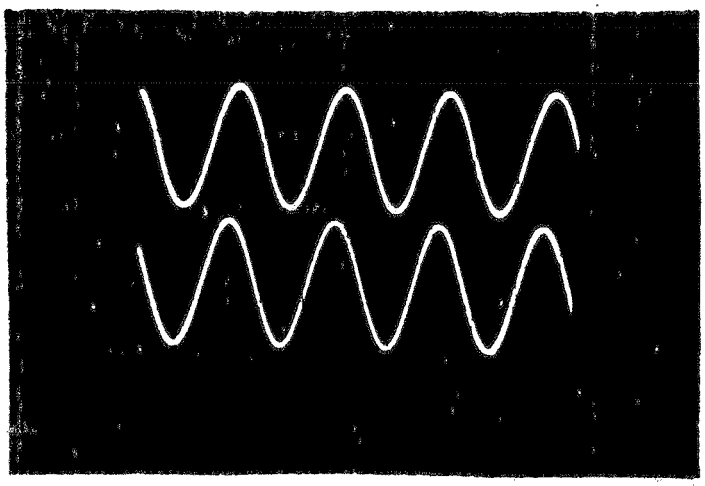

Fig.9b (Top) Input
(Bottom) Output after low-pass filtering, 0.8% distorsion.

A High-Resolution Tunable IR Laser Source

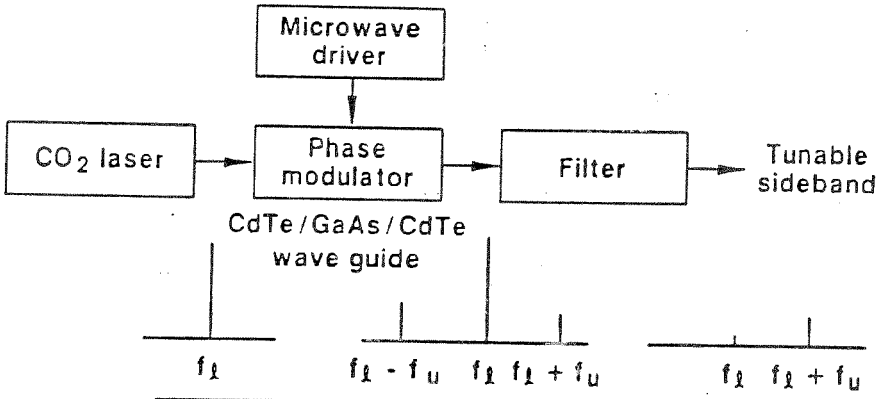

CO_2 laser	Microwave driver	Tunable sideband
10 W	35 W	48.5 mW

Fig.10 CO_2 Laser Electrooptic High Frequency Modulation Experiment

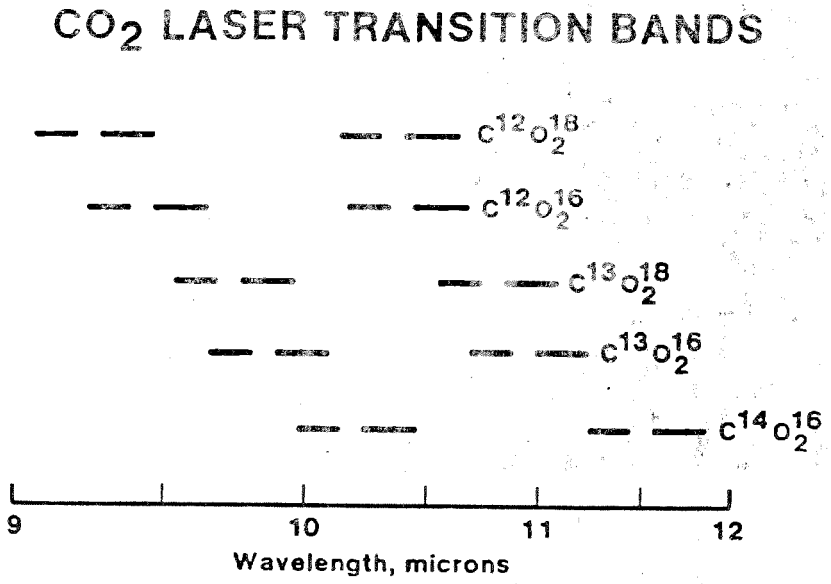

Fig. 11 CO_2 Laser Transition Bands

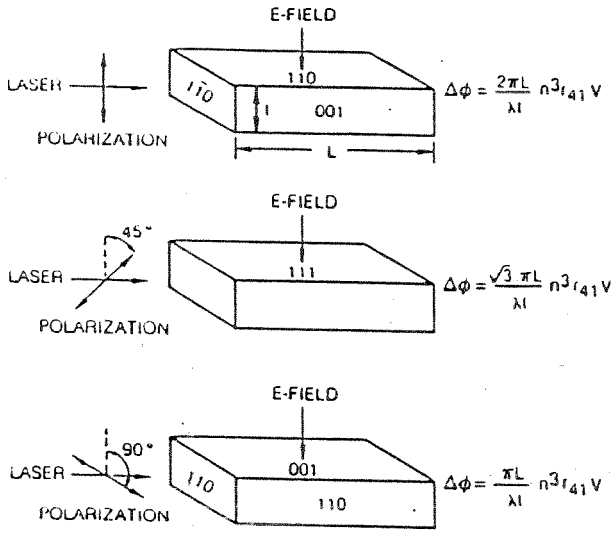

$$E = E_0 J_0(\Delta\phi) \sin(2\pi f_0 t + \phi_0)$$

$$+ \sum_{n=1}^{\infty} E_0 \{J_n(\Delta\phi) \sin(2\pi f_0 t + 2\pi f_m t + \phi_0)$$

$$+ (-1)^n J_n(\Delta\phi) \sin(2\pi f_0 t - 2\pi f_m t + \phi_0)\}$$

Fig.12. Phase Modulation in GaAs

CROSS-SECTION OF CdTe BUFFERED GaAs THIN-SLAB WAVEGUIDE MODULATOR

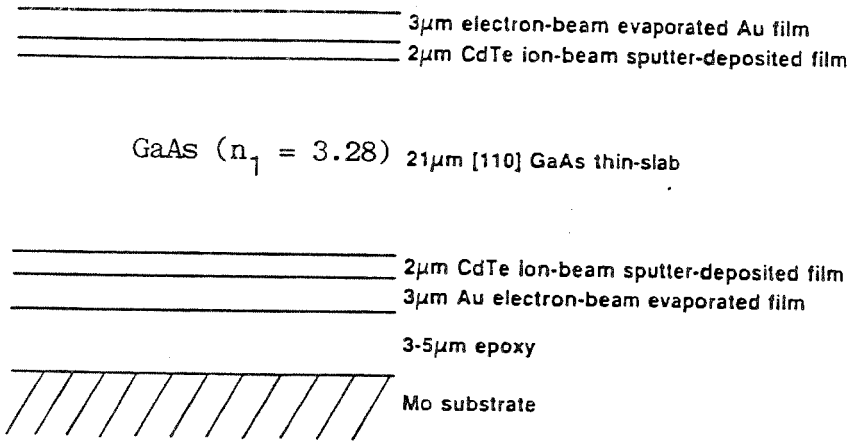

Fig.13. Cross-section of CdTE/GaAS/CdTe waveguide.

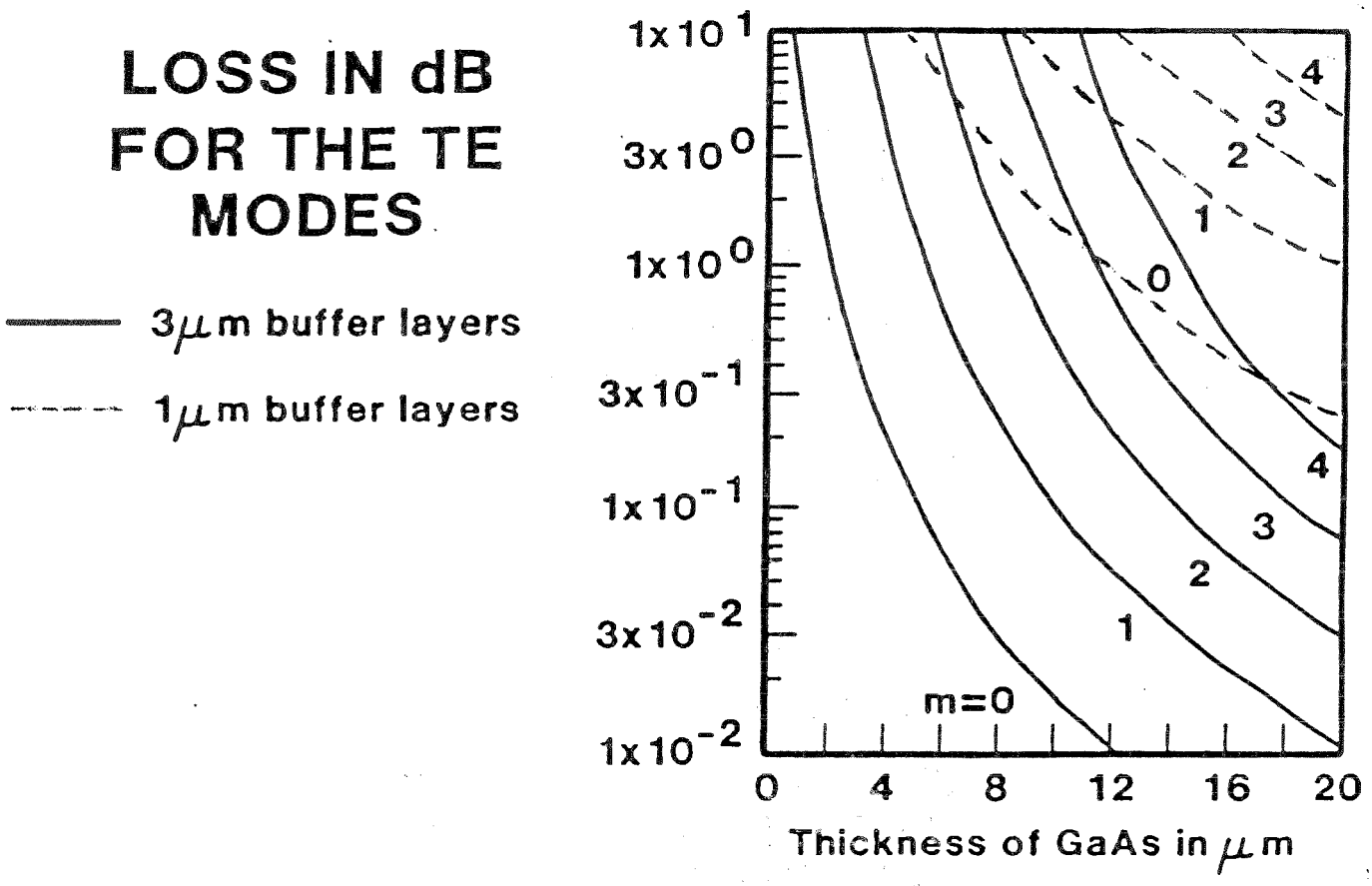

Fig.14. Loss in dB for the TE Modes in CdTe/GaAs/CdTe Waveguide.

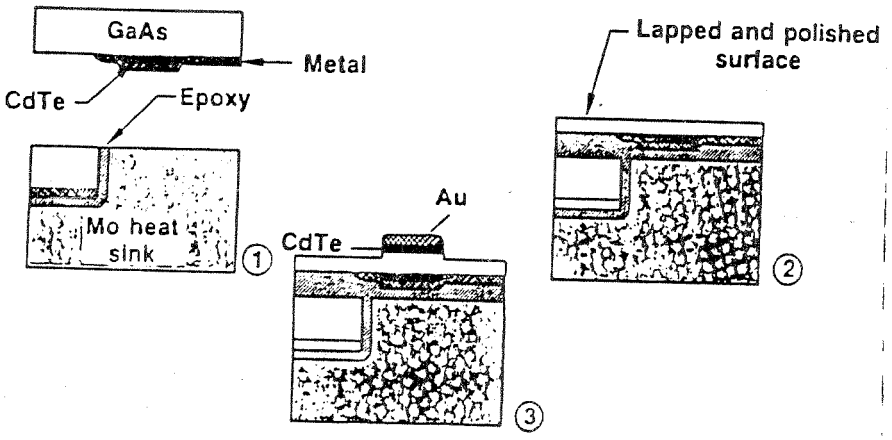

Fig. 15 CdTe Buffered Waveguide Fabrication Cycle

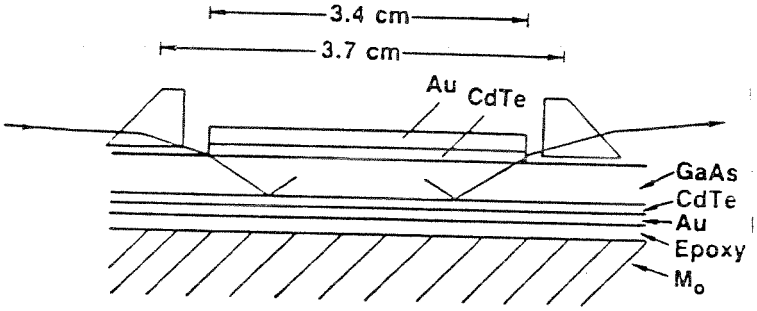

Fig. 16 Optical Path through CdTe Buffered Waveguide Modulator

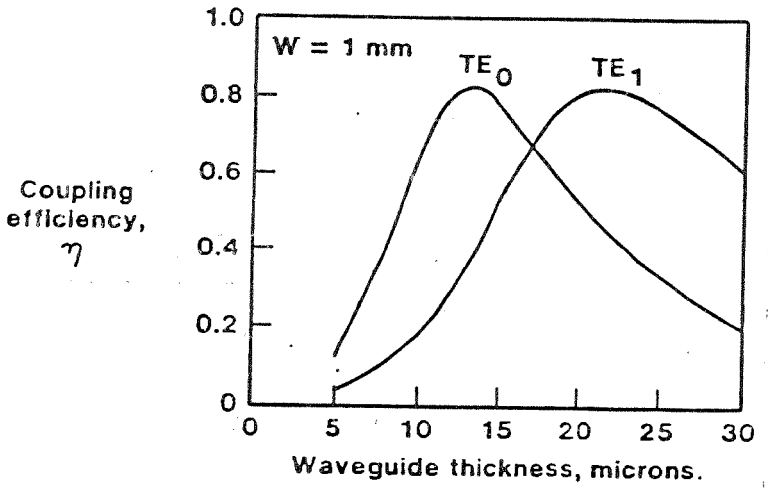

Fig. 17 Input Coupling Efficiency Using a Ge Prism

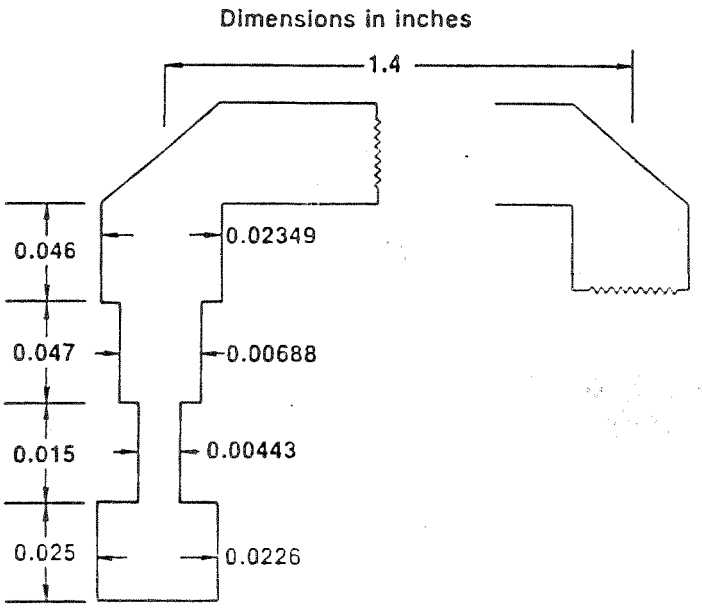

Fig.18. Microstrip Electrode Design For 16GHz Center Frequency.

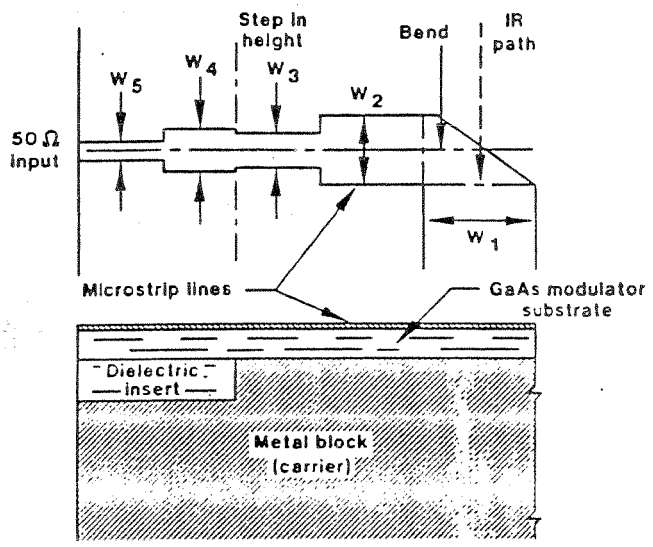

Fig.19. Microstrip Impedance Transformer.

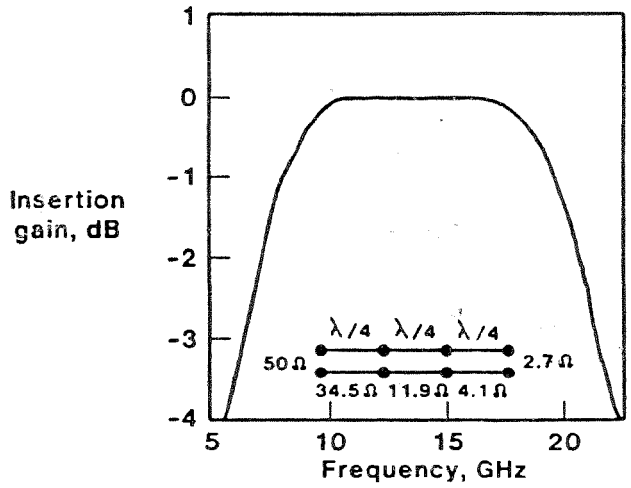

Fig.20. Microstrip Electrode Loss Calculation.

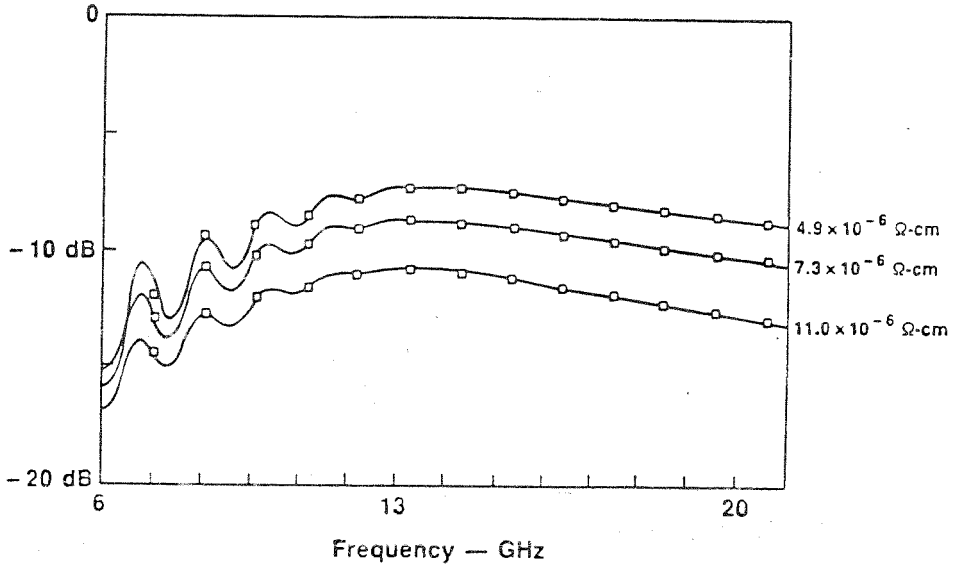

Fig.21 Microstrip Electrode Loss Calculation

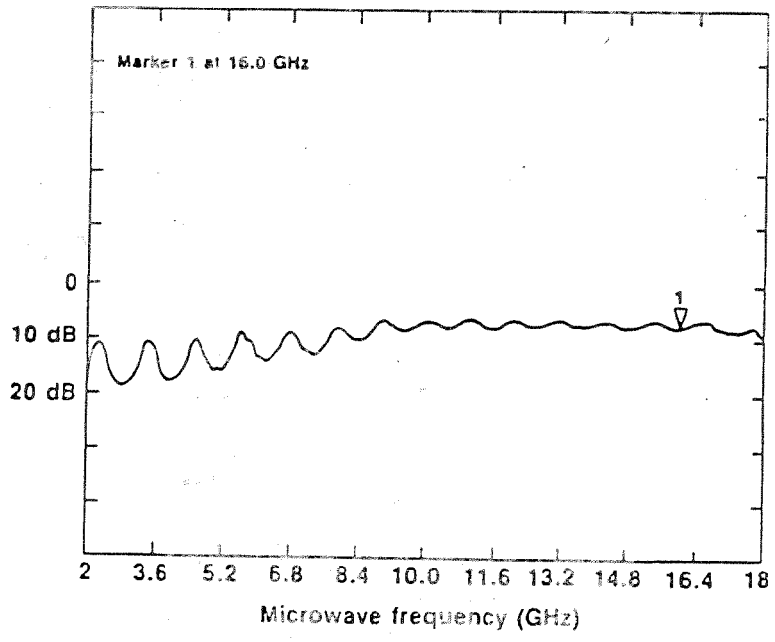

Fig.22 Microstrip Insertion Loss Measurement.

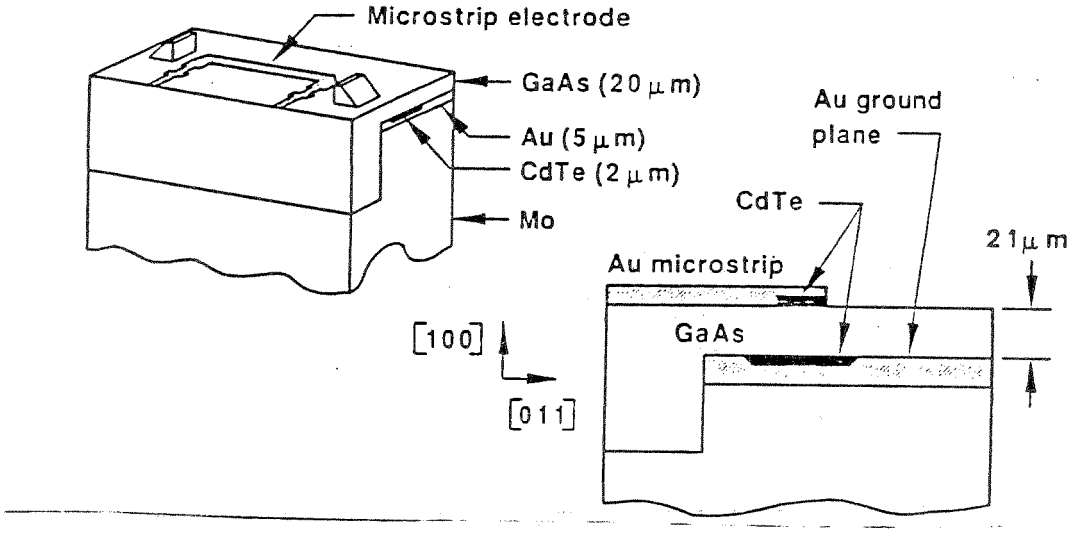

Fig.23. Topology of a Traveling Wave CdTe Buffered GaAs Waveguide Modulator.

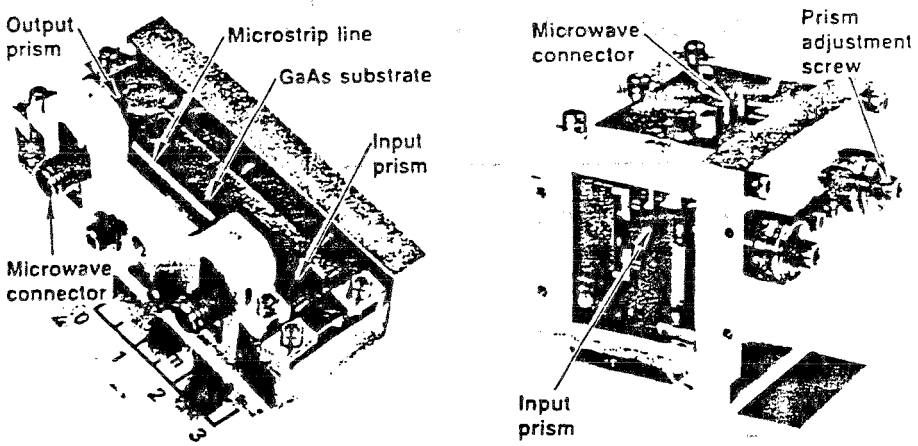

Fig.24. Traveling-Wave Double-Sideband GaAs Modulator Sub-Assemblies.

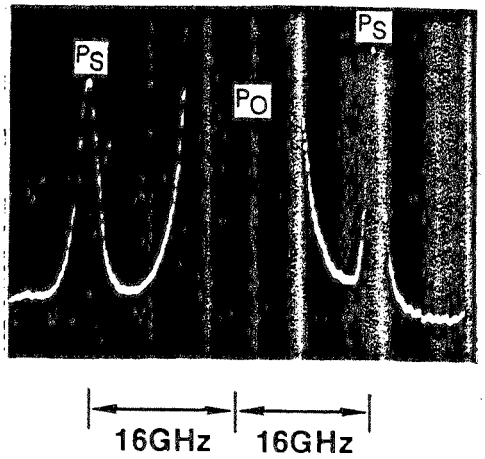

Fig.25. Output Spectrum.

OUTPUT SPECTRA THROUGH A WHITE CELL

(T=60°C, P=35 T orr)

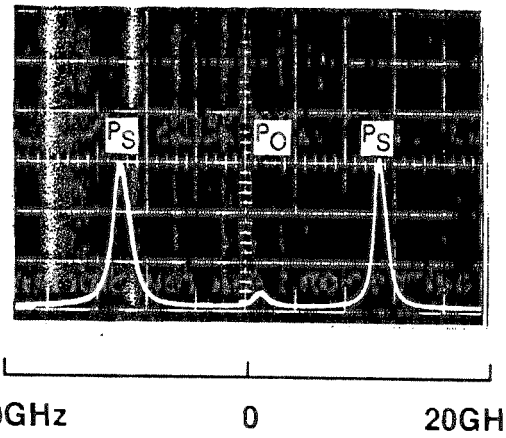

Fig.26. Output Spectra Through a White Cell Filled with Air (T=0°, P=35 Torr).

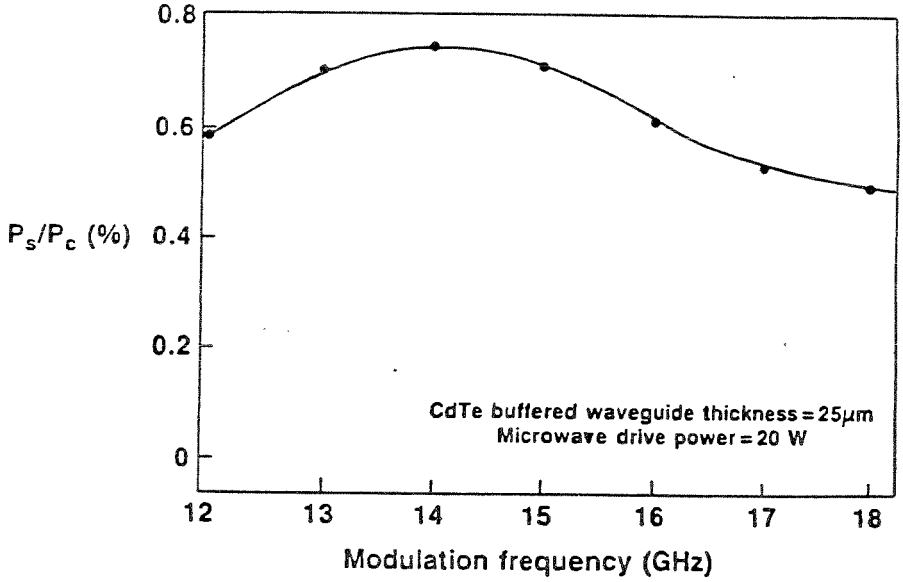

Fig.27. Percent Sideband Power Conversion vs Modulation Frequency.

Input Power (W)		Sideband Power
Laser	Microwave	(mW)
10	20 (CW)	37.7
10	35 (CW)	48.5
10	100 (Pulsed)	138.6

Fig.28. Sideband Power Generation.

TARGET SIGNATURES AND BIASES

Chairperson : Andrew Sinclair

An Analytical Model of Satellite Signature Effects

Reinhart Neubert
GeoForschungsZentrum Potsdam, Dept. Recent Kinematics and Dynamics of the Earth
Telegrafenberg A17, D-14473 Potsdam, Germany

Introduction

The technique of Satellite Laser Ranging (SLR) achieved a precision of about 1 cm per single measurement. Using data averaging, a formal error of a few millimetres is attained at many stations. In this situation, the identification of sytematic error sources which could contribute more than a few millimetres is important. One of these error sources is the asymmetric pulse spreading by the reflector array itself. This pulse spreading is imaged in the histogram of range residuals of a single photon detecting SLR system /1/,/2/,/3/.
The impulse response of spherical satellites like LAGEOS has a sharp leading edge followed by a longer tail. The result of this asymmetry is a systematic shift, depending on the detection hardware, signal level and filtering method.. Appleby investigated the dependence of the effective Centre-of-Mass Correction (CoM) from signal level using a simulation method /1/. In the following we are reporting on the results of an analytical approach to the same problem.

The Model

The calculation of the signal level dependence of the expected range residual distribution is done in the following steps:

First we need a representation of the impulse response (or „optical transfer function") of the reflector array. This function must be convoluted with the laser pulse shape to derive the signal exciting the photodetector. An ideal detection and timing system would contribute no jitter and therefore the distribution of range residuals would be close to the signal shape, as far as a very low return rate is chosen .

In the next step we treat the detector as being ideal and estimate first the distortion of the residual distribution for nonzero signal energy. The distortion is typical for a single stop photon counting system. It results from the fact, that the photons arriving first have a higher chance to produce an avalanche than the photons corresponding to the tail of the pulse. This effect can be easily represented in closed form by a simple application of Poisson statistics.

In the last step we are convoluting with a gaussian distribution representing the limited time resolution of the whole time of flight measuring system.

Let us denote the impulse response of the satellite by I(t) . The signal at the receiver is then:

$$S(t)=\int_{-\infty}^{\infty} g(t-\tau)\cdot I(\tau)\,d\tau \qquad \int_{-\infty}^{\infty} S(t)\,dt=1 \qquad \text{Eq.1}$$

where g(t) is the laser pulse shape. Then the probability distribution for the stop event can be expressed by:

$$P(t)=Q\cdot S(t)\cdot\exp\left[-Q\cdot\left(\int_{-\infty}^{t} S(\tau)\,d\tau\right)\right]=\frac{dW(t)}{dt}\cdot\exp(-W(t)) \qquad W(t)=\int_{-\infty}^{t} Q\cdot S(\tau)\,d\tau \qquad \text{Eq.2}$$

where Q is the energy of the whole pulse measured in terms of the average number of photoelectrons.

This relation follows from the Poisson statistics of the photoelectric process as will be explained later. The integral of P(t) is equal to the total return rate per pulse:

$$R=\int_{-\infty}^{\infty} P(t)\,dt=1-\exp(-Q) \qquad \text{Eq.3}$$

This is the well known relation between the return rate and the average number of photoelectrons. It can be used to estimate Q from the observed return rate.

For our problem sufficient accuracy is obtained using discrete distributions instead of continous signals. Denoting the signal by S_i and the probability of detection in the bin No. i by P_i we can write:

$$P_i=\left(1-Q\cdot S_i\right)\cdot\exp\left(-Q\cdot\sum_{k=0}^{i-1} S_k\right) \qquad R=\sum_k P_k \qquad \sum_k S_k=1 \qquad \text{Eq.4}$$

This formula can be easily explained using the discrete Poisson distribution for the emission of k photoelectrons if the mean pe number is q for the special case of k=0. The probability of the emission of no electron is p(0)=exp(-q). Thus the first factor in Eq.4 is the probability for at least 1 electron within bin i , and the exponential is equal to the probability of no electron in all bins corresponding to earlier time. The formula for continuous signal can be derived going to infinitesimal bin width. The distribution P_i does not include the effect of timing jitter , it can be taken into account by a final convolution with a (discrete) gaussian T_i .

$$D_i=\sum_{k=0}^{n} T_{i-k}\cdot P_k \qquad \text{Eq.5}$$

The range k=0....n must be chosen to include all P_k which are significantly different from zero. The distribution D_i is our model for the distribution of the range residuals. It can be used to compute the moments, especially the mean and the variance:

$$\bar{t}=\Delta t\cdot\frac{1}{R}\cdot\sum_k k\cdot D_k \qquad \sigma^2=\Delta t^2\cdot\frac{1}{R}\cdot\sum_k k^2\cdot D_k-\left(\bar{t}\right)^2 \qquad R=\sum_k D_k \qquad \text{Eq.6}$$

A Numerical Example: LAGEOS

Starting point for the computation is the optical transfer function of the satellite. It can be obtained from publications for most of the laser satellites (see references cited in Tab.1). We are using an analytical approximation proposed by Degnan /4 /. In this representation the satellite's sphere is regarded to be quasi continuously covered by small cube corners.

The signal intensity coming from a zone of equal angle of incidence is then:

$$I\phi(\Phi)=\frac{1}{A}\cdot(\sin(\Phi)\cdot\eta(\Phi)) \qquad A=\int_{\Phi c}^{0} \sin(\Phi)\cdot\eta(\Phi)\,d\Phi \qquad \eta(\Phi)=\left(1-\frac{\Phi}{\Phi c}\right)^2 \qquad \text{Eq.7}$$

where $\sin(\Phi)d\Phi$ is the surface element on the unit sphere and $\eta(\Phi)$ is a function describing the angular dependence of the effective reflectivity of an individual cube corner. The denominator A is necessary for normalisation. The reflectivity function $\eta(\Phi)$ has been calculated by Arnold /5/ for various azimuthal orientations of the cube corner prisms, but the simple quadratic form given above /4/ is a useful approximation if the cutoff angle Φc is well adjusted. For uncoated quartz glass we use the value Φ_c=0.75 radians and for aluminium coated prisms Φ_c=1 in case there is no recession of the prisms. Fig.1 shows a comparison of the simplified reflectivity function with Arnold's results for LAGEOS (Table 4 of Ref. /5/ for 532 nm and averaged over all azimuth angles). It can be seen that $\eta(\Phi)$ approximates the rigorously calculated reflectivity ref(Φ) reasonably well.

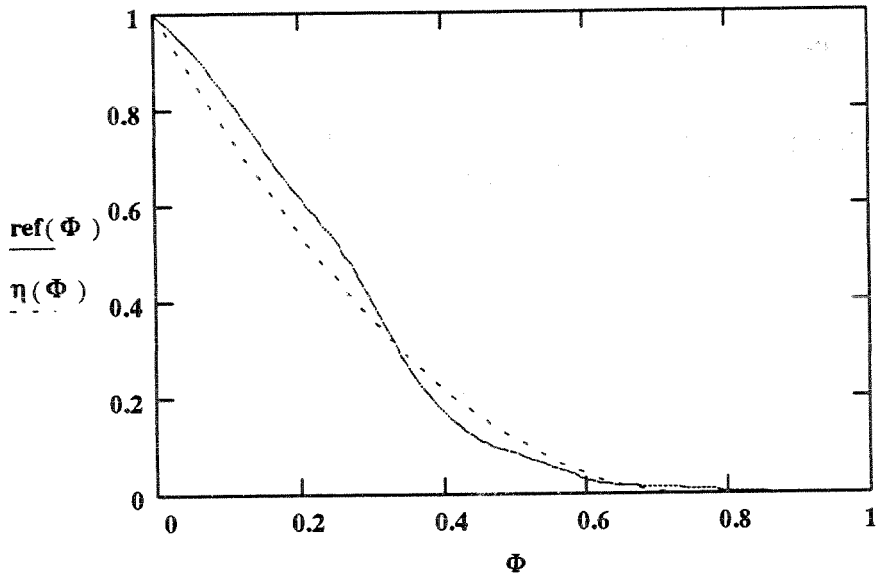

Fig.1: Comparison of $\eta(\Phi)$ with the rigorously calculated reflectivity in the 32...41 µrad annulus of the far field diffraction pattern (Ref./5/).

To derive the impulse response we need the relation between the location of the effective reflection plane and the angle of incidence. Using the satellite centre as the coordinate origin the distance of the reflection plane from the center of the satellite is:

$$x(\Phi) = Rs \cdot \cos(\Phi) - L \cdot \sqrt{n^2 - \sin(\Phi)^2} \qquad \text{Eq.8}$$

where R_s is the radius from the satellite centre to the front face of the prisms, L is the distance of the vertex to the front face of an individual prism and n is the index of refraction. These design paramaters are listed for all spherical satellites in Tab. 1.

In the following we are using the x coordinate instead of time. This corresponds to the use of one way range instead of the time of flight. Note that x is directed from the satellite to the observer. To derive the intensity fraction contained in the interval x, x+dx we have to devide

Iϕ by the first derivative of x(Φ):

$$Ix(\Phi)=\frac{I\phi(\Phi)}{x'(\Phi)}=\frac{\frac{1}{A}\cdot\eta(\Phi)}{Rs+\frac{L\cdot\cos(\Phi)}{\sqrt{n^2-\sin(\Phi)^2}}} \qquad \text{Eq.9}$$

To express Ix in terms of x as the independent variable would require the inversion of Eq.8 which is not possible in closed form. But a picture can easily be obtained by drawing Ix(Φ) versus x(Φ). This is done in Fig.2a using the parameters for LAGEOS. It shoes the expected sharp rise at the point of earliest reflection corresponding to the angle Φ=0 .

The mean value of x , which is just the centre of mass correction CoM (centroid), can easily be calculated using the function Iϕ(Φ) :

$$CoM=\bar{x}=\int_{\Phi c}^{0} x(\Phi)\cdot I\phi(\Phi)\,d\Phi \qquad \text{Eq.10}$$

This quantity is tabulated for all spherical satellites in column 1 of Tab.2 . For the calculations as well as the preparation of most of the graphs MATHCAD 5.0 has been used /16/.

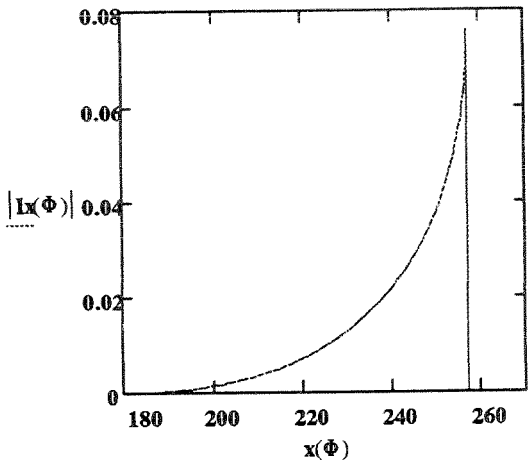

Fig.2a: Optical transfer function of LAGEOS (Eq.9)

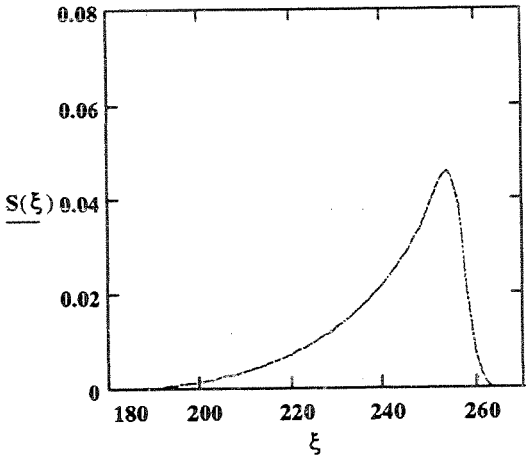

Fig.2b: Same as Fig.2a convoluted with the laser pulse

The convolution with the gaussian laser pulse can be expressed as follows:

$$S(\xi)=\frac{1}{\sigma\cdot\sqrt{2\cdot\pi}}\cdot\int_{\Phi c}^{0}\exp\left[-\frac{(\xi-x(t))^2}{2\cdot\sigma^2}\right]\cdot I\phi(t)\,dt \qquad \text{Eq. 11}$$

This function is plotted in Fig.2b using σ=2.25 mm corresponding to a laser pulse of 35 ps FWHM. The function S depends on ξ , the location of the reflection plane. The letter ξ is used

instead of x to avoid confusion with the function x(t). After execution of the convolution ξ may be renamed to x. The convolution removes the discontinuity of the transfer function. At this point we convert to a discrete distribution sampling the function S(x) at points spaced by Δx:

$$X_i := i \cdot \Delta x \qquad S_i := S(X_i) \cdot \Delta x \qquad \Delta x := 1mm \qquad i := (0, 1 .. N) \qquad \text{Eq.12}$$

The discrete distribution S_i can now be inserted into Eq. 4 to 6 using different values for the average number of photoelectrons. The results are illustrated in the following figures.
Fig.3 is the result of application of Eq.4 on the signal S_i for 3 different values of the average signal strength : Q=0.125 pe, 0.5pe and 4pe resp. The area enclosed by the curves and the x- axis is equal to the total return rate. The asymmetry of the transfer function is clearly visible at low return rate. With higher signal strength the distributions become narrower and less asymmetric. The curves in Fig.3 are the predicted range residual distributions for an ideal single photon detector. In practice, the detector and time of flight electronics have limited resolution. We model this by convoluting with a gaussian. Assuming 50ps timing jitter (standard deviation) the distributions of Fig.4 are obtained. The asymmetry is still visible for low signal strenth, but the curve for 4pe looks like a gaussian because of the limited resolution. For a comparison with observed range residual histograms see Fig.7a and 7b.

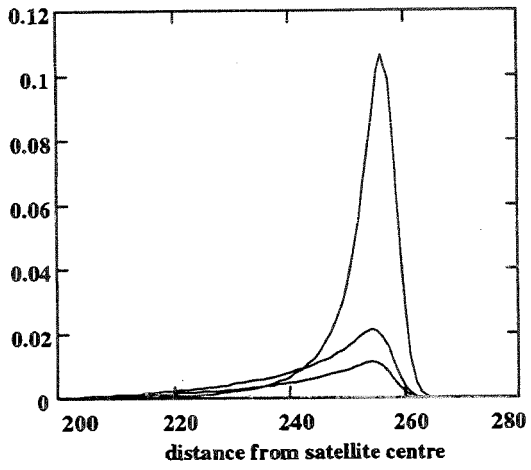

Fig.3: Expected stop event distributions P_i for Q=0.125, 0.5, and 4 pe resp.

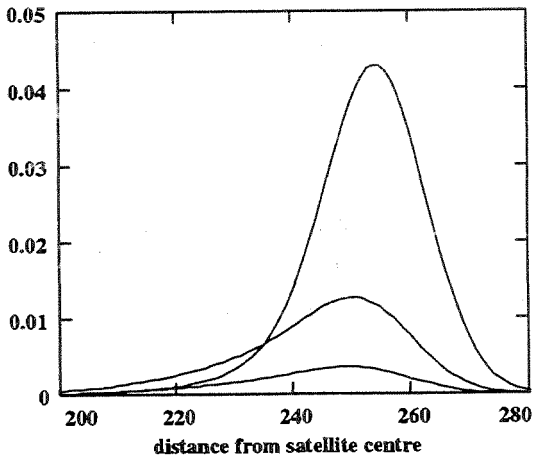

Fig.4: The same as Fig.3 but convoluted with a gaussian of 50 ps = 7.5mm standard deviation

We are now in a position to compute the signal dependence of the centre of mass correction and standard deviation using Eq.6 . The result is represented in Fig.5 . The monotonically rising curves are for CoM- shift whereas the falling curves are for the standard deviation. The dashed lines result by application of clipping to the distributions at 2σ points (one iteration). Clipping is shifting the mean to higher values by about 2mm if the signal level is very low. At high signal levels clipping is not changing the mean significantly, because the distributions tend to become symmetric for strong signal. The standard deviation is always reduced by clipping of course.

The most important conclusion from Fig.5 is that the CoM will be shifted by more than 10mm at high signal levels. The real shift may be even higher because most avalanche diode detectors contribute their own signal dependent shift /7/. Thus it is strongly recommended to work below 1pe where the shift can be reasonably well estimated and corrected.
At return rates <20% the signal induced shift is 1 mm or less. Under these conditions the strength of filtering is more important. This is illustrated in Fig. 6a and 6b showing the dependence of the CoM from the number of filtering iterations for zero level and 0.2 photoelectrons (18% return rate) respectively. The calculations for Fig 6a and b were done using Arnold's reflectivity data /5/. When using the approximation Eq.7 we got about 0.5 mm smaller values for the CoM. It can be seen that for 2.5σ editing the CoM becomes stationary after 5 iterations already and the total shift is 1.8mm only. In contrast, for 2σ editing the CoM is increasing until the 10th iteration and attains a shift of about 5mm.

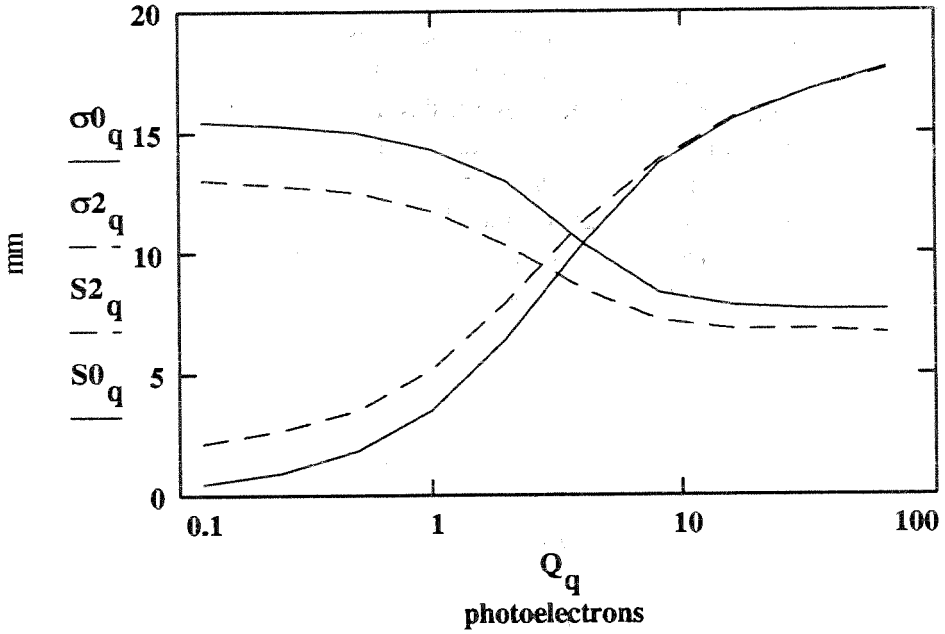

Fig.5: Dependence of standard deviation and centre of mass correction from signal strength. monotonically rising: CoM- shift ; monotonically decreasing: standard deviation dashed curves are for 2σ- clipping.

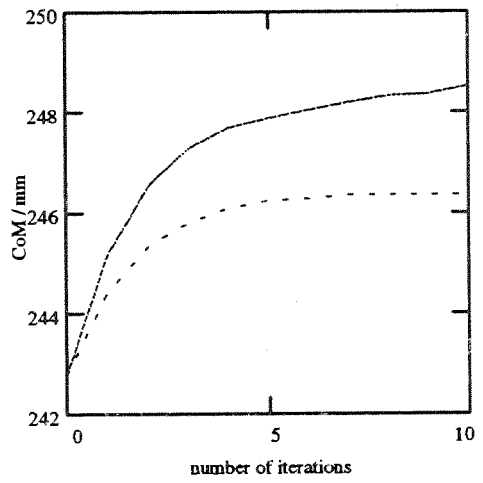

Fig.6a: Depencence of CoM from editing upper curve: 2σ , lower: 2.5σ

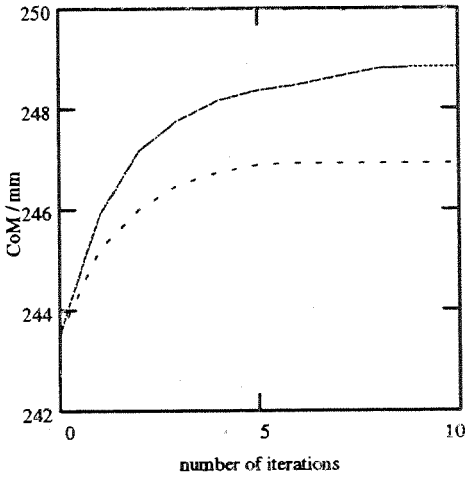

Fig.6b: Same as Fig.6a for Q=0.2 pe (R=18%)

Results for other Satellites

In the following we compile some numerical results for all spherical satellites including the GFZ-1 to be launched in 1995. Tab.1 summarises the main design data of the reflector arrays.

Tab.1: Retroreflector Data of Spherical Satellites

Satellite	Radius mm	Vertex length mm	Cut off angle radian	Recession mm	Coating	Reference
AJISAI	1053.0	25.72	0.75		no	/8/
ETALON	641.5	19.1	0.75 (rec.)	5.5	Al	/9/
LAGEOS	298.0	27.84	0.75		no	/5/
STARL.	118.4	23.3	1.0		Al	/10/
GFZ-1	91.0	19.1	0.70 (rec.)	17 (40 ϕ)	Al	/11/

In Tab.2 we compare the centre of mass correction using Eq.7 and Eq.10 with rigorous computations as far as published and with the value presently adopted by the orbital analysis community. The values of column 1 are for single photon ranging at zero signal level and without clipping (filtering) of the data.
A more realistic value is given in column 2 , which has been obtained for 0.5 pe and 2.5σ filtering using 10 iterations. LAGEOS results have been obtained using the reflectivity values of the cube corners tabulated in Ref. /5/. Therefore it is not surprising that the centroid correction at zero return rate is very close to the value given by the same author.
For all other satellites the simple approximation given in Eq.7 together with the Φc values tabulated in Tab.1 has been used.

Tab.2: Centre of Mass Correction

Satellite	**Analytical model**		**Other source**	**Present standard**
	zero level	0.5 pe, 10x2.5σ		
AJISAI	959.0	978.1	1010.0 /8/	1010.0
ETALON	579	590	576.0 /9/	558.0 /12/
LAGEOS	242.7	247.9	242.5 /5/	251.0 /12/
			251.0 /14/	
STARLETTE	74.6	76.6	74.5 /10/	75.0
GFZ-1	59.4	60	60 /11/	

Comparison with Observations

The precise value of the centre of mass correction can only be checked by laboratory investigations of the satellite prior to launch. To our knowledge this was done for LAGEOS only. On the other hand we can examine the shape of the optical transfer function as well as relative shifts by analysis of the range residuals when the satellite is in orbit. In Fig.7a and Fig.7b we compare the histograms of range residuals with the model in the case of LAGEOS and AJISAI . In this figures the x-axis is directed from observer to the satellite and therefore the satellite signature appears reversed. The return rate has been estimated from the range data.

The timing jitter has been modeled in these cases by convoluting with the histogram of the calibration data . Note the different x-axis scale for LAGEOS and AJISAI resp. It can be seen that the agreement is reasonable.

To estimate power dependent shifts from range residuals, Kirchner /15/ investigated the spacing of individual tracks in a semitrain ranging system. The laser system at Potsdam station is using single pulses. But this laser produces side pulses with about 4% of the main pulse energy. We take advantage of this situation adjusting the signal level such that the return rate from the prepulses is less than 10% and the main pulse corresponds to about 1 photoelectron. Fig. 8 shows the histogram of range residuals for an AJISAI pass as an example. Taking the means for each track separately we expect that the differences of the means from the weak pulses are near to a multiple of the laser pulse spacing. But the mean of the main pulse is shifted to smaller range. This is indeed the case and the shift was in this case about 15mm. This is in reasonable agreement with the model taking into account the possible error in estimating the signal level, which in addition is not constant during the pass. The signal estimation is based on the return rate of the weak pulses. From the known energy ratio of the laser pulses one can then calculate the signal level of the main pulse.

In the case of LAGEOS it is difficult to obtain significant results from Potsdam data because of the low return rate and associated small effects. Therefore we used raw data from Graz station kindly supplied by Kirchner. In the experimental LAGEOS-2 pass at Graz the laser energy was switched periodically between two levels. The ratio between the two levels was 1 to 4 . The average photoelectron number at high level for the first pulse of the semitrain (we used only this for analysis) was between 0.5 and 1 . From the modulation of the averages (normal points) the shift could be determined to be 2...3 mm in good agreement with the expectation.

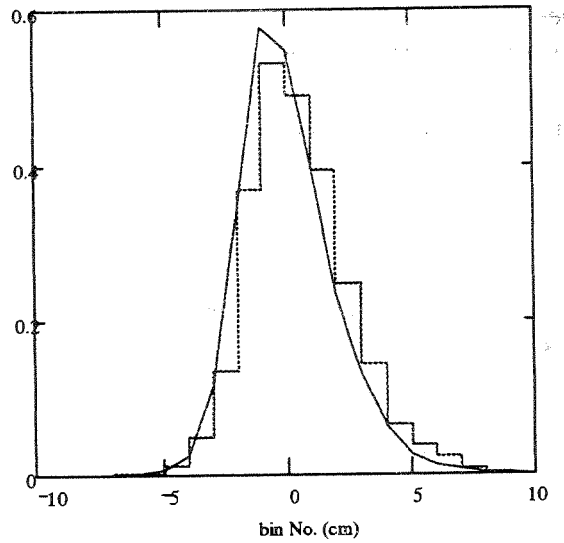

Fig.7a: Comparison of the measured range residual histogram (steps) of LAGEOS (sum of 3 passes) with the modeled pulse shape (line). R=10%

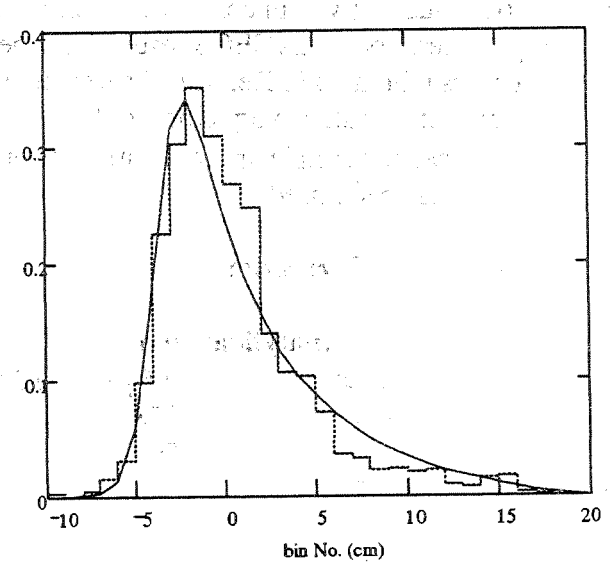

Fig.7b: Comparison of measured and modeled range residuals for an AJISAI pass. R=70% .

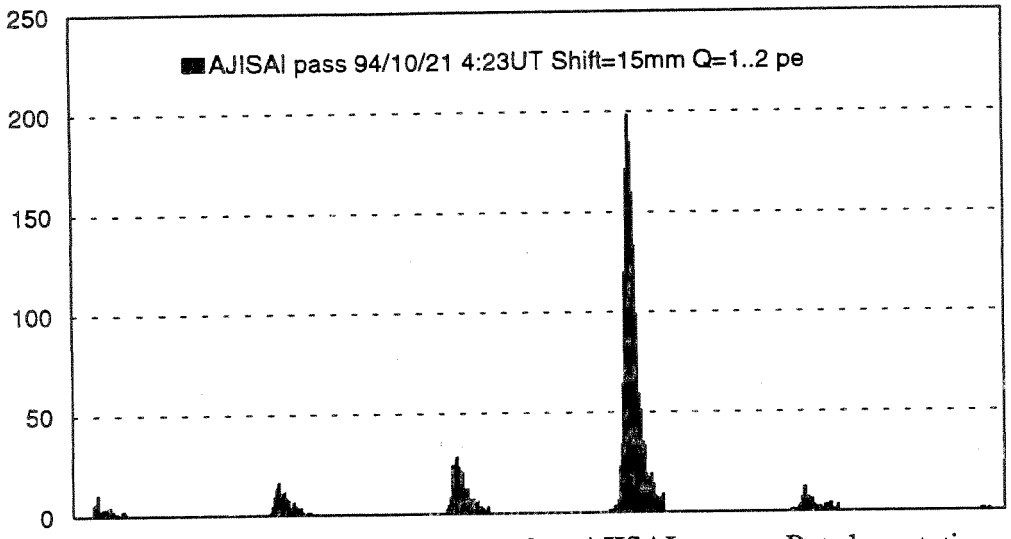

Fig.8 : Range residual histogram of an AJISAI pass at Potsdam station.

Conclusion

It has been shown that the given model well explains the observed satellite signatures as well as the power dependent shift of mean range (normal points). The calculated centre of mass corrections for LAGEOS and STARLETTE are in good agreement with the results of D.A.Arnold /5/,/10/.

For the practical application we conclude/recommend the following:

- single photon ranging systems should adjust the return rate to 50% or less
- the centre of mass corrections for the conditions of single photon detection at low signal level differ from the presently adopted values except for STARLETTE
- it is recommended to maintain the adopted standards for the centre of mass corrections and to correct the data at the stations to remove systematic effects.
- in the most important case of LAGEOS about 3...6 mm must be subtracted from the ranges of a typical single photon detecting system to be in agreement with the standard value of the centre of mass correction. This correction depends on laser pulse width, time resolution, return rate as well as the edit criteria used at the station.

References:

/1/ G.M.Appleby: Satellite Signatures in SLR Observations,
Proc. 8th Worksh. on Laser Ranging Instr., Annapolis (1992), p.2-1...2-14

/2/ A.T.Sinclair: SLR Data Screening; location of peak of data distribution,
Proc. 8th Worksh. on Laser Ranging Instr., Annapolis (1992), p.2-34...2-43

/3/ G.Kirchner, F.Koidl: Work at Graz on Satellite Signatures,
Proc. 8th Worksh. on Laser Ranging Instr., Annapolis (1992), p.2-15...2-22

/4/ J.J.Degnan: Millimeter Accuracy Satellites for Two Color Ranging,
Proc. 8th Worksh. on Laser Ranging Instr., Annapolis (1992), p.7-36...7-51

/5/ D.A.Arnold: Optical and Infrared Transfer Function of the LAGEOS Retroreflector Array,
Final Report, Grant NGR 09-015-002, Suppl.No 57, (May 1987)

/7/ L.Grunwaldt, H.Fischer: Field Experience with Various Detector Types, this Proceedings

/8/ M.Sasaki, H.Hashimodo: Launch and Observation Program of the Experimental Geodetic
Satellite of Japan, IEEE Trans. Geosci. GE-25, No.5, p.526-533 (1987)

/9/ N.T.Mironov et al.: ETALON-1,-2 Center of Mass Correction and Array
Reflectivity, Proc.8th Worksh.on Laser Ranging Instr., Annapolis (1992), 6-9...6-32

/10/ D.A.Arnold: Optical Transfer Function of the STARLETTE Retroreflector Array,
Grant NGR 09-015-002, Suppl. No. 57, Tech.Rep. RTOP 161-05-02, (Feb.1975)

/11/ V.D.Shargorodsky: GFZ-1 Scient.-Techn. Note for the User
Russian Inst. for Space Device Eng., Moscow (1994)

/12/ D.D. McCarthy (ed.): IERS Standards 1992
IERS Tech. Note 13, July 1992, Centr. Bureau of IERS, Observat. de Paris

/13/ D.Egger: private communication

/14/ Th.Varghese et al.: Test Results from LAGEOS-2 Optical Characterization Using Pulsed
Lasers, Proc.8th Worksh.on Laser Rang.Instr., Annapolis (1992),p.6-33

/14a/ P.O.Minott et al.: Prelaunch Optical Characterization of the Laser Geodynamic
Satellite (Lageos 2), NASA Techn. Paper 3400 (Sept. 1993)

/15/ G.Kirchner: presented at the working meeting on satellite signatures, Graz (March 1994)

/16/ Mathcad 5.0, product of Math Soft Inc., Cambridge , Mass., USA

MONITORING POTENTIAL RANGE BIASES IN SINGLE–PHOTON SLR SYSTEMS.

GRAHAM APPLEBY AND PHILIP GIBBS

Royal Greenwich Observatory, Cambridge and Herstmonceux, UK

Abstract. Of prime importance in the SLR technique is the minimization of biases in the distance measurements. As systems achieve millimeter precision, their potential increases for monitoring subtle mm-level geophysical processes, and the accuracy of the observations becomes paramount. It has been established that for single-photon systems the effect of satellite signature can introduce a broadening and an asymmetry into the post-fit range residuals which causes a reduction in the single-shot precision and an uncertainty in the appropriate value of the correction required to reduce the observations to the satellite centre-of-mass (CoM). These effects are particularly important for satellites such as Topex/Poseidon which carry large laser retro-arrays, but are also of significance for geodetic satellites such as Lageos. It is therefore desirable that single-photon systems be able to increase the return signal level beyond that of single photons in order to reduce the target signature effect and increase the single-shot precision. However we must ensure that such a departure from the single-photon regime does not introduce un-modelled range biases.

In this paper we describe an investigation into the stability of range measurements made by the Herstmonceux system employing a SPAD detector, by carrying out experimental target-board and satellite ranging over a wide range of return signal levels. We find significant range biases at high signal levels with respect to the equivalent single-photon values. From an empirical model we estimate that half the bias effect is due to statistical sampling of the temporal distribution of the return pulse. We attribute the remaining effect to a plausible degree of time-walk within the detector system. In addition the satellite observations and models confirm that account must be taken of the return signal level in the calculation of the appropriate CoM correction. A scheme is described for monitoring these effects on an operational basis so that routine ranging may be carried out at higher than single-photon levels, and a recommendation made to enable more precise reduction of normal-point ranges to satellite CoM.

1. Introduction.

For single-photon systems operating at single photon receive levels, satellites with large laser retro arrays (LRAs) place a proportionately large source of ranging jitter into the systems' error budget. The Herstmonceux system uses an un-cooled single photon avalanche diode (SPAD) detector (Cova et al, 1990), working at 3 volts above breakdown, and currently achieves a precision of about 9mm single-shot rms from target-board calibration ranging. However, as is evident from Figure 1, the precision of satellite ranging observations is inferior. The plots show typical distributions of post-fit range residuals for most of the frequently tracked satellites, in ascending order of size of LRA.

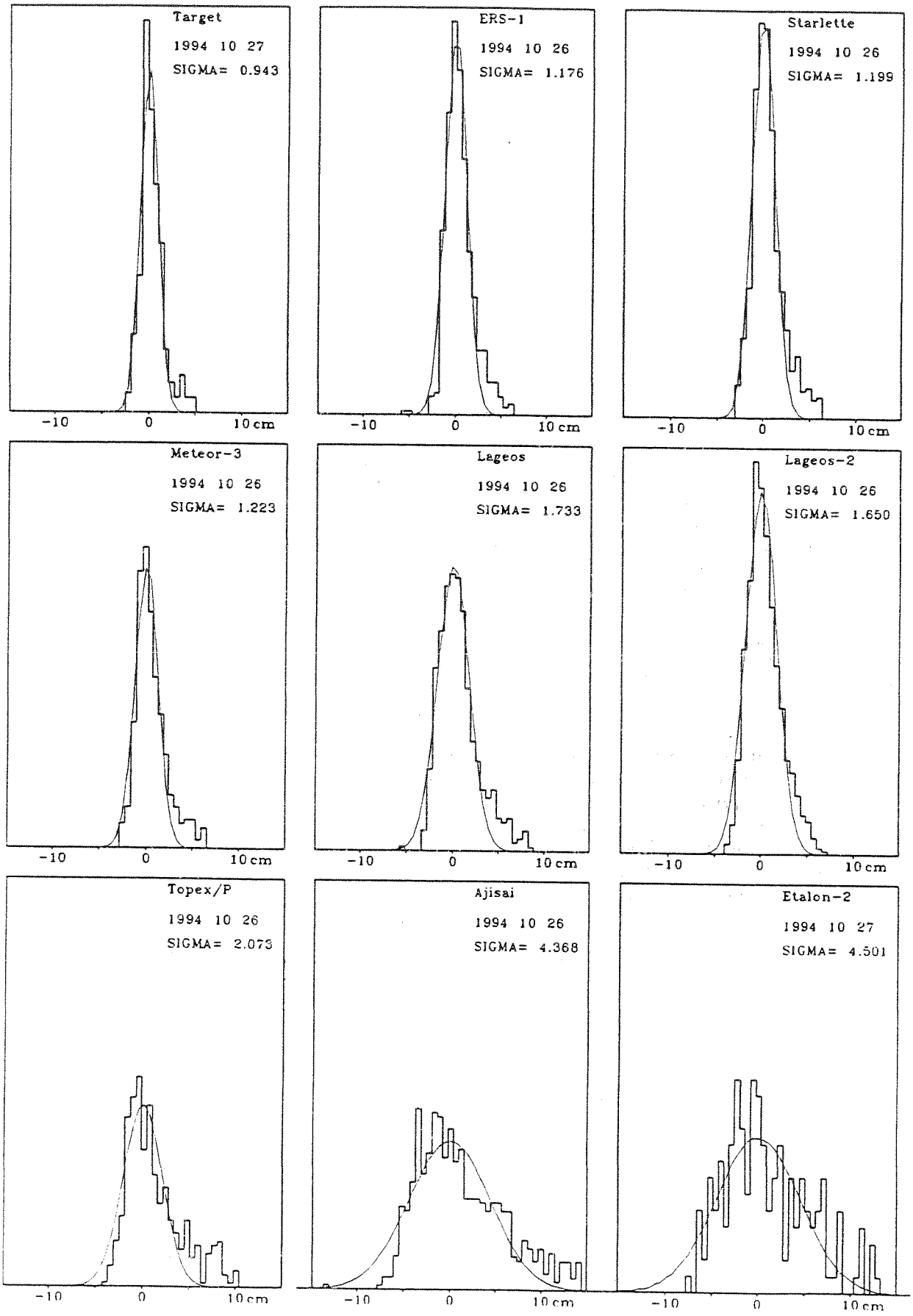

Fig. 1. Distribution of range residuals from target-board and satellites.

The small LRA of ERS-1 has minimum effect on the precision (11mm), typical Lageos precision is 17mm, Topex/Poseidon 21mm and Etalon 45mm. Simple modelling has successfully explained this satellite signature effect in the Herstmonceux data (Appleby, 1993), such models also clearly demonstrating that if large numbers of photons reach the detector, then as photons from the leading edge of the pulse are detected the influence of the LRA is reduced and ranging precision increases. With the launch in 1992 of Topex/Poseidon with its large LRA it was clear that potentially large numbers of photons are readily available, and furthermore it is difficult observationally to remain within the single-photon regime. Thus, although in routine operation we keep all return at the single-photon level by using a set of neutral density filters in the receive path, we have also recently carried out experiments to gauge the bias effects of departing from this level of operating. In particular we wish to measure and model both for target-board and satellite ranging the expected 'time-walk' effects due to intrinsic detector walk and statistical sampling of the return pulse.

2. High Energy Experiments.

2. 1. TARGET-BOARD RANGING.

We compute the return rate from ranging sessions by counting the number of laser shots in a given time interval, say 15 seconds. For each of these shots we check whether a noise event is detected, each of which reduces by one the effective number of laser shots. Given the number of true returns within the interval, we compute the true return rate as a percentage of the corrected number of laser shots. This information is displayed to the observer in near realtime. For a detector with quantum efficiency qe, where $(0 < qe < 1)$, we can relate the return rate to the number n of photons reaching the detector from

$$rate = 100x(1 - (1 - qe)^n).$$

For the SPAD we have qe=0.2. For standard calibration ranging this rate is maintained at about 10-15% by attenuation of the outgoing laser beam, and by selection from a set of ND filters in the receive path, so that $n \leq 1$. For the duration of the ranging experiments the outgoing beam was attenuated such that the highest value ND filter was required to maintain single-photon returns. A series of calibration ranges was performed at different receive levels by selection of different ND filters, such that some 12 return levels of between 1 and 1000 photons were obtained. We note that for n approaching about 15, the observed return rate approaches 100%, so for rates $\geq$ 100%, n is estimated from the known relationships between the densities of the filters. The resulting calibration values and precision (1-sigma) are shown in Figure 2.

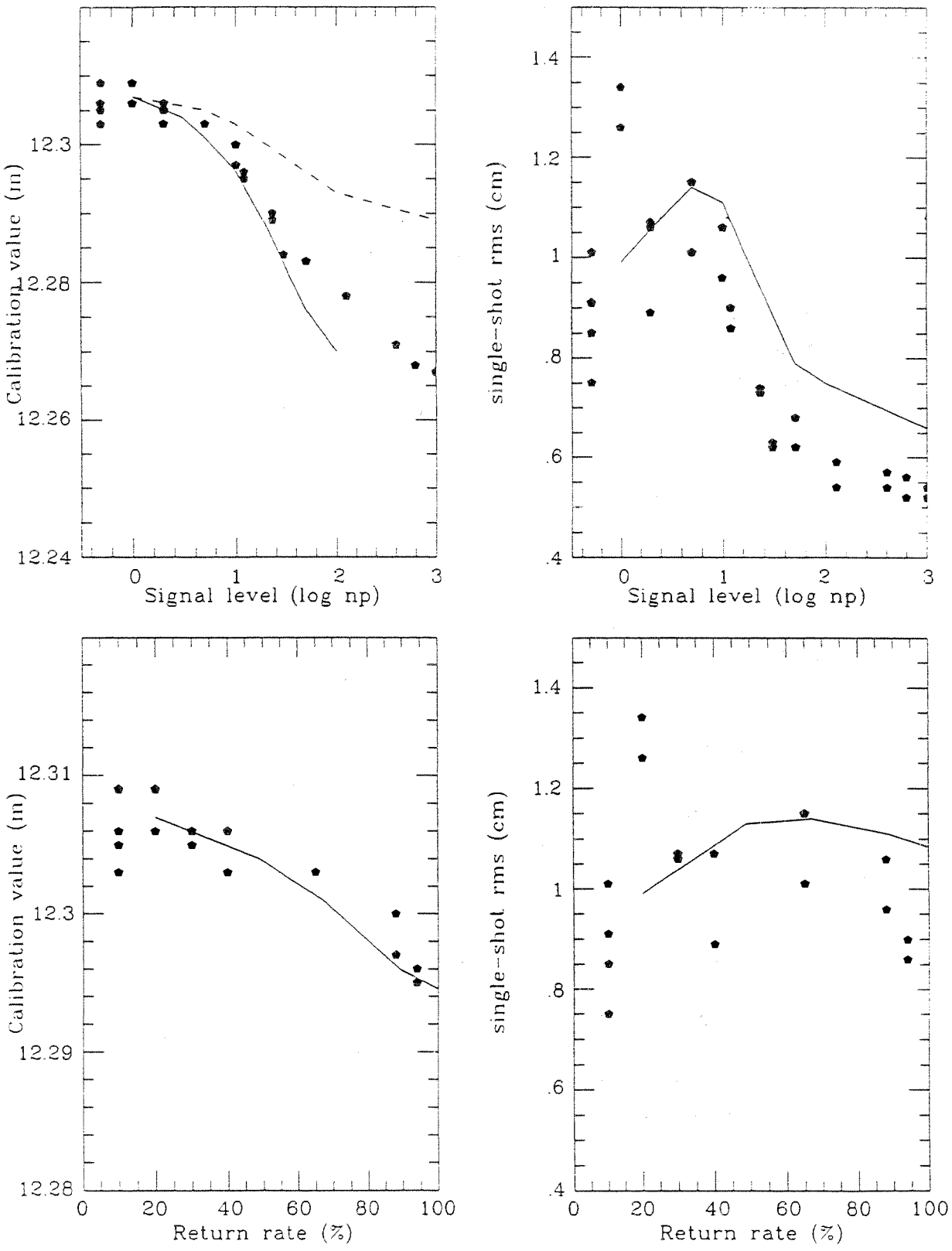

Fig. 2. System calibration *vs* signal level - Observations and models

We have plotted separately the results from the full range of return levels and those for which return rates of between zero and 100% were achieved. For this latter sub-set it is seen that the calibration value changes by about 15mm. The range precision changes little, with mean value about 9mm, but with a temporary decrease to 13 mm at around 20%. This precision decrease has been noted consistently, and is also seen by Prochazka (1993) in laboratory tests of the SPAD. For the results over the full range of the experiment, we see that the calibration value changes by some 40mm, and the single-shot precision increases to about 6mm.

2. 2. MODEL OF TARGET-BOARD RESULTS.

Our estimates of the errors in ps (FWHM) of the ranging system components are as follows. SPAD detector system 70 (Prochazka, 1993), Laser 120 (manufacture's estimate, experimental estimate), start-diode 65 (experimental estimate), Stanford interval timer 65 (manufacture's estimate, experimental estimate). Quadratic combination of these values gives an expected single-shot single-photon rms range precision of 10mm, close to the experimental mean of about 9mm. Using these parameters, we have set up a model of the expected change of calibration value as a function of numbers of returning photons, as described in detail for satellite ranging in Appleby (1993). We assume a Gaussian return pulse of n photons, a detector efficiency qe of 0.2, and sample from the pulse a large number of times, finally forming the peak and precision of the resulting distribution of selected events. We then include an estimate of an energy-dependent timewalk intrinsic to the SPAD system by using the measurements by Prochazka (1993) over a dynamic range of between zero and 200 photons. The results of this model are shown as the full lines in Figure 2. To emphasize the relative effects in our model of the pulse-length and detector time-walk we also plot with a broken line the curve based solely on the contribution from the laser pulse, showing that the laser contributes some 50% of the observed effect over the range of zero to 1000 photons. We find agreement between the observations and the model at the lower return levels, where the model agrees with the observed change at the 1-2 mm level. However, at the higher levels of return, the model over-estimates the total effect by some 8 mm, and does not fully model the observed increase in single-shot precision. Clearly, we have over-estimated the timewalk intrinsic to the SPAD. The results from this experiment suggest that the timewalk for our device is some 15mm, or 100 ps, over a dynamic range of from zero to 200 photons.

2. 3. SATELLITE RANGING.

We might expect that the bias effects measured from target-board ranging would also be present during satellite ranging if we depart from the single-photon regime. For this experiment, we observed nighttime passes of the satellites ERS-1, Meteor-3, starlette, Stella, Lageos and Topex/Poseidon. At intervals throughout each pass the return levels were changed rapidly between single and multi-photons by removing or inserting ND filters in the receive path. For each pass the single-photon

observations were reduced in the standard way, and then the deduced smoothing functions removed from the multi-photon data. The post solution residuals for all six passes are shown in Figure 3, where 'steps' of between 10 and 40 mm are clearly evident. For each pass we have computed separately the peak values and precision of the single and multi-photon sections of the data, and these values are displayed in Figure 4. From the known densities of the ND filters required to maintain single-photon levels we have estimated the numbers Np of photons reaching the detector during the high-level return phases.

2. 4. MODELLING OF SATELLITE RESULTS.

Analogous to our model of the target-board results, we have modelled the satellite 'steps' as a function of the numbers of photons reaching the detector. We digitized the responses for Lageos and ERS-1 from the curves derived by Degnan (1993), estimated the Starlette and Stella responses from the same source, and used the Topex/Poseidon responses of Varghese (Varghese and Pearlman, 1992). We do not currently have a model of the response of the small Meteor–3 LRA. We convolved these responses with our system response as characterized by the temporal distribution of the target-board ranges, and sampled from the resulting probability distributions in order to predict the range 'steps'. The results of the pass–averaged high and low-energy residual peak values and precision estimates, and the observed and predicted steps are shown in the Table, along with the mean numbers of photons Np. In most cases as expected the multi-photon data has the greater single-shot precision, and the predicted 'steps' are in reasonable agreement with the observations, given the quoted observational precision values. We also note that we have observed only one pass for each satellite.

TABLE I

Summary of satellite ranging and modelling results.

Sat	Single-photon		Multi-photon		Np	Step	
	Peak	rms	Peak	rms		Observed	Modelled
	mm	mm	mm	mm		mm	mm
ERS-1	+24	11	0	9	80	-24	-30
Meteor	+18	14	0	11	20	-18	-
Star	+5	19	-10	14	6	-15	-10
Stell	0	12	-20	13	12	-20	-15
Lag-2	0	16	-12	15	5	-12	-9
Topex	+35	25	0	10	100	-35	-50

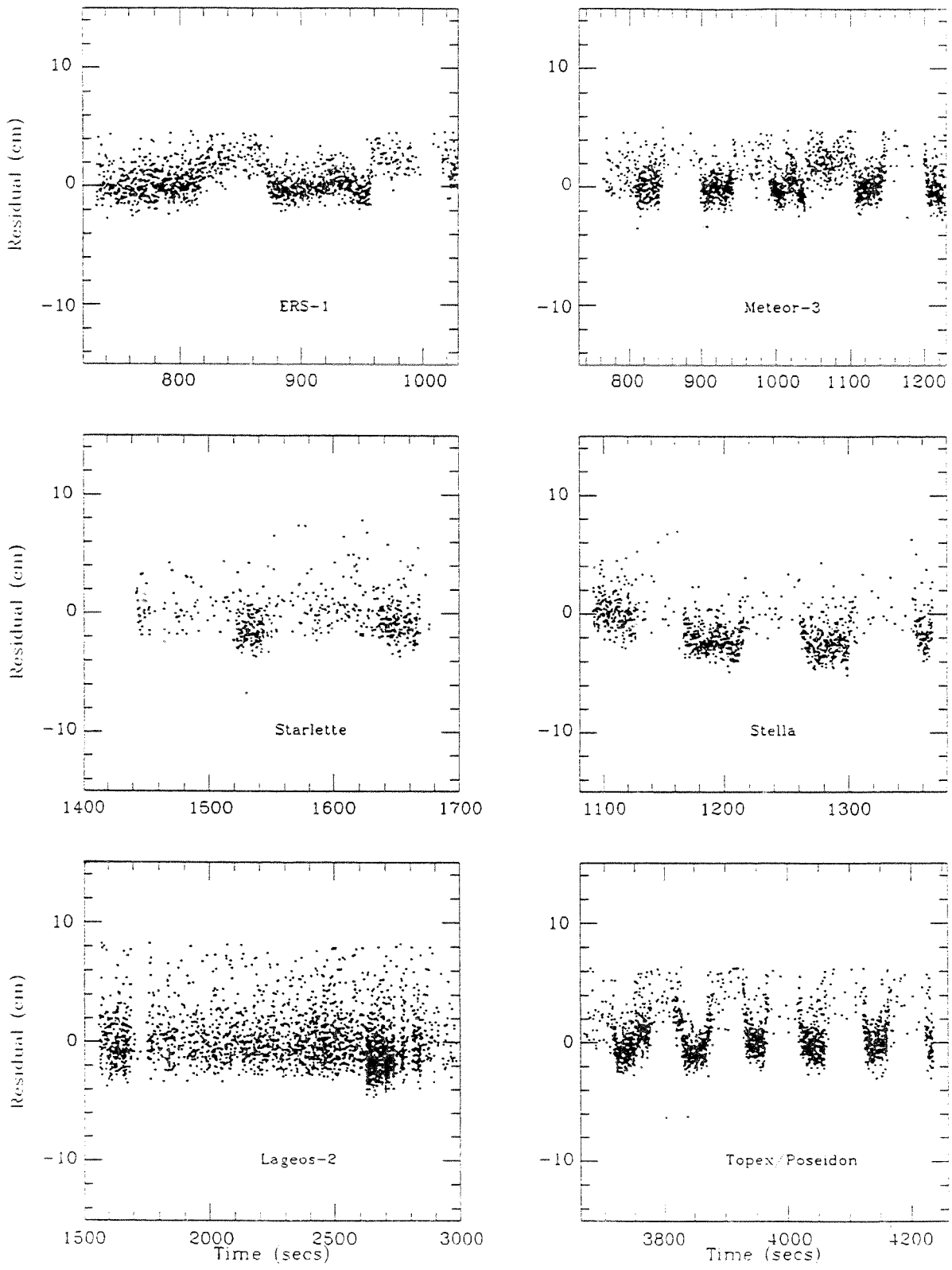

Fig. 3. Satellite range residuals with rapid return-level changes - raw data

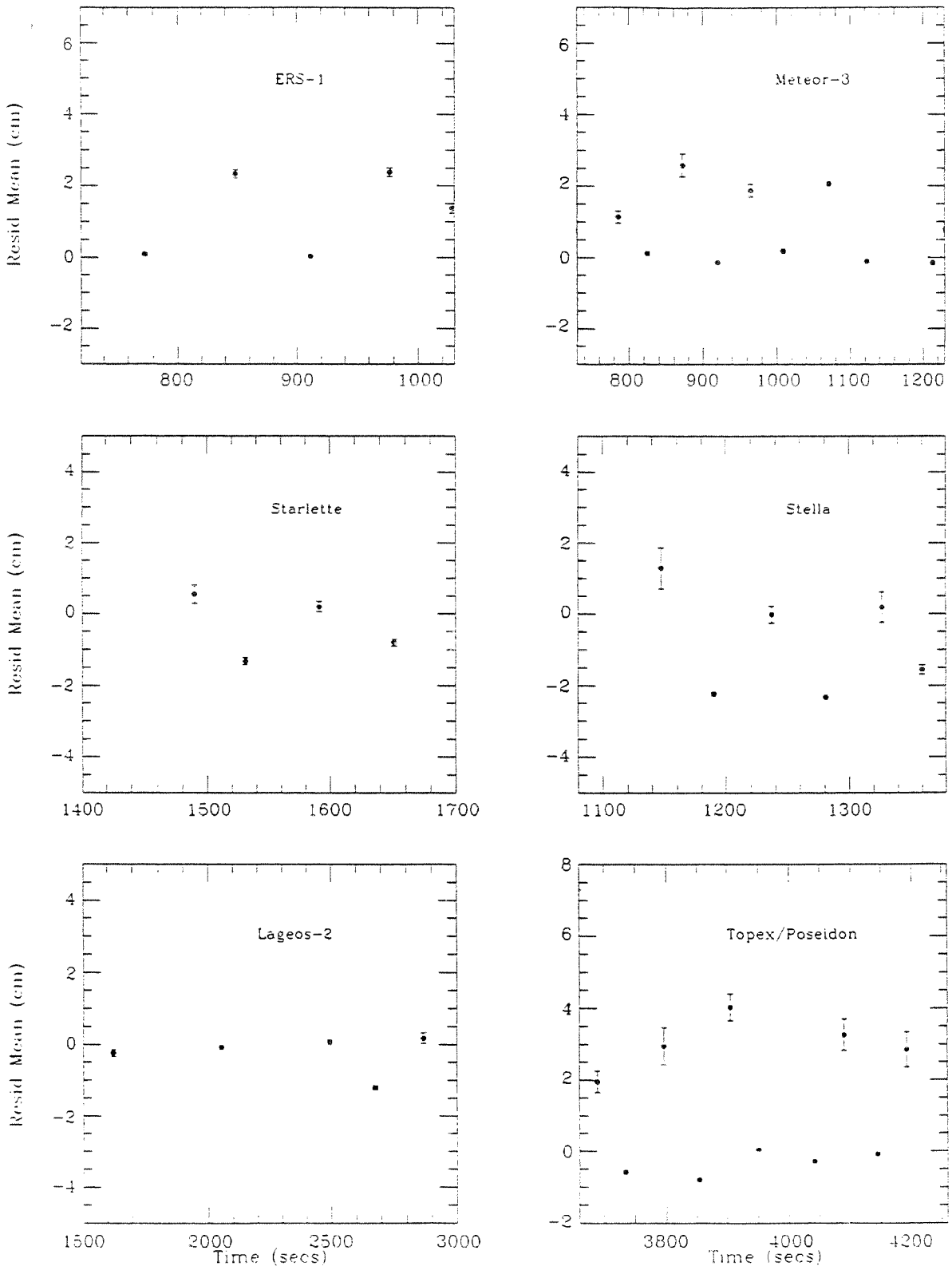

Fig. 4. Satellite range residuals with rapid return–level changes - mean values

3. Operational implications.

3. 1. BIAS REMOVAL

The results of this study imply that unless during all ranging sessions we carefully remain within the single-photon regime, we must take account on a short timescale of the resulting range biases. On an experimental basis, we have tested the feasibility of this approach by carrying out limited satellite ranging during which we allowed the return rate to vary during the pass without the normal practice of insertion of ND filters. During the pre-processing stage, return rates were estimated at intervals corresponding to the quicklook normal point bins. Using a linear fit to the data in figure 2 for the 0-100% level, we have corrected the single-photon calibration value to that appropriate for the particular rate pertaining in each bin. An example of the application of this procedure is shown in Figure 5, where residuals from a pass of Meteor-3 in June 1994 show obvious energy-dependent steps. The steps have been removed by the above procedure as shown in the second plot. We stress that this process was carried out on an experimental basis, and that the corrections to the calibration values are not model-dependent, being derived from the target-board observations.

3. 2. CENTRE–OF–MASS CORRECTIONS.

The above procedure has been shown to successfully remove observational bias from data departing from the single-photon level. However we consider that there is a further complication if account is not properly taken of energy variations. Using our Lageos response model, we find that for returns at the single-photon level the CoM correction is 250 $\pm$2mm which agrees well with the 250.2mm derived by Degnan (1993), and with the 251mm currently recommended to analysts (IERS standards, 1992). However even a modest departure from single photons results in changes of several mm to this value; at a level of 5 photons the CoM correction is 254 $\pm$2mm, at 15 photons the value is 259 $\pm$2mm. For Topex/Poseidon where large return levels are readily available, our simulations indicate that the CoM correction changes by 20mm over a range of return levels from single to about 15 photons. Clearly in order that analysts can apply appropriate CoM corrections to each normal point, the data record will have to include some measure (return rate, number of photons) of the mean return signal levels during each normal point.

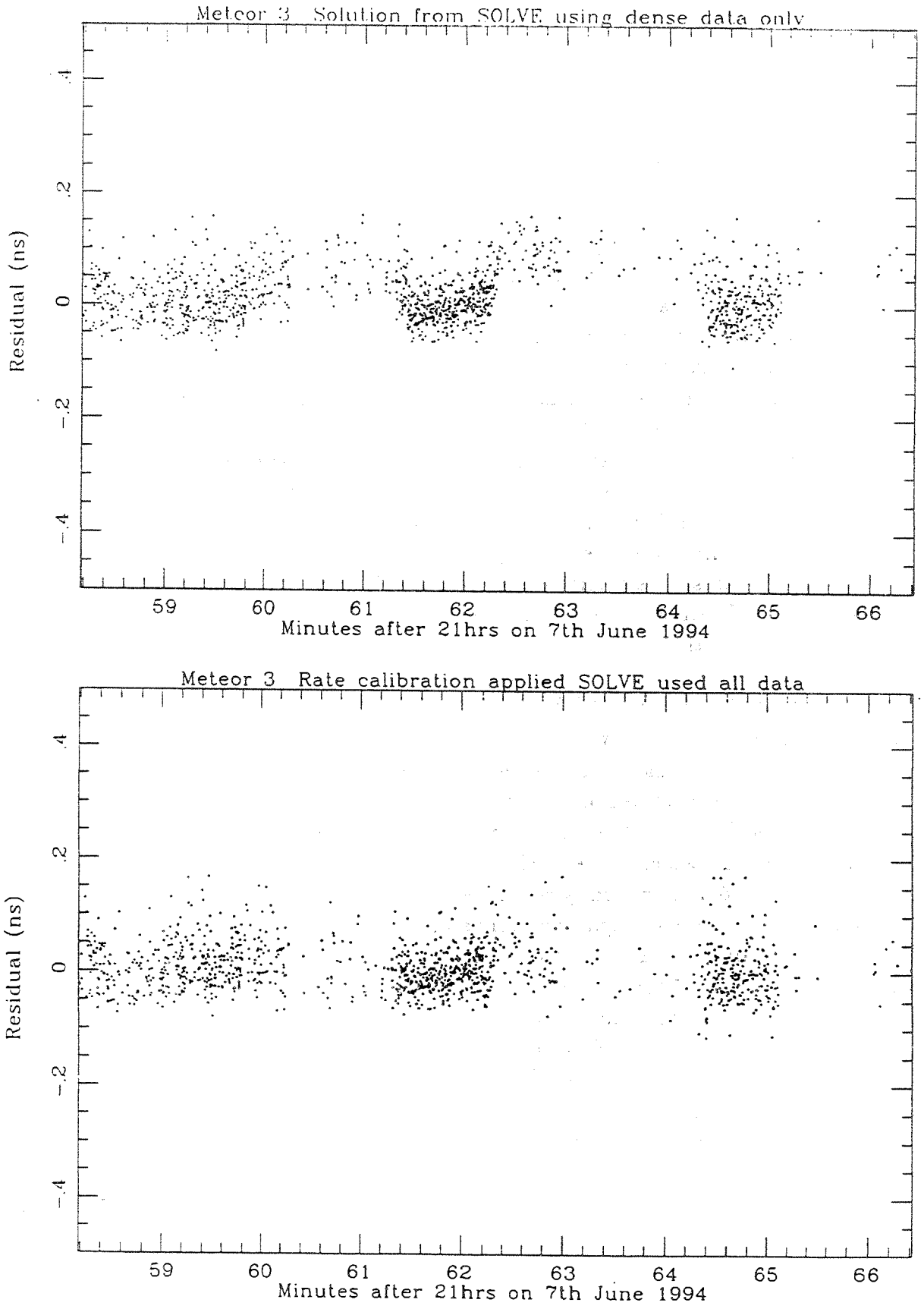

Fig. 5. Meteor-3 pass with return level variations; raw and corrected data

4. Conclusion.

We have shown that for our SPAD-based system, departure from the regime of single-photon return levels will result in range bias. We have experimentally examined the degree of bias as a function of return level, over a range of energy from single to 1000 photons. Simple statistical modelling of the system adequately explains the observational results, and implies that finite pulse-length accounts for about half the bias, and a plausible degree of energy-dependent time-walk within the SPAD system accounts for the remainder. For satellite ranging we find similar energy-dependent biases, which again are adequately explained by our models which include the effect of each satellite's response function. We conclude that if significant departures from single photons do occur during satellite passes, then the data should either be corrected using a measurement of the calibration dependence of the system on receive energy level, or sufficient information on the actual receive energy be included with each raw data point or normal point in order that analysts be able to compute appropriate CoM corrections. We finally note that provided calibration ranging and satellite ranging continue to be carried out at a strictly single- photon level, our normal practice, then range bias is minimal, at the expense of some loss of single-shot precision.

References

Appleby, G.M, 1993. Satellite Signatures in SLR Observations, NASA Conf. Proc 3214, Eighth International Workshop on Laser Ranging Instrumentation, Anapolis, MD, May 1992.

Cova, S, M. Ghioni, A. Lacaita and G. Ripamonti, 1990. Avalanche photodiodes optimized for single–photon detection, proc Seventh International Workshop on Laser Ranging Instrumentation, Matera, Italy, October 1989.

Degnan, J.J, 1993. Millimeter Accuracy Satellite Laser Ranging : A Review. Contributions of Space Geodesy to Geodynamics : Technology, Geodynamics 25, AGU.

IERS (1992). International Earth Rotation Service Technical Note 13, *IERS Standards*, Observatoire de Paris.

Prochazka, I, 1993. Single Photon Avalanche Diode Detector Package; Upgrade kit for RGO, July 1993.

Varghese, T and M. Pearlman, 1992 September. SPAD Operations on the Topex/Poseidon Retroreflector Array, Private Communication.

TARGET CHARACTERIZATION USING SINGLE PHOTON LASER RANGING ON SPAD

I.Procházka, J.Blazej

Faculty of Nuclear Science and Physical Engineering
Czech Technical University
Brehova 7, 115 19 Prague 1, Czech Republic
ph +42 2 85762246, fax +42 2 85762252, prochazk@earn.cvut.cz

Abstract

We are reporting on the capabilities of a Single Photon Avalanche Diode (SPAD) based receiver in target characterization in laser ranging. In an indoor calibration experiment we did determine the ultimate resolution in the "target depth" of the identical corner cube reflectors array. Ranging to the TOPEX satellite in Graz, employing SPAD based receiver, we have demonstrated the possibility to resolve individual corner cubes within the satellite retro array.

General

The single photon response of the SPAD based detectors and the high timing resolution of the whole laser ranging system permit to resolve a non standard data distribution in the satellite laser echoes ([1],[2] and others). To study this effect in detail, an indoor test facility has been established at the Czech Technical University. The goals of the work is to determine the ultimate timing resolution of the SPAD based receiver itself, to record the nonstandard data distribution attributed to the SPAD and to establish a test bed for the corner cube retroreflector array response studies.

Experimental setup

The block scheme is on Fig.1. As a laser source, the Hamamatsu laser diode pulser PLP01, provided by the Satellite Laser Station Graz, is used. The diode produces pulses FWHM=32 picoseconds. Its output is recollimated and spatially filtered, the transmitted / received signal path is separated by 50% beam splitting cube. The beam is expanded to the diameter needed to cover the whole corner cube array of interest : up to 300 millimeters. The short time intervals are measured using the time to amplitude converter and the amplitude analyzer card installed in a personal computer. The timing resolution of this setup is about 30 picoseconds FWHM. In the indoor experiments, the uncooled 100 micrometer SPAD biased 2 to 4 Volts above its break has been used. The repetition rate of measurements is controlled by external pulse generator, the standard value is 10 kHz. The temporal resolution of the whole loop : laser & SPAD & timing system is on Figure 2, the data distribution nonsysmetry inherent to a SPAD based detection may be seen.

Target depth resolution experiment

To measure the ultimate target depth resolution, we placed two identical corner retroreflectors into the flat wavefront. Changing consequently the depth separation of these reflectors, we did monitor the ranging data distribution width and shape, see Figure 3. The target depth of less than 4 millimeters may be detected by broadening the

data distribution curve. Two independent peaks in the data distribution may be resolved for the target depth larger than 10 millimeters.

Examining one large corner cube retrorelfector, we have measured the position of the point invariant to the angle of incidence of the input beam. Rotating the corner cube around this point, the signal propagation delay is not changing. For glass cube, this point is located inside the tube.

Satellite signature resolution

On the Satellite Laser Station Graz, Austria, the SPAD based receiver package is used, the diode is biased up to 10 Volts above its break voltage [3]. Employing the Raman shifted second harmonic of YAG, which is producing the picosecond pulse with extremely steep leading edge, the TOPEX satellite has been ranged. The ranging residuals are plotted on Figure 4. The "undulation" of the leading edge of the data distribution may be seen. This effect has been identified as the contribution of individual corner cubes within the TOPEX retro array. The returns have been obtained at high zenithal distances, larger than 70 degrees, the echo signal was multiphoton. Considering : the laser ranging geometry, the angular dependence Satellite-Observer, the "undulation period" corresponds quite well to the individual cornercubes geometry. The observed effect is a combination of several contributions : target depth, detector time walk effect and effects of partial coherent reflection.

Conclusion

The target signature indoor testing facility based on the SPAD detection technique has been established at the Czech Technical University. Its timing resolution is typically 70 picoseconds FWHM. The target depth bellow 4 millimeters is detectable. The maximum diameter of the target under test is 300 millimeters. Up to now, the tests are limited to the single photon characterization, the energy budget link of the experiment may be improved using the 35 picosecond passively mode-locked NdYAG laser in the future. The contributions of the individual corner cubes of the TOPEX satellite have been identified.

[1] G.M.Appleby, Satellite signatures in SLR observations, Proceedings of the International Workshop on the Laser Ranging Instrumentation, Annapolis, MD, May 1992

[2] A.T.Sinclair, 1992 SLR data screening; location of peak of data distribution, Proceedings of the International Workshop on the Laser Ranging Instrumentation, Annapolis, MD, May 1992

[3] G.Kirchner, SLR Graz, private communication

LASER RANGING TARGET CHARACTERIZATION

Block scheme

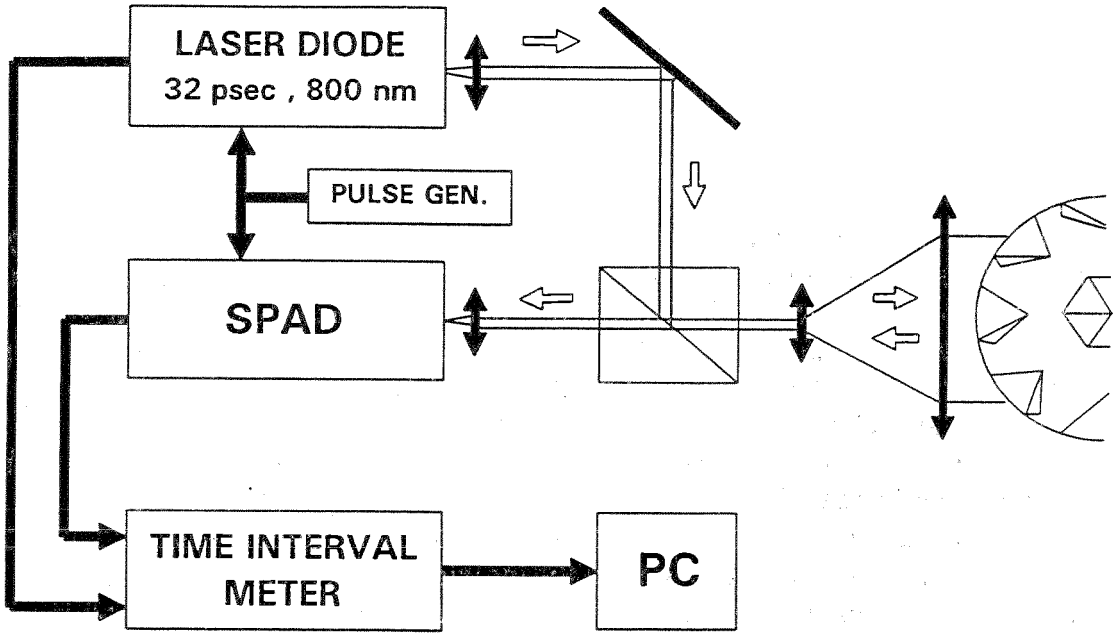

J.Blazej, I.Prochazka, Prague Feb.94

Figure 1

LASER RANGING TARGET CHARACTERIZATION

System temporal resolution, indoor exp.

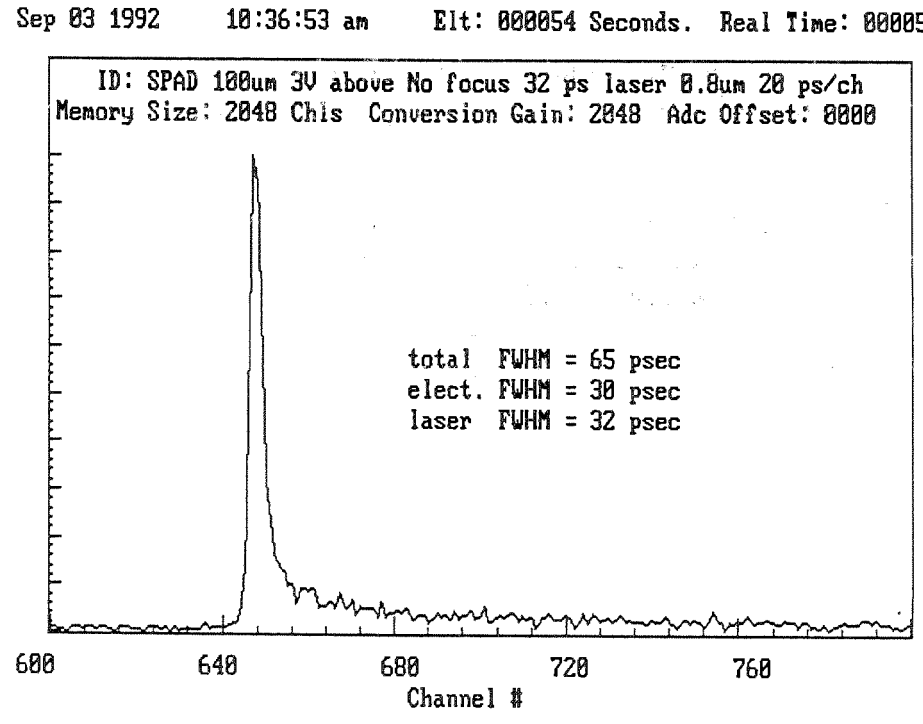

I.Prochazka, J.Blazej, Canberra, 1994

Figure 2

LASER RANGING TARGET CHARACTERIZATION

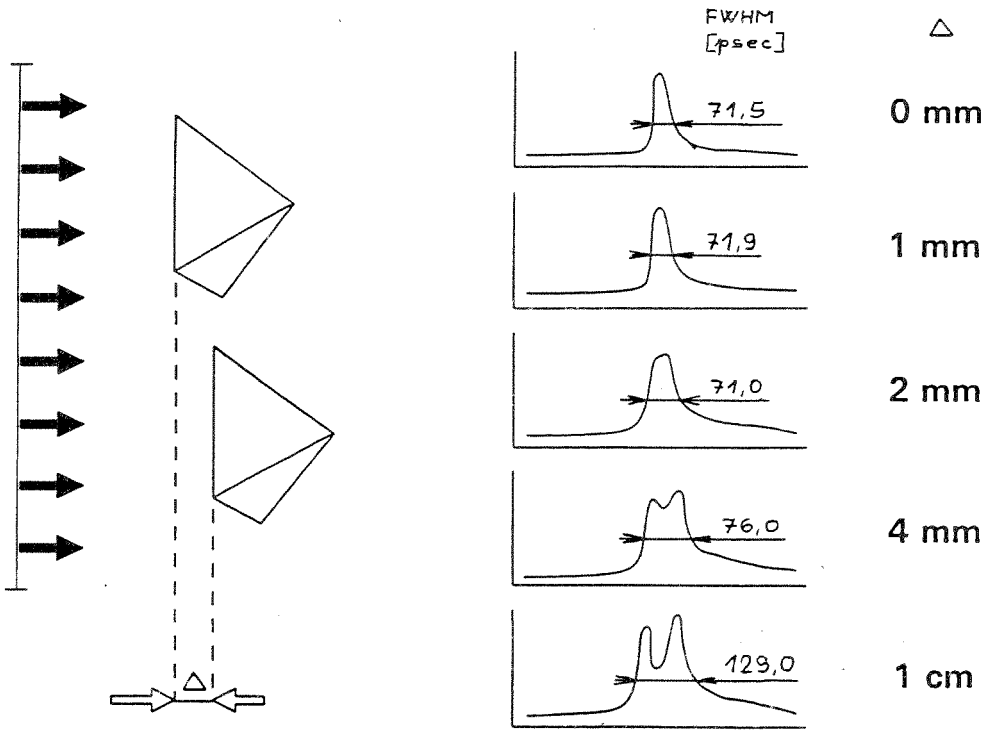

Figure 3

LASER RANGING TARGET CHARACTERIZATION

TOPEX array individual cubes resolution
Zenith dist.>70 deg, Raman pulses 0.68um

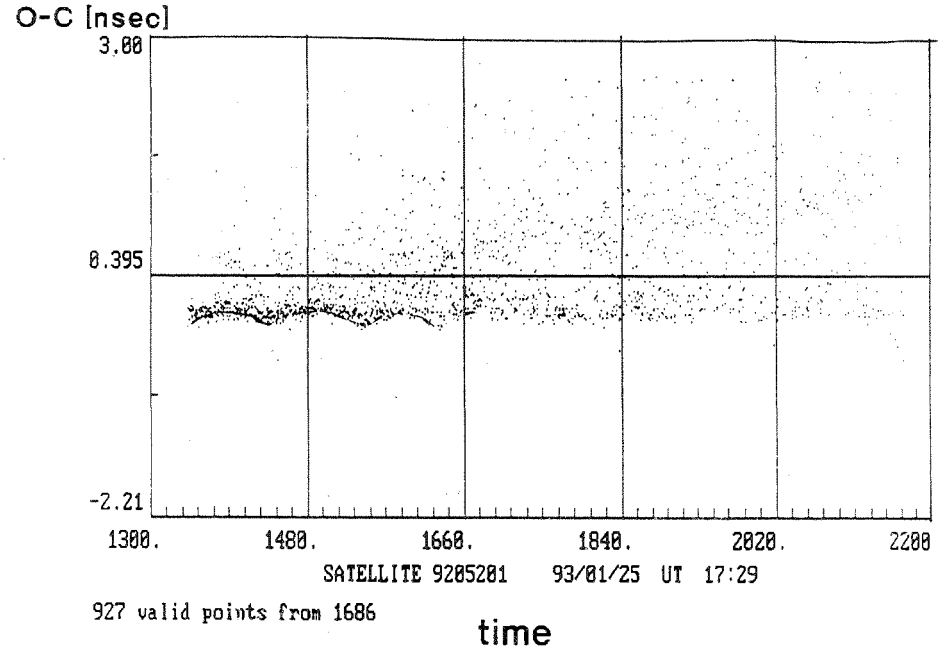

Kirchner,Koidl,Prochazka,Hamal ; Graz'93

Figure 4

Determination of Satellite Signatures and Time Walk Effects in Graz

G. Kirchner, F. Koidl

Institute for Space Research
Observatory Lustbühel
Lustbühelstrasse 46
A-8042 GRAZ

AUSTRIA

Abstract

Using Single-Photon-Avalanche-Diodes (SPADs) as detectors, some stations had measured significant time walk effects (up to nanosecs) at terrestrial target ranging, when using high return signal levels. It can be shown however, that these return levels are unrealistically high and can not be achieved using standard ranging configuration in Graz. Comparison with similar measurements at other stations show that this effect strongly depends on the used SPAD type, range of received energy, satellite signatures etc.

In addition, we use our high return rates (e.g. more than 25.000 returns per LAGEOS pass; worldwide highest average return rate - 1400 returns per pass - from ERS1 etc.) and the routinely used SemiTrain technique, to check for and to determine also any satellite signatures in our data.

1.0 Measuring time walk effects using different energy levels

To verify time walk effects due to different return energy levels, we switched during actual passes between maximum and minimum laser energy by changing the delay of the double pass laser amplifier; the switching was done within 1 s or so; switching times were chosen according to the Normal Point time slots for the specific satellite, so that we observed one NP with maximum energy, the next NP with minimum energy and so on; this allowed easy analysis of any resulting effects by using our standard programs.

We used our standard setup for routine ranging:

- 20 mJ SemiTrain (≈ 15 Pulses max.), 532 nm, 35 ps, 10 Hz; this means that the strongest pulses will have only a few mJ;
- SPAD (Prague, 100 μm, 11 V above Break, Peltier cooled -15°C;
- Improved leading edge trigger board;
- Linear Start Pulse Detector etc.

Maximum energy is our usual operational energy of the Nd:YAG laser (20 mJ SemiTrain; i.e. only a few mJ for the first pulse); the laser divergence was minimized to get highest possible return energy; most satellites were visible in the ISIT camera, allowing optimum tracking.

Minimum energy was adjusted to give reliable Single-Photon-Returns (return rate below 20%, full SemiTrain visible) for each satellite:

- 5.0 mJ in 15 SemiTrain pulses for LAGEOS;
- 0.5 mJ in 15 SemiTrain pulses for ERS1, Stella;
- 0.1 mJ in 15 SemiTrain pulses for TOPEX

All measurements have been handled with our standard post-processing programs; the degrees of all polynomial fits used in the procedures were kept low enough - as compared to the collected number of Normal Points - not to remove any potential signatures.

1.1 Results from LAGEOS measurements

A few LAGEOS passes were observed, with switching the laser energy between 20 mJ and 5 mJ, in the 2-minute NP intervals; no variation could be observed in the residuals (fig.1); there is always the full SemiTrain visible, indicating that return energies are not very far from the few photon level.

After folding of the SemiTrain (fig.2), a slight "modulation" of the return density becomes visible; plotting the Normal Points (fig.4), again a very slight - and interpretative - modulation can be seen; the measured steps are about 1.5 ± 0.7 mm, in the order of the NP accuracy.

To check and verify any influence of the SemiTrain, the same data set was used, but now without SemiTrain (first track only; fig.3); the steps are better pronounced now, about 2.1 ± 0.3 mm); this indicates that the SemiTrain returns are more or less Single Photon-Electrons only, and tend to cover slightly the energy step effect.

These values coincide with the direct results from our SemiTrain statistics (fig. 5), which gives an average of 2 mm between first track (few PE) and SemiTrain tracks (SPE only) of Lageos.

Comparing this with results from calibration runs (where no such variations are visible in this energy range), the modulation could be explained with the weak LAGEOS satellite signature.

1.2 Results from lower satellites

Similar measurements were made with lower satellites; while Starlette and Stella showed only little time walk (similar to LAGEOS), ERS1 showed noticeable effects.

For ERS1-ranging, the SemiTrain energy was switched between 20 mJ and 0.1 mJ; with 20 mJ, minimum divergence, and ERS1 in earth shadow, a fraction of the return energy can be observed with the ISIT; this ensures maximum possible return levels.

After SemiTrain folding, again Normal Points are calculated; most pairs of consecutive NPs here show a standard step, with step size of about 12 ± 5 mm; as the theoretical ERS1 satellite signature should be much smaller, this step can be explained by the laser pulse rising edge (pulse width is 35 ps FWHM).

Ranging to Topex with energy switching (Factor again 1:200) shows similar steps of 15 ± 4.5 mm; due to the strange retro array, a large satellite signature is expected anyway, which hides any SPAD biases etc.

2.0 Measuring time walk and/or satellite signature using the SemiTrain

During the last years, we measured all passes using the SemiTrain technique; this has a number of advantages:

- It increases the number of returns, especially for low return signal conditions (LAGEOS ≈ +70%, GPS35/36 ≈ +350% more returns);

- It allows use of quite low energies per pulse (typically 1 to 3 mJ), thus maintaining SPE levels AND high return rates at the same time;

- It allows simple real-time estimation of return signal strength: At levels significantly higher than a few PEs, the SemiTrain echoes will just disappear.

- It is used to identify and mark possible returns in real-time during ranging within the high noise of our SPE-sensitive system (especially useful during daylight tracking).

- It allows a rough estimate of time walk effects for return signal levels between 1 and a few 10 photons max.; this is described here.

The SemiTrain distance is determined, using calibration rangings to the terrestrial target, with an accuracy of ± 1 ps. The obtained value is used to "fold" also the SemiTrain returns from the satellites; all original information is kept within the result files. This allows later determination of total mean (mean of all "folded" returns), and also the mean of the single "folded" tracks of the SemiTrain. Scanning through these log files allows averaging of all mean values (total mean and single track mean) for the different satellites.

With no bias at all - and the correct SemiTrain distance - there should be no difference between total mean and single track values; but as plotted in fig. 5, the first track shows a significant deviation towards shorter ranges, while all other tracks are on the expected straight horizontal line. This leads to following conclusions:

- All SemiTrain echos (except those from the first track) are close to the SPE range (obviously!), showing no time walk effects at all;

- The first track shows a shift, depending on the satellite, towards shorter range; in most cases, the amount of this shift concides in first order with the theoretical values (as predicted by satellite signature and/or laser pulse width). The value of this shift is:

  - 2 mm for LAGEOS1/2, due mainly to satellite signature;
  - 3 mm for ERS1, due to laser pulse width and/or satellite signature.

For other satellites, the plotted values are higher, but should be interpreted with caution (due to higher signal strenths for the first track, the SemiTrain contributes less to the overall return number).

3.0 Measuring satellite signature using statistics

Due to the large number of returns per pass in Graz (1400 returns on ERS1 average, up to more than 20.000 returns from LAGEOS), we are able to apply statistical tests to all passes routinely; all evaluated values (peak, mean, skew, curtosis, median etc.) are stored also in log files.

The same values are stored for all routine calibrations; this allows us to check for example the Peak-Minus-Mean values also for all routine calibrations (fig.6); with an average value of -0.4 mm, we assume a more or less symmetric distribution of the calibration returns.

In LAGEOS passes, we have obviously a non-symmetric distribution (the skew is NON-Zero); due to satellite signature, the peak of the data is shifted by about 3 mm towards shorter ranges relative to the arithmetic mean (fig.7): While the Normal Points are calculated according to the standard arithmetic mean procedure, the peak is calculated using methods described in [1], and gives an indication of a "mean reflection point", thus directly effecting any Center-of-Mass correction.

Applying this for all passes of all satellites, we get some average peak-minus-mean values (fig.8, lower bars), which give a good indication of the signature of the various satellites:

- GPS35/36: The "ideal satellite" to check the ranging system for any biases: The array itself is flat, the incident angle never is far from 90°, and it only responds with single photons; so we get similar peak-mean (-0.3 mm) and RMS (≈ 6 to 7 mm) as from our flat calibration target; no signature is visible;

- ERS1 and METEOR 3 also have the expected low signature, but higher time walk effects due to higher return signal levels;

- LAGEOS (peak-minus-mean ≈ -3 mm) shows the expected signature;

- TOPEX and AJISAI are listed here for completeness, their signatures are quite high and not well defined; the deviation of their P-M values (fig.8, upper bars) therefore also shows higher values.

4.0 Conclusions and recommendations

The satellite signatures mentioned here are referred only to systems using Single Photon Detectors (SPADs), but multi-photon returns (with an upper limit for "multi" to be tested for each system; a few 10 photons should be the maximum in the Graz setup).

- The systems should check distribution of target measurements for any peak-minus-mean values; these should be low and insignificant;

- Calibration should be done not too far from Single Photon-Electron level; in Graz, a maximum return rate of 70% is used for calibration.

- Keep all returns from satellite below a tested and veryfied limit; a simple indication is the use of SemiTrain (even if the resulting additional returns are not used at all).

References:

[1] A.T. Sinclair: SLR Data Screening: Location of peak of data distribution; Proceedings of Eigth International Workshop on Laser Ranging Instrumentation, Annapolis, May 1992; p. 2-34 ff

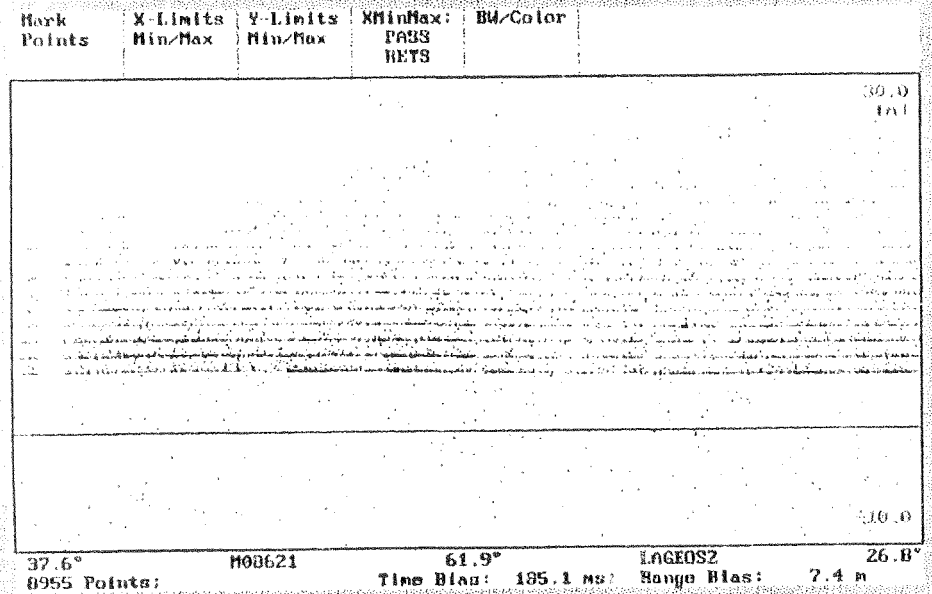

Fig. 1: LAGEOS 2 Residuals; with SemiTrain

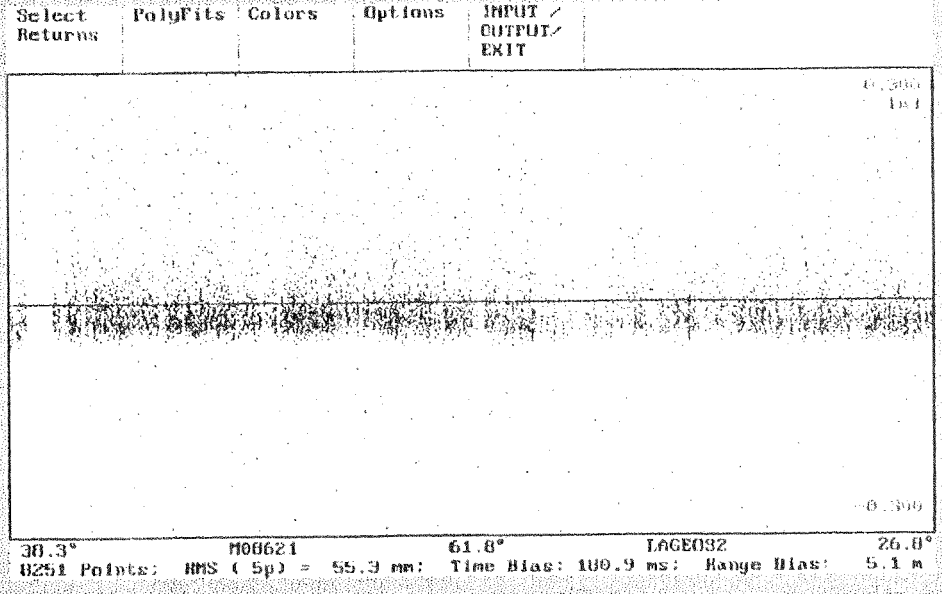

Fig. 2: LAGEOS 2 Residuals, after Folding of SemiTrain

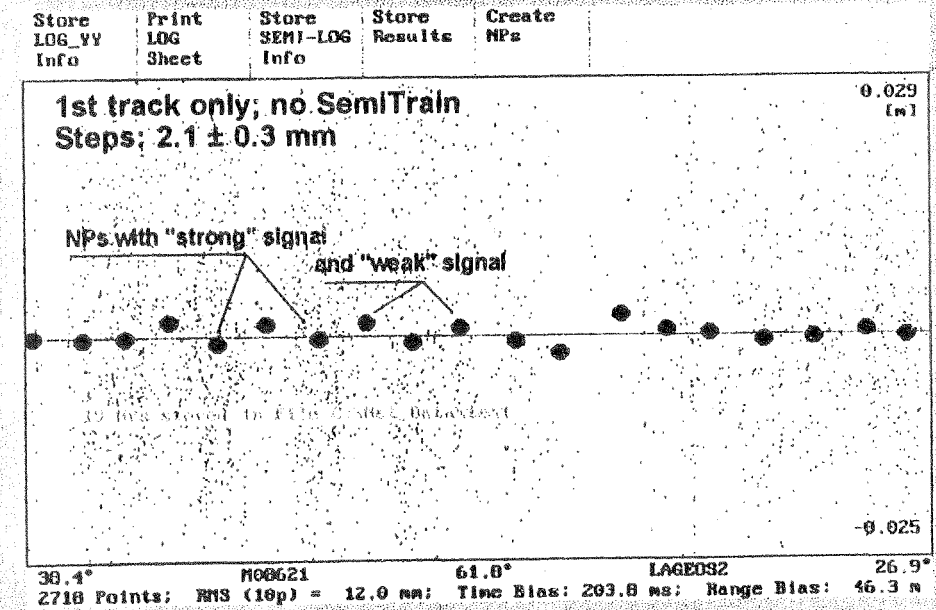

Fig. 3: Same Pass, with Normal Points; No SemiTrain

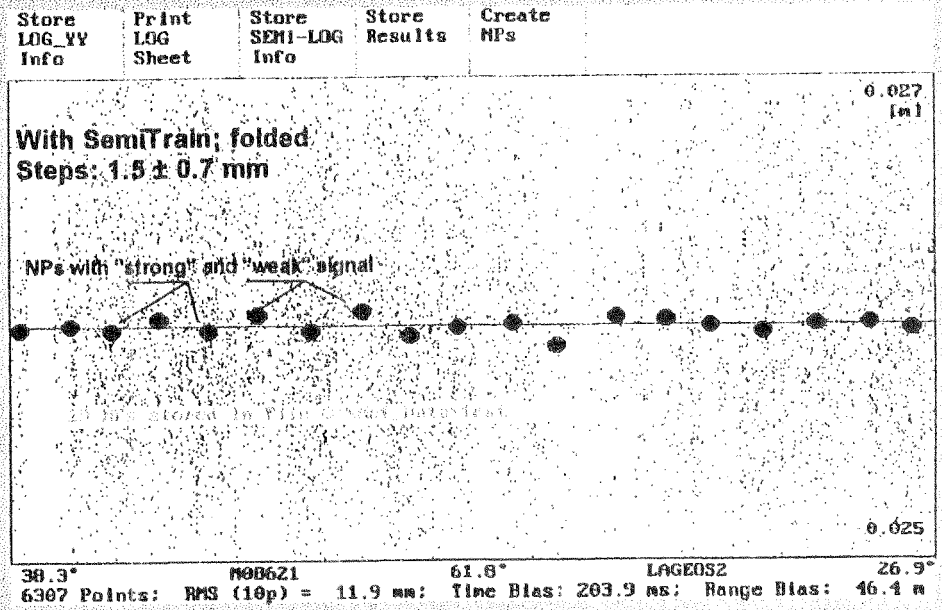

Fig. 4: Same Pass; with SemiTrain Returns

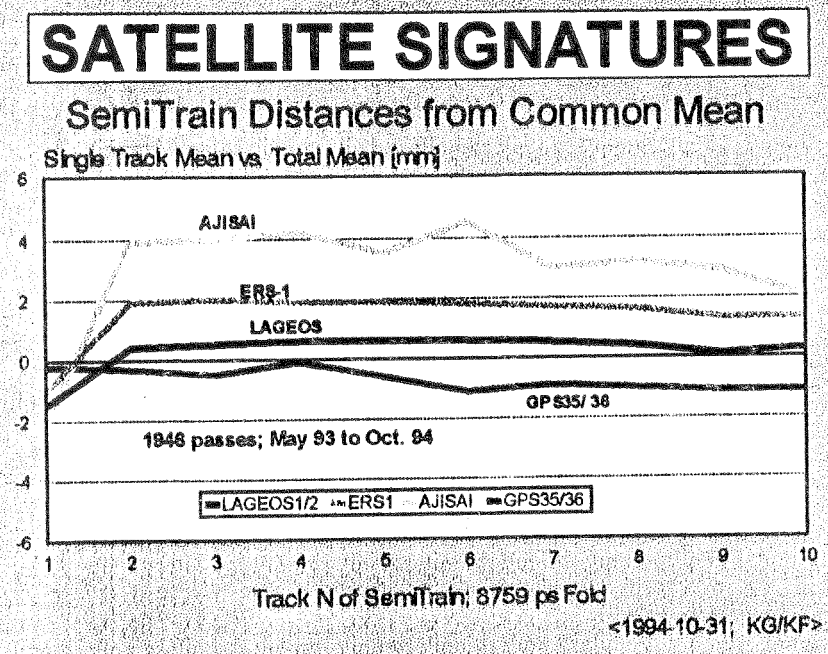

Fig. 5: SemiTrain distances from common mean

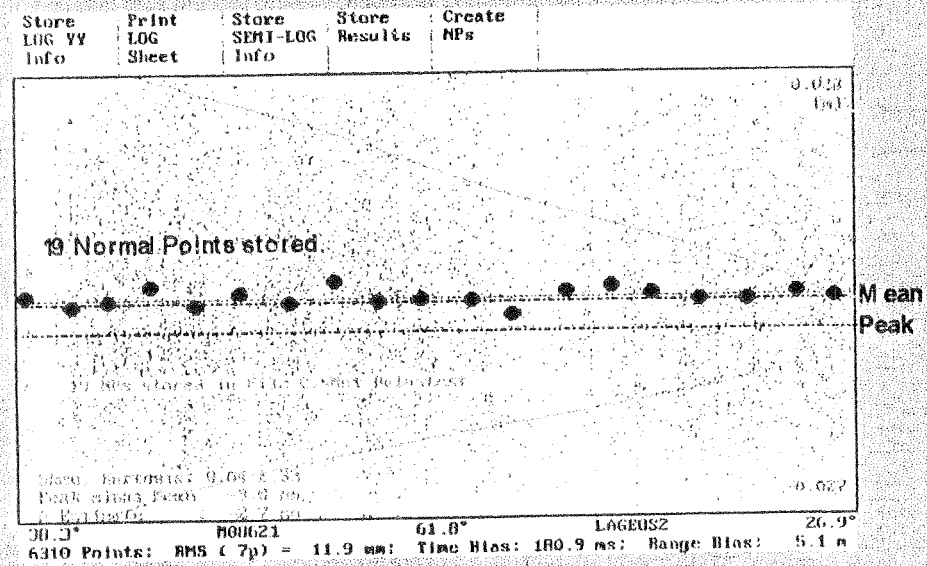

Fig. 7: LAGEOS 2: Peak Minus Mean: -3.0 mm

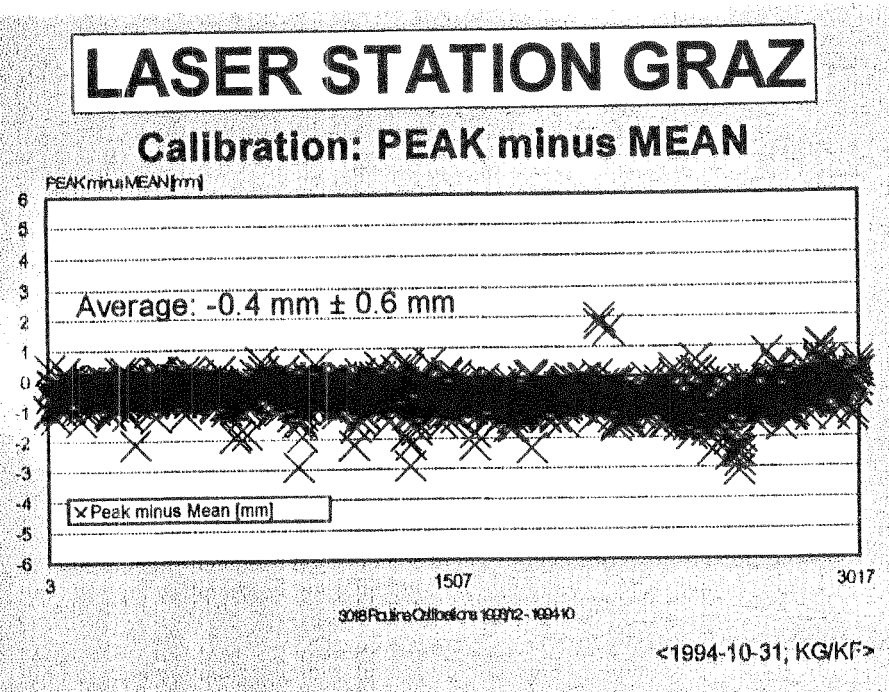

Fig. 6: Routine Calibrations: Peak Minus Mean

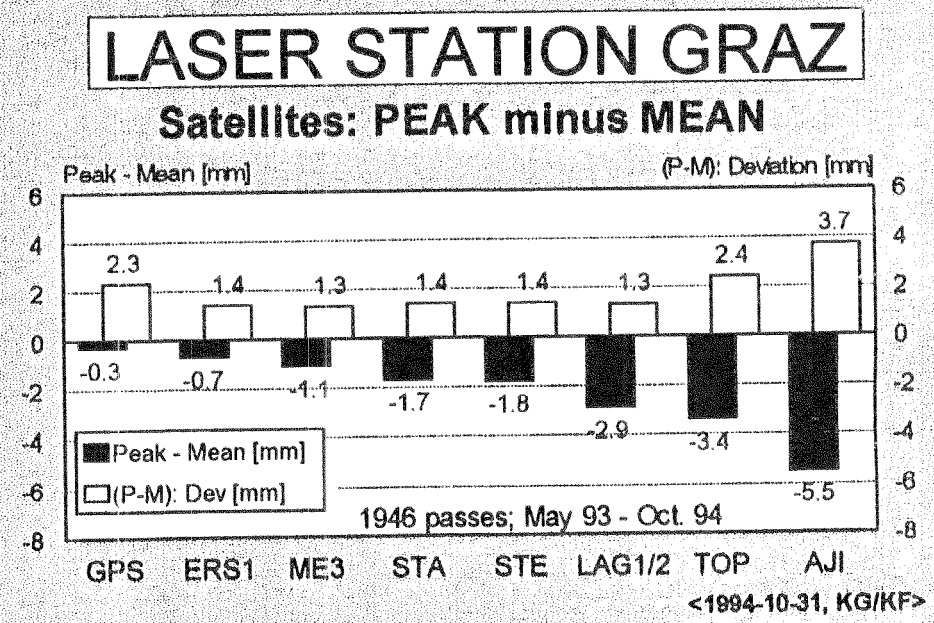

Fig. 8: All Satellites: Peak Minus Mean

Properties of Avalanche Photo Diodes

U. Schreiber, W. Maier
Forschungseinrichtung Satellitengeodäsie
Fundamentalstation Wettzell
D-93444 Kötzting
Germany

K. H. Haufe
Institut für Angewandte Geodäsie
Aussenstelle Wettzell
D-93444 Kötzting
Germany

B. Kriegel
Silicon Sensor GmbH
Ostendstrasse 1
D-12459 Berlin

Abstract

At the Wettzell Laser Ranging System the usefulness of various types of avalanche photo diodes (APD) operated in the Geiger mode has been under investigation since 1989. Their application in laser ranging is analysed and compared to the performance of microchannelplates and photomultipliers. From measurements of local targets at various levels of intensity, a significant offset from the expected range was obtained. The possible cause for this timewalk effect is discussed in this paper.

1. Introduction

One of the most remarkable properties of avalanche photo diodes in general is their high sensitivity for light detection in the single photon domain, which is far beyond that of photomultipliers, particularly in the red wavelength band. Moreover, these diodes do not require high voltages to be operated. Another good feature is, that unlike photomultipliers they can not be destroyed by excessive light exposure. However, there are drawbacks to be considered as well. APDs for ranging applications usually have a small photosensitive surface area. This makes the focussing of the aperture of the ranging telescope onto the chip difficult. Another problem is, that the behaviour of the various types of detectors is significantly different with respect to a precise timing of the detected laser pulse. Under normal conditions the photocurrent of a photomultiplier is proportional to the intensity of the incident signal. This is not the case for an APD operated in the Geiger mode. A

diode always shows a characteristic output signal shape. This is caused by the process of an avalanche breakdown. There is no change in shape or amplitude with the amount of input light.

2. Timing the propagation of light with an MCP and APD

When a MCP is used as a detector in a laser ranging system, variations of the amplitude of the output signal must be compensated, so that they do not cause a jitter in switching the ranging timer. This is achieved by using a constant fraction discriminator. By triggering at the half of the maximum voltage from the rising edge of the detected pulse, the jitter in timing is minimised. However, care must be taken, to adjust the discriminator properly, in order to be safe from systematic walk offs. Figure 1 shows a diagram, where the dependency of the detection of the time of flight of a laser pulse is plotted over the variation of the intensity. From the measurements it can be concluded, that the influence of the received signal strength can be neglected for the given setup. When the same experiment is carried out for an avalanche photo diode an entirely different behaviour can be seen. After some stability in the low light level regime, a dramatic walk off towards shorter ranges can be observed. The offset finally becomes as large as 1 ns. This can be seen in figure 2. Putting together the observed effects, one can find the following summary.

- Below a certain detection threshold, the distribution of the values of range measurements are following the expected statistics, including laser pulse width and jitter of the timing devices and the detectors.
- The return rate itself is proportional to the introduced light intensity. The shape of the obtained histogram is that of a Gaussian.
- Above this detection threshold the previously mentioned timewalk effects can be observed. With increasing amplitude of light, a progressive narrowing of the distribution of the ranges is found as well as an worsening asymmetry of the shape of the histogram. Towards shorter ranges, the slope becomes steeper, while it develops a 'tail' in the direction of longer ranges.

3. Modelling the observations

There have been continued discussions, concerning the idea, that an avalanche diode acts like a fast switch. The observed timewalk reflects the fact, that the duration of the incident laser pulse needs to be considered [1, 2] in the search for a source of the bias. This discussion is assuming one single retroreflector, so that the target geometry in the following can be neglected. At a very low light level, the photon which is causing an avalanche statistically originates from the center of the pulse, where the probability for detection is at a maximum. At higher intensities, a photon from the beginning of the laser pulse already has a high probability to trigger the avalanche. That means, that the observed timewalk is a representation of the laser's pulse shape. In other words, one is "walking" down the slope of the laser pulse, as the light intensity is increased. However this approach fails to

account for all the observations. It is misleading in that it produces unrealistic broad laser pulses too. Therefore some refinements to this model are neccessary.

Now let us consider a given threshold for the detection, which is fixed and located, where the normalised probability of detection becomes 1. As long as the input signal stays well below this threshold, one obtains a symmetric Gaussian shaped distribution of the range measurements. The probability of detection is proportional to the pulse amplitude and no bias is observed. This relation is plotted in figure 3. For amplitudes high above this threshold, the situation becomes different. When the signal exceeds the threshold and assuming, that no avalanche has been generated, then the probability of starting an avalanche in the next moment is again decreasing. In analogy to other processes in physics, such as the decay of an electric field at the boundary to some dielectric material, it is assumed, that the probability of detection also follows an exponential decay function. In figure 4 this behaviour is sketched. The shaded area shows the form of the histogram, that can be expected. It illustrates the observed asymmetry, the increasing sharpness of the measurements (when the intensity is so high, that the domain of the steepest increase in the Gaussian is reached) and it also accounts for a timewalk.

Taking the laser pulse to be of the shape of a Gaussian

$$I_s = I_0 e^{-a^2 \Delta t^2} \tag{1}$$

and solving for an offset Δt from the middle of the curve, one yields

$$\Delta t = \sqrt{\frac{ln \frac{I_0}{I_s}}{a^2}}, \tag{2}$$

or in a more general form

$$\Delta t = -\frac{1}{a}\sqrt{ln(sx)}, \tag{3}$$

where x is introduced, to allow for an adjustment along the horizontal intensity axis. Tuning the parameters s, x and a to the data and calculating theoretical curves for some laser pulses of different length, one obtains figure 5. As can be expected by this approach, there is a strong dependence between pulse width and timewalk. This conclusion however, must be regarded with caution, as we now show.

4. Experimantal Data

Data from five different photo diodes have been taken or was made available [3, 4]. Figure 6 shows a diagram of the same scale as figure 5. Obviously one can group the data into two different detector families. The detectors having less systematic walk off are all SPADs [5]. The other family are diodes such as the RCA 30902s and SSO AD-220 (Silicon Sensor). Different lasers have been used in either detector family for the measurements. This however contradicts the theoretical concept of section 3. Therefore one may conclude, that the

applied pulse width does not have the relevance which may be expected by looking at the problem and which has been considered in the previous section.

There are significant differences in the design of the diodes, which strongly suggest that the reason for the observed timewalk is related to a process within the semiconductor structure. The diode is essentially consisting of two layers relevant for the simplified understanding here. One is the absorption layer, the other the avalanche region. In the absorption layer, a incoming photon is absorbed by creating an electron- hole- pair. Assuming, that no recombination takes place, this pair is entering the avalanche region. In the Geiger mode the electric field in this layer is so large, that the accelerated electrons (holes) are generating secondary electrons (holes) by collision. This is called the multiplication process. A rapid growth of the current is the result. One has to keep in mind, that shortly after entering the avalanche region, electrons are soon moving at their maximum drift velocity. The multiplication process is fast, but not instantaneous. In fact it is dependent on many parameters, such as intensity and wavelength of exposed light intensity and of course to the temperature, composition and structure of the semiconductor chip. The level of the bias voltage, the amplitude of the Geiger pulse and the the external electronic circuit are also of importance. Therefore it is suggested, that the cause of the observed light intensity dependent timewalk is due to a shortening of the avalanche growing process by the injection of more than one photoelectron (hole) into the avalanche region. This process can be very complicated, because on one hand multiple avalanche sources are speeding up the growth, while on the other hand a growing avalanche causes depolarisation inside the avalanche region. This weakens the electric field and therefore the electron acceleration is decreased.

Looking at the observed properties in chapter 2 again, the threshold would then be the level of intensity, where the multiplication factor no longer is constant due to additional avalanche sources. The skewness of the "high intensity" histogram could be interpreted as a probability of recording an event on a low multiplication factor compared to one, caused by a high factor. The sharp rise of the histogram towards shorter ranges reflects the fact, that the multiplication factor can not become infinite.

Figure 7 illustrates another example of a variation in the avalanche growing process. The residual plot shows a LAGEOS pass, tracked simultaneously on two frequencies ($\lambda_1 = 0.532\mu m$ and $\lambda_2 = 1.06\mu m$), using the same avalanche diode as a detector. The elevation angle dependent spacing between the two tracks of residuals is due to dispersion in the atmosphere. However, to adjust the measurement to the atmospheric model, a constant offset value of as much as $200ps$ needs to be inserted.

5. Conclusions

Starting with some experience gained by using avalanche diodes, a theoretical understanding of observed effects has been attempted. The initial model looked at the probability of starting an avalanche with respect to the length of the laser pulse. Unlike other models, it could also account for the observed asymmetry of range histograms at high laser intensities. But it failed to predict the right amount of the observed timewalk.

By grouping all available data from various diodes together, a systematic offset between diodes of different structure became evident. Finally the multipication process of the

avalanche buildup was identified as the cause for the bias. There is also a bias between simultaneous range measurements on two different frequencies for the same reason.

References

[1] R. Neubert, "Modelling Bias Effects of APDs", *Oral presentation from a meeting about the characteristics of APDs*, held in Graz, March (1994)

[2] G. Appleby, "Satellite Signature Effects and APD Characteristics",*Oral presentation from a meeting about the characteristics of APDs*, held in Graz, March (1994)

[3] L. Grunwaldt, R. Neubert, Li Ya, "Operational Characteristics Of Commercial Silicon Avalanche Photodiodes For Use As Laser Radar Receivers", *Proceedings Of 7th International Workshop on Laser Ranging Instrumentation*, (1989)

[4] G. Appleby, private communications (1993)

[5] I. Prochazka, K. Hamal, B. Sopko, "Photodiode Based Detektor Package For Centimeter Satellite Ranging", *Proceedings Of 7th International Workshop on Laser Ranging Instrumentation*, (1989)

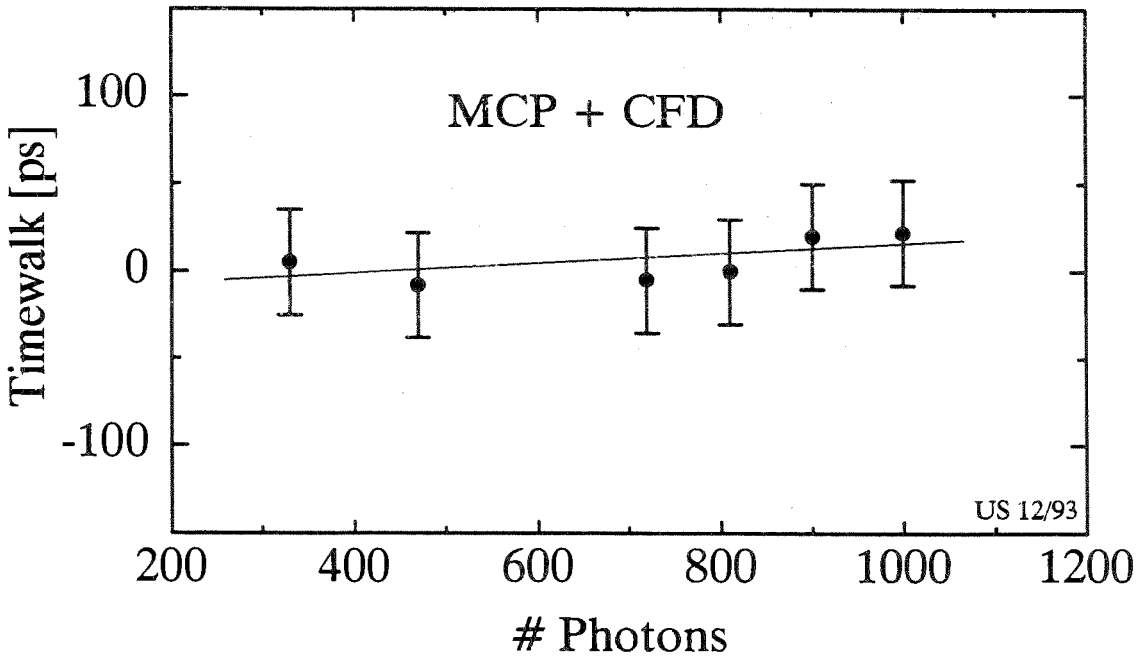

Figure 1: The diagram shows the dependency of the recorded time of flight along a constant path. The intensity of the laser pulse was varied over a critical region. The detector is a microchannel plate (MCP). A constant fraction discriminator is used to compensate changes in the laser amplitude

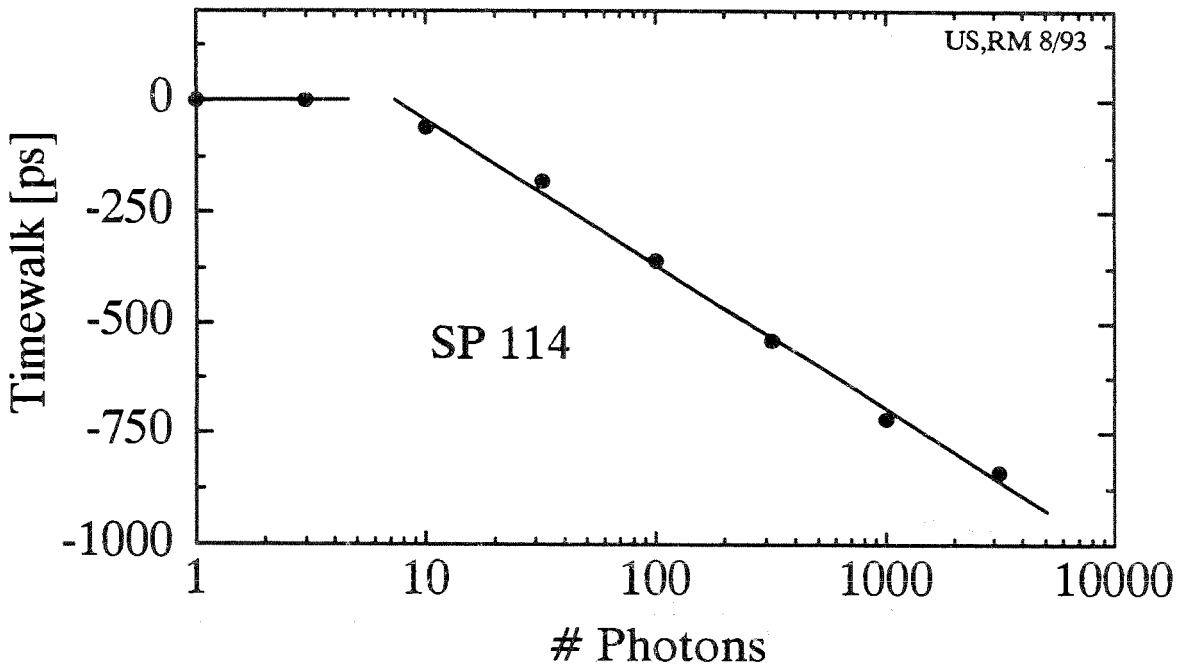

Figure 2: The dependency of the recorded time of flight of a laser pulse over a constant path. The intensity of the laser pulse was varied over a broad region. The detector is an avalanche diode

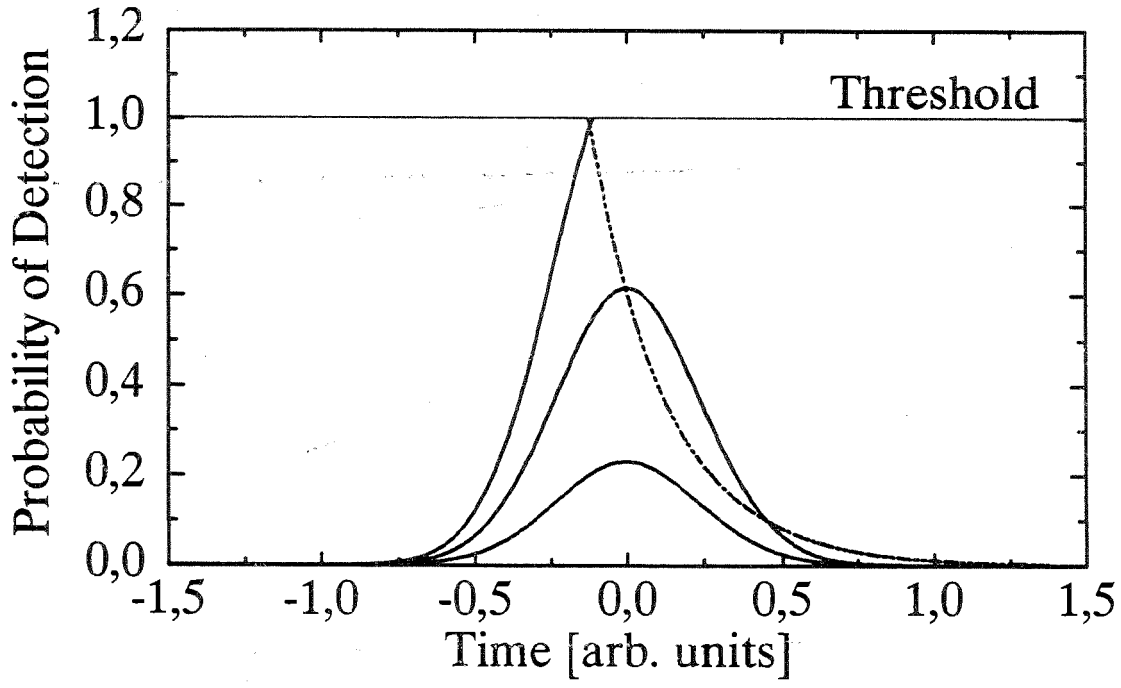

Figure 3: An illustration of the distribution of repeated range measurements for two characteristic situations. For pulse amplitudes well below the detection threshold no bias is observed. The data rate is directly proportional to the light intensity. For pulses exceeding the treshold an asymmetry in the shape of the histogram is obtained, as well as a bias for the range

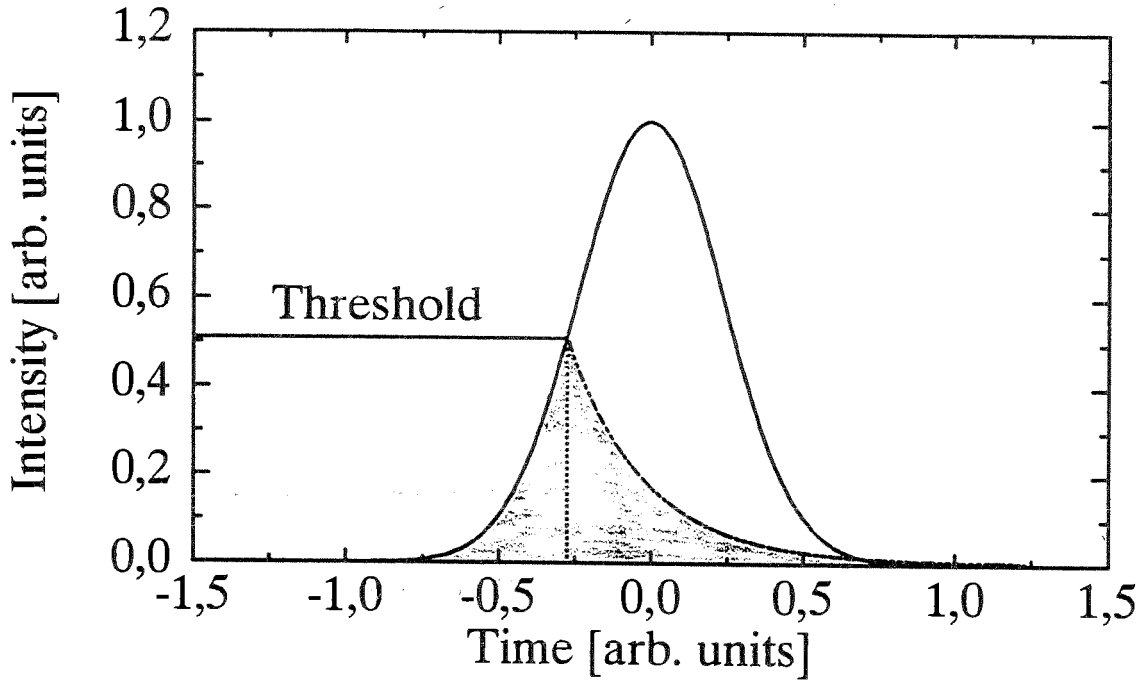

Figure 4: The shape of the modeled histogram for pulses at intensities high above the detection threshold. The falling edge of the histogram (shaded area) is represented by an exponential decay function to account for the observed skewness in the histograms of real measurements

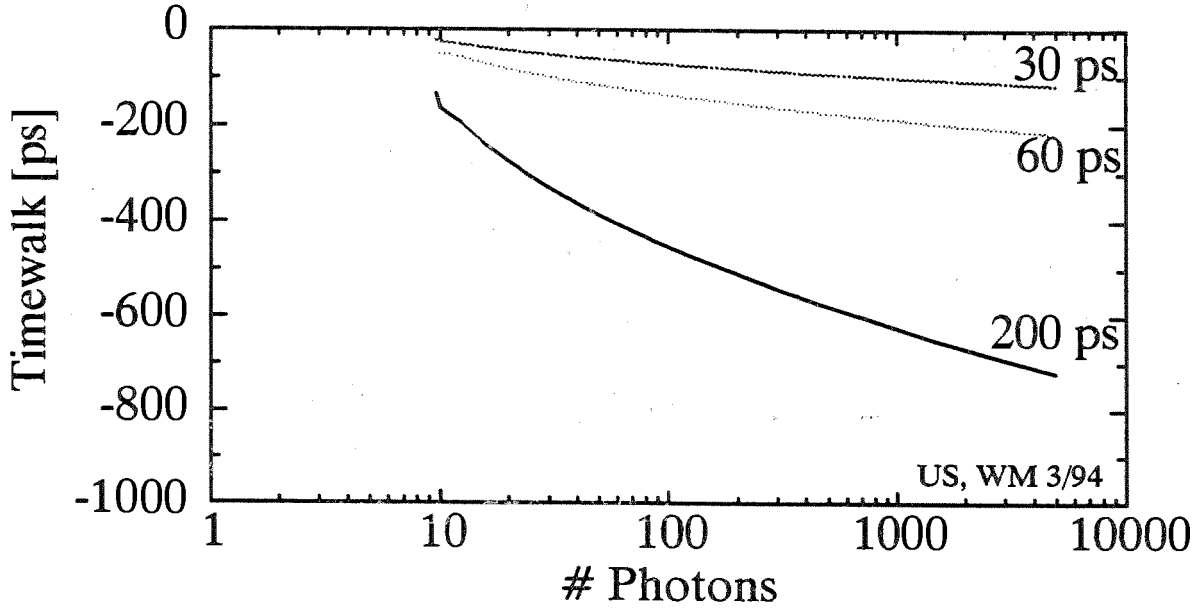

Figure 5: The calculated timewalk for some laser pulses of different length, according to the proposed model

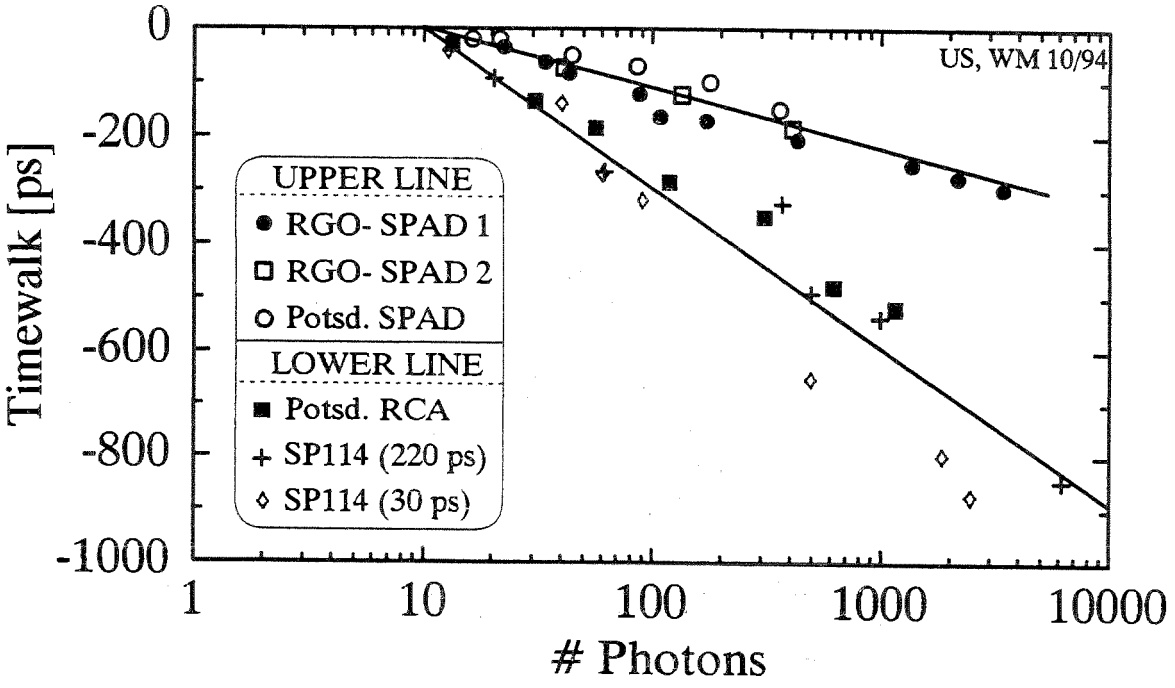

Figure 6: The measured timewalk for some avalanche photo diodes of different structure and with different lasers. One can see, that the obtained bias is depending on the type of diode, rather than the pulse width of the used laser

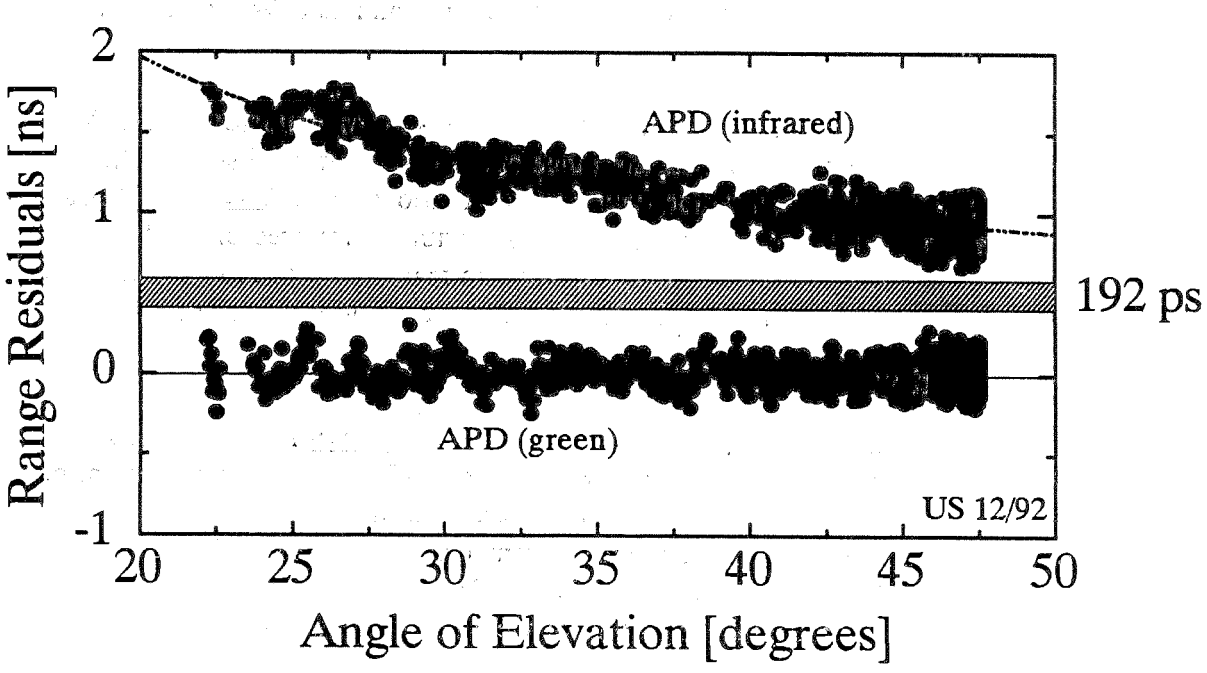

Figure 7: The residual plot of a satellite pass (LAGEOS), tracked simultaneously on two frequencies ($\lambda_1 = 0.532\mu m$ and $\lambda_2 = 1.06\mu m$. The difference in range is due to atmospheric dispersion. However there is a constant deficit of 200 ps in this seperation. This illustrates the frequency dependence of the multiplication process in the avalanche diode.

System Characterization of the NASA SLR Network

Van Husson, Julie Horvath
AlliedSignal Aerospace
AlliedSignal Technical Services Corporation
NASA SLR
7515 Mission Drive
Lanham, Maryland 20706 USA

Richard Eanes
University of Texas at Austin
Center for Space Research
Austin, Texas 78712 USA

Abstract - Orbital analysis techniques have improved significantly over the past 5 years. Three-day arc fits to LAGEOS-1 and LAGEOS-2 data are now consistently at the 1-2cm level. These orbital modeling improvements have enabled international Satellite Laser Ranging (SLR) analysts to identify many cm level range biases in recent and historical global SLR datasets. These improved techniques have been the primary motivation for writing this paper on the characterization of historical biases in the NASA SLR network. The application of these biases may prevent potential geophysical effects to be misinterpreted as data problems and vice versa. This paper is an update to the first paper written on this same subject [*Husson*,1992], which was published in the Proceedings of the Eighth International Workshop on Laser Ranging Instrumentation.

In this paper, we discuss the pre-requisites for doing system characterization. We provide a brief history of data products. We update the range bias information published in the first paper on this topic, and provide characterization data on two additional NASA systems (MLRS and SAO-2). We correlate our knowledge of the ranges biases with the inferred biases from Center for Space Research (CSR) LAGEOS-1,-2 analysis. We summarize the results and encourage other SLR engineering groups to complete a similar characterization of their systems.

1. Introduction

This paper is intended to be a reference document for known LAGEOS systematic errors in the NASA SLR network (MOBLAS 4-8, MLRS and SAO-2) since 1988, determined solely from engineering records and independent of biases determined from orbital analysis techniques. However, sometimes unexplained biases from orbital analysis did lead to an re-engineering assessment of previously published biases. Biases prior to 1988 for the most part are unrecoverable from an engineering point of view due to the nature of the biases [*Husson*, 1992]. These NASA SLR network bias models are available from the Crustal Dynamics Data Information System (CDDIS).

2. PRE-REQUISITES

Recovering historical biases requires a solid understanding of the data chain (i.e. hardware, software, data processing, operational procedures, survey and time keeping) and how every element of the data chain relates to each other. For instance a survey error to the calibration target induces a fixed range bias. Good record keeping is another requirement for system characterization. The configuration of the hardware, software, data processing constants applied to the data and performance statistics (satellite RMS, calibration RMS, system delay) must be known to determine historical biases.

Our understanding of the NASA SLR data chain improved tremendously during the mid 1980's primarily due to numerous collocations, improvements in system precision through hardware upgrades (see Figure 1) and our improvements in collocation analysis techniques. In the early 1980's, many systematic biases were discovered in collocation, but little was done in eliminating the biases because the root causes were unknown and because of pressure from management to deploy the systems into the field. In the mid 1980's, as data precision and data analysis techniques improved, a change in collocation philosophy occurred. If biases were discovered, an intense investigation would begin to determine the root cause of the bias. If the bias could be eliminated, the proper measures were taken. After the bias source was eliminated, collocation would resume to verify the biases were at the sub-cm level. This led to many long and stressful collocations, but was very well worth the effort. Engineering upgrades and modifications were a direct result of these investigations, and led to significant improvements in the data accuracy of the NASA SLR systems. Since the late 1980's, the NASA SLR network have at least ten of the twelve most accurate systems in the world.

Figure 1. Improvements in MOBLAS 6 Data Precision

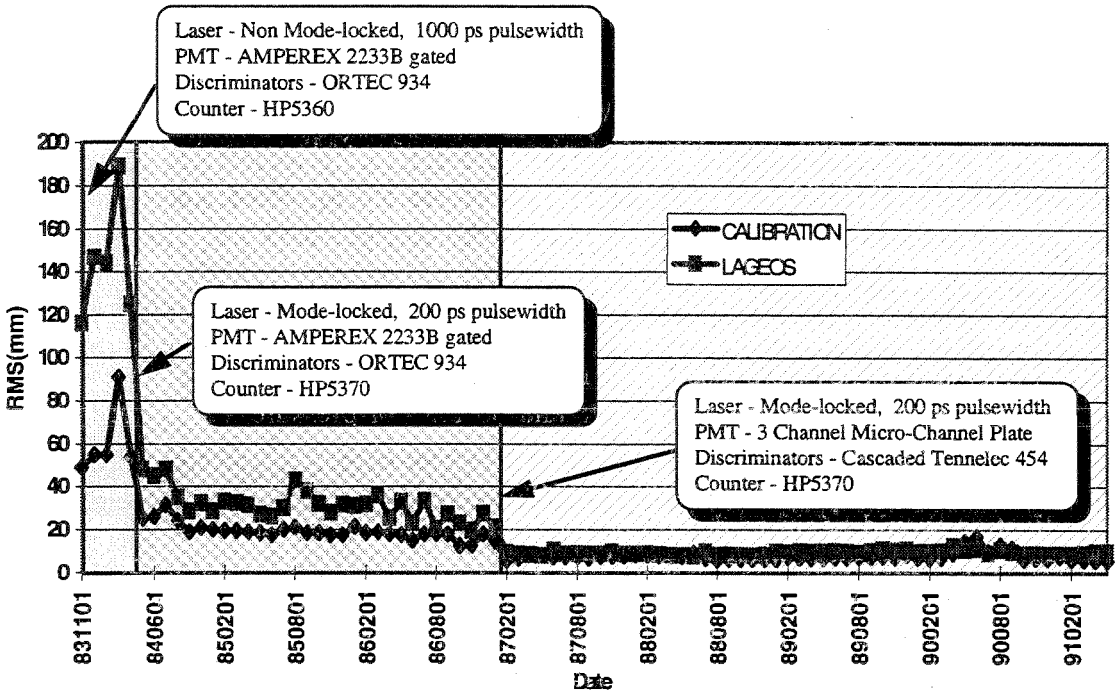

3. SLR DATA PRODUCTS

Since the late 1980's, most global SLR analysts have used two primary data products for their analysis. The two data products are quicklook data and fullrate data. Originally quicklook data was 50 observations randomly sampled across the duration of the pass, was not quality controlled, and was usually available within 24 hours of acquisition. Quicklook data was designed to provide a central facility with a quick assessment of system performance and was used in orbital determination to provide predicts. Quicklook data was not originally intended to be used for scientific purposes. Fullrate data was designed for this purpose. Fullrate data contained all observations; was tightly quality controlled by a central data processing facility; was sort merged by month; and made available to the scientific community after several months . Prior to standardization of normal points, most users of fullrate data designed their own data compression algorithms which converted fullrate data into normal points.

In the late 1980's and early 1990's, normal points became globally standardized [*Herstmonceux*, 1984] and became the preferred scientific data product. There are currently two types of normal points (field generated normal points in the CSTG format and fullrate normal points in the MERIT II format). Field generated normal points are produced at the station and replace the traditional 50 sampled quicklook observations. Global fullrate normal points have been produced on LAGEOS-1 and all satellites since 1987 and 1991, respectively, by ATSC from the global fullrate dataset. The differences between quicklook data and fullrate data have been greatly

diminished over the years through improvements in field data processing capabilities and more timely communication of problems. Our comparison of field generated and fullrate normal points from 1993, indicate very little difference (<1cm in range and <1 microsecond in epoch) between these two datasets for all but a few stations.

4. KNOWN NASA SLR NETWORK BIASES

This section is divided into sub-sections. There is one sub-section for each NASA SLR network station. Biases (range and epoch) for *fullrate* normal points are provided since Jan 1, 1988. Biases for field generated normal points or quicklook sampled data may be significantly different. *Users are strongly encouraged to use the fullrate normal points for their final analysis.* Appendix A contains the bias corrections for *fullrate* normal points. Appendix B contains graphics of each station showing the pass-by-pass range bias corrections along with the inferred range biases from CSR LAGEOS-1 data analysis.

For each station, only significant data problems will be discussed. A problem is considered significant if there is greater than an apparent 1 centimeter level systematic bias in the data.

4.1 MOBLAS 4 at 7110

MOBLAS 4 data (7110) since Jan 1988 had two significant problem periods. The first problem period was Jan 1 through May 4, 1988. Data was degraded due to an unstable calibration target [*Wetzel et. al.*1988]. This problem was resolved on May 5, 1988, when a new stable calibration target was implemented for calibrations. Special daily multi-target ranging tests were very beneficial in recovering the data during this period.

The second problem period was between Dec 29, 1988 and Jan 27, 1989 [*Heinick et. al.* 1989]. The LAGEOS RMS's during this period were twice as high as normal due to a bad counter which was replaced on Jan 28, 1989. The RMS's were also range dependent. Biases induced by this problem are unknown, and therefore, data during this period should not be used for precise geodetic applications.

4.2 MOBLAS 5 at 7090

MOBLAS 5 data (7090) since Jan 1988 had only one significant problem period. This period was from Jan 4 through Jan 11, 1992, inclusive. Data was degraded during this time due to a stuck bit in the measured time-of-flight [*Heinick, et. al.* 1989]. LAGEOS RMS's were twice their nominal value. The bit that was stuck was range dependent. Data during this period should not be used for precise geodetic applications.

4.3 MOBLAS 6 at 7122

MOBLAS 6 data (7122) since Jan 1988 had three significant problem periods. This first problem period was from Jan 1, 1988, through Jun 22, 1989. Data was degraded during this period due to unstable calibration targets and surveys errors [*Husson*, 1992]. This problem was resolved on Jun 23, 1989 when a new stable calibration target was installed and used for operational tracking. This data were recoverable from the regular monthly multi-target calibrations.

The second problem period was between Feb 1, 1989, through May 12, 1989. Barometric data during this period was severely degraded (as large as 30 millibar errors) due to a bad setra barometer [*Heinick*, 1989]. The barometric data was recovered to $\pm$ 2 millibars using barometric data from a local GPS experiment. Data during this time should be used with caution.

The third problem period was between Apr 1, 1990 and Sep 26, 1990. Calibration RMS's continued to increase during this period due to noise on the reference frequency to the time interval unit. Calibration RMS's exceeded satellite RMS's during the last 2 months. However satellite RMS's remained fairly stable during this whole period. The effect of this problem on range accuracy is unknown. The data during this interval should be used with caution.

4.4 MOBLAS 7 at 7105

MOBLAS 7 data (7105) since Jan 1, 1988, had only one significant problem period.
This period was from Aug 25 through Oct 11, 1989, inclusive. Data was originally biased due to an undocumented movement of the MOBLAS 7 reference point. The problem was detected in MOBLAS 7/TLRS-3 collocation analysis [*Varghese et. al.*, 1989]. A subsequent survey on Oct 12, 1988 indicated the system had moved several cm. The data during this period is slightly suspect, because the date the system physically moved is unknown.

4.5 MOBLAS 8 at 7109

MOBLAS 8 data (7109) since Jan 1, 1988 had only one significant problem period. This period was from Jan 1, 1988 through Mar 22, 1989. Data was degraded due to survey errors to the calibration targets [*Wroe et. al.*, 1984-1994]. This problem was resolved on Mar 23, 1989 when a new calibration target was installed, surveyed, and used for operational tracking. The data were recoverable from the regular monthly multi-target calibrations.

4.6 MLRS at 7080

MLRS implemented spider ranging on March 21, 1990 and made no hardware configuration changes prior to the collocation with TLRS-4 beginning in February 1993. During collocation a +25mm azimuth and elevation dependent range bias was detected. The source of this bias was a 25mm error in a fixed internal optical path combined with an unmodeled $\pm$ 5mm angular dependent term in the MLRS geometric correction [*Ricklefs*, 1989; *Husson et. al.*, 1993]. All fullrate data since February 1, 1993, was processed with the new geometric correction. All data

between March 21, 1990 and January 31, 1993 is fully recoverable. Biases prior to March 21, 1990 are not known as of this writing.

4.7 SAO-2 at 7907

SAO-2 data (7907) since Jan 1, 1988 had two problem periods. The first period was from Jan 1, 1988 through May 25, 1988, inclusive. Data was degraded during this time due to an improper calibration range used in data processing and improper modelling of LAGEOS signal strengths [*Heinick et. al.*, 1988]. All fullrate data since May 26, 1988 was processed with a updated calibration range which eliminated a 40mm bias. The second period was from May 26, 1988 through June 15, 1988, inclusive. Data was degraded due to improper modelling of LAGEOS signal strengths. This problem was resolved by implementing new LAGEOS calibration procedures on Jun 16, 1988. SAO-2 collocated with TLRS-3 in the 1990 and the two systems agreed on the average to better than 1cm on LAGEOS.

5. CONCLUSIONS

There are obvious correlations between known biases and inferred biases from CSR orbital analysis. Applying these biases will improve the accuracy of the data. We strongly encourage other engineering groups to perform a detailed bias analysis of their historical data and compare it with orbital analysis results.

6. ACKNOWLEDGMENTS

The material in this paper has been amassed through years of close interaction with highly talented group of colleagues at Allied-Signal Technical Services Corporation, formerly Bendix Field Engineering Corporation, in Greenbelt and Columbia, Md; at the NASA Goddard Space Flight Center in Greenbelt, Md; and at the University of Texas in Austin. Much of their work is referenced here.

7. REFERENCES

Heinick M, Husson V, Wroe S, Brogdon O, Wetzel S, Clarke B, "Six Month Data Processing Report", Bendix Field Engineering Corporation internal report, Nov 1989.

Husson V, "Historical MOBLAS System Characterization", Proceedings of the Eighth International Workshop on Laser Ranging Instrumentation, Annapolis, Md, May 18-22, 1992.

Husson V, Conklin B, Cheng G, Donovan H, Heinick M, Wetzel S, Eanes R, Ricklefs R, Wiant J, "MLRS/TLRS-4 Collocation Results", CSTG meeting, Potsdam, Germany, Oct 26-27, 1993.

Recommendation 84A, Proceedings of the Fifth International Workshop on Laser Ranging Instrumentation, Herstmonceux, UK, 1984.

Ricklefs R, "MLRS Geometric Correction", SLR memorandum, Aug 31, 1989.

Wetzel S, Clarke B, Husson V, Heinick M, Wroe S, Brogdon O, Zanni K, "Six Month Data Processing Report", Bendix Field Engineering Corporation internal report, Oct 1988.

Varghese T, Husson V, "TLRS-3: Engineering Upgrades and Performance Evaluation through Intercomparison with MOBLAS-7 from Oct 88 - Nov 89", Bendix Field Engineering Corporation internal report, Nov 1989.

Wroe S, Heinick M, Brogdon O, Gheng G, Horvath J, "MOBLAS Ground Test Results", Bendix Field Engineering internal reports, 1984-1994.

Appendix A. NASA SLR BIAS CORRECTION TABLE

Note: To correct for these biases, the range and time biases must be subtracted from the one-way time-of-flights (ranges) and timetags (epochs), respectively.

Time Span	Pad	Range Bias(mm)	Time Bias(us)	Revision Date
01-Jan-88 - 28-Jan-88	7110	27	0.0	01-Jan-94
29-Jan-88 - 30-Jan-88	7110	15	0.0	01-Jan-94
31-Jan-88 - 04-Jan-90	7110	-3	0.0	01-Jan-94
05-Jan-90 - 17-Jan-92	7110	-3	-0.4	01-Jan-94
18-Jan-92 - 31-May-92	7110	-1	-0.4	01-Jan-94
01-Jun-92 - 31-Dec-94	7110	0	0.0	01-Jan-94
01-Jan-88 - 29-Jan-90	7090	-3	0.0	01-Jan-94
30-Jan-90 - 31-May-92	7090	-3	-0.3	01-Jan-94
01-Jun-92 - 31-Dec-94	7090	0	0.0	01-Jan-94
01-Jan-88 - 02-May-88	7122	-14	0.0	01-Jan-94
03-May-88 - 16-Aug-88	7122	-8	0.0	01-Jan-92
17-Aug-88 - 31-Aug-88	7122	1	0.0	01-Jan-92
01-Sep-88 - 30-Sep-88	7122	2	0.0	01-Jan-94
01-Oct-88 - 31-Oct-88	7122	3	0.0	01-Jan-94
01-Nov-88 - 30-Nov-88	7122	4	0.0	01-Jan-94
01-Dec-88 - 31-Dec-88	7122	5	0.0	01-Jan-94
01-Jan-89 - 31-Jan-89	7122	6	0.0	01-Jan-94
01-Feb-89 - 28-Feb-89	7122	7	0.0	01-Jan-94
01-Mar-89 - 31-Mar-89	7122	8	0.0	01-Jan-94
01-Apr-89 - 30-Apr-89	7122	9	0.0	01-Jan-94
01-May-89 - 31-May-89	7122	10	0.0	01-Jan-94
01-Jun-89 - 22-Jun-89	7122	11	0.0	01-Jan-94
23-Jun-89 - 10-Jan-90	7122	-3	0.0	01-Jan-94
11-Jan-90 - 30-Apr-91	7122	-3	-0.3	01-Jan-94
01-Jan-88 - 31-Jan-88	7105	-3	0.0	01-Jan-94
01-Feb-88 - 30-Apr-88	7105	4	0.0	01-Jan-94
01-May-88 - 12-Jul-89	7105	-3	0.0	01-Jan-94
13-Jul-89 - 24-Aug-89	7105	-3	-0.5	01-Jan-94
25-Aug-89 - 11-Oct-89	7105	-18	-0.5	01-Jan-94
12-Oct-89 - 27-Sep-90	7105	-3	-0.5	01-Jan-94
28-Sep-90 - 09-Jul-91	7105	-3	-0.3	01-Jan-94
10-Jul-91 - 23-Jul-91	7105	-1	-0.3	01-Jan-94
24-Jul-91 - 17-Oct-91	7105	-3	-0.3	01-Jan-94
18-Oct-91 - 31-May-92	7105	-1	-0.3	01-Jan-94
01-Jun-92 - 31-Dec-94	7105	0	0.0	01-Jan-94
01-Jan-88 - 11-Dec-88	7109	17	0.0	01-Jan-94
12-Dec-88 - 22-Mar-89	7109	6	0.0	01-Jan-94
23-Mar-89 - 21-Nov-89	7109	-3	0.0	01-Jan-94

22-Nov-89	- 30-Nov-89	7109	-3	-0.3	01-Jan-94
01-Dec-89	- 06-Apr-92	7109	5	-0.3	01-Jan-94
07-Apr-92	- 31-May-92	7109	-1	-0.3	01-Jan-94
01-Jun-92	- 31-Dec-94	7109	0	0.0	01-Jan-94
21-Mar-90	- 31-Jan-93	7080	25	0.0	01-Jan-94
01-Feb-93	- 31-Dec-94	7080	0	0.0	01-Jan-94
01-Jan-88	- 25-May-88	7907	-71	0.0	01-Jan-94
26-May-88	- 15-Jun-88	7907	-31	0.0	01-Jan-94
16-Jun-88	- 31-Dec-94	7907	0	0.0	01-Jan-94

Appendix B. NASA SLR RANGE BIASES (KNOWN VS. INFERRED)

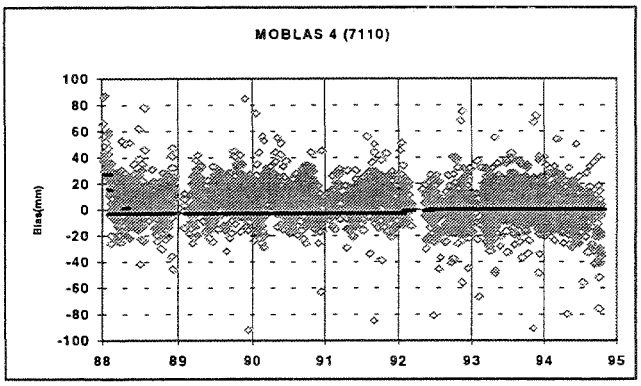

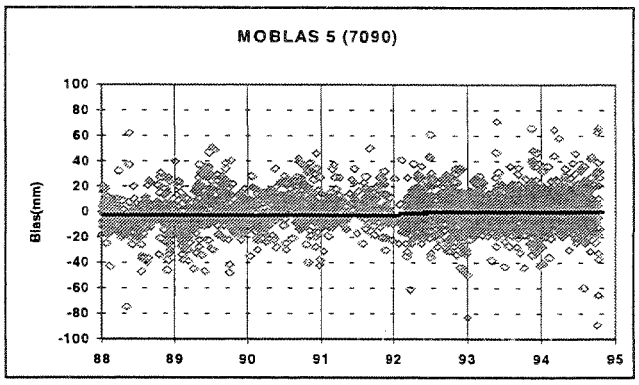

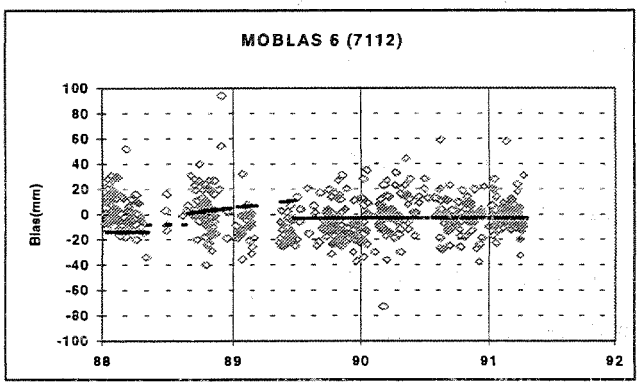

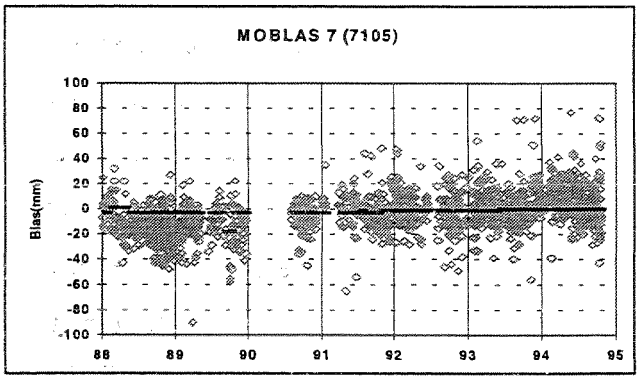

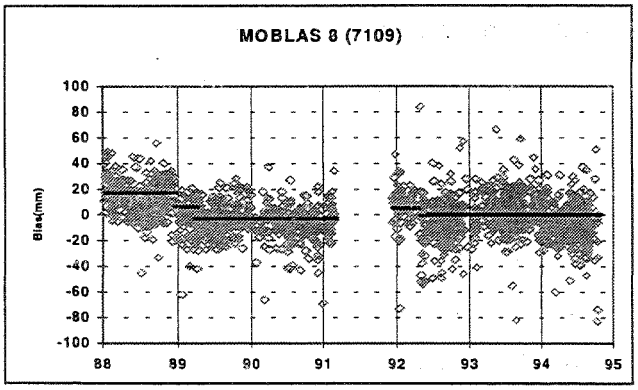

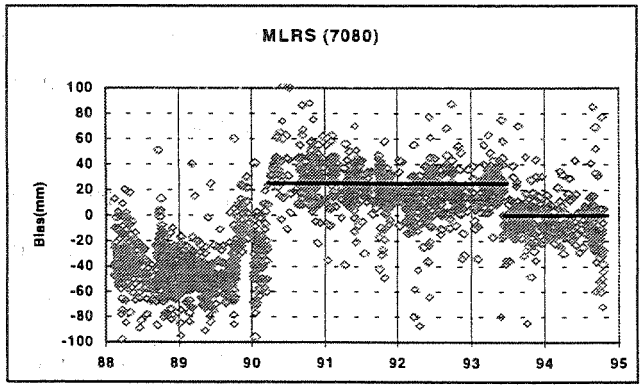

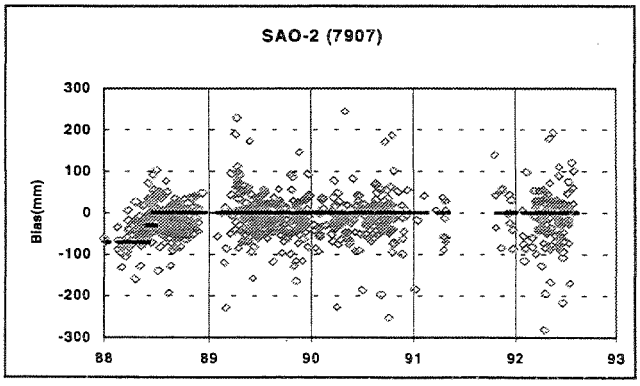

Legend

◇ CSR (Orbital Bias)
- ATSC known bias

MULTI-SATELLITE LASER RANGE RESIDUAL ANALYSIS FOR QUALITY CONTROL OF THE SLR NETWORK

Richard J. Eanes, Srinivas V. Bettadpur, John C. Ries
Center for Space Research, The University of Texas at Austin
Mail Code C0605, Austin, Texas 78712, U.S.A.

1. Introduction

The determination of the coordinates of SLR sites, their velocities, as well as the individual station observation biases and time biases is dependent upon the availability of a long time history of measurements and on the precise determination of the orbits of the satellites. This activity has usually been carried out using the laser range measurements made to the Lageos satellite from tracking sites around the world.

In the last few years, several new satellites have become available for laser ranging, whose orbits are routinely determined to the sub-decimeter level. Examples include Lageos-2, Stella and TOPEX/POSEIDON (T/P). Furthermore, improvements in the modeling and orbit determination of satellites with longer measurement histories, for example Starlette and Ajisai, has also made them viable targets from which to carry out station position determinations.

In this note, we consider the use of laser range measurements to Lageos, Lageos-2, Ajisai, Stella, and T/P satellites to monitor the variations in station biases. In these results, we focus on the use of multi-satellite tracking data to resolve the vertical position errors, range bias, time bias and frequency bias for each station, as well as to monitor mutual consistency of these estimates made from different satellites. In this note, frequency bias is taken to mean the error in the frequency of the oscillator used in the measurements of the time of flight.

Multi-satellite monitoring of station characteristics offers two significant advantages. The range measurements and related biases and errors at each station are dependent upon not only the ground station hardware and software, but also on the individual satellite characteristics, such as its orbital geometry, target size and shape. Targeting multiple satellites with different characteristics from the same station provides an

opportunity to make the estimation of station biases relatively independent of the characteristics of any one satellite.

The second important advantage of multi-satellite estimation of biases is that it allows us to discriminate between a range bias and a frequency bias at each station. The effect on a single satellite range due to a range measurement bias at a station is difficult to separate from the effects of a station frequency bias. Since the equivalent satellite range error due to a frequency bias at a station is proportional to the mean range to a satellite, and since the effects of a range bias are independent of the target altitude, the inclusion of measurements from a second satellite at a different altitude permits the separation of frequency biases from range biases.

The separability between range and frequency biases is illustrated further in Fig. 1. In the top panel, the sensitivities of the range to errors in the vertical station position, a range bias and a frequency bias are shown as a function of the pass elevation angle. The sensitivities of ranges to a frequency bias are clearly seen to be dependent on satellite altitude. These sensitivities (or partial derivatives of the range with respect to station vertical position, range bias and frequency bias) determine the linear system mapping the three errors into equivalent range errors. A singular value decomposition of this linear system from a single satellite clearly shows that one mode is nearly singular, reflecting the inseparability of range and frequency biases from single satellite ranges. If this mode is projected onto the measurement space, as shown in the bottom panel in Fig. 1, we see that it contributes virtually nothing to the measurements. However, if the same analysis is carried out with two satellites at different satellites, the worst singular mode now has a significant observable effects on the range, as also shown in the bottom panel of Fig. 1.

Within the context of the discussions in the last few paragraphs, we now describe the techniques and results obtained from an estimation of station biases from laser range tracking of multiple satellites.

2. The Technique

The orbits of the laser satellites were determined using UTOPIA, The University of Texas Orbit Processor. The initial conditions, empirical drag and 1 cycle per revolution acceleration parameters were estimated in appropriate short arcs fit to the Quick-Look normal points for a 360 day duration from Oct. 1993 to Sep. 1994. This time span was

determined by the availability of data from Stella, and is quite adequate to demonstrate the utility of the techniques, though not enough for a determination of a mean set of multi-satellite station coordinates or velocities. The force models, the arc structure, the number of measurements and the residual laser range rms for each satellite are summarized in Table 1. The orbit fits for Ajisai and Stella are not as good as those for Lageos, Lageos-II and Topex, primarily due to force model inadequacies. It must be emphasized that for these demonstrations, relatively loose data editing criteria were used, so that the residual rms are perhaps a little higher than they would be in an operational orbit determination scheme using well edited laser range data.

The laser range residuals from each satellite were computed about these nominal orbits. All further analysis was done using the measurement residuals. The orbits for each of the satellites were held fixed, and the variational equations for the range residuals with respect to the station positions, station range bias, time bias and frequency biases were written out. The University of Texas Consider Analysis software CONAN was used to provide single and multiple satellite estimates of the various biases and station positions. The station biases were adjusted once every 15 days. In all cases where the station coordinates were estimated, only a single adjustment over 360 day data span was allowed.

3. Results and Discussion

In the first set of tests, the range and time bias for each station were estimated individually from each satellite. These estimates were made both while holding the stations fixed, as well as while allowing the station positions to adjust. In either case, the range biases for each station from a tracking to a particular satellite were the same, showing that the range bias is well separated from the station position using data from a single satellite.

In Table 2, the weighted mean of the 15 day range biases is shown for a selection of tracking stations in the network. The scatter about the mean biases from Lageos show that for the high quality stations, the range biases are monitored with approximately 1 cm precision. The bias estimates from Lageos, Lageos-II and T/P data are seen to be mutually consistent, with the possible exception of Matera (7939), Graz (7839) and Simosato (7838). On the other hand, the biases from Ajisai and Stella show significant differences

in comparison to the other satellites. The is attributable to the lower quality of orbit fits to Ajisai and Stella data. Another interesting feature is that the range biases from Ajisai data are consistently higher than the values obtained from Lageos data. This can be probably attributed to an incorrect center of mass offset correction (1.01 meters) applied to the Ajisai data.

Fig. 2a shows the time variation of the 15 day range bias estimates for Yaragadee (7090) in the 360 day time span. This plot clearly shows the mutual consistency of estimates from Lageos, Lageos-II and T/P data, whereas the estimates from Ajisai data are seen to be consistently offset. Similar offsets can also be seen for the biases (Figs. 4a-c) for the stations at Matera (7939), Graz (7839) and Simosato (7838).

Somewhat different behavior is seen in the estimates of range biases for the station at Haleakala. In late 1993 (the initial part of the time span considered here) the station at Haleakala is known to have had a frequency bias. Due to reasons discussed in Section 1, the range bias estimates for Haleakala from tracking to different satellites shows a large variation in that span, as is seen in Fig. 2b. After the frequency bias was corrected in early 1994, the estimates of range biases are seen to become more consistent between different satellites.

In the second set of results, the variational equations and laser range residuals from the five different satellites were combined into a single set of linear equations. As before, the individual satellite orbits were not readjusted. The relative data weights between satellites are summarized in Table 3. The data weights were determined in inverse proportion to the contribution from each satellite to the total weighted residual sum squared of noise.

Using the multi-satellite measurement residuals, it becomes possible to solve simultaneously for the range and frequency biases for each station. In Table 4, the weighted mean of the 15 day frequency bias estimates are shown, along with their scatter, for few of the stations in the network. The scatter for most stations appears not to exceed a few parts per billion (ppb). Orroral (7843), Riga (1884) and Wettzel (8834) appear to have no systematic frequency bias problems even though the mean estimates are significant in comparison to their scatter or uncertainties. Furthermore, the scatter in the mean range biases, with and without the simultaneous adjustment of the frequency bias, is too large for the change in the mean range bias in the two cases to be very significant. The frequency bias estimates from Graz (7839), Matera (7939) and Simosato (7838) seem to be

significant for two reasons. The mean range bias changes between the two cases seem to be significant in comparison with the scatter of the 15 day biases about this mean. Furthermore, the plots of individual range biases (Figs. 4a-c) for each of these stations from the five different satellites show that the estimates from T/P or Ajisai data are consistently different from the estimates made using Lageos or Lageos-II data.

The consequence of a frequency bias is further illustrated by the case of Haleakala (7210). In Fig 2b, we showed the variation in the range biases in late 1993. The pair of lines in Fig. 3a where the frequency biases were simultaneously adjusted with the range biases using data from all five satellites, clearly show that the range biases seen in Fig. 2b in late 1993 were due to the presence of the frequency bias. Using data from multiple satellites resolves the singularity between the range and frequency biases, and allows a separation between the effects of a range and frequency bias. The plot of the frequency bias for Haleakala (7210) in Fig. 3b shows the expected high frequency bias in late 1993, in the two cases with and without station station height adjustments. Furthermore, Figs. 5a-c show the estimated frequency biases for Graz (7839), Matera (7939) and Simosato (7838) with significant variations over the time span considered here. This is consistent with the variations of range biases for these stations seen in Figs 4a-c.

Finally, we consider the influence of an adjustment of the station coordinates upon the estimates of the station range bias. In Table 5, the mean range bias and their scatter are shown for two cases, with and without simultaneous station coordinate adjustment. Also shown are the station vertical adjustments in the former case. The stations fall broadly into two categories, the first where there is a significant change in the range bias in the two scenario, with an accompanying larger change in the station height; and a second where the differences are significantly smaller. These differences are yet unexplained. The height adjustments from these stations should not be interpreted as actual deficiencies in their nominal values, as almost certainly the presence of relatively lower quality orbits of Ajisai and Stella are corrupting the estimates. Furthermore, as has been seen from a comparison of range biases from the Ajisai data in comparison to Lageos, Lageos-II and T/P, it appears that the satellite or target specific errors are not completely eliminated from the problem. These results do, however, point to the importance of ensuring uniformly good quality orbit computation and relative data weighting while making multi-satellite estimates of station coordinates and biases.

4. Conclusions

Using tracking data to Lageos, the station dependent biases are being monitored to accuracies of about 1 cm for the range bias, 5 μ sec for the time bias, and 1-3 ppb in the frequency biases. The estimates of these biases are generally seen to be consistent when using data from Lageos, Lageos-II or T/P. Estimates from Ajisai and Stella data are seen to be significantly different, largely due to poorer orbits for these satellites. Inconsistencies between estimates from Lageos and T/P satellite data could be due to the presence of frequency biases, as in the case of Haleakala (7210), Graz (7839), Matera (7939) and Simosato (7838). The last three stations also show a very significant interdependence between adjustments to station heights and range biases.

A combination of multi-satellite tracking data is seen to be very useful in resolving the effects of range biases from frequency biases, and also to enhance the accuracy of their estimates. The dependence of these results upon the individual satellite signal strength and the target signature continues to remain a problem.

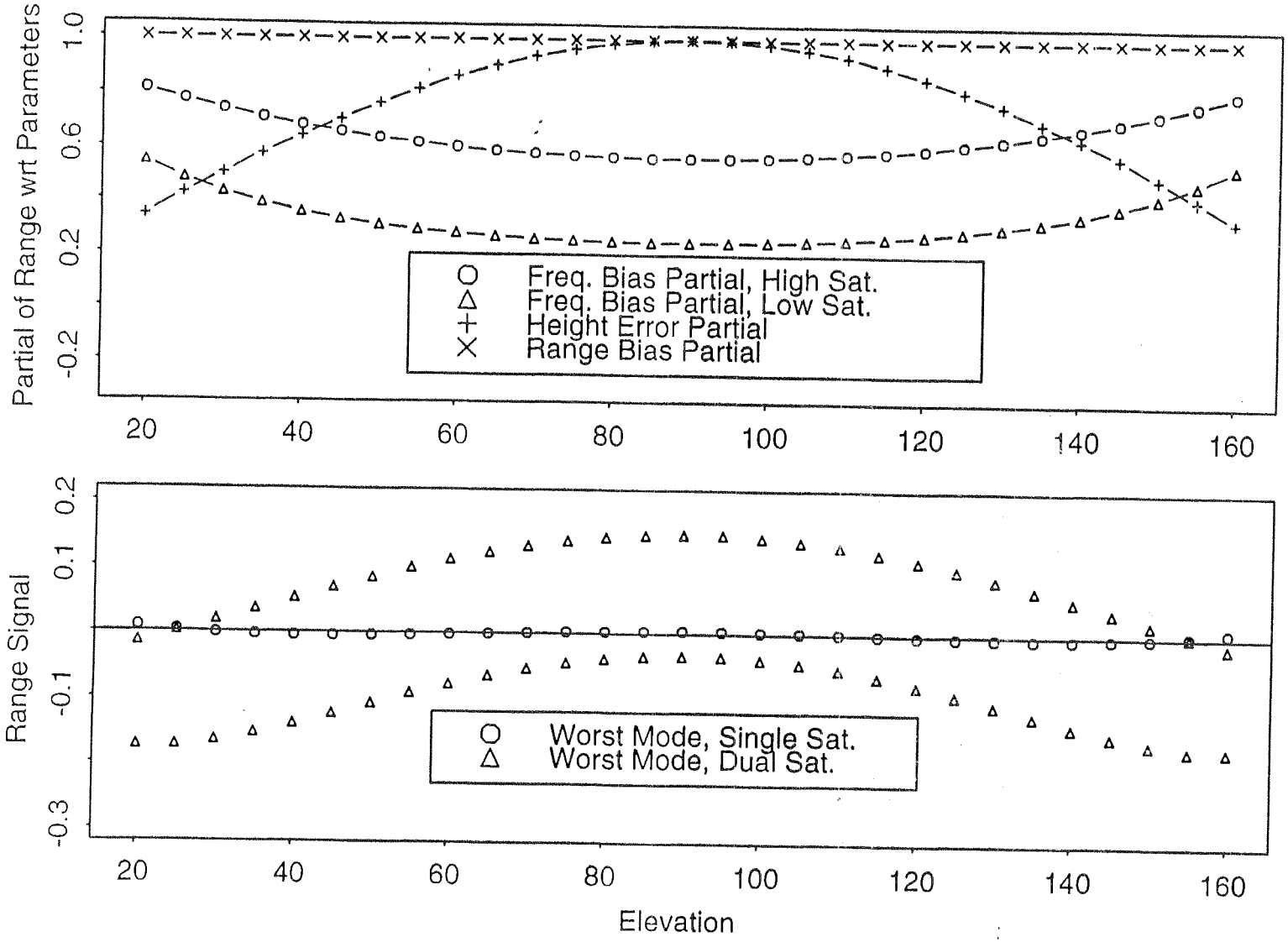

Fig. 1 : Effects of the near singularity between range and frequency biases upon the range to a single satellite; and its resolution using two satellites at different altitudes.

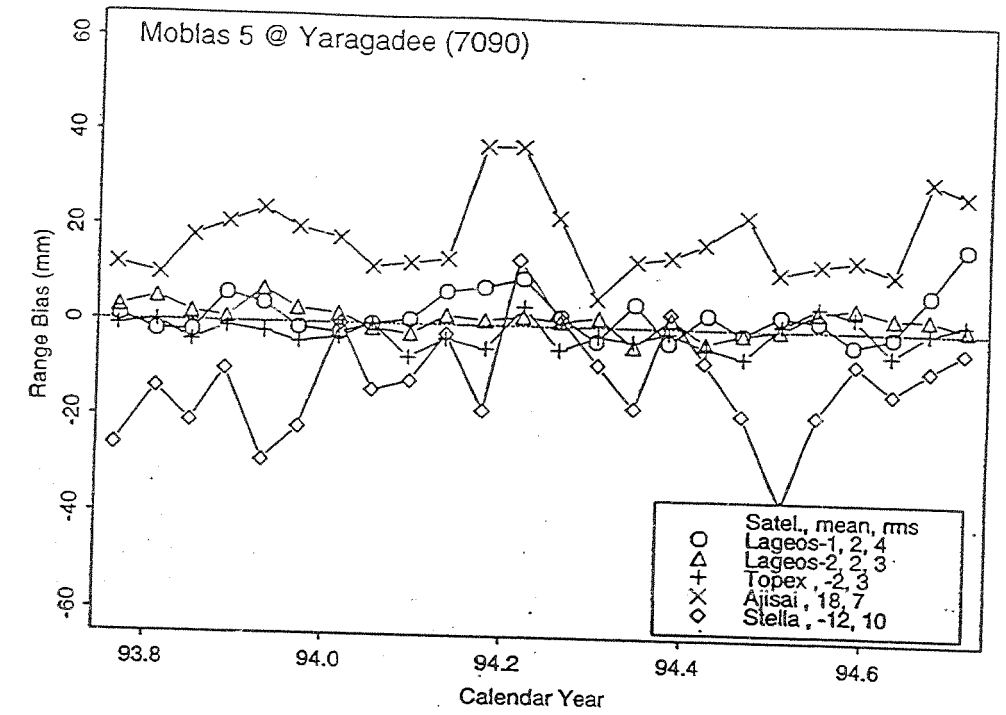

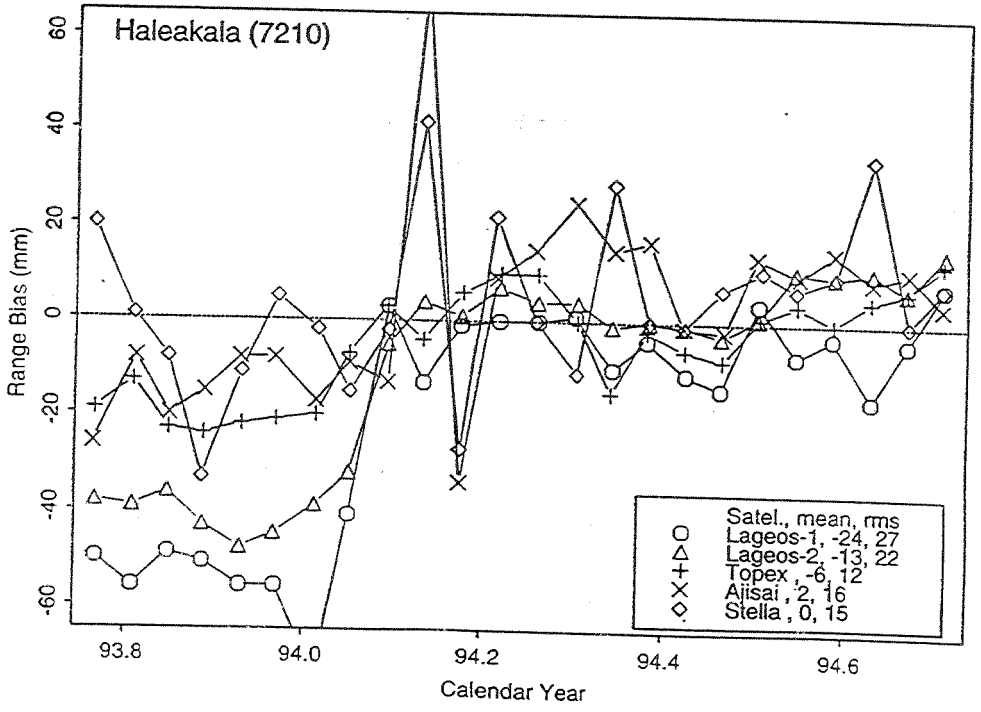

Fig. 2a-b : 15 day range bias estimates for Yaragadee (7090) and Haleakala (7210) from different satellites. The station coordinates were not adjusted.

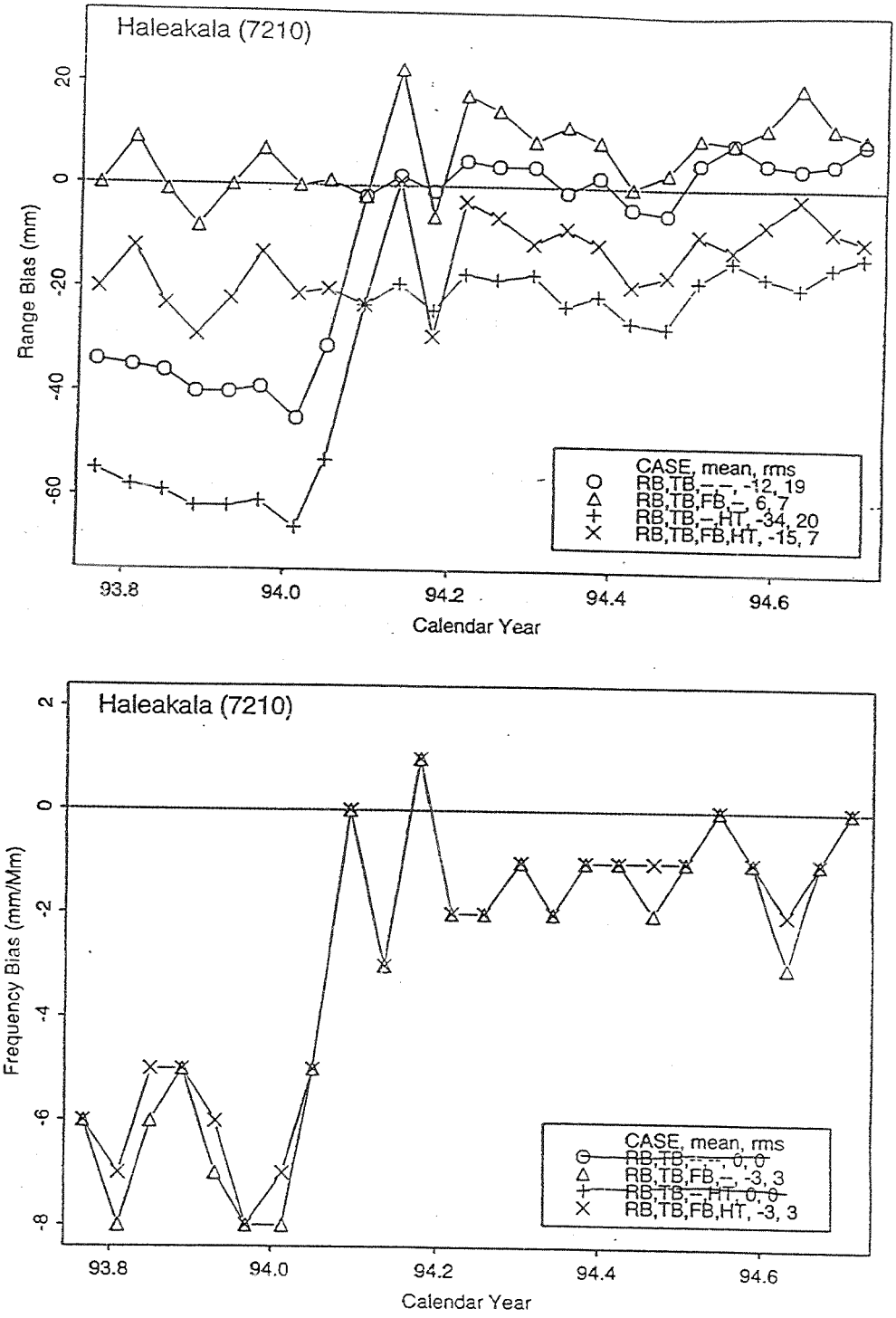

Fig. 3a-b : Multi-satellite 15 day estimates of range and frequency biases for Haleakala (7210) with and without simultaneous height adjustments.

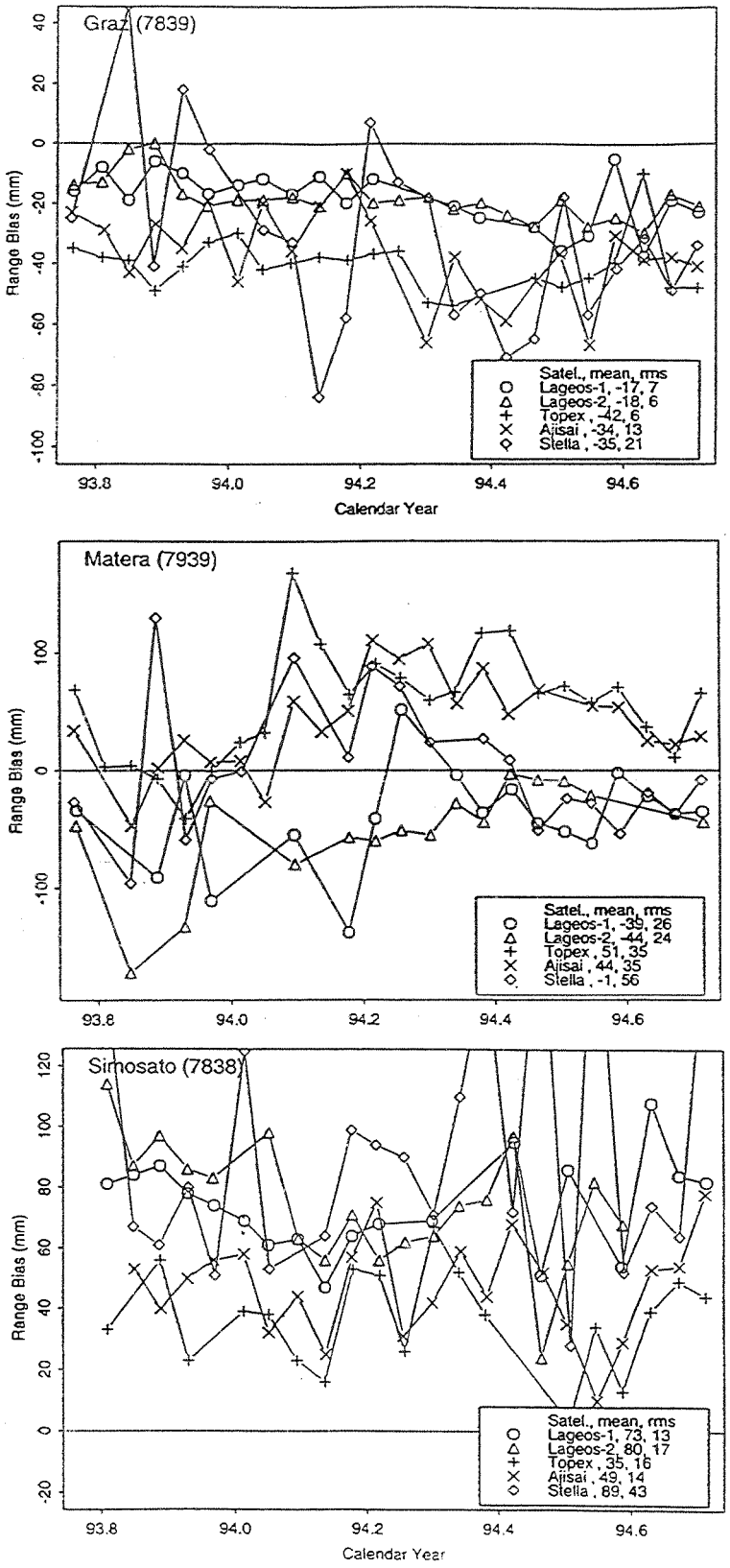

Fig. 4a-c : 15 day range bias estimates for Graz (7839), Matera (7939) and Simosato (7838) from different satellites. The station coordinates were not adjusted.

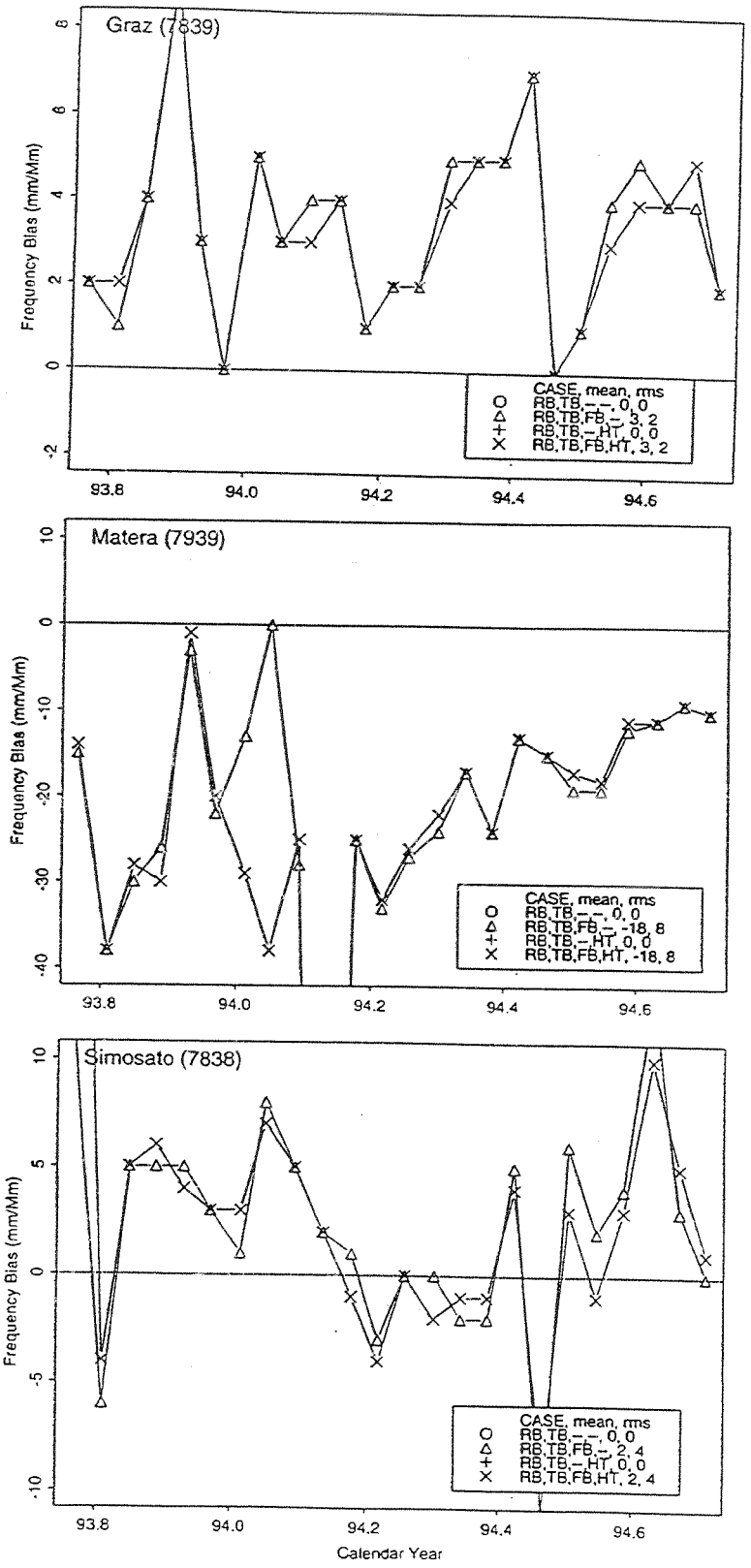

Fig. 5a-c : 15 day multi-satellite frequency bias estimates for Graz (7839), Matera (7939) and Simosato (7838) with and without simultaneous height adjustments.

Table 1 : The size, Time-of-Flight (TOF), orbit fit parametrization and laser range residual rms for the selected SLR target satellites.

Target	Size (m)	TOF (msec)		Range ($\times 10^6$ m)		Orbit Quality	
		Min (90 deg)	Max (20 deg)	Min (90 deg)	Max (20 deg)	RMS (mm)	Arc (d)
Ajisai	1.0	10	19	1.5	2.9	60	9
Lageos	0.3	39	57	5.9	8.5	15	15
Lageos II	0.3	39	57	5.9	8.5	15	15
TOPEX	0.8	8.9	18	1.3	2.7	30	10
Stella	0.08	5.5	12	0.8	1.8	70	6

Table 2 : Average of 15 day range bias estimates and their rms scatter (in parentheses) from selected stations in a 360 day span from Oct. 93 to Sep. 94, using ranges to different satellites. The station coordinates were not adjusted. All units are in mm.

Station	ID	Range Bias (mm)									
		Ajisai		Lageos		Lageos-II		Stella		Topex	
Arequipa	7403	20	(9)	5	(8)	5	(5)	-5	(13)	6	(6)
Bar Giyorra	7530	28	(13)	27	(10)	19	(19)	15	(40)	15	(16)
Borowiec	7811	-3	(24)	-8	(14)	-19	(3)	-33	(31)	18	(17)
Grasse	7835	55	(10)	38	(16)	37	(12)	21	(15)	50	(6)
Graz	7839	-34	(13)	-17	(7)	-18	(5)	-35	(20)	-41	(5)
GSFC	7105	2	(7)	6	(8)	2	(7)	7	(22)	-4	(8)
Haleakala	7210	2	(15)	-22	(27)	-14	(21)	-1	(14)	-5	(12)
Matera	7939	44	(36)	-34	(16)	-43	(19)	-2	(56)	50	(33)
McDonald	7080	3	(11)	-6	(5)	-6	(5)	-8	(21)	-6	(4)
Mon. Peak	7110	4	(4)	1	(5)	3	(3)	14	(12)	-4	(5)
Orroral	7843	60	(9)	42	(5)	46	(5)	64	(22)	49	(9)
Potsdam	7836	28	(18)	17	(9)	12	(6)	8	(15)	11	(11)
Quincy	7109	6	(8)	-4	(5)	-2	(2)	12	(8)	-9	(3)
RGO	7840	7	(9)	0	(6)	-4	(6)	-11	(12)	-5	(7)
Riga	1884	56	(32)	155	(114)	115	(54)	90	(32)	50	(51)
Simosato	7838	49	(14)	72	(12)	80	(18)	84	(35)	35	(17)
Wettzel	8834	40	(25)	22	(23)	19	(24)	31	(53)	40	(32)
Yaragadee	7090	18	(7)	1	(4)	2	(2)	-13	(11)	-2	(3)
Zimmerwald	7810	27	(15)	12	(11)	17	(6)	-12	(17)	33	(11)

Table 3 : Relative data weights, given as scale multipliers to the formal measurement uncertainty (Scale), for laser range measurements made to the selected SLR target satellites.

Target	Num Obs	RMS (cm)	Scale
Lageos	62,220	3.5	1
Lageos-2	59,900	2.9	0.82
Stella	35,300	8.0	1.74
Ajisai	117,500	5.2	2.06
Topex	194,100	3.6	1.83

Table 4 : Average of 15 day multi-satellite frequency bias (FB) estimates and their rms scatter (in parentheses) for selected stations in a 360 day span from Oct. 93 to Sep. 94. Also given are the mean multi-satellite range bias (RB, in mm) estimates with and without the simultaneous estimation of the frequency biases. The station coordinates were not adjusted in any case.

Station	ID	FB (ppb)		RB (with FB)		RB (w/o FB)	
		Mean	RMS	Mean	RMS	Mean	RMS
Graz	7839	3.1	(1.7)	-43	(10)	-25	(6)
Haleakala	7210	-3.1	(2.8)	5	(7)	-13	(20)
Matera	7939	-18.1	(7.9)	79	(43)	-1	(16)
Orroral	7843	-2.5	(0.9)	62	(9)	47	(5)
Riga	1884	13.4	(10.5)	27	(55)	126	(73)
Simosato	7838	2.5	(3.3)	52	(26)	68	(16)
Wettzel	8834	-3.4	(2.7)	47	(32)	29	(25)

Table 5 : Average of 15 day multi-satellite station range bias (RB) estimates with and without simultaneous adjustment of station coordinates (StaCor). Also given are the height adjustments in mm. In each case, the frequency biases were estimated. All units in mm.

Station	ID	Ht Adj	RB (with StaCor)		RB (w/o StaCor)	
Arequipa	7403	-17	0.8	(7)	12	(6)
Borowiec	7811	-31	-3	(26)	27	(28)
Graz	7839	-21	-54	(10)	-43	(10)
Haleakala	7210	-30	-15	(7)	6	(7)
Matera	7939	63	117	(43)	79	(43)
Orroral	7843	-39	37	(9)	62	(9)
Potsdam	7836	-32	-9	(12)	14	(12)
Simosato	7838	-35	33	(24)	52	(26)
Bar Giyorra	7530	10	25	(22)	19	(22)
Grasse	7835	-8	49	(6)	51	(5)
GSFC	7105	-9	-6	(8)	1	(8)
McDonald	7080	-17	-13	(8)	-2	(8)
Mn. Peak	7110	-8	-2	(5)	2	(5)
Quincy	7109	-5	-2	(4)	1	(4)
RGO	7840	-14	-15	(8)	-5	(8)
Riga	1884	-10	16	(57)	26	(55)
Wettzel	8834	-1	46	(32)	47	(32)

Prof.Vladimir P.VASSILIEV, Prof.Leonid I.GUSEV,
D-r John J.DEGNAN, Prof. Victor D.SHARGORODSKY

Russian Institute for Space Device Engineering

EXPERIMENTAL VERIFICATION OF THE FIZEAU EFFECT INFLUENCE ON THE REFLECTED BEAM DIRECTION IN SATELLITE LASER RANGING

1994

A joint US-Russian experiment in satellite laser ranging with cube corner reflectors shows that it is necessary to take into account the influence of the Fizeau effect on the reflected beam direction which partly compensates for the angular displacement caused by the velocity aberration. Data from more than 2000 single measurements are in good agreement with values obtained from calculations based on the assumption that such a compensation really takes place.

- In some recent publications several scientists from the Russian Institute for Space Device Engineering have supposed that the Fizeau effect in the media of cube corner retroreflectors installed on board of a satellite rapidly moving relative to a ground station may cause a substantial angular displacement of the reflected beam which partly compensates for the displacement caused by the velocity aberration.

- According to a resolution adopted by the 8-th International (Annapolis, MD, May 1992) a joint US-Russian experiment has been made for experimental verification of the presence of such an effect.

- On board of a Russian-made satellite (Meteor-2) launched in autumn 1993 in a circular orbit with a height h_s=940 km three cube corner reflectors were placed, the central one pointed along the Nadir axis and two others at 45° angles to this direction in the plane orthogonal to the orbit plane and have near- diffraction-limited far field diffraction patterns (narrow as compared to the velocity aberration angle).

1)

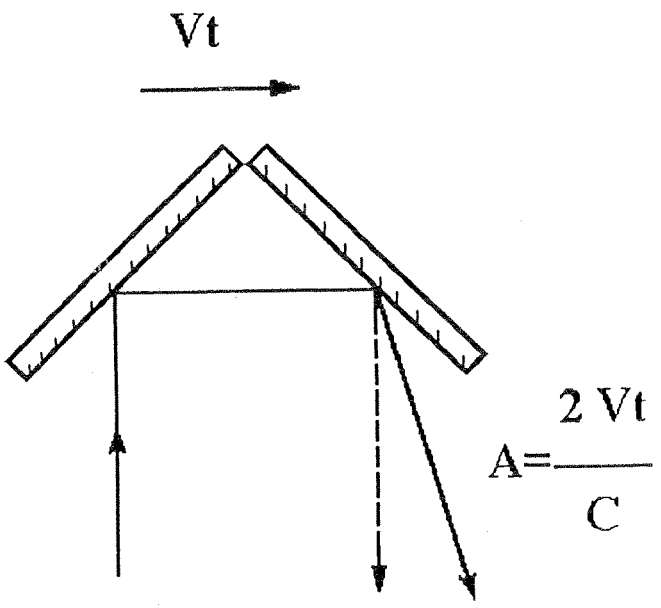

$$A = \frac{2\,Vt}{C}$$

Light reflection from mirror and prizm reflectors

2)

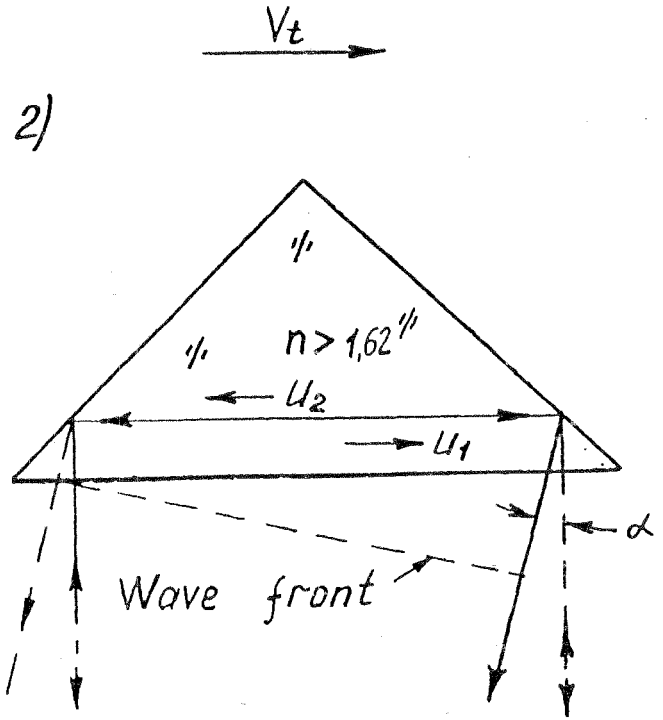

$$U_1 \approx \frac{c}{n} + Vt\left(1 - \frac{1}{n^2}\right)$$

$$U_2 \approx \frac{c}{n} - Vt\left(1 - \frac{1}{n^2}\right)$$

$$\alpha \approx \frac{2\,Vt}{c}\left(n + 1 - n^2\right)$$

For $n = 1{,}618$ $\alpha = 0$

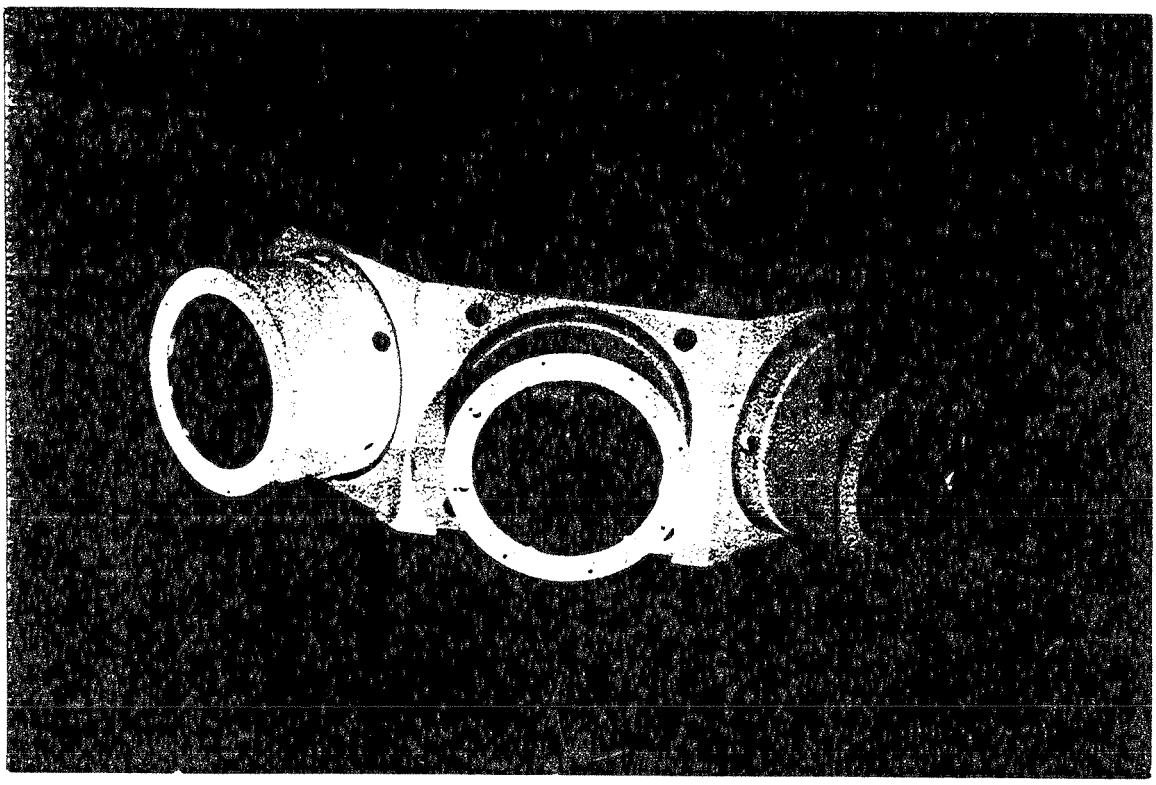

Retroreflector assembly for the Meteor-2 satellite

The central cube corner is made of fused silica and has a two-lobe FFDP providing nearly equal signal inten-sities for both cases (compensated and uncompensated velocity aberration).
One of the side reflectors is made of fused silica (n=1.46), the other of flint glass (n=1.62). Both reflectors have aluminium coatings on the reflecting surfaces and near-diffraction-limited FFDP's.

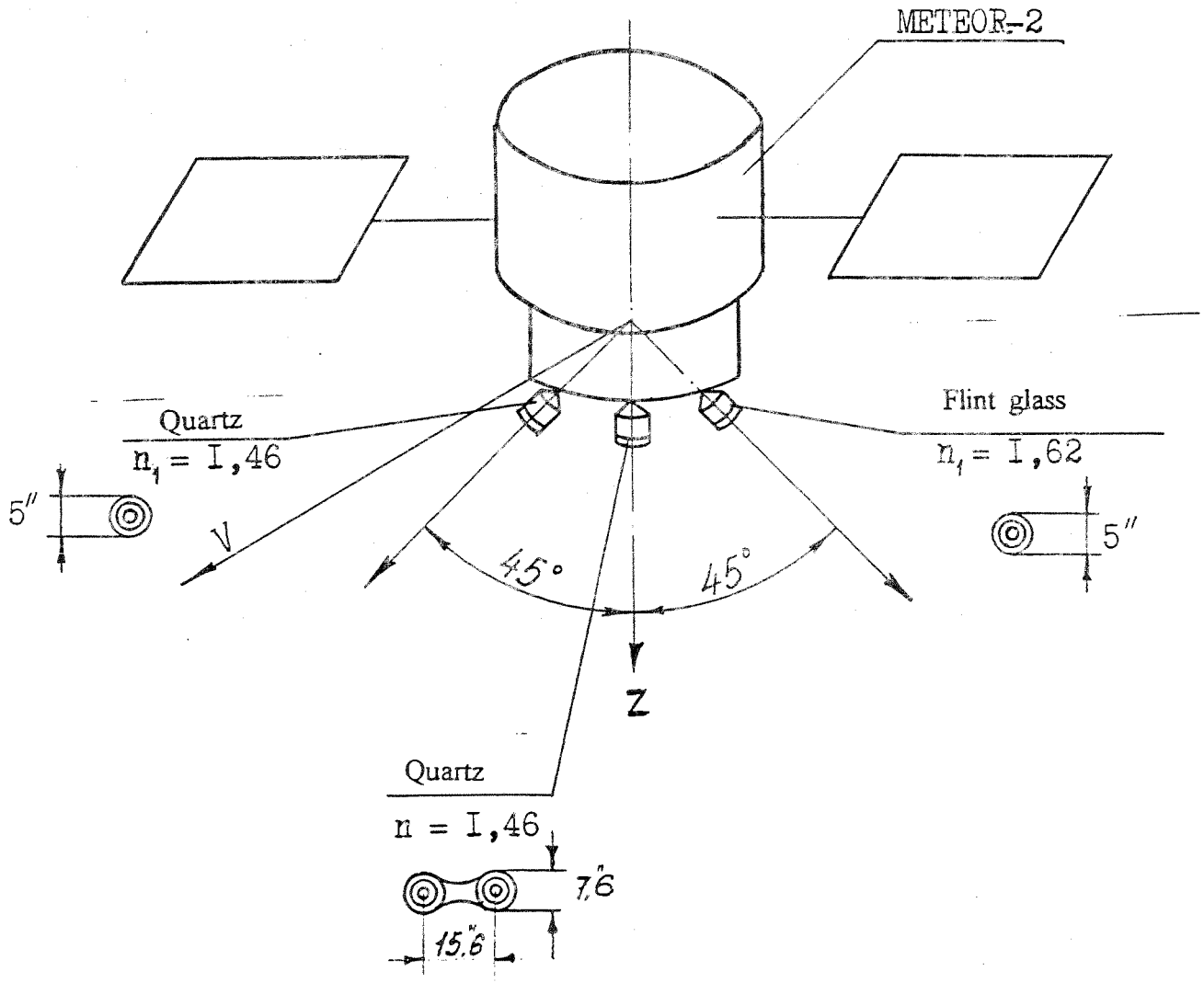

Accomodation of reflectors on METEOR-2

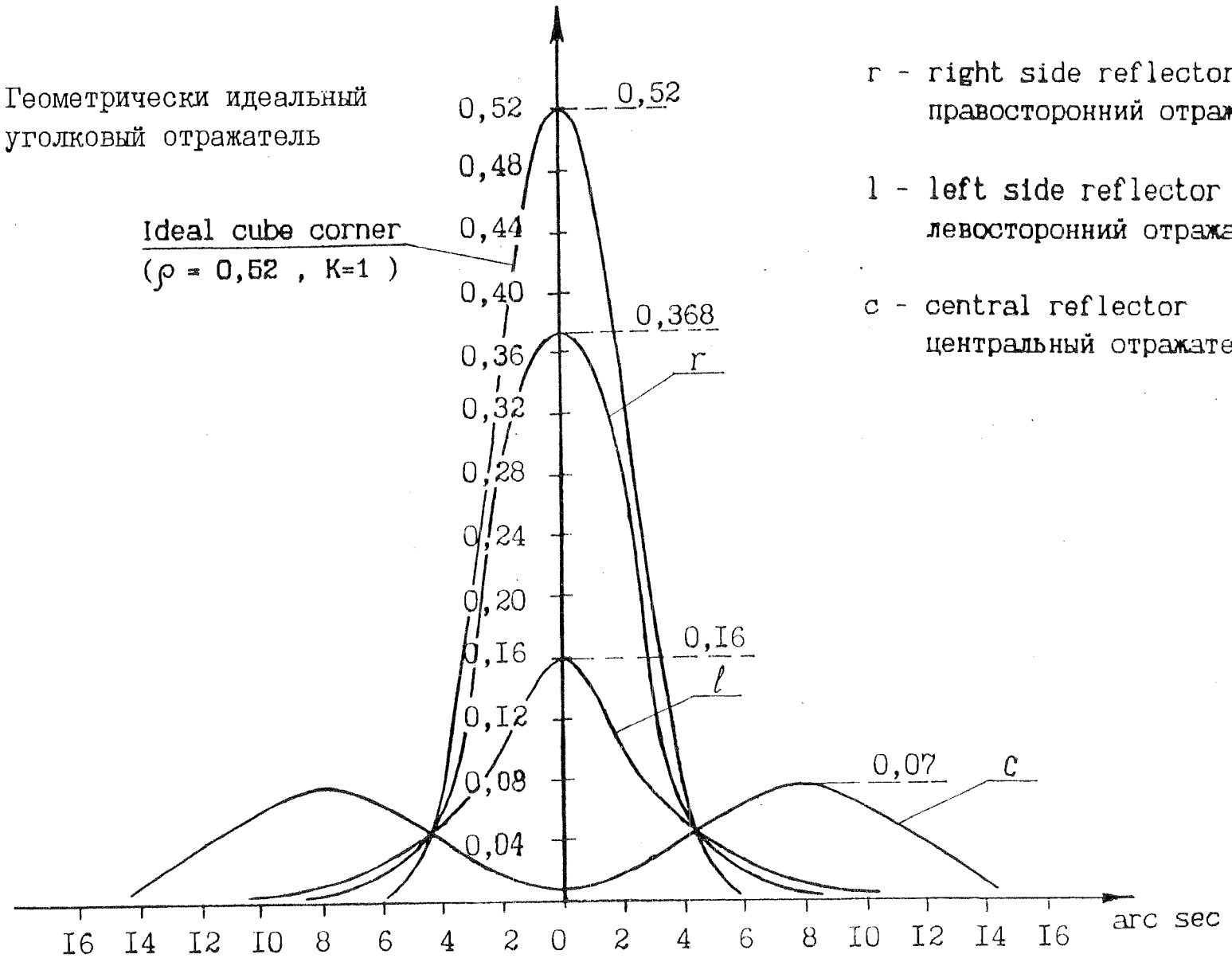

Fig.1. Far field diffraction patterns of cube corner reflectors.
Распределение поля в дальней зоне уголковых отражателей.

- The reflector pointed to the left side (when looking along the velocity vector of the satellite) is made of glass having a refraction index $n \approx 1.62$ so that it would provide a perfect compensation of the velocity aberration by the Fizeau effect (if such a phenomenon really takes place). The reflector pointed to the right side is made of fused quartz ($n=1.461$) and should provide partial compensation of the velocity aberration. The central reflector made of fused quartz is used for calibration. All cube corners have a clear aperture diameter of 47 mm.

- If there is no influence of the Fizeau effect on the reflected beam direction, the probability of signal detection from the side reflectors would be near zero. If a compensation takes place, the signal from the left-side (glass) reflector must be strong (as strong as in a static case), and from the right-side (quartz) reflector it must be an order of magnitude less (but strong enough for registration).

- Calculations were made of the expected levels of reflected signals from all cube corners for two cases (with and without compensating influence of the Fizeau effect), taking into account the parameters of the three stations taking part in the experiment:
  - MOBLAS-4 (Monument Peak, CA);
  - MOBLAS-7 (Greenbelt, MD);
  - Russian-Uzbek station at Mt.Maidanak (Uzbekistan).

Data for the tables 1 and 2 were taken from 7 satellite passes registrated by MOBLAS-4, 3 passes registrated by MOBLAS-7 and 5 passes registrated by the Maidanak station.

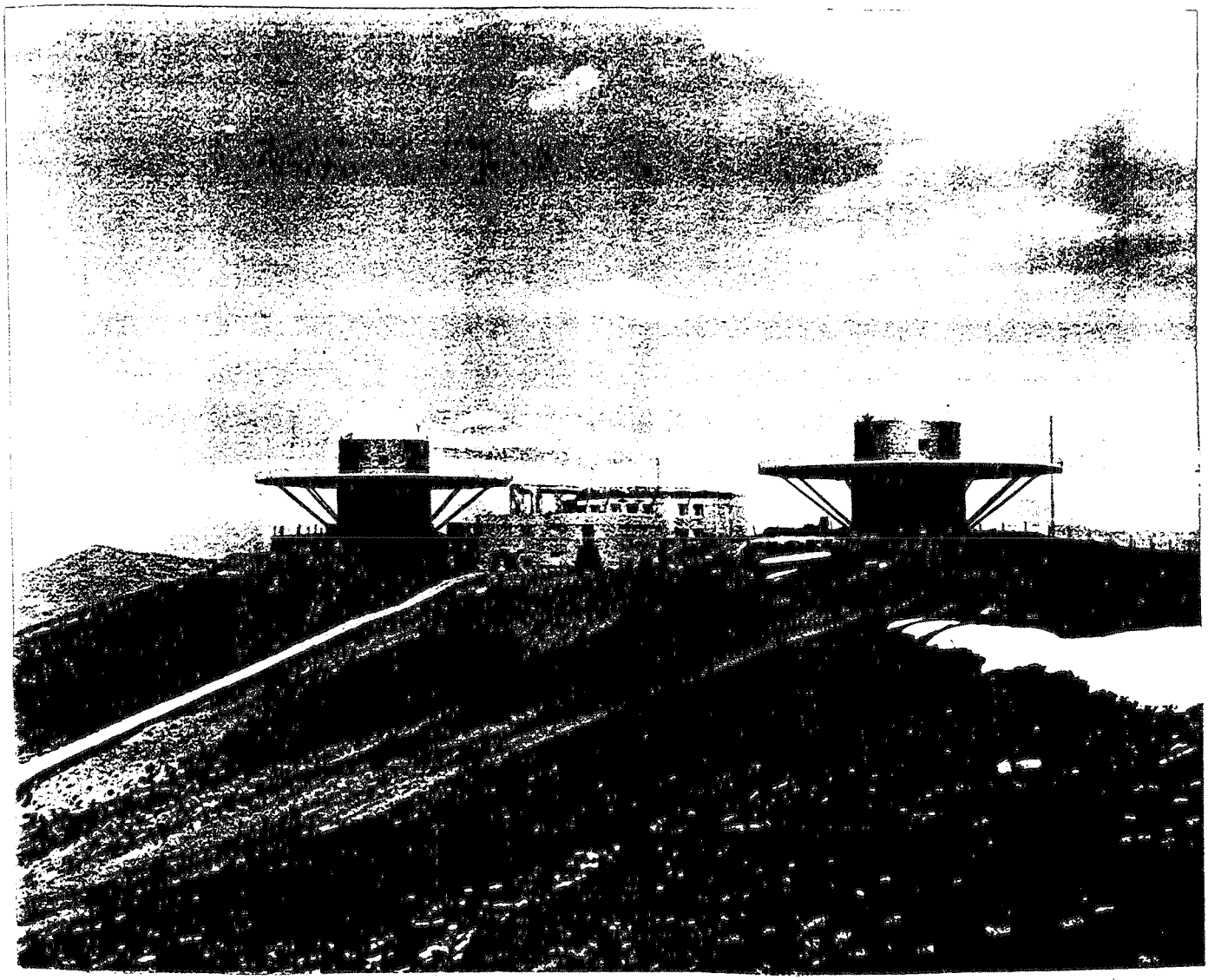

SLR station Maidanak
Outline view of the complex

Table 1

Results of measurements and calculations for the rigth-side cube corner (quartz, n=1.46)

Date	Label	β_{max}	$R_{(km)}$	n_{pe} (measured)	With compensation of velocity aberration		Without compensation of velocity aberration (α_{max}=10.1 arc sec)		Station
					n_{pe} (calculated)	$\frac{n_{pe}(calc)}{n_{pe}(meas)}$	n_{pe} (calculated)	$\frac{n_{pe}(calc)}{n_{pe}(meas)}$	
3/31	d8914	41°	1328	$1.62 \cdot 10^{4}$	$9.84 \cdot 10^{4}$	6.08	9.0	$9.1 \cdot 10^{-5}$	MOBLAS-4
4/1	d9014	24°	1835	$3.0 \cdot 10^{4}$	$2.16 \cdot 10^{4}$	0.72	2.01	$6.7 \cdot 10^{-5}$	MOBLAS-4
4/6	d9523	42°	1308	$1.39 \cdot 10^{4}$	$1.04 \cdot 10^{5}$	7.48	9.6	$6.9 \cdot 10^{-4}$	MOBLAS-4
4/8	g9720	48°	1204	$3.14 \cdot 10^{3}$	$1.04 \cdot 10^{4}$	3.31	1.1	$3.5 \cdot 10^{-4}$	MOBLAS-7
4/8	d9713	44°	1271	$1.16 \cdot 10^{4}$	$1.13 \cdot 10^{5}$	9.72	11.0	$9.5 \cdot 10^{-4}$	MOBLAS-4
4/9	d9813	26°	1754	$6.01 \cdot 10^{3}$	$2.81 \cdot 10^{4}$	4.68	2.28	$3.8 \cdot 10^{-4}$	MOBLAS-4
7/26		29°	1632	33.1	27.2	0.82	$2 \cdot 10^{-3}$	$6 \cdot 10^{-5}$	MAIDANAK
7/27		48°	1208	33.3	81.9	2.46	$1 \cdot 10^{-2}$	$3 \cdot 10^{-4}$	MAIDANAK
7/30		28°	1670	29.6	25.4	0.86	$2 \cdot 10^{-3}$	$7 \cdot 10^{-5}$	MAIDANAK
7/31		46°	1235	42.4	79.5	1.87	$9 \cdot 10^{-3}$	$2 \cdot 10^{-4}$	MAIDANAK

The signals reflected from the right-side (quartz) prism are always in good agreement with those calculated for an assumed partial compensation of the velocity aberration by the Fizeau effect

Table 2

Results of measurements and calculations for the rigth-side cube corner (flint glass, n=1.62)

Date	Label	β_{max}	$R_{(km)}$	n_{pe} (measured)	With compensation of velocity aberration		Without compensation of velocity aberration (α_{max}=10.1 arc sec)		Station
					n_{pe} (calculated)	$\frac{n_{pe}(calc)}{n_{pe}(meas)}$	n_{pe} (calculated)	$\frac{n_{pe}(calc)}{n_{pe}(meas)}$	
3/14	g7200	50°	1176	$1.31 \cdot 10^3$	$5.21 \cdot 10^4$	39.8	6.4	$4.9 \cdot 10^{-3}$	MOBLAS-7
3/18	g7600	51°	1162	$1.17 \cdot 10^3$	$5.3 \cdot 10^4$	45.3	6.8	$5.8 \cdot 10^{-3}$	MOBLAS-7
4/1	d9012	39°	1370	$7.76 \cdot 10^3$	$4.29 \cdot 10^5$	55.3	49	$6.3 \cdot 10^{-3}$	MOBLAS-4
4/2	d9101	36°	1441	$8.3 \cdot 10^3$	$3.78 \cdot 10^5$	45.6	43	$5.2 \cdot 10^{-3}$	MOBLAS-4
7/31		23°	1878	11.3	54.7	4.84	$4.9 \cdot 10^{-3}$	$4.3 \cdot 10^{-4}$	MAIDANAK
7/30		30°	1570	52.8	94.8	1.80	$6.3 \cdot 10^{-3}$	$1.2 \cdot 10^{-4}$	MAIDANAK

The signals reflected from the left-side (glass) prism are in good agreement with those calculated for full compensation of the first effect by the second, but only for the set of measurements taken by the Maidanak station. The MOBLAS-4 and MOBLAS-7 measurements show a 1.5 orders of magnitude lower signal intensity than one calculated for a compensated case. Nevertheless, the measured intensities are always much higher than the calculated ones for the uncompensated case. The difference may be caused by thermal effects arising from the different sun illumination conditions of the Meteor-2 satellite at the sun-syncronous orbit in spring (MOBLAS measurements) and summer (Maidanak measurements).

Conclusion

Strong reflected signals were received during the experiment from cube corner reflectors having near-diffraction-limited far field diffraction patterns, while the FFDP's angular width was far less than the velocity aberration angle. It may be confirmation of the presence of a compensating influence of the Fizeau effect.

On board of a Resourse satellite scheduled for launching in early November two cube corner reflectors with near-diffraction-limited FFDP's are mounted, which are destined for continuation of such experiments.

NEW MOBILE STATIONS

Chairperson : Erik Vermaat

9th International Workshop on Laser Ranging Instrumentation
Canberra, November 7-11, 1994

PORTABLE SATELLITE LASER RANGING SYSTEM

Maris Abele, Janis Balodis, Arvids Kalnins, Augusts Rubans, Janis Vjaters,
Owen West, Ansis Zarinjsh

SLR Research Pty Ltd
Level 3, 30 Kings Park Road
WEST PERTH WA 6005, Australia
Fax: 61-9-257 1892

ABSTRACT

A project to design and construct a portable satellite laser ranging system (PSLR) has been developed and its progress is reported.

It is planned to use the PSLR for the same purposes that mobile SLR instruments are currently used. The size of the PSLR is however dramatically reduced and the construction philosophy allows for the instrument to be dismantled into convenient small, lightweight elements for transportation to observation sites. This modular system allows for easy and quick assembly and adjustment of the instrument at the new location.

The alt-azimuth telescope has a lightened ceramic glass main mirror with a diameter of 620 mm and the optical system is designed to minimize the number of optical surfaces which are supported by a thermocompensated mechanism. The optical system is designed for the use of multi frequency laser transmitters. The telescope mount and control electronics have been constructed to permit a vast range of tracking speeds and high accuracy automated pointing in order to observe all satellites equipped with retroreflectors, including low altitude and geostationary candidates.

A portable lightweight computer performs all control functions and observation logging automatically using the company developed proprietary software.

INTRODUCTION

The main goals pursued for the development of a portable satellite laser ranging system were to reduce the size of the mount and to improve the ability to move the SLR from one site to another in order, amongst other things, to combine GPS and SLR observations in satellite geodesy networks for their absolute positioning improvement (Degnan and Pavlis, 1994).

Some initial approaches to design a mobile SLR telescope concept proceeded from the consideration of the primary mirror technologies (Abele et al., 1988-1989). The horizontal mount is the most convenient construction method for telescope mounts for tracking low altitude satellites, including their observations in the zenith zone (Mihelson, 1961). Experience with this design and manufacturing constraints has been acquired with two similar telescopes, "YUKON" (Abele et al., 1988-1989) and ULIS-630 (Serafimov et al., 1986) and proved the merits and shortcomings of such mounts. Unfortunately the mass and size of these telescopes appears too large for their construction and application as a portable SLR telescope. Used almost exclusively all over the world, the conventional alt-azimuthal telescope mount facilitates certain advantages for portable SLR devices, i.e. both small size and

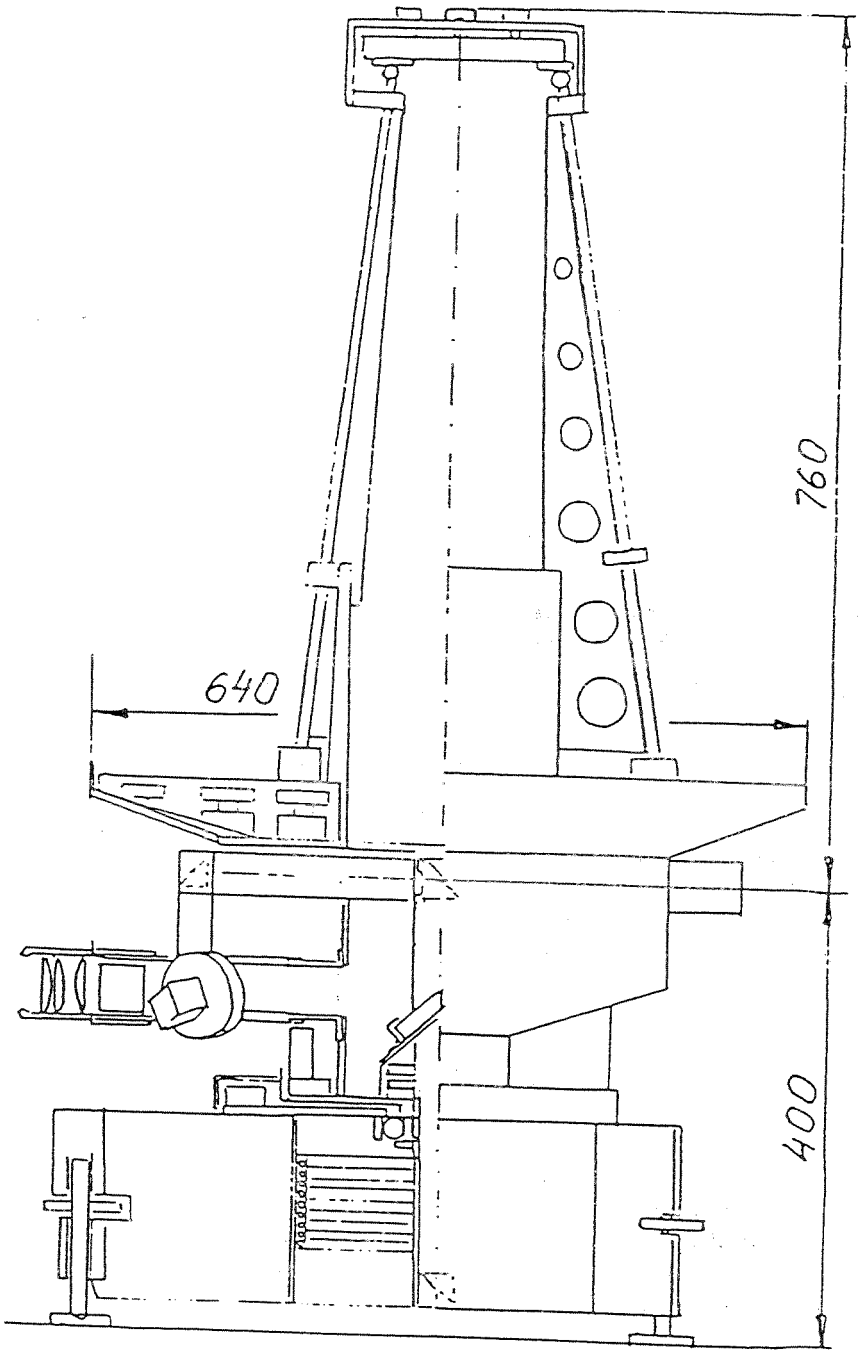

Figure 1. PSLR telescope mount

reasonable weight. These advantages were tested and proved in the form of a stationary SLR (Abalakin et al., 1985). The main optical system was used for all the telescope optical channels : receiving, transmitting and visual. The optical channel's commutator was used (Abele et al., 1988-1989), which gives the ability to create unmoving focal planes for corresponding optical channel devices. The utmost shortcoming of alt-azimuthal telescope is the tracking difficulties of quickly moving objects at the zenith zone. However, even in spite of this, the alt-azimuth mount is used in many other SLR telescopes (Wilson 1982; Johnson et al., 1985; Varghese, 1986; Bauersima et al., 1991; Dassing et al., 1989; Jiang Chongguo 1988).

The common work of Latvians and Australians in attempts to restore the Latvian triangulation network, created a need for the development of a portable satellite laser ranging systems (Abele et al., 1994). Recently a project to design and construct a fourth-generation portable satellite laser ranging system (PSLR) has been developed and shortly a report on its progress will be published.

MECHANICAL CONSTRUCTION

The alt-azimuth telescope mount has lightened mechanical construction with the possibility to easily dismantle it into separate components to allow packaging in several ordinary travelling cases in order to move the telescope from site to site by car or plane. On arrival at a site, it is easy and quick to assemble the telescope and to perform adjustments. No special building for observations is needed. It is expected that the PSLR will be operated in an open air regime where it is mounted on the specially designed very stable tripod, on which also some other devices are placed, such as the laser transmitter, etc. The telescope mount contains a foundation with azimuthal plate, an azimuthal frame, elevation frame and the secondary mirror mount.
A general view of the mount of the PSLR is shown in Figure 1.

OPTICS

The telescope has a lightened ceramic glass mirror (weight 18 kg) with an aperture of 620 mm. The optical system have been designed to minimize the number of optical surfaces. Thermocompensation mechanisms are employed to avoid the expansion effects on the optical handling system. The optical system is achromatic and therefore a multi frequency laser transmitter can be used. The principal optical design is shown in Figure 2.

The optical system permits the following:

* The optical system is able to transmit and to receive both visible light and infrared light without any additional adjustment.
* It is expected that the atmosphere turbulence effects will be eliminated because all of the 620 mm aperture is used for the transmission of double frequency (or multifrequency) electromagnetic beam propagation.
* Eyesafe security for people at any distance from the PSLR (in aircraft as well) because the energy concentration on the area of 1 cm^2 on main mirror is relatively small. The laser beam being distributed over the large area of the main mirror significantly reduces any danger.
* The PSLR can be used also for other purposes, for example lidars, because of the modular construction principle whereby the laser oscillator as well as the receiver modules can be changed quickly and easily.

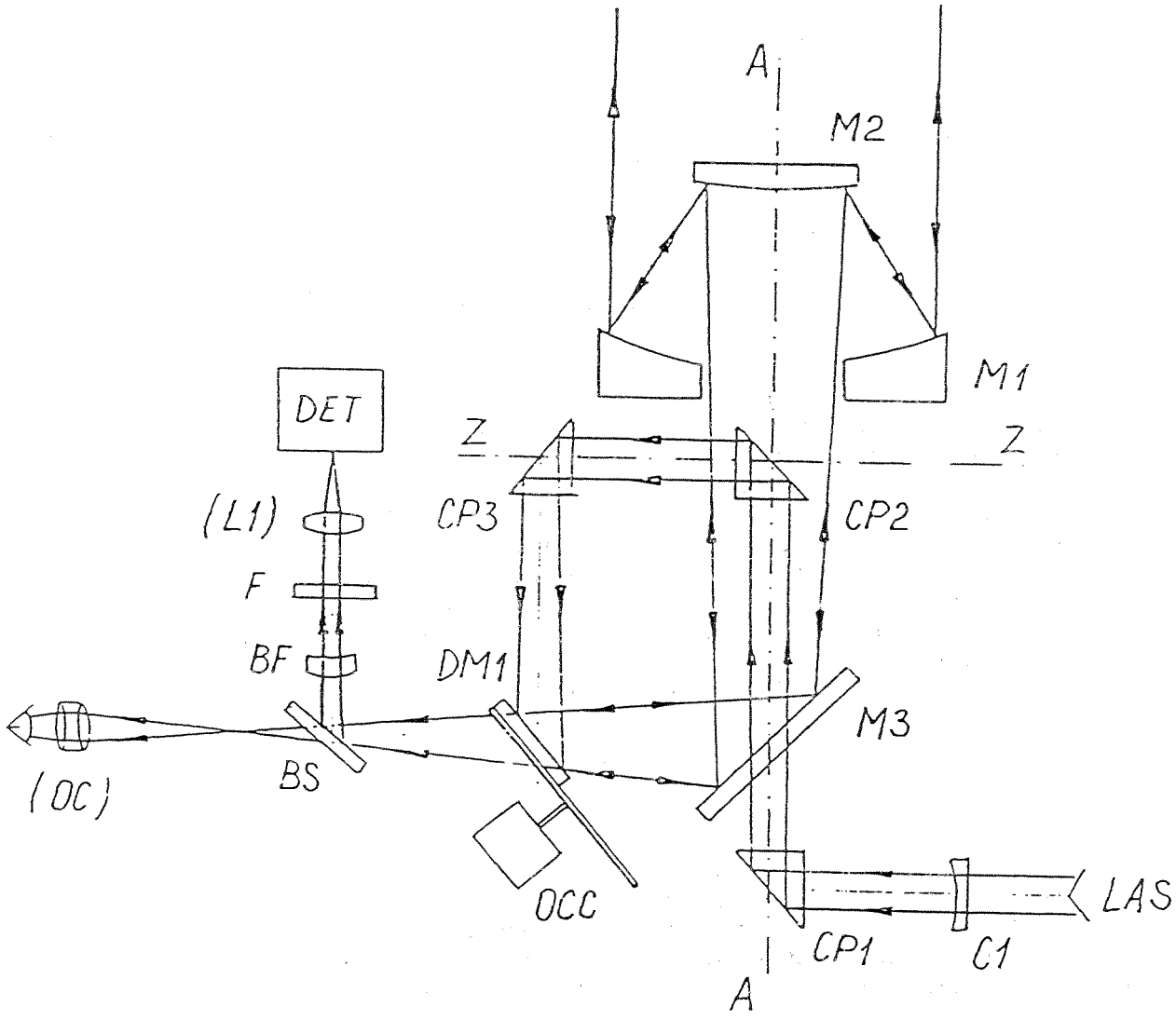

Figure 2. Optical design of PSLR

M1 - primary mirror
M2 - secondary mirror
M3 - diagonal mirror
BS - beam splitter
OC - visual channel
LAS - laser transmitter
AA - azimuthal axis
DET - photoelectrical channel with stop photodetector

CP1, CP2, CP3 - corner prisms
L1 - field lense
DM1 - deflection mirror
OCC - optical channel's commutator
C1 - laser beam collimator
F - dichroic filter
ZZ - elevation axis
BF - lense beamformer of photoelectrical channel

At the time of writing the PSLR optical system has been calculated and constructed but not adjusted and tested in an operational environment.

TELESCOPE CONTROL AND DATA ACQUISITION SYSTEM

An IBM PC compatible computer is used for telescope control and data acquisition systems. Control electronics are designed as ISA compatible extension PCB's, an intelligent docking unit can be used to accommodate them in a notebook PC without extension slots. It ensures a following functionality (Figure 3):

* Provides internal system time scale (station time). To synchronise with external sources a 1 PPS input is required (usually from GPS). Event time recording is supported with resolution of 100 Ns and this will be upgraded to 20 Ns.
* Generates pulses for stepper motor drives. The maximum supported step frequency is up to a few hundreds of Hz. Step generation is synchronised by station time scale.
* Control of the optical channel's commutation (OCC) drive.
* Support of the incremental angular encoder interface for both altitude and azimuth axes.
* Provides the gate and window for both the satellite and calibration ranges. Range gate is supported within the interval $(2^0 - 2^{49})$* 100 ns and window size $(2^0 - 2^{16})$* 100 ns with resolution of 100 ns.
* Laser trigger control. Maximum firing rate is 10 Hz.
* Control of mount end switches.

Interface to all peripherals is decoupled by opto - couplers.

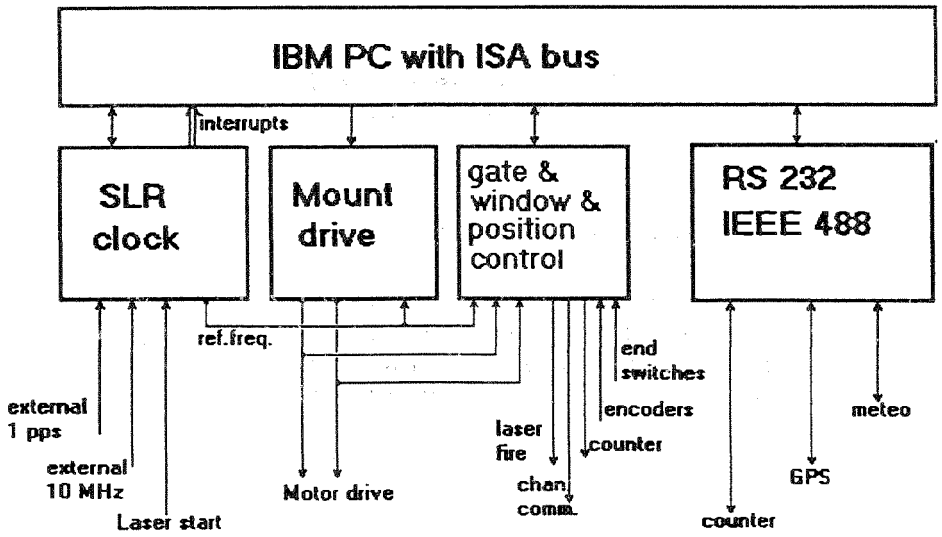

Figure 3. PSLR control data interchange

LASER AND OPTICAL DETECTORS

The computer controlled laser firing rate up to 10 Hz is supported by channel commutator. It is possible to install various kind of lasers; currently the Nd: YAG

laser has been installed with pulse duration 130 ps, wavelength 1064/532/355 nm and pulse energy 250/100/40 mJ respectively. Dimensions of the laser head are 250x190x680mm. Another laser with pulse length 20 - 50 ps has been ordered and will be available soon.

Enhanced photomultipliers will be used as optical detectors as well as internationally approved time interval counters.

SUMMARY

A portable satellite laser ranging system has been constructed and its adjustment and control tests will commence soon.

The total weight of PSLR is approximately 65 kg.

The PSLR is able to be dismantled into lightweight modules for convenient transportation. The modular system allows both the easy and quick assembly and adjustment of instrument at the observation location.

The optical system is able to transmit and receive both visible and infrared light without any additional adjustment.

This design philosophy allows the creation of a fourth-generation laser ranging systems .

The PSLR optical system enables a high degree of eye safety security for people from laser lights.

The PSLR internal time base can be synchronised with GPS or any other external source.

The portable satellite laser ranging system's lightweight computer performs all the PSLR control functions as well as the onsite normal point computation and the result transmission to central archives.

ACKNOWLEDGEMENT

The authors thank the Vice Chancellor of Curtin University of Technology Professor John Maloney and Dr. Mervyn Lynch for their valuable work in the very beginning of this project. Thanks to Igor Altuhov, Juris Katkevitch, Irina Bistrova, Peteris Rozenbergs, Sigurds Trops and Agris Petersons for their technical aid.

REFERENCES

Degnan J.J., Pavlis E.C. Laser Ranging to GPS Satellites with Centimeter Accuracy. In: GPS World, September 1994, pp. 62-69.

Abele M., Balodis J., Vjaters J., Zhagars J., Zarins A., Lapushka K., Rubans A., Salmins K., Tarasova A. Final Report "Elaboration of Automated Satellite Laser Rangers of II and III Generation, Principal Schemes, Matematical Maintenance and Production of their Models". Riga, 1988 - 1989. Vol. 1, 42 p., Vol. 2, 92 p. Dep. VINITI No. 02.88.0077291, Vol. 3, 97 p. Dep. VINITI No. 02.90.0017897, (in Russian).

Mihelson N.N. Horizontal Telescope Mount. In: Proc. of Main Astronomical Observatory, Pulkovo, No. 4, 1961, pp. 131-140 (in Russian).

Serafimov K., Abele M., Vjaters J., Stoykov A. Possibilities, Properties and Characteristics of the Universal Laser System of Third Generation "ULIS-630". Proc. 4th Simposium 26th Plenary Meeting of the Comm. On Space Res. XXVI COSPAR 86. Abstracts. June 30-July 11, 1986, Toulouse, France. p. 23.
Abalakin N.K., Abele M., Artyuk J.N., Basov N.G., Bronnikov V.N., Ignatenko J.V., Kokurin J.L., Kurbasov V.V., Lapushka K.K., Lobanov V.F, Masevich A.G., Sukhanovsky A.N., Shilokhvost J.P., Shubin S.G., Jatskiv J.S. Laser Network Design for the Moon and Artificial Earth Satellite Ranging. Proc. International Conference on Earth Rotation and the Terrestrial Reference Frame. July 31- August 2, 1985, Columbus, Ohio. V. 1, pp. 246-256.
Wilson P. The German/Dutch Mobile Ranging System. Proc. of the 4th International Workshop on Laser Ranging Instrumentation. Geodetic Institute of the University of Bonn, 1982. pp. 468-483.
Johnson T.S., Bane W.L., Johnson C.C., Mansfield A.W., Dunn P.J. The Transportable Laser Ranging System Mark III. IEEE Trans. on Geoscience & Remote Sensing. Vol. GE-23 No. 4, July 1985. pp.324-331.
Varghese T. System Characterization of MOBLAS 7 for Collocation with TLRS 1 & 2. Proc.of the 6th International Workshop on Laser Ranging Instrumentation. Antibes - Juan Les Pins, September 22-26, 1986.
Bauersima I., Utzinger J., Pop E., Gurther W. Konzeptioneller Entwurf eines kombinierten laser und astrographischen Telescops der Satellitenbeobachtungsstation Zimmervald. Satelliten - Beobachtungsstation Zimmerwald, Bericht Nr. 20, Univ. Bern, 1991. p. 51
Dassing R., Schluter W., Schreiber V. Status Report on the New Wettzell Laser Ranging System (WRLS). Proc. of the 7th International Workshop on Laser Ranging Instrumentation. Matera, Italy, 1989.
Jiang Chongguo. The Design of Analysis and Realization Method of LLR and SLR Systems. Publ. of Yunnan Observatory, Academia Sinica No. 3, 1988. pp. 1-9.
Abele M., Balodis J., Balodis M., West O., Vjaters J., Zuments U. Restoration of Geodetic Survey Network in Latvia and Associated Activities. In: Proc. of the XX General Assembly of International Association of Surveyors. Melbourne, Australia, 1994.

TRANSPORTABLE SATELLITE LASER RANGING SYSTEM

Y. Suzaki, K. Aikawa
Telecommunications Division
Hitachi, Ltd.
216 Totsuka-cho, Totsuka-ku
Yokohama 244, JAPAN
Telephone: 81-45-881-1221
Facsimile: 81-45-881-7364

T. Yamaguchi
Denoh System, Ltd.
202 SunCourt Totsuka
167-1 Totsuka-cho, Totsuka-ku
Yokohama 244, JAPAN
Telephone 81-45-871-0026
Facsimile 81-45-871-9650

ABSTRACT

A Transportable Satellite Laser Ranging System for practical use has been investigated. A compact, personal computer controlled tracking mount was developed. The entire system housed in a single van will be proposed.

INTRODUCTION

We developed the HTLRS, a transportable satellite laser ranging system, for the Hydrographic Department of the Maritime Safety Agency seven years ago[1]. The system is used by the Hydrographic Department for determining the precise location of Japanese isolated islands. The location determination has so far been completed on 12 islands. Based on the development experience, we are discussing development of a more durable, smaller, and simpler satellite laser ranging (SLR) system. The goal is to implement a system, which is more compact than, but functionally equivalent to the HTLRS, employing a single photon detection method to allow LAGEOS ranging. The system will feature a tracking mount that is made more compact and lightweight, enabling the entire system to be housed in a single van. We have made a prototype of a tracking mount employing a mass-produced, compact, direct-drive motor with a built-in encoder for its azimuth, elevation axis drive motor. The tracking mount, currently being under tracking test for a fixed star and the AJISAI, has shown performance of 3 seconds (rms) in the automatic TV tracking mode for the fixed star, and 15 seconds (rms) in the calculated tracking mode for the AJISAI.

1. Study of System Size

To what extent an SLR system can be made compact is one of the development subjects, and several prototype systems have been developed[2][3]. We define the size of the SLR system, S, as follows[1]:

$$S = n \cdot Eo \cdot Ar \cdot \alpha\beta\gamma \cdot \eta \quad (1)$$

where, n is the laser repetition rate, Eo is the laser output energy, Ar is the area of receiver optics, $\alpha\beta\gamma$ is the optics efficiency, and η is the quantum efficiency of the detector.

During night operation, the error count due to background noise can be decreased to nearly zero by the range gate and narrow FOV at the single photon level. Figure 1 shows the requirement for the system size to obtain a single photon return per second for the LAGEOS and the AJISAI in single photon detection meeting the above condition. The horizontal axis represents the system size S, while the vertical axis represents beam div. The calculation is based on an assumption that the satellites are seized by 100% in the beam div. range. From this viewpoint, we assume that the vertical axis shows the necessary pointing accuracy. The HTLRS system size was designed to be 3.8W.cm^2, but the theoretical value of beam div. 100 arc sec. shows that reception of one count per second from the LAGEOS can be expected. In the actual use (i.e., in the HTLRS), the reception is performed in the range of beam div. 20 through 40 sec. under favorable conditions. Thus, a factor of 1/25 needs to be included for 20 arc sec. This is perhaps because the atmospheric transmittance is lower than the calculated expected value, since the HTLRS is operated at a low altitude near the seashore. Most SLR systems are operated at a low altitude near the seashore or metropolitan areas in Japan. Since this tendency will continue, it is important to consider a factor of 1/25.

Assuming a system with S = 1W.cm^2 to make a system more compact than the HTLRS will lead to a required pointing accuracy of approximately 50 arc sec. as seen from the diagram. However, the required tracking accuracy (= beam div.) may be 10 arc sec. ($\pm$5 arc sec.), considering the factor of 1/25.

2. Prototype of Compact Tracking Mount

Through the system size discussion, we are contemplating implementation of a system of S = 1W.cm^2 with a pointing accuracy of $\pm$5 arc sec. The system of 1W.cm^2 anticipates:

n: 10 Hz

Eo: 0.01 J (10 mJ)

Ar: 400 cm^2 (25cmØ)

$\alpha\beta\gamma$: 0.4

η: 0.07

Nd-YAG SHG laser and MCP PMT detector are taken into consideration, and yet semiconductor detectors with higher quantum efficiency are also discussed.

To implement such a system, we manufactured a prototype tracking mount of the construction shown in Fig. 2. The tracking mount of azimuth-elevation type is composed of a double-axis drive motor, transceiver telescope, and a transmitting coudé mirror system. The mount employs for its azimuth and elevation axis drive motor, a mass-produced, direct-drive DC motor with a built-in angle encoder and integrated load support bearings.

The hollow-type motor allows transmitting laser beams along the azimuth and elevation axes. The encoder resolution is rated at 5 arc sec., but since it is a mass production model, each has an inherent error, and the accumulated error can be 30 arc sec. at a maximum. The mount allows automatic tracking using a TV set, or calculated tracking under control of a personal computer. The calculated tracking is such that the angle data from the encoder are compared with the calculated values, and the control is made at a rate of 30 Hz by using the differences as error signals. Although the resolution of the encoder is designed to be 1.5 sec., the standard specifications for the production model are ±5 sec. in repeated recurrent accuracy, and ±30 sec. in absolute accuracy. The absolute accuracy of ±30 sec. means the maximum value of the accumulated error, that is, the inherent error which can be corrected with software. At present, automatic tracking testing for a fixed star and calculated tracking testing for the AJISAI resulted in a value of 3 arc sec. obtained for the former, and 15 arc sec. for the latter. The major reason for the error being large in the calculated tracking is that the accumulated encoder error is not compensated for. We will compensate for the error by means of software.

We expect to obtain the accumulated error data, necessary for the software error compensation, through continuous automatic tracking of a fixed star. Figure 3 illustrates a block diagram of the mount control system. The transceiver telescope is separated from the mount. A telescope with a diameter up to 40 cm can be installed through modification to the mount mechanism. The entire tracking mount weighs about 150 kg.

3. Other Hardware Discussions

One of the breakthroughs in implementing a compact and easy-to-operate system is to increase the pointing accuracy to allow operation with narrow beam div., thus enabling a compact, low output laser unit to be employed. We consider that the pointing accuracy will be increased through software modification to the above-mentioned inherent encoder error, and through automatic tracking.

Figure 4 shows the output, dimensions, and weight of the laser units so far employed. The use of a low-output laser contributes greatly to compactness and stabilization of the system. The target values for the time being are 10 mJ, and one half the size of the laser employed for the HTLRS.

A personal computer is employed also for control of the HTLRS. Control by means of a personal computer is considered appropriate, since it is easy to operate, and is expected to become even more compact with higher than ever performance. GPS synchronization unit will be adopted as the clock unit for the system to be developed.

4. Plan of Transportable SLR System

Figure 5 illustrates a conceptual diagram of the transportable SLR System contemplated. The entire system of the configuration will be housed in a single vehicle for transportation. The tracking mount and the laser unit will be integrated on the same optics bench whose three legs can be lifted up and separated from the van for self-supporting installation on the ground. The installation method is the same as the HTLRS. The roof canopy of the van housing the optics will allow opening and closing. All the electronics will be installed on two racks. The goal of the total weight of SLR components is within 1 ton.

5. Future Plan

Now, we completed a prototype of the tracking mount and finished a preliminary test. We are going to improve the tracking precision and add a ranging function to enable satellite ranging. We will also continue studying making the components more compact.

References:

1. M. Sasaki and Y.Suzaki, "Satellite Laser Ranging System at the Simosato Hydrographic Observatory and the Transportable System, HTLRS," Six International Workshop on Laser Ranging Instrumentation, Antibes-Juan Les Pins, September 1986

2. E.C. Silverberg and B. Schuts, "A Proposal for a Very Compact Laser Station for Operational Geodesy," Third International Workshop on Laser Ranging Instrumentation, Lagonissi, May 1978

3. T.S. Johnson, W.L.Bane, C.C. Johnson, A.W. Mansfield and P.J. Dunn, "The Transportable Laser Ranging System Mark-III," Fifth International Workshop on Laser Ranging Instrumentation, Herstmonceux Castle, September 1984

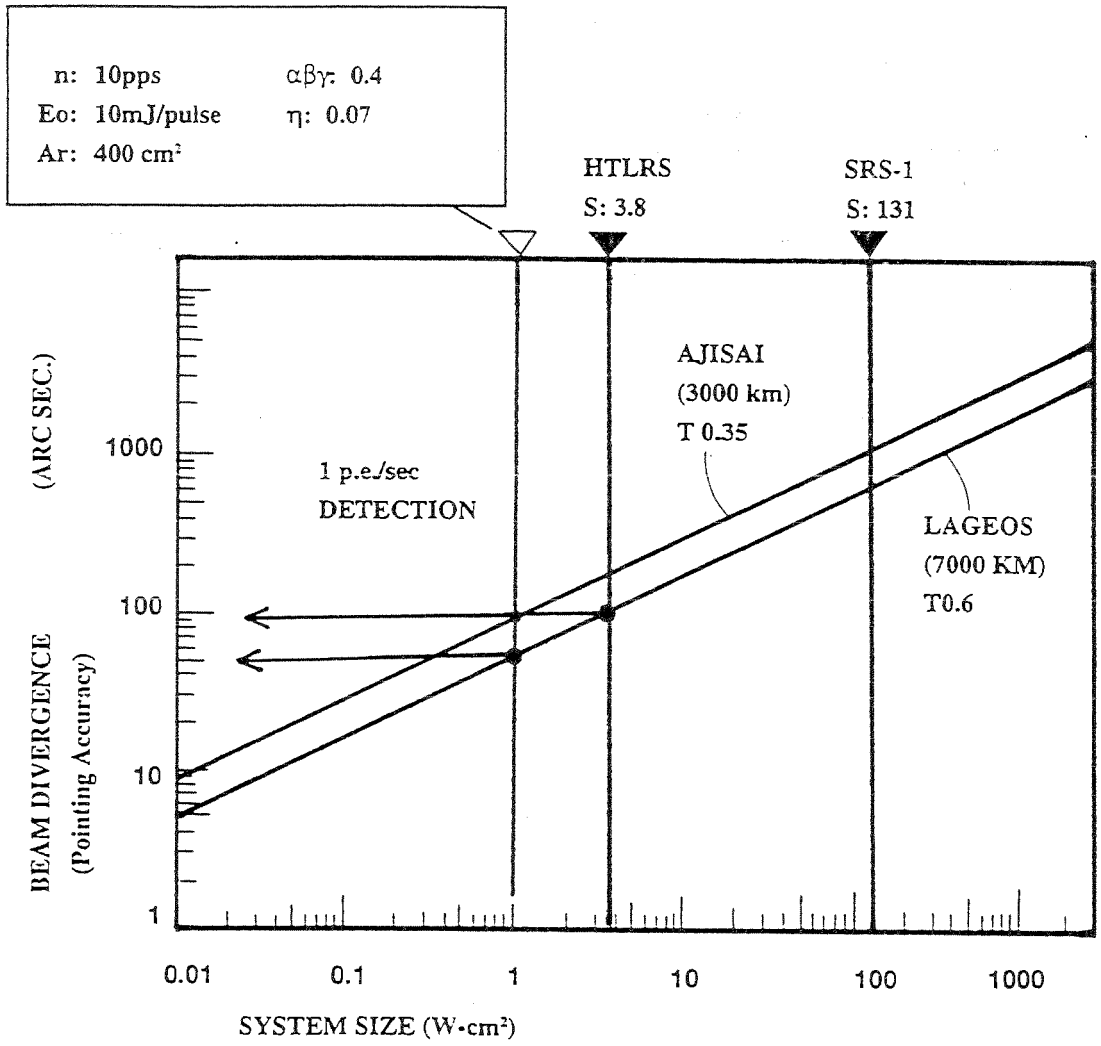

Fig. 1 Study of System Size

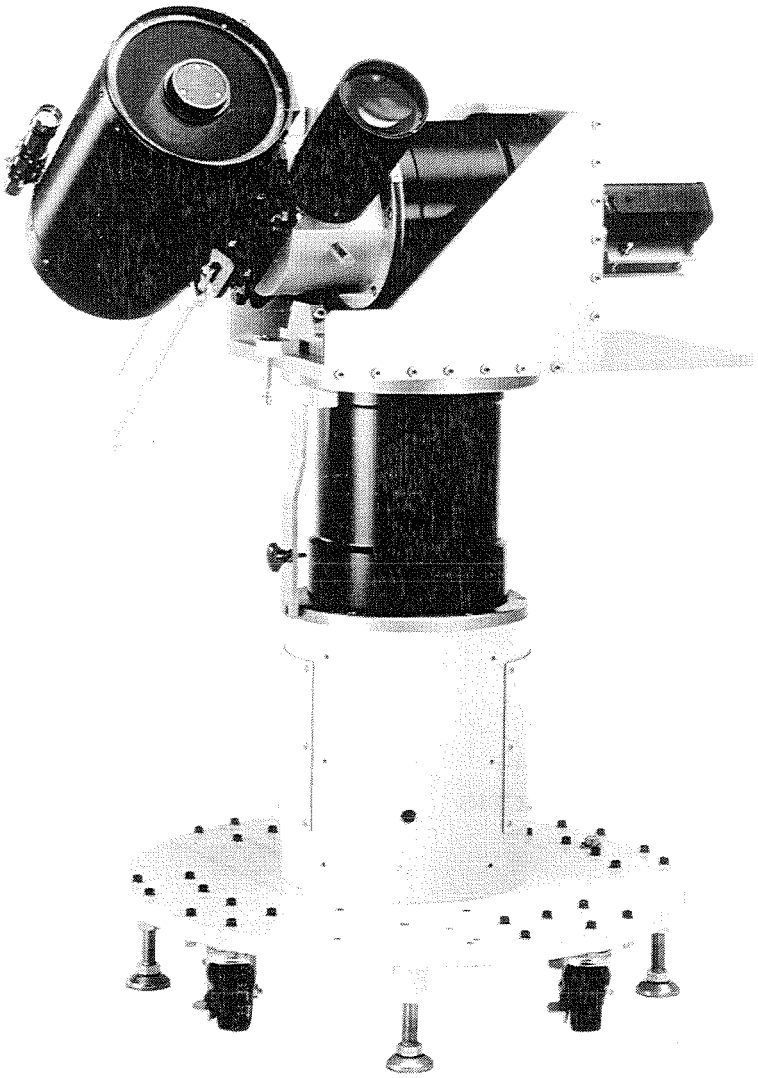

Configuration	Elevation over azimuth
Receiver Optics	25 cmø
Optical Efficiency	0.4
Encoder Resolution	1.6 arc sec.
Range of Tracking	Elevation: 20° to 80°
	Azimuth: ±260°

Fig. 2 Prototype Compact Optical Tracking Mount for SLR

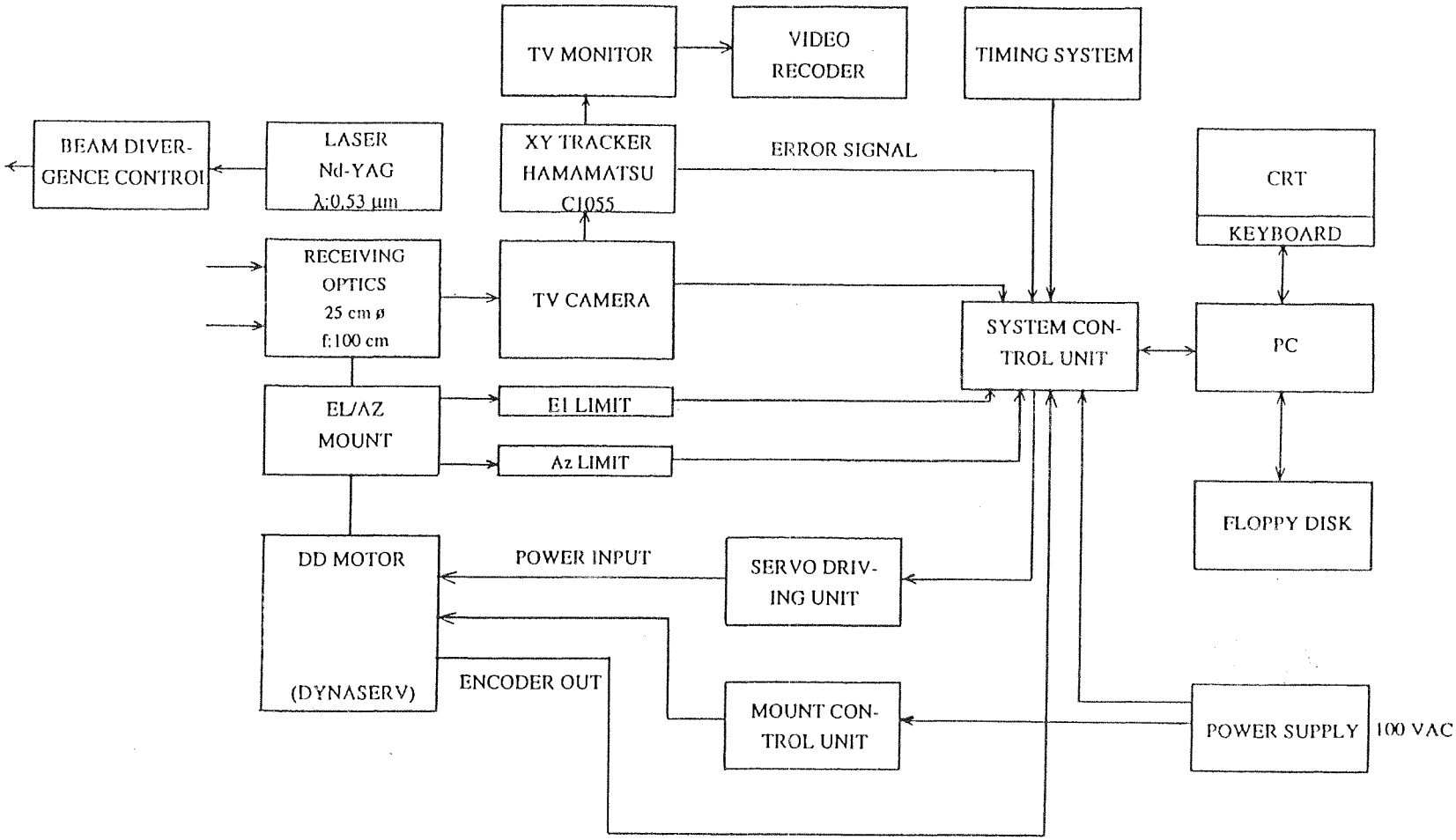

Fig. 3 Block Diagram of the Tracking Mount Control System

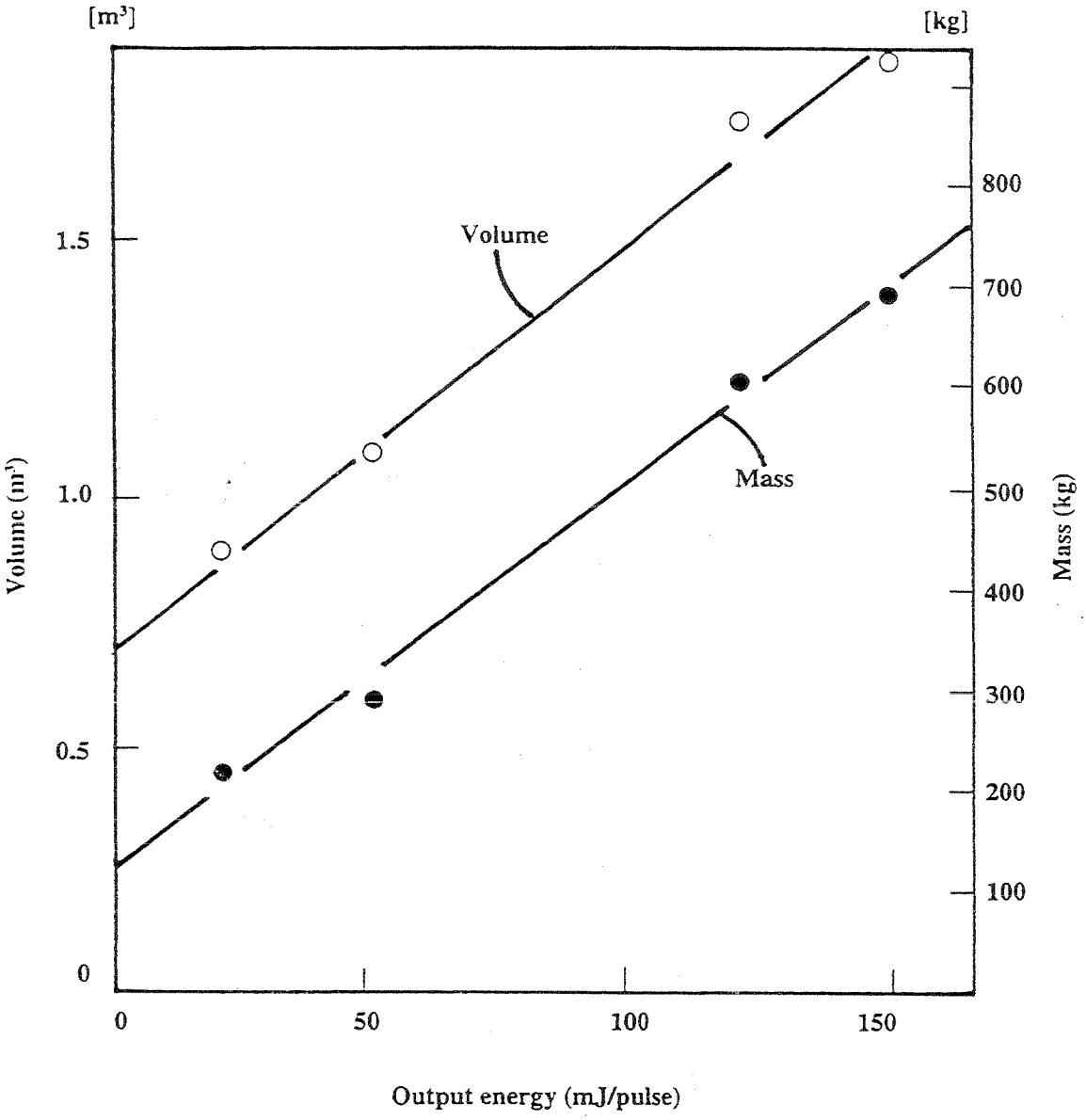

Fig. 4 Relationship between Size and Output of Flash Lamp Pumped Mode Locked ND-YAG Laser

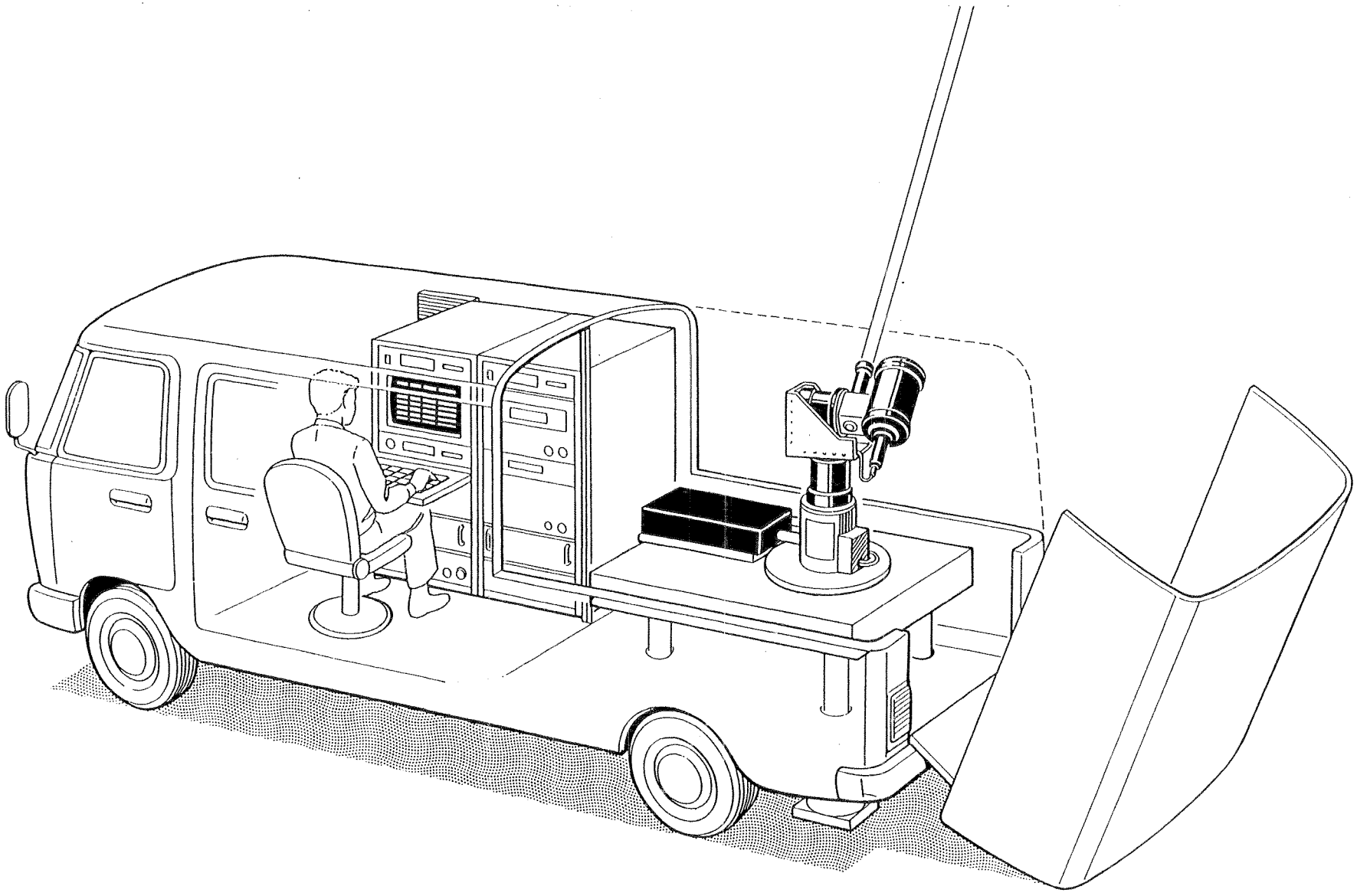

Fig. 5 Transportable Satellite Laser Ranging System

A Developing Transportable Laser Ranging System in China (CTLRS)

Xia Zhizhong, Cai Qingfu, Ye wenwei,
Wang Linhua, Guo Tangyoug
Institute of Seismology, State Seismological Bureau
Xiao Hong Shan, Wuhan 430071, China

Abstract

In order to set up a state geodesy control network and to monitor crustal movement. Since 1992, Institute of Seismology, State Seismological Bureau and Xi'an Reasurch Institute of Surveying and Mapping have cooperated to develop a transportable satellite laser ranging system. The system is composed of a Nd: YAG mode-locked laser, a telescope mount, receiving electronics equipment, time and frequency standard, and a computer etc. The repetition rate of the laser is 1—5pps, the wavelength is 532nm and the main pulse energy is 30mj. The diameter of the receiving telescope is 35cm. All these equipments can be installed in a cross-country vehicle consisted of two rooms, its loaded weight is 3.5 ton. The single shot ranging accuracy of the system will reach 2—4cm for LAGEOS and other satellites. The system will bm completed and put into operation in 1995. This paper proviled with the technical details of the system.

Key wmrds: Satellite laser ranging—TLRS

Introduction

Since 1980's, the 3rd generation satellite laser ringing network has been set up in Shanghai, Wuhan, Changchun, and Beijing in China. Each station can observe satellite ETALON, LAGEOS, ERS-1, TOPEX, etc in generally, the single shot accuracy can come up to 5cm. All station joined the international cooperative project of NASA (U.S.A). But the geographical distribution of the stations is not even, there aren't observation station in the western part of China. Thus, in order to set up a space geodesy network with reasonable distribetaon and monitor crustal movement benificially in China. Since 1992, Institute of Seismology and Xian Reasurch Institute of surveying and mapping have cooperated to develop a transportable laser ranging system which is suitable for China. The system can observe LAGEOS etc. and the ranging precision can reach 2—4cm. It is estimated that the system will be completed and come into operation in 1995.

System Configurations

1. Laser

The laser is a frequency doubled and colliding pulse mode-locked (CPM) Nd:YAG system that produces a mode-locked pulse train with a repetition rate of 1—5pps. The energy of the pulse train is concentrated in three pulses which are located at the center. These pulses are divided into one main and two minor, the energy ratio between the main and the minor is about 6 : 1 for second harmonic generation beam. The main pulse has 30 mj energy with wavelength 532nm and about 100ps width. The diameter of the output laser beam is 8mm. The laser transmitter assembly is located on a table under the mount, the volume of the table is 320×260×1320mm. This laser is developed by Shanghai Institute of Optics and Fine Mechanics.

The optical diagram of the laser is given in figure 1.

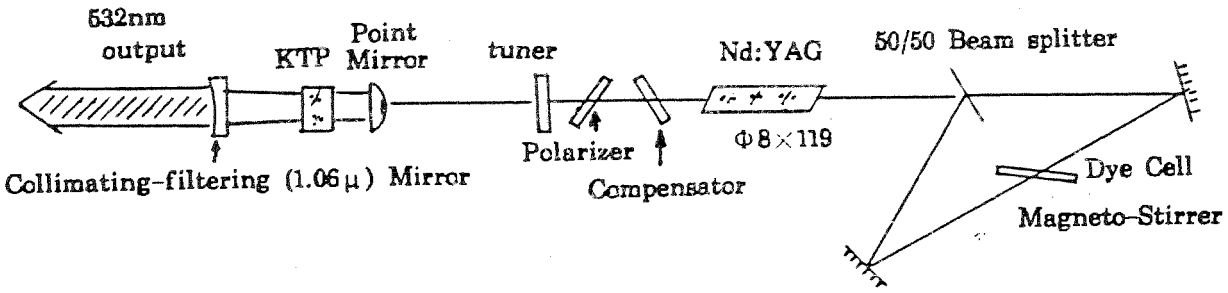

Figure 1. optical diagram of the Nd * YAG laser

2. mount

The mount has a forl of a gimballed elevation axis over the azimuth axis, the receiving and transmitting optics are concentric. A transmitter laser pulse along the azimuth and elevation axes is transmitted to the satellite by using the central part of receiving telescope. A returned signal from satellite is also received by the outer part of the same mirror. The optical block diagram of the system is shown in figure 2. The elevation and the azimuth axes are driven by DC-torque motor and controlled by both a tachometer and a synchronistic inductor (resolution 1 arcsec). The ranges of the azimuth and the elevation axes are ±270 deg. and −10 deg. to +190 deg. respectively. The tracking angular velocities are from sidereal to 2 deg/s for elevation and 15 deg/s for azimuth. The estimation of the tracking accuracy is within 10 arcsec.

2.1 *Transmitting optics*

The laser pulse beam transmitted from Nd:YAG laser with diameter

8mm is expanded to about 80mm by two beam expanders and reflected in a coude path along the azimuth and elevation axes by the mirrors. The divergence for output laser light is controlled from 100 μrd to 1 mrd by a motor. In order to measure the ground target for calibration, a attenuator for output laser beam is installed in the coude path.

2.2 *Receiving optics*

The aperture of the receiving telescope is 35cm and the focal length is 2.3m. The returned light from satellite is splitted in two ways by a split mirror. One light beam with the wavelength 532nm goes to a micro-channel-plate photomultiplier tube along the coude path and the another (except

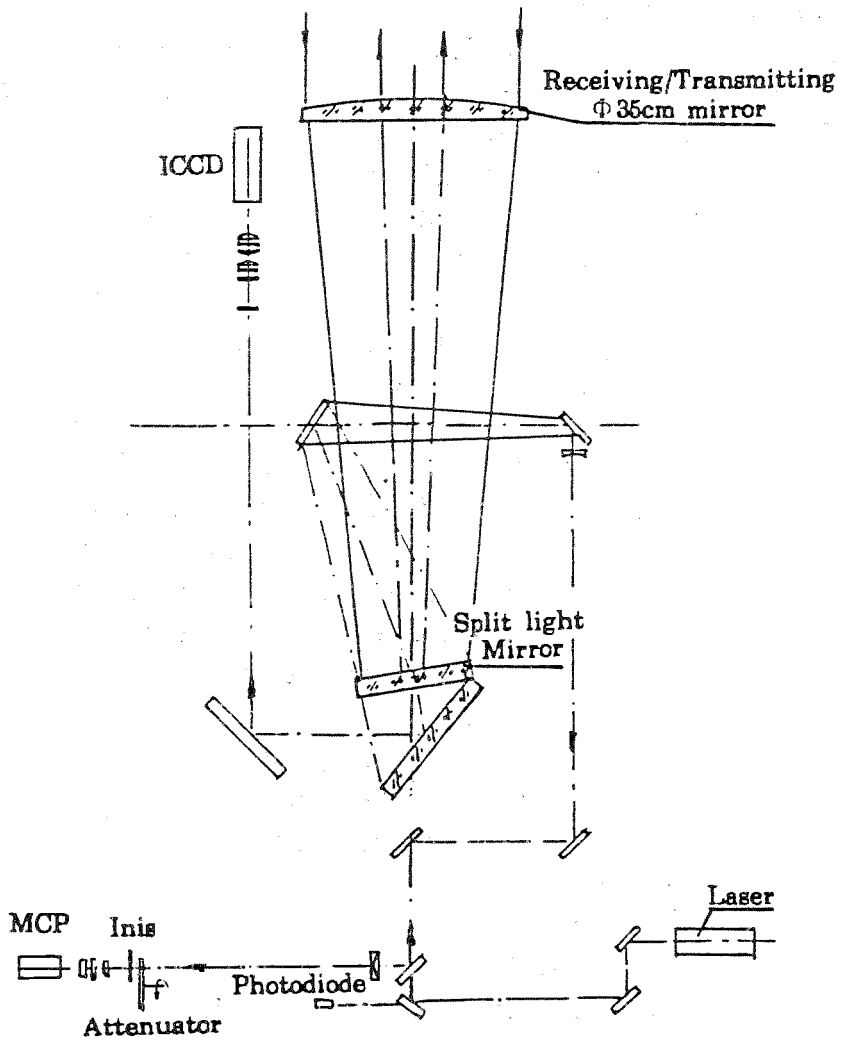

Figure 2. The optical block diagram of the system

532nm) goes to a television with an image intensifier for guiding satellite.

3. **Receiving electronics equipment**

In order to detect returned signal and to measure the flight time, the receiving eluctronics equipment includes a MCP photomultiplier, (Hamamatsu R2566U-07) two amplifiers (B&H DC3003A) a constant fraction discriminator (TENNELEC TC454) and a time interval counter (suanford Research system SR620 resolution 25ps). The external frequency standard of the counter is provided by a Rubidium clock. The MCP-PMT has a gain of 5×10^5(TYP) and a rise time of 100ps, the quantum efficiency is 6% at 532nm of the wavelength. The start pulse is detected by a photodiode (Hamamatsu S-2381 with 200ps risetime) behind the first mirror in the coude path.

4. **time and frequency standard**

A model TTR-6A NAVSTAR GPS Synchronized Time and Frequency standard (Allen Osborne Associates, Inc) is used as time and frequency standard for TLRS. This equipment contains a Rubidium clock which suppiles a 10 MHz signal with the stability of 1×10^{-11}, the timing accuracy of conrected 1pps output is about 100ns. The TTR-6A also includes a navigation, or position and program for refining local coordinates.

5. **Control and computer**

An IBM PC 386 computer will be used in the transportable laser ranging system as control center. Real-time clock range gate controller, data acquisition and laser shooting controller etc. are integrated on two extending circuit boards to be installed on the extension slots of IBM PC computer. Software regarding calculation of prediction, data processing, numerical track guiding, software managing etc. are all transplanted to this computer. While working, the tedescope is automatically guided towards the satellite by the track control part with the calculating result from ephemeris. In order to improve tracking accuracy, the tracking parameter (UTC time, azimuth, elevation) can be displayed and corrected in real-time during the observation, so that some of the status of the system and computed results are shown on the CRT colorfully and in picture. Figure 3 shows the display of some parameters on computer screen during the operation.

6. **Transportable manner**

All equipments are installed in a cross-country vehicle which has loading capacity of 3. 5ton. This vehicle is divided into two rooms. The receiving electronic control and computer, time and frequency standard etc. are set up in the front room with a air conditioner. The mount and laser are installed in the another one located at the back the vehicle. While working, the roof of the vehicle can be moved off and the mount and laser are jacked up by four jacks. The size of the vehicle is 2. 3m×3. 0m×6. 4m. Figure 4 shows the

schematic diagram of the mobile SLR system.

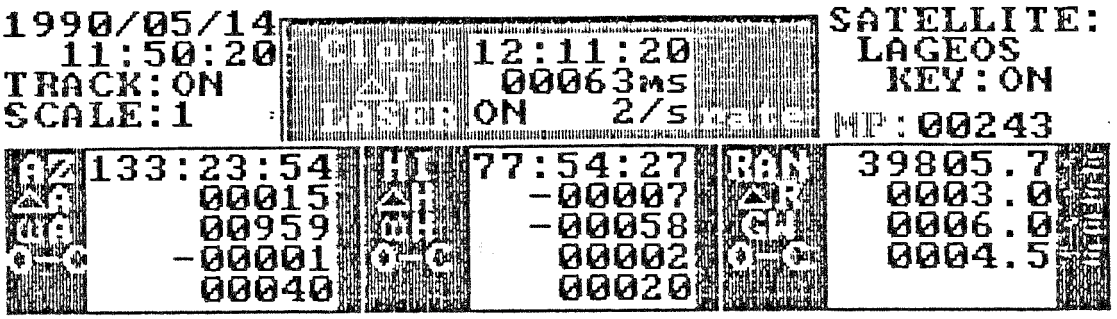

Figure 3. The display of some parameters on computer screen during the operation

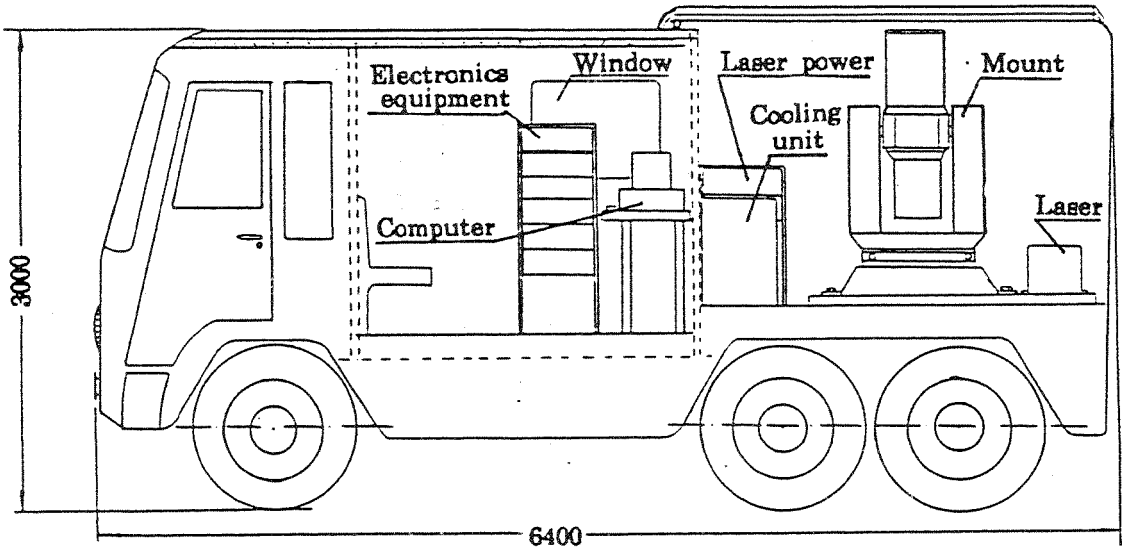

Figure 4. The schematic diagram of the CTLRS

The total specifications of th CTLRS are given in Table 1.

Table 1. Specification of th Transportable Satellite Laser Ranging System (CTLRS)

Subsystem	Specification
Mount	
Configuration	elevation and azimuth axes
Tracking velocity	sidereal to 15 deg/s
Synchronistic inductor	resolution 1 arcsec
Drive	DC torque motors
Orthogonality	3 arcsec
Receiving/Transmitting optics	
Type	common axis
Diameter	35cm for receiver and 10cm for transmitter
Beam divergence	100 μrd—1 mrd
Field of view	20,30,60,120 arcsec
Filter	1 nm
Laser	
Type	Nd:YAG
Wavelength	532 nm
Pulse width	<100 ps
Energy	30 mj(Max single pulse)
Repetition	1—5 pps
Receiving Electronics equipment	
P.M.T.	MCP R2566U-07
Amplifier	B&H DC3003A
Discriminator	TENNELEC TC 454
Time and Frequency	
Type	A.O.A. TTR/6A GPS Receiver
Stability	1×10^{-11}
Accuracy	<100 ns
Time interval counter	
Type	SR620
Resolution	25 ps
Computer	IBM PC 386

Refenence

[1]Xia Zhizhong et al. A Technical Scheme for The Transportable Satellite laser ranging system. 1992. 12 Wuhan (in Chinese)

[2]Xia Zhizhong et al. New progress of Ranging Technology at Wuhan SLR station. Proceedings of Symposium on Eigth International Workshop on Laser Ranging Instrumentation Annapolis U.S. May, 1992.

[3]Sasaki M. Completion of a transportable laser ranging station (HTLRS). Data Report of Hydrographic Observation. Maritime Safety Agemcy TOKYO. JAPAN No. 1, March 1988.

The Transportable Integrated Geodetic Observatory (TIGO)

P. Sperber, W. Schlüter, A. Böer, R. Dassing, H. Hase
Institut für Angewandte Geodäsie
Fundamentalstation Wettzell
D-93444 Kötzting

R. Kilger
Technische Universität München
Forschungseinrichtung Satellitengeodäsie
Arcisstr. 21
D-80333 München

Abstract:

To improve the situation of only few existing geodetic fundamental stations, the German "Institut für Angewandte Geodäsie (IfAG)" decided to set up an "Transportable Integrated Geodetic Observatory (TIGO)", in which all state-of-the-art space geodesy techniques will be available in one mobile configuration.

The main modules (VLBI and SLR) will introduce new technologies in space geodesy to improve data quality and quantity. They will be realized in a cooperation with MAN (VLBI-module, containers), TPD (SLR-module system responsibility, optical telescope), KOSG (SLR control electronics and software) and Quanta Systems (Ti-Sapphire Laser).

The modules of TIGO will be integrated and tested at Wettzell in 1996/97. The whole observatory should be ready for field operation preferable in the southern hemisphere in 1998.

In this paper we will give an overview about TIGO with emphasis to the SLR module.

1. Introduction

For the measurement of the dynamics of earth and for the definition of a terrestrial reference frame a number of techniques like SLR, VLBI, GPS, PRARE etc. were developed in the last years. The experience shows, that these techniques are complementary, for best results a combination is necessary. For the definition of the motion of earth in space and the dynamics of the earth we need a net of globally distributed stations,

- some fundamental station (6-8) for combined solutions to fix the reference frames of the different space techniques and to control the results with independent techniques.

- SLR, VLBI and fixed GPS stations with some thousand km distance for the definition of the terrestrial reference frame, global plate tectonics, fiducial point measurements, precise orbit determination, etc.
  At these stations only a subset of the instruments may be available.

- small highly mobile systems (GPS, SLR) for the measurement of local tectonics.

The main problem is the insufficient global distribution of fundamental stations, mainly in the southern hemisphere. This consideration lead to the basic concept for a "Transportable Integrated Geodetic Observatory (TIGO)" with an observation period of one to two years on selected sites mainly in the southern hemisphere. The design goals were state-of-the-art technology hosted for easy transportation in standard containers. The ideas are summarized in Table 1.

2. TIGO Modules

To fulfil the requirements of a fundamental station, TIGO has to house all available space geodesy techniques (SLR, VLBI, GPS, PRARE, etc.), and additional sensors for gravity, seismic, meteorology, and Time & Frequency standards.

For the operation of the observatory at remote sites a LAN and WAN interface and additional infrastructure like power generator and aircondition systems are necessary (Table 2). For the transport and operation five 40 feet standard containers will be used. The distribution of the instruments in the containers is seen in Fig. 1.

VLBI Module

The VLBI module consists of two 12 m standard containers; one for transportation of the 6 m offset radiotelescope and another one for the VLBI-operation and transportation of the two side panels of the reflector (see Fig. 2).

The antenna was designed for geodetic S/X-wideband observations. The helium cooled low noise amplifier and the Mk IV Data Acquisition Rack and tape recorder shall correspond to the NASA standards.

The setup time in the field on a special plattform for the radiotelescope will be less than 2 days.

Basic Module

The basic module contains the time&frequency standards like cesium clocks, GPS-time receiver and hydrogene masers as well as the central computer for TIGO. The central computer will serve with the auxiliary data e.g. meteorology, absolute time, whenever there is a

request from one of the main techniques. In addition the central computer will be the interface to a wide area network in order to distribute data e.g. of the permanent GPS receiver to international archiving facilities.

SLR Module

The SLR module consists of one 12 m standard container. The SLR instrument is designed as two colour subcentimeter system with day and night capability. The specified ranging distance is 100 to 40000 km. One 50 cm-telescope is used for transmission and receiption of the pulses. The telescope will be mounted on a cart, while the laser transmission and receiption units are located inside the SLR container. The optical beam will be introduced in the telescope through a tube.

The specifications are summarized in Table 3.

For the first time in SLR a Ti:Sapphire Laser will be used in this system.

The wave length of this Laser is 847 nm (Second Harmonic: 423.5 nm). In this wavelength regions the transmission of the atmosphere is very good and the dispersion between fundamental and second harmonics frequency 2.5 times higher than at Nd:YAG wavelengths. This will give the possibility, to calibrate the atmosphere and to test the Murray-Marini modell and therefore reduce the error introduced by the athmosphere.

The SLR module will be realized by coordinated work of TPD, KOSG, Quanta Systems and MAN. The parts of this companies are shown in Table 4-5 and Fig. 3-4, TPD has the overall system responsibility. Details about the telescope, the receiving system, the laser and the control system are given in separate papers in this proceedings.

3. Schedule

In 1992 we started with the general specifications and first contracts.

The integration of the complete observatory is scheduled for 1996, test measurements in Wettzell for 1997. The system should be ready for field campaigns in 1998. The complete schedule is shown in Table 6.

4. Summary

With the Transportable Integrated Geodetic Observatory the "Institut für Angewandte Geodäsie" will set up the first transportable fundamental station. This observatory will help to close gaps in the southern hemisphere and improve the distribution of fundamental stations around the world.

The main modules introduce new techniques in SLR and VLBI systems and may therefore define a new generation of Laser Ranging and VLBI systems.

The situation of

- *only a few existing Fundamental Stations*
- *unsufficient global distribution (Southern Hemnisphere)*

induced the IfAG to set up the T I G O

Basic Characteristics of Fundamental Stations:

- *Permanency (observtions on long term basis)*
- *Complementary (supplementary observations)*
- *Redundancy (independent techniques for control)*

Basic Concept:

- *Observation Period > 1 year on selected sites*
- *preference for Southern Hemnisphere*
- *Cooperation based on agreements with host agencies*

- *Modular Design, State of the Art Technology*
- *High Degree in Automatisation*
- *Set up Time < 1 week*
- *Transportation in 12m Standard Containers*

Realisation Period: 1992 to 1997

Table 1 Transportable Integrated Geodetic Observatory Objectives

SPACE TECHNIQUES

- # *S L R*
- # *V L B I*
- # *G P S (GLONASS)*
- # *P R A R E*

IN SITU OBSERVATIONS

- # *Gravity (abs. or rel. ?)*
- # *Seismic*
- # *Meteorology (Temp., Hum., Press., Rain, Wind,...)*
- # *Time & Frequency*
- # *Supplementary Terrestrial Measurements*

ADDITIONAL REQUIREMENTS

- # *LAN/WAN*
- # *Control Computer for entire system*
- # *Power-System (Generators)*

Table 2 Transportable Integrated Geodetic Observatory
Spectrum of Observations

- Subcentimeter
- range from 500 km up to 40.000 km
- Day- and Night Capabiltity
- Two-Colour System
- High Automatic Operation
- Transmit and Receive Telescope
- High Efficiency in Transmission
- Precise Pointing
- Titan Sapphire Laser

  10 ... 50ps pulslength
  10 ... 50 mJ for 427, 5nm
  30 ... 100 mJ for 847 nm
  up to 100Hz repetition rate

- Avalanche Photo Diode
- 2 day set up time
- Internal Calibration (pulse by pulse) and External Calibration

Table 3 TIGO-SLR-Module Specifications

- Folded Lens Telescope
  without central obscuration
- Diameter: 500 mm
- Aberation Correction for 847 nm and 423.5 nm
- Max. Field of View: 4 arcmin
- Optical Efficiency: 75 %
- Material: Static Part: Granite
  Tube : Stainless Steel
  Fixations : Titanium
- Mass: 1700 kg
- Pointing Accuracy: better than 2 arcsec RMS
- Speed: 6 deg/s (Elevation)
  15 deg/s (Azimuth)
- Encoders: 21 bit absolute
  accuracy: 0.8 arcsec
- Size of Mount: Height : 2 m
  Diameter: 1.3 m

Table 4 Telescope
(Design and realization: TPD, TNO Institute of Applied Physics, Delft)

- Control Electronics compatible to MTLRS
- Four Transputer Configuration
  - Supervisor
  - Mount
  - Timing
  - I/O
- Main Computer: DEC Alpha
- Software: developed by OSG Kootwijk
  - X-Windows Graphic Interface
  - Site Installation
  - Prediction
  - Ranging
  - Processing
  - Utilities, Database
- Ranging Options
  - Event Timing System realized with Stanford Time Interval counters
  - One counter for each detector (two at 847 nm one at 423.5 nm)
  - One counter for start diode

Table 5 Electronics-Software
(Design and realization: TPD, TNO Institute of Applied Physics
TU Delft, Observatory for Satellite Geodesy, Kootwijk)

1992 General Design and Request for Offers

- *First Contracts:*
  - *# VLBI-Antenna*
  - *# SLR-Module*
  - *# Smallsize Maser*

1993 Design

- *SLR-Module*
- *VLBI-Module*

Start for manufactoring

1994 Request for Offers and Contracts for

- *# Titan Sapphire Laser*
- *# VLBI-Receiver, DAT*
- *# Containers*

1995 Set up a Platform at Wettzell

Delivery of SLR-, VLBI-Modules ... Implementation

Request for Offers and Contrats for

- *# T & F*
- *# Meteorological System*
- *# Central Computer, LAN/WAN*

1996 Request for Offers and Contracts for

- *# Gravitymeter*
- *# Power Generators*

Integration of the Components

1997 Final Integration .... Testperiod at Wettzell
Implementation of

- *# GPS ... PRARE*
- *# Seismometer*

1998 Expected to be ready for Fieldcampaign

Table 6 Transportable Integrated Geodetic Observatory Schedule

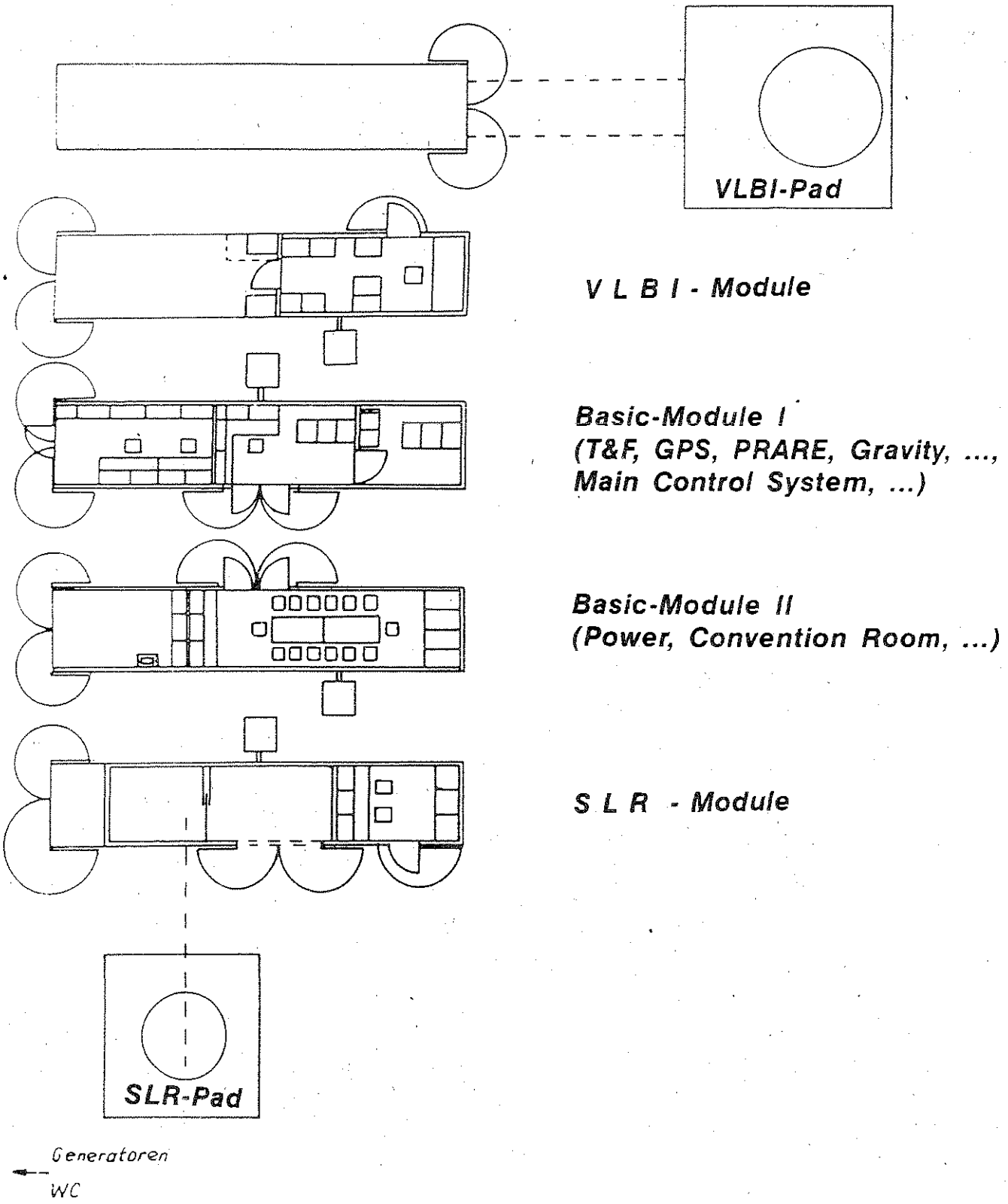

Fig. 1 Transportable Integrated Geodetic Observatory
TIGO-Overview

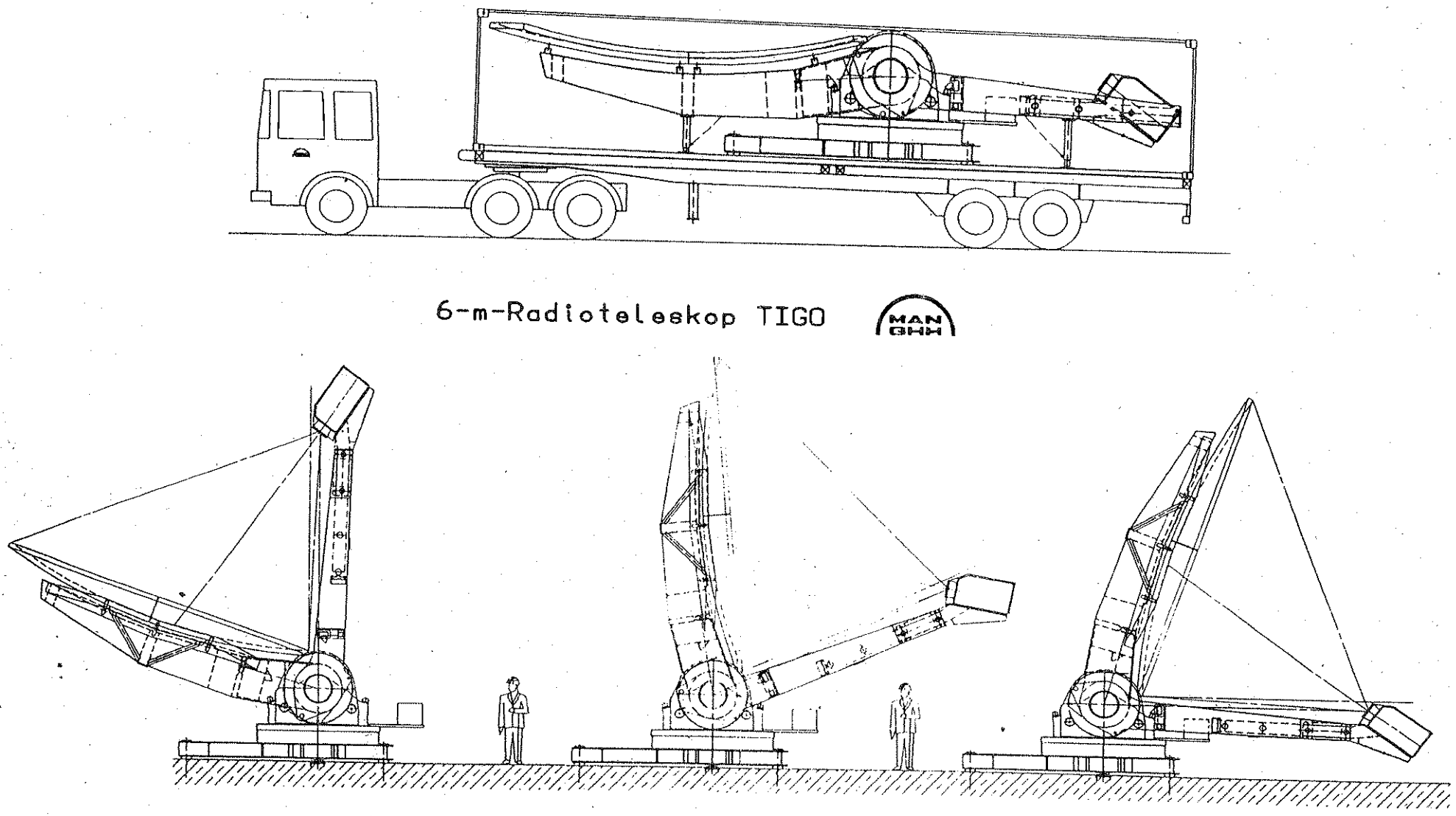

Fig. 2: The VLBI-antenna during transportation in a standard container and in different elevation positions. The feed holder is drawn out for operation.

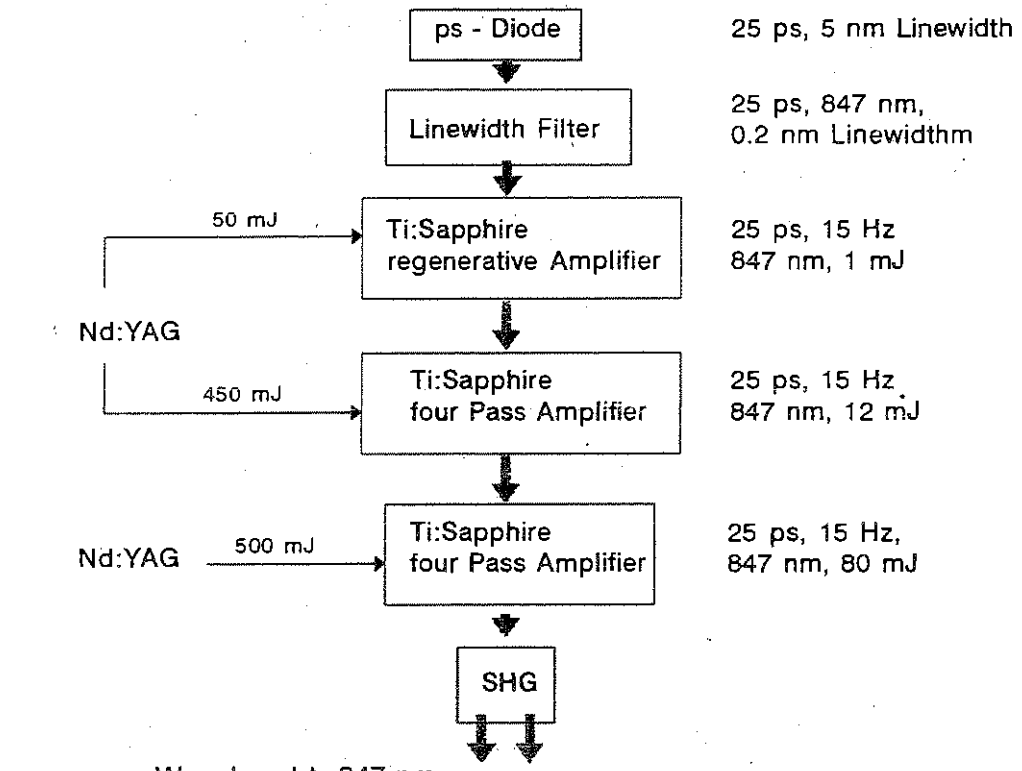

- Wavelenght: 847 nm
  423.5 nm
- Pulse Duration: 25 ps
- Pulse Energy: 30 mJ (at each wavelenght)
- Divergence: 0.4 mrad
- Advantage: - Better Transmission of Athmosphere
  - Good seperation of wavelengths in athmosphere
  - No future limitations in energy, wavelength and pulseduration

Fig. 3 Laser
(Design and Realization: Quanta System, Milano, Italy)

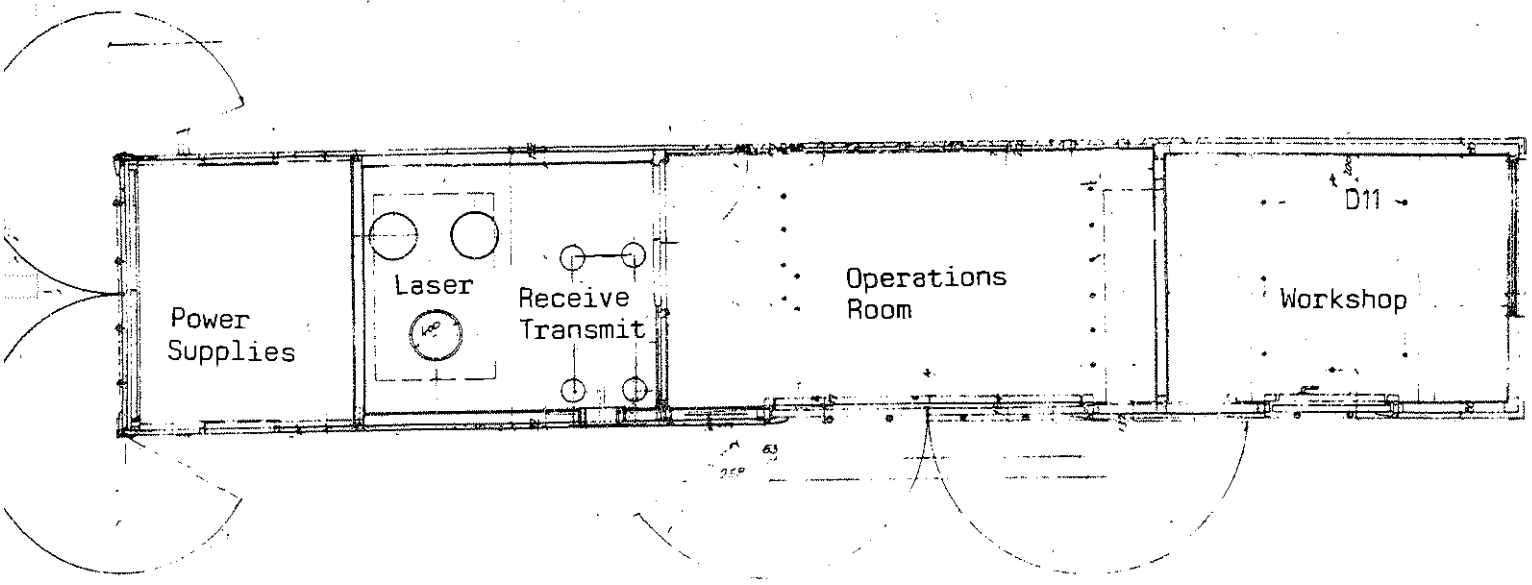

Fig. 4 Cabin
(Design Realization: MAN-GHH, Germany)

TIGO-SLR opto-mechanical configuration

H.W.T. Braakman, M.R. van der Kraan, H. Visser, B.A. van der Zwan
TNO Institute of Applied Physics (TNO-TPD)
2600 AD Delft, The Netherlands
P. Sperber
IfAG, Fundamentalstation für Satellitengeodäsie
Wettzell, 93444, Kötzting, Germany

Abstract

For the German TIGO project ("Transportablen Integrierten Geodätischen Observatoriums") of the "Institut für Angewandte Geodäsie" (IfAG) a new state-of-the-art transportable SLR system is under development.
For this SLR system TPD designs and manufactures major optical/mechanical subsystems (such as the telescope and the transmit / receive optical unit that interfaces with the laser, the telescope and the detectors). TPD also has overall SLR system responsibility.
The SLR system will be capable of ranging to all cooperative satellites (including geostationary orbits) at two wavelengths simultaneously (847 nm and 423.5 nm, generated by a Ti-Sapphire laser).
The design of the system combines a number of features that will give an added value in the sense of expected output, accuracy and user friendliness.
In this paper a general overview on the opto-mechanical configuration of the SLR system will be presented with emphasis on the telescope and its housing.

1. Introduction and general opto-mechanical system overview

In its mobile configuration the TIGO-SLR system is transported in a standard size 12 m container.
At the measurement platform a cart (that contains the telescope) can be rolled out of this container to the measurement position on the platform. In the ranging configuration the nominal distance from the container to the azimuth axis of the telescope is 5.5 meters, as indicated in figure 1. In this configuration the cart is used as telescope housing and the container is used as an air-conditioned cabin for the operator.
The opto-mechanical units of the SLR system are directly supported by the platform as indicated in figure 1 and figure 2.
In figure 2 the three main optical subsystems of the SLR concept can be identified schematically.

- The elevation over azimuth Coudé telescope
- The two-colour Ti-Sapphire pulse laser (847 nm + 423.5 nm)
- The transmit/receive optical unit that interfaces with the laser, the telescope and the detectors.

The schematic overview of figure 2 is a simplification also in the sense that the two optical units inside the cabin (the laser and the T/R optical unit) are, in reality, supported individually by the platform directly.
The optical concept of the transmit/receive optical unit is described in some detail in the "Detectors and Spectral Filters" session of this Workshop.

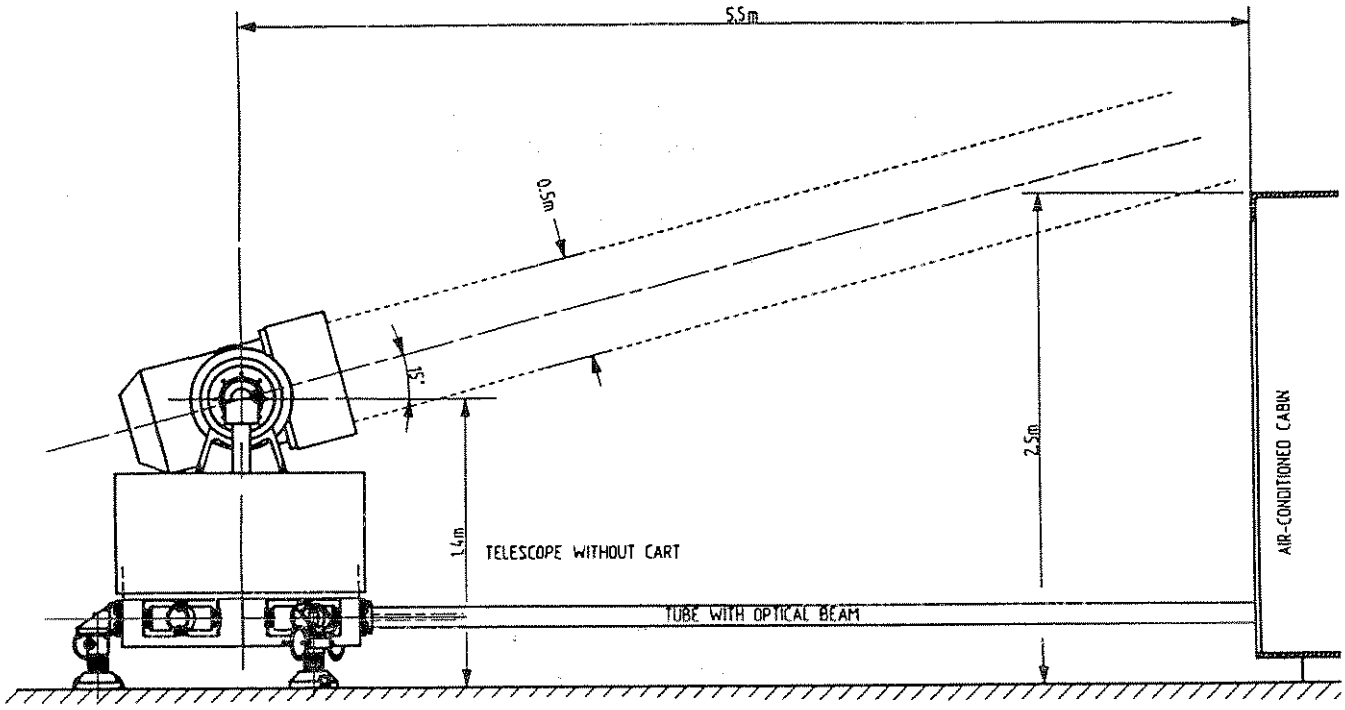

Figure 1 The telescope and its optical interface to the cabin.

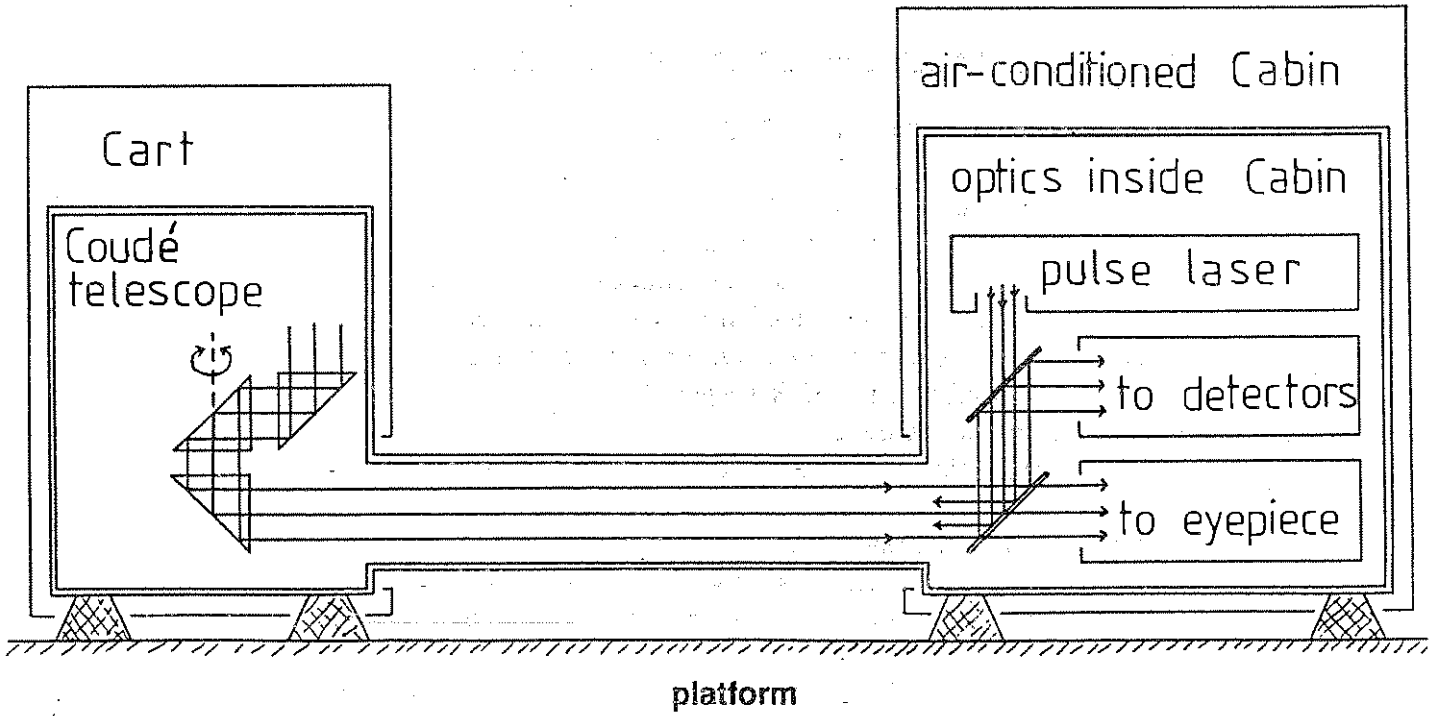

Figure 2 Schematic opto-mechanical configuration.

2. Telescope optics

The general concept of the telescope optics is presented in figure 3. The mount is of the elevation over azimuth type with one common telescope and Coudé optical train for both transmitting and receiving.

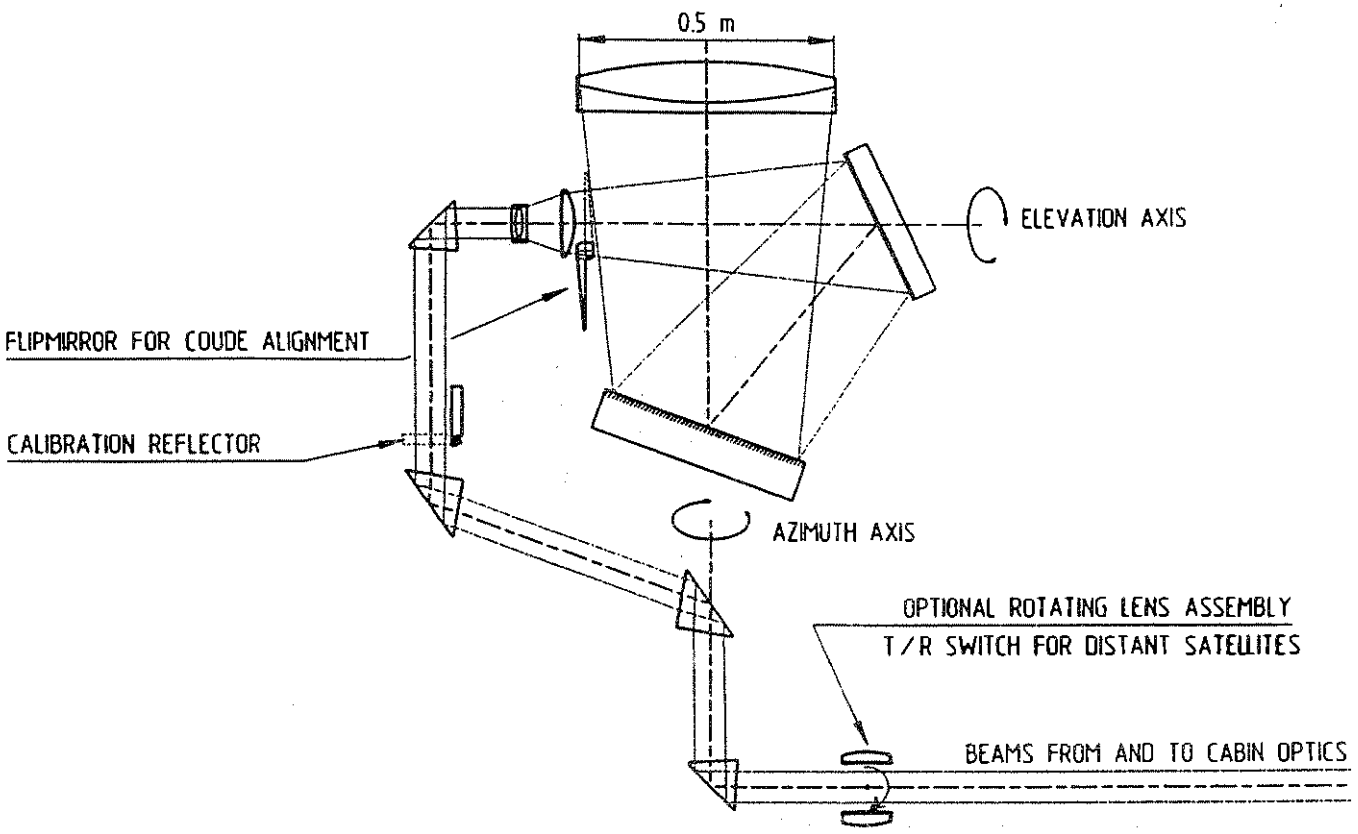

Figure 3 Telescope optics.

A large 0.5 m diameter front lens (a cemented achromatic doublet) and a smaller correcting triplet lens system in the hollow shaft of the elevation axis together form the basic telescope optical concept. The long focal length of the front lens is folded into a compact, mechanically balanced telescope tube by two flat folding mirrors. The triplet lens system exactly recollimates the received beams at both laser wavelengths to a diameter of about 60 mm (magnification 500/60 = 8.33 times).

By means of 4 prisms the received Coudé beam is directed to the cabin as indicated in figure 3.
For visual guidance and alignment purposes an unvignetted telescope field of view of about 0.1 degrees at the sky is transmitted to an eyepiece or a camera inside the air-conditioned cabin.
The telescope system of figure 3 has a theoretical (ray-traced) optical imaging quality of better than 2 arcsec (at the sky) for both laser wavelengths simultaneously. Also an adequately wide wavelength range around 550 nm is well-corrected.

The optical efficiency of the telescope optical train of figure 3 is estimated at 75% for both laser wavelengths and 60% for the visual guidance wavelength range (about 500 - 600 nm).

The optics of the telescope are protected against dust and humidity by
- an almost fully sealed optical train, that is kept at low humidity by small containers with drying agent, and
- a front lens heater that can be switched on to prevent condensation of the outside surface of the front lens.

Besides the actual telescope optics some additional built-in optical features are shown in figure 3.
- An alignment tool called "Flipmirror for Coudé alignment". This, over two axes adjustable, concave spherical mirror can be rotated into the transmitted alignment laser beam (coming from the T/R optical unit inside the cabin) as an alignment aid for the adjustment of the four prisms in the Coudé lightpath.
- A "Calibration reflector" for pre- and post-pass calibration purposes. This calibration feature consists of a retroreflective sheet on a remote control mechanism. By rotating it into the transmitted pulse laser beam (at reduced power) a fixed distance can be measured by the SLR system.
- An "Optional rotating lens assembly" that can be used as a transmit/receive switch for ranging to distant satellites (e.g. in geostationary orbit). It improves the best collimation of the transmitted pulse laser beam from about 5 arcsec at the sky to about 2 arcsec at the sky. This feature is described in another paper entitled "Transmit/receive two-colour optical unit for TIGO" in the "Detectors and Spectral Filters" session of this Workshop.

3. Telescope mount structure and mechanical axes

The telescope is supported by three adjustable feet on the TIGO platform, as already indicated in the figures 1 and 2. These three feet are mounted to a large ring-shaped granite component (out of one single block of granite), that forms the main part of the static structure of the telescope mount. In figure 4 an outline of this granite component is presented. The outside diameter is over one meter, the height is 0.4 meter and the mass is about 600 kg.

The positive properties of the granite component in the static part of the mount are:
- good top surface finish and flatness (better than 4 µm over the entire diameter) to form the static part of an air-bearing that determines the direction of the azimuth axis of the telescope
- good stiffness
- good thermal and temporal stability
- corrosion resistant.

In figure 5 a dimensional drawing and a CAD picture of the telescope mount are presented that show the position of the granite bench and its support to the platform. The dimensions demonstrate the compactness of the mount concept. The total mass of the telescope is estimated at 1700 kg.

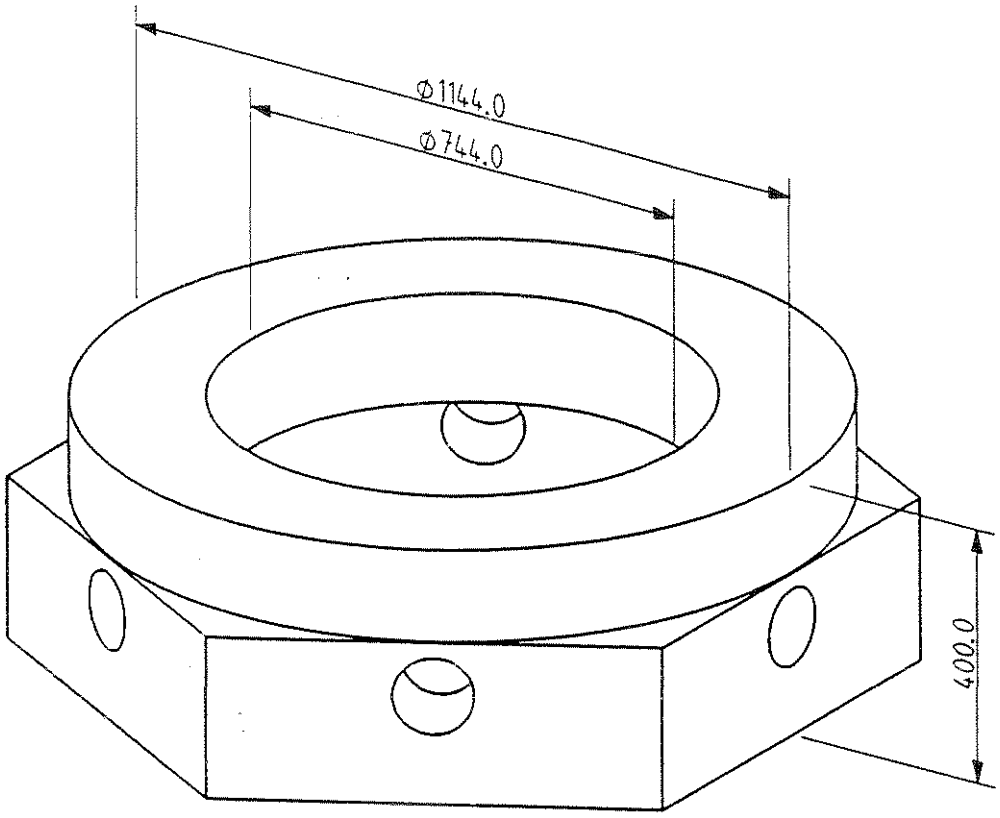

Figure 4 Granite bench (dimensions in mm).

Besides the granite bench the three most important other structural materials of the telescope are:

- Stainless steel,
  for most of the moving structural parts, such as the telescope tube and its support structures, the rotating part of the azimuth axis, fixation of bearings, etc.
- Aluminium,
  for the structure that supports the granite bench with respect to the adjustable feet to the TIGO platform, and for a number of smaller or less critical components.
- titanium,
  for the fixation of optics and for the fixation of the aluminium support structure to the granite bench. Titanium has about the same thermal expansion as granite and as most of the used optical glass materials for lenses and mirrors. The use of titanium helps to maintain critical alignments and fixations over a wide temperature range.

The weight of the rotating part of the azimuth axis is carried by three, relatively small area (2.5 dm^2) flat air-bearings, that "float" on the top surface of the granite bench. These three air-bearings together ensure that the direction of the azimuth axis is fully determined by the flatness of the granite bench (without wobble of bearings or other rotating parts). The lateral position of the azimuth axis, in the center of the granite bench, is defined by a large (0.4 m diameter) pre-loaded ball bearing.
The elevation axis bearing of the telescope tube is accomplished by a combination of a pre-loaded ball bearing at one side of the telescope tube and a pre-loaded hollow-roller bearing at the other side of the telescope tube.
The orthogonality of azimuth and elevation axis will be adjusted to better than 5 arcsec.

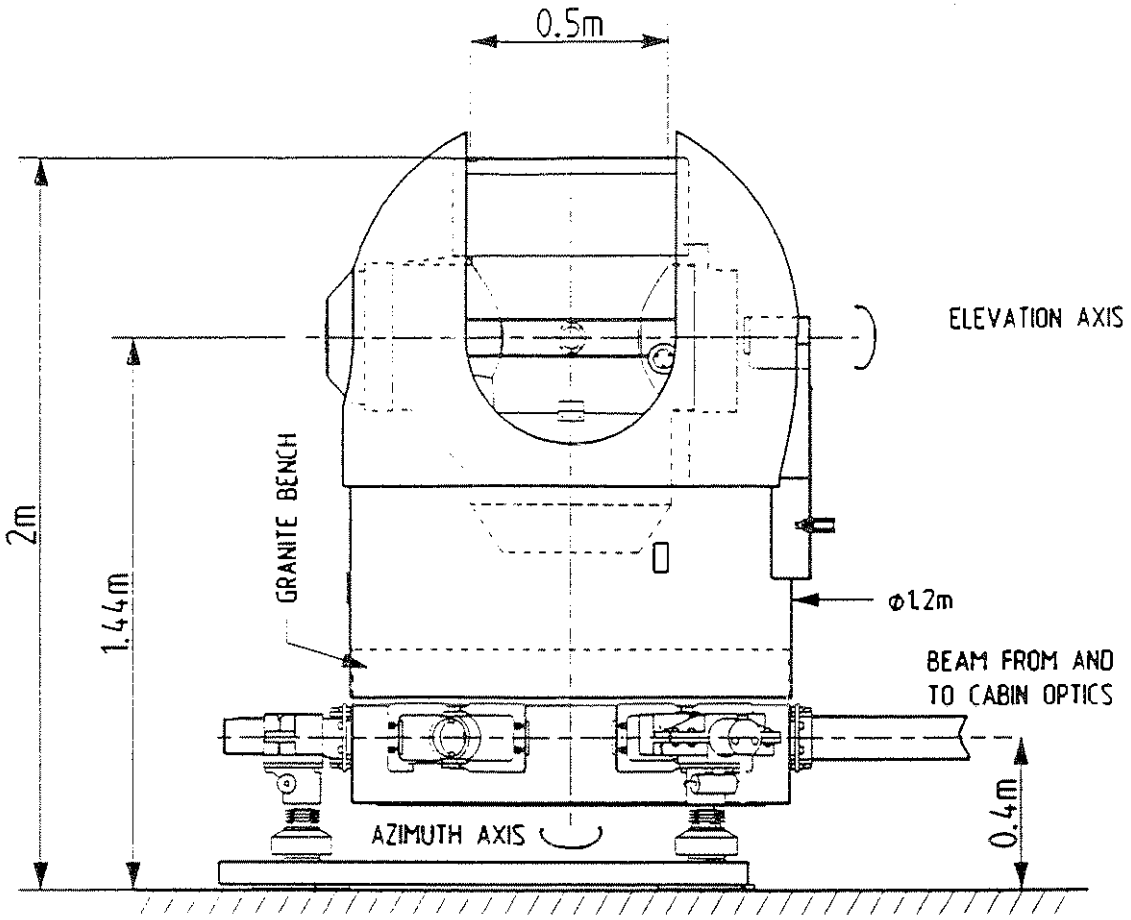

Figure 5
Dimensional drawing and
CAD picture of the telescope

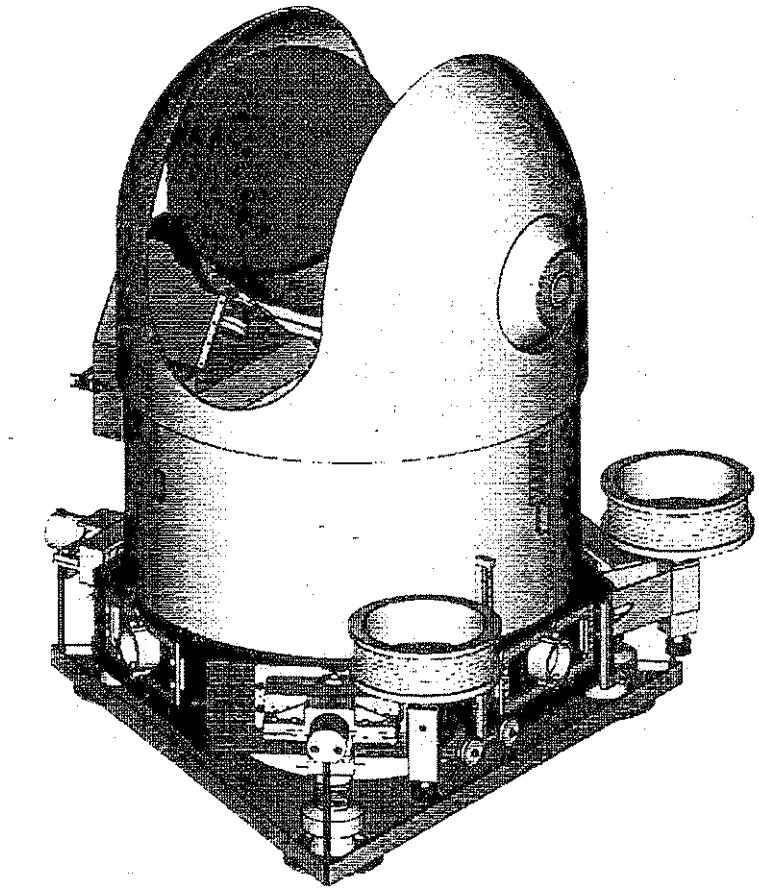

4. Angular read-out and drive system of the telescope

The angular read-out of both telescope axes is accomplished by 21-bits natural binary absolute angular encoders. The encoders are directly coupled to the azimuth and elevation axis (manufacturer BEI, type μS 21/80).
The angular read-out accuracy of these thin, through-hole, absolute optical shaft encoders is 0.8 arcsec RMS and the angular resolution is 0.62 arcsec (2^{21} = 2097152 positions over 360 degrees).

Both telescope axes are driven indirectly, via a pre-loaded, straight-toothed gearing system between the motor axis and the main (azimuth or elevation) axis.
The reduction ratio of the azimuth gearing system is 838.8608 times (= $2^{23}/10^4$), and the reduction ratio of the elevation gearing system is 1677.7216 times (= $2^{24}/10^4$).

The step motors (manufacturer Compumotor, type S83) are used in a micro-stepping mode of 10^4 positions per revolution of the motor axis, so that (on the average) one angular encoder position (0.62 arcsec) corresponds to 4 microsteps of the azimuth motor, or to 8 microsteps of the elevation motor. In this way the micro-steps of the motors can be used to determine angular positions inbetween the angular read-outs of the absolute optical shaft encoders. (The maximum specified interrogation rate of the encoders is 5 kHz).

Because of structural restrictions and cabling the specified angular travel range of the axes is limited to:
- elevation ≥ 180 degrees
- azimuth ≥ 540 degrees

The specified maximum angular velocities are:
- elevation 6 degrees per second
- azimuth 15 degrees per second

These maximum velocities are achieved at motor speeds of 28 revolutions per second for elevation, and 35 revolutions per second for azimuth.
The specified maximum accelerations of the axes are:
- elevation 2 degrees/s^2
- azimuth 5 degrees/s^2

The resulting pointing accuracy of the telescope at the sky is expected to be better than 2 arcsec RMS (inclusive of some mount modelling, to correct for small deviations from axes orthogonalities, for small, angle dependent, flexures in the mount structure, etc.).

5. Cart

In figure 6 the closed cart, that houses the telescope, is shown in its transport configuration. In this configuration the cart can be rolled in and out of the 12 m container. The 8 air-tyres provide vibration and shock protection during transport. The overall dimensions of the cart in this configuration are 2.1 m x 2.2 m x 2.1 m (L x W x H).
In figure 7 the cart is shown in its manouvrable configuration. This configuration can be created outside the container and is used to bring the cart on the desired measurement position at the platform.

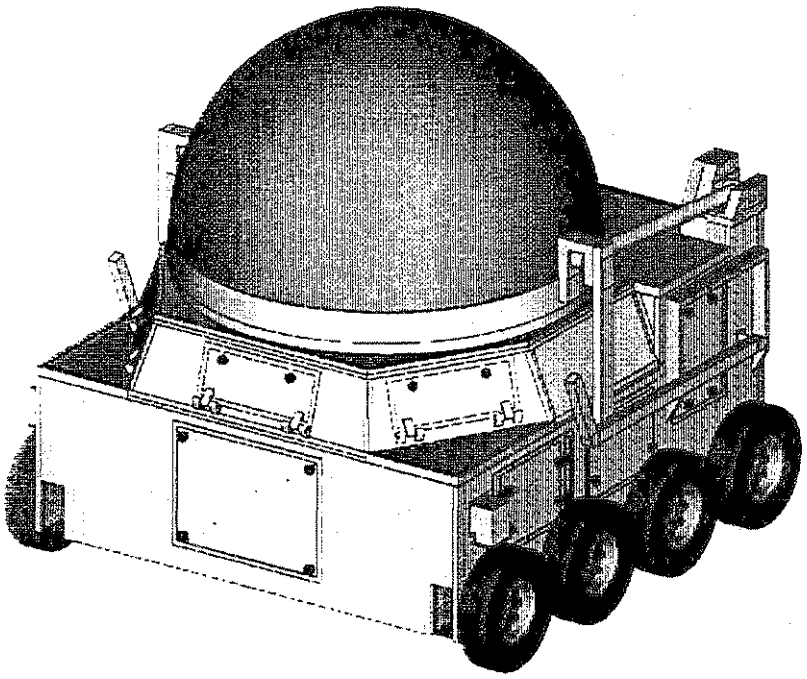

Figure 6 Transport configuration of the cart.

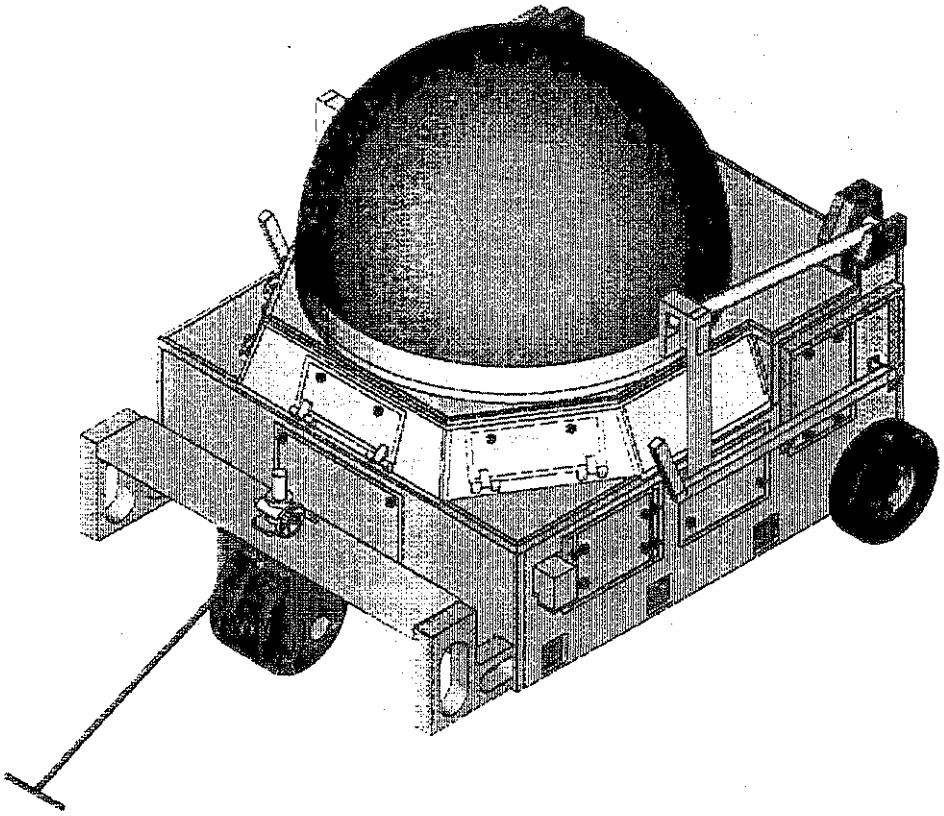

Figure 7 Manouvrable configuration of the cart

In figure 8 the opened cart is shown in the ranging configuration. The cart can be opened and closed by remote control from the control system inside the air-conditioned cabin. In emergency situations the cart can also be opened or closed by a simple 12 volt battery power supply, or by hand.

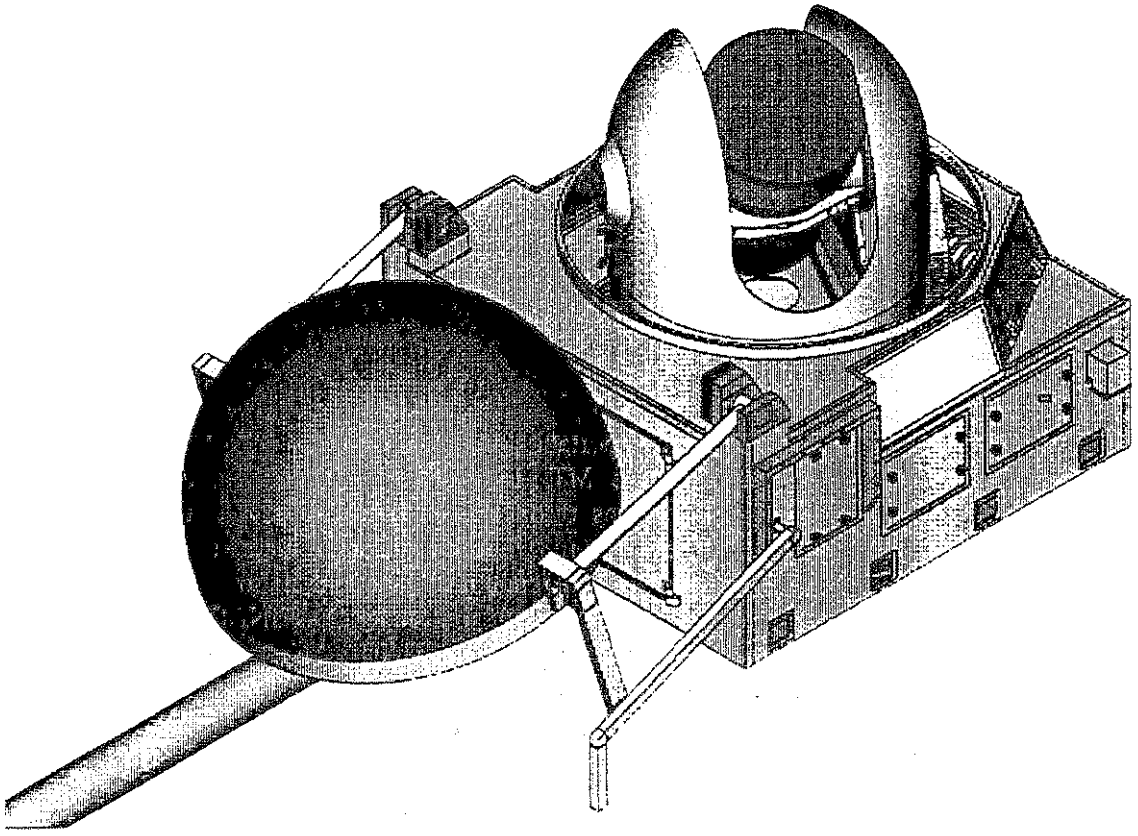

Figure 8 Cart and telescope in ranging configuration.

TIGO-SLR Control System

E. Vermaat
J.W. Offierski

Kootwijk Observatory for Satellite Geodesy
Delft University of Technology
P.O. Box 5030
2600 GA Delft
The Netherlands

1. Introduction

The Control System for the Transportable Integrated Geodetic Observatory (TIGO) is a follow-on development of the MTLRS Control System. The design aims at maximum efficiency of operations through user friendliness and a high level of automation, and at enhanced system reliability through modular and integrated hardware design and definition of a maximum of functions in software in a parallel set-up. The User Interface program will run under X-WINDOW on a UNIX compatible platform which is incorporated in the TIGO LAN. Individual functions in the Real-time system will be identified in parallel tasks, with in particular a rigorous separation of the synchronisation dependent tasks.

2. Overall design

The general layout is shown in figure 1. The *Workstation* (DEC 3000/300LX) hosts the Graphics User Interface (GUI) software and is connected to the *embedded PC* which hosts the Real-time server. The embedded PC is linked to the *network of parallel processors* (T8) in which the Real-time software runs. This network is connected to the hardware of the Laser ranging system.

2.1 Workstation

Advantages of the workstation environment for this application are the multi-tasking / multi-user capability and the access to ANSI standard application software. For this Control System any UNIX compatible operating system can be used (e.g. DEC, SUN, VAX, HP) and for the TIGO the DEC3000/300LX has been chosen. This computer is connected to the TIGO Local Area Network (LAN) with the added advantage, that the Control System can be operated from anywhere in the LAN or even, through an Internet connection, remotely from the site. On the workstation the DEC OSF/1 Alpha

TIGO-SLR control system

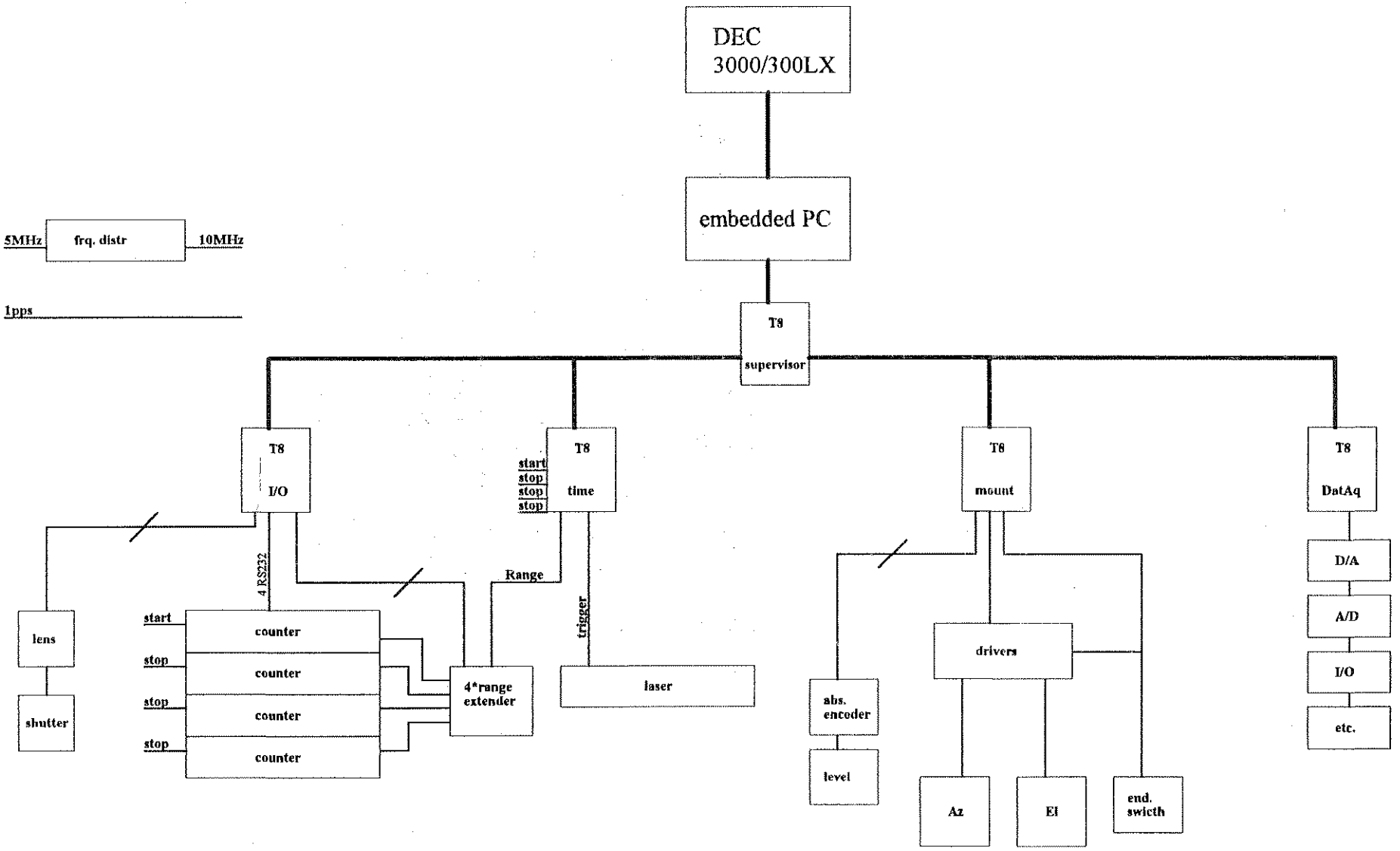

Figure 1 General lay-out

AXP (OSF/Motif and TCP/IP) operating system is installed with the X-WINDOW system. In this environment runs the GUI software which enables the dialog between the Laser Ranging System and the operator. It consists of one master program and a number of application programs running in the background, addressing particular tasks. Communication between the master program and the task programs is performed through PROPERTIES (compare to OLE in the MS environment), semaphores and files.

The principal tasks of the GUI software are the communication with the Real-time system through the standard RS232 connection with the Embedded PC, the monitoring of Real-time data on the display and the execution of all off-line tasks. The design of this software is not rigorously object oriented but the overall layout of this ensemble of programs has this character.

2.2 Embedded PC

The embedded PC hosts the Real-time server and is the intermediary between X-WINDOW (the User Interface) and the Real-time system in the parallel processor network (Figure 2). The RS232 port is in the operational configuration connected to the workstation, or alternatively to a modem for remote control outside the LAN or to another PC for maintenance or engineering. Through the Transputer Link Interface the embedded PC is connected to the parallel processor network. The configuration further consists of a PCMCIA for Flash card and a LCD display with touch screen. Optionally a keyboard and monitor can be connected for software maintenance.

An important function of this intermediary system is to store the command stream between GUI and Real-time system in history files on a storage device. The additional operational functions are:

- to upload the Real-time software from Flash card to the processor network at start-up,
- to perform a system hardware checking procedure initiated by the GUI or by touch screen command,
- to provide a watchdog function for switching on/off of the entire system, initiated by the GUI, by touch screen command or on programmed time (automatic mode),
- to (optionally) control fully autonomous operations when the GUI is not present, in which case the embedded PC software has the highest authority in the Control System.

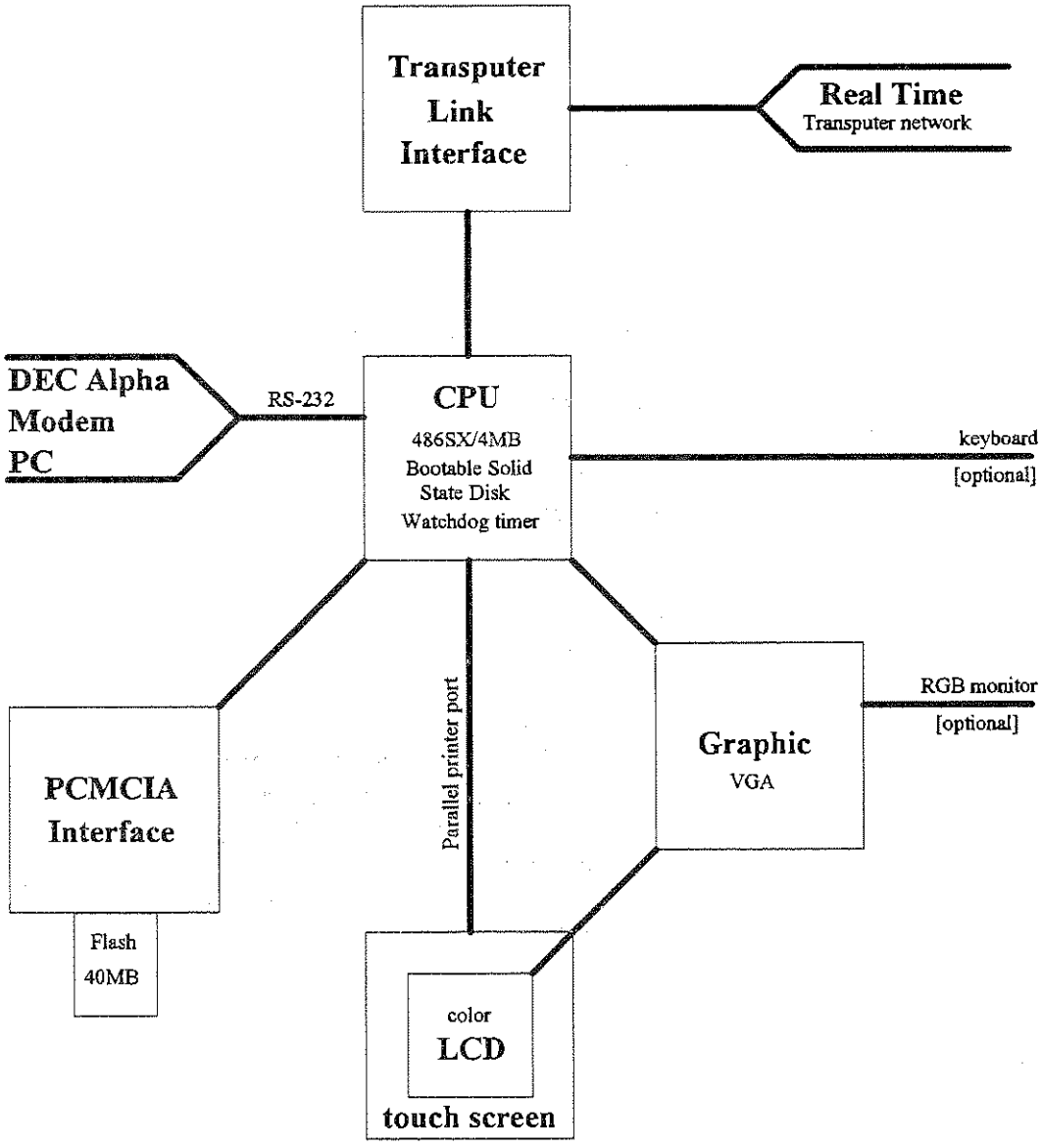

Figure 2 Embedded PC configuration

In addition to these operational functions, the embedded PC will also be used for engineering and maintenance, in particular:

- to run diagnostics tasks initiated by touch screen command,
- to check the operators authority level from Flash card,
- for software development using the optional keyboard and monitor,
- for down-loading new software from one of the systems connected to the serial port.

2.3 Parallel network

This network consists of a number of parallel oriented processors mounted on custom designed Printed Circuit Boards (PCB's) in credit card size format, which are mounted on custom designed functional PCB's in Extended Eurocard format. The processors can be any type of parallel processor and for the TIGO system the T805 INMOS transputer has been chosen, identical to the processors in the MTLRS Control System [Vermaat, E., et. al., 1992]. The T805 processors are interconnected through fast 20 MBaud data links and connected to the Laser Ranging system hardware.

The Real-time system is essentially organised in two parts, one part synchronised to UTC and a part which is not or not critically synchronised.

Synchronised functions

- Network synchronisation
- Time signal generation
- Telescope mount control
- UTC dependent I/O functions

Other functions

- Real-time integrity control
- Data acquisition

Parallelism in the Real-time software which runs in this processor network is obtained through distributing tasks over different processors and by parallel software design inside any processor. The software is written in ANSI-C with parallel extension. It is highly structured and breaks-up into three levels: functional, device dependent and (interface) protocol dependent. This structuring facilitates later upgrades and makes the software system easily transportable to other hardware configurations.

The supervisor program performs the overall control of the Real-time system and enables communication with the outside world. Other programs are dedicated to

specific operational tasks. The Real-time software can simulate each function and hardware unit. This feature facilitates debugging and development and can be engaged manually or automatically when corresponding hardware is not available or doesn't respond correctly.

3. Functionality

The functionality of the TIGO control system can be separated in Real-time and Off-line categories . Below the main features in each of these categories are described.

3.1 Real-time

Network synchronisation

Laser Ranging System control, unlike general robotics applications, requires accurate synchronisation to an absolute time system (UTC) for many of its Real-time functions. Frequency and 1 pps are obtained from the TIGO time module. In every processor runs a synchronisation task with highest, protected priority. After boot-up the network is synchronised and during each UTC dependent task, synchronisation is checked at 1 pps or more often. This process is controlled by the supervisor program for all boards, except for the Mount Control board, which performs its own synchronisation check for maximum accuracy, directly from the 1 pps signal. Actual synchronisation is repeated whenever necessary to maintain synchronisation of the network.

Time signal generation

Time signals are generated for the definition of four range windows with a precision of 500 ps (simultaneous calibration, one blue and two red channels), for synchronisation of the rotating shutter and the rotating lens assembly up to 100 Hz (a T/R switch for distant targets, see [Braakman, H.W.T, et. al., 1994b]) and for laser trigger. Extra signals are generated for pre-gating the detectors. All signals are generated as events (full epoch) based on 500 ps event counters which provide reference to the start detector signal. Therefore the range gate and windows are unlimited in magnitude.

Telescope mount control

The absolute optical encoders on both axes give a read-out precision of 0.8 arcsec RMS. This enhanced precision is obtained under processor control, and therefore the mount control electronics must compensate for a read-out delay. The position routine for synchronised mount control uses both velocity and acceleration, to generate driving signals for the very precise step motors [Braakman, H.W.T., et. al., 1994a]. For reasons of safety, a fast switch-off routine will be developed for electrical de-

coupling of the step motors, triggered by the end switches, the alarm button or in case of a sudden pressure drop in the air-bearing of the azimuth axis. Levelling of the vertical axis is accomplished with the use of a LEICA AARAU NIVEL 20 inclination sensor (see Site Installation below).

UTC dependent I/O functions
Event timing of the start and stop signals is accomplished in two parts, the least significant part is obtained from the 100 ns epoch clock, whereas the remaining most significant part is determined by a time interval counter which records the interval between the event and the next clock signal. This technique has already been successfully applied in the MTLRS Control System [Offierski, J.W., 1994].

The synchronisation of the rotating shutter and the rotating lens assembly is dependent on start and gate signals. Nevertheless the controller maintains this synchronisation even if these signals are temporarily not available.

Hardware status flags are monitored, in particular of those units which are essential during the observation process and require a fast response, e.g. the sun shutter, laser stability, rotating shutter and rotating lens synchronisation, etc.

Real-time integrity control
System reliability is enhanced through error handling routines which have a certain degree of auto-generative capability. These routines are linked to the tracking process but need not necessarily be synchronised. Mathematical errors and unexpected change of state of Real-time programmes will, if necessary, lead to automatic reset and boot-up of the Real-time system and resuming of the current tracking process. Individual hardware units may be automatically switched off and on through the data acquisition system, to attempt to resolve a detected problem with such units. Severe errors or messages will lead to a controlled termination of the tracking process with a message sent to the GUI.

Data acquisition
These functions are either performed independently from the observational process or need not be accurately synchronised to UTC. Examples are the control of calibration and alignment mirrors, opening and closing of the telescope dome, monitoring hardware conditions and status, etc. The data acquisition unit generally receives its instructions from the supervisor programme, but occasionally also from other Real-time programmes. With this capability it will ultimately be possible to obtain an automatic, hands-off ranging system, by computer controlling and monitoring all necessary hardware functions.

3.2 Off-line

Site installation
Astronomical procedures will be available for the rapid and accurate determination of the azimuth orientation of the telescope mount and of astronomical latitude and longitude at the site. A ten-parameter mount model is implemented and can be updated from star observations. Levelling of the mount is software controlled with the use of the LEICA AARAU NIVEL 20 inclination sensor. Within the measuring range of 1.5 mrad of this sensor the software will automatically compensate for a tilt of the telescope mount by correcting appropriate mount model parameters. Because the TIGO is a transportable system, the ground tie vector with respect to site reference markers can be rapidly determined with mm accuracy, using a method comparable to the one used in the MTLRS.

Acquisition data generation
Orbits and derived acquisition data for all artificial satellites can be generated from the standard Inter Range Vector (IRV) predicts. Also alert information for observation scheduling will be generated. Keplerian orbital elements can be used as predict input as well, for low accuracy applications (alerts, graphical representation, etc.). Satellite orbits and visibility can be displayed numerically and graphically in various ways, to facilitate on-site crew planning. In standard mode of operation, acquisition data will be generated automatically through time scheduling of the appropriate tasks.

Data processing
Range data editing can be performed automatically after termination of a pass or manually under operator control. In this process statistical parameters of the resulting residual distribution and estimates for time and range bias will be produced and standard data products such as on-site generated Normal Points and full rate data will be generated in international formats.

Database management
Databases will be available for satellites, sites, IRV's and time bias predicts which contain all relevant data for proper functioning of the ranging system. These databases are conveniently accessible for inspection and editing through dialog windows.

4. User Interface

As indicated above, the main tasks of the GUI are communication with the Real-time system, monitoring data produced by the Real-time system on the display and the execution of the Off-line tasks. The GUI runs on the workstation and enables the

operator to monitor and control the performance of the ranging system. The monitor display and the mouse will be the most important attributes for the operator. The graphics display is entirely windows oriented with dialog boxes, pushbuttons, and other numerical and graphical display features for maximum efficiency and user friendliness. The top part of the display is identical for all applications and addresses counter read-out, telescope status, date/time, joystick status, a target list and pushbuttons for all major tasks. The bottom part will be task dependent.

5. Efficiency of operations

The design of the TIGO-SLR Control system aims at maximum efficiency of the ranging system. The operations can be controlled from the workstation in the SLR module or from any other workstation in the TIGO LAN. The active workstation can also be located remotely when connected via modem or Internet to the TIGO LAN or to the embedded PC of the SLR Control system. Ultimately, the ranging system could run entirely autonomous, with or without a workstation.

References

Braakman, H.W.T., M.R. van der Kraan, H. Visser, B.A. van der Zwan, P. Sperber, (1994a), "TIGO-SLR opto-mechanical configuration". Presented at the Ninth International Workshop on Laser Ranging Instrumentation, Canberra, Australia, November 1994.

Braakman, H.W.T., M.R. van der Kraan, H. Visser, B.A. van der Zwan, (1994b), "Transmit/receive two-colour optical unit for TIGO". Presented at the Ninth International Workshop on Laser Ranging Instrumentation, Canberra, Australia, November 1994.

Offierski, J.W., "Parallel aspects of Laser Ranging Control". Presented at the Ninth International Workshop on Laser Ranging Instrumentation, Canberra, Australia, November 1994.

Vermaat, E., J.W. Offierski, K.H. Otten, W. Beek, C. van Es, (1992), "Transputer Based Control System for MTLRS". In: Proceedings of the Eighth International Workshop on Laser Ranging Instrumentation, Annapolis, USA, May 18-22, 1992, NASA Conference publication 3214, NASA Greenbelt, 1993, p. 12-40 - 12-48.

NEW FIXED STATIONS

Chairperson : Yang Fumin

NAVAL RESEARCH LABORATORY'S SATELLITE LASER RANGING CAPABILITY AT THE PHILLIPS LABORATORY STARFIRE OPTICAL RANGE

A.E. Clement and G.C. Gilbreath
Naval Center for Space Technology, Naval Research Laboratory, Washington, DC

R.Q. Fugate and J.M. Spinhirne
Starfire Optical Range, Phillips Laboratory, Albuquerque, NM

J.J. Degnan
Goddard Space Flight Center, NASA, Greenbelt, MD

ABSTRACT

The US Naval Research Laboratory (NRL) has integrated its ground-based satellite laser ranging system with the Phillips Laboratory (PL) assets at the Starfire Optical Range on Kirtland AFB, Albuquerque, NM. The combined system, which includes a 300 mJ laser and a 3.5 m telescope, is described in detail. Specific critical system parameters are given for this configuration. The laser radar equation is used to evaluate each parameter's impact on overall sensitivity. The configuration is then compared with that for a MOBLAS SLR station. The prospect of using the NRL/PL system to range off of unenhanced satellites is presented and the viability is discussed.

I. INTRODUCTION

In 1992, the Naval Research Laboratory (NRL) and the Phillips Laboratory (PL) created a new laser ranging system at the Malabar Optical Tracking Facility in Palm Bay, FL. [1] The system sensitivity was slightly higher than, but comparable to, the NASA MOBLAS systems. [2] This station was successful in tracking both high and low altitude retroreflector-enhanced satellites (i.e., LAGEOS, GEOS-3, and BEACON-C among others). In 1994, the NRL system was moved to Albuquerque, NM and integrated at the PL Starfire Optical Range (SOR) located on Kirtland AFB. During the transition, several design changes were made as detailed in this article and in Ref 3. The SLR system was moved in order to take advantage of the increased link margins available with the 3.5 meter telescope at SOR.[4]

One of the goals of the NRL satellite laser ranging program is to track targets with small optical cross sections. For unenhanced platforms it may be possible to employ signal processing algorithms to determine points of reflection from returns recorded on wide-band digitizers if the signal is strong enough. These processed returns could, in turn, be used to reduce error in

satellite ephemeris. A large power-aperture product, such as that available with the NRL/SOR system, may provide a means to obtain and identify signals from such points of reflection and from unenhanced targets in general. A second NRL goal is to process precision orbits with data from a single site.[5]

This paper compares the sensitivity of the NRL/SOR system with a MOBLAS system. MOBLAS was chosen for this comparison because it will place the NRL/SOR system in a reference frame which is widely familiar within the SLR community. Although the general trend within the network seems to be heading towards smaller automated systems [6], the high sensitivity shown for the NRL/SOR system is necessary to meet the goals stated above.

II. OPERATIONAL CONFIGURATION

The operational configuration accomodates monostatic acquisition, tracking, and illumination of a satellite. The laser beam is co-aligned with the optic axis of the telescope and the return signal is directed along the same path. Aperture sharing is accomplished using polarization. Two intensified CCD cameras positioned in the recieve optics train assist alignment and tracking.

A. Laser

The NRL laser is a frequency doubled, Nd:YAG radiating at a wavelength of 532nm. The laser cavity has a standard active Q-switch and an active mode-locker, rather than the active-passive configuration used in the MOBLAS lasers. The intracavity design produces a train of high energy pulses with smooth Gaussian temporal beam profiles. The oscillator uses a cavity dumping technique to extract the highest intensity pulse from the pulse train generated within the cavity. This technique is implemented with a second Pockels cell which is triggered by a photodiode. The photodiode senses the intensity buildup inside the cavity and selects a single pulse to pass out of the cavity via polarization rotation and reflection off a linear polarizing beam splitter.

The oscillator and the two single-pass amplifier stages are flashlamp pumped to generate light at 1064 nm. Frequency doubling was achieved using a Type II KD*P crystal, to produce the operating wavelength. The output beam from the laser is approximately 12.5 mm in diameter with a divergence which is approximately 5-10 times the diffraction limit. During ranging operations, the laser emits 300 mJ at a 10 Hz repetition rate for an average power of 3 W. The pulse width is 250 ps, yielding an instantaneous power of 1.2 GW per pulse. Scattered IR light is detected by a PIN diode and the signal is used to trigger the receiver electronics. A streak camera is dedicated to the system for laser diagnostics, but it is not used on a daily basis.

B. Optics

The NRL optics bench is shown in Figures 1 (transmit path) and 2 (receive path). For transmission, the laser light is directed through a pair of lenses (L1 & L2) which generate the beam geometry to both fill the telescope pupil and provide the desired divergence. The range of full angle divergences has been designed to be 10 μRad - 100 μRad in the far-field of the telescope. The light is directed with a right-angle periscope (RAP) which rotates the linear polarization from vertical to horizontal. A 6 inch polarizing beamsplitter (PBS) is used for the transmit/receive switch. The polarizer passes the horizontal light with a 6% loss of energy due to reflection. In the Malabar configuration, an annular mirror was efficiently used as the Tx/Rx switch because the beam was transmitted offset from the optic axis of the telescope. At SOR the laser light is transmitted along the optic axis of the 3.5 m telescope. The beam is then steered with two 6 inch mirrors (M1 & M2) and directed through a quarter wave plate (QWP) to create circularly polarized light.

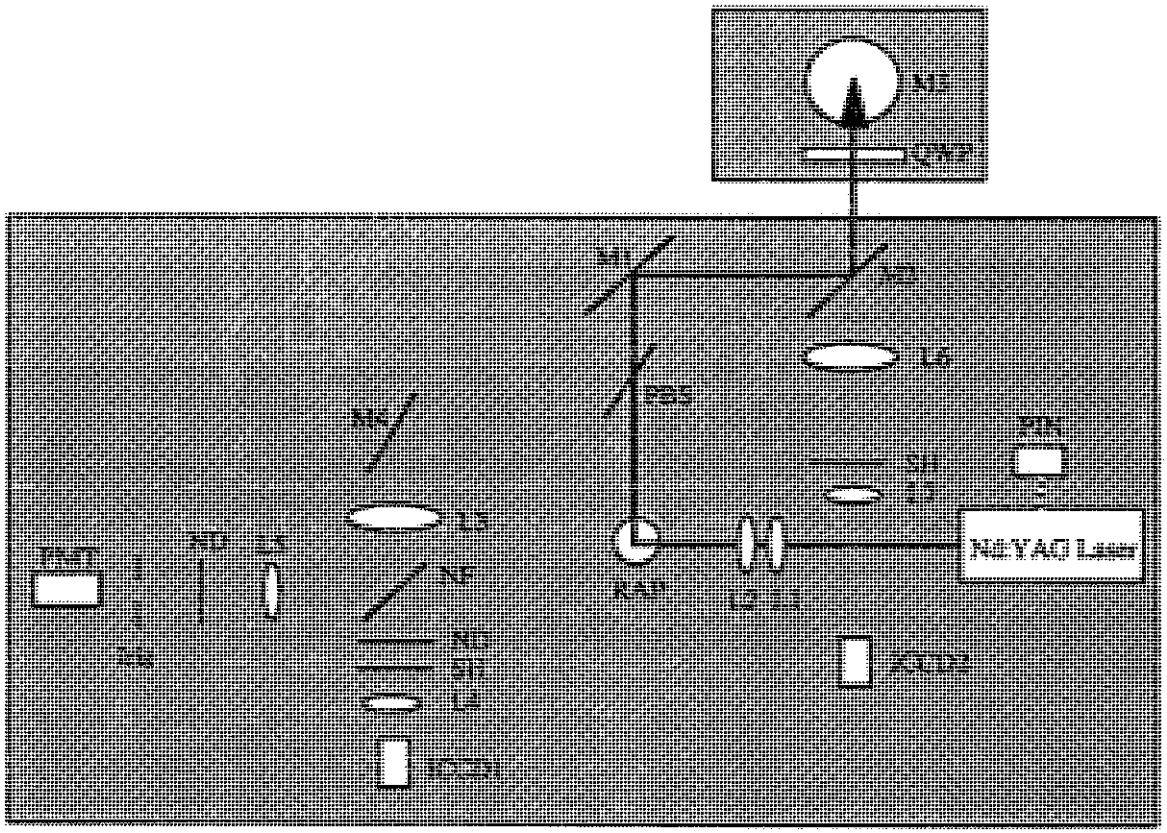

Fig. 1. NRL Optical Bench showing the optical transmit path for laser light.

The next optic encountered is a rotatable mirror (M3) at the base of the telescope pier which directs light from the Coude room or from any one of six laboratories into the telescope. The 3.5 meter telescope consists of four turning flats which direct the light onto the 0.35 meter

secondary and finally the 3.5 meter primary mirrors.[4] The telescope provides a 10x magnification and maintains active optics to control the alignment of the primary and the secondary. In the future, SOR plans to integrate adaptive optics similar to the system on their 1.5 meter telescope. [7] The adaptive optics will allow the propagation of beam divergences which are not limited by the atmosphere. The 1.5 meter telescope has been able to propagate beams with full angle divergence as narrow as 1 μRad.

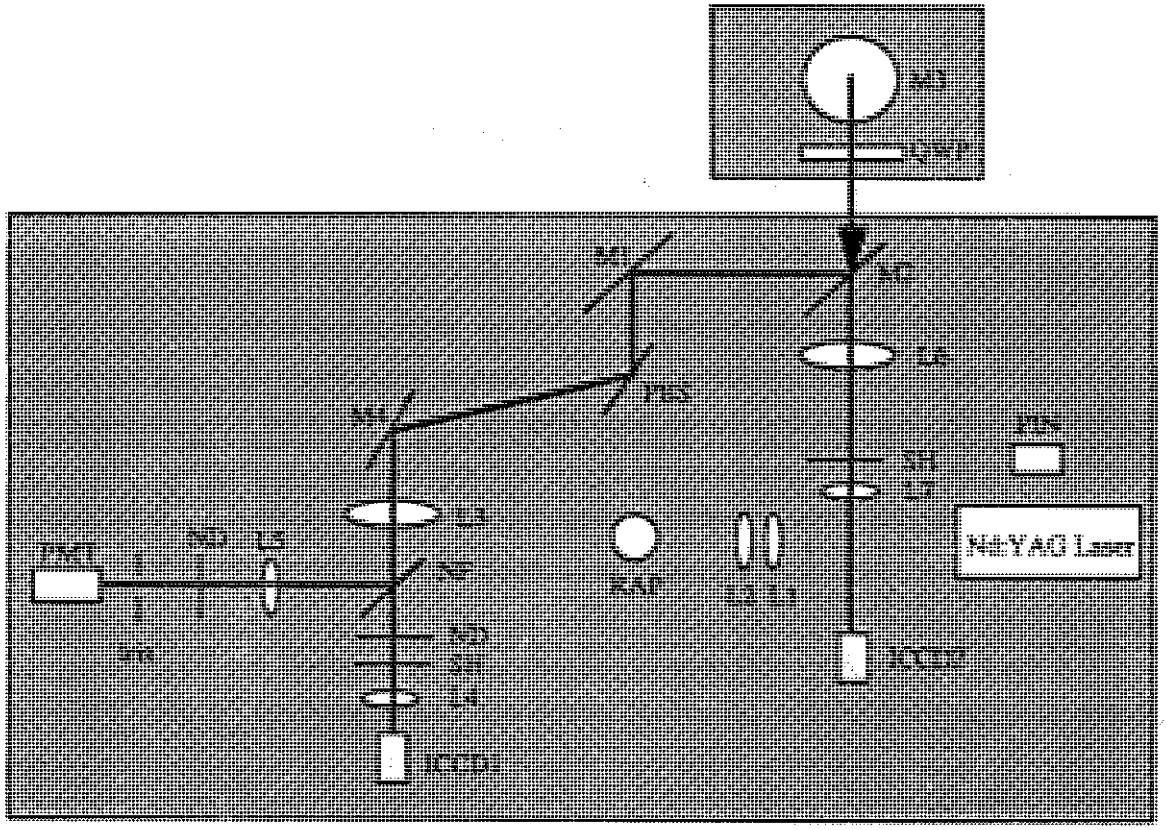

Fig. 2. NRL Optical Bench showing the optical receive path for laser light. and sunlight.

Reflected sunlight and the return laser pulses are collected with the 3.5 meter telescope. The optical path of the received light is shown in Figure 2. In the receive path, the light is circularly polarized in the opposite "handedness" of the transmit path, except to the extent that the target depolarizes the beam. Therefore, the QWP transforms most of the light to a vertical polarization which then reflects off the polarizing beam splitter (PBS). The beam reflects off a mirror (M4) which directs it through a 33 cm focal length field lens (L3) placed at the infinity focus of the telescope. The green light is split from the reflected sunlight with a notch filter (NF) centered at λ=532 nm and with a 10 nm bandwidth. After the green light is reflected off the notch filter, it passes through another short focal length lens (L5). The light is focused through variable neutral density filters (ND) and an iris to spatially filter any stray reflections. The

combination of L3 and L5 creates an 8 mm diameter exit pupil at the surface of the gated photomultiplier tube (PMT) detector.

The white light which passes through the notch filter, neutral density filter, and computer controlled shutter, is focused onto an intensified CCD camera (ICCD1). ICCD1 is used primarily for system alignment. The majority of the white light has passed through M2 (a dichroic mirror optimized for λ=532 nm reflection) before reaching a computer controlled shutter (SH) placed in the exit pupil created by L6. The shutter remains open except for a variable gate set to the time of transmit of the pulse. A short focal length lens (L7), placed directly behind the shutter, focuses the sunlight onto a second gated, intensified CCD camera (ICCD2) which is used for passive tracking in terminator mode. ICCD2 will also collect residual green light which leaks through the M2 and can therefore be used for active tracking as well.

C. Tracking

The NRL/SOR system is monostatic and most often operates in terminator mode (the satellite is sunlit while the ground station is dark). Passive acquisition and tracking of a satellite occurs from horizon break throughout the pass using ICCD1 and ICCD2. Active illumination of the satellites can only occur for elevations above 30° due to local restrictions. Using ICCD2, green returns provide active tracking data whether the satellite is at terminator or in umbra. The telescope operator uses both tracking cameras to center the satellite within telescope's field-of-view.

The telescope pointing software developed at SOR is hosted on a Macintosh Quadra computer. It updates the satellite ephemeris in real time using the ICCD images. The improved orbit arc which can be generated in the first minute of the pass using passive data, allows for nearly "hands-off" open loop tracking throughout the period of active illumination.

D. Data Collection

The timing detector shown in Figure 2 is a gated microchannel plate enhanced photomultiplier tube (MCP/PMT) which provides a gain of 10^6 at λ=532 nm. The receiver system includes a second time-gate on the constant fraction discriminator to negate the effects of electronic noise induced when the PMT is initially turned on. The output voltage from the PMT is split for timing and signal processing.

Figure 3 is a functional overview of the data collection system employed in the NRL/SOR configuration. A detailed description of the equipment and the timing flow are given in Ref 3. The start pulse from the PIN diode is used to trigger the IRIG board and the start channel of the SRC Universal Time Interval Counter (UTIC). The stop pulse from the PMT is used to trigger the stop channel of the SRC UTIC and provides input to the two oscilloscopes: a

1 GHz analog and a 4 GHz digital oscilloscope. The data collected with this system is: (a)the time of transmission; (b)the round trip time delay; (c)the pulse shape; (d)the pulse amplitude; and (e)the pulse position within the gate for each pulse.

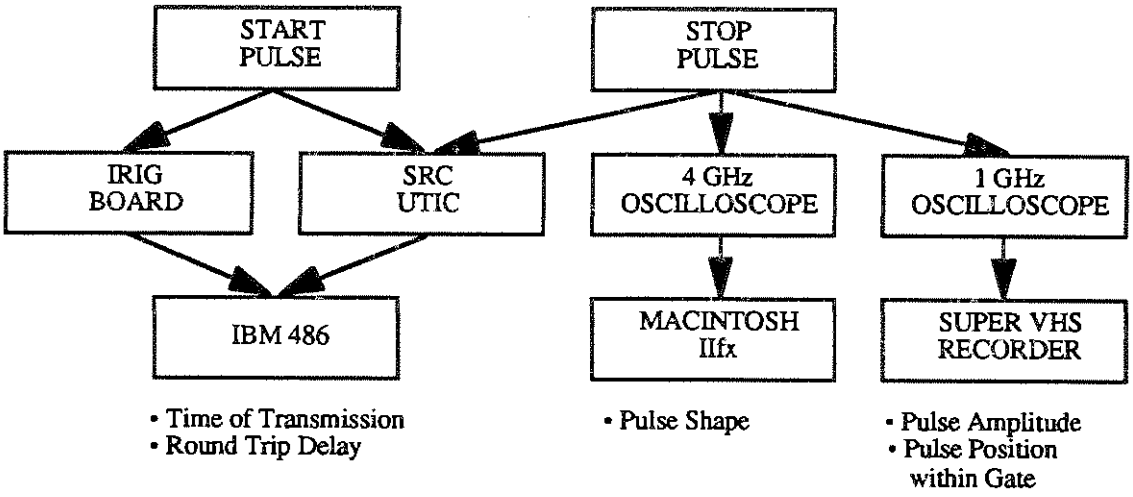

Fig. 3. Functional overview of the NRL data collection system at SOR.

III. SYSTEM COMPARISON

A. Theory

The laser radar link equation is the appropriate tool to compare the sensitivity of SLR systems as well as to establish the viability of a specific system with targets of interest. For an unresolved target (smaller than the beam footprint), the number of photoelectrons, N_{pe}, which will be generated by the detector, is given by [8]:

$$N_{pe} = \eta_d \left(E_T \frac{\lambda}{h c}\right) \eta_t G_t \sigma \left(\frac{1}{4 \pi R^2}\right)^2 A_r \eta_r T_a^2 T_c^2 \qquad (1)$$

where η_d is the quantum efficiency of the detector, E_T is the laser pulse energy, λ is the laser wavelength, h is Planck's constant, c is the speed of light in a vacuum, η_t is the efficiency of the transmit optics, G_t is the gain of the telescope, σ is the target optical cross section, R is the range to the target, A_r is the effective area of the collector, η_r is the efficiency of the receive optics, T_a is the transmission through the atmosphere, and T_c is the transmission through cirrus clouds.

The gain of the telescope, G_t, is given by the following expression for a quasi-Gaussian beam [8]:

$$G_t = \frac{8}{\theta_t^2} \exp\left(-2\left(\frac{\theta}{\theta_t}\right)^2\right) \qquad (2)$$

where θ_t is the half-angle of the far field divergence from the center of the beam to the $1/e^2$ intensity point. The beam pointing accuracy is given by θ. A more general expression for gain is given in Ref. 8 which accounts for radial truncation of the beam as it propagates through the optical train and for the obscuration of the secondary mirror. For the purpose of the comparisons made in this paper, the simplified expression will be used.

This study compares the sensitivity of the NRL/SOR system with a best case MOBLAS system. Because of the geographical dispersion of the MOBLAS systems, it has been assumed for the comparison that a MOBLAS system is operating at the Starfire Optical Range. Therefore, losses due to atmospheric propagation will be constant between the systems. Because the NRL/SOR system has not yet been optimized, it will be assumed the η_t and η_r are also constant between NRL and MOBLAS for this comparison.

Table I. System Parameters used in the laser ranging link equation for this study, Npe = 20.

Assumed Constant	MOBLAS (0.76 m)	NRL/SOR (3.5 m)
η_t=0.66*	A_r =0.4 m^2	A_r =9.5 m^2
η_r=0.54*	θ_t=50 μRad	θ_t=5 μRad
T_c=1.0 **	θ=5 μRad	θ=1 μRad
λ=532 nm	E_T=100 mJ	E_T=300 mJ
Site Alt. = 1864 m	η_d=0.18	η_d=0.1678
$0.91 \leq T_a \leq 0.96$		
* Efficiency of optical train assumed to be the same for NRL/SOR and MOBLAS		
** Cloudless		

The MOBLAS systems are routinely able to operate with CFD thresholds of 3-5 photoelectrons for enhanced targets. For an unenhanced target, signal processing on the returns to determine the points of reflection requires a higher intensity signal. To be conservative, this comparison assumes that twenty photoelectrons must be present in a return so that the signal can be split and the pulse shape can be determined.

The parameters of particular interest in this study are receiver area, divergence, and pointing accuracy. The discussion of these parameters will be accompanied by graphs which plot the optical cross section which would be required of a target in order to detect 20 photoelectrons in the return signal. The target satellite is assumed to be in an 1100 km circular orbit for all cases. Table I lists the link parameters used to generate the following graphs. The MOBLAS parameters are best case values taken from Ref. 8. For each graph in Sections III-B through III-D, the solid curve is generated for a system using all of the MOBLAS values. Each

of the dashed curves were computed using the MOBLAS parameter set except for the parameter of interest for that particular section. For the dashed curves, the parameter of interest was changed to the NRL/SOR value.

B. Receiver Area

The area of the receiver, A_r, was found to have the greatest impact on improving system sensitivity for the two cases described here. A_r is the effective area of the primary mirror on the receiving telescope. The OCS required to produce 20 photoelectrons at different elevations is shown in Figure 4 for an 1100 km orbit.

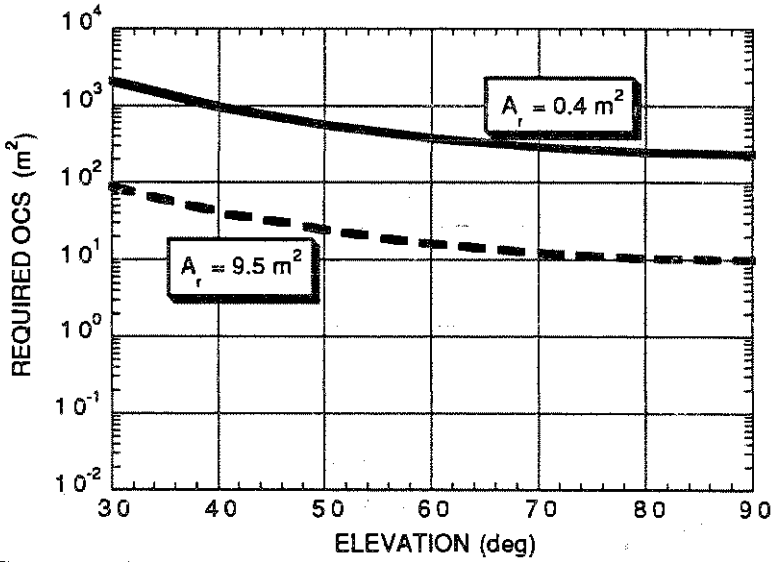

Fig. 4. Effect of Collector Diameter on Minimum Detectable OCS using the MOBLAS Configuration.

The two curves show the impact of receiver diameter on minimum detectable OCS per system as a function of elevation angle. The solid curve was generated using the parameters for the MOBLAS configuration described in Table I. The dashed curve was generated using the same parameters except the receiver diameter of the telescope has been changed from a 0.76 m dish for MOBLAS to a 3.5 m dish for NRL/SOR. As can be seen in the figure, the 3.5 m dish can detect a return signal from a target with a much smaller OCS. The target must have an optical cross section which is more than an order of magnitude larger if it is to be detected using the 0.76 m dish.

C. Transmitter Gain

Transmitter gain is a function of divergence and pointing accuracy. It is inversely proportional to the required optical cross section. Figure 5 shows the improvement in system performance due solely to the smaller beam divergence achievable with the SOR telescope. The analysis reported here assumes the minimum achievable half-angle divergence to be 5 μRad as

reported for the 1.5 m telescope at SOR without atmospheric compensation. As can be seen from the graph, there would be an increase in system sensitivity equal to 11 dB for all elevation angles if the half-angle divergence for MOBLAS could be reduced from 50 μRad to 5 μRad. When the adaptive optics become available on the 3.5 m telescope (1995-96), divergence will become an even more significant factor because SOR will be able to propagate more narrow beams, placing more energy on target. It must be noted that at smaller divergence angles the transmit beam must be accurately pointed ahead of the target by the lead angle.

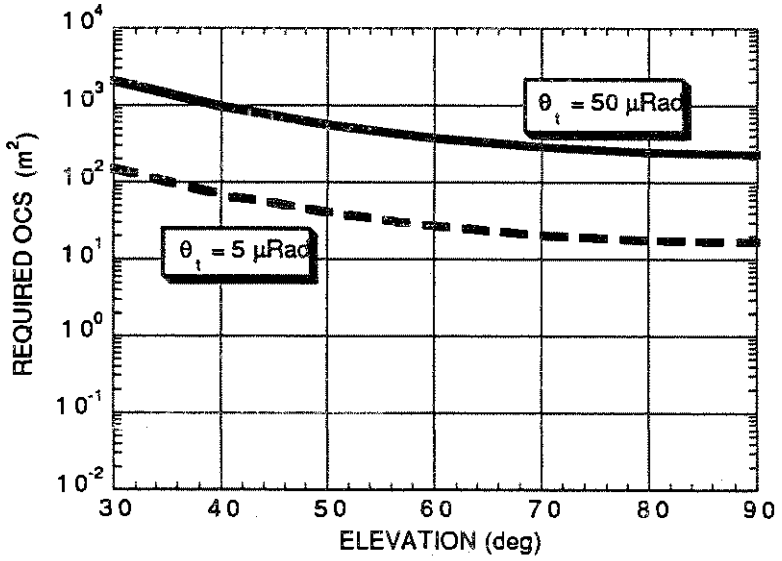

Fig. 5. Effect of Divergence on Minimum Detectable OCS using the MOBLAS configuration.

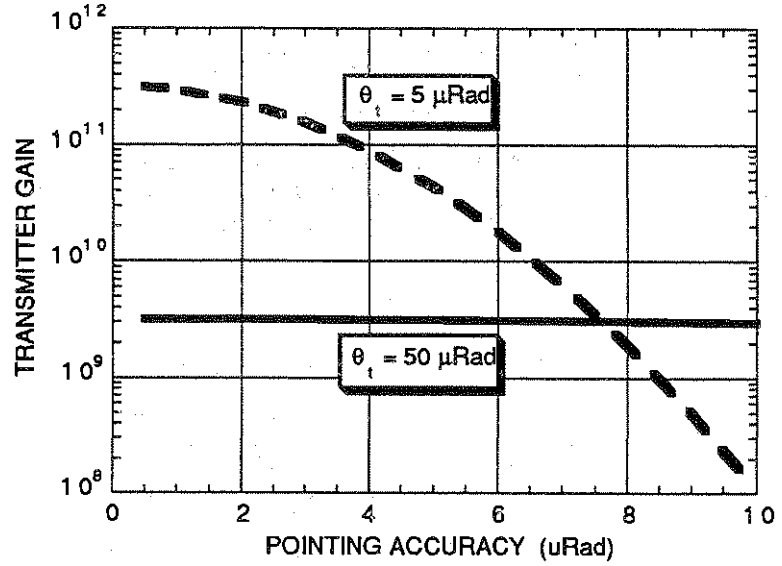

Fig. 6. Gain vs Pointing Accuracy , θ, for NRL/SOR and MOBLAS.

Pointing accuracy also affects system sensitivity through the gain equation. The pointing accuracy, θ, for each system in this comparison (i.e.: 5 μRad for MOBLAS and 1 μRad for NRL/SOR) will provide high gain for the attainable divergences. Because the 50 μRad half-angle divergence typical of MOBLAS is so large, there is a negligible effect on sensitivity if the pointing accuracy is improved to 1 μRad. As seen in Figure 6, the transmitter gain for MOBLAS is nearly constant for pointing accuracies between 500 nRad and 10 μRad. However, the transmitter gain for the NRL/SOR system varies by more than 3 orders of magnitude in this same range due to the small divergence. Between θ=5 μRad and θ=1 μRad, there is an order of magnitude increase in the transmitter gain for a half-angle divergence of 5 μRad.

The improvement in system efficiency includes a contribution from both smaller divergence and better pointing accuracy which are available at SOR. Figure 7 shows the effect of the transmitter gain on the required OCS. The NRL/SOR configuration is almost 20 dB more sensitive than the best case MOBLAS configuration.

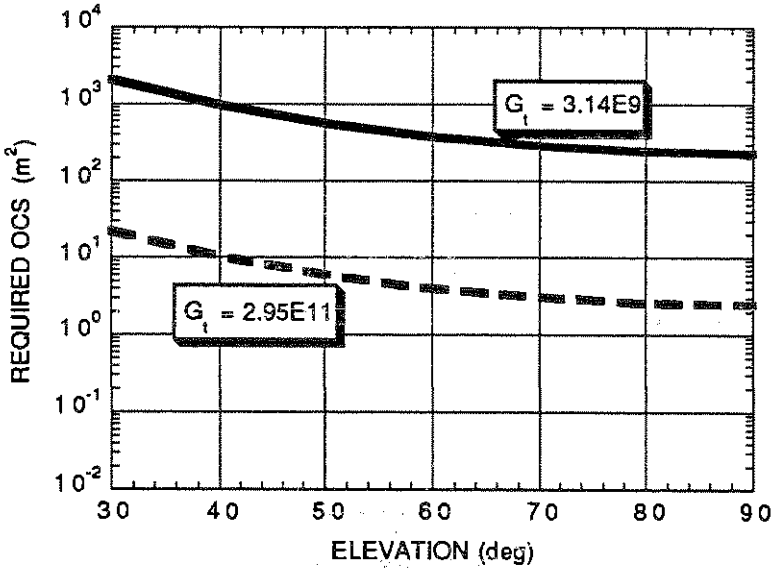

Fig. 7. Effect of Gain on Minimum Detectable OCS using the MOBLAS Configuration. The solid line computes gain based on θ_t = 50μRad and θ = 5μRad, characteristic of the MOBLAS design; the dashed line computes gain based on θ_t = 5μRad and θ = 1μRad characteristic of the NRL/SOR.

D. Composite System

The composite system efficiencies for the best case MOBLAS system and NRL/SOR system can be seen in Figure 8. This figure shows the OCS required to detect a 20 photoelectron return signal with each station. At SOR, the NRL system will be able to detect returns from a target with an OCS which is nearly 4 orders of magnitude smaller than that which could be detected using a best case MOBLAS system in the same location. This graph indicates that with the NRL/SOR system it will be possible to detect returns from an unenhanced object with an

OCS of less than 1 m^2 at all elevation angles. In addition to providing range information for unenhanced satellites, increased system sensitivity may also enable ranging off of space debris.

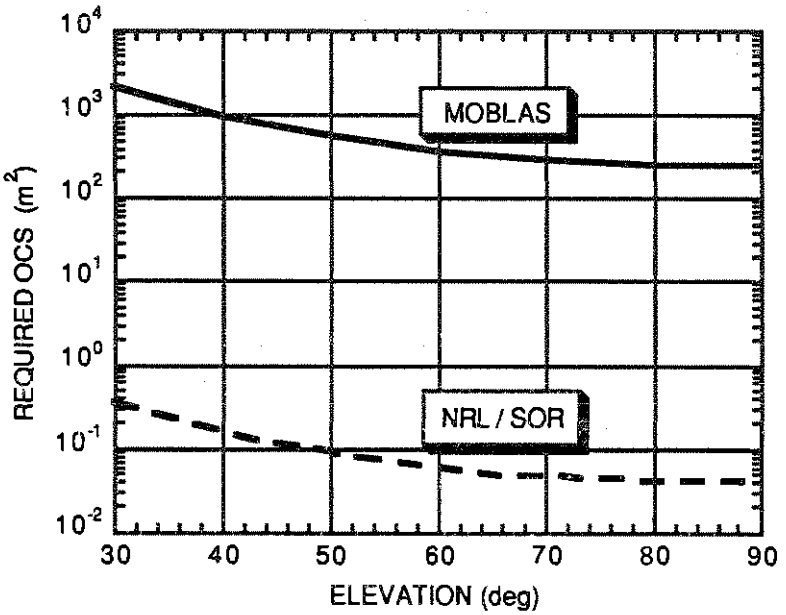

Fig. 8. Minimum Detectable OCS required to detect 20 photoelectrons with NRL/SOR and MOBLAS. The dashed curve shows that with the NRL system integrated at SOR, it may be possible to detect returns off of unenhanced targets with very small cross sections.

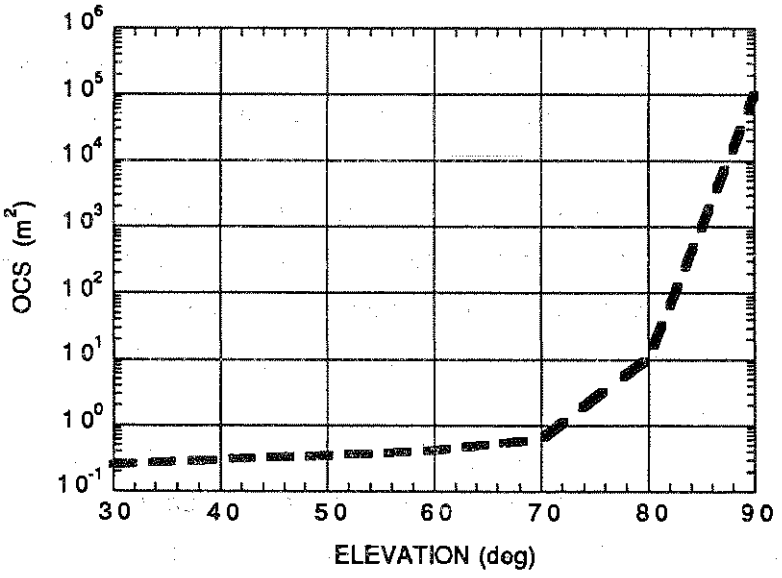

Fig. 9. DELTAS code simulation of the OCS of an unenhanced satellite.

Figure 9 plots the OCS of a generic satellite as modeled by the DEfense Laser/TArget Signatures (DELTAS) code. DELTAS is a program developed by Strategic Defense Initiative

Organization (SDIO) for predicting OCS of objects in flight. The satellite which was modeled had a flat bottom made of shiny aluminum with a surface area of ≈6 m^2. A comparison of Figures 9 and 10 shows that it should be possible to detect returns from unenhanced satellites similar to the one modeled here. For example, at a 40° elevation angle, a satellite like the one modeled has an OCS of $0.3m^2$. At SOR, the NRL system is predicted to detect a $0.1m^2$ target. Therefore, the system should be able to detect and range off the unenhanced target with a high probability of detection.

IV. CONCLUSION

In this paper, a new satellite laser ranging station is described. It is a joint effort between the Naval Research Laboratory and the USAF Phillips Laboratory. The sensitivity of the NRL SLR system as integrated at the Starfire Optical Range has been compared with the sensitivity of a best case MOBLAS configuration. A comparison of NRL's theoretical system efficiency shows that an overall improvement of 38 dB could be obtained over a MOBLAS system at the same site. The three key parameters contributing to this improvement were: collector area, divergence, and pointing accuracy. Contributions to the overall improvement at 90° elevation (overhead) are summarized as follows:

$$13.8\ \text{dB}\ (A_r) + 11.4\ \text{dB (div)} + 8.3\ \text{dB (PA)} + 4.5\ \text{dB (misc.)} = 38\ \text{dB}$$

The single parameter which has the most impact in the laser ranging sensitivity is the increased collector area. The improvement due to the telescope gain is higher, but it contains contributions from both smaller beam divergence and more accurate pointing. As previously pointed out, an improvement in pointing alone will not significantly improve efficiency. There must be a corresponding decrease in divergence. It is anticipated that even greater sensitivity will be achieved when the adaptive optics are integrated at SOR. As the result of this analysis, it was found that, with the NRL system integrated at SOR, laser ranging off of unenhanced satellites may be possible.

Although the effects of weather patterns are not quantified in the laser radar link equation, they do have an impact on the quality of the data. Successful data acquisition per orbit opportunity is extremely important for post-processing. The distribution of returns throughout a pass, as well as the number of consecutive passes collected, significantly weights the final ephemeris produced by orbital models. It is anticipated that the New Mexico site will provide a particularly stable environment and is an optimum location from which to conduct experiments and extrapolate designs for operational use.

V. REFERENCES

[1] G.C. Gilbreath and H.D. Newby, "Ground-Based Laser Ranging for Satellite Location", Proc. of the 8th International Workshop on Laser Ranging Instrumentation (May 1992).

[2] A.E. Clement, G.C. Gilbreath, and A.R. Peltzer, "A Comparison of Two Sites for the Purpose of Satellite Laser Ranging", NRL Memorandum Report #94-7604 (July 1994).

[3] D. Roberts, A.R. Peltzer, A.T. Olson, G.C. Gilbreath, and R.A. McKnight, "Automated Direct Detection Ranging Measurements for US Naval Research Laboratory System", Proc. of the 9th International Workshop on Laser Ranging Instrumentation (November 1994).

[4] R.Q. Fugate, et.al., "First Observations with the Starfire Optical Range 3.5-meter Telescope", in Advanced Technology Optical Telescopes V, L.M. Stepp, ed., SPIE vol 2199, pp. 481-493 (March 1994).

[5] A.R. Peltzer, W.J. Barnds, and G. C. Gilbreath, "Study to Determine the Satellite Ephemeris Accuracy of TOPEX Using a Single SLR Site", Proc. of the 9th International Workshop on Laser Ranging Instrumentation (November 1994).

[6] J.J. Degnan, "SLR 2000 : An Automated, Eyesafe Satellite Ranging Station for the Future", Proc. of the 9th International Workshop on Laser Ranging Instrumentation (November 1994).

[7] R.Q. Fugate, "Laser Beacon Adaptive Optics", Optics & Photonics News, 4 (6), (1993).

[8] J.J. Degnan, "Millimeter Accuracy Satellite Laser Ranging: A Review", Contributions of Space Geodesy to Geodynamics: Technology - Geodynamics Series **25** (1993).

HELWAN 2 SATELLITE LASER RANGING STATION

K.Hamal, I.Prochazka

Faculty of Nuclear Science and Physical Engineering
Czech Technical University, Brehova 7, 115 19 Prague 1, Czech Republic
fax +42 2 85762252

M.J.Tawadros, J.S.Mikhail
National Research Institute of Astronomy and Geophysics
Helwan, Cairo, Egypt, fax +20 2 782683

Considering the increasing number of satellites dedicated for laser ranging launched and planned in nineties on one hand and the increased requirement on the ranging precision on the other hand, it was decided to upgrade the Helwan Satellite Laser Station. The goal of the upgrade is the multiple target subcentimeter laser ranging to the satellites at the distances up to 20 thousands kilometers. Taking into account the resources provided by the National Research Institute of Astronomy and Geophysics, the upgrade has been proposed in two phases. Phase A consisted of a reconstruction of the tracking telescope : the new DC servo and the incremental optical encoders have been implemented, the automatic visual guiding is accomplished using the Cellestron C11 reflector equipped with the ST-4 CCD star tracker. The station is controlled by the new microprocessor based compact control system interfaced to two personal computers for orbit prediction calculations, data analysis, international network communication, etc. The station upgrade Phase A has been completed by July 1994, the satellites up to the distances of 20 thousands kilometers have been automatically tracked. Phase B will consists of system integration with the laser transmitter, assembly on the permanent site, installation of the new receiver detector package and the reconstruction of the Coude transmitter beam path. The Phase B is expected to be completed by the end of 1995.

PROJECT MILESTONES

Helwan 2 Satellite Laser Station

July 92	decision to build the Helwan 2
March 93	J.Degnan + Allied Signal offered the T4 doccumentation
till Dec.93	searchning for sponsor(s)
December 93	alternative concept reflecting available budget from Helwa
till Apr.94	copmonents design and manufact. hard / soft debugging
May 94	shipment
June 94	on site assembly, Phase A satellite laser ranging
June 95	completition, Phase B
July 95	routine operation

Hamal, Prochazka, Tawadros, Mikhail, Canberra 1994

PHASE B 1995 / CONCLUSION

Helwan 2 Satellite Laser Station

- optics subsystem
  Coude path, transmitting telescope, motorised output mirror holder,
- SPAD detector package
- CCD guiding sensor image processing
  automated optical guiding
- control system
  Fully operational, multiple target satellite laser ranging system control, personal computer Prediction, calibration, tracking and ranging, data analysis, archivation, transmittion
- system integration, operational tests
- routine operation

Hamal, Prochazka, Tawadros, Mikhail, Canberra 1994

HELWAN 2 SATELLITE LASER STATION
Az-El mount, Cellestron C11 telescope
DC servo, incremental encoders
K.Hamal, I.Prochazka, 1994

HELWAN 2 SATELLITE LASER STATION
Telescope + detector + guiding package
CCD ST-4 /front/ SPAD /left/
K.Hamal, I.Prochazka, 1994

HELWAN 2 SATELLITE LASER STATION

CCD Satellite image

Cellestron C11,ST-4, 4sec exposure

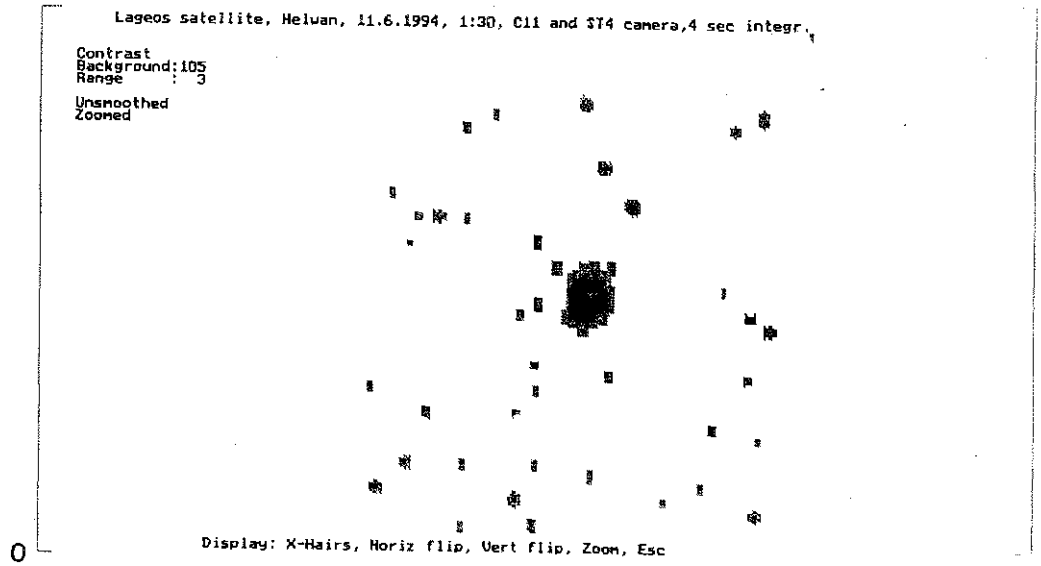

LAGEOS

K.Hamal, I.Prochazka 1994

HELWAN 2 SATELLITE LASER STATION

Experimental laser ranging, SPAD /up/

Helwan 1, PMT /bottom/

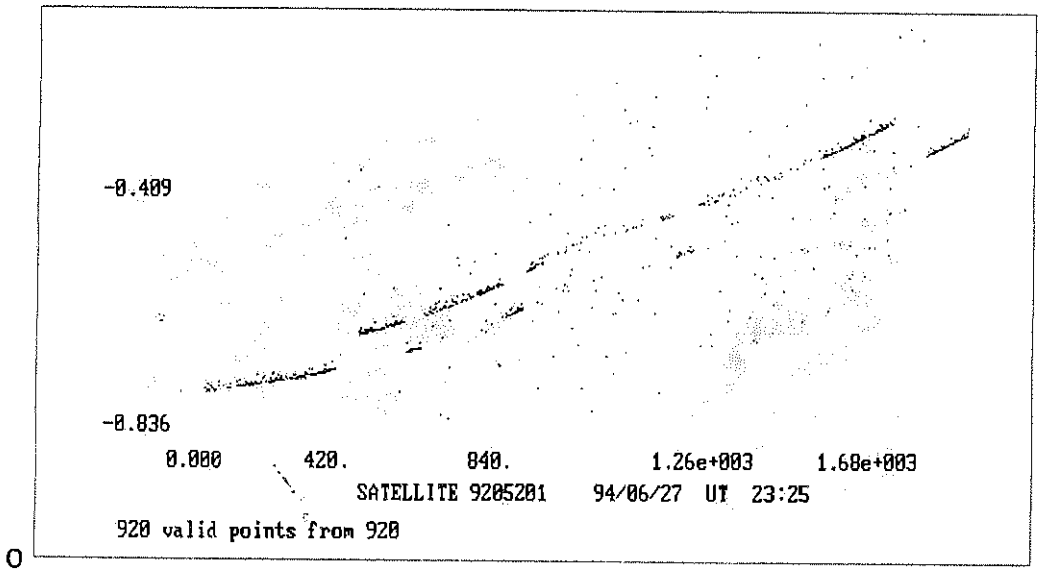

TOPEX

K.Hamal, I.Prochazka 1994

HELWAN 2 SLR STATION

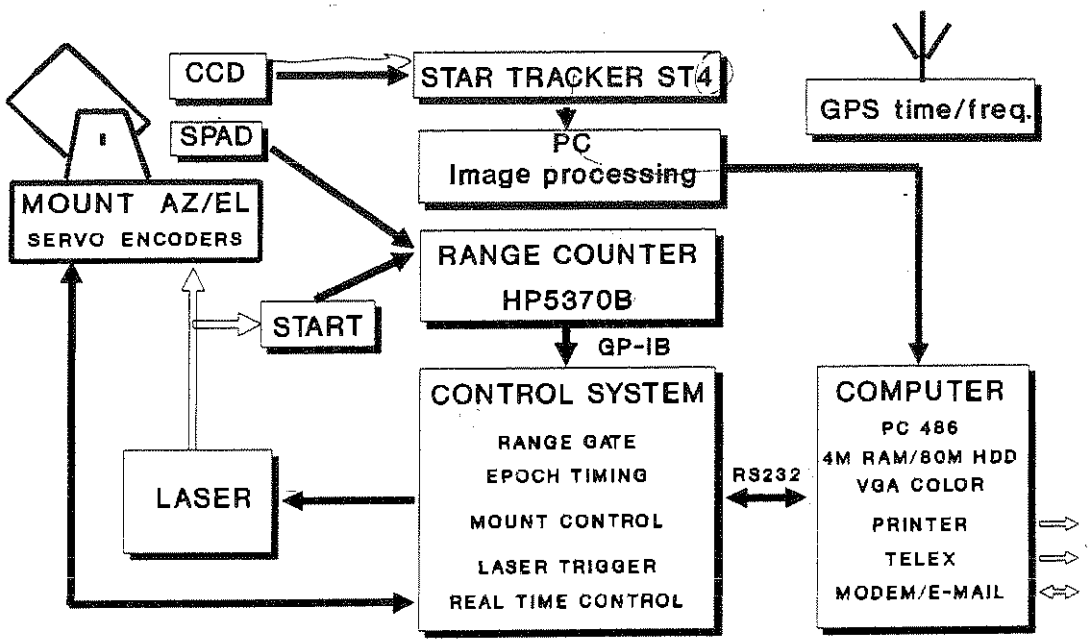

Czech Technical University

HELWAN 2 SATELLITE LASER STATION

Laser tracking telescope optical scheme
Top view

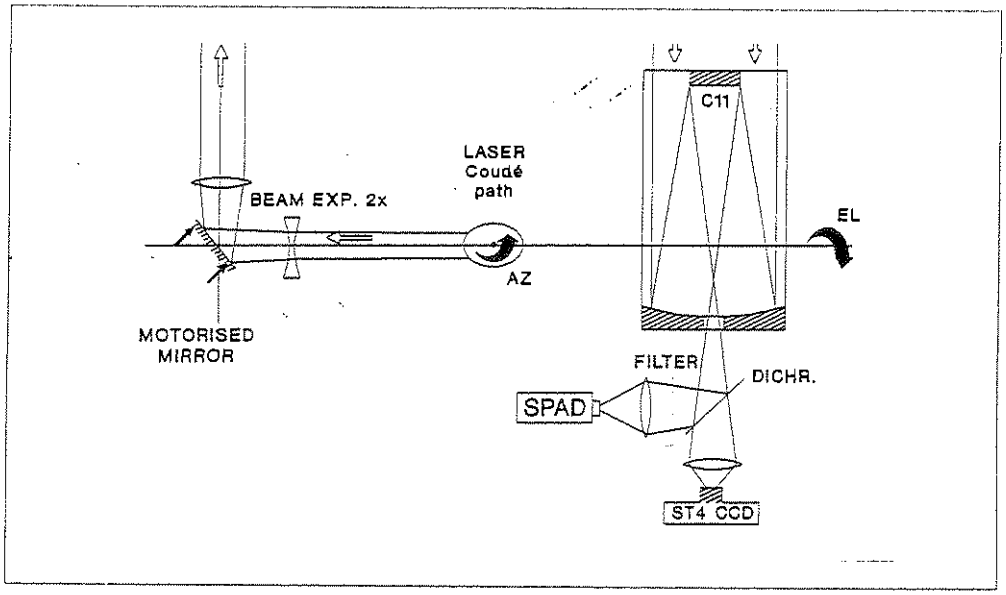

K.Hamal, I.Prochazka, 1994

MOUNT

Helwan 2 Satellite Laser Station

configuration	two axis az - el
Coude path	transmitter
drive	DC motors (Hirsl)
gears	worm gears 1:360 reduction gear 1:16
readout	incremental ecoders on motor axes
control	microprocessor based control unit (Cech)

Hamal,Prochazka,Mikhail, Tawadros, Canberra,1994

MAIN PARAMETRS

Helwan 2 Satellite Laser Station

absolute pointing accuracy	1 arc minute
receiver FOV	1.5 arcmin
pointing resolution	1 arcsec
tracking speeds	0 - 2 degrees/second
guiding sensitivity	CCD star tracking system computer image processing integration 0.5-8 sec
limiting magnitude	14
optical axes paralelity	monitored via CCD sensor cotrolled via remote controlled Coude mirror

Hamal, Prochazka, Tawadros, Mikhail, Canberra 1994

GOALS

HELWAN 2 Satellite Laser Station

- satellite laser ranging to all retro equipped satellites
- measuring range 0 - 20 000 kilometers
- ranging precision
  1 centimeter RMS / single shot/
  1 millimeter /normal points spread/
- automatic optical guiding
- visual guiding capability
- all solid state detector technology
- multiple wavelengths, multiple target capability

Hamal,Prochazka,Tawadros, Mikhail,Canberra,1994

RECEIVER + GUIDING SYSTEM

Helwan 2 Satellite Laser Station

diameter	280 millimeters
configuration	meniscus Cassegrain
optics / housing	Celestron C11
guiding sensor	CCD camera, computer controlled cooled FOV 3 milliradians
ranging detector	Single Photon Avalanche Diode 100 microns, cooled FOV 0.3 mradian
ranging filter	8 nm, 5 %

Hamal, Prochazka, Tawadros, Mikhail, Canberra,1994

Status of satellite laser ranging at Metsähovi

MATTI PAUNONEN

Finnish Geodetic Institute
Ilmalankatu 1A
FIN–00240 Helsinki, Finland
Fax: 358-0-264995, E-mail: geodeet@csc.fi

Abstract. Satellite laser ranging at Metsähovi was restarted in January 1994 after a pause of three years using a 3 ns green Nd:YAG laser and improved tracking. During the year 1994, 462 passes with 42202 accepted observations from 10 satellites were obtained. The average precision of the range measurements to the close-Earth satellites is now about 10 cm. A new, centimetre-accuracy laser ranging system is currently under construction. This report reviews briefly the instrumental status and ranging results.

Introduction

Space geodetic operations at the Metsähovi Observatory of the Finnish Geodetic Institute were begun in 1978 with a satellite laser ranging system (7805) described in [1]. The pulse length of the Q-switched ruby laser was about 20 ns, and the ranging precision was about 0.5 m. As a partial upgrade the ruby laser pulse length was shortened to 4.5 ns by an electro-optical shutter in 1985 [2].

Other relevant activities undertaken included the European mobile VLBI campaign in 1989 at Sjökulla, a site about 3 km north of the observatory, where also a DORIS (Doppler orbitography and Radiopositioning Integrated by Satellite)- orbit determination beacon was started in 1990. Permanent GPS operations were begun in 1991, and the present MiniRogue SNR-8C GPS receiver was connected to the IGS (International GPS Service for Geodynamics) GPS network from the very beginning in June 1992 [3].

The main remaining problems of the laser system were identified as the the slow repetition rate, point-to-point tracking mode and limited computer memory. To improve the capabilities, SLR operations were ceased at the end of 1990, but were restarted in 1994 after a major upgrade to be described in this paper. As a further improvement, construction of a new satellite laser system was launched in 1993.

Equipment

The main specifications of the present satellite laser are given in Table 1. A compact Nd:YAG laser with a positive branch unstable resonator was developed. A passive saturable absorber with colour centres in a LiF crystal is used for short pulse forming. The invisible laser light is converted to green (532 nm) by a DKDP crystal. The pulse length is 3 ns, the pulse energy about 50 mJ, and the pulse rate 0.5 Hz. The entire laser was installed on the tracking telescope. After the collimator the beam width is about 1 arcmin.

The receiver uses a 0.63 m diameter parabolic mirror, a photomultiplier (RCA C31034, now over 20 years old and in autumn period a RCA 8852 without post-amplifiers), an interference filter (3 nm), a constant-fraction timing discriminator (TC 454) and a time interval counter (HP5370B, 55 ps precision). The external frequency comes from the hydrogen maser. Time keeping and pulse epoch timing is based on a GPS station clock. Stop-pulse monitoring in calibration and ranging is done by a digital storage oscilloscope. The voltage of the photomultiplier is varied in fixed steps according to satellite to control the amplitudes. This leads to the use of three different calibration value categories. Saturated pulses, which are often present, cannot be flagged yet. Data screening is expected to strip all marginal pulses. A PC (286 AT) is used for ranging operations and data logging. Weather data is taken once during the pass. The distance to the external calibration target is about 337 m. Operation of this equipment has been

possible down to an ambient temperature of -27 °C.

The telescope tracks a satellite continuously using a slave PC card with a real-time operating system written in the Forth language and step motors connected to worm gears. The mount error model gives about 1 arcmin (rms) accuracy, but it is not sufficient for blind tracking. Therefore visually aided tracking mode is employed (a CCD camera and a TV for bright satellites and an image amplifier and a 20 cm guiding telescope for the others). Tracking commands, i.e., look angles and ranges, were computed with an old semianalytic prediction program [4] and Kepler elements. Recently a more accurate prediction system, which uses predicted daily position and velocity data (so called IRV's, Inter-Range-Vectors) was taken into use. This program is based on the ORBIT program coded in Herstmonceaux [5] with some additions. It takes into account the average travel time to the satellite, the changing hit time interval at the satellite due to range variation [6], the atmospheric delay and the instrument delay. The observed prediction accuracy has been found to be a few metres over the whole pass, provided the time bias is known from the earlier passes or from the time bias reports available in the EUROLAS data centre.

Table 1. Specifications of Metsähovi satellite laser ranging system.

Laser	Nd:YAG, positive-branch unstable resonator, passively Q-switched
Pulse duration	3 ns, in green (532 nm)
Pulse energy	50 mJ, in green
Repetition rate	1/2 Hz (30 pulses per minute)
Beam divergence	1 arcmin (full angle)
Receiving optics	630 mm diameter parabolic mirror
Interference filter	3 nm (as only nighttime observations performed)
Photomultiplier	RCA 8852, RCA C 31034 in spring 1994
Time interval counter	HP 5370B, 55 ps resolution, external 5 MHz frequency from a hydrogen maser
Timing processor	Tennelec TC 454
Range gate	Computer controlled, 100 ns resolution
Telescope mount	Equatorial, offsetting with stepper motors, one step equal to 6 arcsec, continuous tracking, computer controlled (PC), manual offsets
Station computer	PC 486/66
Station timing	TRAK Systems 8810 GPS Station Clock, also used in epoch registration, 100 ns resolution
Calibration	External flat target at a distance of 337.909 m
Pulse monitoring	Tektronix TDS 350, 200 MHz bandwidth
Range noise	10 cm to close-Earth satellites, 15-20 cm to Lageos

Satellite ranging results

The following 10 satellites were observed in 1994: TOPEX/Poseidon, Ajisai, ERS-1, Meteor-3, Stella, Starlette, Lageos-1, Lageos-2, Etalon-1, and Etalon-2. The number of passes and observations with average rms precisions are given in Table 2. The precision is not directly related to the height of the satellite, because detection takes place in multiphotoelectron regime. Data screening of calibration and ranging data are done similarly using median filtering. The observations are first processed by analytical Kepler (Sterne) orbit fitting and then by automatic adaptive median filtering of the residuals with polynomials [7] (generally 5th degree or less, due to some modelling misfit often present). Sometimes it is necessary to use observed – calculated (O–C) range differences. The median filtering is tuned to correspond to the $2.5*\sigma$ rejection level in normal least-squares method. This has led to a 0–10% data rejection, but without excessive truncation of the distribution. The $3*\sigma$ rejection level was thought to be too conservative because of

the low number of the data points, in average about 100 per pass (maximum about 300). Quick-look normal point reports are generally transmitted within one day from acquisition using Internet FTP to the EUROLAS data centre in Germany. So far only full rate Merit-II data is generated, but also field generated normal points can be formed. Normal point rms precision, i.e., the average precision over a certain period (120 s for Lageos, 15 s or 30 s for the close-Earth satellites) has been 2–10 cm according to the Quick-look reports from the Crustal Dynamics Satellite Laser Ranging/NASA/AlliedSignal Technical Services.

Table 2. Statistics for satellite laser observations at Metsähovi in January–May 1994,(**a**), and August–December 1994, (**b**).

Satellite	Passes	Observations	rms (m)
(a)			
TOPEX/Poseidon	78	12060	0.197
Ajisai	35	3715	0.181
ERS-1	33	1561	0.175
Meteor-3	33	1735	0.180
Stella	33	2148	0.185
Lageos-2	17	1795	0.187
Starlette	9	417	0.199
Etalon-1	3	32	0.190
Etalon-2	2	17	0.215
Lageos-1	1	19	0.248
Subtotal	244	23499	
(b)			
TOPEX/Poseidon	52	7335	0.104
Meteor-3	47	2799	0.106
Ajisai	31	3624	0.106
ERS-1	28	1145	0.103
Stella	23	991	0.096
Lageos-1	19	1548	0.164
Lageos-2	9	888	0.177
Starlette	9	373	0.094
Subtotal	218	18703	
Total	462	42202	

Future work

The achieved ranging precision 10 cm is still an order of magnitude lower than that desired or currently possible. Further upgrade of the existing system is not practical, however, so preparation of a new system has been launched. A one-metre laser telescope from the Latvian University, Riga, was installed in November 1994. Because the telescope has the Coudé optics, the laser and receiver electronics can be housed in a warm room next to the telescope housing. The development of a mode-locked Nd:YAG laser to give 50 ps pulses is also under way [8,9]. First measurements may be possible in autumn 1995.

Acknowledgements. The work of J. Vänskä in implementing the telescope tracking program system and the work of M. Takalo in preparing the data logging program are acknowledged. They also carried out the major part of the observations. Thanks are also due to Dr. Petr Zverev and the Laboratory of Laser Spectroscopy of the Institute of General Physics, Moscow, (head Prof. T. Basiev), for providing the passive LiF Q-switches.

References

1. Halme, S.J. and J. Kakkuri, Description and operation of a satellite laser system. *Reports of*

the Finnish Geodetic Institute 77:4, Helsinki 1977, 64 p.

2. Paunonen, M., Performance of the second generation satellite laser ranging system at Metsähovi. *Proc. X General Meeting of the Nordic Geodetic Commission*, Helsinki, 29.9.- 3.10.1986.
3. Paunonen, M., Comparison of globally and locally determined site ties for the Metsähovi GPS station, *Proc. of the 1993 IGS Workshop* (Eds. G. Beutler and E. Brockmann), IAG, IUGG, International GPS Service for Geodynamics (IGS), 25-26 March 1993, Astronomical Institute, University of Bern, Switzerland, pp. 310-317.
4. Vermeer, M., QIKAIM, a fast semi-numerical algorithm for the generation of minute-of-arc accuracy satellite predictions. *Reports of the Finnish Geodetic Institute* 81:1, Helsinki 1981, 17 pp.
5. Sinclair, A.T. and G.M. Appleby, The Royal Greenwich Observatory, Herstmonceaux laser station, England.
6. Paunonen, M., Compensation for the distortion in satellite laser range predictions due to varying pulse travel times. *Proc. 8th International Workshop on Laser Ranging Instrumentation* (Ed. J.J. Degnan), Annapolis, USA, 18-22 May, 1992, NASA Conference Publication 3214, Goddard Space Flight Center, 1993, pp. 9-9...9-12.
7. Paunonen, M., Adaptive median filtering for preprocessing of time series measurements. Ibid., pp. 2-44...2-50.
8. Paunonen, M., Cavity dumping of a mode-locked self-filtering unstable resonator Nd:YAG laser. *Proc. 7th International Workshop on Laser Ranging Instrumentation*, Matera, Italy, Oct. 2-6, 1989, pp. 167-171.
9. Zverev, P.G., T.T. Basiev, M. Paunonen, Mode locking of YAG:Nd^{3+} laser with LiF:F_2^- saturable absorber in coupled cavities. *Conference on Lasers and Electro-Optics 1994 (CLEO'94)*, May 1994, Anaheim, USA, Paper CTuK68.

Status Report of the WLRS

U. Schreiber
Forschungseinrichtung Satellitengeodäsie
Fundamentalstation Wettzell
D-93444 Kötzting
Germany

N. Brandl, K. H. Haufe, G. Herold, M. Gröschel, D. Feil,
R. Dassing, K. Röttcher, R. Stöger, R. Kahn,
G. Pochert, M. Teichmann, A. Vogel, T. Klotke
Institut für Angewandte Geodäsie
Aussenstelle Wettzell
D-93444 Kötzting
Germany

Abstract

The Wettzell Laser Ranging System (WLRS) is routinely tracking all satellites and the moon since 1991. During this time parts of the equipment proofed to be not optimally designed for all the needs. Therefore an upgrade was performed, improving the system and adding some flexibility in supporting future projects. The changes are outlined in this paper and some other experiences gathered by using the ranging equipment are discussed as well.

1. Optimising the Ranging Hardware

The original layout of the WLRS optical setup [1], although constructed to be convenient to use, proved to have some disadvantages. Figure 1 shows this design. The laser pulse was sent to a beam expander (times two), where the negative lens (L1) could be moved along a rail. This allowed ranging operation with either a collimated or with a divergent (≈ 30") beam, by putting L1 to either of the two end positions. After the beam expander, the pulse was passing through a hole in a rotating mirror disc, directed through a wedged window, which extracts a calibration signal from one of the surfaces of this optical component. Then it was guided to the telescope input port by a two mirror adjustment stage. The calibration signal was led along a path on the optical table, hitting a corner cube reflector and was finally focussed onto the MCP- detector. The return echo from the satellite was coming back through the wedged window again, bouncing off the rotating mirror disc and guided through the spatial filter assembly down to the MCP as well. Essentially this setup led to the following problems. First of all, there were a lot of optical components involved, which were deteriorating the total transmission of the system. Then the different settings of the beam expander lens caused different signal levels for the calibration pulses for the collimated

and the divergent mode. This could not be sufficiently compensated by the use of a variable optical attenuator. As the rotating mirror was used heavily through the years, it developed an increasing wobble, which could not be readjusted after some time. This small wobble caused a wandering of the image around the pinhole of the spatial filter of more than 30". Therefore a large field of view had to be used, which increased the noise level considerably. Spurious reflections from the wedged window also caused ambiguous calibration returns. This made routine operation problematic, because the calibration window does not allow for a selective gating.

Guideline for the new design was the goal to simplify the setup as far as possible, to make the field of view adjustable by remote control and to have the best system transmission for the return signals at least for a designated "lunar port". In addition, there needed to be the chance of integrating other detectors and experimental equipment, which could not be housed in the previous assembly. Figure 2 represents the current system. The focal length of the beam expander has been shortened as far as possible, which reduced the amount of required optical components. The rotating mirror disc was substituted by a "one- arm" rotating mirror, thus reversing the previous concept of the transmit/receive-switch. Originally the laser was firing through a hole in the T/R- mirror, now the weak return signal passes through untouched. The problem of laser beam wobble for the transmit section can be neglected, because of the times forty beam expansion of the WLRS telescope. This has the advantage of no moving components for the return path. The spatial filter of the receive section consists of lenses of a long focal length, so that a motor driven iris could be used for filtering, as the waist of the beam is sufficiently wide. The recollimated beam can be guided to an individually selectable detector unit. Motor controlled mirrors are adjusting the appropriate optical path. The arrangement of the detectors was selected such, that the most sensitive detector (LLR- APD) is accessed by moving mirrors out of the way. A high transmission Fabry- Perot of 1 Å bandwidth does the necessary spectral filtering for LLR. All other detectors, MCP (routine SLR), IR- APD, Streak camera and the two test ports were arranged thus, that a minimum of optical components and motor drives is required.

2. Problems in MCP Operation

Most of this upgrade was performed during the beginning of march 1994. It worked well and improved the systems operation considerably. However it did not remove some time varying bias effects, that were causing trouble at the WLRS. The investigation of the problem yielded the following results. As the laser is a dye system, the time of fire jitters with respect to the laser fire command, which generates a gating signal for the MCP by approximately $10\mu s$. The gate for the realtime calibration had been factory preset to be much larger than $100\mu s$. As a matter of fact, the response time of the MCP is depending on the time duration between the beginning of the gate and the detected echo. So there was an unsymmetry between the satellite ranging situation, where short gates are applied only and the calibration being done on long gates. The slowly varying range bias, which resulted out of the fact, that the location of the calibration return within the gate drifted slowly over a period of time, was as much as $5-9cm$. It is worthwhile to note, that this effect can not be identified by target calibration measurements. On a realtime calibration system, such as

the WLRS the time between calibration and target return is of the order of a few hundred nanoseconds. Where ever the calibration return is inside the long gate, the target return is in the vicinity. By subtracting both signals from each other, the bias is taken out. Figure 3 illustrates these properties of the MCP. The upper part of the diagram a) shows the width of the long calibration gate. Usually the laser fire was adjusted such, that it recorded in the middle of the gate, to allow for the roughly $10\mu s$ jitter of the dye laser plus some slow variation over time for the generation of the laser fire command. This variations for example are caused by temperatur changes over some days or weeks. They can be well of the order of the gate size. The section b) of the diagram qualitatively indicates the detection behaviour of the MCP with respect to the applied gate length. Some microseconds after gate opening the MCP starts progressively to delay its response with respect to the incoming laser pulse echo. In c) one can see, that for the satellite echo situation, the MCP never reaches the bias causing "delay region".

The consequence is, that the calibration gate needs to be short and therefore comparable to the satellite recording gate. Taking the laser fire uncertainty into account, there was the requirement of a circuit, which monitors the laser oscillator and switches on the calibration gate a few hundred nanoseconds before the pulse train is generated. This goal could be achieved (see d) in figure 3) and since October 1994 the WLRS is operated in this mode, which stabilised the performance of the tracking station.

3. Conclusion

Heavy use of the ranging equipment and the demand for more experimental flexibility made an upgrade of the receiver section of the WLRS necessary. Care has been taken to optimise the system for higher sensitivity and higher automation. On the other hand, a simpler layout of the optical path was achieved. During the investigation of the cause of a range bias, a dependency of the MCP's signal response to the length of the applied gate was identified. The circuitry of the master ranging controller does not allow to control the timespan between gate open and incoming calibration return. Therefore such an option had to be provided externally. It is important to note, that the source for the bias was not related to a timing critical part of the system, but to the generation of a gating signal. The work for further stabilisation of the system's performance is being continued.

References

[1] W. Schlüter, G. Soltau, R. Dassing, R. Höpfl, "The Concept of a New Wettzell Laser Ranging System with Dual- Purpose Capabilities", *Proceedings Of 5th International Workshop on Laser Ranging Instrumentation*, (1984)

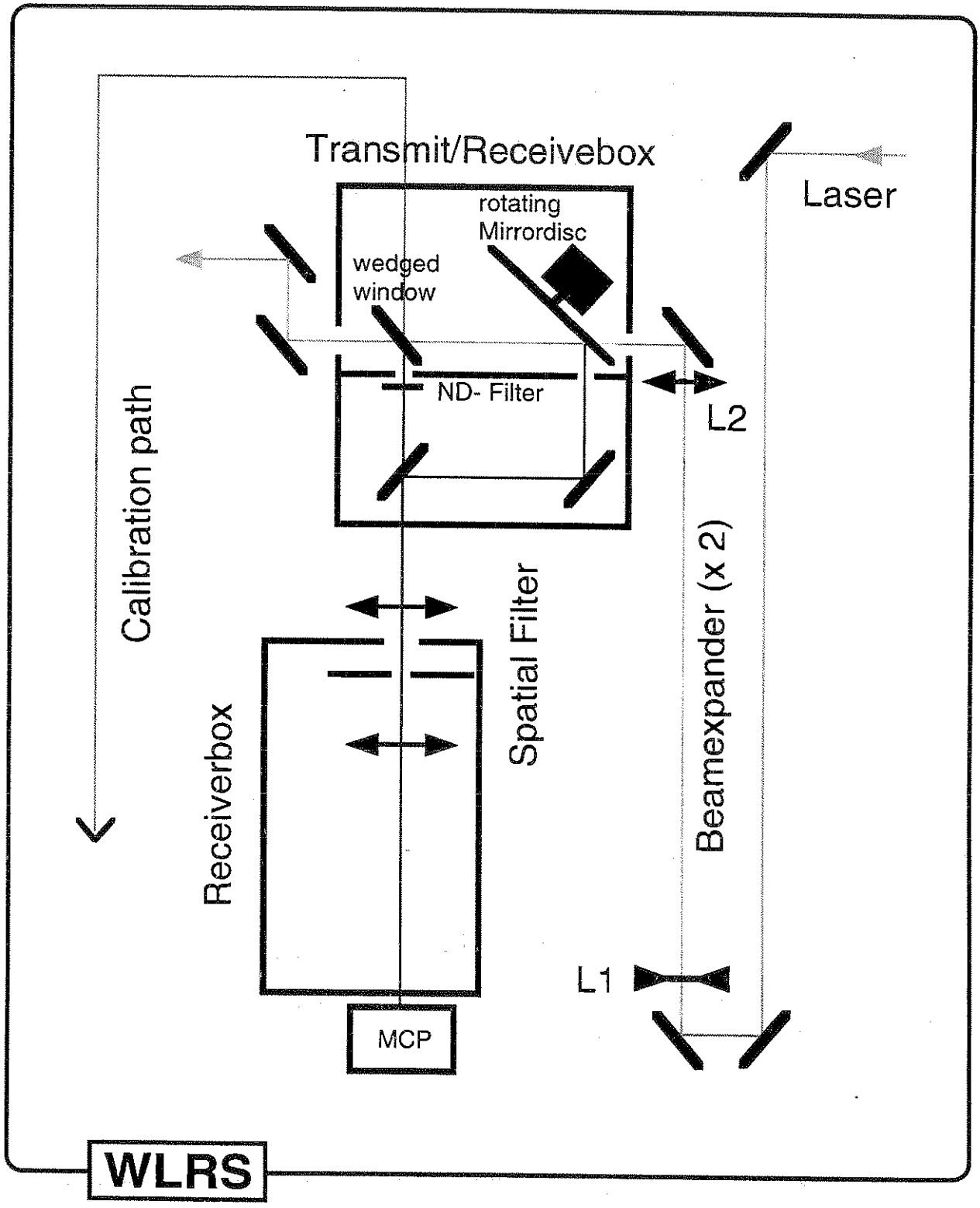

Figure 1: The block diagram of the old design of the WLRS

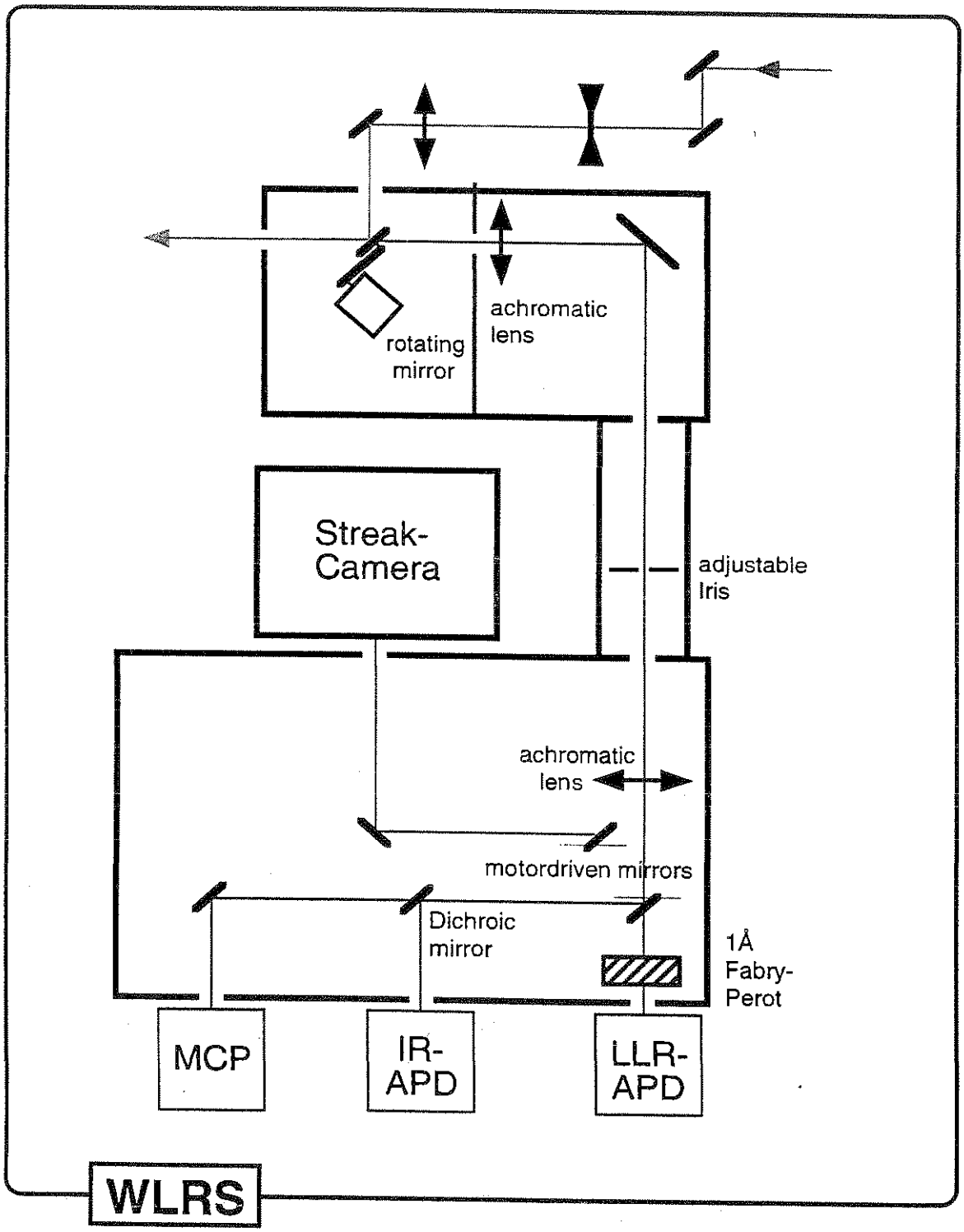

Figure 2: The block diagram of the new design of the WLRS

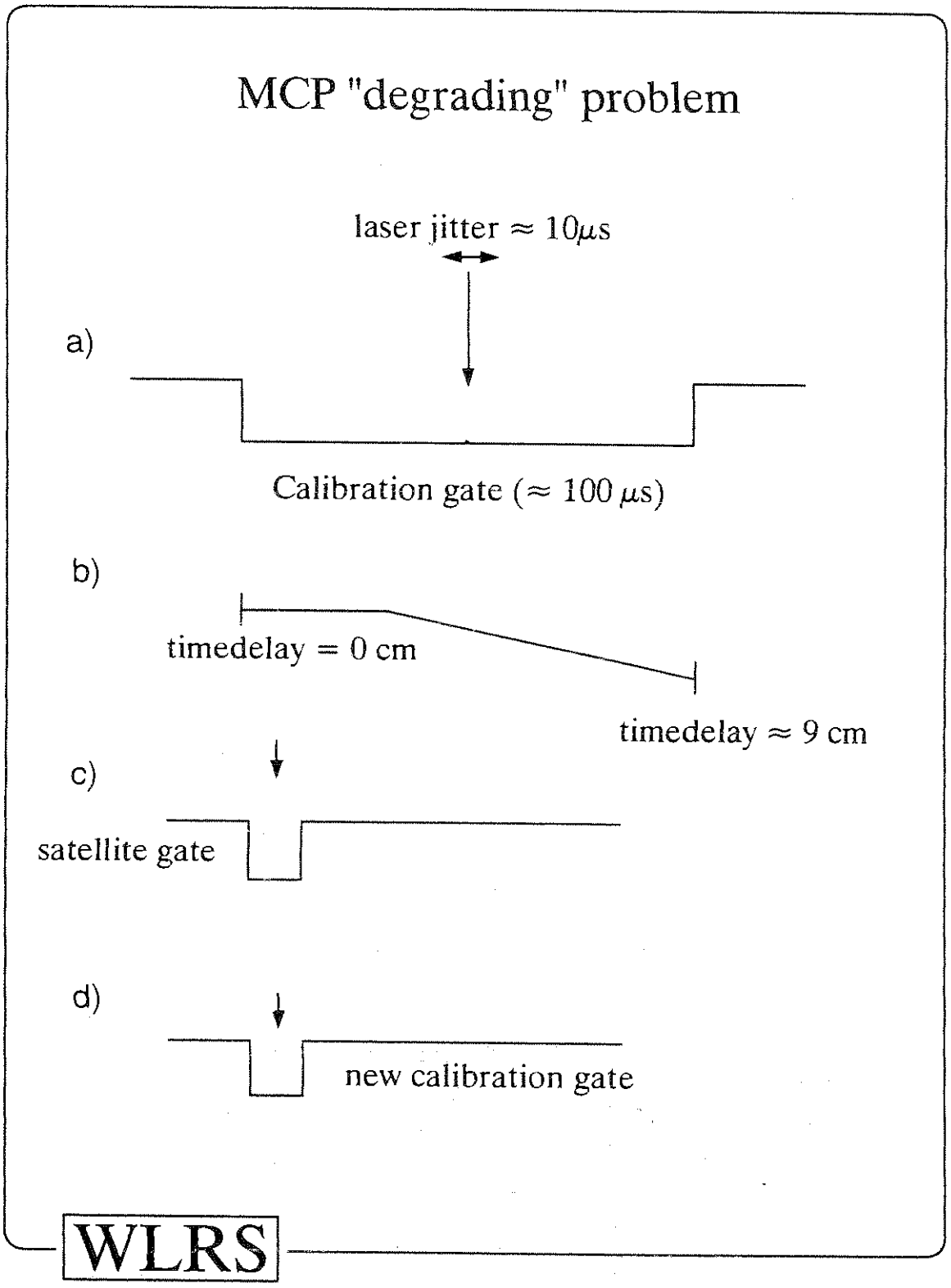

Figure 3: Graphical illustration of the strange MCP behaviour

Current Status of Beijing SLR Station

Tanqiang Wang
The Chinese Academy of Surveying and Mapping (CASM)
16 Beitaiping Road, 100039 Beijing, China
Tel: +86 01 8216335, Fax: +86 01 8218654, Telx: 716 221081

Abstract

The SLR instrumental system of Beijing SLR Station was installed in November of 1988. From that time, the system could not be running for nearly 4 years because of the hardware problems.

Four improvements for the system were finished from May of 1992 to March of 1994. The computer control system with corresponding interface and software, the encoder, the ISIT and the receiving channel were involved in these improvements and all of them were efficent and successful.

Up to now nearly 300 passes of returns were got from all SLR satellites. The precision for all satellites is 4—6 cm.

1: The fundamental informatioms

The Beijing Satellite Station is about 60 kilometers from the city center, south of the city. It is located on a hill in a small town area named Yuegezhuang of Fangshan district. The station was being constructed from 1982 and belongs to the Chinese Academy of Surveying and Mapping (CASM), the National Bureau of Surveying and Mapping (NBSM). the destination of this station is for researching in satellite geodesy and geodenamics. It would be a satellite geodetic station with several methods of observations , but now only Satellite Laser Ranging (SLR) is available.

The station covers about 20,000 square meters and the whole buildings included offices, workshop, laboratory, gararge, boiler house et. have 2500 square meters area.

2: The SLR system

The original SLR system of Beijing SLR Station is made in China and was installed at the station in November of 1988. Because of the hardware problems in the system the regular observations could not be carried out for nearly 4 years. The main problems were in the computer control system, the ISIT, the encoder and the electronic receiving channel. From May of 1992 to March of 1994 some important improvements were finished in succession, and now the new system has the notable difference with the original system and its performance is better than the old one's. Following is the frame diagram of hardware and the list of performance index of some main units for new system:

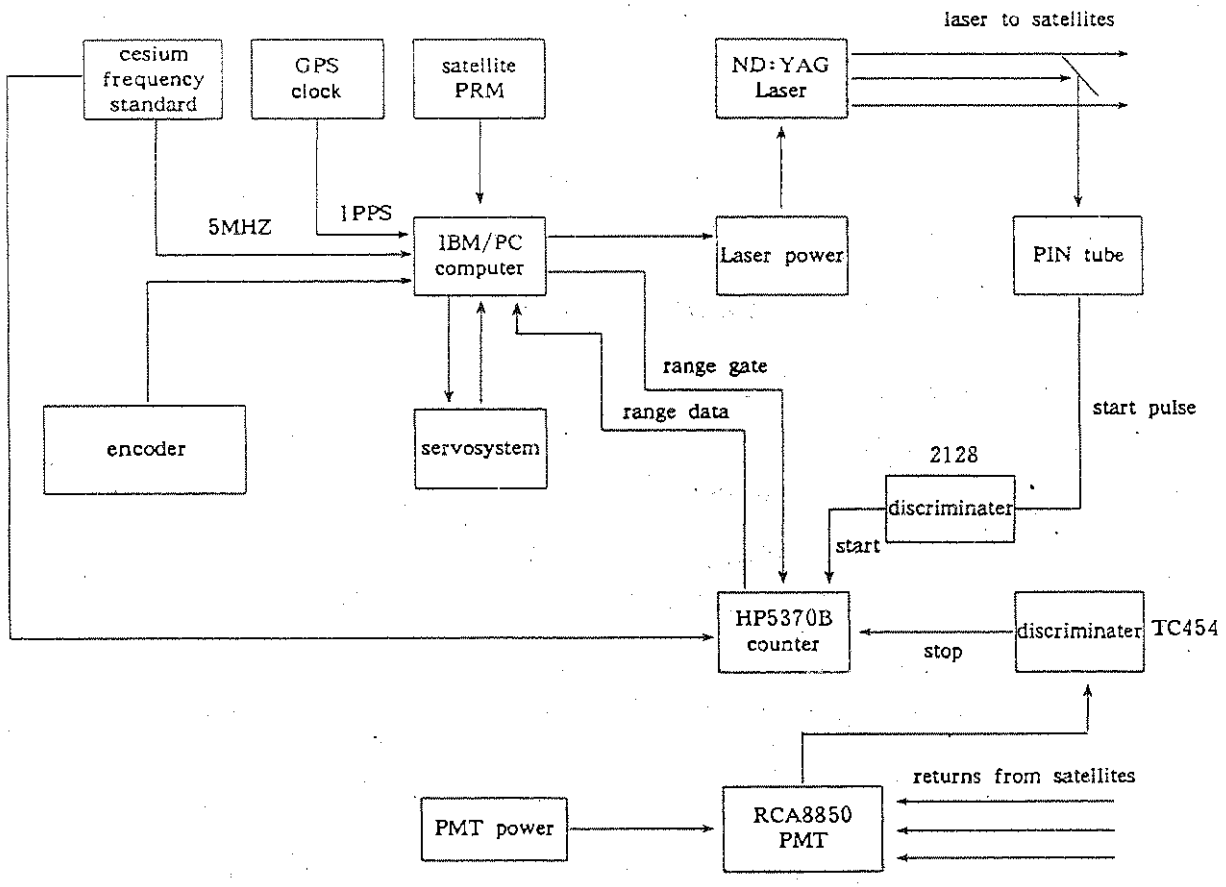

The diagram of SLR system in Beijing

3: Main improvemants

1). The computer control system

The original system based on PDP11－44 computer was strongly dependent on the environment and because of the tracking software problems it was too complicated to operate and a lots of trouble to be made to the observations. It was very often that in the middle of work the computer deaded and it was hard to resume , still worse the digital clock connected with computer made mistakes of seconds undefinitely. So we replaced the computer and corresponding interfaces and software. The IBM－pc is the controller. The new computer system is stable, dependable and has simple structure. This improvement was finished in June of 1992. The frame diagram of the controller is as below.

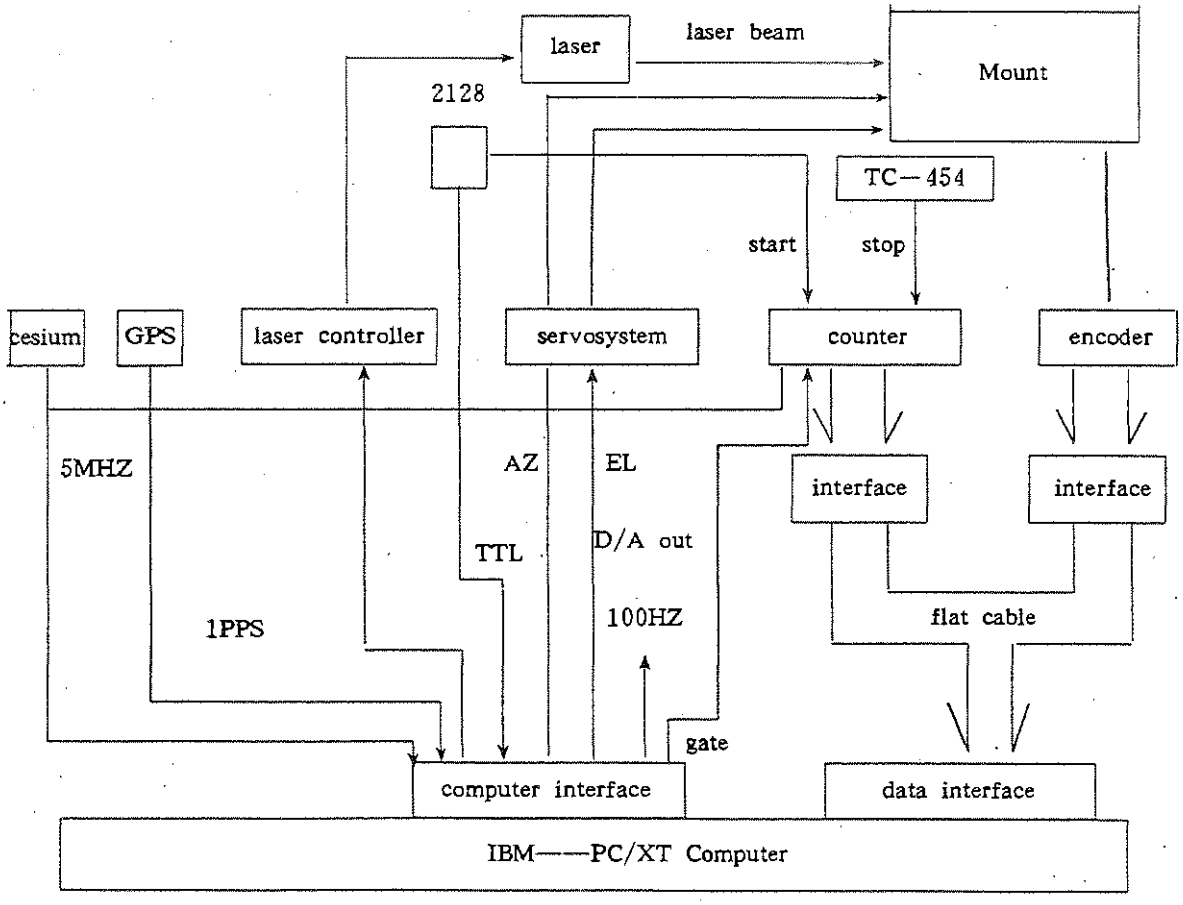

The diagram of control system

The real time clock, range gate controller, data colect controller, laser sending controller and D/A changer of controling mount are compressed onto a circuit plate and it is inserted in an extension channel of the controling computer. The controling system has strong performance and the informations of the performance can be displayed on the screen of the computer and in the same time the performance can be changed and corrected from the keyboard. it is very audio—visual.

2). The encoder

The design of original encoder was reasonable but it was unstable and undependable. it made a lot of troubles to us and there were 185 trouble days in the observation records of 1993 from the encoder.

The improvement for encoder was ended in march of 1994 and the new encoder works very well from that time. Following is the diagram of connections.

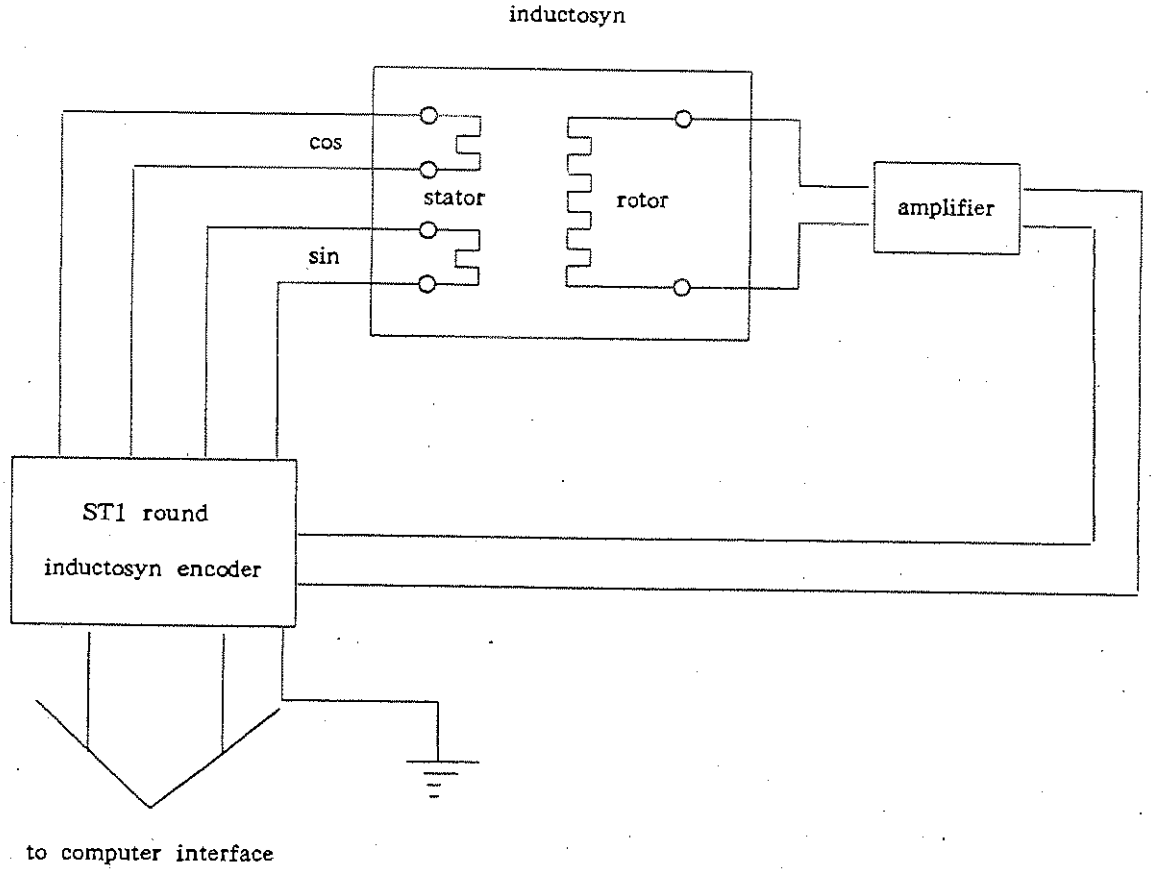

The diagram of encoder connection

3). The ISIT

The old ISIT is a independent optical system , it was difficult to see the image of Lageos on the TV screen and the field of view was 58' ,too big to aim at the satellites properly.

The new one is depending on the main receiving telescope as the diagram showing below.

Use the new ISIT all the high satelltes including the 2 Lageoses and the 2 Etalons can be recognized on the TV screen and the field of view becomes 19' and the aiming pecision is improved a lot.

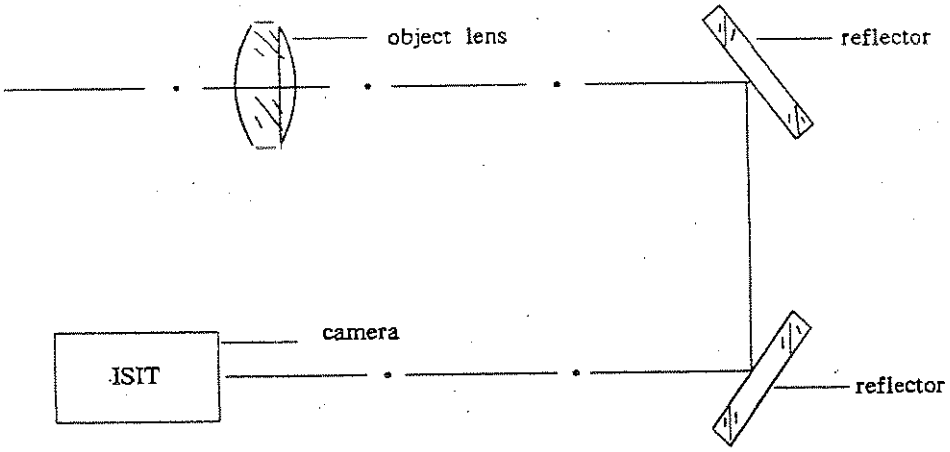

The old ISIT

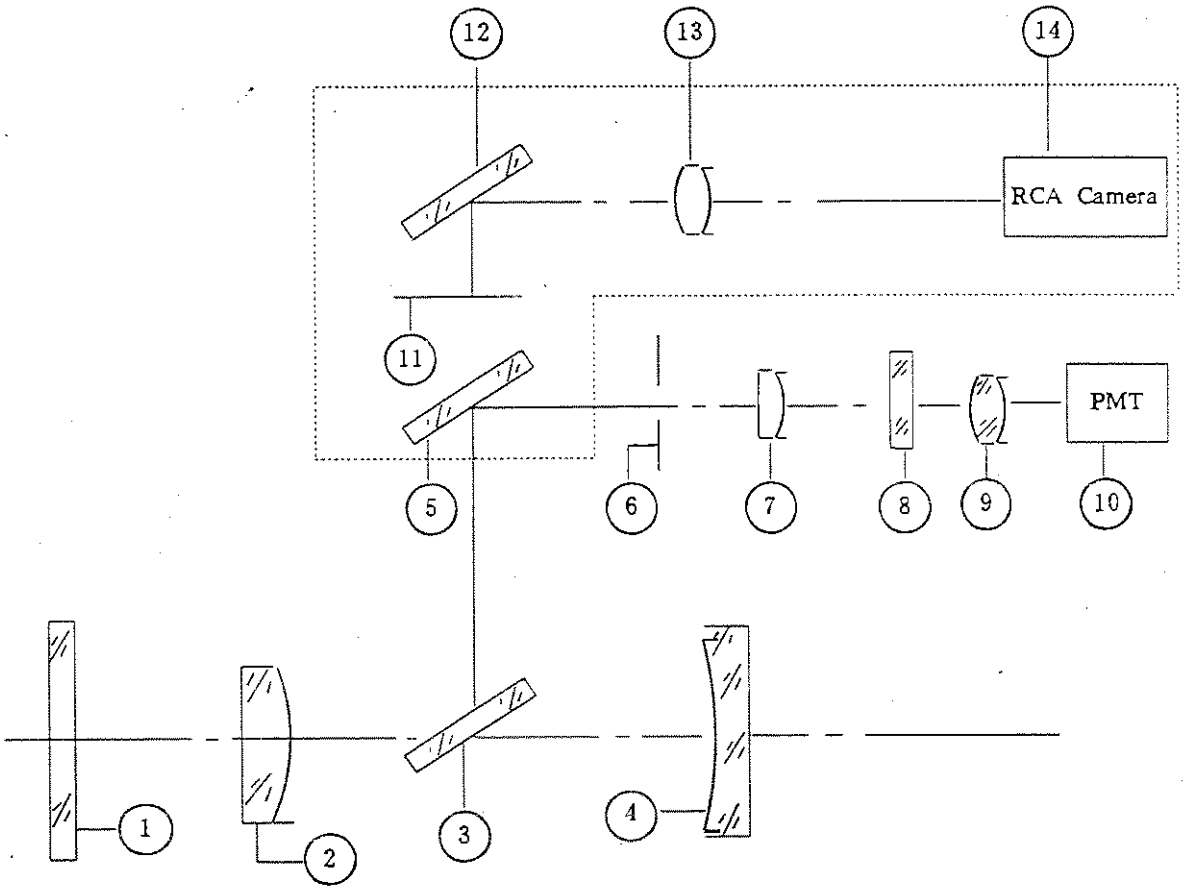

1 safe glass 2 second lens 3 reflector 4 main mirror 5 spectroscope

6 pin- hole 7 collimation lens 8 filter 9 focusing lens 10 PMT

11 scale glass 12 reflector 13 focusing lens 14 camera

The optics principle diagram of ISIT

4). The receiving channel

We replaced the old counter and stop discriminater with a HP5370B and a TC—454 and added a start discriminater Canberra 2128. This was finished in March of 1994 and the new channel works steadily and sensitively now.

4: The observations in Beijing SLR Station

1). In December of 1992

Satellites	Passes	Total Points	Average RMS
Ajisai	16	4160	6. 8cm
Topex	8	1670	6. 9cm
Lageos1	4	360	6. 4cm
Lageos2	2	186	6. 1cm
Starlett	3	260	5. 6cm
TOTAL	33		

2). In the year of 1993

Satellites	Passes	Total Points	Average RMS
Ajisai	42	9920	6. 6cm
Topex	8	1560	6. 8cm
Lageos1	2	230	7. 0cm
Lageos2	4	540	6. 9cm
Starlett	4	320	6. 0cm
TOTAL	60		

3). From March 1 to May 20 of 1994

Satellites	Passes	Total Points	Average RMS
Ajisai	45	10700	6.6cm
Topex	31	6300	6.9cm
Lageos1,2	9	1030	6.2cm
Starlett	6	430	6.1cm
ERS−1	2	90	6.5cm
Meteor−3	17	3200	6.7cm
TOTAL	120		

4). From September 9 to November 2 of 1994

Satellites	Passes	Total Points	Average RMS
Ajisai	20	16230	6.7cm
Topex	11	860	6.8cm
Lageos1	35	13750	6.1cm
Lageos2	19	11340	6.0cm
Starlett	8	1560	5.6cm
ERS−1	1	270	6.6cm
Meteor−3	10	2730	6.7cm
Etalon−1	2	1270	6.9cm
Etalon−2	1	130	6.9cm
Mesti	1	132	6.8cm
Stella	3	462	6.1cm
TOTAL	111		

Note: The large RMS is due to the limitation of 7cm in the data preprocessing programs.

The performance index of main units of SLR system in Beijing

unit	performance index
Mount	
Type	Azimuth and Elevation
Azimuth range	±530°
Elevation range	0°～95°
Elevation precision	⩽2″
Azimuth precision	⩽3″
Resolution of inductosyn	0.618″
Laser	
Material	Nd:YAG
Wave length	0.532um
Energy	150mj
Pulse width	200Ps
Repetition	1～5Hz
Output beam	X≈10mm
Receiving telescope	
Type	Galileo
Calibre	600mm

unit	performance index
Focal length	5500mm
Field of view	2.0mr
Sending telescope	
Type	Galileo
Calibre	160mm
Divergency	0.15～2.0mr(Adjustable)
PMT	RCA－8850
Start discriminater	Cambbra2128
Stop discriminater	TC454
Counter	HP5370B
Frequency standard	HP 5061A(Cesium)
Computer	IBM PC
ISIT	
Calibre	600mm
Focal length	5500mm
Field of view	17′
Encoder	
Type	Round inductosyn encoder
Precision	1″

THE MATERA LASER RANGING OBSERVATORY: CURRENT STATUS

Giuseppe Bianco
Agenzia Spaziale Italiana
Centro di Geodesia Spaziale
p.0. box 11
75100 Matera, Italy
E-mail: bianco@asimt0.mt.asi.it

Thomas Varghese
AlliedSignal Aerospace
ATSC/SLR
7515 Mission Drive
Lanham, MD 20706, USA
E-mail: varghese@atscv1.atsc.allied.com

ABSTRACT

Matera Laser Ranging Observatory (MLRO) is a high performance, highly automated optical and astronomical observatory currently under design and development by AlliedSignal, for the Italian Space Agency (ASI). It is projected to become operational at the ASI's Center for Space Geodesy (CGS) in Matera, Italy in 1997. MLRO, based on a 1.5meter astronomical quality telescope, will perform ranging to spacecrafts in earth-bound orbits, lunar reflectors and specially equipped deep space missions. The primary emphasis during design is to incorporate state-of-the-art technologies to produce an intelligent, automated high accuracy ranging system that will mimic the characteristic features of a fifth generation laser ranging system. The telescope has multiple ports and foci to support future experiments in the areas of laser communications, lidar, astrometry, etc.. The key features providing state-of-the-art ranging performance include: a diode-pumped picosecond (50ps) laser, high speed (3-5GHz) opto-electronic detection and signal processing, and a high accuracy (6ps) high resolution (<2ps) time measurement capability. The above combination of technologies is expected to yield millimeter laser ranging precision and accuracy on targets up to 300,000km, surpassing the best operational instrument performance to date by a factor of 5 or more. Distributed processing and control using a state-of-the-art computing environment provides the framework for efficient operation, system optimization and diagnostics. A computationally intelligent environment permits optimal planning, scheduling, tracking and data processing. It also supports remote access, monitor and control for joint experiments with other observatories.

INTRODUCTION

Ever since the first deployment of laser ranging for space geodetic applications in the mid-sixties, the techniques of Satellite Laser Ranging (SLR) and Lunar Laser Ranging (LLR) have significantly contributed to the advancement of a number of scientific disciplines [Degnan, 1991; Schutz, 1992; Smith, et al., 1993]. Today a network of over 40 globally distributed systems support space geodetic efforts. The primary reason for the success and maturity of the measurement technique is the progressive use of advanced technologies as they evolved [Degnan, 1985; Varghese, et al, 1986; Veillet, et al., 1993; Shelus, et al., 1993]. The adaptation of newer technologies over the years yielded significant improvement in the instrument performance. The quality of the SLR and LLR data has improved by two orders of magnitude during the last two decades. The accurate data over the years coupled with improved scientific understanding through measurement and modeling of phenomenon such as gravity field, tides, and the dynamics of earth's

interior allows computation and maintenance of precision orbits to a few centimeters. The precise apriori knowledge of the orbit in turn permits the computation of precise acquisition and pointing vectors for tracking, thus allowing tighter target coupling of the laser beam through smaller beam divergence. The combination of precise pointing, high repetition rate laser systems and high opto-electronic detection capability has also led to vastly improved data quantity over the years.

There are, however, increased demands on laser ranging technique due to competing techniques and fiscal constraints. The future of SLR and LLR will depend on the scientific data quality as well as the cost of producing such data. High quality globally distributed measurement on a number of satellites, supporting various scientific applications, at low operational cost is a critical requirement for the future. Automation and multiple use of the facility are key aspects to be considered for the reduction and distribution of the cost.

In the global network, fiducial observatories play a fundamental role for the high accuracy measurements of geophysical properties. MLRO with its wide target coverage and ranging performance will become a part of a suite of geophysical and astronomical instruments at Matera obtaining critical measurements for a variety of applications. The targets for these measurements include satellites in earth orbits from ~200km to geosynchronous distances, the lunar reflectors (left by Apollo and Lunakhod missions) and deep space mission spacecrafts. With the significant coverage offered by MLRO together with the potential for other astronomical and optical experiments, optimal use of the observatory during the 24 hour daily cycle is essential. The capability to configure, monitor and perform experiments in an expeditious manner without operator intervention is vital to the most effective collection of scientific data. The ability to perform intelligent decision making based on the observing conditions and the critical requirements of various experiments is a highly desirable feature. Thus, the precision, accuracy, reliability and ability to perform automated expeditious intelligent operations are emerging as the system goals a state-of-the-art system. MLRO detailed design is currently performed in the context of these emerging scientific requirements.

The system specification calls for millimeter precision and accuracy on ranging to targets as far as 300,000km. The absolute accuracy of laser ranging is limited by the measuring accuracy of the SLR instrumentation, the refraction model of the atmosphere, and the knowledge of the spacecraft optical reference to the center of mass. The spacecraft induced errors can be significantly reduced through modeling and correcting the laser data [Varghese, 1992; Minott, 1993]. The unique hardware characteristics of the ranging system can be corrected to the submillimeter level to obtain accurate range to the center-of-mass(CM) of the spacecraft. It is estimated that the atmospheric model induced errors can be reduced to the 1-2mm level using multi-wavelength ranging [Abshire, et al., 1985]. A high accuracy receiver system was developed to measure atmospheric dispersion very accurately in "real-time" [Varghese, et al., 1993]; the real-world operational performance of this receive system is currently under evaluation at the NASA 1.2meter telescope facility. If it demonstrates operational success, this feature will become part of the future millimeter system, thus solving the atmospheric model dependent problems. The ranging instrument performance is determined by the laser transmitter, opto-electronic technologies, time measurement system, telescope and the computing technologies. Each of these disciplines is examined in detail in the current design phase to reduce ranging errors and exceed the system specifications.

SYSTEM DESCRIPTION

The laser ranging instrumentation of MLRO incorporates a number of highly desirable features [Varghese, 1992] that is expected of a fifth generation [Varghese, 1994] laser ranging system. The system and sub-system features are carefully chosen to exploit the best of currently available

technology. In addition, design and integration of certain hardware components in the system is strategically scheduled to incorporate the best of evolving technologies. Major system hardware features are as follows:

- Multipurpose optical and astronomical observatory.
- 1.5 meter astronomical quality telescope with a high resolution imaging system for astronomy applications.
- Day/night laser ranging capabilities to dynamic targets in orbits of 200 km to geosynchronous distances, the moon and deep space missions.
- Design features to accommodate multi-wavelength ranging to directly measure atmospheric refraction effects.
- State-of-the-art computing and ranging instrumentation
- Easy referencing of telescope axes to external datum to further reference it to the center(CM) of the earth and the latitude and longitude.
- Hazard reduction of radiation on aircrafts using a radar.
- 10-20 Hz Operation at high laser powers; KHz operation using lower powers.
- High resolution(<2ps) time measurements of all critical times associated with various events.
- Aggregated instrument limited ranging precision of ~2mm and accuracy of ~1 mm.

The system software provides a number of highly desirable features. These include:

- Computational intelligence tools for decision making.
- Sophisticated GUI for expeditious diagnostics and operations monitoring functions.
- Autonomous operation of the system for tracking, instrument calibration and optimization.

The MLRO hardware and software modules are designed at the present time to provide an integrated framework for high performance automated operations. The hardware elements for ranging consists of the telescope, laser, transmit/receive optics, transmit/receive electronics, computing and control, timing, and safety. The 1.5meter aperture Cassegrain telescope has a pointing accuracy of ~1arcsecond and is based on a parabolic primary, hyperbolic secondary and a flat tertiary. It has a truly rotatable/removable tertiary to switch to Coude, Nasmyth or the Cassegrain focal planes for coupling to various instrumentation. The provision to "truly" rotate the tertiary mirror and position it within 1arcsecond allows easy interchange of Nasmyth and Coude foci. The telescope has been accepted in June 1995; it meets or exceeds all the specifications. In particular, the primary mirror quality has been measured in terms of wavefront error, which turned out to be 0.054λ RMS (λ=0.633 μ); the secondary mirror's wavefront error is 0.024λ RMS (λ=0.633 μ). The overall wavefront error at the Coudé focus is better than 0.1λ RMS (λ=0.633 μ). The primary mirror features a UV-enhanced aluminum coating with an average reflectivity of 94% from 0.4μ to 1.2μ wavelength.

A state-of-the-art digital state space control system employing 32bit RISC processors for each axis control ensures smooth tracking and pointing operation while allowing self diagnostics and computer access to the telescope. The telescope jitter of <1arcsec RMS combined with the 1arcsec accuracy after star calibration allows precise tracking of distant targets. Since the observatory will be a multi-experiment research and observational site, safety measures for instruments as well as humans is given prompt consideration in the overall design of the system. The safety features include: radar, flashing warning lights, displays, alarms, video cameras, and computer-inhibited operations.

A diode-pumped picosecond (50ps) master oscillator and flash lamp pumped power amplifiers generate ~125mJ in a 50-70ps pulse at 532nm to provide adequate link especially to very distant targets. The laser system has been accepted in March 1995; its performances meet or exceed the specifications. The pulsewidth at λ=0.532μ has been measured to be about 43 ps, with an energy of 110 mJ. This configuration is carefully chosen to address the future

possibility of high duty cycle (>KHz) operation. The common Transmit/Receive (T/R) optics and the telescope transfer the laser beam to the target and also couple the retroreflected signal from the target to the detectors in the receiver system. The receive optics assembly couples the reflected light from the polarization discriminating T/R switch to the detectors after spatial and spectral filtering. The spatial filter has an adjustable field of view (FOV) from 1 to 60 arcseconds and its geometrical positioning is adjustable to accommodate defocus and decenter. The precise value will depend on laser beam divergence and background conditions. A CCD camera coupled to an image digitizer analyzes the transmitted laser beam quality; this feature is especially desirable for ranging to very distant targets. The narrow bandpass filter (0.1-0.3nm) allows tracking of the satellites/moon under high background conditions of day or night. The 1.5 meter telescope aperture and the superior optical quality of the telescope allows the coupling of the laser beam to the target at a beam divergence of 1-2arcsec with good wavefront quality. This beam divergence will be maintained for tracking all satellites whose orbits are computed and maintained precisely. The beam divergence control feature will be exercised to expand the beam divergence to accommodate prediction errors or when the initial acquisition was not successful. This is also true when the system attempts to track a newly launched satellite whose ephemeris is not known precisely. The data collected in real-time will be used to compute the short arc and propagate forward the improved real-time pointing information. An intensified CCD camera will optically track sun-lit earth orbiting satellites. It will also acquire lunar craters for ranging to the lunar retro-reflectors. These images will be processed in near real-time to permit target recognition and allow optimal guiding of the laser beam to the retro-reflectors.

The data quality of ranging instrumentation is primarily determined by the T/R Electronics subsystem and therefore, plays a crucial role in determining the overall ranging performance. The opto-electronic detection and measurement of the time associated with each event is performed by the T/R Electronics. Special attention is taken to obtain the highest opto-electronic detection efficiencies (30%) and bandwidths (3GHz). The signal processing bandwidths will match the detection bandwidths to generate the most precise definition of the signal for time measurement process. The time and frequency subsystem is a critical part of the overall system. It provides the critical frequencies (10MHz, 500MHz) and timing (1, 10, 20, 100pps) signals from an ultrastable maser to support the generation of the high accuracy data. A multiple channel, multiple vernier event timer measures the time of occurrence of all critical events associated with each laser transmission to the target. The 28 bit event timer operating at a clock frequency of 0.5GHz measures the time from 100millisecond down to ~2picosecond. This 'local' precise time measurement is referenced to universal time (UT) within the uncertainty of UT. The optical events associated with each frame filtered spatially (1-60arcsecond), spectrally (0.1-.3nm) and temporally (~10-300ns) will provide the highest SNR for collected data. This feature is extremely useful for tracking of very distant targets with low link budget in the presence of high background count rate.

As stated earlier, the computing/control system architecture is partitioned to provide the users with the capability to perform multiple experiments/measurements. The software exercising control of the system and providing automation will be versatile in configuring the system for various applications. The emphasis of software engineering is on the ease of maintainability, upgradability and expandability. This will accommodate future expansion and allow optimal use of the system features and capability. The advanced computing environment in MLRO will permit smooth integration of all control and data related hardware functions and facilitate a very high level of automation. The software domain is divided into (1) man machine interface (MMI), (2) computing/decision making and (3) computing/control subsystems. The primary emphasis of the MMI will be to support

monitoring, diagnostics and optimization of the system. The MLRO computer hardware configuration will consist of several state-of-the-art Hewlett Packard computers networked to form an efficient and effective computing environment with significant I/O capability. A VME-based real-time interfacing approach and a POSIX 1003.4 compatible real-time HP-RT operating system are special features of the real-time computing environment. The UNIX based HP-755 workstation permits a state-of-the-art man machine interface (MMI) and supports high end computing. Thus, compute-intensive applications such as GEODYN can be run with relative ease using this computing configuration. This capability is extremely useful for near real-time computing of orbits for improved satellite acquisition and pointing as well as processing the data. Currently, an apriori estimate of the orbit is used to discern the data from noise followed by statistical filtering and polynomial regression. With the ability to compute near real-time orbits from actual laser data, the filtering and data fitting processes can be implemented with greater effectiveness.

The real-time control and data related functions are addressed in the design using modern software engineering practices. Object-oriented programming techniques are conceived to facilitate speed of development as well as improve maintainability. Integrated performance monitoring of all processes constitutes a step toward identifying real-time process bottlenecks and highlight potential problems for scalability in the future. A key aspect of an automated system is also the ability to monitor the performance of the system continuously. Device performance as well as data queue utilization, memory utilization, etc., will be included for routine monitoring.

The system performance to a large extent is monitored by numerial and statistical processing of various process parameters. For tasks involving numerical computation, conventional programming and analysis techniques offer superior speed over that of humans. However, in certain types of decision making problems, straightforward numerical computing alone is insufficient to deduce the pertinent scientific or technical conclusion. This is also true in cases where the problem is extremely complex and intuition is required for reaching decisions. If the exact rules for solving the problem is ill-defined or fuzziness exists such that conventional logic will not suffice to adequately and unambiguously define the answers to the problem, then "intelligent" decision making capability resident within the system will be an asset. Mission planning, scheduling, optimizing, sparse image and data analysis are areas where an expert system or computational intelligence tools(or their hybrids) can significantly offer help. Implementation of such tools are expected to further enhance the automation of operations and speed the evolution of MLRO towards a truly autonomous system. The availability of significant computing power is thus included in the current design of the system for the implementation of these capabilities.

SUMMARY

MLRO project is currently underway with the goal of designing a state-of-the art system. Software and hardware architectures are carefully chosen to meet and exceed the projected specifications. The ability to perform automated intelligent tracking and ranging of dynamic targets at high accuracy will offer vastly improved capability for a number of scientific applications. In the meantime, the final design of the new building at the ASI/CGS is underway; the construction is projected to start at the beginning of 1996.
The significant improvement in the quality and quantity of both SLR and LLR data will further advance the science in all associated disciplines.

REFERENCES

Abshire, J.B. and C.S. Gardner, Atmospheric Refractivity Corrections in Satellite Laser Ranging, *IEEE Transactions on Geoscience and Remote Sensing*, GE-23(4), 1985.

Degnan, J.J., Satellite Laser Ranging: Current Status and Future Prospects, *IEEE*

Transactions on Geoscience and Remote Sensing, GE-23(4), 398-413, 1985.

Degnan, J.J., Applications of Laser Ranging to Ocean, Ice, and Land Topography, *Proc. of SPIE*, 1492, 176-186, 1991.

Degann, J.J., Millimeter Accuracy Satellite Laser Ranging: A Review, *Contributions of Space Geodesy to Geodynamics: Technology;* Geodynamic Series, Vol.25, 1993

Minott, P.O., T.W. Zagwodzki, T. Varghese, M. Selden, Prelaunch Optical Characterization of the Laser Geodynamic Satellite (LAGEOS-2), *NASA Technical Paper 3400*, Sept. 1993.

Schutz, B.E., Applications of SLR, *Proc. of Eighth International Workshop on Laser Ranging Instrumentation*, Annapolis, Maryland, May 18-22, 1992, NASA Conference Publication 3214.

Shelus, P.J., R.L. Ricklefs, A.L. Whipple, and J.R. Wiant, Lunar Laser Ranging at McDonald Observatory, 1969 to the present, *Contributions of Space Geodesy to Geodynamics*, Technology, Geodynamics Series, Volume 25, 1993.

Smith, D.E., D.L.Turcotte, Editors, *Contributions of Space Geodesy to Geodynamics*: Technology; Geodynamic Series, Vol.23 and 24, 1993

Varghese, T. and M. Heinick, Subcentimeter Multiphotoelectron Satellite Laser Ranging, *Proc. of Sixth International Workshop on Laser Ranging Instrumentation*, Antebes, France, September 1986.

Varghese, T. and M. Selden, Towards High Accuracy(millimeter) Satellite Laser Ranging using Laser Geodynamic Satellites, *Proc., 10th Annual International Geoscience and Remote Sensing Symposium*, vol. II., 1427-1430, 1990.

Varghese, T., Analysis of Topex Laser Retroreflector Array Characteristics, *Proc. of Eighth International Workshop on Laser Ranging Instrumentation*, Annapolis, Maryland, May 18-22, 1992, NASA Conference Publication 3214.

Varghese, T., Decker, W., Crooks, H., Bianco, G., Matera Laser Ranging Observatory (MLRO): an Overview, *Proc. of Eighth International Workshop on Laser Ranging Instrumentation*, Annapolis, Maryland, May 18-22, 1992, NASA Conference Publication 3214.

Varghese, T., C. Clarke, T. Oldham, M. Selden, Streak Camera Based SLR Receive System for High Accuracy Multiwavelength Atmospheric Differential Delay Measurements, *Contributions of Space Geodesy to Geodynamics*: Technology; Geodynamic Series, Vol.25, 1993

Varghese, T., Matera Laser Ranging Observatory (MLRO): An Advanced High Accuracy Satellite and Lunar Laser Ranging Observatory for Agenzia Spaziale Italiana (ASI), *Proc. First International Symposium on Laser and Optoelectronics Technology and Applications*, Singapore, pp. 460-465, Nov. 11-13, 1993.

Veillet, C., J.F. Mangin, J.E. Chabaubie, C. Dumolin, D. Feraudy, and J.M. Torre, Lunar Laser Ranging at CERGA for the Ruby Period (1981-1986), *Contributions of Space Geodesy to Geodynamics*, Technology; Geodynamics Series, Volume 25, 1993.

Varghese, T., Bianco, G., Advanced Technologies in the ASI MLRO towards a New Generation Laser Ranging System, *Third International Symposium on Space Mission Operations and Ground Data Systems*, Greenbelt, Maryland, November 14-18, 1994.

STATUS REPORT ON THE BOROWIEC LASER RANGING SYSTEMS

S.Schillak, J.K.Łatka, J.Bartoszak, E.Butkiewicz, D.Schillak, S.Zapaśnik

Space Research Centre of Polish Academy of Sciences

Borowiec, ul.Drapałka 4, 62-035 Kórnik, Poland
Phone: (48) 61 170 187
Fax: (48) 61 170 219
E-mail: aoslas@pozn1v.tup.edu.pl

ABSTRACT This poster presentation describes status of two Borowiec SLR systems. Since last Workshop number of passes and returns per pass increased very rapidly . BOROWIEC-2 SLR system is operational and it is waiting for construction of a new geodynamical station in Tunisia.

BOROWIEC-1 SLR

The several important tasks have been made during the last two years to increase performance of the BOROWIEC-1 SLR system:

- 1992, October; new pre- and post- observation software on PC-386, including IRV predictions has been introduced,
- 1993, February; the upgraded version of real-time satellite tracking program with graphic system has been implemented,
- 1994; avalanche photodiode experiments,
- 1994; daily passes experiments,
- 1994; computer exchange (to PC-486), new interface and new continuous tracking system are under final realization (engineering tests).

The scheme of the system after computer replacement is presented in Fig.1. The increase of satellite passes and number of returns per pass (Fig.2, 3) result from software upgrading (better tracking control). The single shot RMS is on the same level (±4 cm), mainly due to old PMT (Fig.4, 5). The present hardware specifications are shown in Table 1.

Table 1. Hardware specifications

	BOROWIEC-1	BOROWIEC-2
Laser:	Nd:YAG, CONTINUUM PY-62	Nd:YAG, WAT
wavelength	532 nm	532 nm
pulse energy	100mJ	250 mJ
pulse width	100 ps	4 ns
repetition rate	10 Hz	1 Hz
divergence	0.4 mrad	0.7 mrad
Mount and Telescope:	Az-El, Cassegrain	Az-El, Cassegrain
diameter	65 cm, spherical	65 cm, spherical
field of view	5 arcmin	5 arcmin
encoder resolution	1.8 arcsec	1.8 arcsec
transmitting optics	No	8x gain
Receive Optics and Electronics:		
T/R coupling	separate	separate
interference filter	0.15 nm, 30% transmission	7 nm, 50% transmission
detector	PMT RCA-8852	PMT FEU-87
discriminator	B-6, maximum likelihood	B-6, maximum likelihood
time interval counter	PS-500, ±100 ps	PS-500, ±70 ps
Time Base:		
time comparison	GPS receivers	GPS receiver
frequency standard	cesium, rubidium	rubidium
accuracy	200 ns	200 ns
Calibration:	external, pre and post	external, pre and post

BOROWIEC-2 SLR

First satellite echos (TOPEX/POSEIDON): 25 March 1994

First Lageos echos (LAGEOS-2): 6 April 1994

The history of installation of BOROWIEC-2 SLR is presented in Table 2. The scheme and parameters of the system are shown in Fig.6 and Table 1. Engineering observations performed from March to July 1994 (Table 3) showed proper work of all subsystems. The large RMS and small number of returns result from old 4 ns 1 Hz laser transmitter. BOROWIEC-2 SLR is ready for transport to Tunisia. The system installation in a new geodynamical station at Medenine depends on Tunisian side. Immediately before or after transfer of the system, laser will be replace to third generation. Software and hardware are ready for operating with 10 Hz repetition rate and narrower pulse.

Table 2. History of BOROWIEC-2 SLR installation.

YEAR	TASK
1990	Mount installation Installation of the optical elements of the telescope Manual driving of the mount
1991	Installation of computer PC-286 Mount driving from computer Adjustment of optical elements
1992	Pre- and post-pass software Laser installation
1993	Real-time software Adjustment of Coude path Installation of start photodiode package Alignment of mount optical axis Installation of detector package Installation of laser ranging electronics All devices under computer control First ground target calibrations First visual satellite tracking (ERS-1)
1994	Installation of GPS time receiver Installation of epoch recorder and rubidium frequency standard Determination of mount model errors First successful laser ranging (TOPEX/POSEIDON)

Table 3. Borowiec-2 - engineering observations (1.03.94 - 1.07.94)

SATELLITE	PASSES	RETURNS	RETURNS/PASS	RMS (cm)
LAGEOS-2	7	248	35	22.2
TOPEX/POSEIDON	19	2130	112	22.9
ERS-1	3	101	34	20.6
METEOR-3	2	27	13	24.8
AJISAI	4	228	57	21.6
TOTAL	35	2734	78	22.4

This work was supported by Grants from Polish Committee of Scientific Research:
PB 2 Z6Z6 012 03p12 and PB 2 2150 92 03p09.

BOROWIEC-1 LASER RANGING SYSTEM

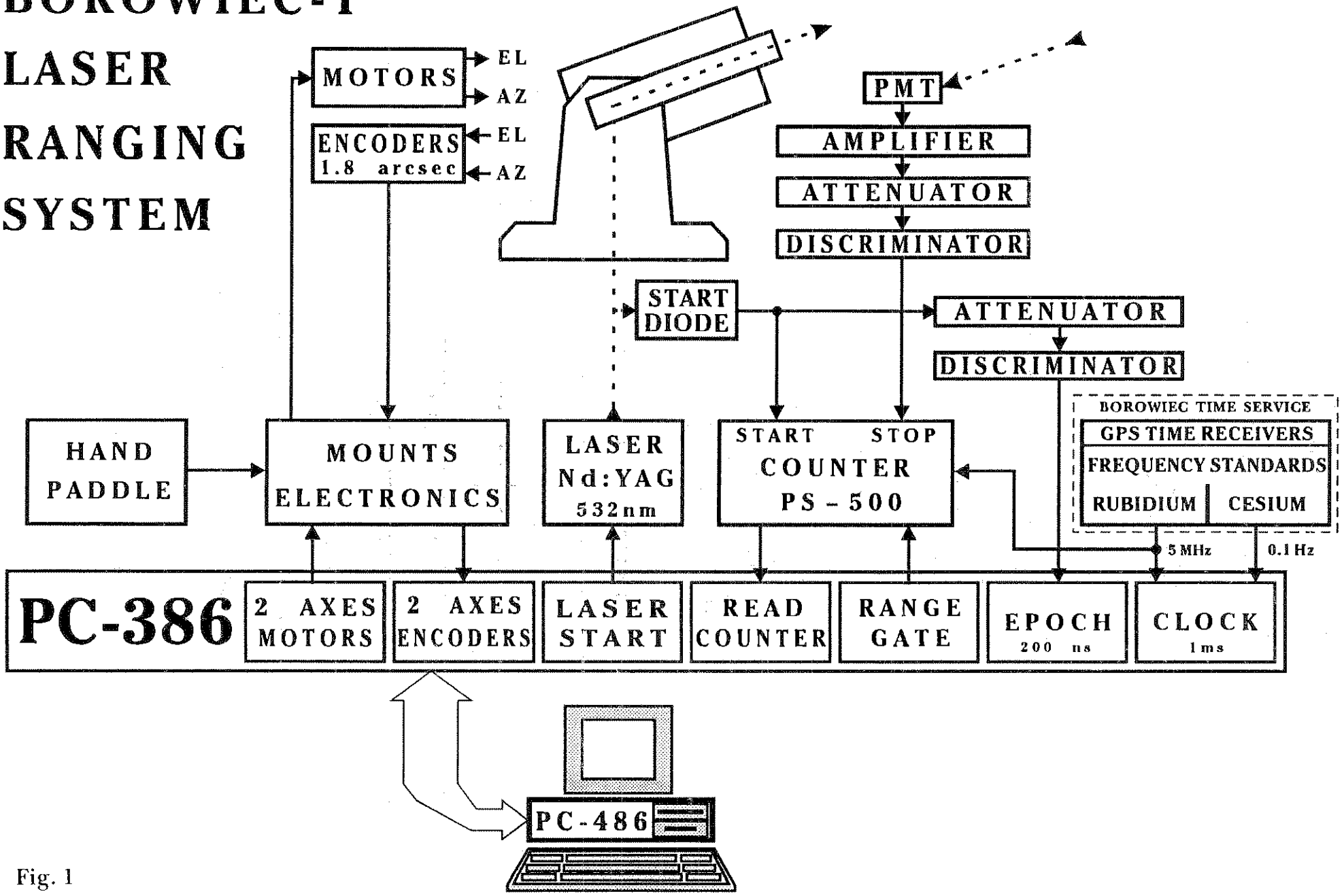

Fig. 1

NUMBER OF PASSES: 1988 - 1994

SLR BOROWIEC

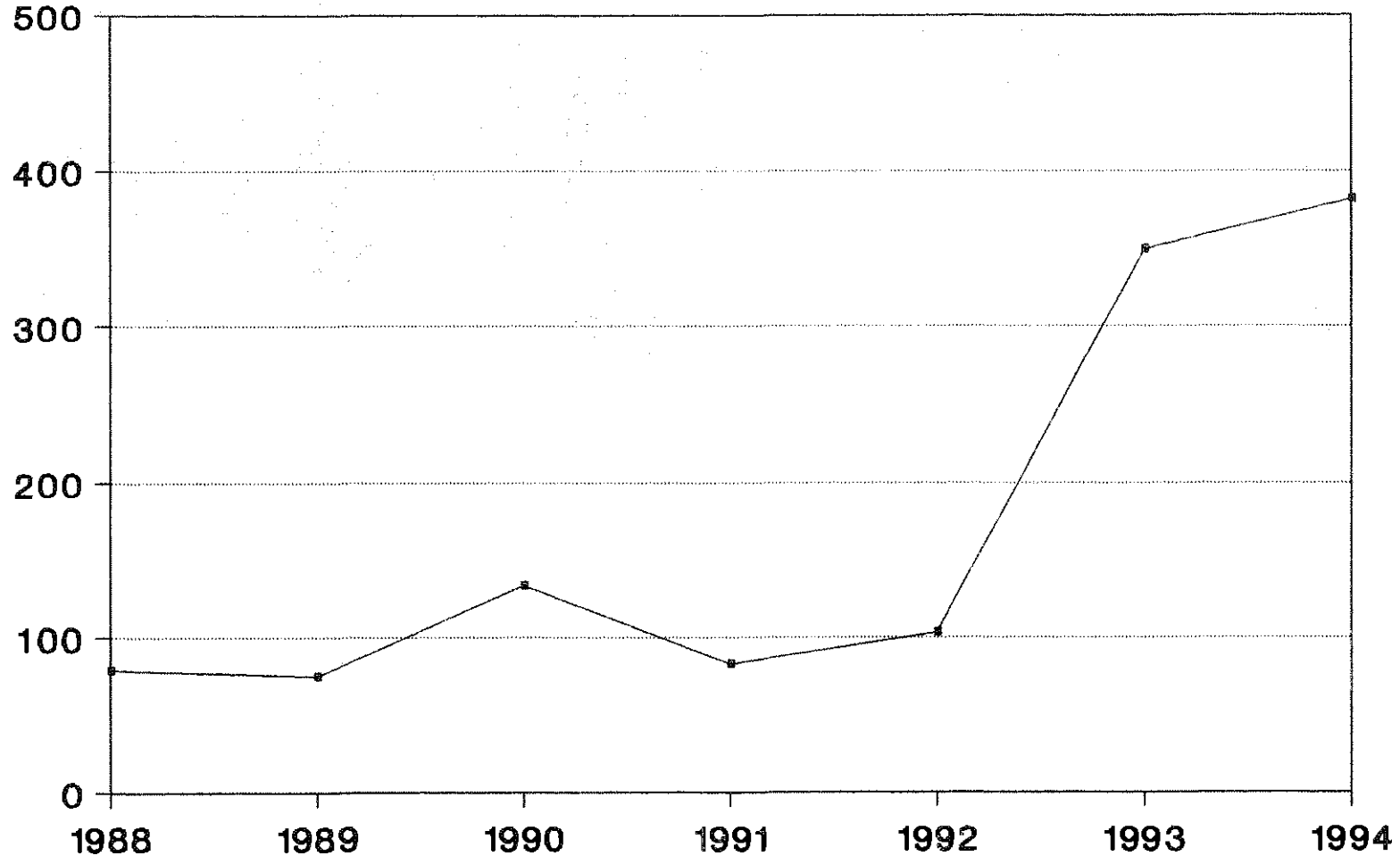

Fig. 2

RETURNS/SATELLITE PASS
BOROWIEC SLR

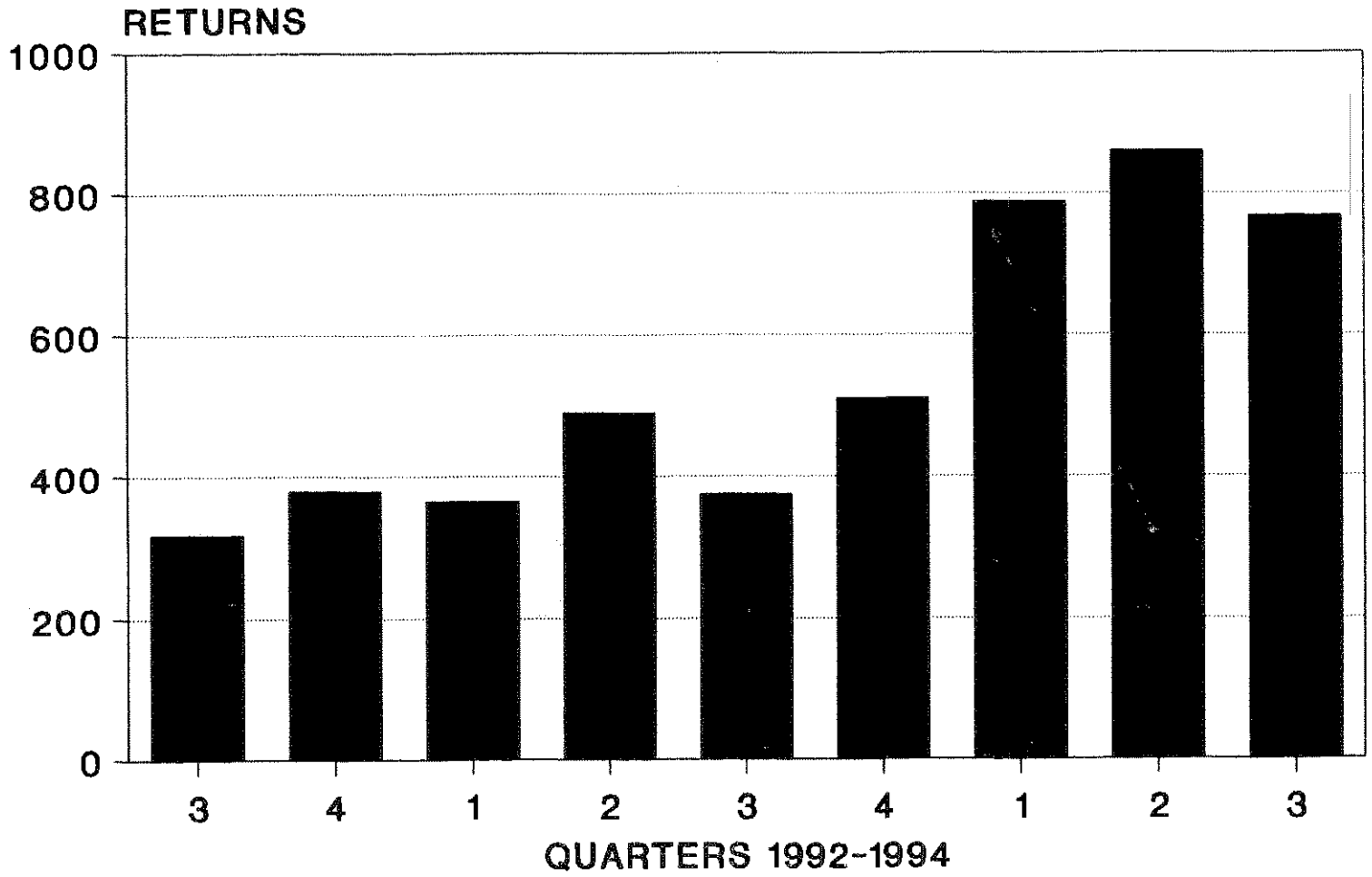

Fig. 3

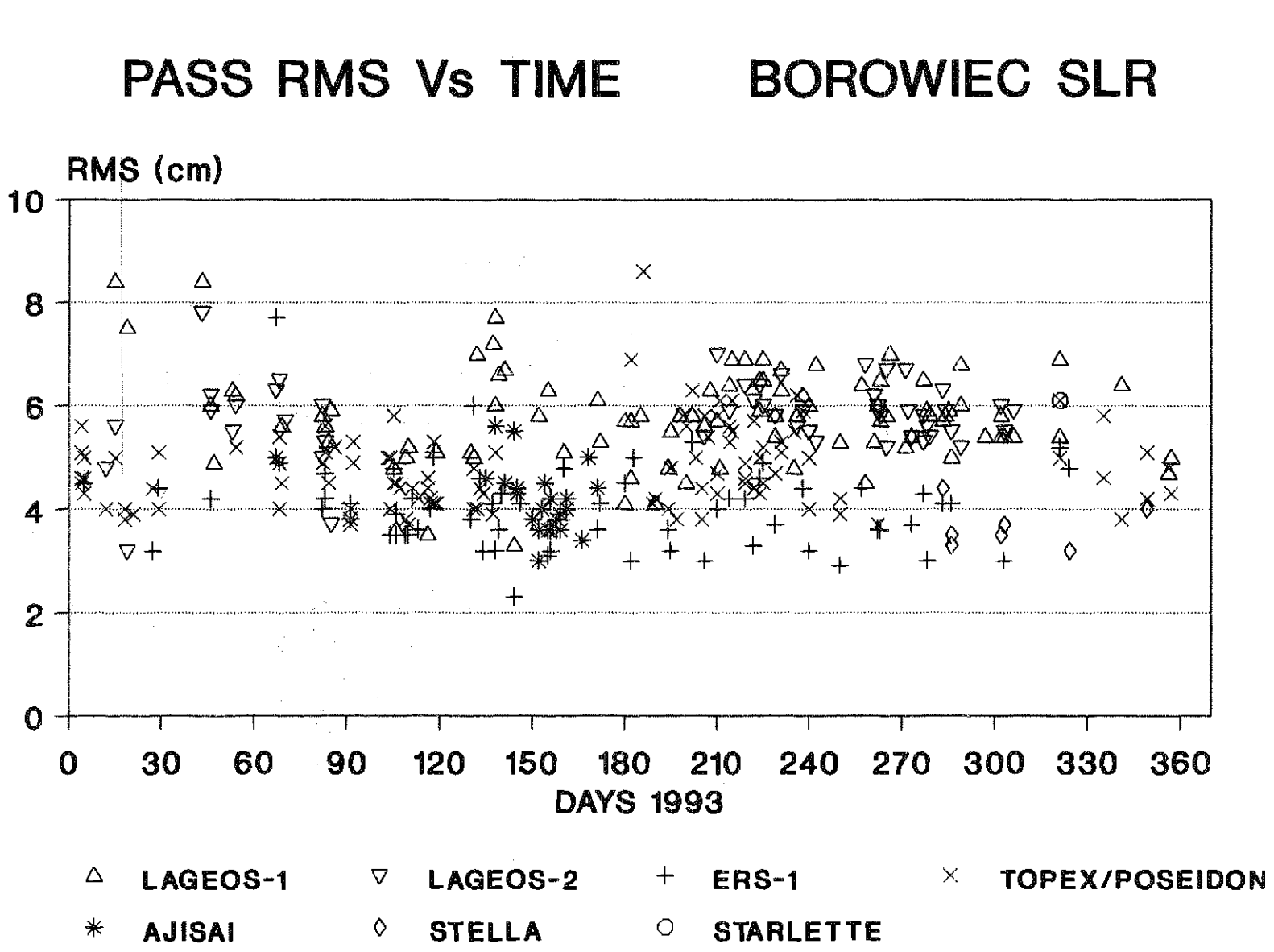
PASS RMS Vs TIME BOROWIEC SLR
RMS (cm)
10
8
6
4
2
0
0 30 60 90 120 150 180 210 240 270 300 330 360
DAYS 1993
LAGEOS-1
LAGEOS-2
ERS-1
TOPEX/POSEIDON
AJISAI
STELLA
STARLETTE

Fig. 4

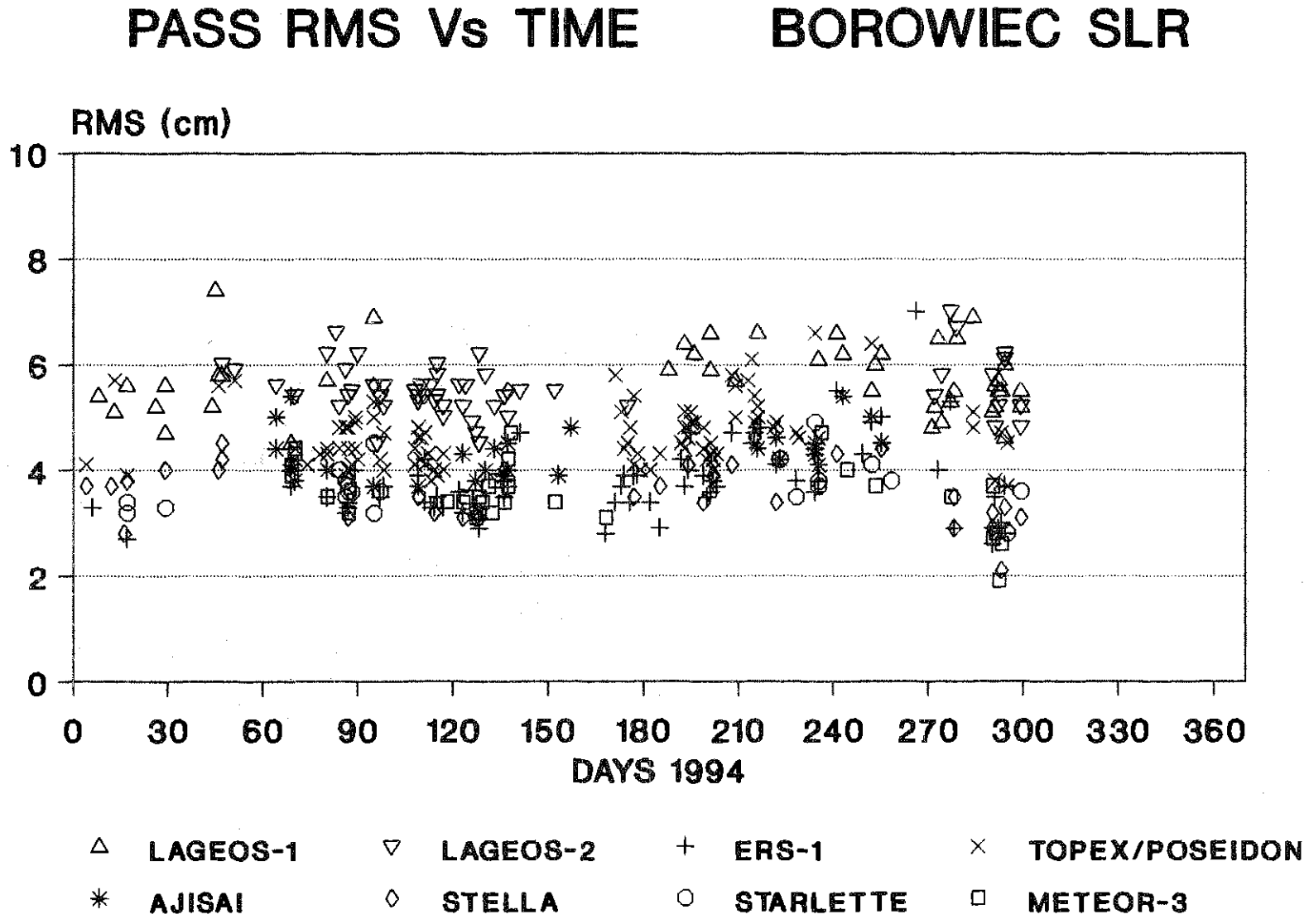
PASS RMS Vs TIME BOROWIEC SLR
RMS (cm)
10
8
6
4
2
0
0 30 60 90 120 150 180 210 240 270 300 330 360
DAYS 1994
LAGEOS-1
LAGEOS-2
ERS-1
TOPEX/POSEIDON
AJISAI
STELLA
STARLETTE
METEOR-3

Fig. 5

BOROWIEC-2 LASER RANGING SYSTEM

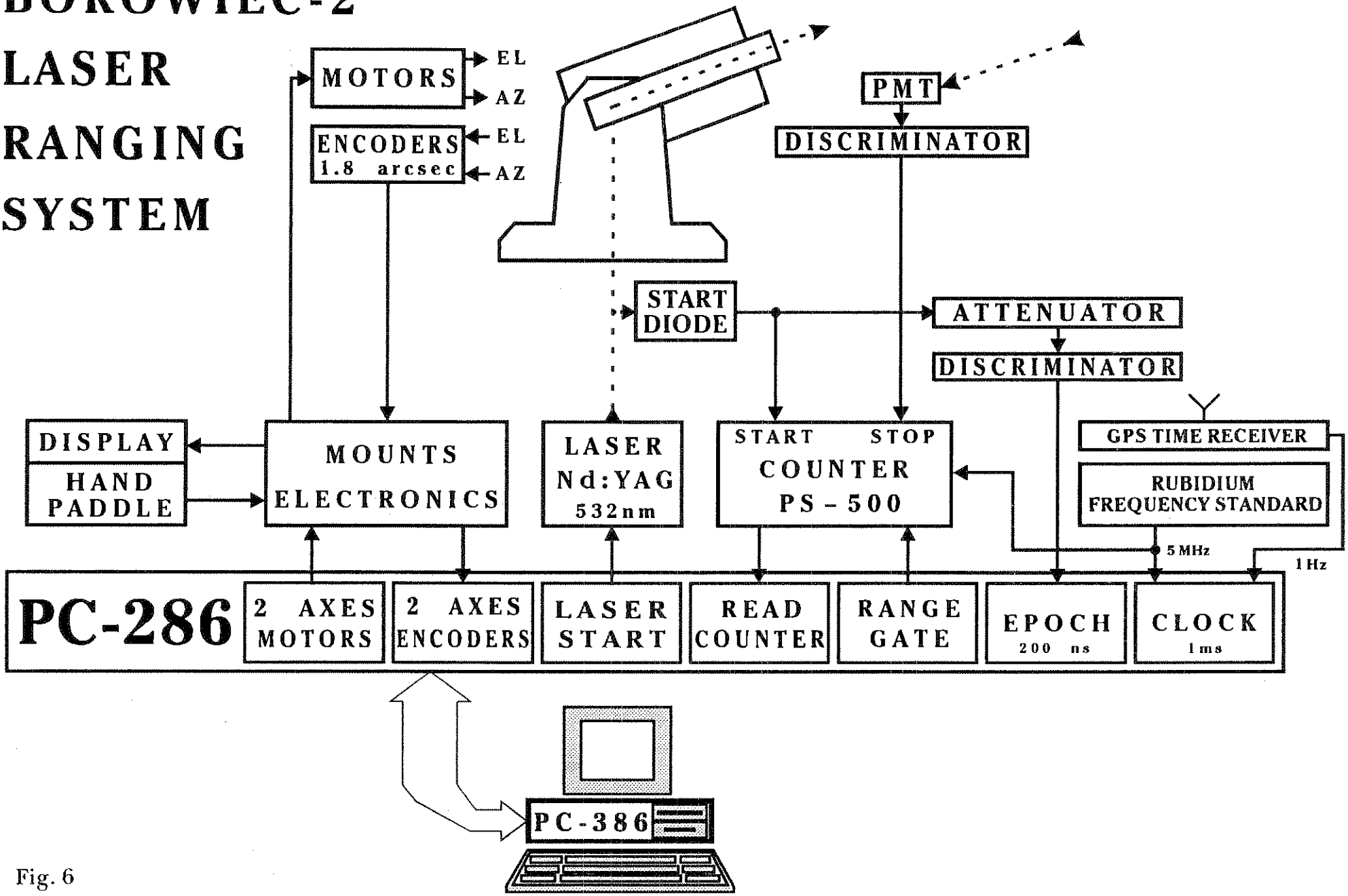

Fig. 6

TIMING DEVICES AND CALIBRATION

Chairperson : Hiroo Kunimori

Investigation of a small range-dependent bias of two Stanford SR620 time interval counters

P. Gibbs, A.T. Sinclair

RGO Herstmonceux, Herstmonceux Castle, Hailsham, East Sussex BN27 1RP. England.

1. Normal SLR operations

For the routine SLR operations at Herstmonceux each range measurement is timed by two Stanford SR620 time interval counters. This is done both for calibration and satellite ranging. The start signal from the start diode is split and fed to the start channel of both SR620s, and the stop signal from a SPAD detector is split and fed to both stop channels. Thus the timers are used in a mode where they time the whole of the time interval, and not as is sometimes done by using clock pulses as the stop events, where just the smaller intervals from the start or stop event to the next clock pulse would be timed. The reason for adopting this mode is that internally the SR620 uses an analog timing method for the small intervals from the start and stop events to the next clock pulse, and uses a digital count of clock pulses for the remainder of the time interval, and so there did not seem much point in duplicating this process externally.

Ideally the difference of the two range measurements should be constant for all ranges, apart from the scatter caused by the jitter of the two timers. The rms scatter of the range differences is found to be about 40 ps for ranges up to about 10 ms, rising to about 50 ps for longer ranges (note that the laser, start diode and detector do not contribute, as we are looking at the *differences* of the same event seen by the two timers). This implies that at best the performance of each SR620 is about $40 / \sqrt{2}$ ps = 28 ps, assuming that their performance is about equal. The mean difference of the measurements was indeed found to be fairly constant for all satellites, but was found to be about 20 ps different from the value for calibration ranging. This effect is very small, equivalent to 3 mm in one-way range, and it speaks highly of the precision of the SR620 that it is able to resolve such a small effect. However the effect did seem to be well-defined, and so further tests were carried out in order to eliminate the possibility that the hardware configuration or the method of processing were treating calibration and satellite ranging differently.

2. Further tests

For more detailed tests of the effect the SLR system was used as if it was carrying out calibration ranging to a target at an arbitrary distance. The start of the range gate is set by a Stanford DG535 time delay generator, and the SPAD detector is gated on at the start of this range gate.. This was set to a chosen range, from very short, typical of calibration ranging ($\sim$ 4 μs) to ~ 50 ms, typical of Lageos ranging. The SPAD was exposed to a high light level, so that an external noise event was generated very shortly after gating on the SPAD, and this provided the stop event for the two SR620s. A large number (several thousand) of measurements were made at each range. The distribution of these measurements at each range was examined and found to be reasonably normal, so that statistical determination of the mean and its standard error are reasonably meaningful. The error bars for plotting these mean values are calculated from $\pm 3 \times RMS / \sqrt{N}$, where RMS is the root-mean-square difference of the measurement differences from the mean, and N is the number of readings. Thus this corresponds to a level of confidence of 95% that the actual value lies within these error bars.

Figure 2 shows a plot of the mean differences of the two SR620 timers. The zero point of the vertical scale has been chose to give a difference of zero for short ranges. The plot shows a distinct rise of the mean difference as the range is increased to 10 ms, and thereafter it is reasonably constant. This plot is actually a composite of two measurement runs, over the ranges 0 to 20 ms, and 10 to 50 ms, and the vertical scales have been adjusted so that the data match over the overlap portion. This is necessary because these runs are lengthy, and are carried out when other activities permit. Any minor change to the system between runs (e.g. unplugging and re-plugging a connector) will change the measurements by considerably more than 20 ps. Various other runs have been carried out, and a rise of about 15 - 20 ps was found in all, but in some the rise occurred over a much smaller change of range, sometimes over 0 to 2 ms rather than 0 to 10 ms, and in some runs the differences would fall again as the range was increased. Thus this plot is indicative of the typical behaviour of the system, but it is not intended and cannot be used as a correction curve.

In one of the tests an HP5370A timer was included in addition to the two SR620s. Figure 3 shows the differences of it from one of the SR620s, and these are much larger than the differences between the two SR620s. There are two interpretations that could reasonably be made, that the HP timer is considerably worse than the two SR timers and so this variation is mainly due to the HP, or that the two SR timers are both poor but have a large variation in common, so that all we see in figure 2 is the smaller difference of this larger variation. This HP5370A is a very early model, and has previously given problems in comparison with the Maryland timer that was used at Herstmonceux up till November 1993. Thus we think it is most likely that the variation shown in figure 3 is primarily due to the HP timer.

3. Comments

Running the internal calibration procedure of the SR620 timers made no difference to this performance. During the course of the tests it was found that the RMS scatter of the differences of the range measurements increased from about 40 to 200 ps for ranges above about 10 ms. This was large enough to be seen as an increase of RMS of the ranges to the satellite measured by one of the timers only, and thus the source of the poor performance could be located. Thus our suspicion is that just one of the SR620s is the cause of the bias problem also.

The method of operation of the SR620 is that it measures the short time interval between an event and the next clock pulse by charging a capacitor, and the voltage of the capacitor is subsequently read by an A/D converter to give a measure of the time interval. It does not state in the manual when the A/D conversion is done. If this is done only after the stop event has arrived, then perhaps the longer time delay that occurs for longer ranges before reading the start channel may allow some dissipation of the charge on the capacitor.

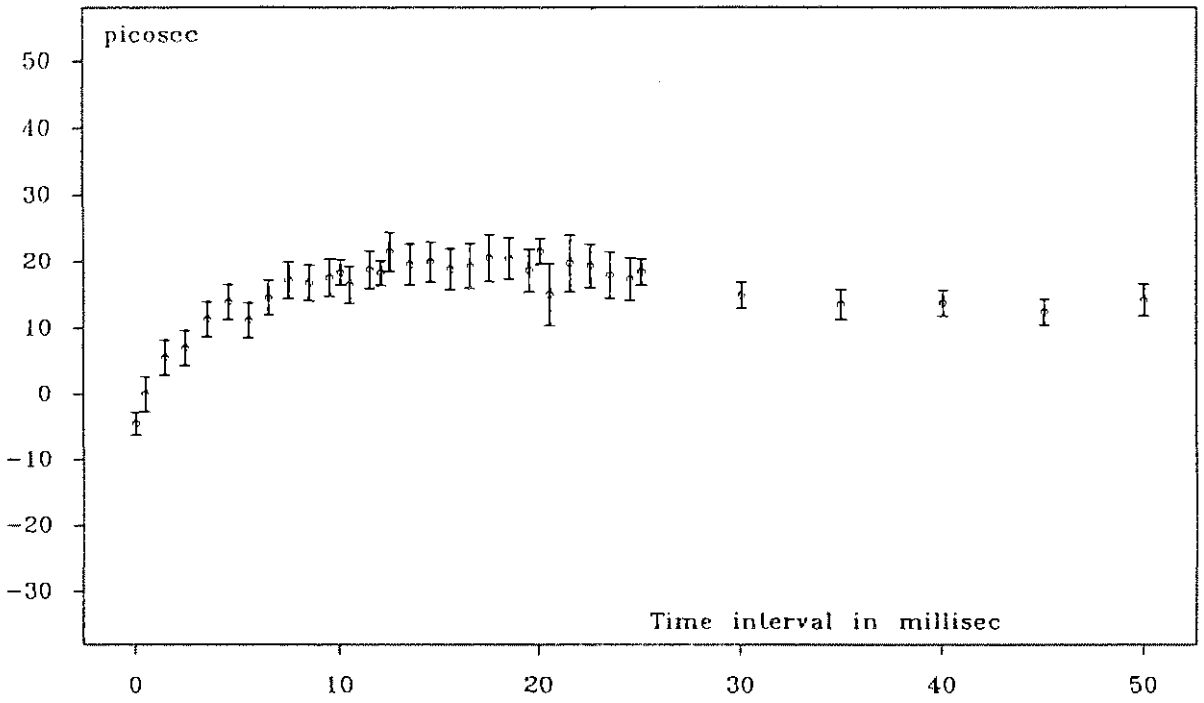

Figure 1. Mean differences of readings of two SR620 timers

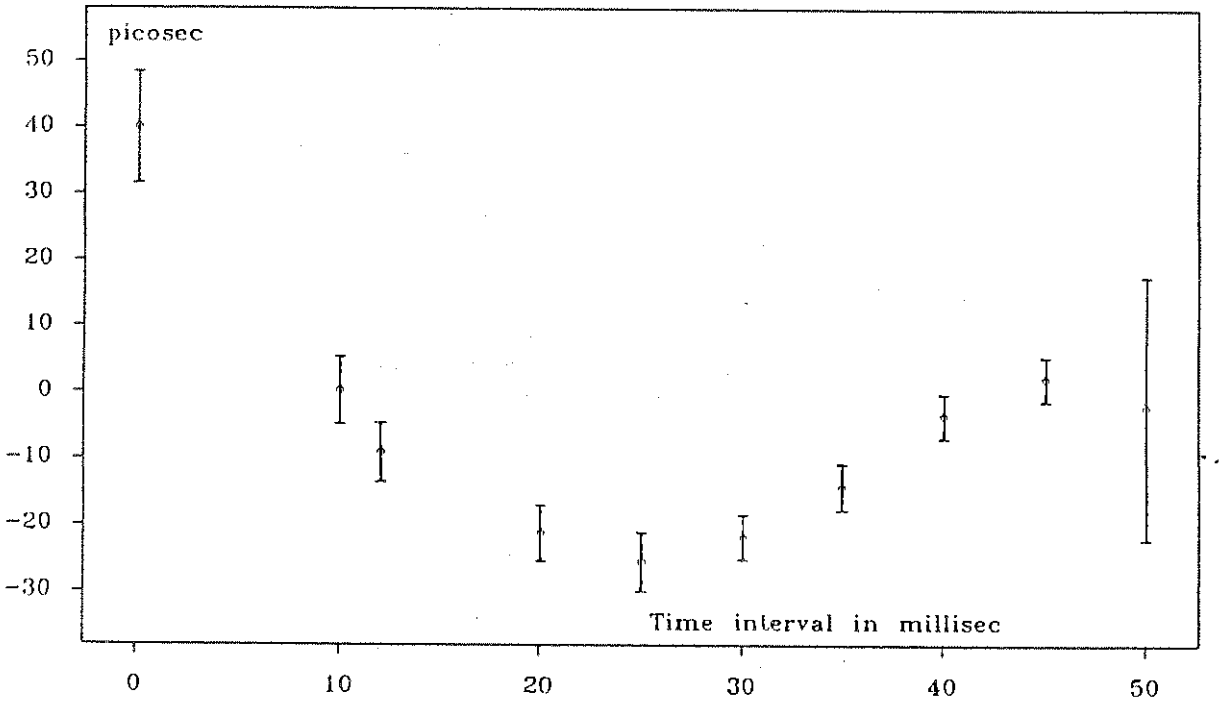

Figure 2. Mean differences of SR620 and HP5370A timers

GPS Steered Rubidium Frequency Standard for the NASA SLR Network

Jeff Ingold, Richard Eichinger, Howard Donovan, Thomas Varghese
AlliedSignal Technical Services
Lanham, Maryland 20706, USA

Wayne Dewey
TrueTime, Inc.
Santa Rosa, California 95407, USA

John Degnan
NASA Goddard Space Flight Center
Greenbelt, Maryland 20771, USA

Abstract

The replacement of the high performance cesium beam tubes in the NASA Satellite Laser Ranging (SLR) Network as well as the automation of the current time and frequency systems are prohibitively expensive. This paper describes an alternative approach towards achieving high precision and automation of the time and frequency systems by using a Global Positioning System (GPS) time and position receiver to steer a rubidium oscillator. The steering is accomplished by using a frequency correction loop to control the C-field of a rubidium oscillator. After a 24 hour acquisition period, the maximum incremental frequency change is constrained to 6 E-14 in no less than one minute intervals. Time and frequency from the steered rubidium provide acurate frequency reference signals and time synchronization for the telescope and transmit/receive electronics. Accurate time reference to the US Naval Observatory for precise laser epoch measurement is also provided. Results from laboratory and field tests will be presented.

Introduction

Cesium beam frequency standards have been the cornerstone of the NASA SLR time and frequency systems for the past eighteen years. Within the past eight years, all of the original cesium beam frequency standards have been refurbished with updated electronics and new cesium beam tubes. The current price for a high performance cesium beam tube is US $25,000. Many of these standards will require a replacement cesium beam tube in the next few years. A viable alternative to cesium standards is to use a low cost multi-channel GPS receiver to slowly steer a rubidium oscillator.

Background

Two methodologies for frequency control used by many manufacturers of GPS disciplined rubidiums are: 1) continuous correction, and 2) single correction every 24 hours. [1,2] Continuous correction via a twelve bit digital to analog converter (DAC) causes an abrupt frequency change of 1 E-12, impacting short term frequency stability and possibly reducing satellite laser ranging accuracy. Single corrections once every 24 hours allows a frequency offset to accumulate for 86,400 seconds, then executes a large frequency step. If this correction occurs during satellite laser ranging, data could be compromised.

Most commercial manufacturers are targeting the much larger telecommunications industry and do not address the impact these methods have on short term stability over any epoch. The main objective of our steering process is to combine the relatively good aging characteristics of the rubidium oscillator with fine frequency adjustments of 6 E-14 continuously without degrading short term stability.

GPS Selective/Availability and SatHop

The Global Positioning System is the standard used to steer the rubidium oscillator. Many references to the operation and use of GPS can be found in published literature. [3,4] Time transfer via GPS to the United States Naval Observatory (USNO) with Selective/Availability (S/A) enabled has been observed to be +/- 300 nanoseconds using single channel receivers. (S/A is the intentional degradation of accuracy for commercial applications.) To reduce the effects of S/A on frequency steering processes, TrueTime developed the Satellite Hopping (SatHop) algorithm. [5]

Once a three dimension position determination has been successfully completed, the antenna's coordinates are retained in non-volatile memory and the receiver considers all range errors to be clock biases only. If the GPS antenna is moved, a new position must be determined.

The next step of the SatHop algorithm is comprised of two components, a satellite sequencer and a solution averager. The sequencer scans the list of satellites in view and selects one satellite for the GPS receiver to use for a timing solution (user deselected and unhealthy satellites are ignored). Because the GPS receiver is capable of tracking up to seven satellites simultaneously, virtually all visible satellites are on the list. After a dwell period of 30 seconds which generates 30 samples for the selected satellite, the next satellite in the sequence is selected. The sequencer continuously loops through the satellite list and is updated by the GPS receiver as satellites rise and set.

The solution averager creates a composite satellite clock bias solution by averaging the phase solution from all of the tracked satellites into a single 400 sample average. The decorrelation time of GPS has been determined to be 400 seconds. [6] After ten sample averages from the SatHop solution averager have occurred, a frequency error is calculated and an adjustment control word is stored in a register. The control word is divided into segments representing one binary bit of the 16 bit DAC. The segments are queued and executed on a 60 second timer, one at a time. The output of the DAC then adjusts the magnetic field (C-field) of the rubidium. One DAC bit is equal to 6 E-14 of frequency change and is an order of magnitude below the noise floor of the rubidium oscillator.

System Hardware

The oscillator being steered is an FRK-H-LN rubidium oscillator manufactured by Ball Corporation, Efratom Division. The oscillator has a 0 to 5 volt electrical tuning input that controls the C-field. The frequency can be controlled +/-1 E-9 via this input. Option H refers to an improved aging rate of 1 E-11/month. The LN option improves the short term stability and lowers the single side band phase noise. The frequency change due to temperature is 1 E-10 from -25 degrees C to +65 degrees C. [7]

The GPS receiver front end is a Tans Timing Module (TTM), manufactured by Trimble navigation. The remaining portion of the receiver is a TrueTime GPS-DC-MKIII. The receiver uses the steered rubidium oscillator as its timebase to synthesize the local oscillator to acquire and track the GPS satellites. Clock bias in meters is reported from the TTM and is directly converted to seconds using the speed of light in free space (3.335640952 E-9 seconds/meter) as the conversion factor. Clock bias contains the rubidium oscillator error, selective availability, variations in the GPS signal path, and system noise. [5]

The rubidium oscillator and associated RF electronics use a single linear power supply with board level DC filtering and voltage regulators for low noise and RF isolation. An external DC input is supplied for continuous operation during power outages of up to eight hours. The 10 MHz sinewave signal from the rubidium oscillator is distributed by low noise, 90 dB isolation amplifiers to drive the GPS receiver, one pulse per second (1PPS) generator, low noise 10 MHz to 5 MHz frequency divider and user output. The 5 MHz sinewave signal from the divider is distributed to four user outputs by low noise, 90 dB isolation amplifiers. These RF techniques are required to achieve minimum overall system phase noise and short term stability.

Two isolated 1PPS user outputs are generated from the 10 Mhz for phase coherency and are synchronized to the GPS 1 PPS after the 24 hour acquisition period. This technique maintains the epoch to USNO within +/-500 nanoseconds, thereby eliminating human intervention to make time steps or time bias corrections.

A user RS-232 port is available for Time of Day time-stamp as well as monitor and control.

IRIG-B modulated time code is also available to the user.

Figure 1 shows the block diagram of the GPS steered rubidium.

Short Term Stability

One of the major design goals of this project was to produce a system with good frequency stability at taus (sampling times) of 20 milliseconds to 50 milliseconds. These taus are the roundtrip time of flight of the laser pulse for most of the satellites tracked by the NASA SLR. These short taus are outside the normal scope of time domain metrology. [8] Frequency domain phase noise measurements were performed from 0.01 Hz to 2 MHz from the carrier using a Hewlett/Packard 3048A phase noise analyzer. The results were normalized from single sideband to double sideband, then converted to the time domain using the US National Institute of Standards and Technology (NIST) approved power-law spectra equations. [9] Use of this metrology proved useful during the development and testing cycle, as near real time results were available while the GPS receiver was correcting the rubidium. Measurements indicated no appreciable difference in phase noise or short term stability between corrected and uncorrected rubidium operation. Figure 2 is a comparison of short term stability of various 5 MHz oscillators.

Laboratory Tests Results

The Time and Frequency Office at AlliedSignal Technical Services in Columbia, Maryland, USA, maintains a time base traceable to USNO within +/- 50 nanoseconds via TV line 10 for the NASA Goddard Space Flight Center. From a group of several cesium beam frequency standards, the best performing unit is used as the "House Standard". The House Standard is compared to the USNO via TV line 10 in common view mode five days a week. All standards are compared to the House Standard daily. Three single channel GPS receivers are also monitored daily as depicted in figure 3. Any 5 MHz frequency oscillator can be evaluated using this system.

The GPS Steered Rubidium was compared to the House Standard at ten minute intervals for seventeen consecutive days from July 26, 1994, to August 12, 1994.

The 24 hour acquisition period of the GPS Steered Oscillator is obvious at the beginning of figure 4. The three small breaks in the data are from short power interruptions in the monitoring equipment. The worst case peak to peak frequency change after the 24 hour acquisition period is less than 2 E-12 over several hours. The worst case epoch error was less than 500 nanoseconds.

Field Tests Results

Mobile Laser System (MOBLAS) 7 located at Goddard Space Flight Center, was the field test site for the GPS steered rubidium. Figure 5 depicts the interconnections between MOBLAS 7 and the GPS steered rubidium. TV line 10 is used to measure the cesium beam frequency standard to USNO in common view mode. The Time and Frequency Office in Columbia, initiates and analyzes the measurements between USNO and MOBLAS 7. Any 5 MHz oscillator can be measured to MOBLAS 7 and traced to USNO using this method. A linear phase recorder and a single channel GPS receiver were also used to evaluate and analyze the performance of the GPS steered rubidium.

Long term frequency stability data is shown in figure 6. The data indicates that the GPS steered rubidium maintains epoch to +/- 500 nanoseconds to USNO. The maximum frequency change is less than 2 E-12 over several hours.

Figure 7 is SLR data taken at MOBLAS 7 on July 12, 1994. The MOBLAS 7 timebase for this Lageos-2 pass started with the cesium frequency standard. As scheduled, the GPS steered rubidium was substituted for the cesium halfway through the pass. The residuals indicate that replacing the cesium standard with the GPS steered rubidium did not impact NASA SLR data.

Summary

The data and techniques presented above indicate that it is feasible to replace cesium beam frequency standards in the NASA SLR network with GPS steered rubidiums.

Acknowledgment

The authors are grateful to John Arnold, Bea Belovarich, Paul Kushmeider, Robert Price, and Harry Sadler, AlliedSignal Technical Services for the data analysis used in this paper.

References Cited

1. McNabb, Jack "A Precise GPS-Based Time and Frequency System" Proceedings of the 24th Annual Precise Time and Time Interval (PTTI) Applications and Planning Meeting December 1992.

2. Dewey, Wayne "A GPS Disciplined Rubidium Clock" Proceedings of the 21st Annual Precise Time and Time Interval (PTTI) Apllications and Planning Meeting November 1989.

3. The Institute of Navigation, "The Global Positioning System" Volumes I and II.

4. Ingold, Jeff et al.,"An International Time Transfer Experiment" Proceedings of the 37th Annual Frequency Control Symposium June 1983.

5. Dewey, Wayne "Disciplined Rubidium Oscillator With GPS Selective Availability" Proceedings of the 24th Annual Precise Time and Time Interval (PTTI) Applications and Planning Meeting December 1992.

6. Allan, Dave, and Dewey, Wayne, "Time-Domain Spectrum of GPS SA" Proceedings of the 1993 Institute of Navigation 1993.

7. Precise Time and Frequency Handbook, Ball Efratom Division, Eighth Edition, 1991.

8. Detoma, Edoardo "Translation of Frequency Stability Measurements from the Frequency Domain to the Time Domain" AlliedSignal (formerly Bendix Field Engineering) Internal Report October 1987.

9. Temple, Robert "HP 3048A Option 301 Phase Noise Measurement System" Reference Manual Volume I.

Additional References

1. Goldman, Stanley "Phase Noise Analysis in Radar Systems" Wiley and Sons 1989.

2. Jespersen, Jim "Introduction to the Time Domain Characterization of Frequency Standards" Tutorials from the Twenty-third Annual Precise Time and Time Interval (PTTI) Applications and Planning Meeting December 1991.

GPS Steered Rubidium I

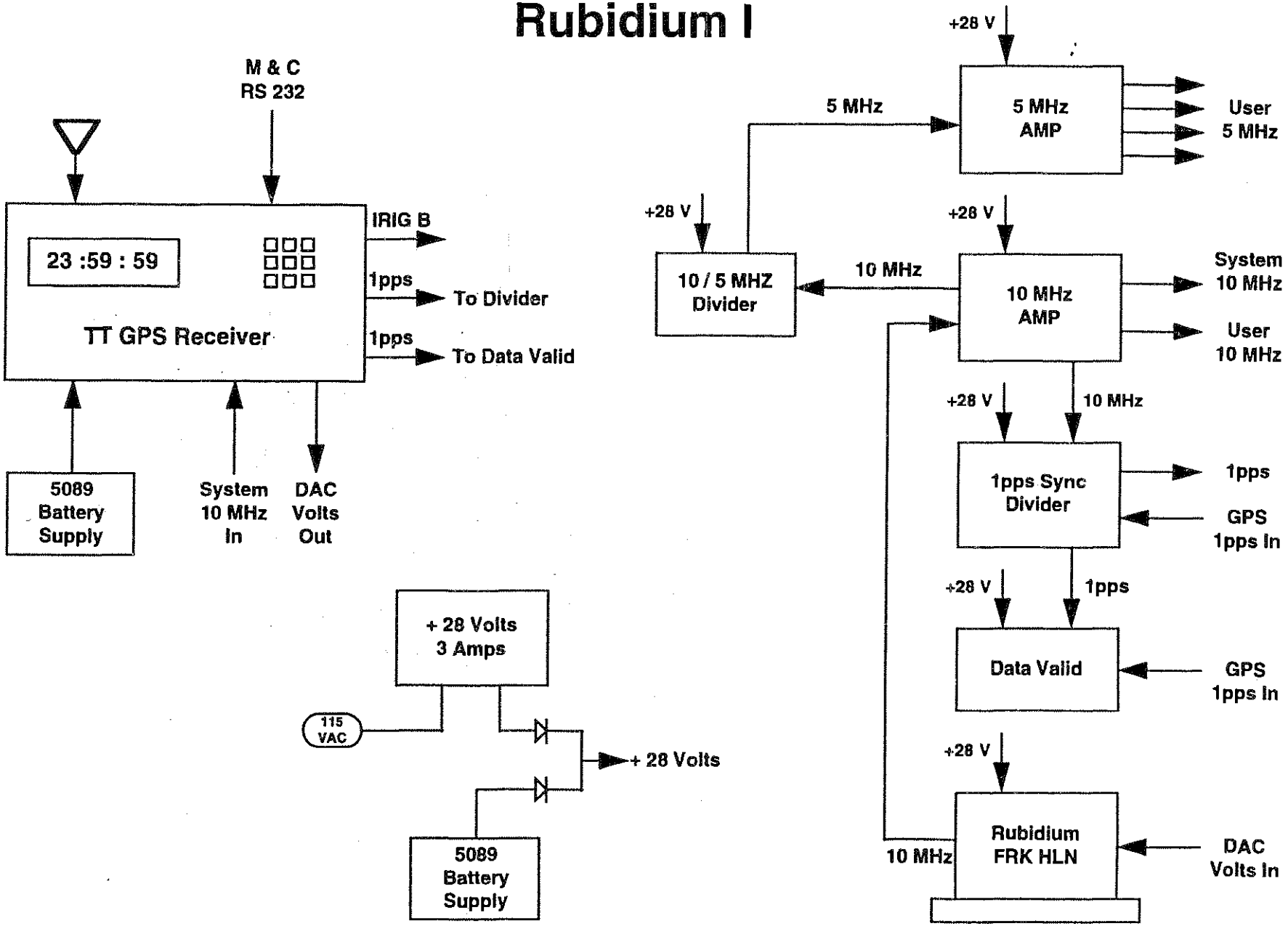

FIGURE 1

SHORT TERM STABILITY

TAU (sec.)	ATSC/TT	ONCE/DAY	857 FTS	5061A 004	5061B 004
.02	80.4	409.0	107.0	81.4	92.4
.05	32.3	165.0	43.0	33.2	36.9
.10	17.0	83.4	21.0	17.0	18.5
.20	11.0	42.6	12.0	9.4	9.5
.50	6.5	17.6	9.4	5.7	5.0
1.0	4.2	9.5	9.9	4.2	4.4
2.0	3.0	5.3	9.7	3.9	4.2
5.0	2.1	2.8	8.0	4.1	3.6
10	1.4	2.0	5.6	4.0	2.7
20	1.3	1.7	3.8	3.6	1.9

SIGMA Y TAU IN E-12

FIGURE 2

GPS Steered Rubidium Laboratory Test Facility

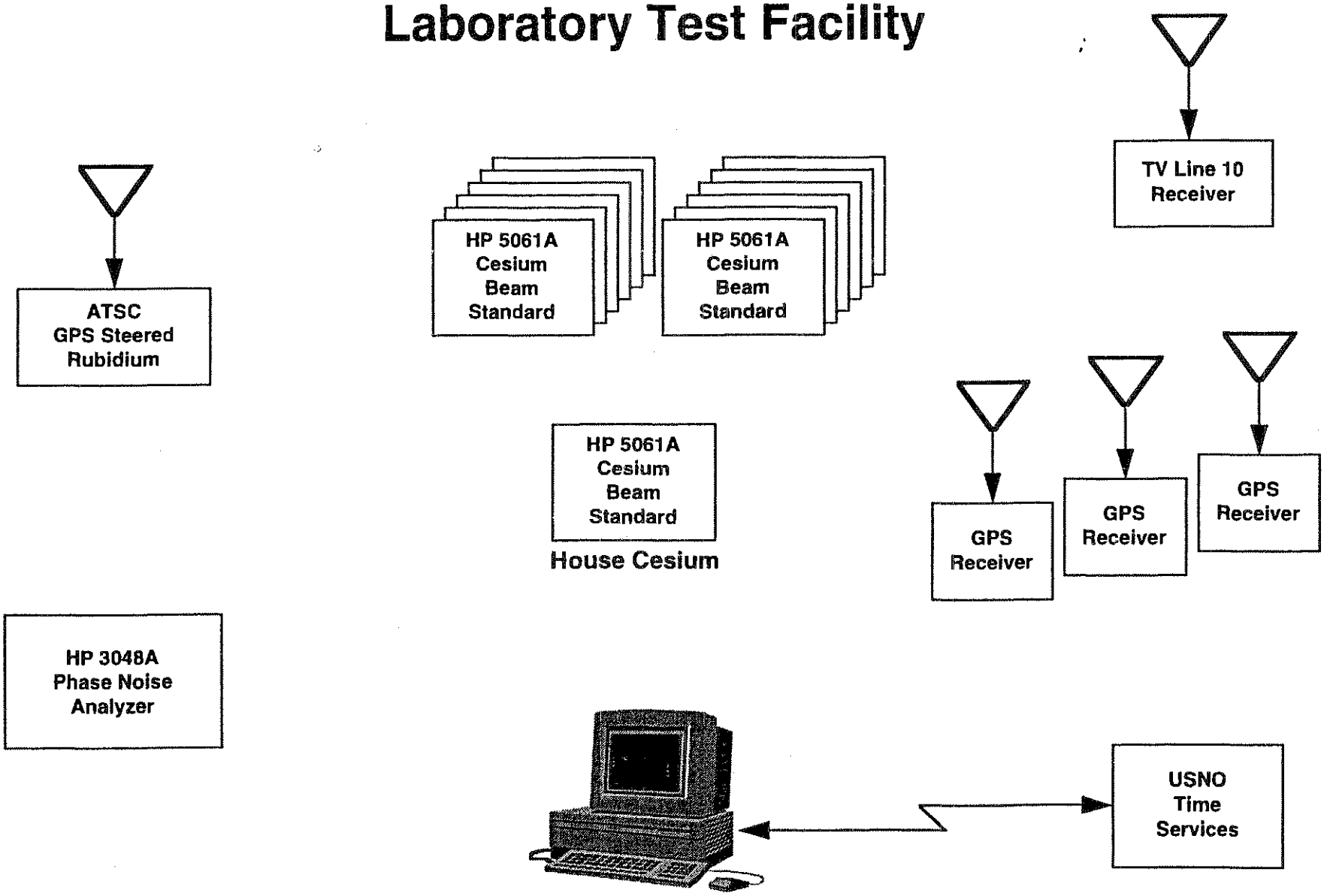

FIGURE 3

7/26 - 8/12/94

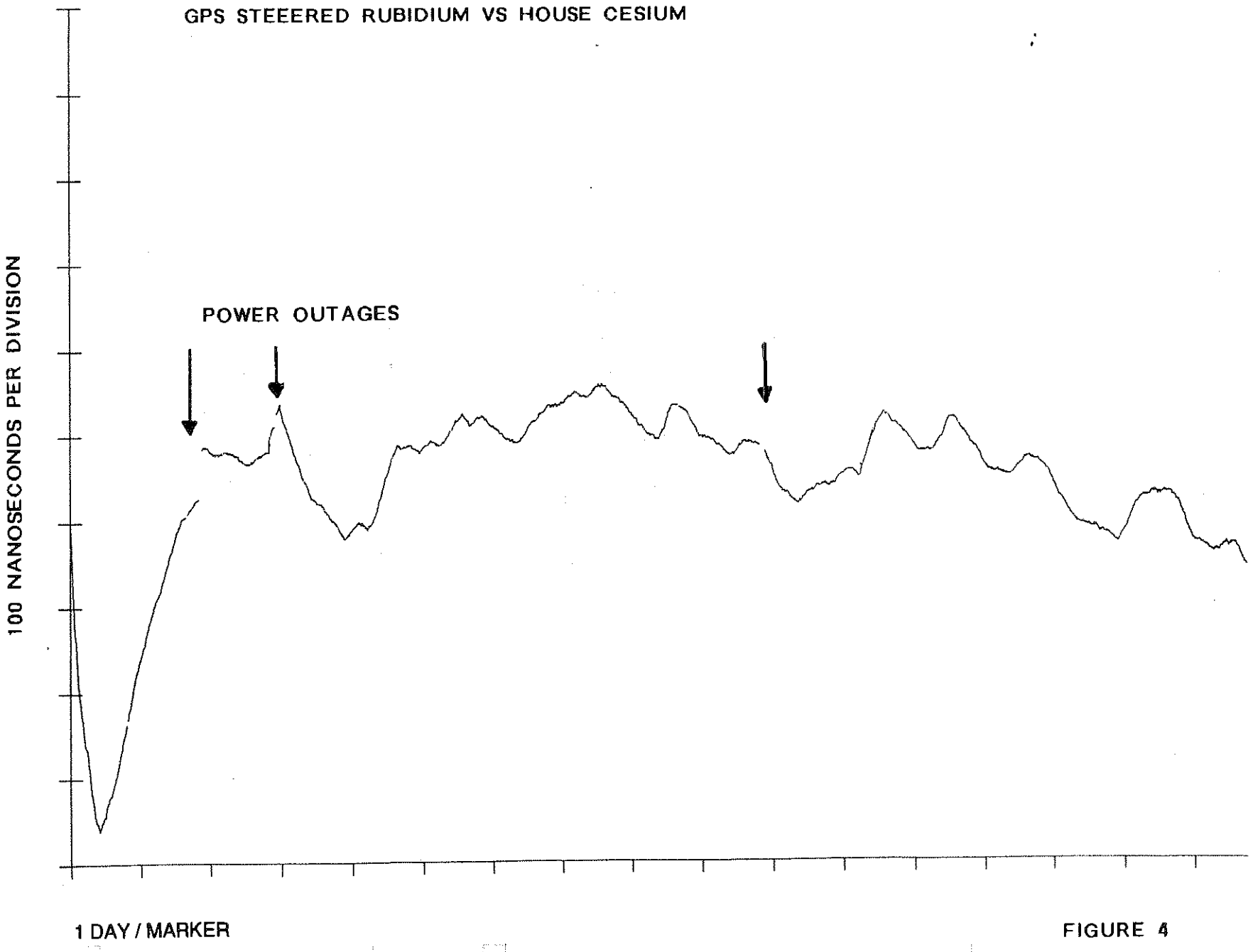

FIGURE 4

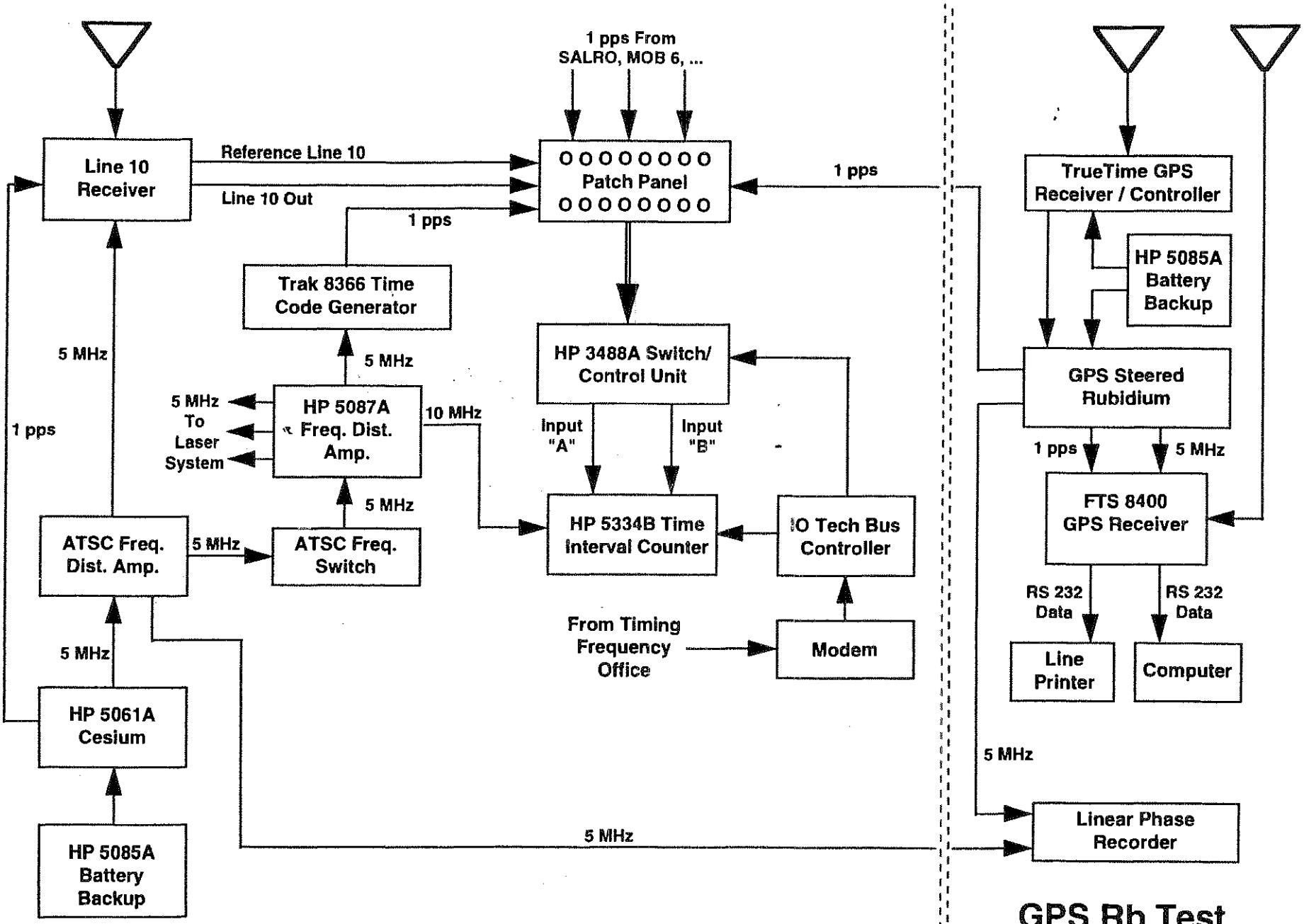
1 pps From
SALRO, MOB 6, ...
Line 10
Receiver
Reference Line 10
Line 10 Out
1 pps
Patch Panel
1 pps
TrueTime GPS
Receiver / Controller
HP 5085A
Battery
Backup
Trak 8366 Time
Code Generator
5 MHz
HP 3488A Switch/
Control Unit
GPS Steered
Rubidium
5 MHz
To
Laser
System
HP 5087A
Freq. Dist.
Amp.
10 MHz
Input
"A"
Input
"B"
1 pps
5 MHz
1 pps
5 MHz
ATSC Freq.
Dist. Amp.
5 MHz
ATSC Freq.
Switch
HP 5334B Time
Interval Counter
IO Tech Bus
Controller
FTS 8400
GPS Receiver
From Timing
Frequency
Office
Modem
RS 232
Data
RS 232
Data
Line
Printer
Computer
5 MHz
HP 5061A
Cesium
5 MHz
HP 5085A
Battery
Backup
5 MHz
Linear Phase
Recorder
MOBLAS 7 Timing Subsystem
GPS Rb Test
Subsystem

FIGURE 5

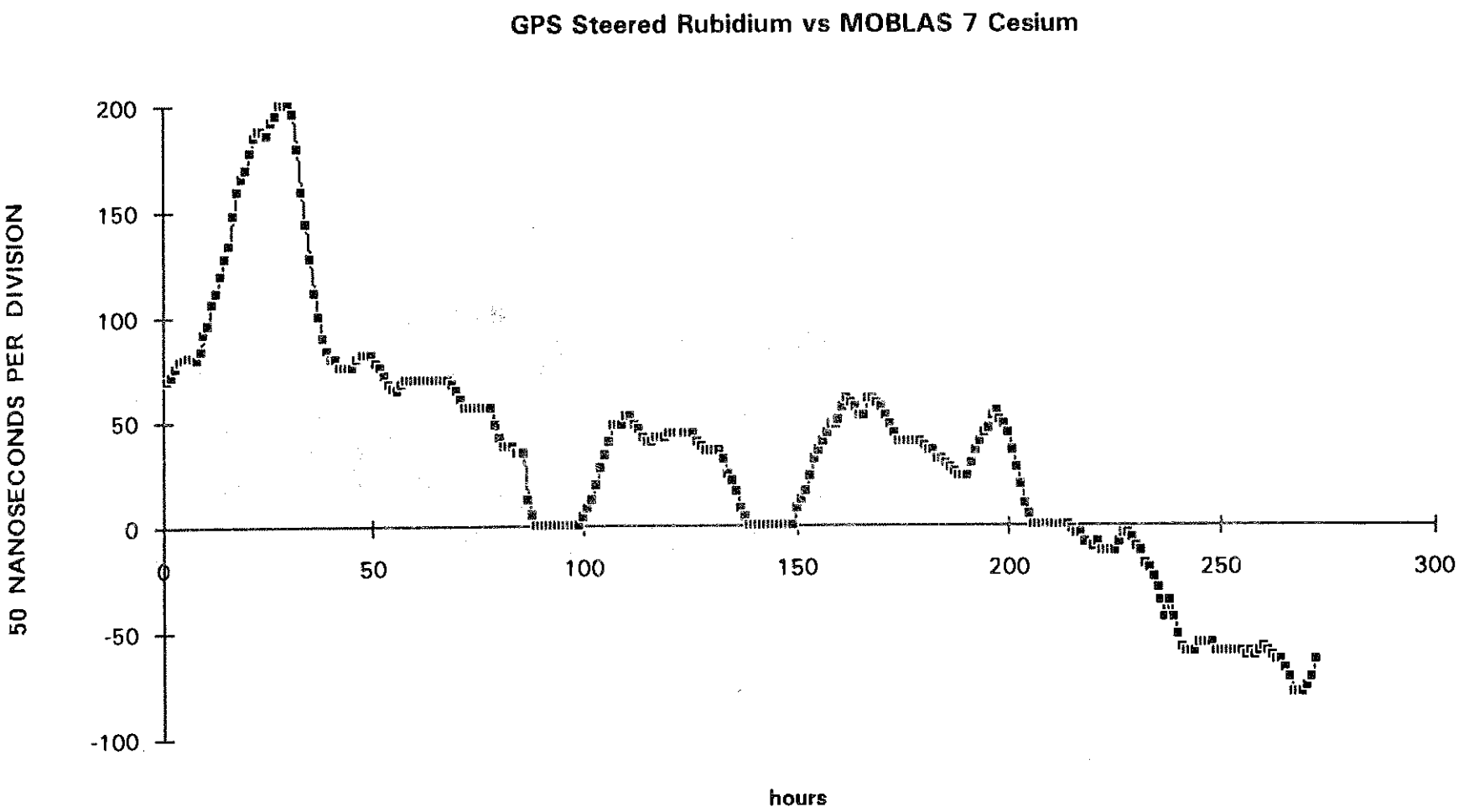
GPS Steered Rubidium vs MOBLAS 7 Cesium
50 NANOSECONDS PER DIVISION
200
150
100
50
0
-50
-100
0
50
100
150
200
250
300
hours

FIGURE 6

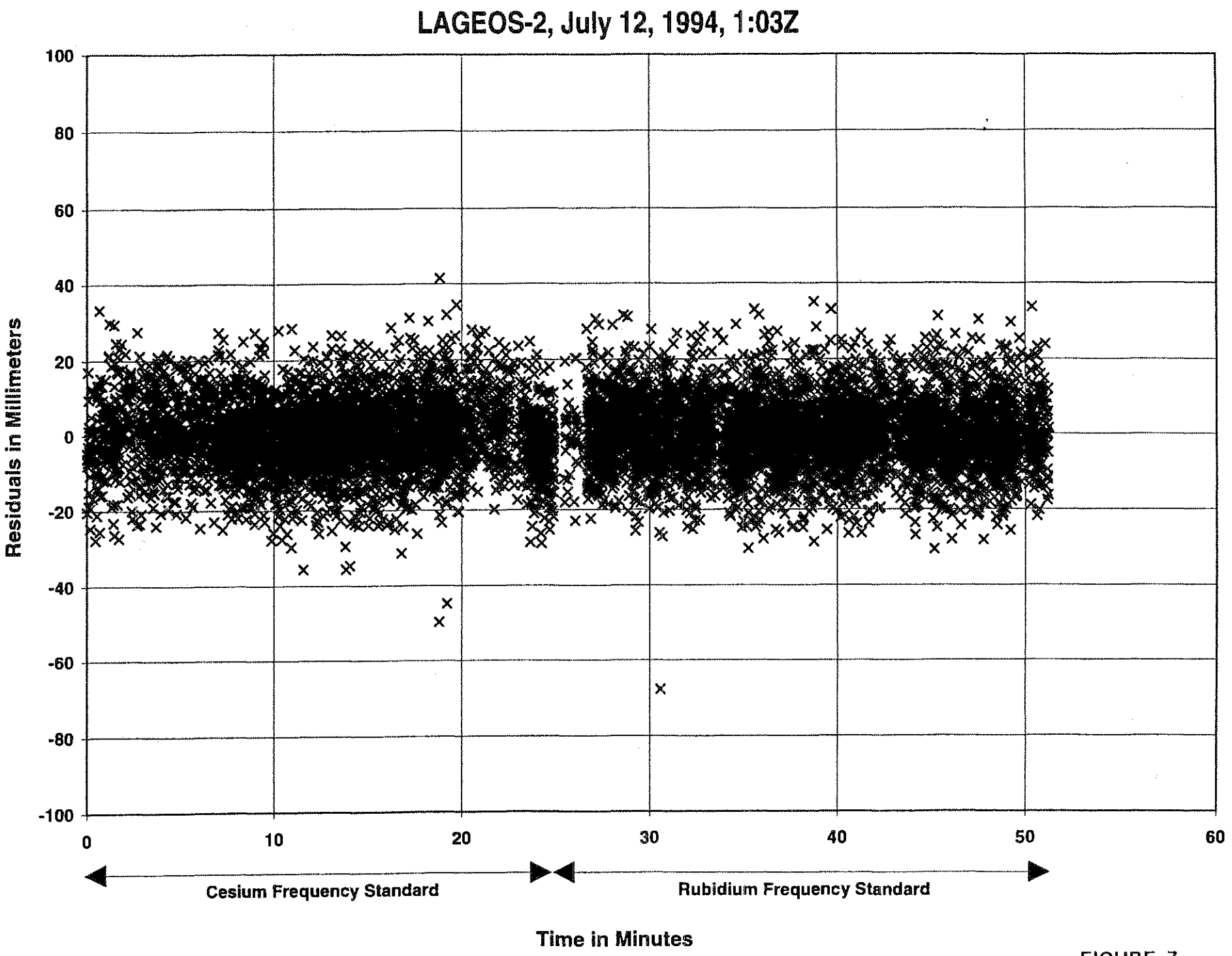
LAGEOS-2, July 12, 1994, 1:03Z
Residuals in Millimeters
100
80
60
40
20
0
-20
-40
-60
-80
-100
0
10
20
30
40
50
60
Cesium Frequency Standard
Rubidium Frequency Standard
Time in Minutes

FIGURE 7

GPS STEERED RUBIDIUM FREQUENCY STANDARD

MODEL 9515

GPS Receiver	C/A code, L1 carrier 6-channel, Parallel tracking
Frequency Accuracy	+/- 2.5 E-12 22 degrees C to 28 degrees C
Time Accuracy	+/- 500 nanoseconds to USNO Coherent to 10 MHz
Frequency Outputs	10 MHZ +10 dBm, 1 each 5 MHz +10 dBm, 4 each
Isolation output to output	5 MHz, 90 dB
Spurious	-100 dBc

Short term stability

Tau (sec)	Sigma y tau
.05	4 E-11
.10	2 E-11
.50	7 E-12
1.0	5 E-12
10	5 E-12

Phase Noise

Offset from Carrier (Hz)	SSB Phase Noise (dBc)	
	5 MHz	10MHz
.1	-70	-65
1	-90	-85
10	-120	-115
100	-145	-140
1K	-150	-150
10K	-150	-150

Time Code Output	IRIG B modulated, 1 each
Power	AC 120 volts 50-66 Hz 2.5 amps DC +24 to +32 volts 2 amps
Maximum frequency step after 24 hours operation	6 E-14 60 seconds or longer
Monitor and Control	RS-232
Size	19" x 5.25" x 19" deep
Weight	less than 40 pounds

LUNAR LASER RANGING

Chairperson : Peter Shelus

LLR at OCA
on the way to millimetric accuracy

C. Veillet, J.E. Chabaudie, D. Feraudy, P. Fridelance,
M. Glentzlin, J.F. Mangin, J. Pham-Van, E. Samain, J.M. Torre

Observatoire de la Côte d'Azur
Av. Copernic F-06130 Grasse

Introduction

Since the end of 1990, the Observatoire de la Côte d'Azur (OCA) Lunar Laser Ranging (LLR) station is operational with a YAG laser on all the lunar retroreflectors illuminated or not. In 1992 started a four year upgrade plan. Its goal is to bring the data (normal points on a lunar target) to an accuracy of 3 mm. The measurements will then be limited mainly by the atmosphere, as the tropospheric correction is not modelled better than 5 mm at a reasonable elevation.

Such an accuracy, according to the low number of individual returns acquired for a normal point (typically 25), requires strong improvements in all the domains of the hardware. We will list these domains, and explain what is he status of the upgrades at he end of 1994, one year before the end of the upgrade period.

1 - Computer/software environment

In order to improve the capabilities of the computer/software environment, the old computer (PDP 11/73 under RSX 11M+) has been replaced in 1993 by a PC 486/50MHz taking in charge all the station except the telescope. The new real time programmes can handle multi-pulse ranging to the Moon, and automated recognition of the echoes by correlation with the theoretical pattern of the returns according to the shape and separation of the pulses in the train.

Extensively used, and permanently improved with the acquisition of more experience, it provides a friendly environment for the observers. A similar effort has been made for the pointing/tracking computer ([1]).

2 - Laser

If we need a LLR normal point precision of 3 mm for 25 returns, the single shot precision has to be 15 mm, which means 100 ps on the round trip time measurement. With a pulse length of 300 ps, there is no way to reach this single shot precision. We need to move to shorter pulses. The Quantel laser has been used for years with 350 ps / 350 mJ (green), leading to a poor single shot precision. It is able to work with much shorter pulses (down to 35 ps). But if we decrease the pulse length, the amount of light sent to the Moon is decreasing also, and the number of returns in 10 mn (the duration of a normal point at our station) is too low. In order to compensate for this low energy in a pulse, we send more than one pulse. Presently, we send two pulses (180 ps) separated by 2.2 ns through a delay line on the laser table. An example of a series of echoes is given in Fig. 1.

At least four 35 ps pulses will have to be sent. Two pulses will be selected by the laser slicer (7.2 ns separation), and each will be doubled through the 2.2 ns delay line. The theoretical pattern, taking into account the respective energy levels of the individual pulses, is automatically computed, and the correlation recognition process is applied in the post processing. This process could perhaps be included in the real time acquisition programme, providing an important help to the observer.

3 - Detector

The photomultiplier (PMT) we used for years (since the early times of the ruby laser) cannot be used any longer with short pulses for a 100 ps single shot

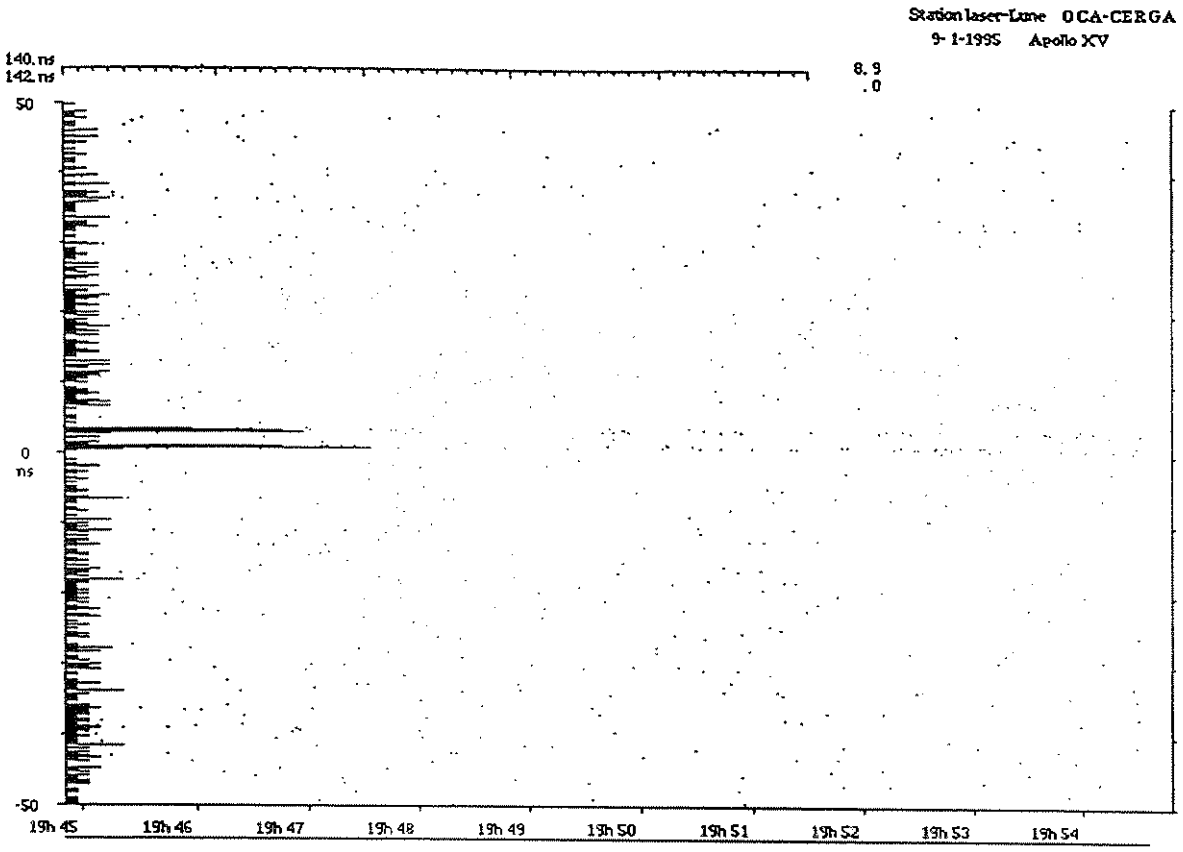

Figure 1 - A series of shots to the Apollo 15 retroreflectors. X-axis is time running for ten minutes. Y-axis is the gate centred on the predicted return time (+/- 50 ns). The two pulses of the train are seen on the histogram where are added all the events in a 250 ps bin.

precision. Its transit time is depending highly on the arrival point of the photons on the cathode, and varying a lot with the environment. It has been replaced by an avalanche photodiode (coming from the former East Germany through U. Schreiber) used in Geiger mode. Its quality is probably not sufficient for the goal we have, and further studies have been made for comparing photodiodes from various origins. More details on this point can be found in another paper ([2]).

4 - Event timer

The event timer we use now has a 50 ps resolution, and a precision/accuracy estimated to be around 100 to 120 ps. This is again insufficient for our 3 mm accuracy normal points. As we want to work with a timer instead of a counter (for other applications like time transfer), we need to replace it by another device.

Taking the opportunity of a preliminary study of a new generation time transfer experiment using light, a ground version of a space qualified event timer able to reach an accuracy better than 10 ps has been ordered to the firm Dassault Electronique which made the LASSO equipment. It should be delivered to our station at the beginning of 1995, and used with our equipment on a routine basis on the Moon and satellites.

The first tests made at the factory demonstrated that this new event timer has a precision of nearly 2 ps. The accuracy, still to be carefully measured, seems to be well below 10 ps. Our 100 ps single shot precision will then be reached...

5 - Waiting for the completion of the upgrades...

All these upgrades have to be made while trying to maintain the station operational. This is not an easy task, and it makes the work progressing slowly. These last years, the station has been quite productive, with variations according to the weather, highly variable at our site from one year to another.

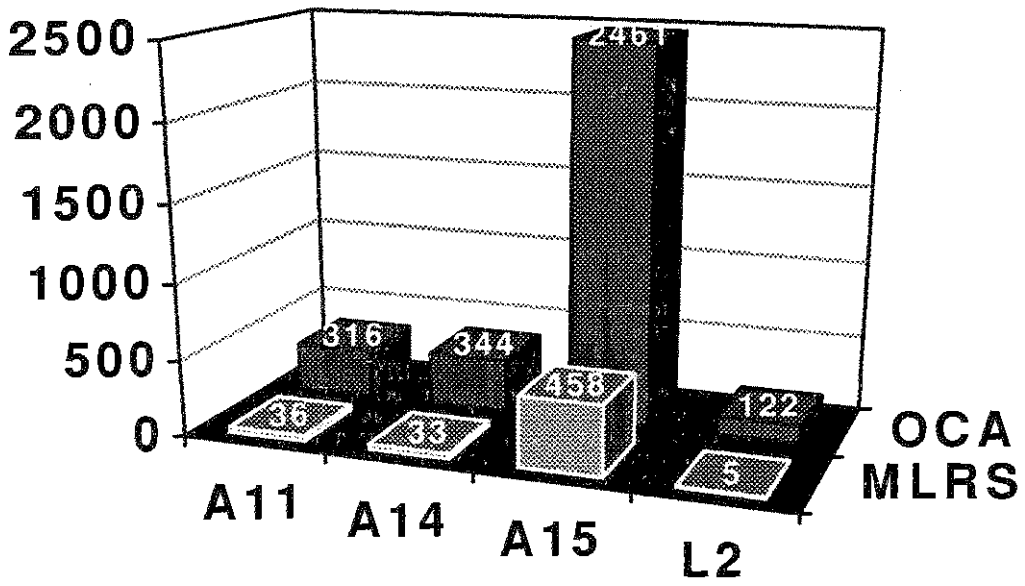

Figure 2 - The number of normal points acquired over the 1987-1994 period. MLRS (McDonald, Texas) improved its data rate in 1994 by enhancing the pointing capabilities on targets in the dark or far from known features ([3]).

The Fig. 2 shows a statistics of the data gathered at the two operational sites (McDonald, Texas, and OCA) for the 1987-1994 period.

In order to achieve a collocation between the satellite and the lunar stations at OCA, an effort has been made to make the satellite observations easy at the LLR station. Prediction software has been included, and real time capabilities added in the software (time bias, if its proximity to OCA is not the best for science. The Wettzell SLR/LLR station seems to focus mainly on satellites, in spite of the strong efforts of the crew. A few normal points have been obtained in 1994, and we hope to see more observing time spent on the Moon. Looking to the very dense SLR network in Europe, science should not miss too much some satellite passes from WLRS, but should benefit from more LLR data...

Chinese efforts, as well as Orroral coming back into the LLR business, could also contribute to a LLR network distributed all other the world. The LLR community has learned to be very patient... Let us wait for the next workshop !

6 - A Lunar Laser Ranging network sill to be done

Five years before the end of the century, and 25 years after the landing of Apollo 11 and the first retroreflector array on the Moon, there are still more retros on the lunar surface than operational stations on the Earth, and LLR is, as on the Moon, essentially a US-French affair !

As the IERS Coordinating Centre is at OCA, it is our duty to stress again the importance of LLR for all the scientific applications it has ([3]). A new station is being built in the USA for Italy, to be installed in Matera. Dedicated of the Moon as well as to satellites, it could enhance the LLR capabilities of Europe, even

Bibliography

[1] C. Veillet, J.M. Torre, 1995. Ranging the Moon with two PC's. ***These Proceedings.***

[2] E. Samain, J.F. Mangin, J.M. Torre, 1995. Detector Studies for Millimetric Lunar Laser Ranging at OCA. ***These Proceedings.***

[3] J.O. Dickey, P.L. Bender, J.E. Faller, X X Newhall, R.L. Ricklefs, J.G. Ries, P.J. Shelus, C. Veillet, A.L. Whipple, J.R. Wiant, J.G. Williams, and C.F. Yoder, 1994. Lunar Laser Ranging : A Continuing Legacy of the Apollo Program. **Science**, 265, pp. 482-490.

Lunar Laser Ranging at McDonald Observatory: An Upgrade to Start the 2nd Quarter Century

PETER J. SHELUS, RANDALL L. RICKLEFS, JUDIT GYÖRGYEY RIES, ARTHUR L. WHIPPLE, AND JERRY R. WIANT

McDonald Observatory and Department of Astronomy, University of Texas at Austin, Austin, Texas 78712-1083, U.S.A.

The MLRS has experienced remarkable success in lunar and artificial satellite laser ranging operations during its many years of operation, in spite of its relatively small receive aperture. We continue to strive, however, for a greater volume of data, together with better accuracy and precision. We are in the final stages of a three-year MLRS LLR up-grade. Lunar data volume in 1993 and 1994 is almost triple that obtained in 1992; the number of UT0 Earth rotation points has increased by more than a factor five; and, for the first time since 2.7-m lunar operations in the mid-1980's, we are obtaining multi-corner data, i.e., ranges to more than one lunar surface retroreflector during a single observing session. This paper describes this recent upgrade and summarizes the effects on the lunar data .

INTRODUCTION

The McDonald Laser Ranging Station, the MLRS (Shelus 1985), was built to range to artificial satellites and to the Moon. It was constructed to replace the McDonald Observatory 2.7-m lunar system (Silverberg 1973), used until the mid 1980's. The MLRS was designed around a 0.76-m x-y mount Cassegrain/Coudé reflecting telescope and a short pulse, frequency doubled, 532-nm, neodymium-YAG laser with appropriate computer, electronic, meteorological, and timing interfaces. The station, initially placed in the saddle between Mt. Locke and Mt. Fowlkes at McDonald Observatory, near Fort Davis, Texas became operational in 1983. Wind tunneling effects in and around this saddle site had produced very serious problems with atmospheric seeing and the MLRS was moved to the top of Mt. Fowlkes in early 1988.

MLRS observing emphasis has always been placed upon ranging to artificial satellites (see Figure 1) but the Moon has remained an important part of routine operations (Shelus 1987). The MLRS's epoch timing system makes all targets equal to the observer and a crew will routinely range to virtually all targets from ERS-1 to the Moon during a single shift. The differences among targets are the angular speed of the target across the sky and the return signal strength. Of course, low targets move quickly and high targets move slowly. Return signal strength is dictated by the inverse-fourth-power of the distance, laser beam divergence, atmospheric effects, and telescope tracking. It is important to realize that the return signal strength ratio, neglecting all parameters except the distance, for a near-Earth artificial satellite and the Moon is something like 3×10^{12}. It is more than a trillion times more difficult to range to the Moon than it is to range to Topex/Poseidon.

In spite of the handicaps of low signal strength and small receive aperture, the MLRS has enjoyed success in its lunar laser ranging (LLR) observations (Shelus et al, 1993a), and the computation of lunar orbit and Earth orientation information (Whipple et al 1991). We have always striven for increased numbers of observations as well as better accuracy and precision. We can increase MLRS LLR data volume in at least three ways: 1) spend more time on target; 2) transmit more energy; 3) increase receive aperture. The last three years have been spent in upgrading the MLRS, particularly as far as LLR is concerned. This paper summarizes that work.

MLRS LLR-RELATED UPGRADES

x-y Offset-Guiding Stage

The initial LLR up-grade at the MLRS was the installation and integration of an x-y offset guiding stage. As used for LLR operations at the MLRS, an offset guiding stage allows an observer to guide on a sun-lit, off-axis lunar surface feature, or, perhaps, even a star, while the retroreflector is on the shadow side of the lunar terminator. Not only does this provide for a greater number of observing opportunities during a lunation, ranging to a retroreflector in the dark produces virtually noise free data. The MLRS instrument (Shelus et al, 1993b) is a two-axis translation stage that provides for the simultaneous mounting of two electronic cameras, with turning optics to direct the telescope's Cassegrain beam to either of the cameras. The cameras are selectable under computer control or manually. A DC servo motor/encoder combination drives each axis of the stage in a range 0-8 mm/sec and each axis is directly encoded using digital linear encoders. The positioning of each stage is accurate and repeatable to 5 microns and each has a travel of more than 125 mm along each axis, centered on the optical axis. The electronics control package includes a dedicated PC-type computer, a motor controller board inside the PC, and all electronic and computer interfaces and controls. Software provides a closed servo loop between the encoders and the motors and communicates with the external control computer through an ordinary serial port. Routine operation began in the spring of 1993 with a dramatic increase in the amount of LLR data obtained.

Optical UpGrades

A typical outgoing MLRS laser pulse contains some 3×10^{17} photons. In lunar mode, only a few of them make it back to the telescope, to pass through the receive system. At the MLRS a typical lunar return rate is a few signal photons per minute. This mandates the use of single photoelectron detection devices and as large an optical throughput in the green as possible. With the large number of noise sources at the single photon level it is impossible

to identify a returning photon from the moon without adequate filtering, both physical and mathematical. Range gating provides a temporal filter and a pin-hole aperture provides a spatial filter. It is vital to also use a spectral filter, to allow only the proper color photons to pass through to the receive system. A spectral filter must be as narrow as possible in wavelength to eliminate as many noise photons as possible, but must adequately transmit as many proper photons as possible. Spectral requirements change with lunar phase and local sky conditions. We specified and purchased a third spectral filter, of intermediate specifications between the two filters already being used. We received this new filter in the spring of 1993 and immediately placed it into service. Further, in August 1994, because of aging and laser induced damage over the many years of observing operations, the telescope's #3 mirror, a dichroic, was replaced. We believe that the added scheduling flexibility and the extra energy throughput that this new filter and #3 mirror provided, during changing lunar phases and local sky conditions, resulted in a significant increase in the amount of LLR data observed at the MLRS.

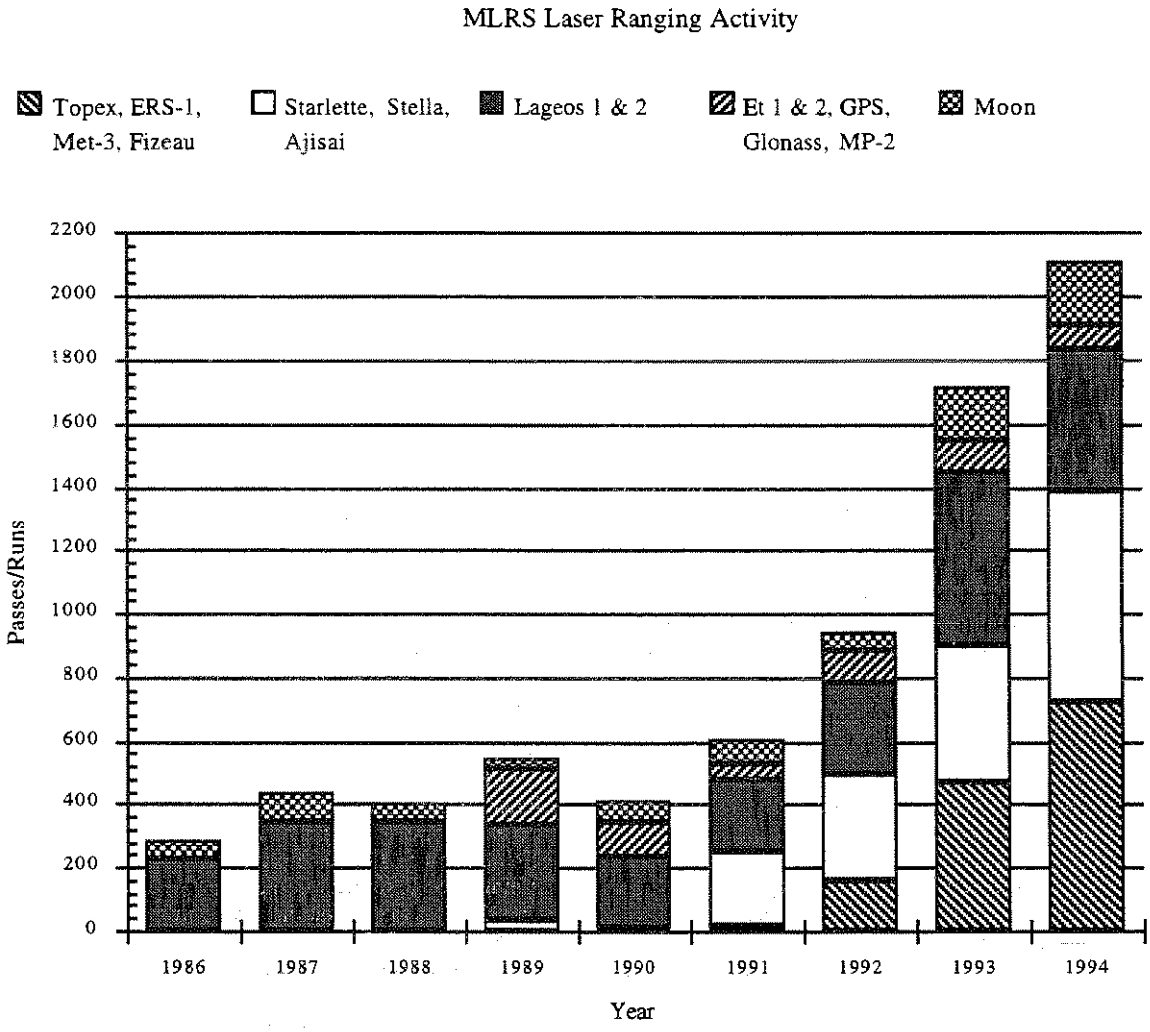

Figure 1. MLRS artificial satellite and lunar laser ranging data throughput.

Auto-Guiding and Image Enhancement System

Certainly, the longer the LLR transmitter/receiver system remains on target during laser firing, the more returns will be detected. Our experience with the MLRS is that present pointing and tracking stability requires intensive manual guiding to keep the telescope aimed at a specific target. Providing the operator with guiding tools or even removing the operator completely from manually guiding the telescope will dramatically increase time on target. In the spring of 1993, we specified and contracted for purchase what is now called the MLRS Auto-Guiding and Imaging

System (AGIS). The AGIS is an integrated hardware and software system that accepts real-time, video signals as input, i.e., a highly magnified image of a small portion of the lunar surface, or a stellar or artificial satellite point-source image. The AGIS performs real-time image processing allowing the user to select among various levels and types of image enhancement. Further, the AGIS produces raw and filtered tracking error signals, that under user selection, are communicated to the MLRS control computer for guiding control. We issued the AGIS construction contract in March 1994. The vendor held a Critical Design Review in May 1994. We expect delivery of the unit at McDonald Observatory in early 1995. We expect that there will be several additional months of effort from MLRS hardware and software personnel before the AGIS can be totally implemented and integrated into the routine observing operation. We expect a marked increase in the amount of MLRS LLR data.

Avalanche Photodiode Detector

Both the French (CERGA) and the German (Wettzell) laser ranging stations have the capability of ranging to the Moon. The Wettzell group has been involved in the design and construction of an avalanche photo-diode (APD) detector. Such an APD detector, now in use at the French CERGA LLR station, has exhibited a significant increase in sensitivity as well as improved accuracy and precision of CERGA LLR data. Another type of avalanche photo-diode device is being used for artificial satellite laser ranging operations in the United Kingdom. In the spring of 1993, we entered into a cooperative effort with our German colleagues to build such an avalanche photo-diode detector for use at the MLRS for LLR operations. Jerry R. Wiant, chief engineer of laser ranging operations at the MLRS, traveled to Wettzell, Germany in late November 1993. During a several week stay at the Wettzell laser ranging station, Wiant became familiar with the intricacies of the APD detector and participated in the design of a unit that could successfully interface with the MLRS's unique hardware and software systems. He brought a completed unit back to McDonald Observatory for integration within the MLRS lunar operation. Final implementation at the MLRS is being currently being performed (see Wiant's paper in the Workshop's Proceedings). We expect completion in early 1995.

Disciplined Oscillator

The present MLRS station clock is a commercial Hewlett Packard cesium-beam standard. These timing units are extremely expensive and must undergo considerable preventive maintenance on a time-critical basis. With the presence of a Global Positioning System (GPS) timing receiver on site at the MLRS, we have been considering a move to a more cost-effective manner, with much lower maintenance responsibilities, to obtain more precise station timing. A so-called disciplined oscillator can provide excellent short-term timing stability, while a suitable GPS receiver is used as a fly-wheel to provide good long-term timing stability. A significant cost and time savings in station operation and maintenance could result, with a reasonable improvement in timing accuracy and precision.

MLRS Control Computer

Finally, we are in the midst of replacing the MLRS's 15 year-old Data General NOVA control computer system with a LynxOS based, X-windows, real-time Unix system running on PC hardware. This is being coordinated with similar upgrades at other NASA-based laser ranging systems. It will create a system with compatible hardware and software architecture in an open-systems (POSIX) environment. The approach allows a maximum amount of software portability and sharing. Data from several satellite passes has already been acquired with the new system in shake-down mode. We expect complete conversion to the new system by early 1995.

MLRS LLR DATA RATES

During the past three years, McDonald Observatory laser ranging operations has pursued a significant and substantial LLR up-grade at the MLRS. The effort has enjoyed a truly remarkable success. Lunar data rates for each year 1993 and 1994 are triple those obtained in 1992; the number of UT0 Earth rotation points has increased almost a factor six; and, for the first time, since 2.7-m lunar operations in the mid-1980's, MLRS LLR operations are obtaining, on a routine basis, multi-corner data, i.e., ranges to more than one lunar surface retroreflector during a single observing session. These increases are a direct result of the optical improvements and the x-y offset guiding stage that were placed into operation during the past two years. The implementation of the MLRS auto-guiding and image-enhancement (AGIS) system and the avalanche photo-diode (APD), in 1995, will accomplish at least as much improvement in MLRS lunar data volume. In addition, the exceptional noise qualities of the APD are expected to bring about a factor two or more increase in data accuracy and precision.

To fully understand the tremendous advances that have been accomplished under this MLRS up-grade effort, it is important to recognize how the MLRS now compares with the French LLR effort, the flagship of the lunar network. To make such a comparison, it is vital to put the MLRS and the CERGA stations in their proper contexts. The French lunar station is essentially a dedicated lunar facility with little or no artificial satellite laser ranging (SLR) commitments. On the other hand, the MLRS is one of the premiere SLR stations in the world. Further, the MLRS has only 25% of the collecting area and only 50% of the laser power of the CERGA station. Several ways of comparing the MLRS to CERGA, and to itself, in lunar capability, appear in Table 1. In every statistic referenced, the up-graded MLRS looks excellent in its own right and compares very well with the French LLR station. In short, while being one of the most prolific producers of SLR data in the world, the MLRS, in 1993 and 1994, also produced about 1/3 the lunar data as the lunar dedicated CERGA station. Perhaps an even more telling statistic is that the MLRS gathered lunar data on up to 86% as many nights that CERGA did. Thus, the multi-faceted MLRS has accomplished a great deal vis-a-vis LLR operations with the LLR upgrade, while still maintaining all of its regular SLR observing responsibilities. Of even greater importance is the fact that several additional up-grades

remain to be done for the MLRS, i.e., a more sensitive and noise free photon detection device and a sophisticated lunar surface automatic guiding system.

Figure 2 provides another view of the effects of the recent improvements of the MLRS LLR data gathering system. The total McDonald Observatory LLR data set comprises lunar observations spanning two-and-a-half decades. For the first 16 years, the 2.7-m system was used; since then, the MLRS. There were several months of overlapping data in 1985. Further, the data has been obtained successively at three different locations: 1) the 2.7-m system on Mt. Locke; 2) the MLRS in the saddle between Mt. Locke and Mt. Fowlkes; and 3) the MLRS on Mt. Fowlkes. The figure summarizes, on an annual basis, the number of McDonald normal points from all of the lunar retroreflectors. Also included is the annual weighted root-mean-square, rms, of the post-fit residuals from our own analyses of these observations. To insure a large enough sample, to be statistically significant, these rms values are calculated from ranges to the Apollo 15 retroreflector only. As can be seen, the 2.7-m system routinely produced more than 200 LLR normal points per year, with a weighted rms of 9-15 cm. When the MLRS first came on line, crew scheduling logistics caused the number of 2.7-m system LLR normal points to drop. When the MLRS attained lunar capability and the 2.7-m lunar system was de-commissioned, the McDonald LLR data throughput dropped to somewhat less than 100 normal points per year. However, the weighted rms of that data also dropped to something like 3-5 cm.

Table 1.

MLRS/CERGA Comparison (1992-1994)
Lunar Laser Ranging Data Throughput

		MLRS			CERGA		MLRS/CERGA	
		1992	1993	1994	1993	1994	1993	1994
LLR Normal Points	Apollo 11	-	3	25	53	55	6%	45%
	Apollo 14	-	8	17	53	44	15%	39%
	Apollo 15	58	151	160	433	499	35%	32%
	Lunakhod 2	-	1	3	12	17	8%	18%
	Total	58	163	205	551	615	30%	33%
Minutes of LLR Data	Apollo 11	-	28	382	561	484	5%	79%
	Apollo 14	-	141	242	485	383	29%	63%
	Apollo 15	757	1,953	2,122	4,156	4,603	47%	46%
	Lunakhod 2	-	3	40	105	142	3%	28%
	Total	757	2,125	2,776	5,307	5,612	40%	49%
Nights when LLR Data was Taken	Apollo 11	-	2	16	27	23	7%	70%
	Apollo 14	-	5	12	26	17	19%	71%
	Apollo 15	23	56	61	75	71	75%	86%
	Lunakhod 2	-	1	3	11	9	9%	33%
UT0 points		5	26	30	49	44	53%	70%

It can be seen easily that the use of two different ranging systems and two different observing philosophies has led to very different quantities and qualities of McDonald LLR data. The 2.7-m system was a lunar-only station that was built around a Korad 3 joule/pulse, 3 nanosecond pulse-length ruby laser, firing at 1/3 hertz. The epoch timing system resolution was approximately 125 picoseconds. However, the present MLRS system is a joint lunar/artificial satellite station that is built around a Quantel 120 millijoule/pulse, 200 picosecond pulse-length Neodymium-YAG laser, firing at 10 hertz. Its epoch timing system precision is approximately 25 picoseconds. Further, the 2.7-m system had a much stronger lunar return signal by virtue of its 2.7-m receive aperture, as opposed to the 0.76-m receive aperture of the MLRS. Moving laser operations from the 2.7-m system to the MLRS should have produced a reduction in the volume of lunar data. The trade-off, of course, which made the transition acceptable, lay in the accuracy of the MLRS data. Laser ranging data accuracy, to first order and with everything else being held constant, scales inversely with the pulse length of the laser. The much shorter pulse length of the MLRS's Nd-YAG laser has led to almost a factor of four improvement in the accuracy of the modern MLRS ranges. Since the total weight of a set of observations scales linearly with improvements in data accuracy, but only as the inverse square of the number of observations, the current MLRS system data is scientifically much stronger than the 2.7-m system, in spite of its lower volume. The significant point is that now, with the various MLRS LLR-related up-grades, not only has the accuracy and precision of the LLR observations been mightily improved, the LLR data volume of the MLRS is now approaching that produced with the 2.7-m system.

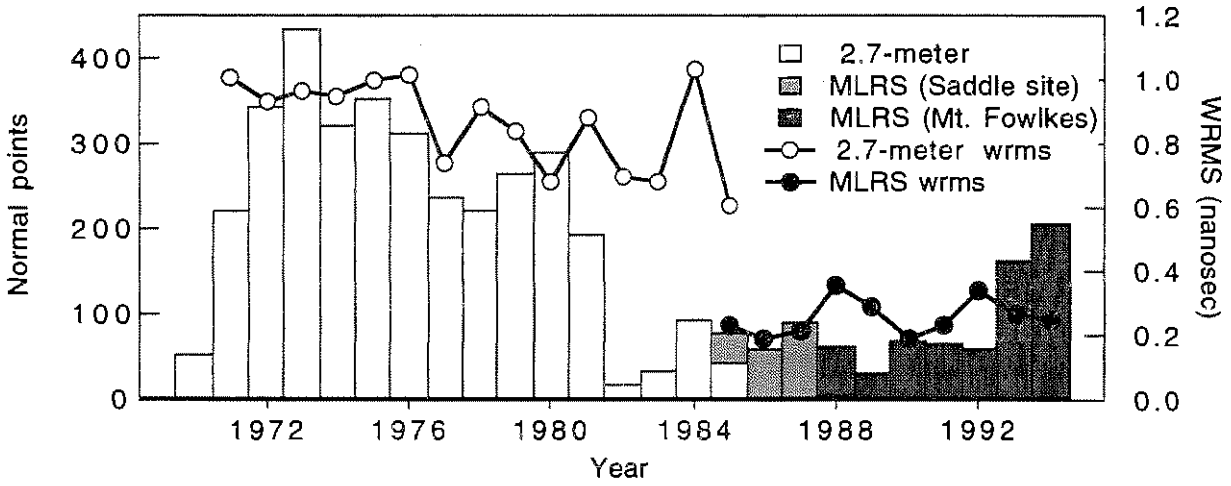

Figure 2. McDonald Observatory LLR Data Quantity and Quality

CONCLUSION

It must be clearly understood that the much-improved MLRS LLR/SLR station and the CERGA LLR station constitute only a bare minimum network that is required for the best use of the LLR data type. More LLR stations are a necessity. Certainly, as a minimum, more stations will improve observational coverage, will tend to eliminate correlated weather data drop-outs, and will allow the easier determination of systematic errors. There are also many important scientifically related reasons for multiple station LLR data (Dickey et al, 1994).

It is especially noteworthy that we have just celebrated the 25th anniversary of the first Apollo manned placement of a retroreflector package on the lunar surface. The lunar laser ranging experiment is the only remaining active Apollo experiment that is obtaining new data. And, it is still marching at the forefront of science. During these times of extremely tight budgets, it is extremely important to point to examples of the efficient and cost-effective progress of research over the years. The lunar laser ranging experiment, and the science it is able to accomplish, should be a source of special pride to the entire scientific community in general. We hope that the MLRS will continue to improve and will continue to provide a constant stream of more and better LLR data into that scientific community.

Acknowledgments. We acknowledge with gratitude grant and contract support from the National Aeronautics and Space Administration and the U. S. Naval Observatory.

REFERENCES

Dickey, J. O., Bender, P. L., Faller, J. E., Newhall, X X, Ricklefs, R. L., Ries, J. G., Shelus, P. J., Veillet, C., Whipple, A. L., Wiant, J. R., Williams, J. G., and Yoder, C. F. 1994, Science, Vol. 265, p. 482

Shelus, P. J. 1985, IEEE Trans. on Geosci. and Rem. Sens., Vol. GE-23, No. 4, p. 385

Shelus, P. J. 1987, Discovery, Vol. 10, No. 4, p. 33

Shelus, P. J., Ricklefs, R. L., Whipple, A. L., and Wiant, J. R., 1993a, AGU Geodynamics Series, Vol. 25, p. 183

Shelus, P. J., Whipple, A. L., Wiant, J. R., Ricklefs, R. L., and Melsheimer, F. L., 1993b, NASA Conf. Publ. 3214, p. 10-1

Silverberg, E. C. 1974, Appl. Opt., Vol. 13, p. 565

Whipple, A. L., Györgyey-Ries, J., Ricklefs, R. L., Shelus, P. J., and Wiant, J. R. 1991, IERS Tech. Note 8, p. 87

Ranging the Moon with two PC's

C. Veillet, J.M. Torre

Observatoire de la Côte d'Azur
Av. Copernic F-06130 Grasse

Abstract

This short contribution will describe briefly the software/hardware environment of the Lunar Laser Ranging station at OCA. Its originality comes from the two processors (PC's) used one for the telescope, and the other one for the real time monitoring of the ranging operations. Running under DOS without multitasking, it proved to be efficient, reliable and easy to implement and modify.

Introduction

The rapid development of computers and workstations using multitasking operating systems leads very often to the implementation on a single machine of huge programmes for taking care of the tracking, ranging and processing tasks to be performed in laser ranging. Such implementations tend to be very sophisticated. Most of the time, they are efficient, but difficult to debug, and also to modify.

The choice made twenty years ago at the OCA (Observatoire de la Côte d'Azur) LLR station has been maintained in spite of the developments mentioned above : a computer is devoted to the telescope, and another one to the real time operations of the station, and the post processing of the data.

1 - Why two computers ?

The telescope of the OCA LLR station is a good 1.5-m astronomical telescope, which can be used for various observations. It is mainly devoted to laser ranging, but other experiments are performed :

- Observations of stellar occultations by the Moon is the oldest one. By observing the light curve at the immersion or the emersion, one can see diffraction fringes which pattern allows, if the star has an apparent diameter high enough, to measure it. One can also detect very close binary stars. For this kind of observations, one needs very good pointing/tracking capabilities, especially for the emersion

where one follows a star without seeing it (it is behind he Moon).

- Observation of mutual phenomena between satellites of Jupiter and Saturn are based also on photometric observations of mutual occultation or close approach. The telescope follows Jupiter and is offset onto the observed satellite.

- Adaptive optics feasibility using an artificial star (laser focused in the atmosphere). Again, one needs a very good optics, and a good tracking of the observed star. Automatic guiding when tracking can be a necessity.

These applications obliged us to develop specific software, not related to any laser ranging operation. The dedicated computer made possible easy implementations of new features, easy to do as the real time ranging software is not embedded in the tracking one.

When the telescope is used for these no-ranging astronomical observations, the observers can then use a very simple system, friendly interfaced. In the same time, the crew can perform internal calibrations, tests on the timer or other tasks on the station computer.

For automatic ranging, the station and telescope computer can be linked through a parallel line. The telescope can then be driven by the ranging software. The station is running in a multi (two) processor environment (the two PC's...).

2 - The telescope computer

The first computer used for the telescope has been a Data General Nova, with very basic routines for the pointing (predictions of the requested target entered through a punched tape...). Later on, linked to the station computer (Data General Eclipse), it received the pointing data directly, but using the telescope was not very friendly.

In 1984, we replaced the Nova by a 8088 based computer (Victor Technologies). The telescope user was really able to use the telescope interactively for any astronomical use. The predictions for lunar pointing were still received from the station computer, but all the basic astronomical routines were implemented on the Victor. It has been a key evolution in the pointing capabilities of the telescope. Automatic generation of very accurate positions of stars taken from various catalogues allowed to map the mount errors with an overall rms of 1 to 2 arc-seconds on all the sky. It made easy the acquisition of retroreflectors in the dark on the Moon surface.

In 1991, the Victor was replaced by an IBM PS/2. The prediction software has been implemented very soon after, giving to the telescope the full capabilities of standing alone for any astronomical use, including LLR. CCD automatic pointing/centring of stars through an image digitizing board made possible automatic ranging sessions. SLR prediction software, and pointing/tracking upgrades were added in 1994. The old IBM has been changed for a 80486/66MHz PC in mid-1994.

3 - The station computer

Back to the beginning of the LLR operations at CERGA in 1980, the station computer was a Data General Eclipse, which has been used for all the ruby operations, up to 1985. Before moving to a YAG laser and a completely different mode of real time operations (10 Hz firing rate instead of one shot every 6 seconds), the Eclipse has been replaced by a DEC PDP 11/73 under RSX 11M+. The new software in this multitask environment has been implemented and tested with the ruby for months before

switching to YAG. This PDP has been the station computer up to 1993.

The low speed of the CPU, joined to high maintenance costs and long compilation times when modifications had to be made incited us to move to a more modern computer. The experience acquired with the telescope monitoring, and the increasing capabilities of the PC's, led us to the choice of a PC (80486 - 50MHz) under DOS. The operations to be made even in real time are in sequence, and, through a careful analysis of the PDP real time software, it was possible to implement a succession of routines chained through a batch file. For the observer, a single programme seems to be running for all the night. Function keys and the mouse are used to take any desired action.

This single task approach could seem more difficult at the beginning, as it obliges to know what has to be done at which moment through a careful analysis of the requirements. Multitasking should not allow to miss this part of the software work. And when done, this analysis shows that there is no need for multitasking, especially if the telescope control is taken by another processor. This approach makes easy any modification, and prevents from any conflict in interrupts, and any trap of the system. Debugging is easy, as one knows what is running at any moment in the CPU.

The station and the telescope computers are now similar at the OCA LLR station. They use the same boards for interfacing with the equipment, and the same basic routines. This standardization in software and hardware enhances the reliability of the station.

Conclusion

The OCA PC-based telescope monitoring software has been, and will be, used for other telescopes. Its very simple hardware and software architecture makes it very easy to modify by its owner. It is installed on the 1.8-m South Korean telescope at Mt. Bohyun. It will also equip the French Solar telescope THEMIS (to be erected in the Canary Islands), and the new Zimmerwald laser and astrometric telescope.

The two-PC's system has been running now for nearly two years, with many changes made easily in the ranging modes (multiple pulses, satellite ranging added, ...). It is a good alternative to bigger and more sophisticated systems, providing simplicity and low acquisition and development costs...

Operating the APD SP114 at the LLR-Station in Grasse

Ulrich Schreiber
Forschungseinrichtung Satellitengeodäsie
Fundamentalstation Wettzell
D - 93444 Kötzting
Germany

Karl Heinz Haufe
Institut fuer Angewandte Geodäsie
Aussenstelle Wettzell
D-93444 Kötzting
Germany

Jean Francois Mangin, Jean Marie Torre and Christian Veillet
Observatoire de la Cote d' Azur
Avenue Copernic
F - 06130 Grasse
France

Abstract

At the Wettzell Laser Ranging System [1] (WLRS, Germany), the Avalanche Photodiode SP114[1] was operated successfully at a wavelength of 532 nm as well as at 1.064 μm. The detector was found to have a high sensitivity, a high accuracy and was convenient to use. To analyze it's sensitivity in detail, a common experiment was planned and carried out, at the Lunar Laser Ranging Station in GRASSE [2] (France). This ranging experiment to the most demanding targets allowed a direct comparison between the well known characteristics of the RCA 31034a photomultiplier and the SP114. Under varying configurations, measurements were taken from all lunar targets. It was found, that the SP114 had a sensitivity and accuracy far above the photomultiplier.

1. THE EXPERIMENTAL SETUP

Figure 1 outlines the optical receive path of the LLR- Station GRASSE. The field of view of the 1.5 m aperture telescope is focused onto a diaphragm for spatial filtering. A dichroic mirror separates the two different laser frequencies used, before the beam is collimated with a lens. The parallel beam then passes a Fabry - Perot spectral filter having a high efficiency

[1] manufactured by: Silicon Sensor GmbH, Ostendstr. 1, D-12459 Berlin

of 80 % and a bandwidth of 0.12 *nm*. To select the laser wavelength only, a 8 *nm* wide filter around the wavelength of 532 *nm* (efficiency 70 %) is passed, before the beam is focused onto the cathode of the photomultiplier RCA 31034a. There is the same optical assembly behind the dichroic mirror, in order to do the filtering and imaging onto an avalanche photodiode (RCA 30954e) for the infrared part of the signal. In the here reported common experiment, this detector was substituted against the avalanche photodiode SP114 which was placed into the "Geiger mode" [3]. As both detectors under this comparison were operated on the second harmonic frequency of Nd:YAG, the following changes to the optical setup had to be made. The dichroic mirror was replaced by a 1 to 1 beamsplitter cube. However, it was found, that the beamsplitter showed a ratio of 1 to 2 in favor of the PMT. The reason may be the fact, that due to lack of space, the incident beam on the splitting cube could not be collimated. To compensate for this, the various spectral filters and the two Fabry-Perots were combined in a way, that the spectral transmission along each path was about the same. In figure 2 the setup is outlined.

2. SIMULTANEOUS RANGING WITH BOTH DETECTORS

After all the components were aligned carefully, LLR- measurements preferably to Apollo 15 have been carried out. The following results were obtained (Table 1). To judge the perfor-

First night of observations (14. - 15. Oct. 1992)

# of Series		1	2	3	4	5	6	7	8	9	10	11	12	13
Identified	PMT	16	0	18	0	0	16	19	20	18	0	22	0	14
Echoes	APD	29	29	38	30	55	45	48	97	68	64	35	35	46

Second night of observations (17. - 18. Oct. 1992)

# of Series		1	2	3	4	5	6	7	8	9	10	11	12	13
Identified	PMT	0	0	12	0	7	0	8	18	3	15	11	0	8
Echoes	APD	12	18	22	13	25	41	33	68	16	34	38	24	31

Second night continued

# of Series		14	15	16	17	18	19	20	21	22	23	24
Identified	PMT	0	8	7	0	0	0	0	0	0	0	0
Echoes	APD	22	18	19	7	17	18	7	27	27	39	33

Table 1: Amount of lunar echoes per series for both of the two simultaneous operated detectors for 2 nights. Each series consists of a 12.5 minute interval of firing at the lunar target at 10 shots per second.

mance of the experiment, the results achieved with the PMT are analyzed first. Under normal ranging conditions around 50 echoes per sequence (12.5 min) are obtained on average. Extremely good or bad series are not considered in this raw estimation. The beamsplitter and the different filter arrangement caused the signal level to go down to a level of 25 % of the usual value. This was found, when the total transmission of the modified system had been measured. Therefore a similar decrease in the average return rate from 50 to 12 echoes

per sequence was expected and actually found. Hence, it could be concluded, that the system worked properly after the rearrangement. Now, looking at the avalanche photodiode (APD) port of the receive section, one can see, that each sequence contained more lunar echoes than the parallel recording PMT. On average a three times higher return rate was found in spite of the fact, that the entire system's transmission was a little in favor of the PMT. As the lunar echoes were recorded simultaneously, it can be concluded, that there was no disadjustment in the optical alignment of the two receive branches with respect to each other. In figure 3 the range residuals of series 8 of the first night is plotted. During the sessions of this night the used lunar reflector was illuminated by the sun. A higher noise level of the APD measurements is obvious, when comparing the plots of the different detectors. This has two reasons. The spectral filter, blocking unwanted light in front of the APD was a little broader, than the one in front of the PMT and the APD was cooled down to 0° C only. This caused a higher thermal noise from the avalanche diode. After that, the operating temperature of the APD was lowered down to $-8°$ C, which reduced the noise considerably. It was not possible to lower the temperature further down to $-20°$ as was desired, because there was no suitable power supply available. However this is no general problem. Ranging to a target being in the shadow the measured range residuals (2. night, series 8) are plotted in figure 4. Comparing figure 3 to figure 4 one can see the considerable decrease of the collected noise in the dataset of the latter series. Analyzing the histogram of repeated range measurements to a local calibration target, it was found, that the scatter of the PMT was higher than that of the APD. The following values were obtained:

$$\sigma_{PMT} = 0,58ns$$
$$\sigma_{APD} = 0,28ns$$

This result is caused by a faster signal risetime and less jitter in the APD operated in the Geiger mode.

3. OPERATING THE AVALANCHE DIODE RCA 30902 TC

Once several comparison measurements have been carried out between the SP114 avalanche diode and PMT, the APD was removed and replaced by another diode type RCA 30902 TC. The advantage of the RCA 30902 TC is the direct mounting of the silicon chip onto a peltier element. So the cooling of the unit is fast, effective and does not show heat conducting problems. During operation the thermal noise level was very low, as expected. As the weather conditions were not favorable, there are not so many sequences of measurements carried out as with the SP114. The quantum efficiency of this detector is lower than that of the SP114 too. There is only one sequence, which is good for comparison. The number of echoes obtained are 8 for the PMT and 10 for the APD. In the other 15 sequences taken, there are no definite echoes identifiable. So one can conclude, that this APD and the PMT are about equal with respect to sensitivity. The distribution of the calibration measurements show, that with regard to the accuracy ($\sigma_{RCA} = 0,45ns$) the RCA diode is placed between SP114 and PMT. However the thermal properties of the 30902 TC are excellent.

4. LUNAR RANGING WITH A SINGLE DETECTOR

In a last experiment, lunar ranging was performed, where the ranging system was operated in its usual way, using the PMT as a detector. After acquiring a few series with lunar echoes, operation was switched to the SP114 diode. The average difference in the number of echoes is a good estimation for the sensitivity of the detector. This allowed the setup of an ranging environment, which was optimal for each detector. The left part of fig. 5 shows a typical result, obtained with the PMT. All the four sequences measured at night time (darkness) contained 4 to 5 echoes. After that, the receive path was adjusted for the SP114 and two more sequences of LLR- measurements could be tracked. The result is shown on the right part of fig. 5. The noise level is quite high, which was mainly caused by light from the rising sun. However the total of 50 lunar echoes gathered in this sequence was beyond all expectations.

5. CONCLUSION

In order to analyze the performance of the detectors from the returns, obtained from the moon, the data was superimposed over the calculated mean for each series. Figure 6 shows the final result. The solid bars are corresponding to all the identified echoes from the PMT, while the open bars represent the distribution of the APD returns. Filtering both data sets at a 2.5σ criterion, an rms of $400ps$ for the PMT and $360ps$ for the APD are obtained. This is caused by the higher noise level of the APD. However, when a 2σ filter is applied, the rms changes to $360ps$ for the PMT and $270ps$ for the APD. Looking at figure 6 again, the better distribution of the APD returns becomes obvious. On average 9 returns went into forming a normal point for lunar ranges from the PMT data, while 22 returns could be used in the case of the APD.

The usage of the avalanche photodiode SP114 in Geiger mode at the lunar station GRASSE showed, that the diode was more sensitive, than the normally used PMT. The SP114 also improved the accuracy of the ranging measurements. As a sideeffect the APD proofed to be the more stable detector, which was attributed to the unit being thermally stabilized with the cooling system.

References

[1] U. Schreiber, K. H. Haufe, R. Dassing, "Measuring Atmospheric Dispersion With WLRS In Multiple Wavelength Mode", *Proceedings Of 8th International Workshop on Laser Ranging Instrumentation*, (1992)

[2] Ch. Veillet, E. Bois, J. E. Chabaudie, C. Dumoulin, D. Feraudy, M. Glentzlin, J. F. Mangin, J. PhamVan, J. M. Torre; "The Cerga Lunar Laser Ranging Station", *Proceedings Of 7th International Workshop on Laser Ranging Instrumentation*, 1989

[3] A. W. Lightstone, R. J. McIntyre; "Avalanche Photodiodes for Single Photon Detection", *IEEE Trans. Electron Devices*, **ED-28**, 1210 (1981)

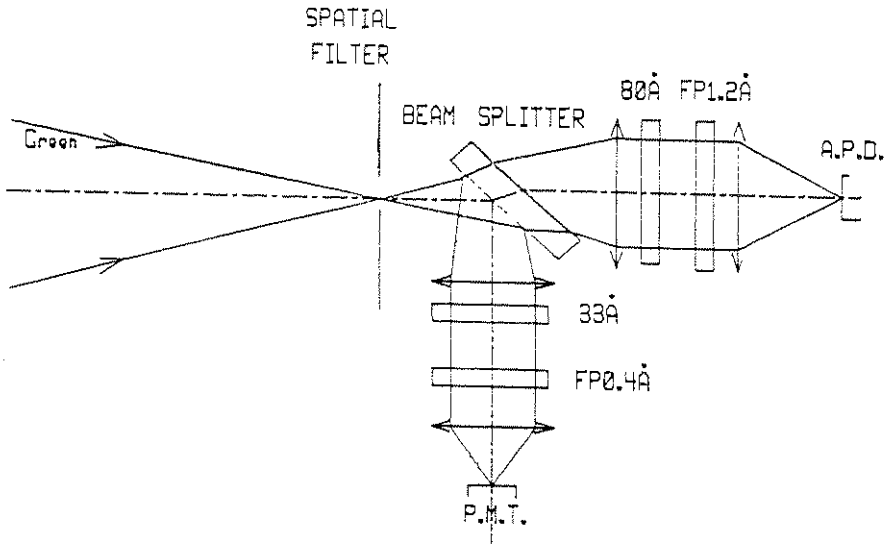

Figure 1: The principle of the optical setup of the receive section of the LLR- Station in Grasse

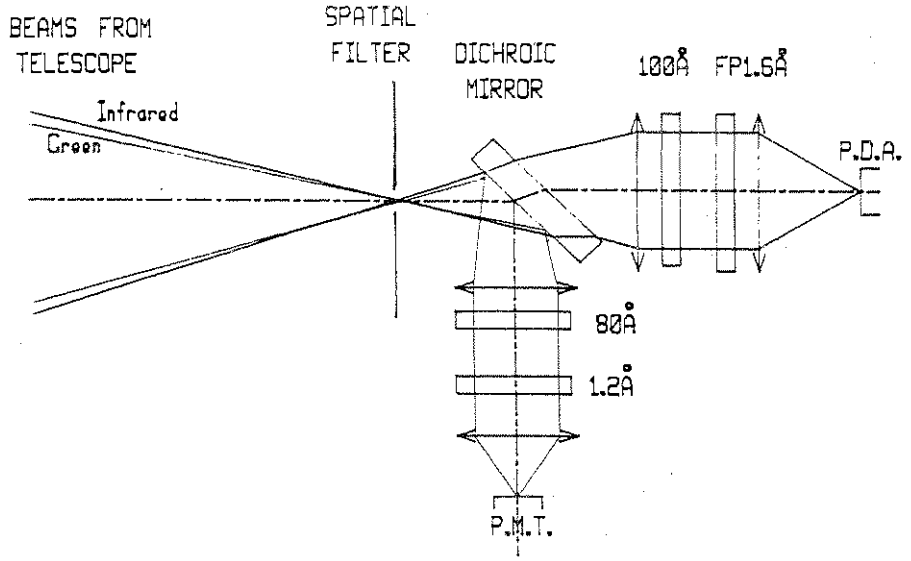

Figure 2: The principle of the optical setup of the whole receive section as used under the common experiment

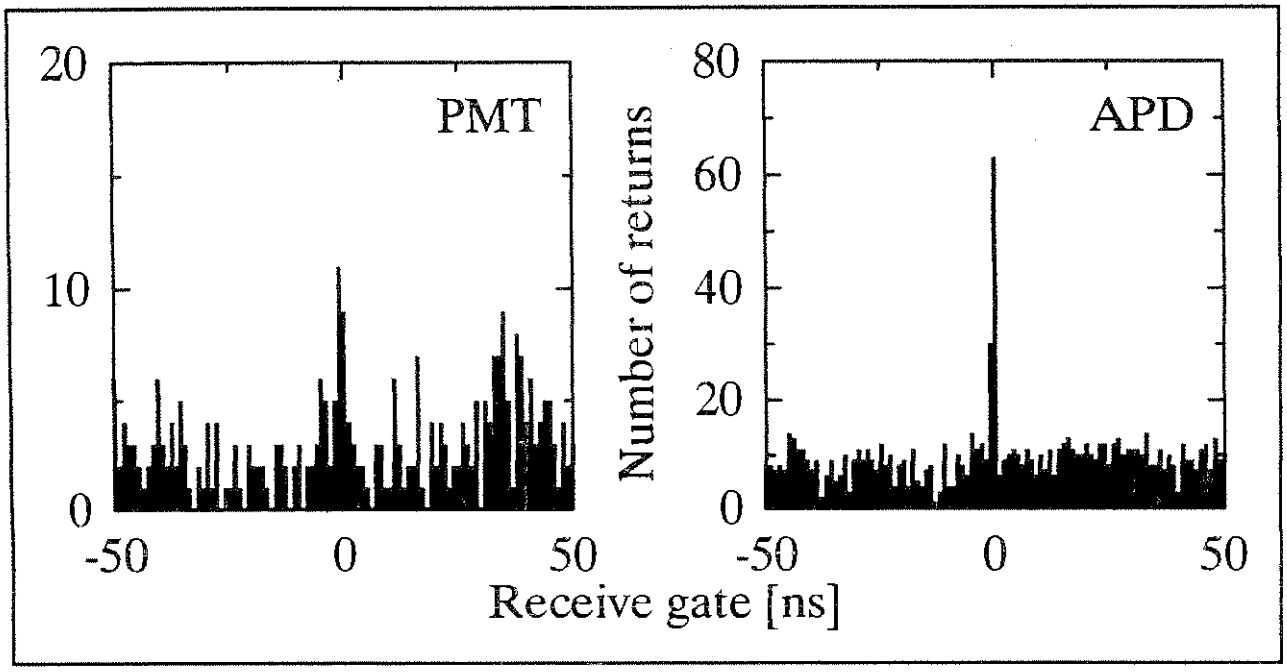

Figure 3: Histogram of the lunar returns for both detectors (the lunar reflector in sunlight)

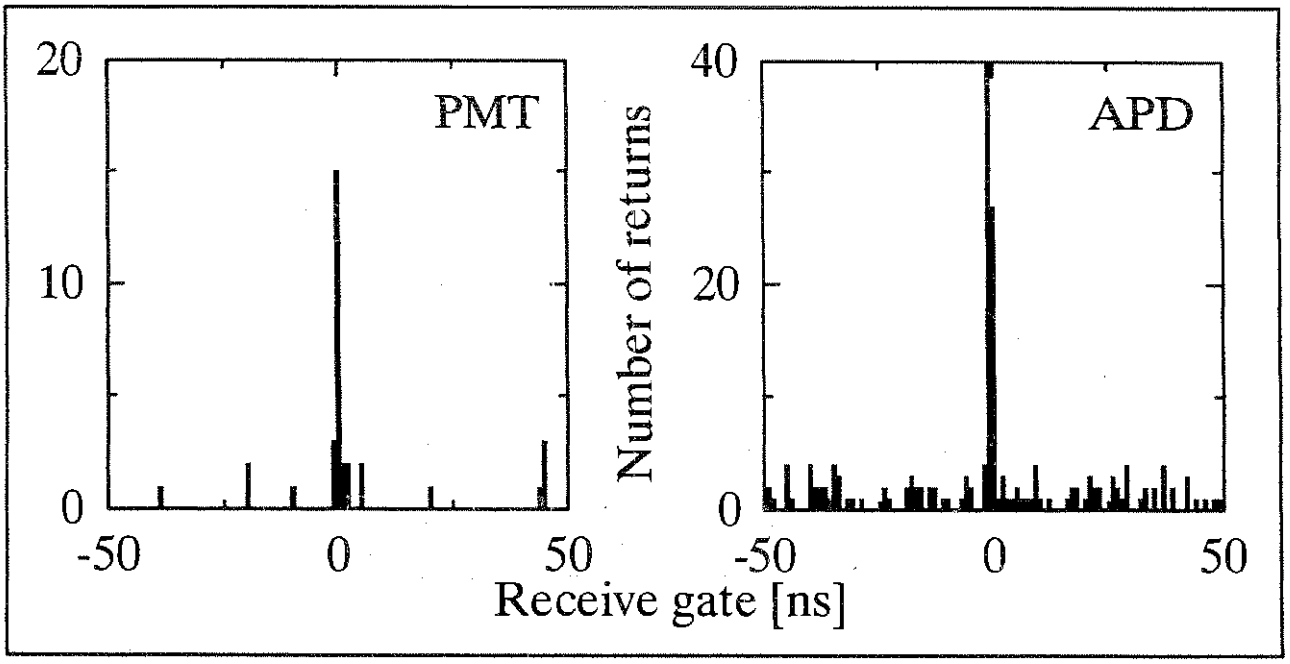

Figure 4: Histogram of the lunar returns for both detectors (the lunar reflector in darkness)

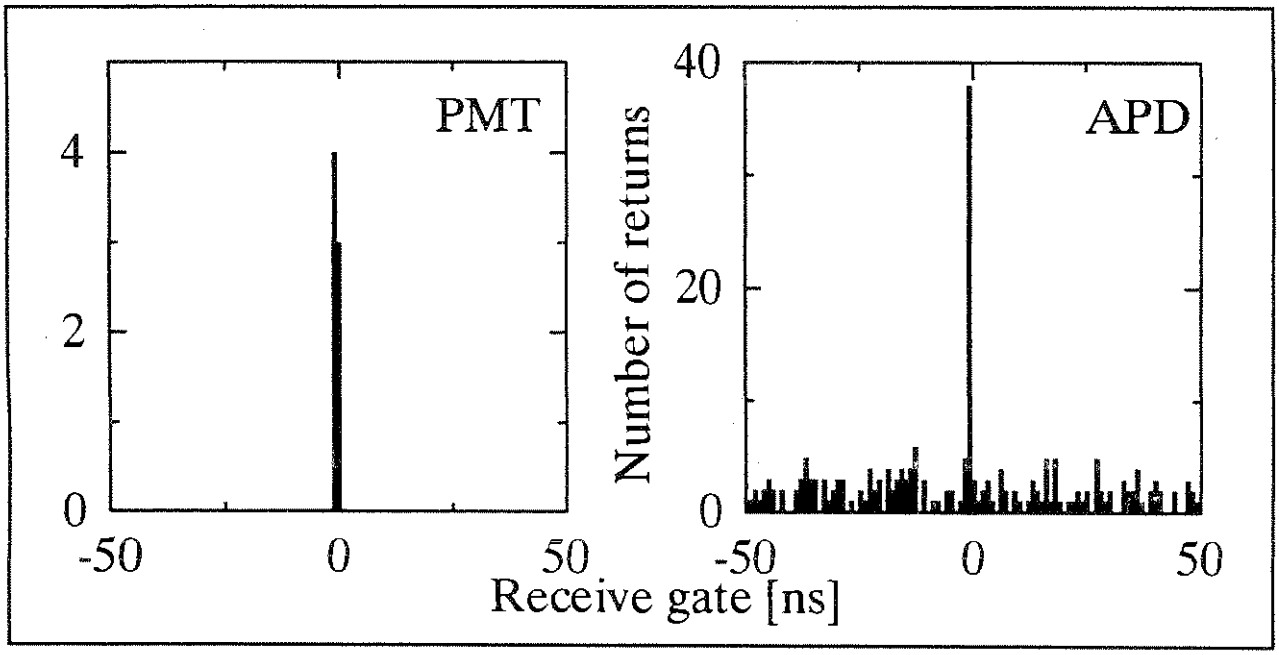

Figure 5: Histogram of the lunar returns for PMT and APD obtained by using the standard configuration of the station

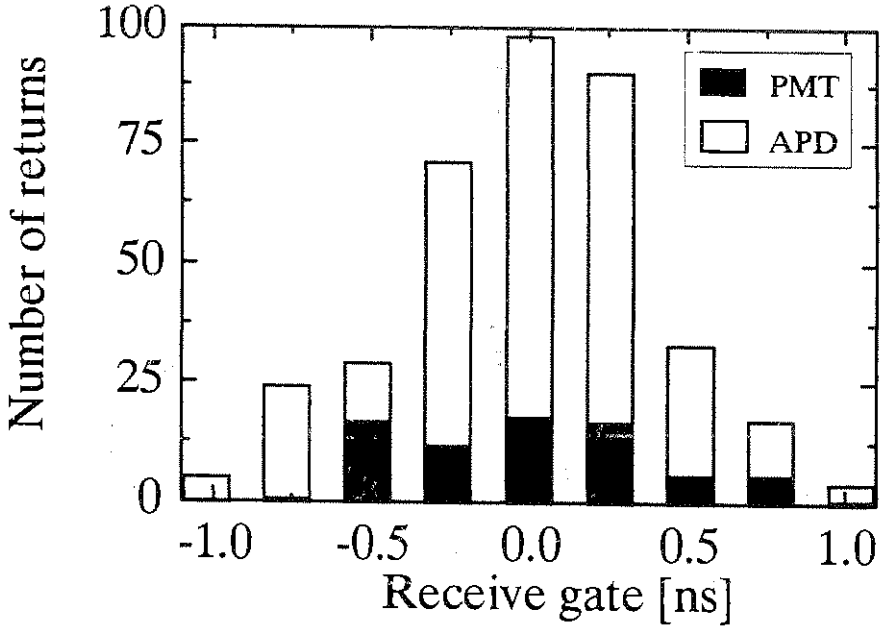

Figure 6: Histogram of the superimposed echoes over all the data collected throughout the experiment for both detectors

EYESAFE SYSTEMS

Chairperson : John Luck

SLR 2000: AN AUTONOMOUS AND EYESAFE SATELLITE LASER RANGING STATION

John J. Degnan
Code 920.1
Laboratory for Terrestrial Physics
NASA Goddard Space Flight Center
Greenbelt, MD 20771 USA

ABSTRACT

SLR 2000 is a system concept for an autonomous, unmanned satellite laser ranging station with a single shot range precision of one centimeter or better. The goal of the program is to provide 24 hour tracking coverage and to reduce both capitalization and operating and maintenance costs by an order of magnitude relative to current outlays. The dominant cost driver in present systems is the onsite manpower required to operate the system, to service and maintain the complex subsystems (most notably the laser), and to ensure that the transmitted laser beam is not a hazard to onsite personnel or overflying aircraft. In performing initial tradeoff studies of the SLR 2000 system, preference was given to simple hardware over complex and to passive techniques over active resulting in the concept described here. The SLR 2000 system consists of an optical head mounted to a concrete pier which in turn contains a single rack of electronic equipment. Temperature inside the pier and instrument is controlled by a small heat pump. The system communicates via Internet with a central scheduler/data processor for the purposes of obtaining updated satellite schedules and orbits and transmitting range and ancillary data and general housekeeping information.

To keep the cost of the tracking telescope and mount subsystems within reasonable bounds, the SLR 2000 telescope aperture is being constrained to diameters between 30 and 50 cm, which is comparable in size to present transportable systems. Single pulse energy is maximized, within eye hazard constraints, by filling the available aperture with the transmit beam and by using passive aperture sharing or polarization techniques, rather than active transmit/receive switches, to separate the transmitted and received beams. Taking into account cumulative multiple pulse effects on the human retina, the maximum allowable transmitted energy per pulse is only 350 microjoules and 90 microjoules for the fundamental (1064 nm) and frequency-doubled (532 nm) wavelengths of Nd:YAG respectively. Our baseline design assumes use of the green wavelength with APD or MCP/PMT detection, but final selection will depend on the success of external NASA programs in developing a high speed, high quantum efficiency infrared detector.

To counteract the negative effect of a roughly three order of magnitude reduction in laser energy relative to present systems, SLR 2000 must operate at roughly Khz pulse repetition rates with a narrower beam divergence on the order of 10 arcseconds (between $1/e^2$ intensity points) in order to achieve a minimum 100 range measurements within a two minute LAGEOS normal point bin. Such rates and energies can be achieved by relatively simple diode pumped and Q-switched microlasers and passive multipass amplifiers, thereby eliminating the need for unreliable flashlamps and associated high voltage power supplies, complex switching and modulation electronics, and long., thermally stable resonators. Furthermore, microlaser packages are sufficiently lightweight and compact that they can be mounted to the same structure as the telescope, eliminating the need for multimirror Coude systems and vastly improving alignment stability. Beam divergence can be adapted to the satellite being tracked.

To handle the higher repetition rates, event timers similar to those used in lunar laser ranging (LLR) will most likely displace single stop time interval counters in present systems. Station epoch time will be maintained to better than 50 nsec by a GPS-steered quartz or rubidium oscillator. More effective spectral, spatial, and temporal filtering will be required to maintain desirable signal to noise ratios during daylight ranging to LAGEOS. Real time data processing techniques, such as Poisson filtering (adapted from LLR), are being used in combination with frequently updated orbits from the central processor to isolate data from noise and to narrow the range gate.

1. INTRODUCTION

SLR 2000 is a system concept for an autonomous, unmanned satellite laser ranging station with a single shot range precision of one centimeter or better. The motivation for developing SLR 2000 stems from the realization that:

SLR provides unique and important science
SLR is more expensive than competing radio techniques
SLR costs can be reduced through increased reliability, standardization, and automation
New technologies are available which can greatly reduce system complexity and cost

The goal of the SLR 2000 program is to provide full 24 hour tracking coverage and to reduce both capitalization and operating and maintenance costs by an order of magnitude relative to current outlays. The dominant cost driver in present systems is the onsite manpower required to operate the system, to service and maintain the complex subsystems (most notably the laser), and to ensure that the transmitted laser beam is not a hazard to onsite personnel or overflying aircraft. Thus, the primary technical goals of the SLR 2000 system are:

Unmanned, eyesafe operation
24 hour tracking of LAGEOS and lower satellites
One centimeter (RMS) single shot precision or better
Minimum 100 ranges per normal point
Mean time between failures: > 4 months
Automated two-way communications with a central data processor via Internet
System free of optical, electrical, and chemical hazards

Secondary goals for the system, presently viewed as highly desirable but perhaps difficult to achieve, include a capability to range to high altitude satellites such as GPS, GLONASS, and ETALON and the ability to retrofit two color technology at some later date.

In performing initial tradeoff studies of the SLR 2000 system, preference was given to simple hardware over complex and to passive techniques over active resulting in the concept to be described here. In our current technical approach, the SLR 2000 system consists of an optical head mounted to a concrete pier which in turn serves simultaneously as the basic geodetic monument and as an environmental shelter housing a single rack of electronic equipment as in Figure 1. The temperature inside the pier and instrument is controlled by a small heat pump. The system communicates via Internet with a central scheduler/data processor for the purposes of obtaining updated satellite schedules and orbits and transmitting range and ancillary data and general housekeeping information.

In this paper, we perform some fundamental system level analyses which have guided the preliminary design of SLR 2000 and provide an overview of the system. Greater engineering detail is given in companion papers located elsewhere in these proceedings.

2. EYE SAFETY CONSIDERATIONS

To keep the cost of the tracking telescope and mount subsystems within reasonable bounds, the SLR 2000 telescope aperture is presently constrained, at least initially, to about 30 cm, which is comparable in size to present NASA transportable systems. Furthermore, it was decided early in our deliberations that eyesafe beams are to be preferred over active aircraft radars in ensuring eye safety. Taking this passive approach has several important advantages. From an engineering and economic standpoint, the passive eyesafe approach is absolutely failsafe and eliminates the need for an additional large and expensive aircraft radar subsystem. Furthermore, from a political and legal standpoint, it should be easier to obtain approval from local regulatory agencies, such as the Federal Aviation Administration (FAA) in the United States for such a system to operate in an unattended mode. The principal disadvantage is that combining

SLR 2000 STATION FRONT VIEW

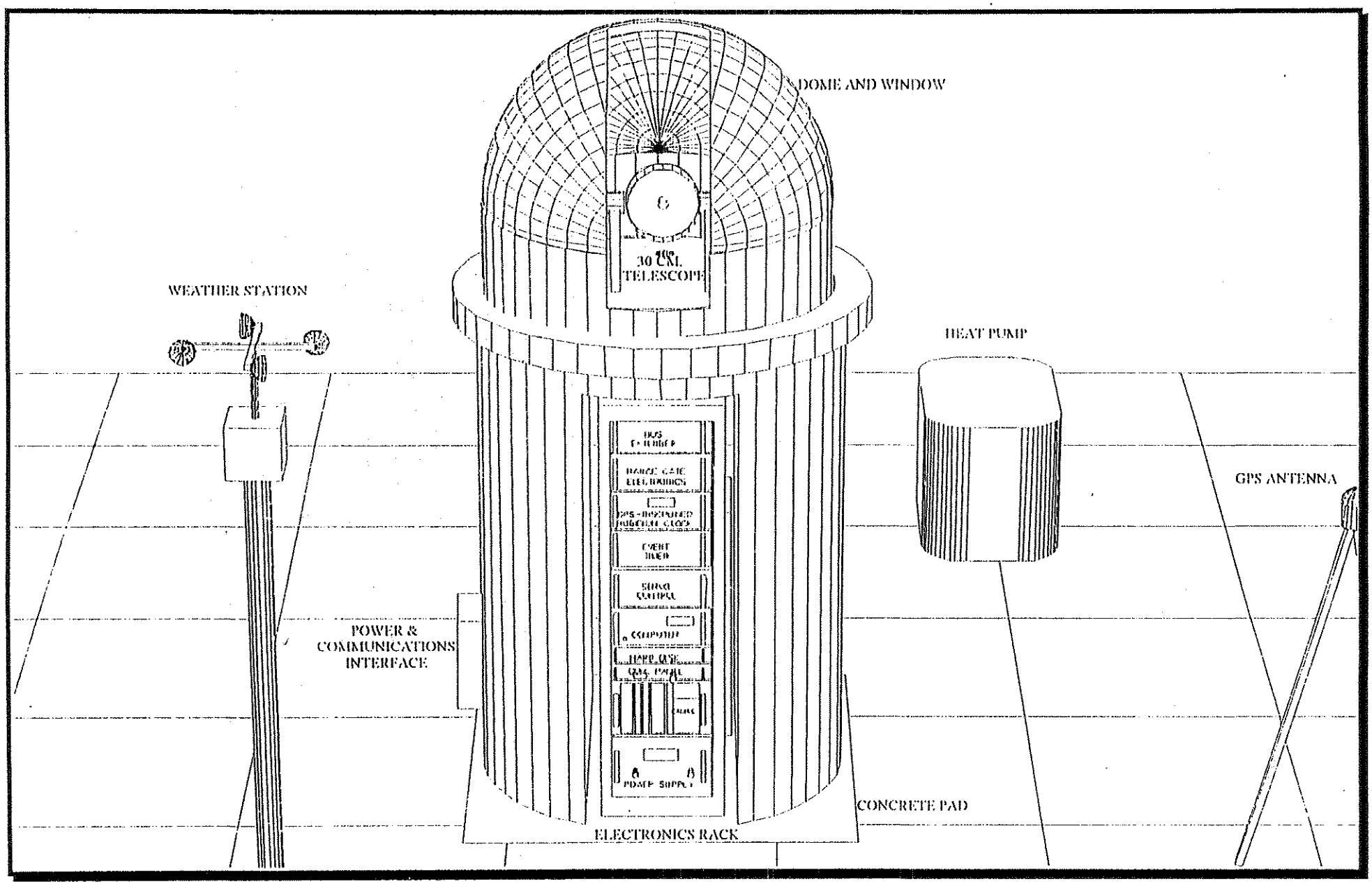

FIGURE 1

the eyesafe requirement with the small aperture results in a maximum single pulse energy which is significantly less than a millijoule at the visible and near infrared wavelengths commonly used in SLR. As we shall see shortly when we discuss probability of detection, SLR 2000 must operate at roughly Khz pulse repetition rates with a narrower beam divergence on the order of 10 arcseconds (between $1/e^2$ intensity points) in order to counteract the negative effect of a roughly three order of magnitude reduction in laser energy relative to present systems and to achieve a minimum 100 range measurements within a two minute LAGEOS normal point bin. However, such rates and energies can be easily achieved by a relatively simple Q-switched microlaser followed by a single multipass amplifier. It is demonstrated elsewhere that a Nd:YAG microlaser operates most efficiently at roughly a 2 Khz rate when pumped by a CW diode [Degnan and Dallas, 1994].

Microlasers can be efficiently pumped by low voltage CW laser diodes, thereby eliminating the need for unreliable flashlamps and their associated high voltage triggering circuits and power supplies, water-to-air heat exchangers and their associated plumbing, complex switching and modulation electronics, and long., thermally stable resonators. Microlasers can passively generate single picosecond pulses due to their extremely small lengths on the order of a mm and hence do not require fast, high voltage electro-optic switches or modulators or carcinogenic dyes as do conventional modelocked systems. Furthermore, these microlaser packages are sufficiently lightweight and compact that they can be mounted to the same structure as the telescope, eliminating the need for multimirror Coude systems and vastly improving long term alignment stability.

Clearly, single pulse energy is maximized, within the eye hazard constraints, by filling the available aperture with the transmit beam. In calculating the eyesafe energy at a particular wavelength according to U.S. ANSI standards , one must take into account cumulative multiple pulse effects on the human retina. For visible wavelengths, readily seen by the observer, a reaction or integration time of 0.25 seconds must be assumed. For infrared wavelengths, invisible to the observer, the ANSI standards require longer integration times on the order of ten seconds.

Assuming a repetition rate of 2 Khz and a 30 cm telescope aperture and taking into account cumulative multiple pulse effects on the human retina as required by current U.S. ANSI eye safety standards, one obtains a curve for the maximum allowable energy as a function of laser wavelength given in Figure 2. The maximum allowable transmitted energy per pulse is only 350 microjoules for the fundamental (1064 nm) and about 90 microjoules for the frequency-doubled (532 nm) wavelengths of Nd:YAG respectively. Our baseline design assumes use of the green wavelength with SPAD or MCP/PMT detection, but final selection will depend on the success of external NASA programs directed at developing a longlived, high speed, high quantum efficiency detector for use at infrared wavelengths beyond 1 micron.

In the author's opinion, the use of so-called "eyesafe" wavelengths longer than about 1.06 microns does not, at least at the present time, offer any real advantages to SLR 2000. These wavelength regions suffer from relatively inefficient, low gain, and technologically immature laser materials and exotic detector materials typically characterized by relatively low quantum efficiency and high internal noise. Furthermore, going to longer wavelengths to take advantage of the higher eyesafe pulse energies reintroduces many of the undesirable features of high energy laser systems which are largely eliminated by the use of the low energy, diode-pumped microlaser. For example, high energy lasers must be pumped either by flashlamps (with their accompanying large high voltage power supplies and cooling systems) or by rather expensive high power laser diode arrays. Furthermore, these larger lasers are more likely to damage optics and cannot be directly mounted to a small telescope which then requires the use of a more complex Coude or similar multimirror system, further increasing cost and endangering the long term reliability and alignment stability in an unattended mode.

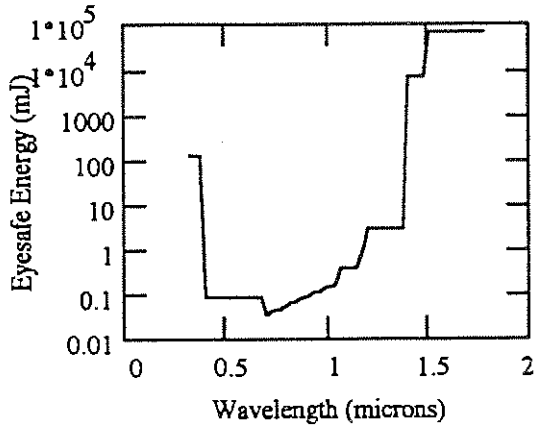

Figure 2: The eyesafe energy as a function of wavelength for a system operating at a repetition rate of 2 Khz with a transmitting aperture of 30 cm.

3. PROBABILITY OF DETECTION

The probability of detection is governed by Poisson statistics according to the equation

$$P_D = 1 - e^{-n_s} \sum_{m=0}^{m=n_t-1} \frac{n_s^{\,m}}{m!} \qquad (1)$$

where n_s is the mean number of received signal photoelectrons and n_t is the detection threshold in photoelectrons [Degnan, 1993]. In designing the SLR 2000 system, we have imposed the requirement that at least 100 single range measurements are obtained in constructing a normal point. Thus, if we have a single shot range with a random uncertainty of $\pm$ 1 cm, the resulting normal point will have a random uncertainty of $\pm$ 1 mm. An SLR 2000 system operating at a repetition rate of 2 Khz sends out a total of 240,000 ranging pulses over the two minute normal point bin for LAGEOS. Hence, only a very small fraction of these (0.042%) must be detected to satisfy the 100 minimum ranges per normal point criteria. Figure 3 is a plot of the number of range returns per normal point as a function of the mean number of received photoelectrons, n_s, and the detection threshold (n_t = 1, 2 and 3 pe) for a LAGEOS normal point time bin of two minutes and a system repetition rate of 2 Khz. Under our criteria of a minimum hundred ranges per normal point, a threshold of 1 pe can accomodate mean signal strengths below 0.001 pe, a 2 pe threshold requires a mean signal strength of about 0.03 pe, and a 3 pe threshold requires a mean signal strength of about 0.15 pe.

4. FALSE ALARM RATE

It is clear from Figure 3 that a lower detection threshold implies a greater number of range returns in the normal point bin, but it also increases the number of false alarms generated by the background and detector noise rates. Noise in a laser ranging system can generally be reduced through four types of predetection filtering - spectral , spatial, temporal, or amplitude filtering [Degnan, 1985]. However, powerful post-detection discrimination can also be provided by Poisson filtering techniques which have long been used by the lunar ranging community [Abbott et al,1973], and these algorithms are currently being adapted for SLR 2000 [McGarry et al, 1994].

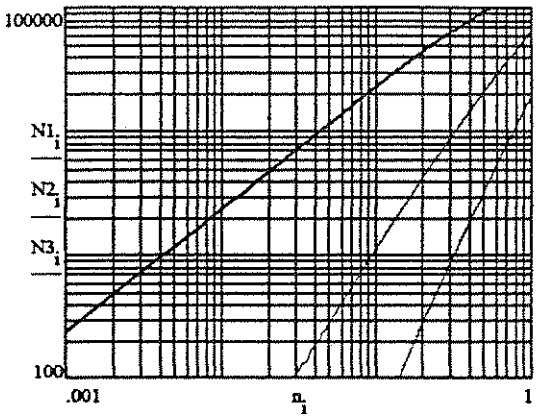

Figure 3: The number of range returns per normal point is plotted as a function of the mean number of received photoelectrons, n_s, and the detection threshold (n_t = 1, 2 and 3 pe) for a LAGEOS normal point time bin of two minutes and a system repetition rate of 2 Khz. Under our criteria of a minimum hundred ranges per normal point, a threshold of 1 pe can accomodate mean signal strengths below 0.001 pe, a 2 pe threshold requires a mean signal strength of about 0.03 pe, and a 3 pe threshold requires a mean signal strength of about 0.15 pe.

The following table lists some spectral filters produced by various manufacturers along their minimum bandpasses, typical throughputs, and field-of-view (FOV) or acceptance angle.

TABLE 1: Some spectral filters and their characteristics.

DEVICE	SOURCE	TRANSMISSION (%)	BANDWIDTH (nm)	FOV (Deg)
Bandpass	Omega	70	1.0 nm	
Bandpass	Omega	53%	0.3 nm	
Photo-refractive	Accuwave	15%	0.0125 nm	1.6
SADOF*	Shay,NMSU	60%?	0.002 nm	2-5?

*SADOF = Stark Anomalous Dispersion Optical Filter

The bandpass of a static spectral filter must be wide enough to accomodate the laser pulsewidth and any Doppler effects created by the moving satellite. Figure 4a shows the laser pulse bandwidth as a function of pulsewidth while Figure 4b describes the maximum Doppler shift induced by the satellite motion as a function of altitude. Both curves are bounded in the vertical by the relatively inexpensive and polarization-insensitive 0.3 nm Omega bandpass filter and by the significantly more expensive and polarization-sensitive Accuwave photorefractive filter. It is clear from Figure 4 that the photorefractive filter begins to reduce signal throughput for laser pulsewidths less than about 80 picoseconds and for satellite altitudes less than about 4000 Km. An "ideal" static filter, with a bandpass on the order of a few hundredths of a nanometer, would accomodate both effects for the current range of satellite altitudes between 400 and 20,000 Km. Active tunable filters, which can track out the Doppler shift based on a priori knowledge of the satellite motion, were also briefly considered for SLR 2000. However, computer simulations [McGarry et al, 1996] have demonstrated the ability of postdetection Poisson filtering techniques to easily cope with SNR ratios smaller than 0.05. Thus, in keeping with our preference for passive over active techniques and

commercially available components over R&D components, our baseline design assumes a simple static filter with a readily attainable bandpass on the order of 0.12 nm.

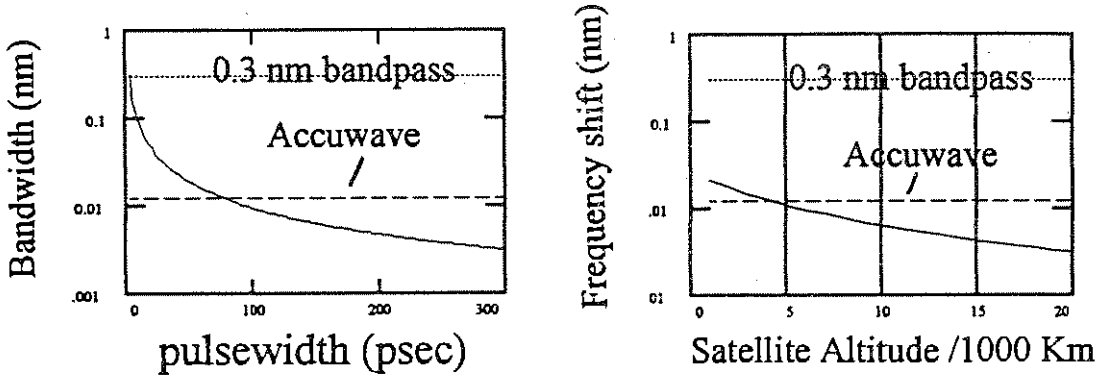

Figure 4: The effect of laser pulsewidth (a) and satellite Doppler (b) on the spectral filter specifications. The Doppler shift produced by low satellites places a lower bound of a few hundredths of a nanometer on the bandpass of a static spectral filter. The same filter could accomodate microlaser pulsewidths greater than 50 psec.

Link calculations suggest that a beam divergence of about 40 microradians (full angle between Gaussian $1/e^2$ intensity points) is appropriate for reliable and robust tracking of LAGEOS. If we design the receiver spatial filter to approximately match this transmitter field of view, we obtain the false alarm rates due to typical daylight background noise shown in Figure 5. We have assumed a detection threshold of one photoelectron and have allowed the range gate to vary between 10 and 1000 nsec. The upper and lower curves represent the number of false alarms generated within one two minute LAGEOS normal point using the Omega 0.3 nm and Accuwave 0.0125 nm spectral filters respectively.

The curves in Figure 5 include background noise effects but do not include false alarms generated by internal detector noise. While this is a negligible effect for microchannel plate photomultiplier (MCP/PMT) detection, it can be a significant factor for Single Photoelectron Avalanche Photodiode (SPAD) detection. On the other hand, SPADs are compact, offer improved sensitivity and quantum efficiency, and are easily adapted to the Khz repetition rates needed by SLR 2000. Furthermore, signal related biases, often observed in larger more energetic systems which currently use SPAD's, are not an issue for SLR 2000 because of its low mean signal strengths which typically fall well below 1 pe for most satellites.

5. SYSTEM OVERVIEW

Figure 6 provides a block diagram of the overall SLR 2000 system. Orbital predicts are generated by a central processor using the latest available data from the global network and provided to the onsite Data Processing/Scheduling computer via the Internet. The latter computer sends back laser range data and other system information over the Internet link to the Central Processor. The InterRange Vectors (IRV's) are passed to the onsite Control Computer which generates realtime pointing commands to the telescope via the dual axis servo drivers as well as range gates to the receiver subsystem. Incremental inductasyn encoders and resolvers on the mount axes pass the absolute pointing information back to the Control Computer. As an illustration of a commercial product which meets the functional requirements of SLR 2000, the Aerotech's Model 360-D series of tracking mounts and their Unidex 500 series of driver/controllers is designed for a PC-bus interface, has subarcsecond resolution, few arcsecond absolute accuracy, and can handle telescope apertures up to 50 cm.

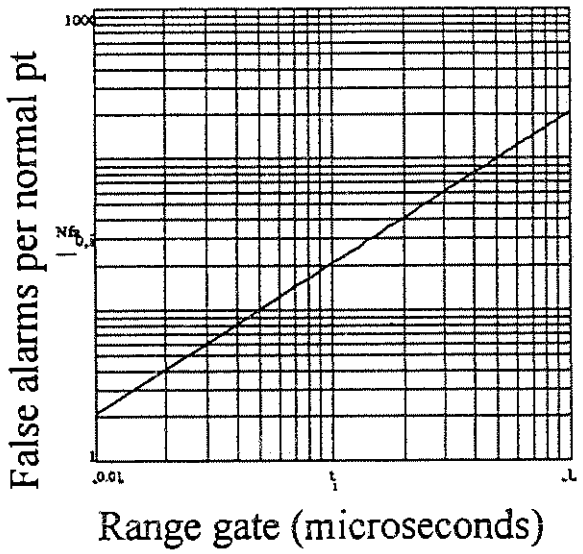

Figure 5: The number of false alarms produced in a sincle LAGEOS normal point frame (2 minutes) by solar scattering in the atmosphere during daylight tracking on a clear day. The curves assume matching transmitter and receiver FOV's (40 microradians), a 1 pe detection threshold, a range gate operating at 2 Khz with a variable window between 10 and 1000 nsec. The curve assumes the Accuwave 0.0125 nm spectral filter and scales linearly with spectral bandpass.

Absolute pointing accuracy is maintained over long intervals through periodic automated star calibrations using a CCD array within the optical pointing assembly. Epoch time is passed to the control computer by a GPS-disciplined oscillator. The best commercial device at present is the Hewlett-Packard Model 58503A GPS Time and Frequency Reference Receiver which combines the excellent short term stability of the internal quartz oscillator with the long term stability provided by GPS time intercomparison and frequency updating. With a GPS satellite in view, the unit provides a 1 pps output synchronized to better than 100 nsec relative to USNO. Jitter is less than 50 nsec. It also provides a 10 Mhz signal with a frequency accuracy better than 1 part in 10^{12} (one day average) when locked. We are also investigating the possible use of a GPS-disciplined rubidium oscillator which would have improved stability characteristics [Ingold et al, 1994].

The PC-based Control Computer enables the microlaser/amplifier by switching on a programmable DC power supply. The repetition rate of the passively Q-switched microlaser can be controlled by adjusting the power of the diode laser that pumps the oscillator. This feature can be used, if necessary, to ensure that returning pulses from the satellite do not arrive coincidentally with the blanking of the receiver during pulse transmission by varying the PRF over a narrow range. The passively Q-switched microlaser is discussed elsewhere in these proceedings [Degnan and Dallas, 1994].

In some instances, it may be beneficial to increase the beam divergence to acquire and track the lower satellites for which orbit predictions are generally poorer but signal strengths are higher. A simple, low-risk approach to accomplishing this is to adjust the spacing in the transmitter magnifying optics by inserting AR coated etalons with different thicknesses via a rotating wheel assembly activated by the Control Computer. Alternatively, an electronically controlled zoom lens assembly can be used to decollimate the beam prior to entering the fixed telescope.

Mechanical Transmit/Receive (T/R) switches, such as rotating mirrors or coated disks, are commonly used in the laser network where typical laser fire rates are between 5 and 10 Hz. However, mechanical

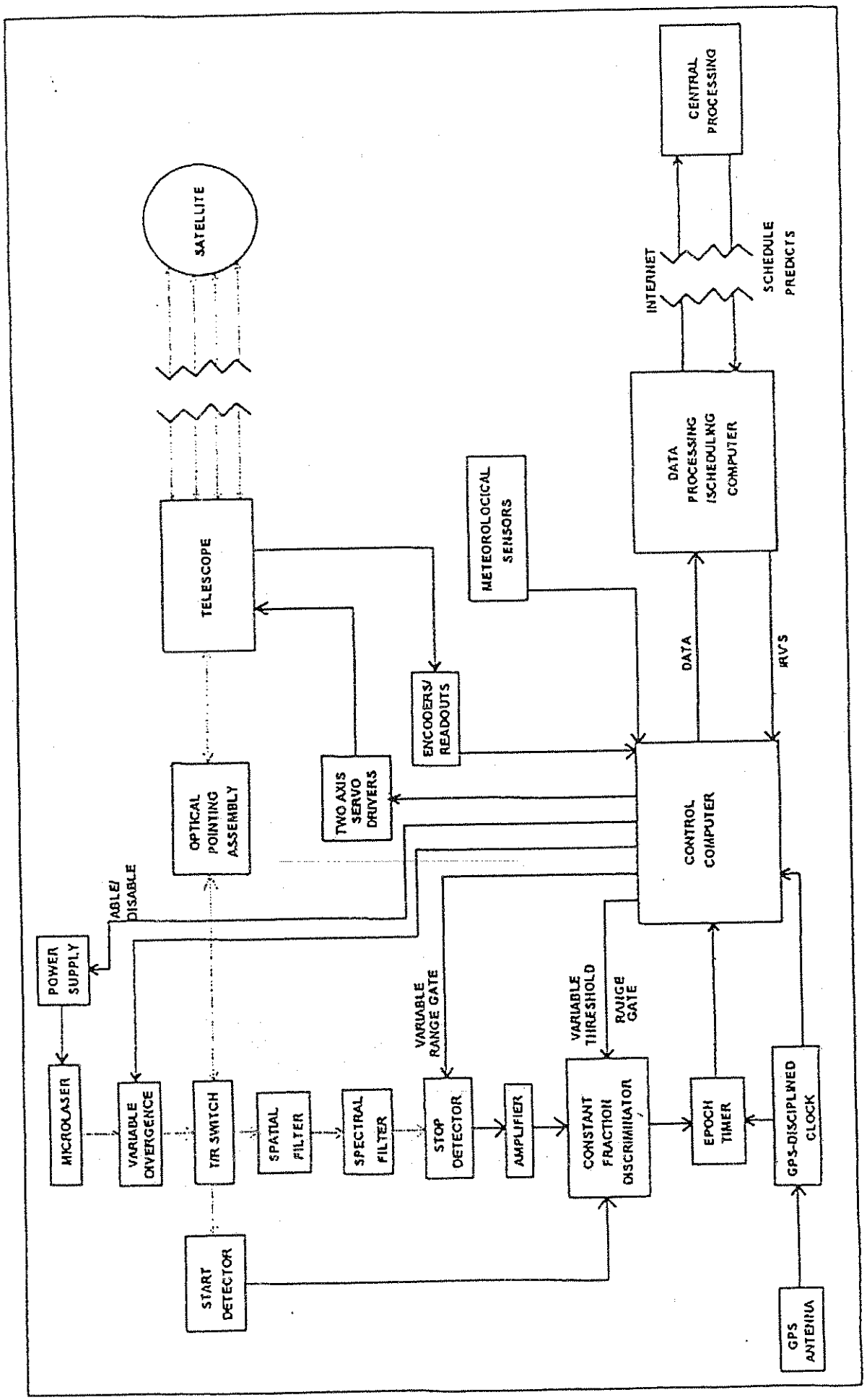
SATELLITE
CENTRAL PROCESSING
INTERNET
SCHEDULE PREDICTS
TELESCOPE
METEOROLOGICAL SENSORS
DATA PROCESSING SCHEDULING COMPUTER
DATA
IRV'S
ENCODERS/ READOUTS
OPTICAL POINTING ASSEMBLY
TWO AXIS SERVO DRIVERS
CONTROL COMPUTER
ABLE/ DISABLE
POWER SUPPLY
VARIABLE RANGE GATE
VARIABLE THRESHOLD
RANGE GATE
MICROLASER
VARIABLE DIVERGENCE
T/R SWITCH
SPATIAL FILTER
SPECTRAL FILTER
STOP DETECTOR
AMPLIFIER
CONSTANT FRACTION DISCRIMINATOR
EPOCH TIMER
GPS-DISCIPLINED CLOCK
START DETECTOR
GPS ANTENNA

FIGURE 6

techniques are not readily adapted to the Khz pulse rates required by SLR 2000. Furthermore, mechanical devices often lose synchronization and require field maintenance. However, other non-mechanical active T/R switch approaches exist which do have the requisite switching speed and include electro-optic, acousto-optic, and frustrated internal reflection. However, our design philosophy of simplicity and reliability drives us to examine totally passive options first.

Two totally passive approaches to the T/R switch are aperture sharing and polarization rotation. Aperture sharing, in which different regions of the primary are used by the transmitter and receiver respectively, has been used successfully on NASA's TLRS-2 system for 10 years . While feasible, aperture sharing may not be the most efficient option for the eyesafe SLR 2000 system since the received signal is maximized by having both the transmit and receive beams use the full aperture of the primary and increases as D^4 where D is the diameter of the telescope primary.

The principal disadvantage of the polarization rotation approach, shown in Figure 7, is that the receiver is polarization-sensitive, i.e. it will only see the linear component of polarization transmitted to the detector. This is not an issue if the circular polarization of the laser beam is faithfully maintained during its flight to and from the satellite, but recent theoretical calculations [Arnold, 1994] suggest that satellites with uncoated retroreflectors (at this time, just LAGEOS 1 and 2), which rely on total internal reflection, can severely depolarize the incoming laser light resulting in a substantial loss of throughput to the detector at some satellite orientations. The majority of satellites have retroreflectors with metallized back surfaces and apparently do not exhibit this effect. Care must also be exercised in designing the transmit/receive optics since the reflection of beams with arbitrary polarization properties off dielectric interfaces at nonzero incidence angles can also lead to polarization changes. The final T/R switch approach will be decided on following further experimental investigations at GSFC of the magnitude of the depolarization effect using our 1.2 meter telescope ranging off LAGEOS.

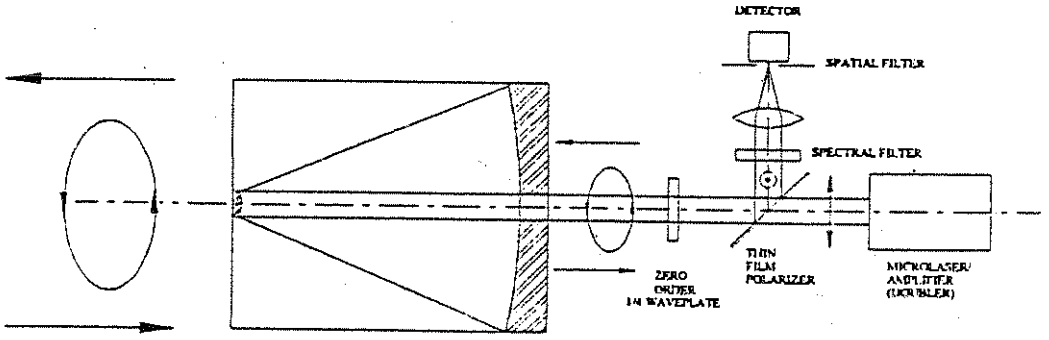

Figure 7: A polarization rotation T/R switch. The p-polarized laser radiation is transmitted through a polarizer and a quarter-wave plate converts it to circularly polarized light. Upon returning from the satellite, a second passage through the quarter wave plate converts the photons to s-polarization which are then reflected by the polarizer into the detector.

In our baseline concept, the received beam at 532 nm will pass through a conventional 0.3 nm Omega narrowband spectral filter (or possibly a 10 nm filter augmented by a Sigma Corporation 0.12 nm etalon filter), a focusing lens, variable spatial filter, and a gated SPAD detector with a quantum efficiency between 20 and 40%, as presently used by the Wettzell and Helwan SLR stations. An epoch timer and programmable range gate generator, currently being developed by AlliedSignal Technical Services Corporation (ATSC) for the Italian Matera Laser Ranging Observatory (MLRO), can be adapted to operate at 2Khz rates for SLR 2000 [Varghese et al, 1994]. Our baseline approach to range calibration is the use of external targets although internal calibration schemes will also be considered.

The system will also incorporate external meteorological sensors (see Figure 1) for the accurate measurement of pressure, temperature, and humidity and return these data over the Internet along with the range data. The tracking mount and optical head will be equipped with military-style connectors and seals to protect the system bearings and electrical connections from the environment. Temperature within the system shelter will be controlled by a small heat pump serviced and maintained through a local service contract. The site host or a local cleaning service will be enlisted to periodically inspect and clean the optics, and a skilled technician will visit the system every four to six months to perform higher level maintenance tasks. Internal sensors and diagnostic subroutines will continuously monitor the health of the various subsystems and report anomalies over the Internet link so that repairs can be initiated either remotely or through an onsite visit by a field technician. Although SLR 2000 will typically be housed at protected military, government, or university sites, additional automated sensors will monitor motion, wind speed, visibility, and rain to provide additional system security.

Using the latest data available, the central data processor will update the orbit parameters and time biases for the various satellites, and the updated data will be accessed via the Internet by the onsite Data Processing/Scheduling computer. This, combined with periodic automated star calibrations, will greatly reduce the initial angular uncertainty in pointing and speed acquisition. Poisson filtering techniques will be used in both the initial acquisition and autotracking of the satellite. The autotracking algorithms will distinguish the satellite data from the background and detector noise and then center and narrow the range gates to further enhance the SNR. System simulations have demonstrated the ability to lock onto the satellite within seconds [McGarry et al, 1996]. We are also investigating whether or not detection of the unused radiation at 1064 nm by a small infrared array might aid in the acquisition and autotracking process without robbing too much energy from the green ranging beam [Titterton et al, 1995].

6. SUMMARY

We have described some preliminary concepts for a fully automated, eyesafe satellite laser ranging system Most of the subsystems can presently be acquired commercially at a relatively low cost, and we believe that, following the initial development of some specialized components and the system software, the total system can be replicated in kit form for under $250,000 USD. Approximately 40% of the total cost is associated with the high resolution, high accuracy tracking mount. Unique subsystems, for which we have not yet identified a commercial source, include the microlaser transmitter, high repetition rate epoch timer and range gating circuitry, and the gated array used in acquisition and pointing. These will be developed inhouse or on contract as extrapolations of existing commercial devices which nearly meet our requirements.

ACKNOWLEDGEMENTS: The author wishes to acknowledge several people who have contributed to the SLR 2000 concept: Jan McGarry and Joseph Dallas of the NASA Goddard Space Flight Center; Paul Titterton and Harold Sweeney of EOO, Inc.; Brion Conklin, Tom Oldham, Howard Donovan, Tom Varghese, and Bill Bane of AlliedSignal Technical Services Corporation; and Peter Dunn of Hughes STX.

REFERENCES

Abbott, R. I., P. J. Shelus, R. Mulholland, and E. Silverberg, "Laser Observations of the Moon: Identification and Construction of Normal Points for 1969-1971", The Astronomical Journal, 78, pp. 784-793 , 1973.

Arnold, D., Smithsonian Astrophysical Observatory, private communication, 1994.

Degnan, J.J., "Satellite Laser Ranging: Current Status and Future Prospects", IEEE Trans. on Geoscience and Remote Sensing, GE-23, pp. 398-413, 1985

Degnan, J.J., "Millimeter Accuracy Satellite Laser Ranging: A Review", AGU Monograph Series, Contributions of Space Geodesy to Geodynamics: Technology, Geodynamics 25, pp. 133-162, 1993.

Degnan, J. J. and J. L. Dallas, "The Q-switched Microlaser: A simple and reliable alternative to modelocking", these proceedings, 1994.

Ingold, J, R. Eichinger, H. Donovan, T. Varghese, W. Dewey, and J. Degnan,"GPS-steered Rubidium Frequency Standard for the NASA SLR Network", these Proceedings, 1994.

McGarry, J. F., B. Conklin, W. Bane, R. Eichinger, R. Rickleffs, and P. J. Dunn, "Tracking Satellites with the Totally Automated SLR 2000 System", these Proceedings, 1994.

McGarry, J. , J.J. Degnan, P. Titterton, H. Sweeney, B. P. Conklin, and P. J. Dunn, "Automated Tracking for Advanced Satellite Laser Ranging Systems", to be presented at the Spring SPIE Meeting , Orlando Florida, April, 1996

Titterton, P. , H. Sweeney, and T. Driscoll, "SLR 2000 Analytical Study of 1060 nm Aided Acquisition and Tracking", Final Report NASA PO # S-61158-Z, November, 1995.

Varghese, T., R. Eichinger, C. Steggerda, H. Donovan, and J. Degnan,"Transmit/Receive Electronics for SLR 2000", these proceedings, 1994.

DATA ANALYSIS AND MODELS

Chairperson : Giuseppe Bianco

FOUR DIMENSIONAL TRACKING STATION POSITIONING FROM SLR DATA

D. E. Smith, R. Kolenkiewicz, Laboratory for Terrestrial Physics, NASA Goddard Space Flight Center, Greenbelt, MD 20771
M.H. Torrence, J.W. Robbins and P.J.Dunn, Hughes STX Corporation, Greenbelt, MD 20770

ABSTRACT

Satellite Laser Ranging (SLR) data to the LAGEOS satellite enables us to make accurate estimates of the motion of many of the tracking sites within the global laser network. Using data acquired between January 1980 and October 1994 we have made simultaneous estimates of site positions and their velocities within a pre-defined kinematic frame. Relative poles of rotation, which are used to model the motion of one plate relative to another, were then computed from the SLR estimated velocities for sites known to be well away from deformation zones. The rotation poles differ slightly from those of NUVEL-1, but in general, indicate that the magnitude of the SLR velocities is slower than those predicted by NUVEL-1, consistent with the 4-5% slowing in relative spherical rates noted in our earlier comparisons. Spherical rates between sites in western North America support models of extension in the Basin and Range Province and the rotation of the Sierra Nevada microplate. An analysis of the spherical rates crossing the North Atlantic shows that estimated extension between North America-Eurasia sites is generally smaller than those implied by NUVEL-1; on the other hand, rates between North America and Africa are in better agreement with NUVEL-1, although they are not so well determined. The maintenance and ongoing monitoring of global SLR site kinematics provides a well defined global reference which will aid in global kinematic solutions where information from other technologies are merged with SLR results, and in densification studies of regional kinematics derived from terrestrial and Global Positioning System observations.

INTRODUCTION

A fundamental geophysical process detectible by space-based geodetic technologies is the large-scale motion of the Earth's major plates. Over time, Satellite Laser Ranging systems, located at key positions around the globe, provide a sequence of measurements from which the tracking site motions can be deduced. SLR site motion results reported to date have been based on range measurements to the Laser Geodynamics Satellite (LAGEOS). These results showed recovery of time averaged positioning at the 4-5 mm level and horizontal linear motion at the 2-3 mm/yr level (Smith et al., 1990, Reigber et al., 1990 and Biancale et al., 1991). Since the publication of Smith et al. (1990), several improvements have been made in the analysis strategy to give a more rigorous solution for horizontal tracking site motion. These improvements, combined with the accumulation of four more years of tracking data, considerably strengthen the results.

Range observations acquired before January 1980 were omitted since the precision of the data deteriorates for the period before January 1980 (Smith et al., 1991). Improved performance after 1980 is mainly due to laser tracking hardware and software upgrades to the NASA tracking systems which were deployed in late 1979 and hardware changes made within the network originally operated by the Smithsonian Astrophysical Observatory. The resulting SLR data set comprises over 700,000 two-minute average range observations acquired by a network of over 70 tracking sites. A measure of the quality of the data and hence the solution through time is provided by the monthly root mean square (RMS) fit of the data to the orbit which, since 1985, has remained steady at the 30 mm level.

ANALYSIS AND RESULTS

The new analysis method differs from the process reported in Smith et al. (1990 and 1991). Instead of following a series of analysis steps to derive velocity estimates from a sequence of tracking site positions, advantage is taken of new software capabilities that allow the direct estimation of three-dimensional site velocity parameters simultaneously with epoch positions and other geodetic parameters. Velocities are estimated in all three dimensions, but only the horizontal components are directly interpretable as tectonic motion. The data are reduced in a least squares estimation scheme using the GEODYN II and SOLVE analysis packages (Putney et al., 1990). The model parameters adopted in the solution follow the 1992 standards of the International Earth Rotation Service (McCarthy, 1992) with principal upgrades in the geopotential (Lerch et al., 1993) and in the modeling of more complete non-resonant ocean tidal terms.

The analysis begins by segmenting the data into monthly orbital arcs of 30 or 35 days in duration. All two minute average range observations are given equal a priori weights since we assume that each laser system performs at the same level of accuracy. For each month, a single set of LAGEOS orbit parameters is estimated and a set of normal equations is created to be used in the final solution that includes all parameters of interest. The 13.5 year sequence of these matrices is brought together into one single SOLVE solution in which site positions (for epoch January 1, 1988), site velocities, daily Earth orientation and Earth rotation rates (5 day values before January 1983), monthly orbit state vectors, bimonthly average along-track acceleration, and bimonthly values of a once-per-revolution acceleration parameter are estimated. All polar motion parameters were freely adjusted, whereas an initial A.1-UT1 value per month was fixed at values obtained from the IERS series (specifically, the 90 C 04 series). The remaining values of A.1-UT1 through the month were estimated yielding excess length of day measurements over that month. Estimation of the once-per-revolution acceleration essentially removes unmodeled effects acting upon the satellite and dramatically improves the overall orbital fits to LAGEOS.

Since the solution is formed simultaneously, all parameters which define the static and kinematic aspects of the geodetic reference frame are internally consistent. The maintenance of the reference frame over the time span of the observations in SL7.1 by a series of rigid-body transformations was described in Smith et al. (1990). These transformations to rectify reference system misalignments with respect to the computation surface (i.e. the ellipsoid) are no longer required since the velocity estimation is no longer dependent on the computation of geodesic lengths and rates. The static part of the terrestrial reference frame is defined by adopting an epoch latitude and longitude for the tracking site at Greenbelt, Maryland and only the latitude of the site on Maui, in the Hawaiian Islands. The kinematic portion of the reference frame is established through the adoption of no net rotation NNR-NUVEL1 (Argus and Gordon, 1991a) implied motion for the north and east components at Greenbelt and only the north component at Maui. The east/west component of Maui's position and motion is freely estimated, providing a parameter to absorb any deviation from NUVEL-1 that may exist for the rate between Greenbelt and Maui. Application of NNR-NUVEL1 motion components for these sites defines the evolution of the terrestrial reference frame in time. No constraints were applied in the directions of the local vertical.

The Earth orientation and length-of-day parameters, as well as the epoch geodetic positions and linear motion for each unconstrained site are all estimated within this reference frame. The statistics of the site velocities determined in earlier solutions did not use the full covariance information in the calculation of the geodesic rates and their uncertainties. These compromises and approximations have been eliminated in the new solution (designated SL8.3) yielding a much stronger solution with improved error statistics. The horizontal components of the estimated motion vectors are given in Table 1 and shown in Figure 1.

PLATE-SCALE IMPLICATIONS

Global comparisons of space geodetic results (i.e., SLR alone or SLR combined with VLBI) to "present-day" models of plate motion derived from geophysical evidence (e.g. AM0-2 of Minster and Jordan (1978) and NUVEL-1 of DeMets et al. (1990)) have been made by several authors (e.g., Smith et al., 1990, Cazenave et al., 1993 and Robbins et al., 1993). Relative rates of motion between sites located well away from plate boundaries were utilized in these studies to provide samples that were free from site motions in deformation zones. These studies showed that the relative rates implied by the "geologic" models were generally faster in magnitude, on the order of 4-5%, than those determined from space geodesy.

Recently, new evidence has suggested that earlier K-Ar derived time scales were ~5% "too young" spanning the Pliocene (Hilgen, 1991, Wilson, 1993 and Baksi, 1994), which includes the period of magnetic anomaly 2A, the normal polarity anomaly used to define the rate scale for NUVEL-1. The average difference seen between the rates implied by NUVEL-1 and those determined from space geodetic observations can largely be reconciled by these adjustments in the geochronologic time scale. This is true in general, but not all plate pair rotational velocities benefit from a single scaling factor. Broad scale plate motions and relative plate motions are conventionally modeled by poles of rotation and rotation rates. Given the horizontal components of motion for a set of locations well distributed across a particular plate and sufficiently far away from boundary zone deformation, relative poles of rotation between four plates (Eurasia, North America, Pacific and Australia) can be determined.

Parameters describing a pole of rotation for Eurasia were based on the velocities of five northern European sites: Graz, Austria; Herstmonceux, England; Potsdam, Germany; Wettzell, Germany and Zimmerwald, Switzerland. Inclusion of the velocity of Shanghai, China, as an additional site nominally located on the Eurasian plate, was precluded since the spherical rates between Shanghai and sites in northern Europe exhibited statistically significant shortening. The pole of rotation for North America was based on velocities from six sites: Bear Lake, UT; McDonald Observatory, TX; Mazatlan, Mexico; Platteville, CO; Richmond, FL and Westford, MA. The velocity of Greenbelt was omitted since its motion is defined a priori by NNR-NUVEL1. The poles of rotation for the Australia and Pacific Plates were each based on velocities from only two sites and hence are more weakly determined than those for Eurasia and North America. The Pacific pole of rotation was determined without redundancy since only the east component of motion at Maui, Hawaii and both velocity components at Huahine Island were used in the calculation. The relative poles of rotation between plate pairs were formed by taking differences of the individual plate poles of rotation. This eliminates the effects of any possible kinematic frame misalignments between the SLR frame and the NNR-NUVEL1 frame and yields poles which can be compared with the relative plate motion model NUVEL-1 of DeMets et al. (1990). The results are shown in Table 2.

In terms of their location, the SLR and NUVEL-1 relative poles of rotation are generally positioned within 4 degrees or less in spherical angle (equivalent to <450 km in distance) with the exception of two of the relative poles of rotation that include Eurasia as one of the plate pairs. In all cases the respective pole locations agree well within the 3 sigma (99% confidence) uncertainties. For the Australia-Eurasia pole of rotation, the SLR pole lies 850 km to the southeast of the NUVEL-1 pole. The SLR determined Eurasia-North America pole of rotation lies 1500 km to the north-northeast of the NUVEL-1 pole. This differs somewhat from a VLBI determined Eurasia-North America pole of rotation (Ward, 1994) which was determined to lie 1000 km northwest of the corresponding NUVEL-1 pole of rotation. However, the results from both SLR and VLBI agree that the Eurasia-North America pole of rotation is located about 10 degrees further north of the corresponding NUVEL-1 pole.

With respect to the rotational velocities, NUVEL-1 is faster than SLR for four plate pairs (Australia-Eurasia, 3% faster; Australia-North America, 5%; North America-Pacific, 1%; Pacific-

Australia, 3%), the same as SLR for the Eurasia-North America plate pair and 3% slower than SLR for the Eurasia-Pacific plate pair. Based on the uncertainties in rotation rate, none of the SLR Euler rotation rates differ significantly from those of NUVEL-1. On the other hand, the velocity of a site relative to another plate is a function of both the angular rate of the rotation pole and the perpendicular distance from the site to the axis of rotation. The difference between the magnitudes of motion vectors calculated for locations on the rotating plate between SLR and NUVEL-1 poles of rotation provide a more meaningful way to assess scale differences than by simply examining the rotational rates. The difference (in terms of percentage, shown in the last column of Table 2) of how much faster NUVEL-1 is relative to SLR varies between 1% and 6%, with the exception being the North America/Pacific plate pair. The discussion here has involved a subset of the ten plate pairs used in Robbins et al. (1993) and largely corresponds with the 4-5% scale difference noted therein.

CONCLUSIONS

An improved analysis of more than 13 years of laser range observations to LAGEOS has yielded horizontal site velocities approaching a precision of 1 mm/yr for those sites with the longest histories of continuous operation. Estimating parameters within a simultaneous least squares solution removed the need for approximations and reference system alignment adjustments made in earlier studies, and provided robust statistics for the results. The tectonic motion results for the sites having longer tracking programs have not deviated significantly from those in Smith et al. (1990) and the geophysical interpretations offered there remain valid. The vectors estimated for sites that are intermittently occupied benefit tremendously from the new solution design. These improvements enable the recovery of motion for twelve such sites that until now have received little attention in the literature. Future solutions with additional laser tracking observations of LAGEOS and LAGEOS II, as well as other geodetic satellites, will further strengthen the results of the overall solution. The maintenance and ongoing monitoring of the global SLR site kinematics is important for it provides a well defined global reference to aid densification studies of regional kinematics derived from terrestrial and Global Positioning System observations.

REFERENCES

Argus, D. F. and Gordon R. G., 1991a, No-Net-Rotation model of current plate velocities incorporating plate motion model NUVEL-1, Geophys. Res. Lett., 18, 2039-2042.

Baksi, A. K., 1994, Concordant sea-floor spreading rates obtained from geochronology, astrochronology and space geodesy, Geophys. Res. Lett., 21, 133-136.

Biancale, R., Cazenave A. and Dominh K., 1991, Tectonic plate motions derived from LAGEOS, Earth Plan. Sci Lett., 103, 379-394.

Cazenave, A., Gegout, P., Soudarin, L., Dominh, K, Barlier, F., Exertier, P. and Boudon, Y., 1993, Geodetic Results from Lageos 1 and Doris Satellite Data, in Space Geodesy and Geodynamics, AGU Geodynamics series, 23, ed. by D. E. Smith and D. L. Turcotte, 81-98.

DeMets, C., Gordon, R. G., Argus, D. F. and Stein, S., 1990, Current plate motions, Geophys. J. Int., 101, 425-478.

Dunn, P. J., Torrence, M. H., Kolenkiewicz, R and Smith, D. E., 1993, Vertical positioning at laser observatories, in Space Geodesy and Geodynamics, AGU Geodynamics series, 23, ed. by D. E. Smith and D. L. Turcotte, 99-106.

Hilgen, F. J., 1991, Extension of the astronomically calibrated (polarity) time scale to the Miocene/Pliocene boundary, Earth Plan. Sci. Lett., 107, 349-368.

Lerch, F. J., Nerem, R. S., Marshall, J. C., Putney, B. H., Pavlis, E. C., Klosko, S. M., Luthcke, S. B., Patel, G. B., Pavlis, N. K., Williamson, R. G., Chan, J. C., Tapley, B. D., Shum, C. K., Reis, J. C.,

Eanes, R. J., Watkins, M. M., Schutz, B. E., Biancale, R and Nouel, F., 1993, Gravity Model Improvement for TOPEX/Poseidon (abstract), EOS, Trans. Am. geophys. Un., 74 (16 suppl.), 96.
McCarthy, D. D. (ed.), 1992, IERS Standards (1992), IERS Tech. Note 13, Paris Observatory.
Minster, J. B. and Jordan, T. H., 1978, Present-day plate motions, J. geophys. Res., 83, 5331-5354.
Minster, J. B. and Jordan, T. H., 1987, Vector constraints on western U. S. deformation from space geodesy, neotectonics and plate motions,J. geophys. Res., 92, 4798-4804.
Putney, B., Kolenkiewicz R., Smith D., Dunn P. and Torrence M. H., 1990,Precision orbit determination at the NASA Goddard Space Flight Center, Adv. Space Res., 10, 197-203.
Reigber, C., Ellmer W., Müller H., Geiss E., Schwintzer P. and. Massmann F. H, 1990, Plate motions derived from the DGFI 89 L03 solution, in Global and Regional Geodynamics, P. Vyskocil, C. Reigber and P. Cross (eds.), Springer-Verlag, New York.
Robaudo, S. and Harrison, C. G. A., 1993, Plate Tectonics from SLR and VLBI Global Data, in pace Geodesy and Geodynamics, AGU Geodynamics series, 23, ed. by D. E. Smith and D. L. Turcotte, 51-71.
Robbins, J. W., Smith D. E. and Ma C., 1993, Horizontal Crustal Deformation and Large Scale Plate Motions Inferred from Space Geodetic Techniques, in Space Geodesy and Geodynamics, AGU Geodynamics series, 23, ed. by D. E. Smith and D. L. Turcotte, 21-36.
Smith, D. E., Kolenkiewicz R., Dunn P. J., Robbins J. W., Torrence M. H., Klosko S. M., Williamson R. G., Pavlis E. C., Douglas N. B. and Fricke S. K., 1990, Tectonic motion and deformation from satellite laser ranging to LAGEOS, J. geophys. Res., 95, 22 013-22 041.
Smith, D. E., Kolenkiewicz R., Dunn P. J., Klosko S. M., Robbins J. W., Torrence M. H., Williamson R. G., Pavlis E. C., Douglas N. B. and Fricke S.K., 1991, LAGEOS geodetic analysis – SL7.1, NASA Tech. Memo. 104549.
Wilson, D. S., 1993, Confirmation of the astronomical calibration of the magnetic polarity timescale from sea-floor spreading rates, Nature, 364, 788-790.

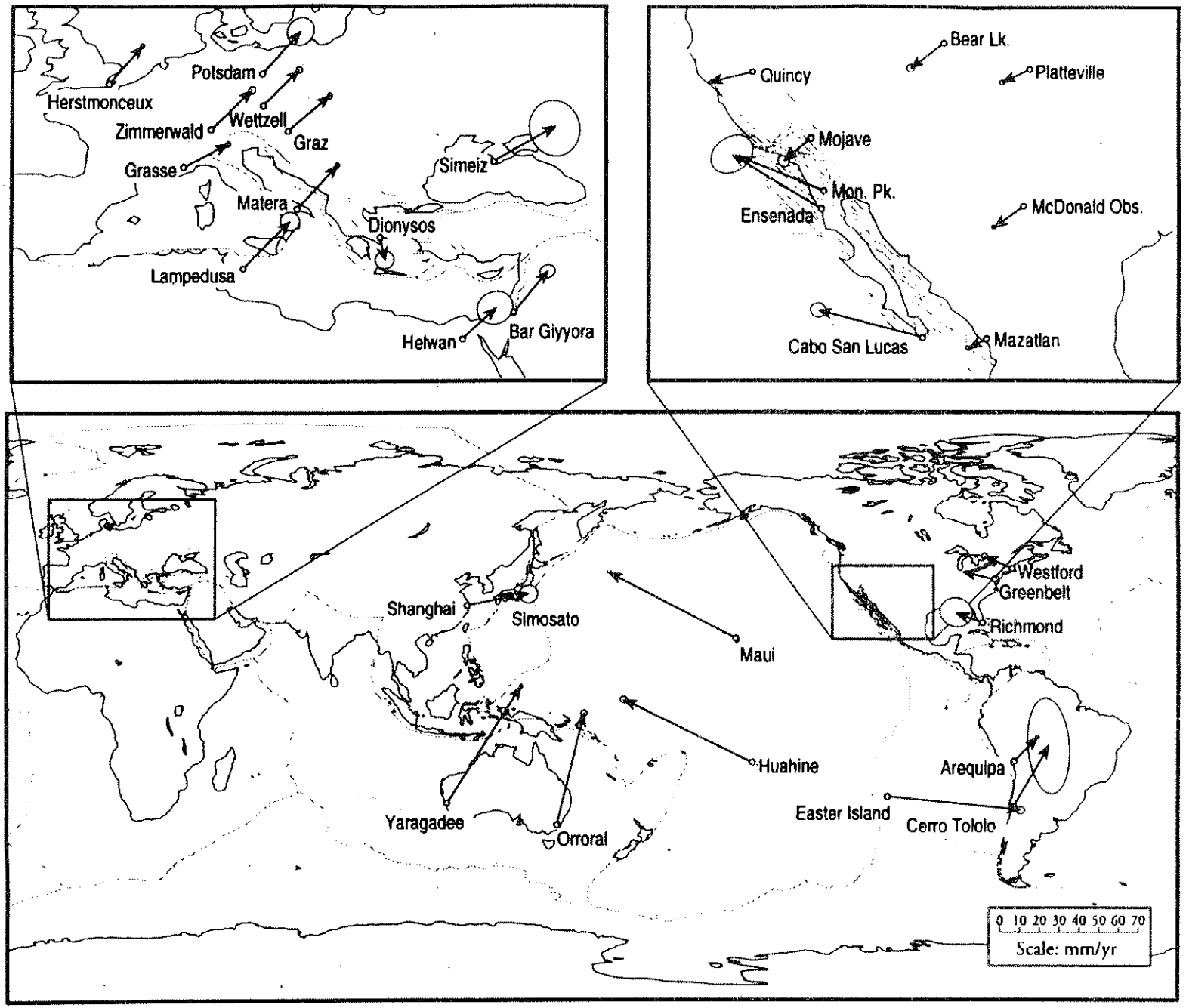

Figure 1. Horizontal vector motion estimated for SLR tracking sites. The kinematic frame is defined by adopting NNR-NUVEL1 motion in the north and east direction of motion at Greenbelt (hence, no error ellipse is shown at Greenbelt) and only the north direction at Maui. Error ellipses are $1-\sigma$. The inset maps use the same vector scale as the main map.

Table 1. SL8.3 determined tracking site motions.

Station Name	SLR Velocities Azimuth (°)	Rate (mm yr^{-1})	Error Ellipse Parameters Semi-Major (mm yr^{-1})	Semi-Minor (mm yr^{-1})	Orientation (°)	NNR-NUVEL Model Azimuth (°)	Rate (mm yr^{-1})
			North American Plate				
Bear Lake†	232	21.5	2.2	2.1	81	236	18.7
Greenbelt*	284	16.5	0.0	0.0	0	284	16.1
Mazatlan	242	10.8	1.3	1.1	-77	230	13.2
McDonald Obs.	234	18.5	0.9	0.8	-69	239	14.8
Mojave†	231	17.5	3.0	2.7	-59	226	18.0
Platteville	245	14.8	1.3	1.2	-74	243	17.5
Quincy	256	22.6	0.8	0.6	-62	224	19.5
Richmond†	289	14.4	8.2	7.4	-68	282	11.7
Westford†	292	15.0	1.4	1.4	-71	290	17.8
			Eurasian Plate				
Dionysos†	168	12.0	4.8	4.3	75	64	26.5
Grasse	64	25.5	1.3	1.1	5	54	25.4
Graz	50	27.7	1.5	1.2	8	58	25.5
Herstmonceux	40	26.1	1.2	1.0	3	49	23.9
Potsdam	42	29.2	7.4	6.5	33	56	24.6
Shanghai†	79	31.9	4.7	4.5	72	121	26.6
Simeiz†	62	35.8	13.6	12.7	-22	69	26.3
Simosato	262	4.7	1.7	1.4	63	127	26.0
Wettzell	45	25.8	1.6	1.5	12	57	25.1
Zimmerwald	47	28.4	1.8	1.6	11	54	25.0
			African Plate				
Bar Giyyora	40	27.2	4.0	3.3	70	52	32.5
Helwan†	48	23.3	9.1	8.1	70	51	32.4
Lampedusa†	46	33.3	4.9	4.6	46	44	29.3
Matera	43	30.1	1.3	1.0	12	43	29.0
			Australian Plate				
Orroral	14	57.4	1.7	1.5	-87	18	59.5
Yaragadee	33	69.2	1.0	0.7	-6	33	74.5
			Pacific Plate				
Cabo San Lucas†	285	54.3	4.0	3.6	-75	292	54.8
Ensenada†	300	52.0	11.2	8.7	61	298	50.0
Huahine	296	72.7	2.1	1.7	-69	297	73.5
Maui	298	72.5	0.8	0.0*	90*	299	69.6
Monument Peak	291	45.2	0.8	0.6	-70	299	48.7
Otay Mtn.	298	47.9	2.9	2.8	76	299	49.1
			Nazca Plate				
Easter Island	96	67.9	2.3	1.8	83	96	83.9
			South American Plate				
Arequipa	44	17.0	1.0	0.7	76	340	10.3
Cerro Tololo†	30	35.9	24.0	10.7	-5	352	9.8

* Contains some components constrained to NNR-NUVEL1 values.
† Results not previously published in Smith *et al.* (1990).

Table 2. Relative poles of rotation implied from SL8.3 and from NUVEL-1 (DeMets *et al.* 1990). First plate rotates clockwise relative to second. One sigma error ellipses are specified by the angular lengths of the principle axis, their orientation (ζ) from north and in the uncertainty of the rotational rate. The percentage difference shows the average increase of the magnitude of the NUVEL-1 inferred velocities with respect to those implied by the SL8.3 poles of rotation for those regions where the tracking sites are located on the rotating plate.

	SL8.3 determined							NUVEL-1							
plate pair	ϕ (°)	λ (°)	ω (°/Ma)	σ_{max} (°)	σ_{min} (°)	ζ (°)	σ_ω (°/Ma)	ϕ (°)	λ (°)	ω (°/Ma)	σ_{max} (°)	σ_{min} (°)	ζ (°)	σ_ω (°/Ma)	% Diff. vect. mag.
au-eu	10.8	47.0	0.70	4.2	0.9	-57	0.05	15.1	40.5	0.72	2.1	1.1	-45	0.01	5%
au-na	27.4	52.2	0.75	4.3	3.2	-77	0.04	29.1	49.0	0.79	1.6	1.0	-53	0.01	5%
eu-na	73.3	157.6	0.22	11.3	7.8	-14	0.05	62.4	135.8	0.22	4.1	1.3	-11	0.01	6%
eu-pa	60.3	-79.0	0.93	2.9	0.7	72	0.04	61.1	-85.8	0.90	1.3	1.1	90	0.02	1%
na-pa	49.9	-72.8	0.77	2.9	1.1	80	0.05	48.7	-78.2	0.78	1.3	1.2	-61	0.01	-10%
pa-au	-59.3	-175.0	1.09	2.7	1.5	76	0.02	-60.1	-178.3	1.12	1.0	0.9	-58	0.02	4%

Inter-continental Plate Motions Derived from SLR Analysis

Minoru Sasaki
Hydrographic Department
3rd Regional Maritime Safety Headquarters
5-57, Kitanaka-doori, Naka-ku, Yokohama 231 Japan
Tel:+81 45 211 0771, Fax:+81 45 212 1597

Masayuki Fujita
Hydrographic Department, Maritime Safety Agency
5-3-1, Tsukiji, Chuo-ku, Tokyo 104 Japan
Tel:+81 3 3541 3811, Fax:+81 3 35415 2885

1. Introduction

In 1982 the Hydrographic Department of Japan (JHD) started to operate a satellite laser ranging (SLR) station at the Simosato Hydrographic Observatory in order to measure the precise relation between the Japanese Geodetic System (Tokyo Datum) and a satellite-derived geocentric coordinate system and also to be the base station of an expanding marine geodetic controls around Japan (Sasaki et al. 1983). In mid-1986, the Japanese Geodetic Satellite, AJISAI, was launched for the purpose above (Sasaki and Hashimoto 1987) . An transportable laser ranging station was developed and named HTLRS by JHD in 1987 (Sasaki 1988) and the field observation was started in early 1988. The observation status of JHD including Simosato and HTLRS is presented by Fujita et al. (1984) as another paper in this issue.

2. Data processing in use of orbital processor/analyzer HYDRANGEA

The development of an orbital processor/analyzer to process the SLR data was started in 1980 (Sasaki 1981) and preliminary results of the SLR station coordinates were obtained in 1984 (Sasaki 1984a; 1984b). The development was completed and the processor/analyzer was named HYDRANGEA in 1988. HYDRANGEA was used to estimate baseline lengths between nearby SLR stations in a specific short arc method with use of several sets of SLR data obtained simultaneously at the two stations for successive passes of a satellite. The precisions of the resultant lengths of stright baselines of Simosato-Chichi shima (938km) and Simosato-Minamitori

shima (2025km) with use of LAGEOS and AJISAI SLR data attain to 4 mm and 7 mm, respectively (Sasaki et al. 1989, Sasaki 1990).

The semi-long arc method is also applied. By using eight five-day-arcs of LAGEOS (5965 normal point data) from Sep. to Nov. 1984 and GEM-T1 gravity field, four geodetic parameters were derived as GM=398600.4452 $\pm$0.0003 km^3 /s^2 , J_2=(1082.571$\pm$0.015)$\times 10^{-6}$, γ (solar reflectivity coefficient of LAGEOS) = 1.111$\pm$0.008 and Δa (mean along track acceleration of LAGEOS) = (-2.5$\pm$3.7)$\times 10^{-12}$ m/s^2. The mean range residual for the estimation is 7.1 cm.

The pole position (x_p,y_p) and excess rotation per day ($\Delta \omega$) of the earth in five day intervals from September 1983 to October 1984 are estimated by means of 85 five-day-arcs of LAGEOS SLR (49,576 normal point) data . The standard deviation of each five-day result is (δx_p, δy_p, $\delta \Delta \omega$) = ($\pm$1.1mas, $\pm$1.4mas, $\pm$0.42ms/d) and mean range residual is 9.8 cm.

3. Estimation of terrestrial reference frames and motion of SLR sites

In order to establish a SLR terrestrial reference frame, the geocentric coordinates of the reference point of each worldwide SLR stations are estimated. As the first case, the LAGEOS normal point data of 5965 ranges in the successive eight five-day-arcs from late-Sept. to early - Nov. in 1984 (mean epoch is 1984.80) are used. The solved-for parameters are 61 unknowns of initial position and velocity of LAGEOS, GM, J_2, reflectivity coefficient, along track acceleration, earth rotation parameters and three dimensional station coordinates for 16 sites. The gravity model used is GEM-T1 of the lower degrees and orders than 21$\times$21. Several station coordinates are fixed based on SSC (CSR) 85L07 (Tapley et al. 1986) in order to avoid uncertainty of solution. The same procedures are made for all LAGEOS range data of forteen five-day-arcs in late 1985 to early 1986, eight five-day-arcs in mid-1986 and nine five-day-arcs in early-1988, nine five-day-arcs from early-Nov. 1989 to late-Jan. 1990 and six five-day-arcs from mid-1990 to late-Jan. 1991.The total numbers of raw range or normal point data and mean residuals are 31933, 7.6cm for 1985.99, 87275, 5.3 cm for 1986.76 and 91634, 4.7 cm for 1988.11, 7168, 5.7cm for 1989.95 and 5051, 5.3cm for 1990.97, respectively. The fixed stations are the same as the previous case but their station positions are slightly shifted by using the plate motion models of AM 0-2 given by Minster and Jordan (1978). The data lists and resultant station coordinates named JHDSC-2(Sasaki 1990), JHDSC-2.5(Tatsuno and Fujita 1994), JHDSC-3 and -4(Sasaki 1990), JHDSC-5 and -6(Sasaki and Sengoku 1993) are given in **Tables 1--12**. Averaging the six heights of these coordinates the height from geocenter (gravity center) is given as : 6371735.476$\pm$0.012m.

4. Change of baseline arc lengths and estimation of plate motions

The change of baseline arc lengths between any two stations of the determined stations and four major fixed stations of Yaragadee, Quincy, Wettzell and Matera were estimated by using the terrestrial reference frame of JHDSC-2, -2.5, -3, -4, -5 and -6. The results for relative baseline arc length change derived are shown in **Table 13** with plate motion models of AM-02 (Minster and Jordan 1978) and NNR 1(DeMets et al. 1990) and some typical cases are given in **Figure 1**. The

Table 1. Data table for JHDSC-2 and range residuals

mean date	station number	normal point	RMS
1984			cm
Sep. 26.26	10	841	7.3
Oct. 1.53	12	569	5.6
Oct. 5.51	13	623	5.9
Oct. 10.71	16	750	6.8
Oct. 16.37	12	821	7.8
Oct. 20.57	13	639	7.2
Oct. 25.71	13	821	8.9
Oct. 31.31	12	901	6.9
		(total 5965)	(mean 7.1)

Table 2. JHD SLR station coordinate set 2 (JHDSC-2) for 1984.80

STATION	U	V	W	SU	SV	SW
	m	m	m	mm	mm	mm
Greenbelt, Maryland	-1130720.328	-4831352.954	3994108.568	28	32	55
Monument Peak, Calif.	-2386279.158	-4802356.889	3444883.211	14	6	13
Huahine, Polynesia	-5345868.277	-2958248.487	-1824625.026	14	14	25
Mazatlan, Mexico	-1660090.188	-5619103.211	2511639.243	16	21	19
Maui, Hawaii	-5466007.043	-2404428.299	2242188.416	24	9	29
Zimmerwald, Switzerland	4331283.534	567549.240	4633140.238	18	41	18
Grasse, France	4581691.869	556159.276	4389359.474	32	13	11
Shanghai, China	-2831087.666	4676203.584	3275172.901	43	24	43
Simosato, Japan	-3822388.330	3699363.577	3507573.186	27	40	29
Graz, Austria	4194426.797	1162693.822	4647246.852	41	60	61
Herstmonceux, Britain	4033463.840	23662.263	4924305.153	18	11	14
Orroral, Australia	-4446476.890	2678127.310	-3696252.010	35	26	43
Quincy, Calif.	-2517244.864	-4198552.155	4076572.977	17	7	12
Arequipa, Peru	1942791.901	-5804077.812	-1796919.276	30	35	38

Table 3. Data table for JHDSC-2.5 and range residuals

date	station number	raw range	RMS
1985			cm
Nov. 1 - 5	13	1757	5.7
Nov. 7 -11	14	3224	8.2
Nov. 12-16	10	3029	7.0
Nov. 24-28	9	1199	8.7
Nov. 29 - Dec. 3	10	1802	10.1
Dec. 9-13	12	1785	6.3
Dec. 15-19	12	2936	8.9
Dec. 20-24	10	1250	7.3
1986			
Jan. 4 - 8	12	2330	6.0
Jan. 9-13	13	3628	9.0
Feb. 2 - 6	10	1899	5.8
Feb. 8-12	11	2299	7.6
Feb. 16-20	11	2194	7.2
Feb. 21-25	14	2661	8.6
	(total 31933)		(mean 7.6)

Table 4. JHD SLR station coordinate set 2.5 (JHDSC-2.5) for 1985.99

STATION	ID	U	V	W	arc used
GSFC105	7105	1130720.246	-4831352.955	3994108.704	8
MNPEAK	7110	-2386279.202	-4802356.844	3444883.273	13
HUAHINE	7121	-5345868.393	-2958248.532	-1824624.880	6
MAZTLN	7122	-1660090.184	-5619103.252	2511639.295	12
HOLLAS	7210	-5466007.073	-2404428.183	2242188.431	11
ZIMMER	7810	4331283.597	567549.650	4633140.055	3
GRASSE	7835	4581691.799	556159.340	4389359.556	7
SIMOST	7838	-3822388.388	3699363.577	3507573.154	14
GRAZ	7839	4194426.882	1162693.883	4647246.692	2
RGO	7840	4033463.820	23662.334	4924305.213	12
AREQPA	7907	1942791.545	-5804077.599	-1796919.011	6

Table 5. Data table for JHDSC-3 and range residuals

mean date	station number	raw range	RMS
1986			cm
Sep. 17.37	10	9033	4.0
Sep. 23.98	11	8462	5.0
Sep. 29.32	13	7665	7.8
Oct. 2.72	13	11046	5.1
Oct. 8.51	12	6062	5.1
Oct. 14.25	13	16561	4.3
Oct. 18.16	12	14436	6.2
Oct. 22.88	10	14010	4.5
		(total 87275)	(mean 5.3)

Table 6. JHD SLR station coordinate set 3 (JHDSC-3) for 1986.76

STATION	ID	U	V	W	SU	SV	SW
		m	m	m	mm	mm	mm
GRF105	7105	1130720.392	-4831353.012	3994108.478	46	30	60
MNPEAK	7110	-2386279.216	-4802356.794	3444883.240	27	18	21
MAZTLN	7122	-1660090.204	-5619103.192	2511639.131	53	24	40
HOLLAS	7210	-5466007.001	-2404428.137	2242188.454	47	69	46
SIMOST	7838	-3822388.362	3699363.594	3507573.190	31	48	44
GRAZ	7839	4194426.800	1162693.823	4647246.696	28	66	39
RGO	7840	4033463.875	23662.353	4924305.137	42	71	47
AREQPA	7907	1942791.795	-5804077.799	-1796919.213	35	38	48

Table 7. Data table for JHDSC-4 and range residuals

mean date	station number	raw range	RMS
1988			cm
Jan. 12.58	14	11638	3.9
Jan. 19.33	10	3887	4.0
Jan. 25.73	14	9865	5.1
Jan. 30.75	11	9391	4.1
Feb. 4.21	11	17370	5.2
Feb. 9.77	11	12228	5.3
Feb. 14.11	12	12817	7.0
Feb. 18.96	12	9885	3.1
Apr. 13.01	9	4553	4.3
		(total 91634)	(mean 4.7)

Table 8. JHD SLR station coordinate set 4 (JHDSC-4) for 1988.11

STATION	ID	U	V	W	SU	SV	SW
		m	m	m	mm	mm	mm
GRF105	7105	1130720.259	-4831353.100	3994108.475	70	49	70
MNPEAK	7110	-2386279.222	-4802356.792	3444883.277	22	32	25
MAZTLN	7122	-1660090.255	-5619103.286	2511639.256	20	25	27
HOLLAS	7210	-5466007.127	-2404427.947	2242188.711	17	37	50
GRASSE	7835	4581691.850	556159.423	4389359.610	47	34	59
SIMOST	7838	-3822388.307	3699363.540	3507573.232	21	60	50
GRAZ	7839	4194426.760	1162693.831	4647246.703	20	15	21
RGO	7840	4033463.833	23662.357	4924305.282	28	36	34

Table9. Data table for JHDSC-5 and range residuals

date	station number	normal point	RMS
1989			cm
Nov. 8-12	12	704	5.7
Nov. 17-21	14	738	5.6
Nov. 26-30	14	1089	6.0
Dec. 2 - 6	11	721	8.0
Dec. 7 -11	13	523	4.4
Dec. 13 -17	12	607	4.0
Dec. 18 -22	12	930	5.7
1990			
Jan. 7 -11	9	908	5.5
Jan. 16 -20	12	948	6.5
	(total 7168)		(mean 5.7)

Table 10. JHD SLR station coordinate set 5 (JHDSC-5) for 1989.95

STATION	ID	U	V	W	arcs used
		m	m	m	
FRTDVS	7080	-1330021.474	-5328403.357	3236481.769	6
GRF105	7105	1130720.270	-4831353.037	3994108.385	7
MNPEAK	7110	-2386279.359	-4802356.701	3444883.313	9
MAZTLN	7122	-1660090.269	-5619103.300	2511639.234	8
HOLLAS	7210	-5466007.168	-2404427.966	2242188.619	4
ZIMERW	7810	4331283.660	567549.688	4633140.115	6
GRASSE	7835	4581691.767	556159.346	4389359.538	8
SIMOST	7838	-3822388.270	3699363.562	3507573.195	9
GRAZ	7839	4194426.692	1162693.938	4647246.719	9
RGO	7840	4033463.803	23662.265	4924305.224	6
AREQPA	7907	1942791.869	-5804077.710	-1796919.170	8

Table 11. Data table for JHDSC-6 and range residuals

date	station number	normal point	RMS
1990			cm
Nov. 11-16	12	1139	4.9
Dec. 3 - 7	17	1224	6.6
Dec. 10-14	14	731	4.2
Dec. 15-19	10	399	4.2
1991			
Jan. 13-17	13	836	7.0
Jan. 26-30	14	722	4.7
		(total 5051)	(mean 5.3)

Table 12. JHD SLR station coordinate set 6 (JHDSC-6) for 1990.97

STATION	ID	U	V	W	arcs used
		m	m	m	
FRTDVS	7080	-1330021.454	-5328403.394	3236481.628	3
HAYSTK	7091	1492454.098	-4457280.297	4296819.599	3
MNPEAK	7110	-2386279.346	-4802356.775	3444883.296	6
MAZTLN	7122	-1660090.330	-5619103.269	2511639.214	6
HOLLAS	7210	-5466007.215	-2404427.735	2242188.599	4
CEROTL	7401	1815517.951	-5213466.979	-3188000.671	5
GRASSE	7835	4581691.744	556159.415	4389359.574	5
SIMOST	7838	-3822388.241	3699363.615	3507573.160	5
GRAZ	7839	4194426.714	1162693.886	4647246.740	4
RGO	7840	4033463.800	23662.324	4924305.269	5
AREQPA	7907	1942791.869	-5804077.710	-1796919.170	8

names of SLR stations with the plate names in each bracket are given in the table and figure. The zero length is the mean length in each figure and each dot shows difference of arc length from the mean length. The change rate of each yearly arc length estimated by means of a line fitting is shown by a solid line and the value with "SLRJHD". The calculated values of the AM02 and NUVEL 1 models are given by broken lines and values with "MJ" and "NVL" for comparison in the figures. The results of the yearly arc-length-change of worldwide SLR stations through the analysis, namely derived plate motions, are shown on a world map in **Figure 2.**

According to discussions by geologists in Japan Simosato is believed on the edge of the Eurasian plate. Therefore, in order to derive the motion of Simosato within the Eurasian plate only the position of Simosato is assumed to move as same as the motion of AM-02 model and other stations are moved as the SLR results above at first. And the arc length changes between Simosato and other stations are calculated. The values are given as (Simost fix in Eura) in right side in **Table 13.** Next, the each value that the actual arc length change derived by SLR analysis given as Sasaki et al. in **Table 13** minus the value of (Simost fix in Eura) for each baseline arc is understood as the effect of the Simosato motion on the Eurasian plate. The subtracted values are given as (Siost within Eura) in **Table 13.** From an arithmetic calculation derives from the subtracted values the mean motion of Simosato in the Eurasian plate is 20mm/year toward 294 degrees of azimuth (WNW). This direction of the Simosato motion almost coinside with the motion of Simosato within the Eurasian plate given by Smith et al. (1990) and recent GPS results in the nearby south part of Shikoku (Tabei 1994). The Simosato centered location of SLR sites projected on the globe, virtual arc length changes between Simosato and other sites which are assumed on the Eurasian plate, and motion vector of Simosato referred on the Eurasian plate are given in **Figure 3.**

Table 13. SLR derived plate motions

<HYDRANGEA results> 1984.80 - 1990.97

stations	Sasaki et al. (Simost within Eura)	DeMets et al. (Simost fix in Eura)	M/J
	mm/y	mm/y	mm/y
Simosato [EURA] -- Quincy [NOAM]	+5 (+16)	-9	-19 (-11)
Simosato [EURA] -- Mon. Pk [PCFC]	-32 (+18)	-56	-64 (-50)
Simosato [EURA] -- Hawaii [PCFC]	-78 (+36)	-89	-99 (-114)
Simosato [EURA] -- Yargde [AUST]	-69 (+8)	-80	-77 (-77)
Simosato [EURA] -- Wetzel [EURA]	-40 (-40)	0	0 (0)
Simosato [EURA] -- Matera [AFRC]	-43 (-43)	-3	0 (0)
Hawaii [PCFC] -- Quincy [NOAM]	+23	+7	+8
Hawaii [PCFC] -- Mon. Pk [PCFC]	+22	0	0
Hawaii [PCFC] -- Yargde [AUST]	-119	-97	-103
Hawaii [PCFC] -- Wetzel [EURA]	-37	-35	-40
Hawaii [PCFC] -- Matera [AFRC]	-40	-46	-43
Mon. Pk [PCFC] -- Quincy [NOAM]	-37	-45	-53
Mon. Pk [PCFC] -- Yargde [AUST]	-97	-97	-103
Mon. Pk [PCFC] -- Wetzel [EURA]	+9	+5	+1
Mon. Pk [PCFC] -- Matera [AFRC]	+12	-0	+5

5. Conclusions

The motions of worldwide SLR stations derived above indicate that the motions of SLR sites almost well coincide with the plate motion models of Minster and Jordan and DeMetz et al. except Simosato. The mean motion of Simosato, 20mm/year toward 294 degrees of azimuth within the Eurasian plate, is understood as followings. Considering the contraction of the arc length between Simosato and Wettzell within the same Eurasian plate, there should exist any reasons for the contraction in some places between the two areas. There may be many microplates on the line from Simosato to Wettzell and it is considered that simple plate model may not be applied. However, in roughly saying, the north part of Europe seems almost stable geologically and the northward penetration of India on the Indian plate toward Siberia causes thrust faulting at Himalaya and Tien shan, and strike-slip faulting, primarily left-lateral, on faults emanating from Tibet and cross Mongolia. The effect thrusts the crust of North China eastward. In this sense the arc length between Simosato and Europe should be rather expanded than contraction . However Simosato is located at around 100 km northwest from Nankai Trough and the distance is

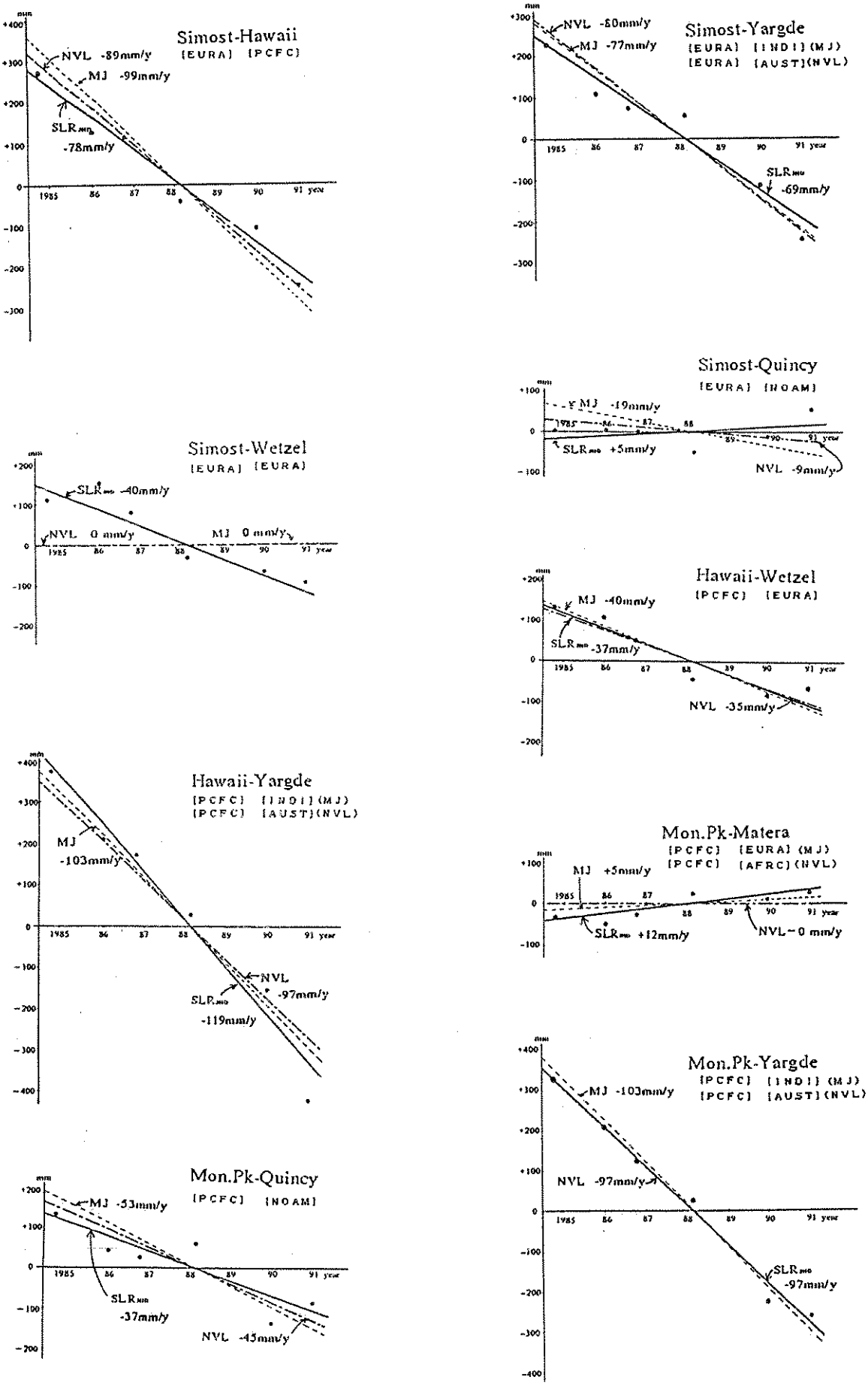

Figure 1. Baseline arc length changes derived from LAGEOS SLR analysis.

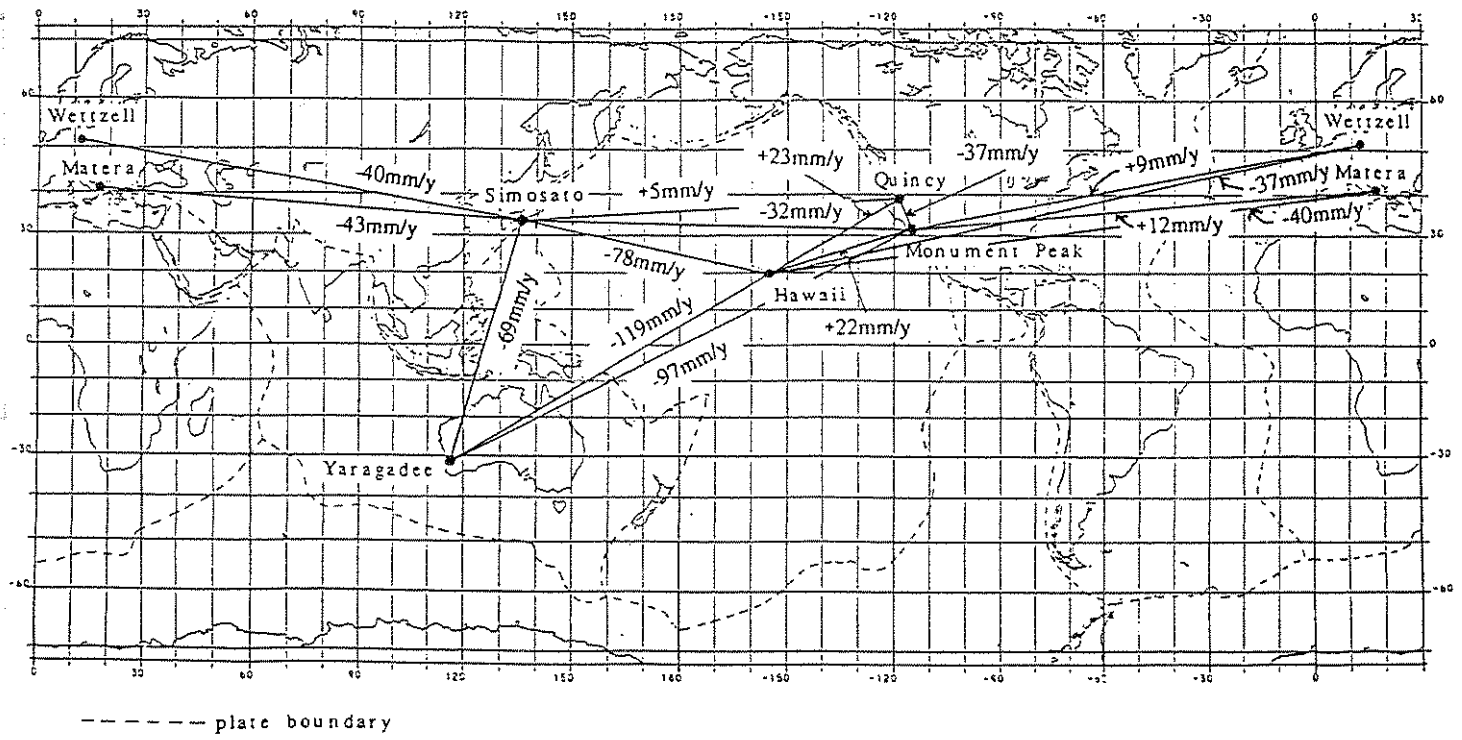

Figure 2. Worldwide plate motions derived from LAGEOS SLR data in 1984 - 91. <HYDRANGEA results>

sufficiently far from the subduction zone of the Nankai Trough. According to Seno (1977) Philippine Sea plate moves to the northwest in the rate of 4 cm/year. Therefore the major reason of the motion of Simosato site obtained is understood as the strain caused by the stress of the Philippine Sea plate at the edge of the Eurasian plate in Nankai Trough. However the direction of the motion is almost 10 degrees different to westward. As for the deflection Smith et al.(1990) indicated that it is associated with the Median Tectonic Line which is right-lateral strike slip feature crossing the Kii Peninsula ~50 km north of Simosato. For precise discussion more SLR data analysis and local crustal information is necessary in the area.

References

DeMets, C., R. G. Gordon, D. F. Argus and S. Stein (1990) : Current plate motions, Geophys. J. Intl., **101**, 425-478.

Fujita, M., M. Suzuki and M. Sasaki [1994] : SLR status in the Hydrographic Department of Japan. Proc. of Simposium on Western Pacific Satellite Laser Ranging Network (WPLS '94), [This issue].

Minster, J. B. and T. H. Jordan (1978) : Present-day plate motions. J. Geophys. Res., **83**, 5331-5354.

Sasaki, M. (1981) : On a baseline measurement by satellite laser rangings. J. Geod. Soc. Japan, **27**, 333-337.

Sasaki, M. (1984a) : Algorithm for determination of satellite orbit and geodetic parameters by using laser ranging data and preliminary results of its application. Rep., Hydrogr. Researches, No. 19, 107-133.

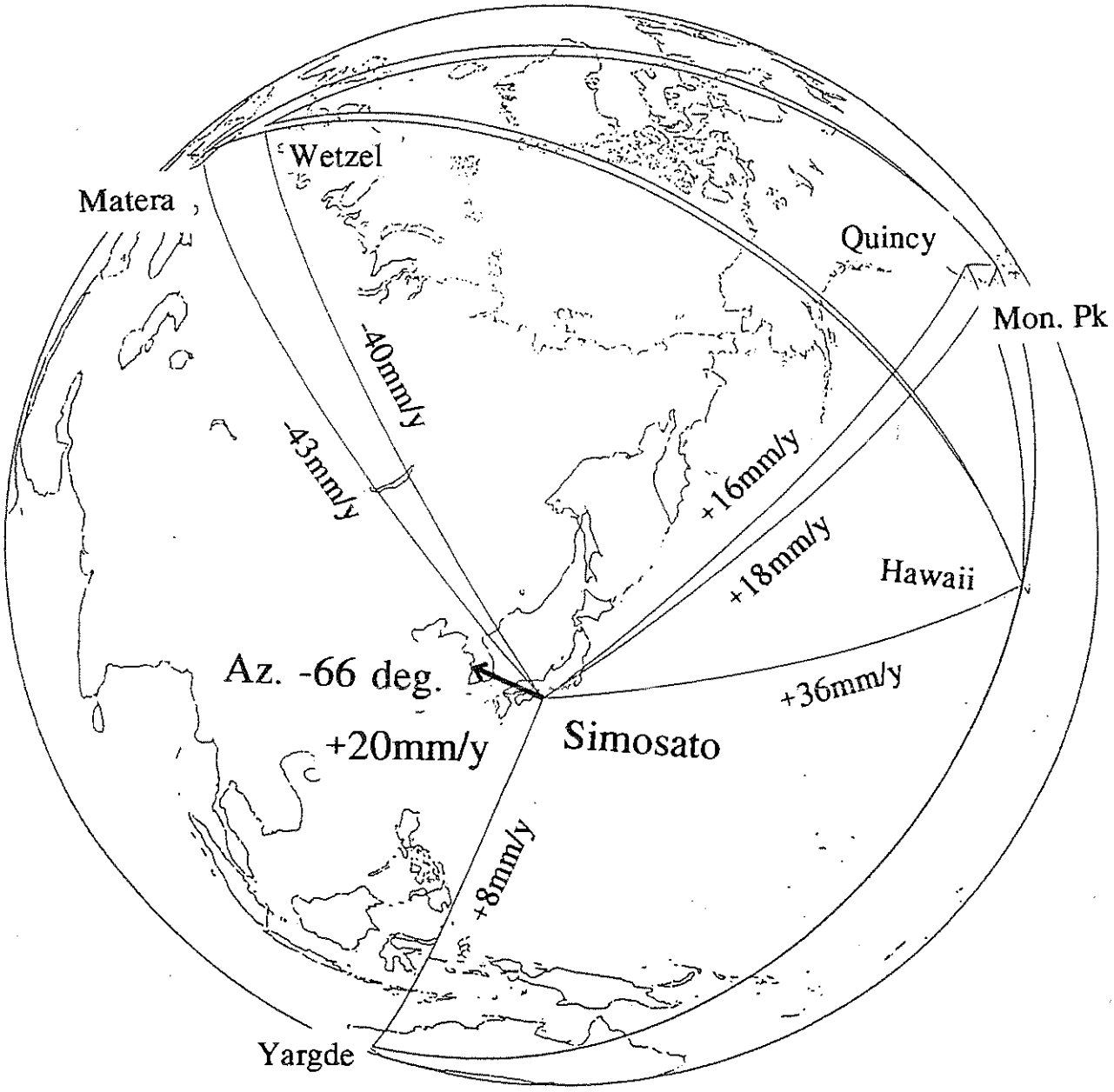

Figure 3. Motion of Simosato in the Eurasian plate.
The arc length changes are virtually derived by assuming all SLR sites on the Eurasian plate.

Sasaki, M. (1984b) : Satellite laser ranging at the Simosato Hydrographic Observatory and its preliminary results. J. Geod. Soc. Japan, 30, 29-40.

Sasaki, M. (1988) : Completion of a transportable laser ranging station (HTLRS). Data Rep. Hydrogr. Obs., Series of Satellite Geodesy, JHD, No. 1, 59-69.

Sasaki, M. (1990) : Study of the earth's dynamics by means of satellite laser ranging techniques. Rep., Hydrogr. Researches, No. 26, 99-187.

Sasaki, M., Y. Ganeko and Y. Harada (1983): Satellite laser ranging system at Simosato Hydrographic Observatory. Data Rep. Hydrogr. Obs., Series of Astronomy and Geodesy, JHD, No. 17, 49-60.

Sasaki, M. and H. Hashimoto (1987) : Launch and observation program of the Experimental Geodetic Satellite of Japan. IEEE Transactions on Geoscience and Remote Sensing, GE-25, 526-533.

Sasaki, M., A. Sengoku, Kubo, Y. and T. Kanazawa (1989) : Baseline determination by a short arc satellite laser ranging technique, J. Geod. Soc. Japan, 35, 117-126.

Sasaki, M. and A. Sengoku (1993) : SLR observation and data analysis made by the Hydrographic Department of Japan in the last decade and the motion of the simosato site, Proc. Intl. Wksp for Reference Flame Estbl. and Tech. Devl. in Space Geodesy, iRiS 93 Tokyo, CRL, 134-141.

Seno, T. (1977) : The instantaneous rotation vector of the Philippine Sea plate relative to the Eurasian plate. Techtonophysics, 42, 209-226.

Smith, D.E, R.Kolenkiewicz, P. J. Dunn, J. W. Robbins, M. H. Torrence, S. M. Klosko, R. G. Williamson, E. P. Pavlis, N. B. Douglas and S. K. Fricke (1990) : Tectonic motion and deformation from satellite laser ranging to LAGEOS, J. Geophys. Res. 95, 22013.

Tabei, T. (1994) : private communication.

Tapley, B. D., R. J. Eanes and B. E. Schutz (1986) : Earth rotation from laser ranging to LAGEOS ; ERP (CSR) 85L07. Rep. MERIT-COTES Campaign on Earth Rotation and Reference Systems, Part III, M. Feissel (ed.), IHB, Paris,B67-B73.

Tatsuno, T. and M. Fujita (1994) : Determination of the position of the mainland control point in the marine geodetic control network, Data Report of Hydrogr. Obs., Series of Satellite Geodesy, JHD, No. 7, 102-106.

STUDY TO DETERMINE THE SATELLITE EPHEMERIS ACCURACY OF TOPEX USING A SINGLE SLR SITE

by

A. R. Peltzer*, W. J. Barnds†, and G. C. Gilbreath*

ABSTRACT

In this paper, we will present the results of an analysis of TOPEX precision orbit determination using a reduced number of sites from the international SLR network. The study provides insight into the position accuracy which can be achieved for an extremely well specified satellite. The study was conducted to determine the viability of using a single SLR site to provide an independent method of verifying GPS navigational performance. Insight was gained into the instantaneous and averaged ephemeris errors. Computational simulations included varying the number and distribution of sites, and empirical modeling of non-conservative forces to determine the limitations of this SLR-based reduction strategy.

*Authors are with the Naval Center for Space Technology, US Naval Research Laboratory, Code 8123, 4555 Overlook Ave. SW, Washington, DC 20375, USA.

†Author is with Swales & Associates, Inc., 5050 Powder Mill Rd, Beltsville, MD 20705, USA.

I. INTRODUCTION

The goal of this study was to determine the satellite ephemeris accuracy of TOPEX/POSEIDON using a reduced number of Satellite Laser Ranging (SLR) ground sites. Our approach was to use GEODYN[1], DELTA, and orbit determination and analysis programs generated by the Naval Research Laboratory (NRL) to gain insight into averaged and instantaneous ephemeris errors using the NASA Precision Orbit Ephemeris (POE) as the "truth" model[2]. The goal of the study was to determine the efficacy of SLR as an independent means of validating Global Positioning Satellite (GPS) navigational performance using a subset of the international SLR network.

II. BACKGROUND

The study focused exclusively on the TOPEX/POSEIDON satellite. The POE was generated in 10 day cycles for the satellite and was derived from SLR and DORIS data. The stated Root Mean Squared (RMS) position accuracy of the POE was 3 cm to 4 cm radial, 8 cm to 10 cm cross-track, and 10 cm to 15 cm along-track[2]. These estimates were based, in part, by comparing orbital differences between the POE and GPS.

Although a number of analytical tools were used in the study, GEODYN provided the primary means of analysis. GEODYN updated the TOPEX orbit by using SLR observations to minimize the residual errors between the observed and calculated ranges. GEODYN used state-of-the-art force models in its solution. The most significant models were as follows: JGM2 for the geopotential, GEM-T3 for ocean tides, DTM for atmospheric drag, and a box/wing "macro-model" for radiative effects. TOPEX specific platform parameters were provided by NASA/Goddard.

The outputs from GEODYN included ephemeris, RMS range residuals and normal points. The GEODYN ephemeris files were used as inputs to DELTA. DELTA would then calculate the average RMS differences in radial, cross-track, along-track, and total position between the GEODYN ephemeris and a baseline ephemeris over a specific period of time. The absolute position error would have been determined by taking the rss of the position "differences" and the POE ephemeris error for the specific radial, cross-track, or along-track component. However, the correlation was unknown, so the computation could not be made accurately. Therefore, we reported position differences with respect to the POE, where POE was considered the truth.

NRL-generated programs developed for this study were utilized to determine instantaneous orbit position errors and the minimum SLR station configuration requirements for achieving sub-meter accuracy. Specifically, parameters such as number of passes and time occuring, zenith elevation, revisit times, and site distribution were accessible through the NRL processing tools.

III. METHODOLOGY

A subset of the international SLR network was examined for suitability in single site orbit determination. Using laser observations from TOPEX, the ephemeris was generated using GEODYN. This computed ephemeris was then compared with the POE to establish instantaneous and orbit-averaged position errors. This methodology was then repeated for the multiple site analysis. Building on the single site orbit determination result, the observations from additional sites were added incrementally to examine the improvement in the ephemeris solution. This study examined three TOPEX 10-day cycles numbered (39,40, and 41) for the period of 4 Oct. 1993 - 4 Nov 1993.

TOPEX orbit estimates were normally optimized at NASA/Goddard using empirically adjusted anomalistic accelerations (AA) with fixed atmospheric drag and solar radiation pressure (D/R) modeling. The AA compensated for the unexplained but observable perturbations acting on the satellite in its orbit. The background model of fixed D/R values were calibrated by NASA/Goddard based on prior observations from the global SLR network. Due to the abundance of data, the AA could be determined effectively from the complete network. However, our analysis indicated that solving for AA from a single site was not possible. In all cases, the solution was "ill-behaved" due to the paucity of observations and single site's coverage gaps.

A series of cases were run for comparison which included: fixed AA and fixed D/R; no AA and fixed D/R; and no AA and varying D/R, for both single and multiple sites. These cases were summarized in Table 1 of Section V. Additional computational simulations were conducted to determine the impact of the number of passes, data density, and optimization of solution intervals. The effectiveness of performing sequential GEODYN runs without apriori knowledge from existing POE ephemerides was also examined.

An important implicit consideration throughout this analysis was the necessity for TOPEX passes to cover both ascending and descending portions of the orbit. In all of our single site results, the individual site passes were approximately evenly distributed between the two portions of the orbit. Similarly, in the trials involving improvements to single site accuracy by the addition of passes over a second site, care was taken to ensure that the passes over the second site did not result in one portion of the orbit arc being over-weighted with respect to any other part.

IV. RESULTS

A. SINGLE SITE ANALYSIS

In the first part of the analysis, nine globally distributed SLR site observations were individually compared using GEODYN and DELTA. Figure 1 shows RMS total position differences versus number of observations for each of the nine sites. The ephemeris from each single site was compared with the POE to determine the RMS position differences. Results for cycle 39 demonstrated that approximately 500 observations were necessary for sub-meter ephemeris accuracy. Total position differences were graphed for each of the nine sites. In the first set of results, D/R were fixed. In the second set, the D/R were allowed to vary, which permitted GEODYN to

more accurately model the trajectory. For both cases, no AA adjustments were made to the orbit, for the previously described reasons. Results show a substantial improvement in the solution by recovering the D/R parameters. For example, the position difference for Yarragadee (7090) was 126 cm RMS with no D/R adjustment and 38 cm RMS with recovered D/R terms. When recovering the D/R parameters, two consecutive D/R terms were solved for during the 10 day cycle with their boundary set after half the total number of passes.

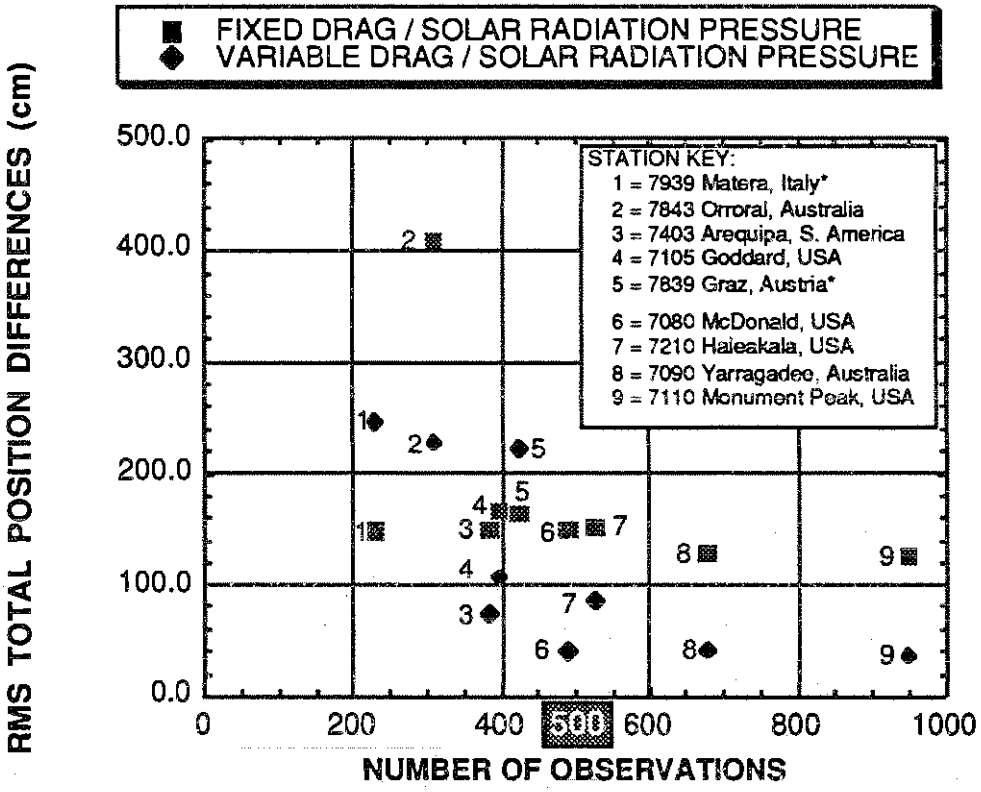

Figure 1. Results from nine independent SLR sites show approximately 500 observations are needed for sub-meter accuracy over the 10-day cycle examined. Each estimate is the position difference with respect to the POE.

Figure 2 shows the same information with the x-axis expressed in terms of the number of passes. This plot shows that approximately 15 passes were necessary for sub-meter accuracy. As shown, the number of passes was a better variable for predicting position accuracy than the number of observations. The generalization that the distribution of data was more important than the density of data proved to be true for each of the cycles examined.

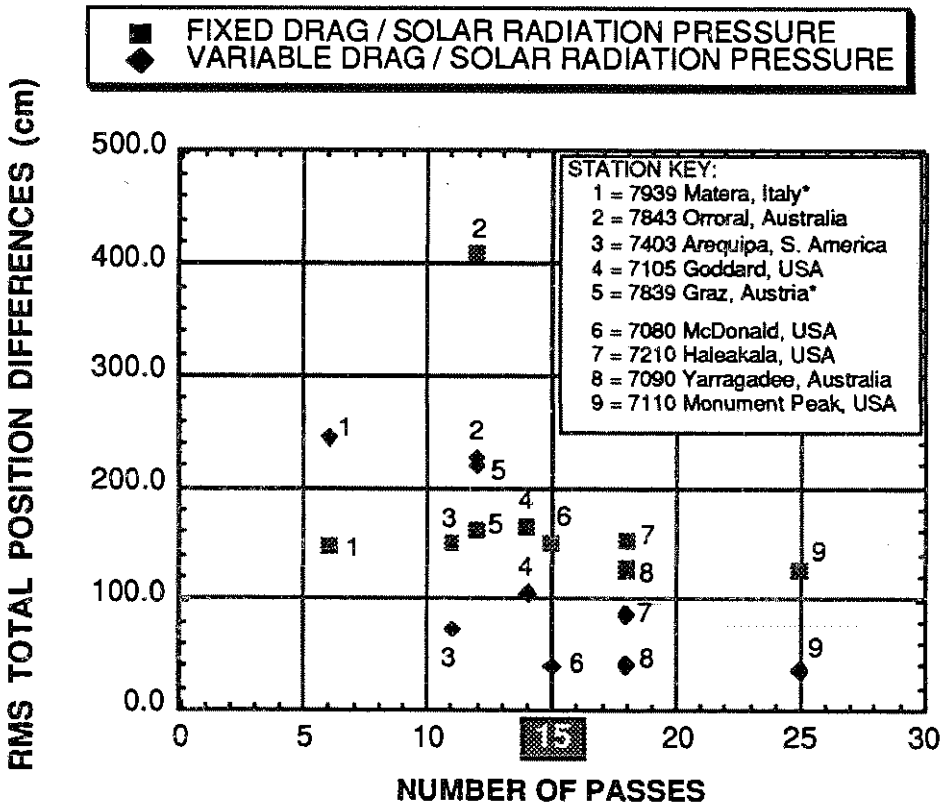

Figure 2. Results from nine SLR sites show a minimum of 15 passes are necessary for sub-meter accuracy over the 10-day cycle examined.

The next part of the study was to assess whether or not consecutive cycles of GEODYN could be run using a single SLR ground site. The three cycles chosen were numbers (39,40, and 41). For this case, there were no AA, two D/R parameters were recovered per cycle, and initial conditions (IC) for succeeding cycles were determined from the previous cycle. Figure 3 shows the Root Sum Squared (RSS) instantaneous total position difference over the 30 day period for the global SLR network and for Monument Peak (7110). The plot demonstrated that a single site was capable of producing sub-meter ephemeris for three consecutive 10-day cycles using the TOPEX satellite. The diamond markers on the plot show when measurements were made during a pass. There was a strong dependence on the number of passes and their distribution as shown in the results. For example, cycle 41 had fewer observations and one less pass than cycle 39, but it produced a better solution (33 cm vs. 42 cm) rms, due to its more uniform distribution of data. Peaks in the plot occur where data was sparse and at the beginning and end of each 10 day cycle as often seen from the "bow-tie" effect[3]. These effects were inherent charcteristics of all least-squares estimators.

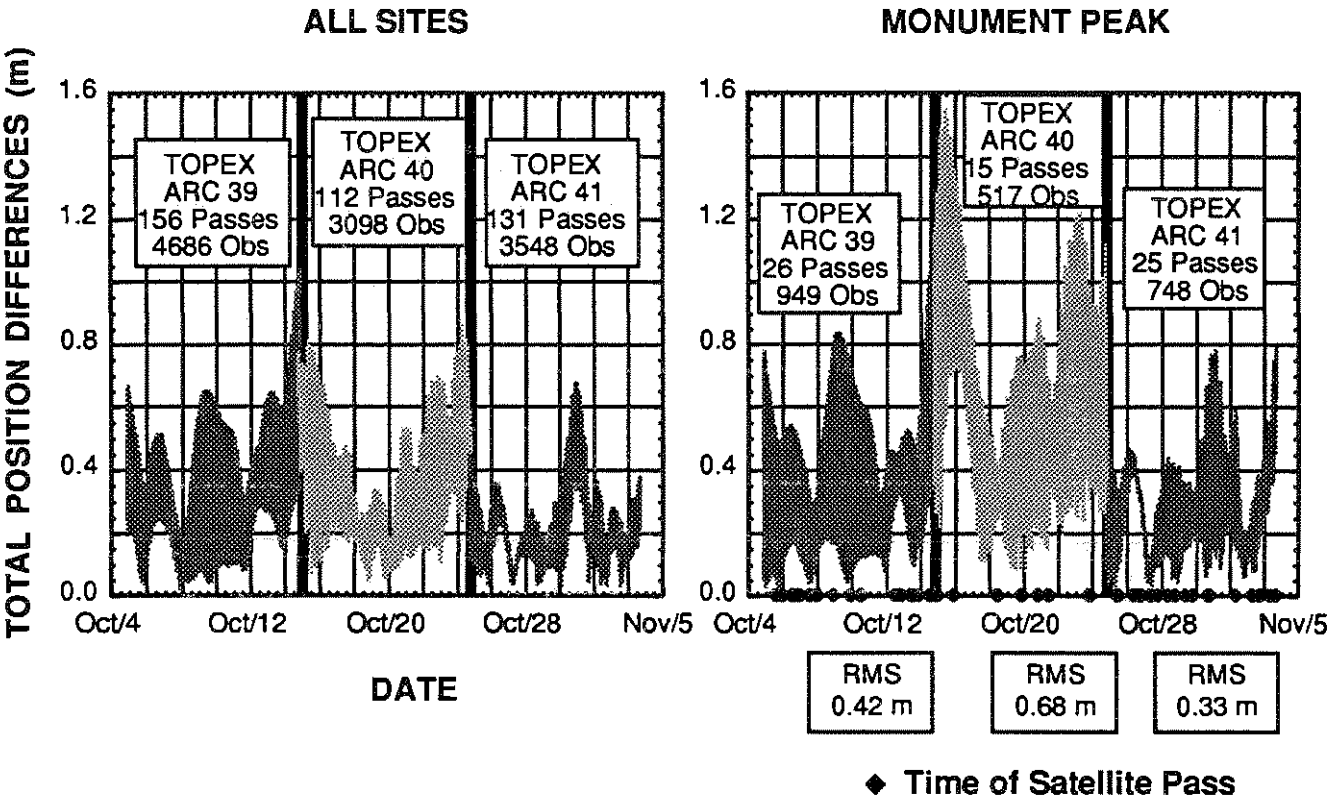

Figure 3. Total position difference with respect to POE for three consecutive 10-day TOPEX cycles for all SLR sites and Monument Peak (7110).

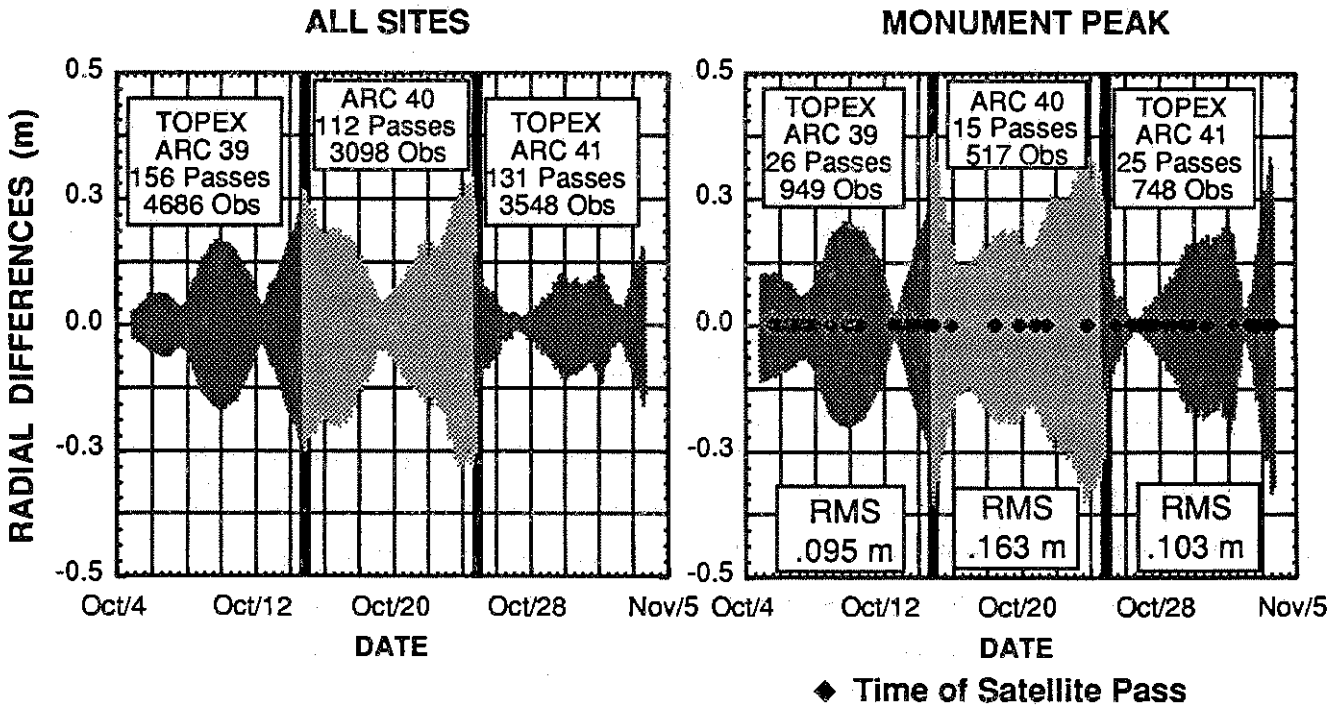

Figure 4. Radial position difference as compared to POE for three consecutive 10-day TOPEX cycles for all SLR sites and Monument Peak (7110).

Cycle 40 had only 15 passes and poor pass distribution, producing a substantial increase in RSS difference from 42 cm to 68 cm. A close comparison of the two cases demonstrated the strong influence of Monument Peak on the all site ephemeris solution. As seen in Figure 3, the difference plots for both cases display some similar features. This was due to the large number of observations contributed to the solution by Monument Peak as compared with the other stations in the network for that specific period of time. Figure 4 shows the same part of the study, with the radial difference component of the solution being graphed. A strong dependence on number of passes and their distribution was evident again for the solution of Monument Peak. Cycle 40 had a larger RMS radial difference (16.3 cm) as compared to the other two cycles (~10.0 cm).

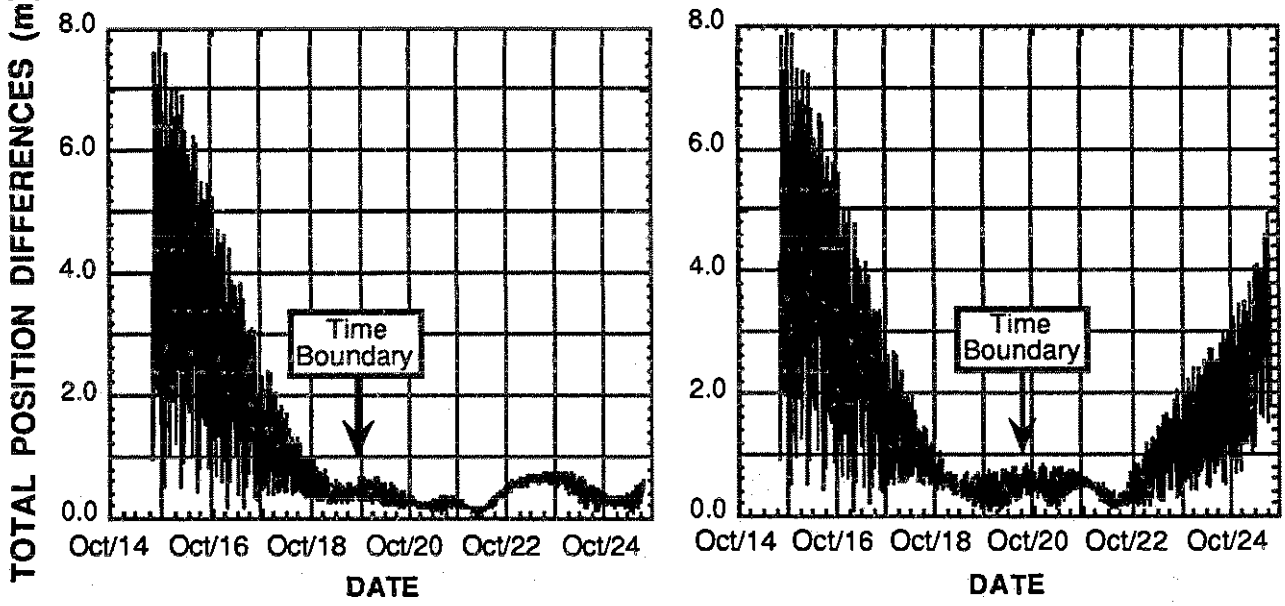

Figure 5 (a&b). Figure 5a displays results of total position difference with the boundary for adjustments of the two D/R terms set halfway in time through the 10-day TOPEX cycle-40. Figure 5b shows the solution with the boundary of the D/R terms shifted to half the total number of observations.

The TOPEX cycle 40, beginning 14 October 1993, initially had an instantaneous RSS total position difference of 7.5 m at the beginning of the cycle, as compared to the POE. Initial conditions predicted from the previous cycle were used. Figure 5 shows the procedure used to reduce the observation residuals for cycle 40. D/R and ICs were varied during the solution interval. Figure 5a shows the original solution with an instantaneous difference of 7.5 m at the beginning of the cycle. Two consecutive D/R terms were being solved for with their boundary set halfway in time through the cycle. Plot 5b shows the two D/R terms boundary centered at half the total observations. The position difference

increased in the beginning and end of the cycle. The third plot, 5c, shows the solution with one D/R being solved for over the 10 day cycle. This result reduced the magnitude of the peak difference to 5.8 m. Plot 5d shows the result from adding two passes to the beginning of the cycle. Two D/R terms were solved for in this case with the boundary set at the midpoint of the total number of observations. The total position rms difference was reduced to 0.68 m. These results demonstrated the need for more observations at the beginning of the cycle to balance the data distribution.

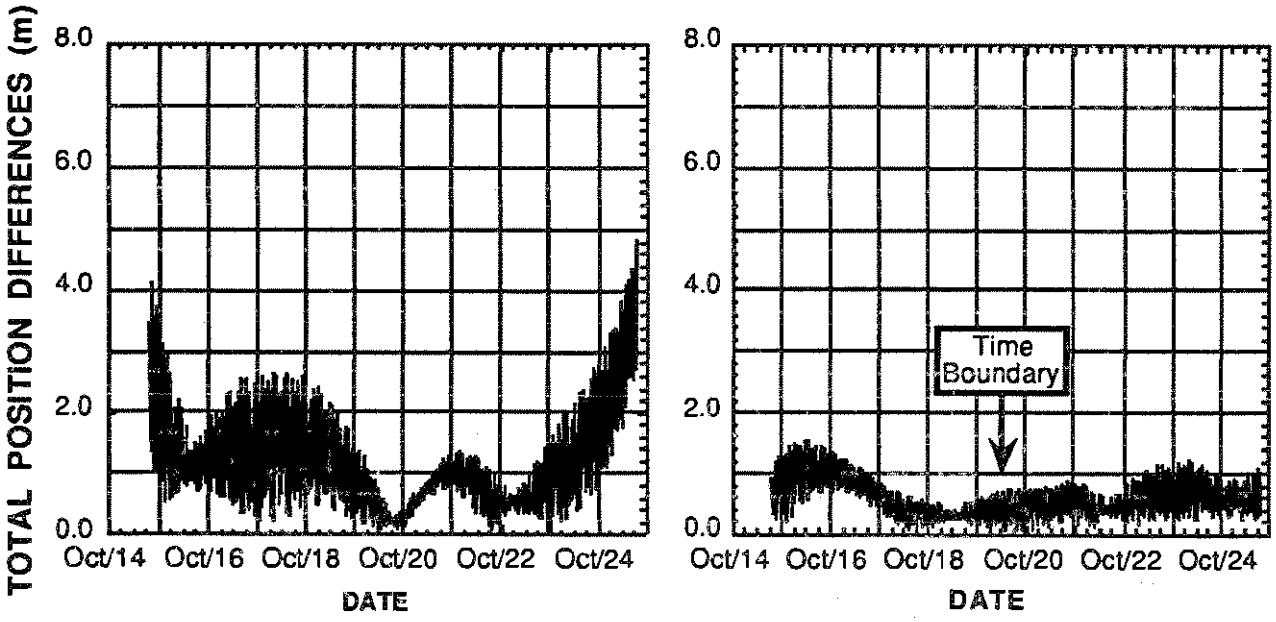

Figure 5 (c&d). Figure 5c is total position results using one D/R term over the 10-day TOPEX cycle-40. Figure 5d demonstrates improvement in solution by adding two passes to the beginning of the 10-day cycle and setting the boundary of the two D/R terms by half the total observations.

B. MULTIPLE SITE ANALYSIS

In the next part of the analysis, the observations for additional sites were added incrementally to those of the initial single site to examine the improvement in the ephemeris solution. Figure 6 shows the total position RMS difference versus an increased number of sites. The D/R were estimated for all cases and no AA parameters were adjusted. The initial site chosen in this case was an average site from the global SLR network. Typically, such a site had less than 15 satellite passes over the 10 day cycle, which was less than the number of passes deemed necessary for sub-meter accuracy. We observed a significant reduction in the RMS position difference after adding the observations from the second site to those of the initial site (from 105 cm to

35 cm). No significant improvement resulted from using the observations from additional sites given this empirical orbit parameterization. With more sites however, additional parameters can be recovered as was done when NASA produced the POE, which achieves ~15 cm overall position accuracy.

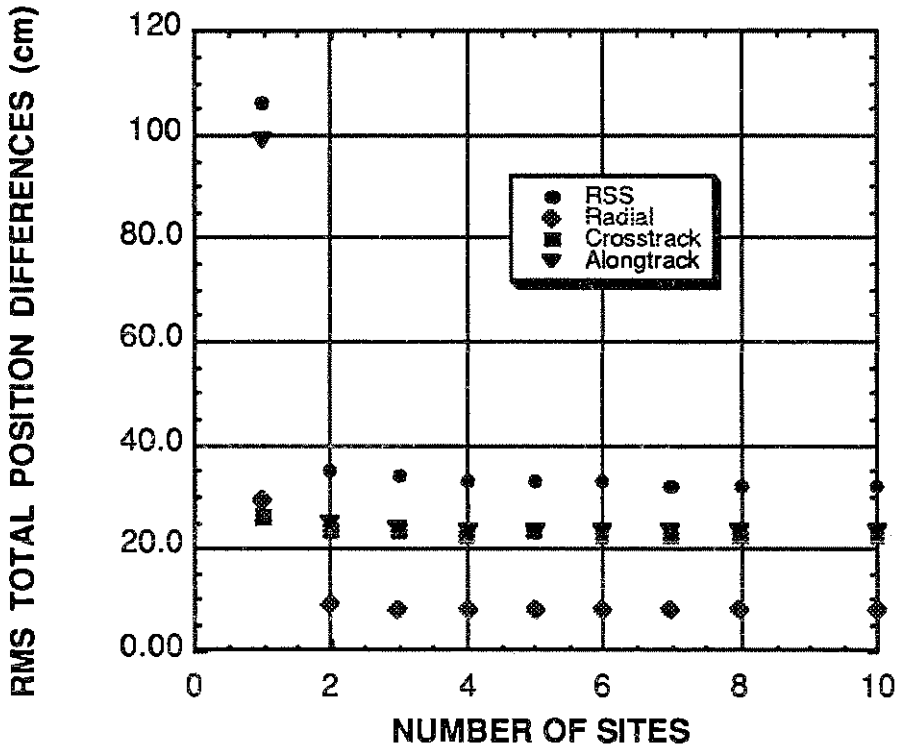

Figure 6. Total position difference versus an increased number of sites demonstrates that two SLR sites, that are non- coincident during measurements, provide 40 cm orbit accuracy.

V. SUMMARY OF RESULTS FOR SINGLE AND MULTIPLE SITE ANALYSIS

The cases and results from this analysis are summarized in Table I. All results were represented as total position differences in ephemeris as compared to the POE. The total position error of the POE was 15 cm.

In summary, single site ephemeris accuracy in the sub-meter range was achieved. This was shown for a number of independent sites. Furthermore, we demonstrated the ability to achieve this accuracy using a specific site for three consecutive TOPEX 10-day cycles, with self-generated initial state vectors. The conditions for this solutions were as follows: a well specified satellite (TOPEX); a minimum of 15 passes of SLR data; and a

relatively even distribution of ascending and descending satellite passes (maximum revisit time of less than 2 days) throughout the solution interval.

Table I.

CASE	AA	D/R	COMMENTS	TOTAL POSITION RMS (cm)
All Sites	Fixed	Fixed (1)	NASA's Apriori Values	15
All Sites	None	Fixed (1)	Used to Compare with ->	123
All Sites	None	Adjusted (2)	Single/Multiple Site Cases	38
Single Site	Adjusted	Fixed	Could Not Converge	****
Single Site	None	Fixed (1)	Best Single Sites	125
Single Site	None	Adjusted (2)	Best Single Sites	39
Single Site	None	Adjusted (2)	3 Consecutive Cycles	42/68/33
Single Site	None	Adjusted (2)	Average Single Sites	100 to 200
Two Sites	None	Adjusted (2)	2 Average Sites	43
Three Sites	None	Adjusted (2)	Reached Boundary **	42
Nine Sites	None	Adjusted (2)	"	42

The results from the multiple site analysis demonstrated that in most cases, two SLR sites were sufficient for 43 cm RMS total position accuracy. Further, they showed that if a given single site had fewer than 15 passes, the addition of non-coincident passes from a second site reduced total position differences to less than 50 cm. The only qualification to this last statement was that these additional passes from a second site should cover a portion of the TOPEX trajectory which had not previously been tracked. To repeat, these cases did not use AA parameter adjustments which have demonstrated the ability to improve the ephemeris solution using the available observations from the complete SLR network. Solving for AA was an under-determined problem for a reduced number of sites.

VI. CONCLUSION

The results from this study were TOPEX/POSEIDON specific. Sub-meter ephemeris was produced using the best single SLR sites. The distribution and density of observations and passes had a significant effect on the ephemeris solution. The study demonstrated the ability to estimate satellite position using a single SLR site by optimizing the solution interval. Orbit differences, as compared with the POE, were

reduced to 40 cm RMS total position for good SLR sites. Adding a second SLR site reduced ephemeris differences substantially, from 100 cm to 40 cm RMS, when the single site had less than 15 satellite passes of data or a non-uniform distribution of passes. This study demonstrated the ability of select single and dual sites to perform orbit determination to provide an independent method of verifying GPS navigation at the sub-meter level.

VII. REFERENCES

1. B. H. Putney, *GEODYN II Description*, NASA/GSFC/HSTX Contractor Report, 1991
2. B. D. Tapley, et. al., "*Precision Orbit Determination for TOPEX/Poseidon*", J. Geophys. Res, 99, (C12), 24,383 - 24,404, 1994.
3. O. L. Colombo, "*Ephemeris Errors of GPS Satellites*", Bull. GEOD., 60, (64-84), 1986.

ERS-1 PRECISE ORBIT DETERMINATION WITH SLR DATA

G.Bianco[1],A.Cenci[3],R.Devoti[2],M.Fermi[3],C.Luceri[2],P.Rutigliano[2],C.Sciarretta[3]

[1] Agenzia Spaziale Italiana, Centro di Geodesia Spaziale, Matera, Italy
[2] Telespazio, Centro di Geodesia Spaziale, Matera, Italy
[3] Telespazio, Roma, Italy

Introduction

This paper shows the results of a series of ERS-1 orbit determination tests from SLR data carried out at the Italian Space Agency's Center for Space Geodesy (CGS) located in Matera, Italy, to support the Synthetic Aperture Radar (SAR) interferometry activities of the Italian Processing and Archiving Facility (I-PAF) and to develop know-how for future LEO missions (e.g. ERS-2, ENVISAT). Due to the failure of the PRARE space segment, the precise orbit determination for ERS-1 is entirely based on SLR data. Three orbit arcs, each 5.5 days long, have been analysed with a dynamic approach using a state-of-the-art software (GEODYN II) developed at the NASA Goddard Space Flight Center, and a force model which takes into account the complex form of the satellite.
After the internal consistency check of the solution, our orbit has been compared with the precise orbit coming from the German Processing and Archiving Facility (D-PAF) and the orbit estimated at the Delft University of Technology (DUT).

The data set

A period of 13.5 days of May 1993, going from the 14th at 12:00 UTC to the 27th at 00:00 UTC, has been selected and divided into 3 arcs, each 5.5 days long, having a 2-days overlapping time span. The analysis has been done using both full-rate (FR) data and on-site quick-look normal points (QL/NP). The temporal distribution of the FR data set is shown in Figure 1. The number of observations and the fit residuals root mean square of each arc are underlined; the numbers between parentheses are the corresponding parameters of the normal point analysis. The temporal distribution is a critical factor; it, and above all its "large holes", strongly affects the quality of the estimated orbit. Even in this test case, with a particularly good data coverage, we will see how the lack of data for a time span (e.g. the interval in May 22th) can play an important role in the orbit determination.

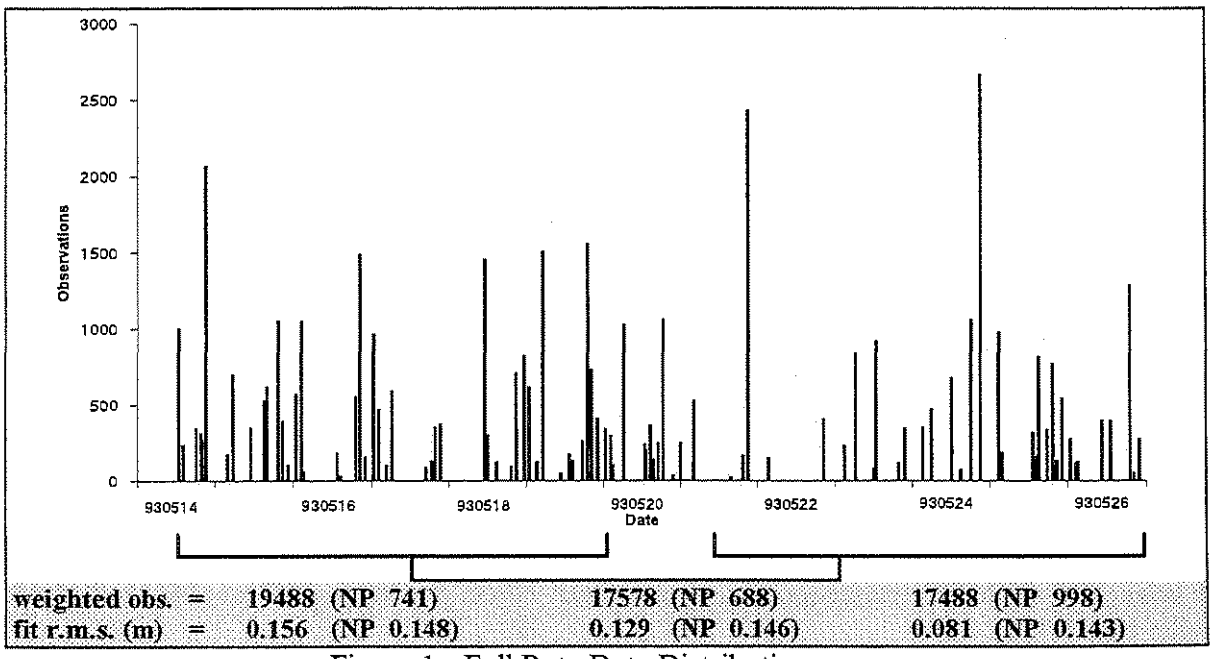

Figure 1 - Full Rate Data Distribution

The model

A summary of the main features of the model is given in the table below (Table 2). Some aspects must be underlined: the use of the full JGM-2 model for the gravity field and ocean tides, the modelling of the air density with the Thermospheric Drag Model (DTM) that uses 3-hourly Kp terms and the modelling of aerodynamic drag and solar radiation pressure using the description of the satellite shape.
All the estimated parameters are listed in the above mentioned table.

Model and constants	
Reference frame	
- Precession	IAU 1976
- Nutation	IAU 1980
- Planetary ephemerides	DE-200
- Station coordinates	ITRF91 advanced to May 1993 using Nuvel-1 Tectonic Model
- Reference ellipsoid	ae = 6378136.3 m 1/f = 298.257
- Pole tide	IERS
Dynamical model	
- Earth gravity field and associated tides	JGM-2 (NASA/GSFC - UTC/CSR) 70x70
- Third body attraction	Sun, Moon + all the planets
- Atmospheric drag	DTM Model 3-hourly Kp and daily F10.7 (NOAA values) Panel modelling
- Solar radiation pressure	Panel modelling
Estimated parameters	
- State vector - 12 hourly CD coefficient - solar reflectivity coefficient - Once per rev acceleration	

Table 1

The results

The consistency of the orbit has been verified by comparing the orbit of two contiguous arcs in the overlapping period. The differences of the estimated positions have been expressed in terms of radial, cross-track and along-track components and are shown in Figures 2a-2b. These graphs, as all the other in this paper, refer to the orbits resulting from the analysis of SLR full-rate data; the analysis performed using normal points gave similar results, as we expected, and only some statistical parameters of the orbit quality check have been included here.
Looking at the previously mentioned graphs, it's evident that the highest differences involve the along-track component and they dramatically increase when the lack of data becomes critical. The large differences at the beginning of the first overlap (fig.2a) are explained by the lack of data at the beginning of the second arc. This "hole" of observations belongs to both the first and the second arc but the orbit is better "constrained" in the first case by the measurements which preceed and follow the interval. On the contrary, the radial and cross-track differences are much smaller and behave in the same way: their root-mean-square is better than 10 cm and their peak-to-peak value is always smaller than 30 cm.

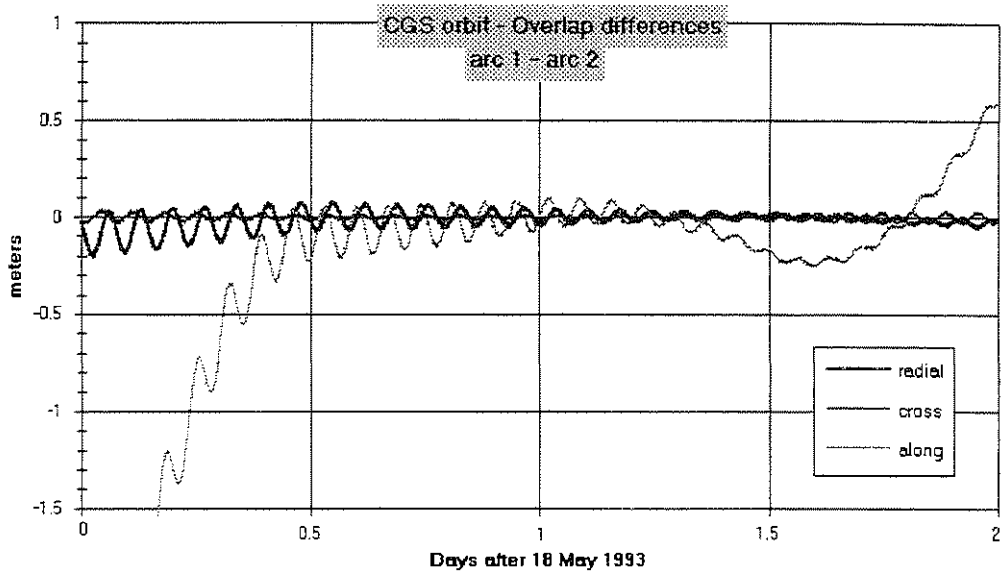

Figure 2a

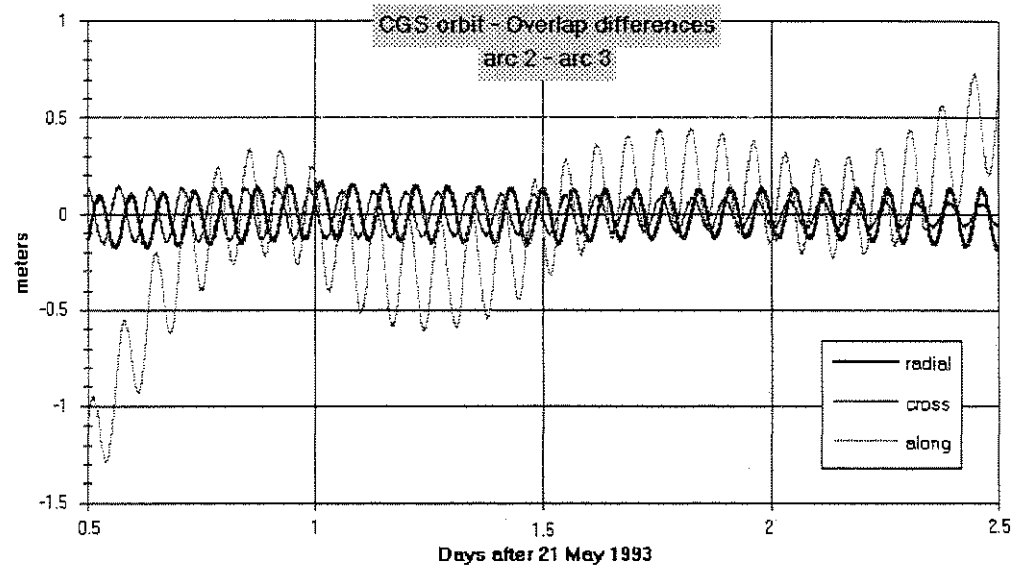

Figure 2b

The internal consistency check is not sufficient to state the quality of the orbit; external comparisons are necessary to be more confident that the estimated orbit is the "real" orbit of the satellite.
This has been accomplished by performing two spot by spot comparisons: one with the precise orbit coming from the D-PAF and the other with the ERS-1 orbit estimated at the DUT.
The first comparison (the differences for each arc are plotted in the figures 3a, 3b, 3c) showed a good agreement between the orbits, the differences being larger when there is a lack of data for a long period (tens of hours), which results in a poorer estimation of the parameters. As stated before, the along-track component is strongly related to the data distribution as pointed out by the deep negative peak in the second and third arc (May 22th). A summary of the comparison is in Table 2.

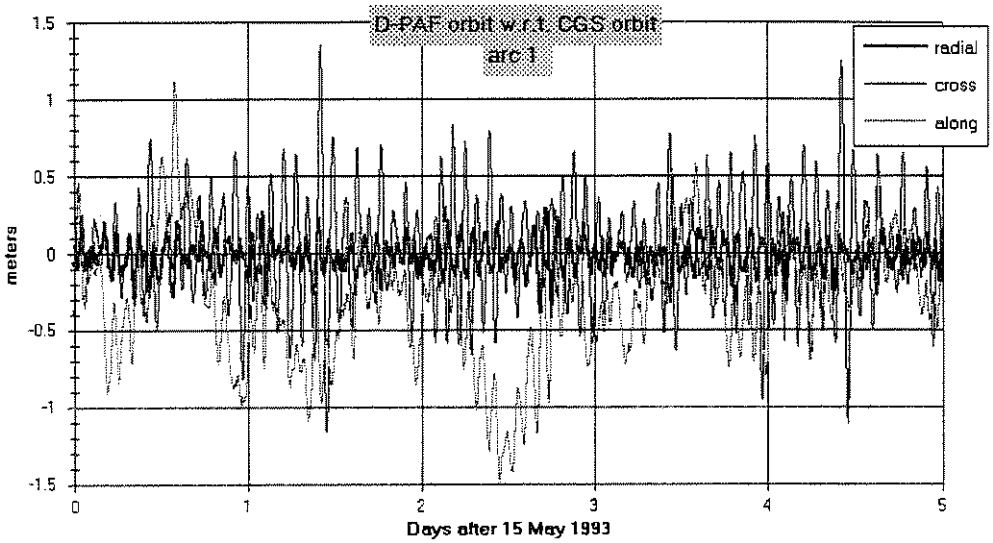

Figure 3a

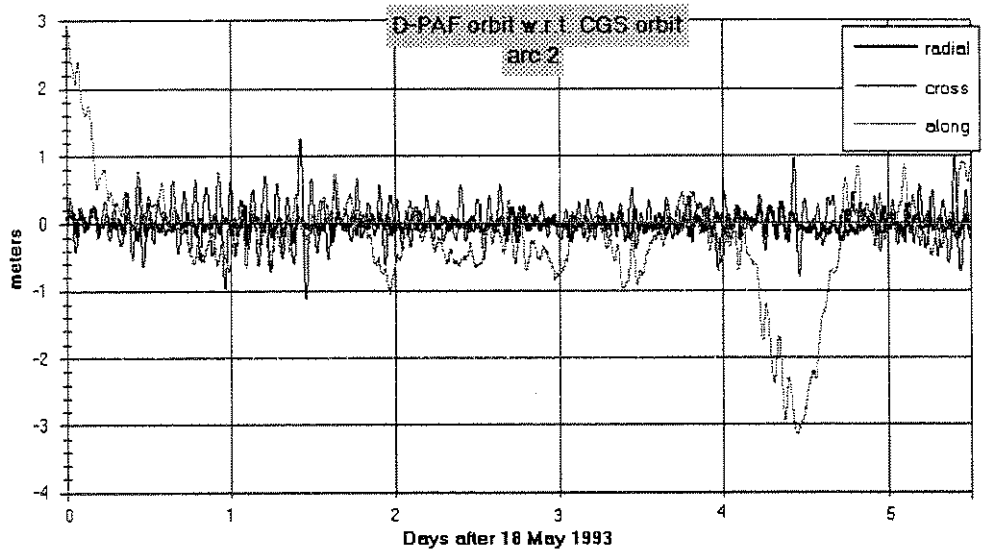

Figure 3b

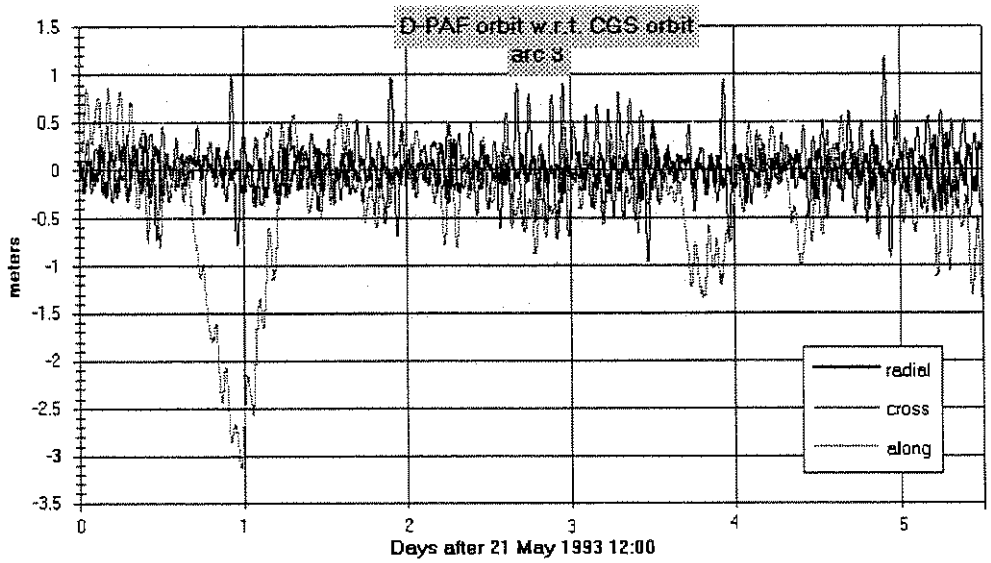

Figure 3c

Summary of orbit differences : D-PAF w.r.t. CGS

	Arc 1			Arc 2			Arc 3		
Position diff. (m)	**Radial**	**Cross**	**Along**	**Radial**	**Cross**	**Along**	**Radial**	**Cross**	**Along**
Minimum	-0.433	-1.162	-1.496	-0.368	-1.113	-3.145	-0.439	-0.954	-3.143
Maximum	0.290	1.363	1.123	0.310	1.257	2.995	0.374	1.190	0.860
Mean	**-0.018**	**0.028**	**-0.298**	**-0.012**	**-0.033**	**-0.221**	**-0.019**	**-0.038**	**-0.304**
Rms	**0.103**	**0.356**	**0.497**	**0.100**	**0.298**	**0.820**	**0.129**	**0.326**	**0.726**

Table 2

The second spot by spot comparison, made with the orbit from DUT, gave, at first glance, worse results (about 20 meters in the X and Y differences) that were unexpected because the same software and substantially the same models were used on the same kind of data (only SLR data) to determine the satellite ephemerides.
With a more accurate analysis of the differences, the reason was found in the coordinate reference systems adopted by the two groups. The rotation angles between the two systems were calculated and a rotation of 0.7 arcsec about the Z-axis, that cannot be traced to the used of a different set of *a priori* station coordinates, was discovered.
After the back rotation of the DUT satellite state vectors, to have two consistent sets of ephemerides, the comparison has given very good results (Figures 4a, 4b, 4c and Table 3), even in those intervals without data because of the similarity of software and models.

Summary of orbit differences : DUT w.r.t. CGS

	Arc 1			Arc 2			Arc 3		
Position diff. (m)	**Radial**	**Cross**	**Along**	**Radial**	**Cross**	**Along**	**Radial**	**Cross**	**Along**
Minimum	-0.222	-0.354	-0.629	-0.361	-0.570	-0.961	-0.1959	-0.387	-0.600
Maximum	0.178	0.378	1.005	0.325	0.603	0.853	0.1580	0.421	1.050
Mean	**-0.037**	**0.000**	**0.014**	**-0.039**	**0.000**	**-0.022**	**-0.036**	**0.001**	**0.085**
Rms	**0.083**	**0.173**	**0.268**	**0.112**	**0.210**	**0.326**	**0.075**	**0.209**	**0.311**

Table 3

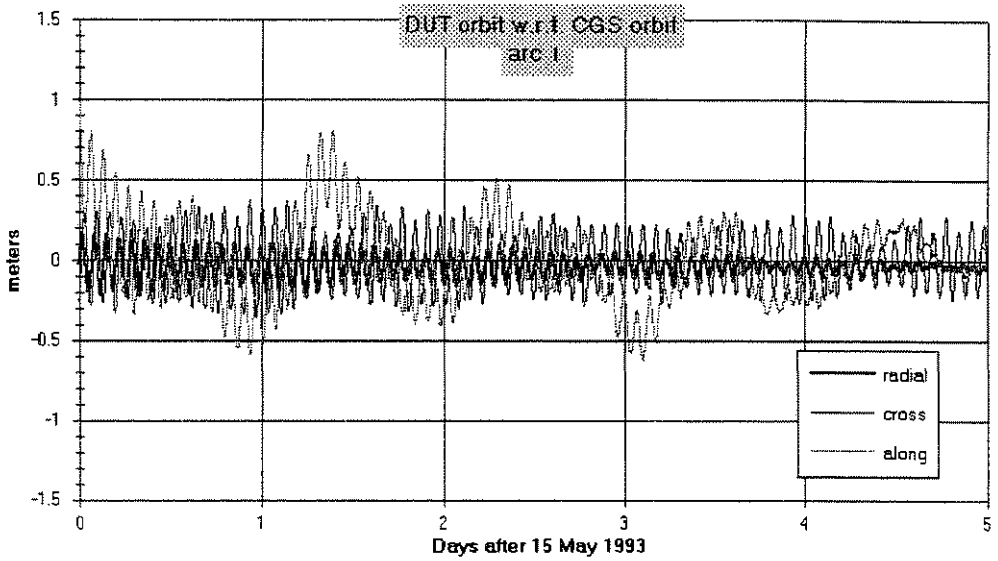

Figure 4a

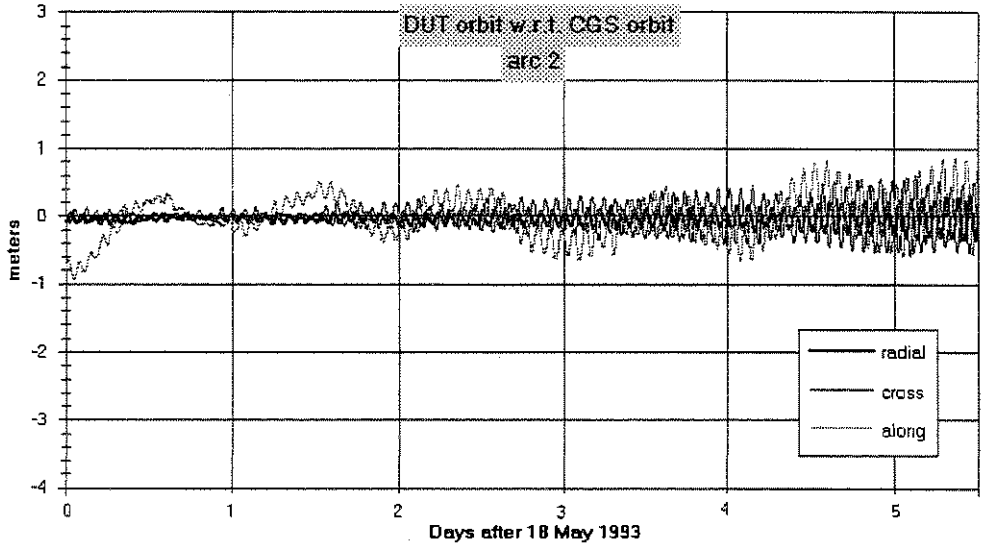

Figure 4b

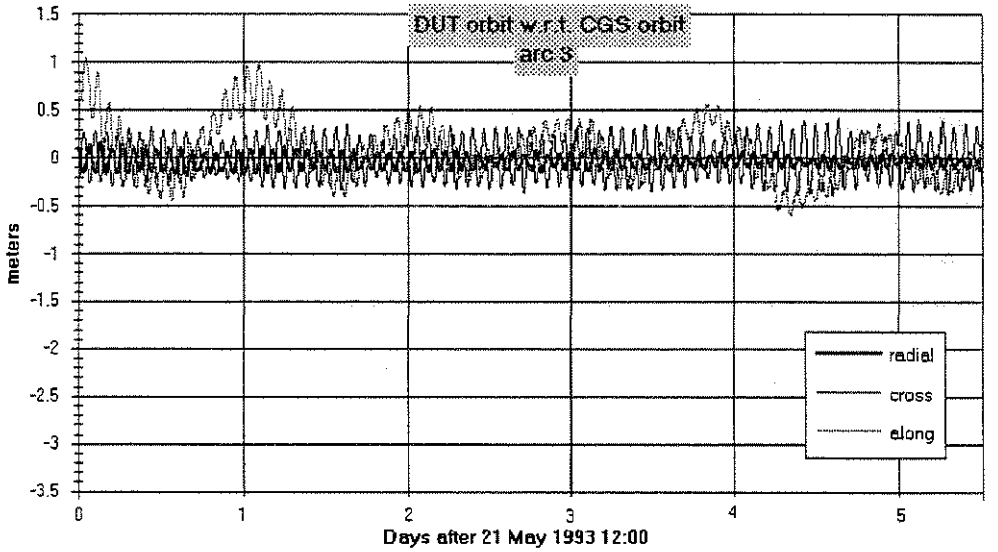

Figure 4c

Concerning the analysis based on the QL/NP data, some results of the internal consistency checks and the comparison with the D-PAF orbits are summarized in the Table 4 below.

Summary of orbit differences (QL/NP data): Overlap analysis

	Arc 1 - Arc 2			Arc 2 - Arc 3		
Position diff. (m)	**Radial**	**Cross track**	**Along track**	**Radial**	**Cross track**	**Along track**
Minimum	-0.134	-0.139	-0.861	-0.116	-0.145	-1.343
Maximum	0.109	0.141	0.774	0.097	0.142	0.309
Mean	**-0.005**	**0.000**	**-0.057**	**-0.005**	**-0.001**	**-0.123**
Rms	**0.046**	**0.074**	**0.234**	**0.059**	**0.066**	**0.329**

Summary of orbit differences (QL/NP data) : D-PAF w.r.t. CGS with QL/NP

	Arc 1			Arc 2			Arc 3		
Position diff. (m)	**Radial**	**Cross**	**Along**	**Radial**	**Cross**	**Along**	**Radial**	**Cross**	**Along**
Mean	**-0.017**	**0.030**	**-0.330**	**-0.015**	**-0.032**	**-0.426**	**-0.012**	**-0.037**	**-0.393**
Rms	**0.119**	**0.324**	**0.537**	**0.110**	**0.299**	**0.794**	**0.169**	**0.306**	**0.826**

Table 4

Conclusion

These tests indicate the ability to estimate the orbit of ERS-1 with a radial precision better than 10 cm using SLR data; the agreement with the D-PAF and DUT precise orbits is acceptable. Probably, the agreement with the D-PAF orbits could be improved using the same terrestrial reference system and the same force model, but this is beyond the scope of this preliminary work. It has to be pointed out that the D-PAF includes in its analysis cross-over data from the ERS-1 Radar Altimeter which have not been considered here.
The overlap analysis gives worse results, above all in the along-track component, when the data distribution in the period of interest is not so dense but the r.m.s. of the radial differences is less sensitive to the lack of data.

Acknowledgement

We would like to thank Ron Noomen (DUT) for his support.

Geophysical Signal or Instrument Noise?

Peter Dunn and Mark Torrence
Hughes STX, Greenbelt, Maryland, U.S.A.

Introduction

The best current SLR systems provide range measurements with an accuracy at their noise level of a few millimeters, but the satellite position determined from these observations is limited by force and Earth model errors to a few centimeters. On the other hand, the influence of model error on station position is low enough to determine the three-dimensional location of the best stations with millimeter repeatability. However, certain kinds of instrument errors, such as calibration bias, clock offset, TIU oscillator drift, and some detector characteristics can bias the station location estimate if they are neglected in the data analysis.

Satellite Ranging Data Applications

The technical applications of SLR data cover a variety of scientific areas. The accurate satellite position defined by a network of SLR stations enables us to improve the gravity model of the Earth and to investigate other force model effects on the orbit. The network also allows high resolution of Earth orientation parameters from observations of geodetic satellites in stable orbits, such as the LAGEOS and ETALON constellations. The scale of the measurements allows very accurate definition of the center of mass of the Earth, as well as the dimensions of the planet and its gravitational constant. Individual stations can define specific position information to yield tectonic motion measurements and deformation in certain regions, and to monitor height variations to improve measurements of sea level.

The SLR instruments are carefully calibrated in their routine operations, and are occasionally cross-checked in collocation comparisons, but there is a need to remain alert to the possibility of instrumental errors affecting the scientific parameters produced by the most modern systems operating at millimeter accuracy. The usual procedure in SLR data analysis is to concentrate on maintaining the integrity of the observations, and to estimate only those orbit and station location parameters which are of technical interest. The basic criterion for the separation of these estimates from instrument errors is to maintain a large volume of passes within the time span of interest, and provide a variety of orbital geometries. In order to accurately define horizontal position, it is important to cover the sky in both latitude and longitude, and this can be accomplished efficiently with day/night tracking systems and intelligent shift scheduling. On the other hand, vertical position is improved by covering a large

range of pass elevations, and this requires versatile tracking mounts with no mechanical limitations.

In order to conduct the measurements in a short period of time, geometric analysis approaches can be used, but depend on both the precision and the accuracy of the observations. These methods require concentrated simultaneous observations from a critical configuration of stations, which is usually difficult to schedule in advance. The use of dynamic data analysis techniques, in which orbital as well as Earth and station position parameters are simultaneously estimated is more widely employed. This approach can be adopted for routine data analysis and is more dependent on the accuracy of the observations than their precision, as the orbital fit to the observations does not usually match their noise level.

SLR Measurements of the Vertical

The powerful capability of SLR systems to use the scale of the ranging observations to monitor station height is useful in a variety of geophysical and engineering applications. For example, the systems can monitor tectonic processes in the region for indications of pre- or post-seismic events. The time grain of the height variations that can be detected at the millimeter level ranges from hours (for atmospheric pressure loading) to decades (for post-glacial rebound), and includes strong signals at the semi-diurnal and diurnal frequencies caused by Earth tides and ocean loading. The absolute scale upon which the SLR measurements are based allows us to accurately define scale in an Earth-centered reference system, and to establish a global vertical datum. The vertical resolution of SLR systems facilitates the calibration of altimeter instruments, as well as defining the radial orbit component in altimeter missions, to fully exploit the accuracy of the calibrated instruments.

The factors which limit the vertical resolution of the SLR systems include the orbital reference system, the local survey (for optical axis eccentricity and for horizontal target distances in externally calibrated instruments), as well as the model for atmospheric refraction and the data processing system to properly accommodate known satellite signature and detector characteristics. Instrument characteristics which remain uncalibrated will directly influence the systems' vertical resolution and the characteristic signature of the most common errors must be separated from station height.

Station Height and Range Bias

The effect of engineering changes in a continuously developing SLR system can be seen in the first figure, which shows the history of monthly height determinations of the MOBLAS-7 instrument at Greenbelt, Maryland during the period between 1980 and 1990, in which several up-grades were made. Most of the obvious changes in the vertical behavior at the site can be reduced with

corrections based on the analysis of engineering data collected during the upgrade process, but the ability of the data analysis to separate height variation from unexpected ranging system error is also strong in the most accurate modern systems. The signature of the engineering error must be different from that of the height signal if it is to be detected in the absence of external information.

The effect on the range residuals to a monthly fit of data from the Global Laser Tracking Network if a station's measurements are all biased by 10 mm is shown in the second figure. The range residuals at the example station (Yarragadee), shown as a function of elevation, are displaced by a little less than the full range offset, which is partly shared by participating stations in the network through the orbit. The effect on two of these supporting stations is only a millimeter or two with a sign which depends on the station' s position: a site close to the example station will share the sense of the displacement and a remote station will balance the bias in the orbit. The equivalent residual signals for a height displacement at the example station is shown in the next figure, and here we see a different function of elevation from the range bias, with again a very small effect at the supporting stations. We can therefore be confident that, with a reasonable data yield, a simple range bias can be separated from height at the offending station and that other stations in the network will be largely unaffected by the error. On the other hand the height signature is similar to that given by a range scale error, and this similarity is shown in the final figure, in which range residual is plotted against range value for the station whose height is displaced. The ability of the observations to detect a range-dependent TIU oscillator frequency error is thus weaker than their sensitivity to a straight ranging offset, but the separation of the two effects can usually be achieved if a concentrated data span is collected. Epoch timing errors, on the other hand, may be linked to orbit characteristics, but will not usually be confused with height and are easily separated from horizontal position with a few passes of data.

Summary

In SLR measurements to stable targets like LAGEOS I and II, any significant instrument bias can be separated from location error, particularly in the vertical component, where SLR systems have a powerful resolution capability compared to other space techniques. It is important, for example, to discriminate between range bias and eccentricity error (which is physical if not really geophysical) for stations which have been moved or disturbed, or which have undergone no collocation test. The concentration of observations required to separate geophysical from engineering signal depends on the nature and magnitude of the offending error, and subtle effects will require a large data set to be accurately resolved.

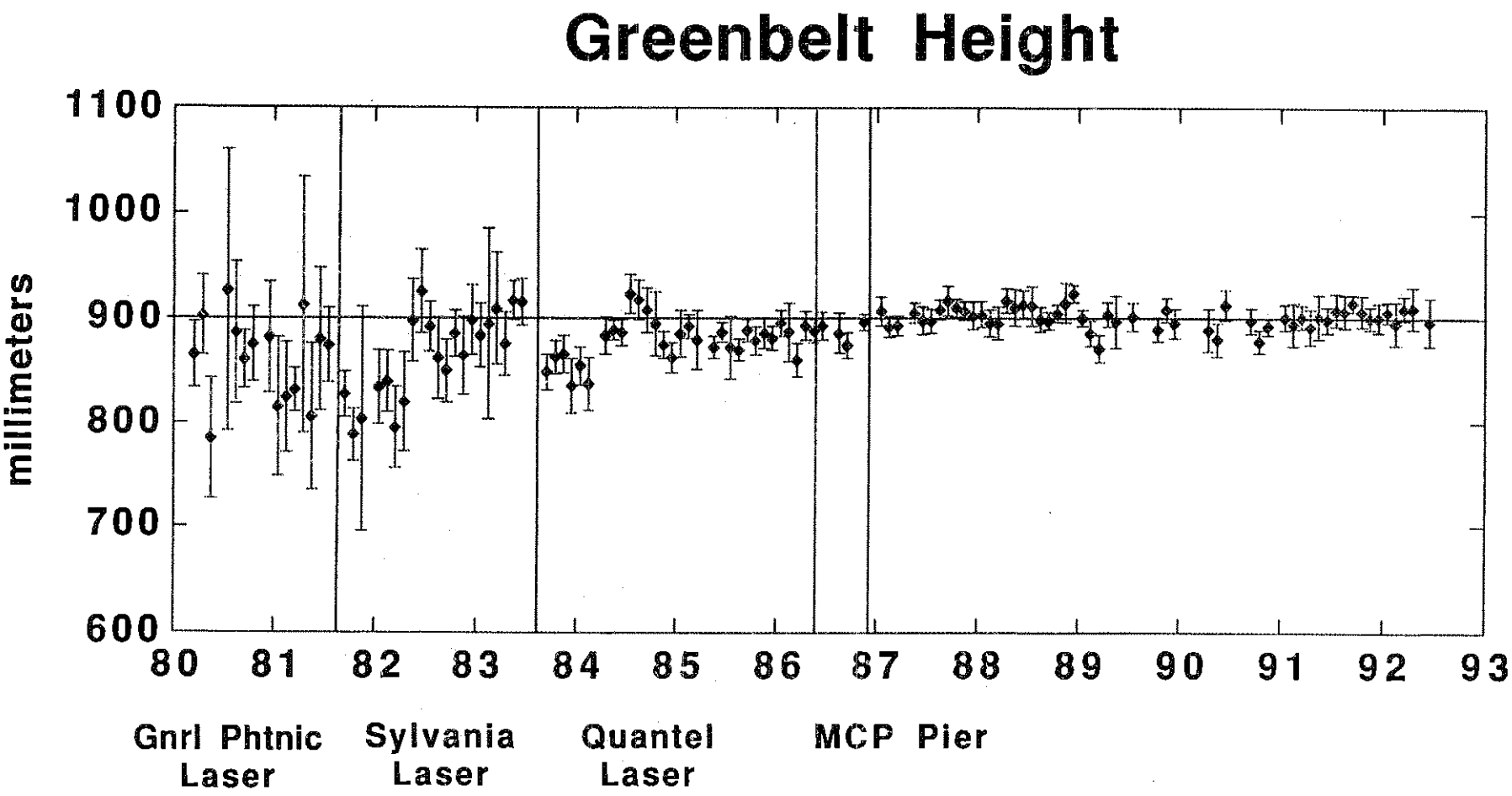
Greenbelt Height
millimeters
1100
1000
900
800
700
600
80
81
82
83
84
85
86
87
88
89
90
91
92
93
Gnrl Phtnic Laser
Sylvania Laser
Quantel Laser
MCP Pier

Effect of Yarragadee Range Bias on Residuals

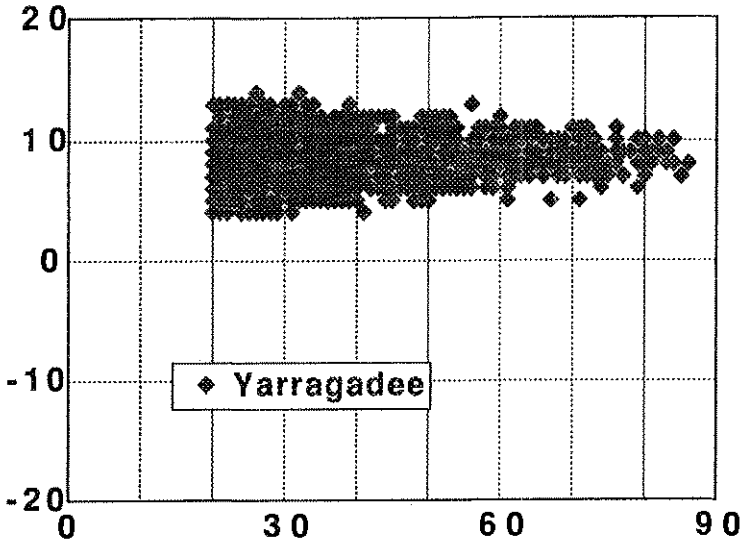

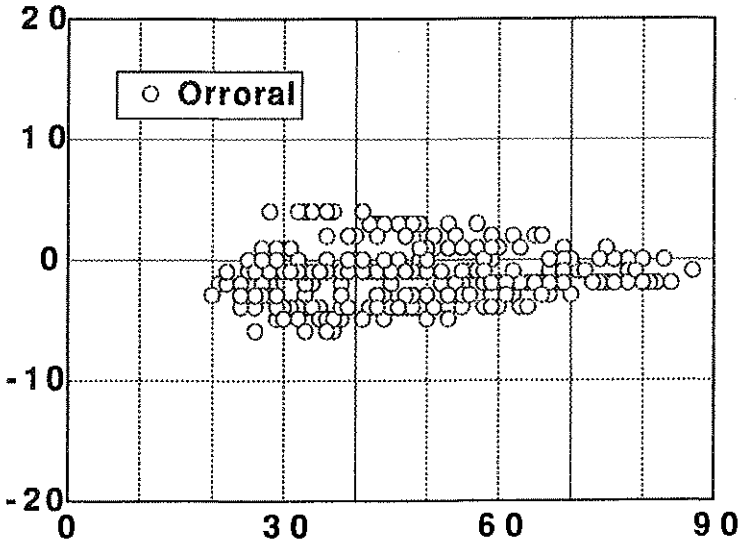

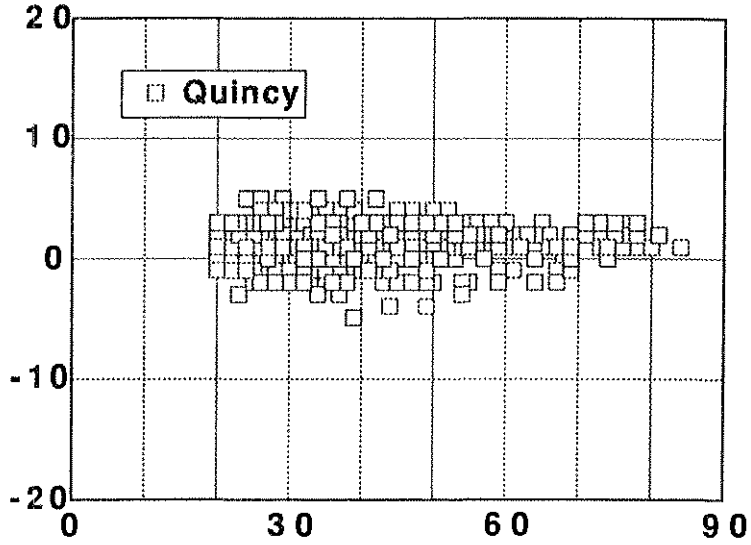

LRW '94

Effect of Yarragadee Height Offset on Residuals

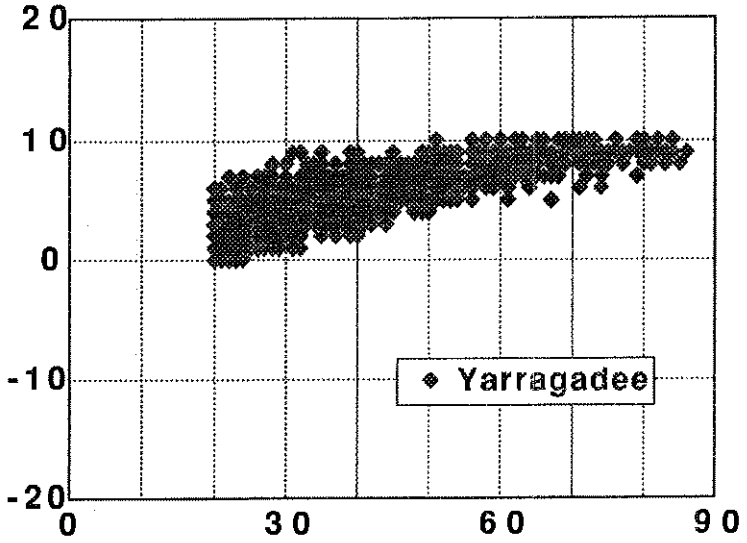

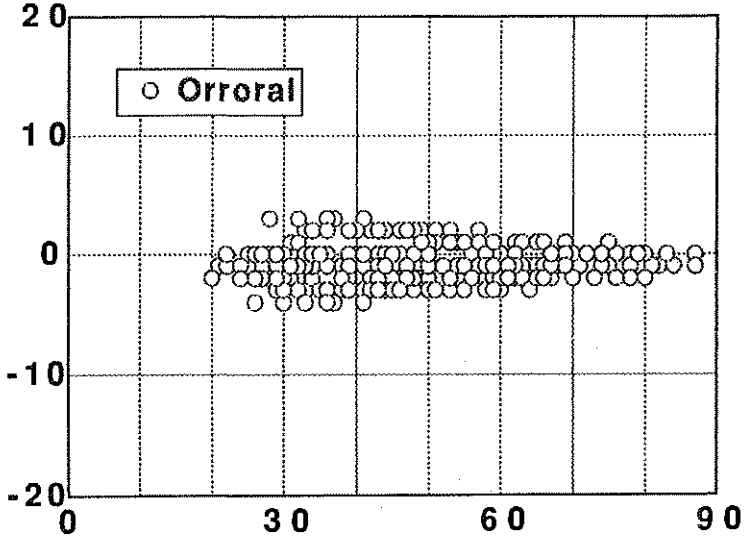

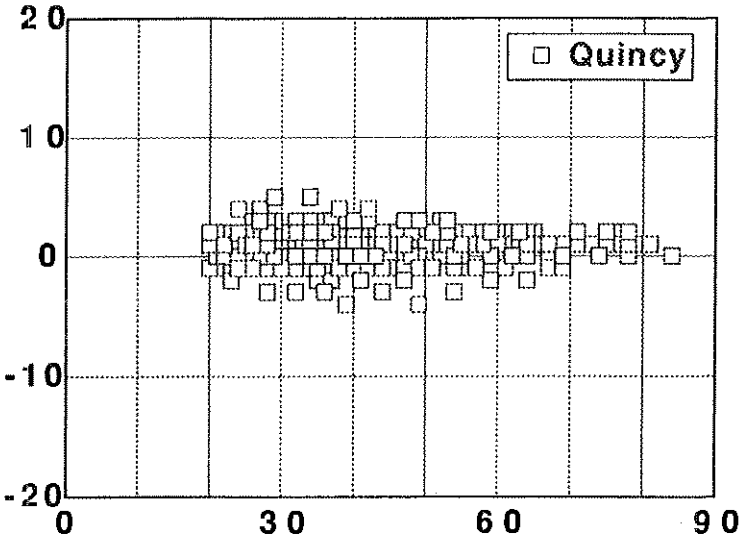

Effect of Yarragadee Height Offset on Residuals

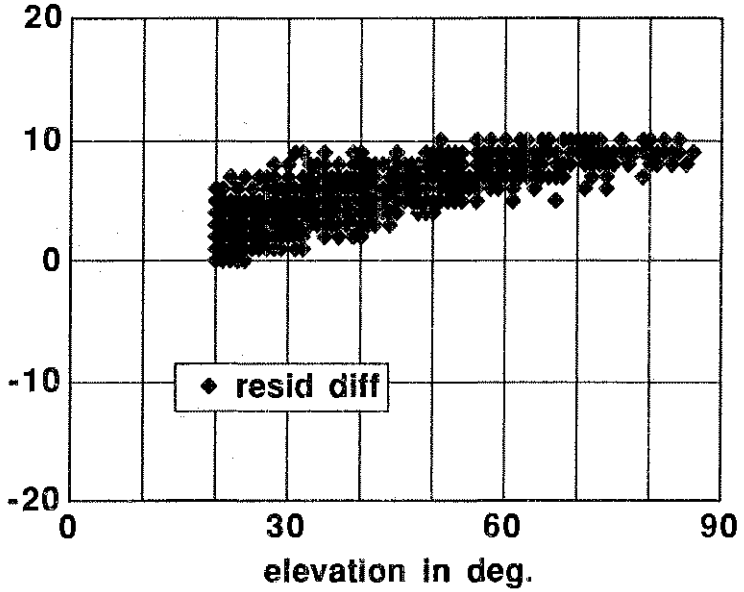

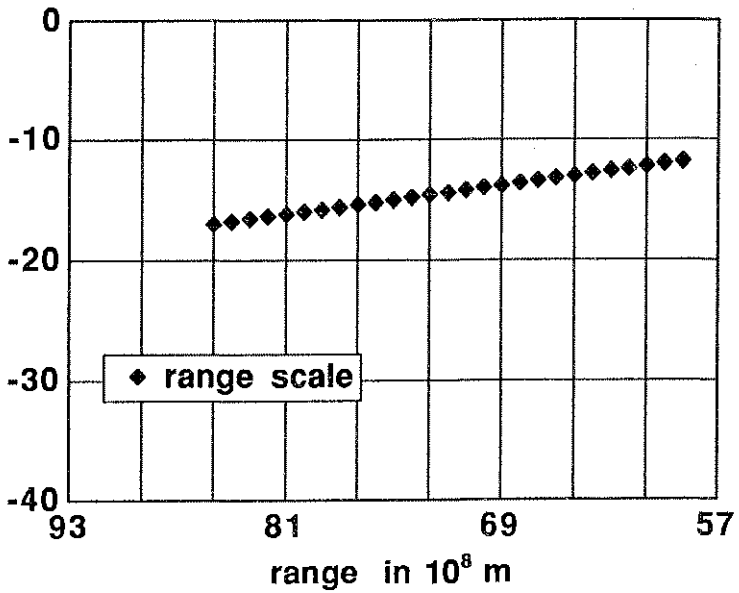

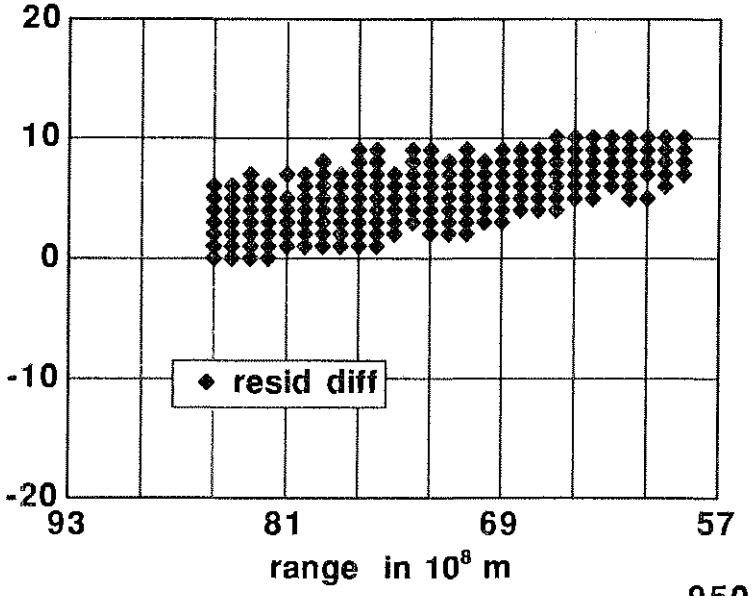

950109

PROBABLE QUALITIES OF GFZ-1 ORBIT PREDICTIONS

R. König, Z. Chen
GeoForschungsZentrum Potsdam (GFZ), Dept. Kinematics and Dynamics of the Earth, Potsdam, Germany

The new laser satellite GFZ-1, being built under GFZ contract, will be launched in March 1995. This gravity mission will have the lowest altitude, i.e. 400 km and less, among the geodetic satellites. GFZ will generate and distribute orbit predictions to the SLR (Satellite Laser Ranging) community. Surface forces, besides gravity, will cause major perturbations of the orbit. The prediction errors of the atmospheric models will result in considerable along-track errors of the predicted orbits. Particularly the dependence of the orbit prediction accuracies on the prediction errors of the solar and geomagnetic activities is analyzed. Also the influence of the prediction errors of polar motion and Earth's rotation rate is investigated.

1. INTRODUCTION

GFZ will generate orbit predictions for the new laser satellite GFZ-1 and provide them to the SLR community. GFZ gained already a lot of experience in producing orbit predictions for the ERS-1 and METEOR-3 satellites flying at altitudes of 800 km and 1250 km respectively. The GFZ-1 mission will put new demands on the orbit prediction process because the orbit has an initial altitude of 400 km only and will then decay to 300 km within about 5 years. More details on the mission may found in *Reigber et. al.* [1994].

The surface forces at the altitudes of the GFZ-1 orbit create enormous orbit perturbations (see *Reigber and König* [1994]). All a priori model errors being introduced to the orbit prediction process will pile up rapidly in the predicted period. Particularly the errors made in the prediction of solar and geomagnetic activity will influence the orbit prediction accuracy. Also ERPs (Earth rotation parameters, i.e. polar motion and lengths of day) have to be predicted for the orbit prediction period. Their errors will also affect the orbit prediction accuracy.

In the following the errors of solar and geomagnetic activity predictions and of predictions of ERPs are determined. The data are based on the past ERS-1 orbit prediction work over a period of nearly three years. With the results of this error assessment, the influence on the GFZ-1 orbit predictions is investigated.

2. ERRORS OF SOLAR AND GEOMAGNETIC ACTIVITY PREDICTIONS

Solar and geomagnetic activity prediction data are taken from the ERS-1 orbit prediction work done since launch in July 1991 until May 1994. In the following the errors are compiled and some features highlighted.

2.1 *Errors of Solar Flux Predictions*

The errors of solar flux predictions are computed from the differences between the values used in the ERS-1 orbit prediction processes and the final values available later on. The errors are shown in the upper part of Figure 1. The lower part of Figure 1 compiles the solar flux magnitudes for the same period.

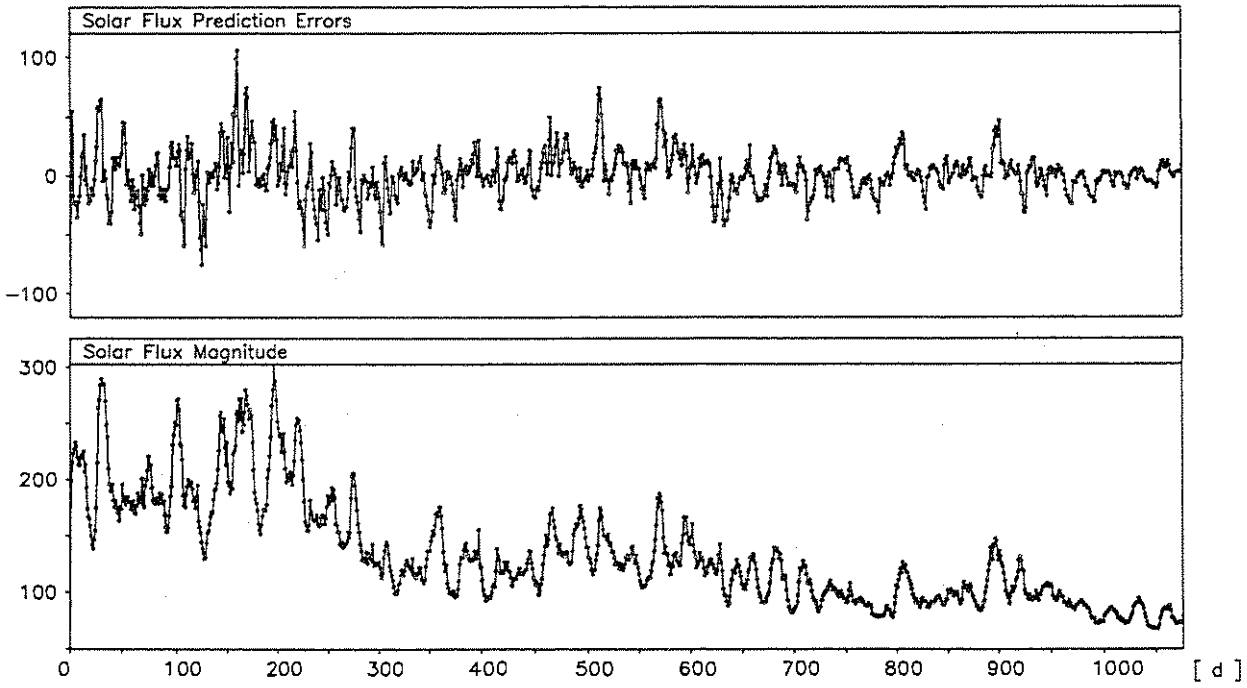

Figure 1 Errors of solar flux predictions and solar flux magnitudes

The errors of the solar flux predictions are highly correlated with the magnitude of the solar flux. The solar flux prediction errors have therefore been sampled in classes of certain solar flux magnitudes. The result is graphically displayed in Figure 2.

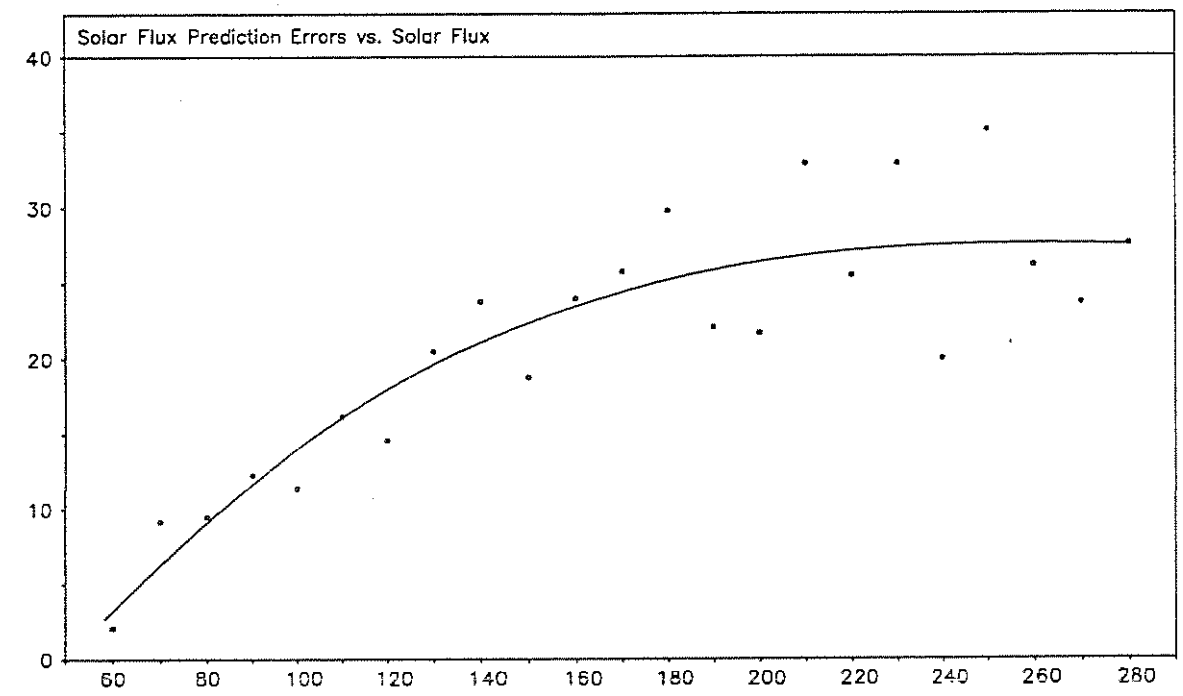

Figure 2 Solar flux prediction errors w.r.t. solar flux magnitude

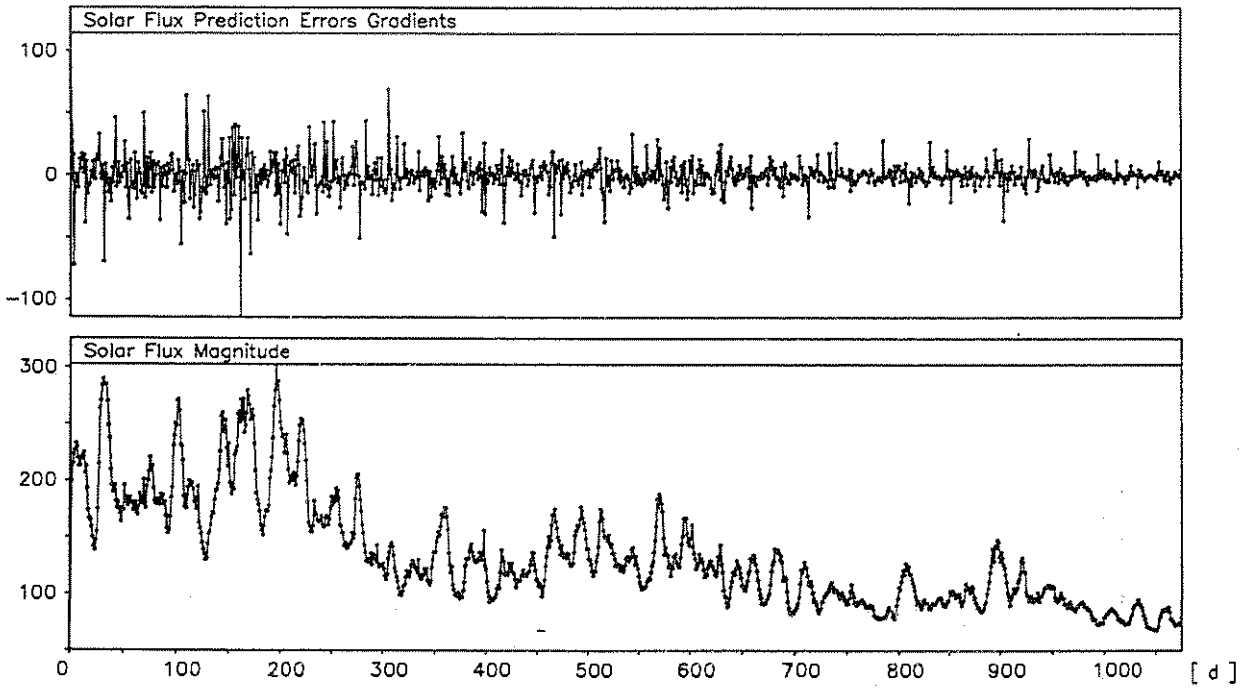

Figure 3 Gradients of the solar flux prediction errors

At high solar activities the errors of the solar flux predictions are large. A line is fitted to the values providing a general relation between solar flux prediction errors and solar flux magnitude.

If the solar flux prediction errors are viewed in greater detail, one can notice consecutive errors developing in a more or less linear way within certain periods. So the error curve shows a sawtooth like behaviour. Therefore gradients from error point to error point are determined providing one more error feature besides extrema, mean and RMS values. The computed gradients are compiled in Figure 3.

Again the dependence on the magnitude of the solar flux can be seen. The overall level of error development can be represented by the median of the absolute values of the gradients being 5.0. The median is taken in order to exclude any impact of the large gradients resulting at leaps between successive prediction sets. A gradient of 5.0 means that the prediction error of solar flux values increases in general by 5 units from day to day. Besides the median of the absolute values of the gradients, extrema, mean and RMS values for the solar flux prediction errors are compiled in Table 1.

Table 1: Errors of solar flux predictions

	Min	Max	Mean	RMS	grad (1/d)
Flux (10**-22 J/s/m**2/Hz)	-75	106	1.4	19.9	5.0

2.2 *Errors of Geomagnetic Activity Predictions*

The errors of geomagnetic activity predictions in terms of Ap values are displayed in Figure 4. The errors are determined by comparing the predicted values, used in ERS-1 orbit prediction work over 3 years, with the final values.

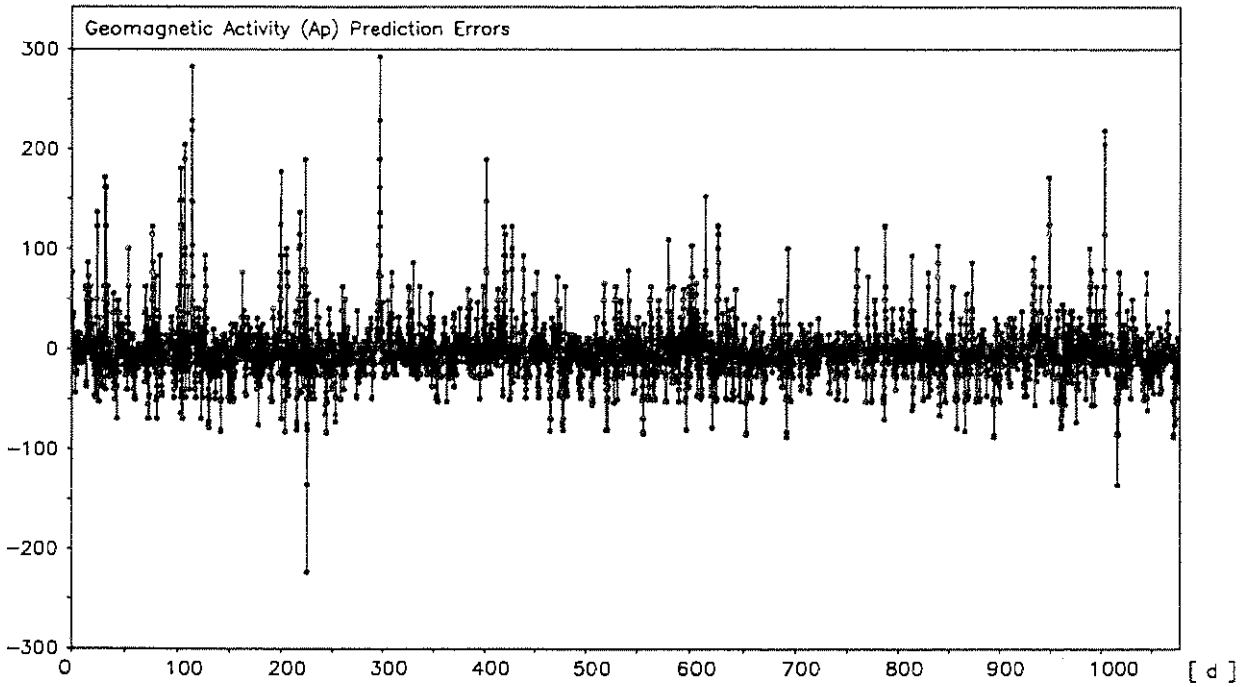

Figure 4 Geomagnetic Activity prediction errors

Large correlations between consecutive errors can be noticed. This becomes visible in the correlation matrix given in Table 2. Columns and rows from 1 to 8 are respective to the three-hourly Ap errors at 0 hours to 21 hours of all days.

Table 2: Correlations of three-hourly Ap errors

	0 h	3 h	6 h	9 h	12 h	15 h	18 h	21 h
0 h	1.0							
3 h	0.8	1.0						
6 h	0.6	0.8	1.0					
9 h	0.4	0.5	0.7	1.0				
12 h	0.2	0.4	0.5	0.7	1.0			
15 h	0.2	0.2	0.4	0.5	0.7	1.0		
18 h	0.3	0.3	0.4	0.4	0.5	0.7	1.0	
21 h	0.3	0.2	0.3	0.3	0.4	0.5	0.7	1.0

An interesting feature of geomagnetic activity prediction errors can be found if the error analysis is carried out for each Ap error at 0 hours, 3 hours, 6 hours etc. separately as compiled in Table 3.

Table 3: Errors of geomagnetic Ap predictions

	Min	Max	Mean	RMS
0 h	-223	219	-8.9	26.8
3 h	-135	229	-2.6	25.7
6 h	-80	219	0.0	24.0
9 h	-69	293	1.6	21.6
12 h	-53	229	3.1	21.5
15 h	-85	190	0.7	22.7
18 h	-87	205	3.9	25.9
21 h	-135	283	-10.6	27.8
all	-223	293	-2.6	25.0

The Ap predictions around noon are more accurate than around midnight. There seems to be no obvious physical reason for this. The overall RMS value amounts to 25 units.

3. ERRORS OF ERP PREDICTIONS

The ERP predictions considered in the following have been used in the orbit prediction work done for ERS-1 from July 1991 until May 1994. Their errors are computed from the differences of the predicted values to the later on available final values.

The errors of ERP predictions show in general similar features as the solar flux prediction errors above. Figure 5 compiles the errors for polar motion predictions in X- and Y-direction and for the lengths of day predictions in terms of UT1R-TAI differences.

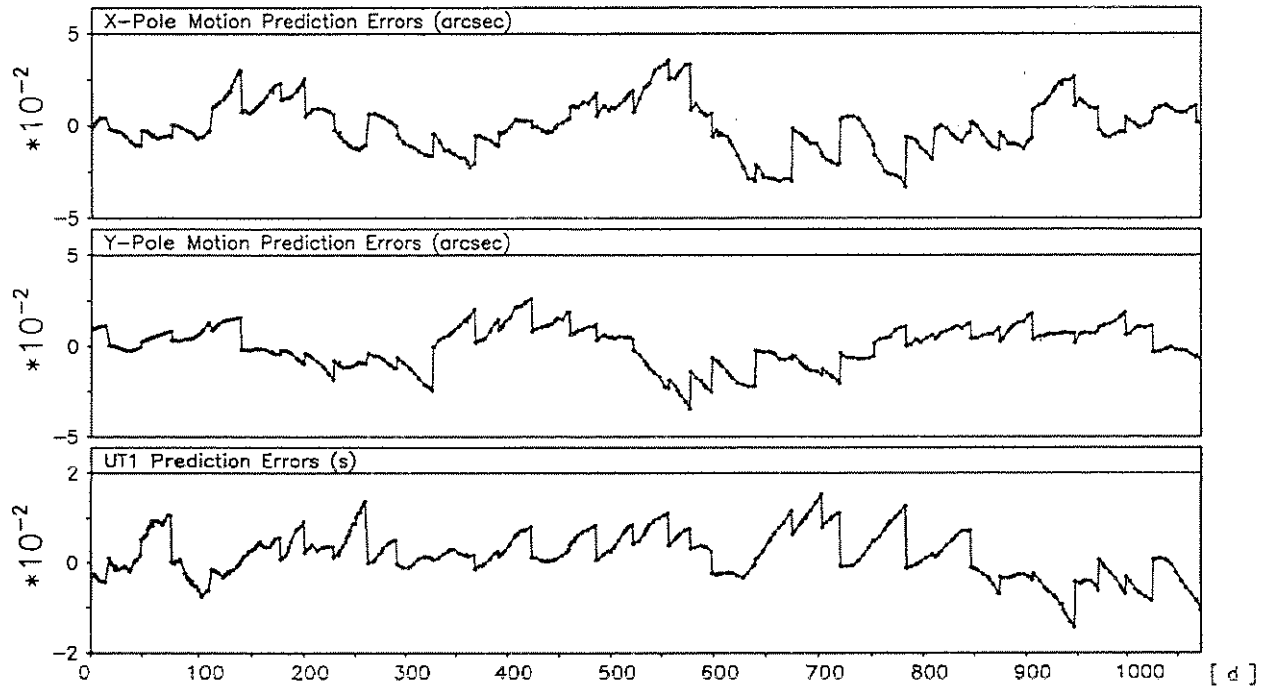

Figure 5 ERP prediction errors

The sawtooth behaviour of the errors is clearly visible. Polar motion prediction errors seem to have a slight seasonal dependence. The UT1R prediction errors have been mainly positive during the first two years.

Table 4 gives the extrema, the mean and RMS values and the median of the absolute values of the gradients.

Table 4: Errors of ERP predictions

	Min	Max	Mean	RMS	grad (1/d)
X-Pole (mas)	-33.0	35.6	-0.2	13.4	0.5
Y-Pole (mas)	-34.6	26.1	0.7	10.8	0.3
UT1R (ms)	-14.4	15.3	1.7	5.2	0.2

4. IMPACT ON GFZ-1 ORBIT PREDICTIONS

On the basis of the results of the previous error analyses, simulations are carried out in order to estimate the influence of solar and geomagnetic activity prediction errors and of ERP prediction errors on the orbit predictions in the GFZ-1 mission scenario.

Two reference orbits are generated, one with an altitude of 400 km and with a low solar activity model representing the environment at beginning of the mission in March 1995. The second reference orbit has an altitude of 350 km and is integrated with models reflecting the high solar activity towards the end of the mission in November 1999.

The influence of the prediction errors of solar activity on the orbit predictions is determined by changing the flux values of the reference orbit models according to the prediction error features found above. For the first of the original flux values within the orbit prediction period a random error is generated with a standard deviation depending on the flux magnitude as given in Figure 2. The consecutive flux values within the orbit prediction period are altered by this random error plus an increase computed with help of the gradient. So the sawtooth shape of solar flux prediction errors is preserved. With the erroneous model the orbit is integrated and compared to the reference orbit. The differences represent the orbit prediction error due to solar flux prediction errors. The results for the two mission phases are listed in Table 5.

Table 5: Orbit prediction errors due to flux prediction errors

Scenario	Maximum errors after 3 d		
	Radial (m)	Cross-track (m)	Along-track (m)
400 km, Low SolAct	37	386	7573
350 km, High SolAct	83	1257	25116

In the worst case for low orbital altitudes in conjunction with high solar activity the solar flux prediction errors lead to an along-track error or a time bias respectively of the orbit predictions of more than 3 seconds in time after 3 days already. This is a demanding new level of error development in orbit predictions not experienced so far with satellites familiar to the SLR community.

In order to keep track of the time bias development once GFZ-1 will be in orbit, a few laser range observations each day are required. A further help will be to determine the solar flux prediction errors as soon as updated values are available and the resulting time bias thereof. In this case the atmospheric model errors, which may also lead to considerable orbit prediction errors (see *Reigber and König* [1994]), are still present. Therefore a proper time bias evaluation will always rely on sufficiently dense laser tracking.

The prediction errors of the geomagnetic activity may also have a major effect on the orbit prediction accuracies. In order to investigate this, the original Ap values of the reference orbit model are altered by random errors with a standard deviation according to the error analysis above. With the erroneous models the orbits are integrated and compared to the reference orbits. Table 6 provides the maximum orbit prediction errors after 3 days resulting from the simulated geomagnetic activity prediction errors.

Table 6: Orbit prediction errors due to Ap prediction errors

Scenario	Maximum errors after 3 d		
	Radial (m)	Cross-track (m)	Along-track (m)
400 km, Low SolAct	7	53	1027
350 km, High SolAct	33	454	8990

The influence on orbit prediction accuracies from geomagnetic activity prediction errors seems to be not as large as from solar activity prediction errors. Nevertheless the along-track orbit prediction error or time bias respectively may reach values of 0.1 to 1 seconds in time and more after 3 days. Again this is a level where laser tracking is already heavily affected. For the geomagnetic activity prediction errors the same comments apply as for the solar flux prediction errors. If the time bias can not be estimated from laser tracking, an indication of the time bias could be gained from geomagnetic activity prediction errors as soon as updated Ap values are available. As the atmospheric model errors will still be present, this method can not be a substitute for dense laser tracking of the satellite.

Finally the influence of ERP prediction errors on GFZ-1 orbit predictions are determined. The original values of the reference orbit models are altered by random errors with standard deviations according to the error analysis of the previous chapter. Additionally some error increase within the orbit prediction period on the basis of the previously derived gradients is introduced.

As now the solar activity models are kept fix and as the difference of the orbital altitudes is small, the following holds approximately for both mission scenarios. Table 7 summarizes the orbit prediction accuracies depending on ERP prediction errors.

Table 7: Orbit prediction errors due to ERP prediction errors

ERP	Maximum errors after 3 d		
	Radial (m)	Cross-track (m)	Along-track (m)
Polar motion	0	1	1
UT1R	0	4	3

Indeed the influence of ERP prediction errors is small. Therefore no need can be seen to watch the ERP prediction errors very carefully within the GFZ-1 mission.

5. SUMMARY AND CONCLUSIONS

The errors of solar and geomagnetic activity predictions and the errors of ERP predictions are analyzed on the basis of nearly 3 years of orbit predictions for ERS-1. Solar flux and ERP error series show a sawtooth like behaviour. Extrema, mean and RMS values as well as correlations and gradients describing the dynamical behaviour of the errors are compiled. The results are used to estimate the influence of the errors on GFZ-1 orbit predictions within two contrary mission scenarios within the expected lifetime of GFZ-1. It turns out that errors of solar and geomagnetic predictions will heavily affect the orbit prediction accuracy at a much higher level than what the SLR community is used to. Particularly the time bias will increase very rapidly and can only be controlled if at least a few laser range observations can be acquired day by day.

REFERENCES

Reigber, Ch., König, R., Massmann, F.-H., "The GFZ-1, the ERS-1 and the ERS-1/ERS-2 Tandem Mission," this volume (1994)

Reigber, Ch., König, R., "Gravity and Atmosphere Aspects by the Low Altitude Target GFZ-1," this volume (1994)

An assessment of the IRV model for very low and very high satellites

A.T. Sinclair

Royal Greenwich Observatory, Madingley Road, Cambridge CB3 0EZ, England.

1. Introduction

The IRV format, coordinate system and force model were adopted by the Center for Space Research (CSR), University of Texas in about 1982 as a means of providing predictions for Lageos. They adapted the IRV system from a system previously in use by NASA. The IRV system has now been adopted for all satellites, but using a different degree and order for the gravity field for lower satellites. This system is working well for the satellites ranging in height from ERS-1 to Lageos. In this paper we examine its effectiveness for very low satellites such as MSTI-2 and GFZ-1, and for very high satellites such as GPS35 and GPS36. We find that it does not work too well for very low satellites. There are two possible solutions, either to use a more elaborate force model or to use the same force model but generate the IRVs over a shorter span than the 1-day in use for other satellites. We consider that the second option is the easier to implement.

2. The IRV force model

The IRV force model uses the GEM10 gravity field model, evaluated to degree and order 7 for Lageos 1 and 2 and higher satellites, and to degree and order 18 for lower satellites. Lunar and solar perturbations are applied, with the positions of the Moon and Sun being calculated from simple precessing-ellipse orbital models, and no drag or solar radiation pressure forces are included in the model.

There are much better gravity field models now available than GEM10, but it has not been considered worthwhile to make a change, due to the difficulty of ensuring that the changes are properly carried out in the wide variety of software that is in use throughout the SLR network, and anyway the present model seems to be perfectly adequate for all the SLR satellites prior to the launch of MSTI-2.

3. The orbit of MSTI-2

MSTI-2 (9402801) had a short life of being tracked by SLR. It was launched on 9th May 1994 into an orbit with inclination 97.11° and height 435 km. It carried a retro-reflector on the lower side of its 3-axis stabilised body. It was in a Sun-synchronous orbit, with the Sun at close to 90° to the orbit plane. This made it virtually impossible to observe from highish latitudes during the summer months. The satellite became unstabilised in early October 1994, and then attempts to range to it ceased. Thus there never was an opportunity for ranging to it from European stations.

The SLR tracking data that were obtained were very sparse, but there were a few periods of a few days with sufficient data to give a moderately good orbit. We have selected the period July 19.0 to July 23.0 with a total of 9 passes from the stations Haleakala, Monument Peak, Quincy and Yarragadee. The JGM-2 gravity field model was used, to degree and order 70, and a solar radiation pressure and a drag parameter were solved-for, in addition to solving for the state vector. This gave an RMS range residual of 3.78 m. This was adopted as our precise

reference orbit for the purpose of testing the IRV process - for this purpose it does not matter whether or not it is a particularly accurate orbit.

IRVs were formed from this precise orbit. The IRVs use the standard force model described above, and are tuned to give the best fit to the precise orbit over one-day spans. The differences of the IRV orbits from the precise orbit are resolved into the along-track, across-track and radial directions, and are plotted in Figure 1. The along track components shows a strong quadratic variation over the span of each day, with an amplitude of about 400 m. This is clearly due to the strong drag forces on the satellite which are not included in the IRV model. The total error of a set of IRVs used for a predicted orbit would consist of this quadratic component plus a probably much larger secularly increasing along track error due to the error of predicting drag. So does the quadratic component of the error matter, if the total error is likely to be much larger? We consider that it does. In recent years there has been a big increase in the success of tracking the lower satellites by the SLR network due to the use of time bias (i.e. along-track) corrections to the current set of IRV predictions. From every pass of a satellite that is tracked anywhere in the network a time bias correction is determined, and this is distributed to the stations. For the normal satellites this time-bias correction is found to vary smoothly, and it is possible to extrapolate with reasonable accuracy to estimate the time bias for a coming pass. However if this quadratic along-track error is present in the IRVs then it will affect the time bias determination made from each pass that is tracked, and if only a few passes are available over a short time span then the attempt to fit a smooth curve through these determinations could give a very inaccurate determination of what the trend in the time bias is actually doing.

4. Use of an improved IRV force model

We first consider the option of reducing the differences between the IRV orbit and the precise orbit by improving the force model used in the IRV integrator. The first stage of improvement of the IRV model is to include a drag force. (The same drag term as in the precise orbit was used, and soit was not found to be necessary to solve for a drag term in the tuning process.) With this drag force included, the differences of the IRV orbit from the precise orbit is shown in Figure 2. The strong quadratic variation has been removed, and the RMS of the remaining differences is 31.2 m.

The next stages of improvement are to use the JGM-2 field for the IRVs, to increase the degree and order, and to include a solar radiation pressure force in the IRV model. Inclusion of the solar radiation pressure force had little effect. Changing to JGM-2 field, still at 18x18, reduced the RMS differences to 23.8 m, and then increasing the degree and order to 26 reduced the RMS to 14.6 m. The differences with all of these improvements applied to the IRV model are plotted in Figure 3.

5. Use of a shorter time span for the IRVs

We next consider the option of reducing the differences between the IRV orbit and the precise orbit by reducing the time span over which the IRV orbit is tuned to fit the precise orbit. For all satellites before the launch of MSTI-2 a one-day span is used. The drag term causes a quadratic error in the IRV orbit, and so we would expect that if the time span is reduced by a factor h the error due to drag would be reduced by a factor h^2. So we expect that use of a 0.25-day span will reduce the drag error by a factor of 16, which should be adequate. The errors due to some of the other limitations of the IRV force model will also be reduced by restricting them to act over the shorter time span.

Using the standard force model for the IRV orbits, but restricting them to spans of 0.25 days, the differences of the IRV orbits from the precise orbit are shown in Figure 4. The RMS of the differences is 17.2 m.

We note that there are two possible ways to produce IRVs that are valid for a fraction of a day (we will consider the case where the span being used is 0.25 days). The first is to produce the IRVs with epochs 0.0 day, 0.25 day, 0.50 day, 0.75 day, and , for example, the set with epoch 0.50 would be used to generate orbits over the span 0.50 to 0.75 days. The second way is produce all four sets with epoch 0.0 days, and so, for example, if an orbit was required within the span 0.50 to 0.75 days the relevant set of IRVs would have to be integrated from 0.0 days up to a most 0.75 days, but the orbit thus generated would only be used within 0.50 to 0.75 days.

The first of these ways is computationally more efficient, but computational efficiency is of little importance these days, and anyway, all these processes are very fast. The second way is much easier to implement. For the stations no changes to software are needed other than to select which of the four sets of IRVs to use. The first way involves using a fractional day for the epoch, and this has probably never been tested in much of the IRV software that is in use, and would most likely cause problems. Also there would need to be some discussion as to whether the meridian of 0^h of the fraction of the day should be used as reference point. In the tests for this paper we have used the second way for the formation of IRVs over a fraction of a day, and we have found this to be quite straightforward; one simply limits the period of the tuning to the required fraction of a day.

6. Recommendations

We have shown that, for the very low satellite MSTI-2, the standard IRV model using 0.25 day spans gives an RMS difference of the IRV orbit from the precise orbit of about 17.2 m, and using a more elaborate force model over one day spans gives an RMS of about 14.6 m. The plots of the differences in each case of the IRV orbits from the precise orbits are shown in figures 3 and 4, and are farly similar. Thus we consider that either of these methods would produce IRVs of sufficient precision for use in practice. However it would be a difficult task to ensure that the software modifications needed to include a drag and solar radiation force model in the on-site integrators throughout the network, and we consider that the option of reducing the time span of the IRVs is much simpler. Further, we consider that if this scheme is adopted then the epochs of all of the sets of IRVs used for a day should be 0^h.

The plot of along-track differences in Figure 4 (standard IRV model at 0.25 day span) shows a high frequency signature, which is due to the limitations of the gravity field model used. Thus one may question whether it is worth making some improvements to the force model as well as using a shorter time span for the IRVs. It would be very easy to replace the dated gravity field model GEM10 by a modern gravity field model such as JGM-2, and not too difficult to increase the degree and order of the coefficients used, although this would mean some changes to array dimensions. The following lists the mean RMS of the differences of the IRV orbit from the precise orbit for MSTI-2 for various choices of the gravity field, all using IRVs over 1/4 day spans:

GEM10	18x18	RMS	17.2 m
JGM-2	18x18	RMS	15.3 m
JGM-2	26x26	RMS	7.9 m

7. Use of the standard IRV model for other satellites

ERS-1 is the lowest of the SLR satellites in normal use, and for it the RMS difference of the standard IRV model using one day spans is about 14.2 m. A plot of these differences is shown in Figure 5. These are fairly similar in nature to those shown for MSTI-2 in figures 3 and 4. In practice the IRVs for ERS-1 are found to work well, and in particular the noise level of them is sufficiently low to permit time bias corrections to be determined with sufficient accuracy. However if it were decided to use a better gravity field model than GEM10 for very low satellites, then it would no doubt be used for all other satellites also, and we have examined what improvement this change would make for ERS-1. We find that the improvement is small, because the IRVs of ERS-1 are at present limited about equally by the deficiencies of the GEM10 field and by the omission of drag from the IRV model. Thus both of these factors need attention in order to improve the IRVs. If a 1/2 day span is used in order to reduce the drag effect, and the JGM-2 field is used to degree and order 26, then the RMS of the differences of the ERS-1 IRVs from the precise orbit is 2.7 metres.

At the other extreme of height of the usual SLR satellites, we have considered Lageos, and the RMS difference of the IRVs using the standard model over one day spans is about 3.0 m. We expect that the satellites of height in between ERS-1 and Lageos will have IRVs with RMS differences somewhere between these values of 14.2 and 3.0 m, and indeed it is found that the IRVs for all of these satellites work well in practice.

For the GPS satellites the situation is a little worse, due to the comparatively large solar radiation pressure forces which are not included in the IRV model. Figure 6 shows a plot of the differences of the IRV orbit for GPS36 from the precise orbit. The RMS difference is 34.0 m. This rather high noise level of the IRV orbit does cause a little uncertainty in the values determined for the time bias correction from a satellite pass, but this is not a severe problem. The broadcast elements can be used to give a mean daily value for the time bias correction, which bye-passes the problem of a poor determination from a single SLR pass.

Figure 1. Differences of tuned IRVs (standard model) from precise orbit

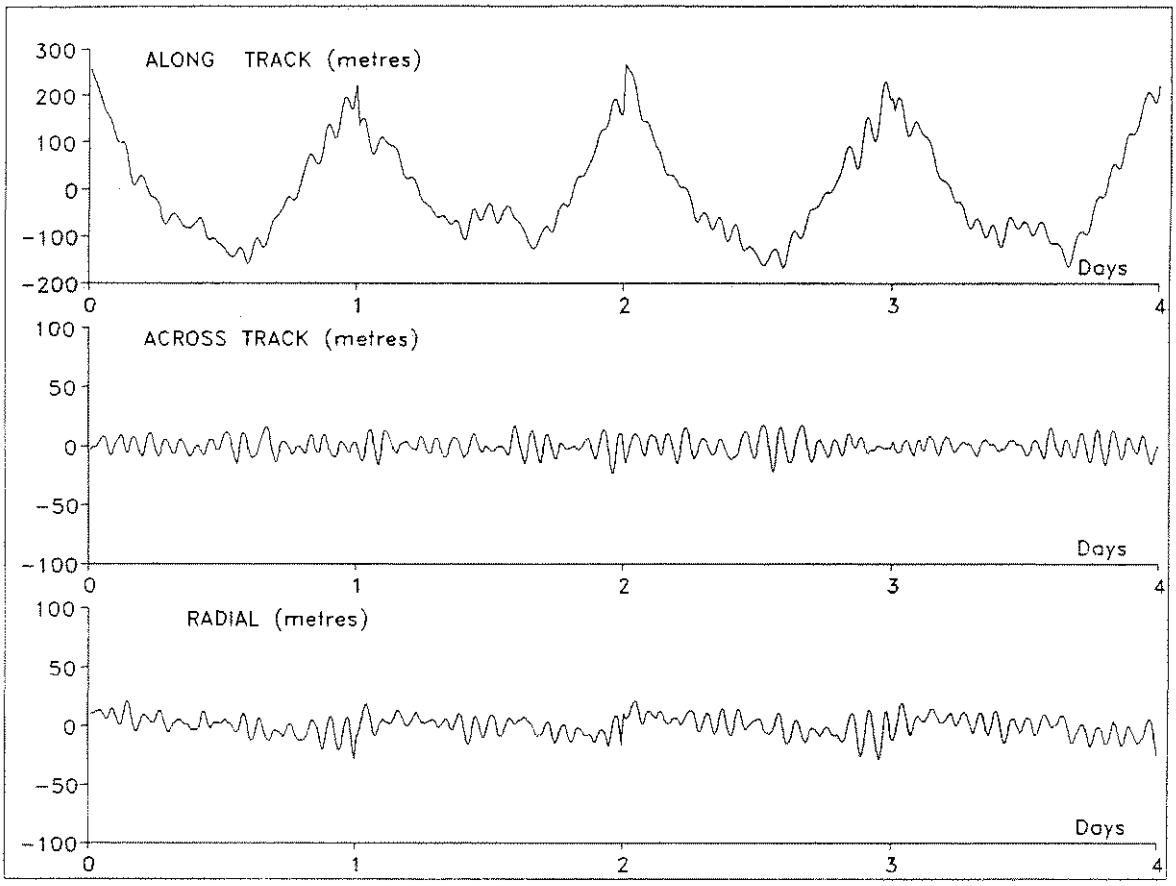

Figure 2. Differences of IRVs (including drog) from precise orbit

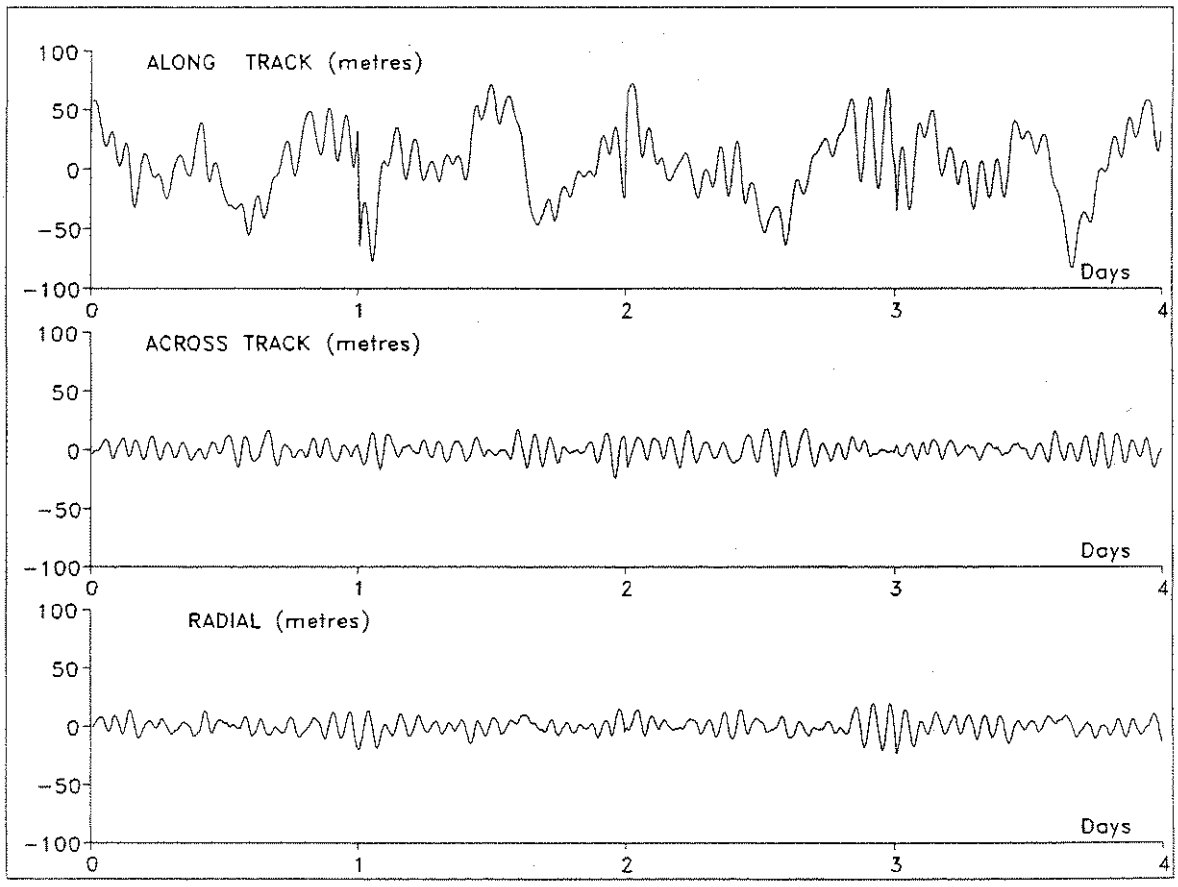

Figure 3. Differences of IRVs (drag, JGM2 26x26, SolRad) from precise orbit

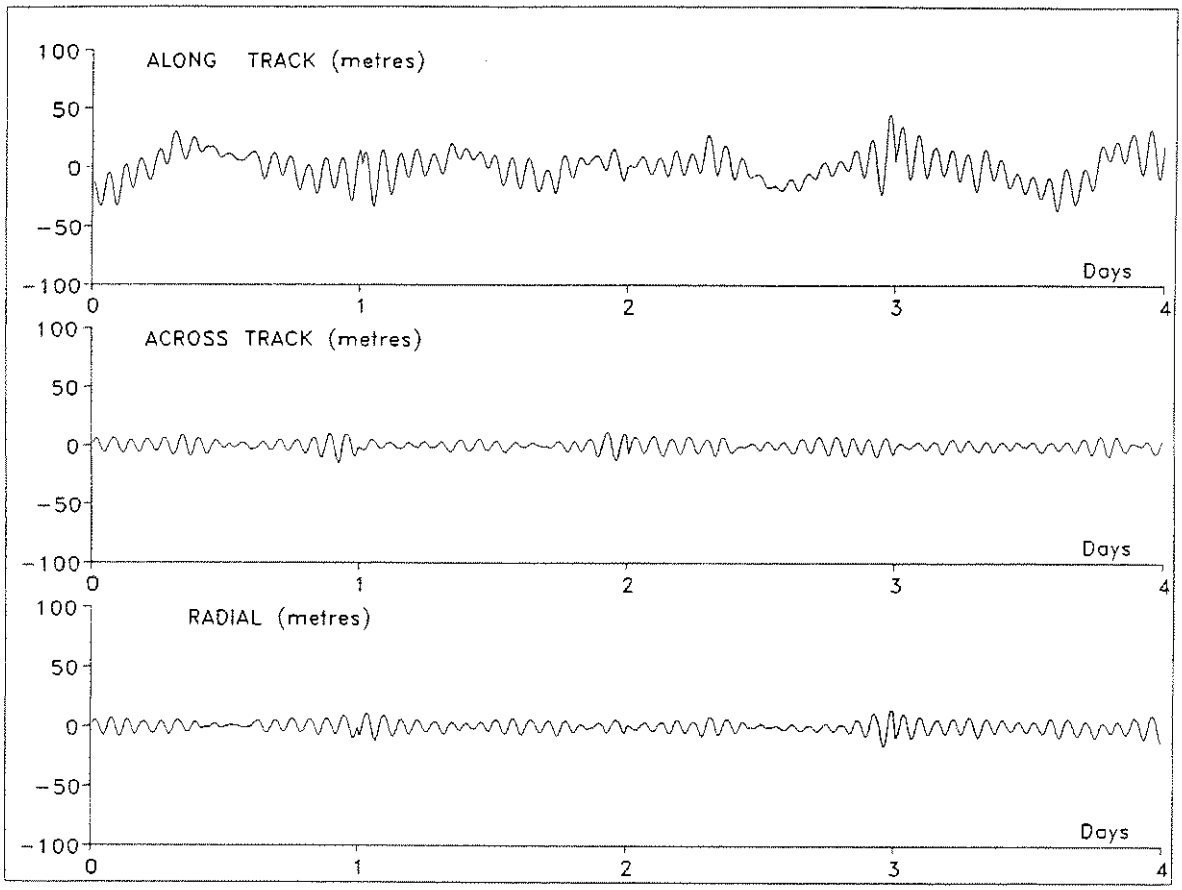

Figure 4. Differences of IRVs (standard model, 0.25 day span) from precise orbi

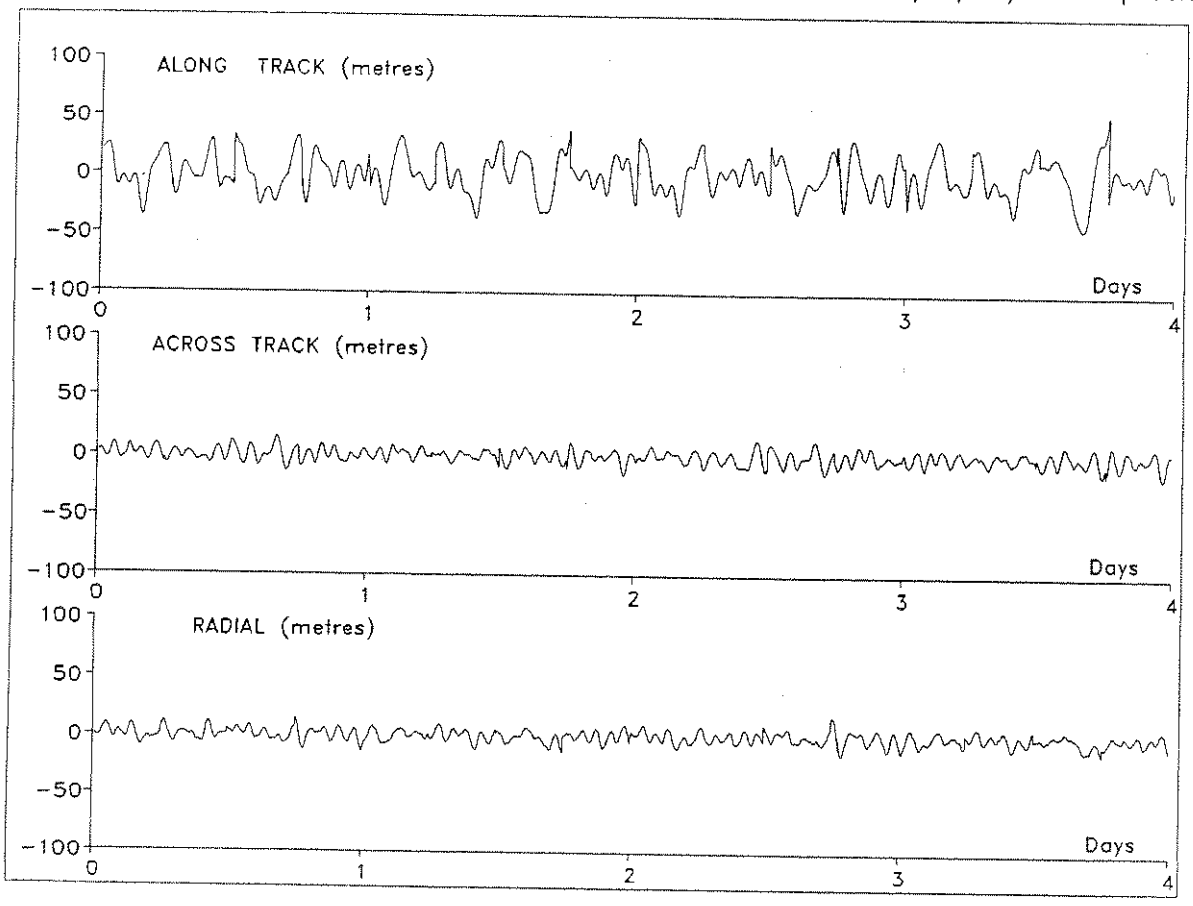

Figure 5. Starlette. Differences of IRVs (standard model) from precise orbit

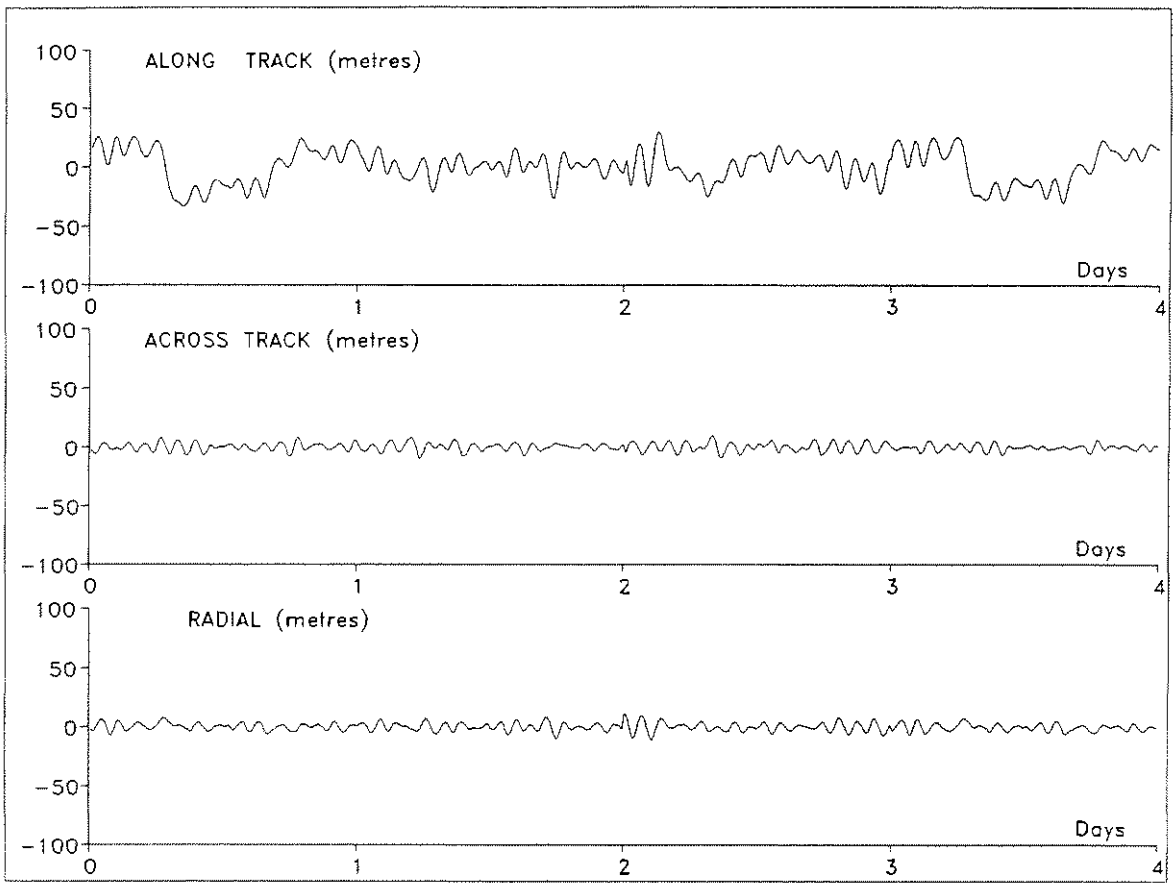

Figure 6. GPS36. Differences of IRVs(standard model) from precise orbit